

NEW APPLICATIONS OF ANALYTICAL TECHNIQUES TO FOSSIL FUELS
Introduction to the Symposium

H.L. Retcofsky and M.B. Perry

U.S. Department of Energy
Pittsburgh Energy Technology Center
P.O. Box 10940
Pittsburgh, PA 15236

The "New Applications of Analytical Techniques to Fossil Fuels" symposium was envisioned as a forum for researchers to describe (1) new twists to established techniques, (2) techniques only recently applied to fossil fuels, and (3) potentially useful techniques that have not as yet been applied to such materials. The response to our call for papers was overwhelming, the result being a four-day symposium consisting of thirty-six technical presentations. The podium will be shared by speakers from industrial, government, and university laboratories. We are pleased to acknowledge participation by three countries -- Canada, United Kingdom, and the United States -- all of which have well-established, on-going fossil fuel programs.

ORGANIZATION OF THE SYMPOSIUM

We resisted the urge to organize the papers into sessions according to analytical technique by structuring the symposium so as to place primary focus on the materials examined and the type of information obtained. Thus, one session is devoted to coal or coal macerals as total (unseparated) materials, while other sessions emphasize analyses for particular functional groups. Another session deals with compound identification, while others address process-oriented analysis and measurements of dynamic processes. Logistical consideration dictated that the three invited magnetic resonance papers be organized into a single session.

Most of the symposium papers deal with instrumental methods of analysis. This was not unexpected because applications of modern instrumental techniques have experienced phenomenal growth since their introduction in the mid- and late-1940's. Figure 1 depicts historically the introduction of a few such techniques into the coal research programs at the Pittsburgh Energy Technology Center; the timetable of Figure 1 closely parallels that for other fossil fuels research organizations located throughout the world. The large number of techniques that will be described during this symposium suggests that periodic updates of such plots are appropriate at relatively short intervals. Among the many techniques included in the symposium are laser induced fluorescence, inverse gas chromatography, ultraviolet resonance Raman spectroscopy, and zero field nuclear magnetic resonance, as well as many of the hyphenated techniques, such as TGA-FTIR, GC-FTIR, and LC-MS. Classical wet methods, nonetheless, are not ignored.

SOME THOUGHTS FOR THE FOSSIL FUEL ANALYST

The current role of the fossil fuel analyst in the research environment is one in which he functions as an integral member of the research planning team. The analyst faces a number of technical challenges that require a very broad scientific knowledge covering a number of different disciplines. The lack of such knowledge may very well leave the fossil fuel analyst vulnerable to a variety of "perils and pitfalls" that in some cases are unique to the fossil fuel area. The following thoughts are given (with perhaps a degree of "tongue in cheek") to draw attention to several of these.

Perils and Pitfalls

Thou shalt have many samples before thee, and no one shall be considered sacred is, for example, good advice for the coal analyst. In a study of sixty-four vitrains from coals originating from nine countries, a quite viable explanation for the electron spin resonance (ESR) characteristics of the samples was presented (1,2). Despite the large number of samples and the wide geographical distribution, a more recent study revealed "unusual" coals that do not adhere to the correlations established during the earlier study (3). Needless to say, such findings often lead to new research opportunities and improved understanding of coal structure.

In a similar vein, **Thou shalt have a variety of analytical methods before thee, and again, no one shall be considered sacred.** This statement is motivated by results from an extensive laboratory study of five methods that are commonly used for the determination of asphaltenes (4,5). In their initial study, which was confined to a coal-derived liquid, Schultz and Mima found (not unexpectedly) that the results were dependent on the method that was used (4). The method dependency was further confirmed (again, not unexpectedly) in their second study, which extended the testing of the methods to a coal-derived solid (5). Subsequent analysis of the data for both samples (Figure 2) revealed a sample dependency in addition to the method dependency, thus precluding the use of a constant factor to compare the results of analyses performed by the different procedures (6).

With respect to the coal analyst's need for a broad knowledge of a variety of scientific disciplines, it is well that **Thou shalt remember thy physics and honor its relevance.** Drawing again from the ESR literature, it has been shown that misleading g values and spectral intensities may result from the lack of attention given to the physical bases that underlie both the ESR phenomena and the microwave techniques employed to observe the resonances (7).

Fossil fuel analysts should no longer permit themselves to be viewed as conveyers of data, and they must **Recognize that "data, however fascinating, is not insight"** (8). The present authors feel that coinage of the phrase "data base" is unfortunate in that it fails to communicate that it is the storage of information or the translation of data into useful information that should be emphasized.

Analysts, in general, strive to achieve results of high precision. It is our feeling that a more appropriate goal is to strive for that precision

necessary to solve the problem at hand. It is important that analysts **Know thy data and thy precision, and use both wisely.** Some recent work undertaken in our laboratory to respond to a challenge of the doublet state free radical interpretation of the ESR behavior of coals (9) serves to illustrate this point. Careful reanalysis of the data from reference 9, the results of which are summarized in Table 1, showed no reason to choose a model that includes both doublet and triplet states over the Curie law model, which is, in part, the basis for the doublet state free radical interpretation (10).

Fossil fuel analysts often face the problem of long-term storage instability of samples. Although the problem has been well documented (11-13), it is appropriate to remind analysts that they should **Honor thy sample, for its integrity (or lack thereof) may very well reflect upon their own.** Long-term sample stability is but one of many concerns. Certainly, analytical results on second-hand samples are suspect, and those on samples of questionable origin should be rejected outright. Additionally, short-term sample stability has received little attention despite a study that showed measurable changes in spectral properties of coal within a few hours after removal from the mine atmosphere (14). The lack or improper use of sampling protocols is yet another problem that often confronts the fossil fuel analyst. Unless he asserts himself as a member of the research team, the problems associated with improper sampling are likely to be ignored.

A Closing Thought

The final thought that we would leave with the audience is that analytical methods that have been applied successfully to other materials frequently are not directly transferable to the analysis of fossil fuels. Rare is the coal analyst who has not on occasion identified with Figure 3. We offer this closing thought for consideration by the speakers as we open this symposium.

ACKNOWLEDGMENTS

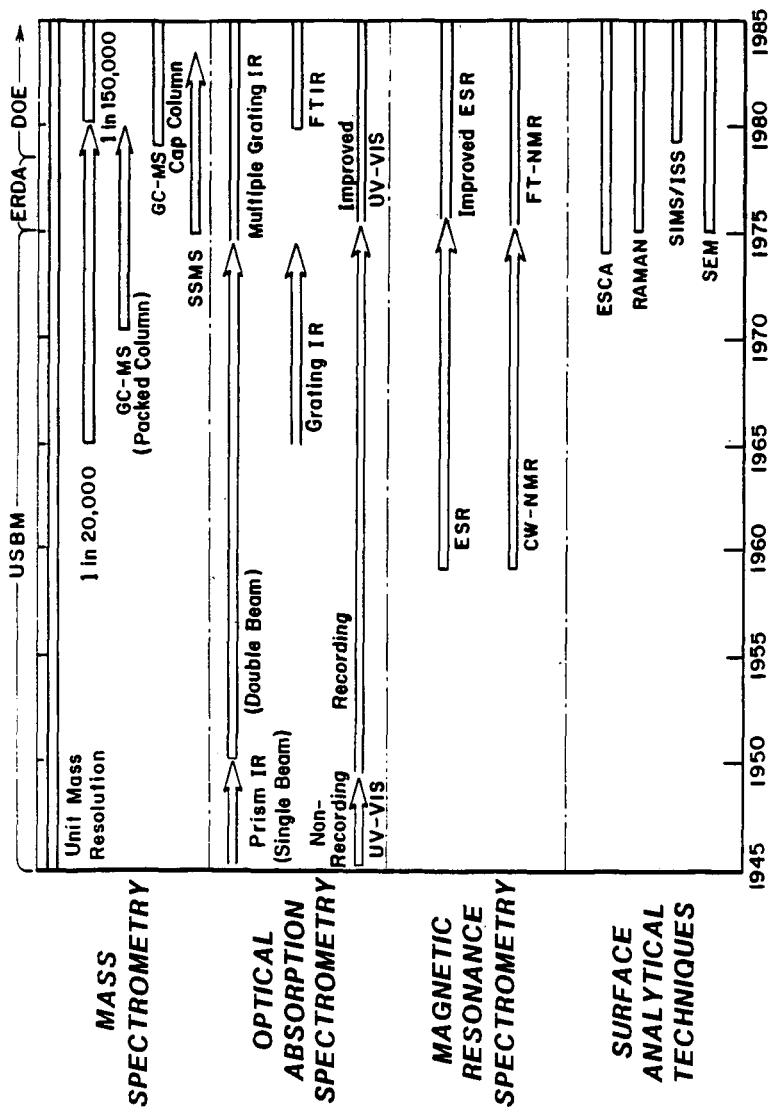
Helpful discussions with D.H. Finseth, R.F. Sprecher, H. Schultz and S. Castellano and editorial assistance by M.S. Edmunds are gratefully acknowledged.

Table 1. ESR Intensity-Temperature (IT) Behavior for a Single Coal

Temperature Range, K	126	to	264
IT (Measured), Arbitrary Units	23.4	to	28.95
IT (Measured) - IT (Predicted) (CURIE LAW MODEL)	-0.45	to	0.25
IT (Measured) - IT (Predicted) (CHARGE TRANSFER MODEL)	-0.47	to	0.37

REFERENCES

1. Retcofsky, H.L.; Thompson, G.P.; Hough, M.; Friedel, R.A. In "Organic Chemistry of Coal," ACS Symp. Ser. 1978, 71, 142.
2. Retcofsky, H.L.; Hough, M.R.; Maguire, M.M.; Clarkson, R.B. In "Coal Structure," (Gorbaty, M.L.; Ouchi, K., eds.) ACS Advances in Chemistry Ser. 1981, 192, 37.
3. Retcofsky, H.L. In "Coal Science," (Gorbaty, M.L.; Larsen, J.W.; Wender, I., eds.) Vol. 1, Academic Press, 1982, 43.
4. Schultz, H.; Mima, M.J. "Comparison of Methods for the Determination of Asphaltenes, Oils and Insolubles: Part 1-A Coal-Derived Liquid," PETC/TR-8013, Technical Information Office, U.S. DOE.
5. Schultz, H.; Mima, M.J. ACS Div. Fuel Chem. Preprints 1980, 25(1), 18.
6. Synfuels Characterization (A Publication of the Pittsburgh Energy Technology Center, H.L. Retcofsky, ed.), October, 1982.
7. Retcofsky, H.L. Appl. Spectrosc. 1980, 31, 116.
8. Quotation attributed to Richard Kluger.
9. Duber, S.; Wieckowski, A.B. Fuel 1984, 63, 1474.
10. Castellano, S. Carnegie-Mellon University, Personal Communication.
11. Brown, F.R.; Karn, F.S. Fuel 1980, 59, 431.
12. White, C.M.; Jones, L.; Li, N.C. Fuel 1983, 62, 1397.
13. Jones, L.; Hazlett, R.N.; Li, N.C.; Ge, J. Fuel 1984, 63, 1152.
14. Ohuchi, H.; Shiotani, M.; Sohma, J. Fuel 1969, 48, 187.



**FIGURE 1. Spectrometric Instrumentation at PETC
(Partial Historical overview)**

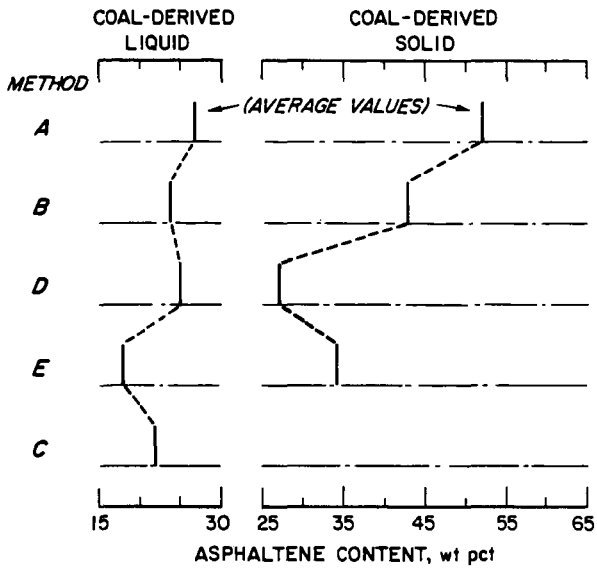


FIGURE 2. Comparison of Methods for the Determination of Asphaltenes in Liquid and Solid Products from Coal Liquefaction

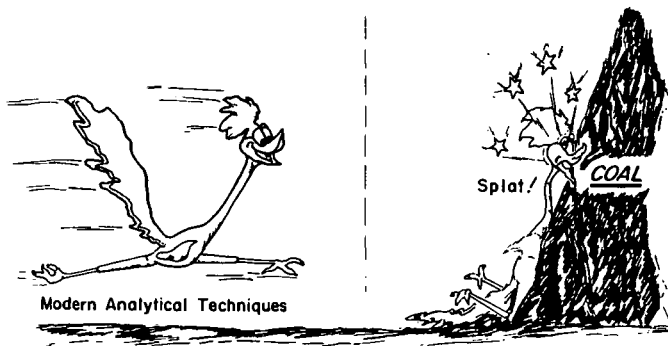


FIGURE 3. The Study of Coal Structure

LASER-INDUCED FLUORESCENCE MICROSCOPY OF COAL MACERALS
AND DISPERSED ORGANIC MATERIAL

W.L. Borst, M.W. Pleil,
and G.W. Sullivan
Department of Physics
Texas Tech University
Lubbock, Texas 79409

and

J.C. Crelling and C.R. Landis
Department of Geology
Southern Illinois University
Carbondale, Illinois 62901

INTRODUCTION

Fluorescence microscopy has been a useful analytical tool for characterizing organic material in various coals and rocks (1-9). Teichmuller and Wolf (3,7) discovered new fluorescing coal macerals, which also were found by Spackman (6) in U.S. coals. Ottenjahn et al. (9) related the fluorescence properties of macerals to technological properties of coal. Van Gijzel (8) has organized spectral fluorescence properties for comparison. Since 1983, we have extended fluorescence microphotometry from the spectral to the time domain by using a pulsed laser for fluorescence excitation. Fluorescence decay times are measured as the new characterizing parameters for the dispersed organic material. Simultaneously, individual spectra of the various fluorescing components in the material are obtained. This paper describes the new time-resolved fluorescence microscopy and its application to coal and shale characterization.

SYSTEM DESCRIPTION

The laser fluorescence microscopy system is represented schematically in Figure 1. Further specifications are given in Table 1. A pulsed laser and three sources of continuous wave (c.w.) illumination are interfaced with a Leitz MPV3 microscope. The tungsten lamp is used for spectral calibration and surveying the sample under white light. The mercury and xenon arc lamps are used for fluorescence excitation and are coupled to the excitation monochromator. The EG&G nitrogen pumped dye laser with a BDBP dye provides intense near-ultraviolet light pulses. The laser is coupled to the microscope via a liquid light guide. The modular construction of the microscope allows various optical components to be readily interchanged. The emitted fluorescence is detected by a fast two-stage multichannel plate (MCP) photomultiplier tube (Hamamatsu R1564U-01) with an enhanced red response. The output of the MCP is directed either to a picoammeter when acquiring conventional c.w. spectra or a Tektronics 7912AD fast waveform digitizer when acquiring time-resolved spectra. The digitizer sums a number of MCP output pulses and passes the average to the 4052A Tektronics desk top computer. The extensive software, developed in-house, constitutes a large portion of the development time.

TABLE I - Instrument Parameters and Fluorescence Signals

Size of coal maceral	10-50 μm
Diameter of analyzed area	5 μm
Tuning range of emission monochromator	220-800 nm
Range used	380-800 nm
Monochromator bandwidth	1-7 nm
<u>Continuous Fluorescence Excitation</u>	
Tuning range of excitation monochromator	220-800 nm
Typical excitation wavelength	365 nm
Monochromator bandwidth	1-7 nm
<u>Fluorescence Excitation by Pulsed Laser</u>	
Dye laser pulse duration (FWHM)	0.7 ns
Pulse energy (BDBP dye, 373nm, 10Hz)	10 μJ
Peak power	10 kW
Laser bandwidth (FWHM)	0.04 nm
Dye laser tuning range	360-800 nm
Excitation wavelength used	373 nm
Pulse repetition rate	1-100 Hz
Number of photons emitted per pulse (BDBP dye)	2×10^{13}
Photons onto sample	1×10^{13}
Photons onto measured region of sample ($\sim 5 \mu\text{m}$)	$10^{11} - 10^{12}$
Typical fluorescence yield	0.001
Photons reaching MCP photomultiplier after passing emission monochromator	10^4
Typical number of photoelectrons per pulse	$10^2 - 10^3$
Instrument function risetime (laser pulse + photomultiplier + digitizer preamplifier)	0.7 ns
FWHM of instrument function	1.1 ns
Single pulse digitization rate	10-100 GHz
Number of pulses signal averaged, typical	64

METHOD

Time-resolved fluorescence emission spectra are obtained in 10 nm steps by scanning the emission monochromator of the MPV3 from 400 to 700 nm and acquiring the fluorescence decay at each wavelength. This takes about 10 seconds at each wavelength or 5 minutes total. The data reduction yields the multiple decay times, component spectra, and relative intensities and takes about 4 minutes at one wavelength or 1-2 hours total. Conventional spectra are obtained with c.w. illumination and continuously scanning the emission monochromator. This takes about 60 seconds, including correction for optical system response and smoothing. Very similar spectra, as expected, are obtained by integrating the time-resolved results.

For routine data collection, a tungsten lamp is used to determine the spectral response of the system. The lamp is cross calibrated with a standard lamp of a known spectral output. This is done by measuring the raw spectrum, which includes the system response of both the tungsten and standard lamps. The ratio of the raw tungsten spectrum $T_r(\lambda)$ to the raw standard lamp spectrum $E_r(\lambda)$ is independent of the system response, and, when multiplied with the known standard lamp spectrum $E(\lambda)$, results in the true tungsten spectrum $T(\lambda)$

$$T(\lambda) = \frac{T_r(\lambda)}{E_r(\lambda)} E(\lambda)$$

1)

The determination of the relative spectral response $S(\lambda)$ of a chosen optical configuration (objective, dichroic filter, apertures) is done routinely by measuring the raw tungsten spectrum $T_p(\lambda)$ and dividing by the true tungsten spectrum $T(\lambda)$:

$$S(\lambda) = \frac{T_p(\lambda)}{T(\lambda)} \quad 2)$$

The corrected fluorescence emission spectrum $R(\lambda)$ from a sample is then determined by taking the ratio

$$R(\lambda) = \frac{R_p(\lambda)}{S(\lambda)} \quad 3)$$

where $R_p(\lambda)$ is the raw fluorescence spectrum. The above calibration procedures are built into the software. In this way, normalized fluorescence spectra are obtained independently of the particular optical components chosen.

The acquisition and reduction of the pulsed fluorescence data require much care. The individual anode pulses from the MCP PMT contain the fluorescence decay $F(t)$ and the temporal instrument response $I(t)$. The measured signal $M(t)$ is given by the convolution integral

$$M(t) = \int_{-\infty}^t I(\tau) F(t-\tau) d\tau \quad 4)$$

The task is to obtain the fluorescence decay function $F(t)$ and, from this, the various decay times and percentage contributions from the individual fluorescing components. This is done with an iterative deconvolution technique and least squares fitting (see below). First, the instrument function has to be determined. If $F(t-\tau)$ in the above integral is a delta-function $\delta(t-\tau)$, then the measured signal $M(t)$ is $I(t)$. Experimentally, a mirror is used in place of the sample, which corresponds to replacing $F(t-\tau)$ with $\delta(t-\tau)$. Thus the instrument response is obtained and contains the contributions from the laser pulse, photomultiplier response and preamplifier bandwidth (1GHz) of the waveform digitizer.

Various deconvolution techniques have been examined by other investigators (15,16,17). We have looked into three such techniques. The software developed allowed us to mathematically model the fluorescence experiments by convoluting a synthesized instrument response, including random Gaussian noise, with an assumed multi-exponential fluorescence decay. The synthesized signal $M(t)$ was then deconvoluted using the different techniques to see how the calculated parameters (decay times and pre-exponential coefficients) compared with the known parameters set at the beginning. We found that the Fourier transform method requires intensive operator interaction and its ability to discern a sum of two or more exponentials was questionable. The method of moments could resolve single and double exponential fluorescence decays. However, extension to three exponential waveforms has proved to be difficult. The technique we found to give the best results is the iterative reconvolution method, which was also found to be most satisfactory by O'Conner et al. (15). We are able to successfully deconvolute data containing up to three different fluorescence decays.

The iterative reconvolution method assumes that the fluorescence decay $F(t)$ from the sample is a sum of exponential terms corresponding to emission from n individual fluorophores:

$$F(t) = \sum_{i=1}^n A_i \exp(-t/\tau_i) \quad 5)$$

Combining this with Equation 4 gives the fitting function

$$M^0(t) = \sum_{i=1}^n A_i \int_{-\infty}^t I(\tau) \exp[-(t-\tau)/\tau_i] d\tau \quad (6)$$

where A_i and τ_i are the parameters to be adjusted until a best fit to the measured signal $M(t)$ is found.

This best fit is obtained when the error sum χ^2 is minimized, where

$$\chi^2 = \sum_{i=1}^N \frac{1}{\sigma_i^2} [M(t_i) - M^0(t_i)]^2 \quad (7)$$

and N is the total number of channels (128 or 512) used.

The weight σ_i^2 is the square of the uncertainty in the measurement of the i th channel and is given by

$$\sigma_i^2 = \sigma_0^2 + C \cdot M(t_i) + \left[\frac{\partial M}{\partial t} \right]^2 \sigma_t^2 + \left[\frac{\partial M}{\partial t} \frac{\Delta t}{2} \right]^2, \quad (8)$$

where σ_0^2 is the baseline noise (0.01 mV^2), $C M(t_i)$ is the counting error (1 mV^2), σ_t is the time axis jitter caused by small fluctuations in the trigger pulse ($\sigma_t \sim 40 \text{ ps}$) and Δt (~ 0.25 channels) is the fractional channel shift in our time axis lineup routine. Typical values for the last two terms in Equation 8 are 2 mV^2 and 0.25 mV^2 , respectively.

Minimizing the χ^2 error sum is an iterative process, which involves incrementing the parameters A_i and τ_i and thus successively reducing χ^2 . The method employed (20) is a combination of a gradient search along the χ^2 hypersurface and linearization of the fitting function. When far from the surface minimum, the gradient plays the dominant role in determining the increment changes. As the search closes in on the minimum, the linearization of the fitting function dominates. The parameter increments are given by

$$\delta B_j = \sum_{k=1}^{2n} \beta_k \alpha_{jk}^{-1} \quad (9)$$

where $B_j = (A_i, \tau_i)$, and β_k and α_{jk} are given by the relations:

$$\beta_k = \sum_{i=1}^N \frac{1}{\sigma_i^2} [M(t_i) - M_e^0(t_i)] \frac{\partial M_e^0(t_i)}{\partial \beta_k} \quad (10)$$

$$\alpha_{jk} = \sum_{i=1}^N \frac{1}{\sigma_i^2} \frac{\partial M_e^0(t_i)}{\partial \beta_j} \frac{\partial M_e^0(t_i)}{\partial \beta_k} (1 + \lambda \delta_{jk}) \quad (11)$$

$M_e^0(t_i)$ is the best fit from the preceding iterations, λ is a weighting factor and δ_{jk} is the Kronecker delta. The weighting factor determines the relative contribution to the increments from the gradient search on the hypersurface to the linearization of the fitting function.

APPLICATION TO COAL MACERAL ANALYSIS

An example for time-resolved fluorescence analysis is given in Figure 2 for a sporinite coal maceral (SIU sample 1444). The top part shows a signal-averaged fluorescence pulse (solid line) and the best 2-exponential fit (dashed line). The emission monochromator was set at 500 nm. The fit yields the pre-exponential coefficients A_i and decay times τ_i . The component percentages are given by

$$P_i = \frac{A_i \tau_i}{\sum_i A_i \tau_i} \quad (\text{here } i=1,2) \quad 12)$$

The accuracy of the fit can be assessed from the residuals and the reduced χ^2_V (20), where $\chi^2_V < 1$ indicates a good fit. Ideally, the residuals should be random. They are not because of a finite number of channels, interpolation between channels, small time axis jitter, and small pulse shape variations. A 2-component decay fits the present data well, and the assumption of a 3-component decay would show redundancy in the third component. The quantity τ_m is the mean decay time as defined by $\tau_m = \sum P_i \tau_i / 100$ and has proved useful for comparisons.

The bottom of Figure 2 shows a complete time-resolved spectral analysis, where the parameters A_i , τ_i , and P_i are plotted versus emitted wavelength. The coefficients $A_i(\lambda)$ are the individual component spectra. The individual decay times τ_i often remain nearly constant over the spectral range, as would be expected for pure substances.

In order to determine the usefulness of time-domain fluorescence analysis as an extension of conventional fluorescence analysis of organic materials, two sets of samples were studied. One set was a series of kerogen-rich shale samples at different levels of maturation from the New Albany Formation from the Illinois Basin. In these samples Type I kerogen is abundant as alginite Tasmanites, and all measurements were taken on this material. While the maturation trends of this material in the Illinois Basin have been studied using vitrinite reflectance and qualitative and quantitative fluorescence techniques (21,22,23), nothing previously was known of the time-resolved fluorescence properties of these (or any) samples. The other set was a series of samples from the lower Kittanning seam from Pennsylvania and Ohio, which range in rank from high-volatile bituminous C to medium-volatile bituminous.

One obvious advantage of the time-resolved analysis is illustrated in Figure 3. The continuous-type fluorescence spectrum for a sample of the alginite Tasmanites (upper diagram) can be time-resolved into two separate spectra (lower diagram). The time-resolved analysis indicates that the continuous spectrum derived from standard fluorescence contains, in this case, the combined contributions from (at least) two fluorescing components with their own distinct spectra.

The fluorescence decay times of organic materials in both sets of samples showed some surprising similarities. First, in all material studied, Tasmanites in the New Albany shale, and fluorinite, sporinite, resinite, and cutinite macerals in the Lower Kittanning seam, the time-resolved data showed good agreement with a two-component decay model. Thus, the fluorescence of all of these materials appears to be composed of two fluorescing components with lifetimes in the subnanosecond and nanosecond ranges. In addition, the fast lifetime component (about 200 ps) seems to be constant in all samples and maceral types. Although these results are preliminary, a working hypothesis is that the two fluorescence lifetimes are from two different fluorophores, one of which is common to all the materials studied (alginite, fluorinite, resinite, cutinite and sporinite).

When the fluorescence decay times were plotted against rank (as defined by vitrinite reflectance), the alginites and sporinites showed the clearest trends as seen in Figures 4 and 5. The decay times do not seem to change much with increase in thermal maturation or rank. However, the percentage contribution of each component to the overall spectra do show a systematic change as illustrated in the same figures. In the case of the alginite, the fast component increases with rank, the slow component decreases, and the trends are reversed for the sporinites. Although these data are preliminary, the hypothesis (being investigated further) is, that in the maturation process one fluorophore is transforming into another.

To further test our experimental procedures, model compounds (e.g. PPOPOP, anthracene) in solution and their mixtures were studied. We found that two compounds can be distinguished in a mixture and the correct fluorescence decay times and spectra are obtained.

CONCLUSIONS

1. Time-domain analysis is a powerful extension of continuous fluorescence analysis.
2. Characteristic lifetimes, percentages, and intensities can be determined.
3. The spectra of a variety of organic materials can be resolved into two distinct components, one in the subnanosecond range and one in the nanosecond range.
4. Within the resolution limits of the system (100 ps), it appears that the fast lifetime component is the same in a variety of organic materials.
5. With the new technique, mixtures of short and long lifetime model compounds can be resolved into their original component spectra and fluorescence decay times.
6. In alginites and sporinites, fluorescence lifetimes appear to be nearly constant with changes in rank.
7. In alginites and sporinites, the percentage contribution from each component changes with rank.

Time-resolved laser spectroscopy improves the specificity of conventional fluorescence microphotometry of coals and oil shales. We have been using the new technique in studies of dispersed organic matter in shales and expect to understand better the maturation of the organic material in source rocks (24).

ACKNOWLEDGEMENTS

Support from the U.S. Department of Energy (Grant DE-FG22-82PC 50801) and E. Leitz, Inc., is gratefully acknowledged.

REFERENCES

1. P. van Gijssel, "Autofluorescence of Fossil Pollen and Spores with Special Reference to Age Determination and Coalification", *Leidse Geol. Meded.*, Vol. 50, pp. 263-317 (1967).
2. H. Jakob, "Lumineszenz-Mikroskopie der Organo-Petrographischen Bestandteile von Sedimentgesteinen", *Leitz-Mitteilungen Wiss. u. Tech.*, Vol. 4, no. 8, pp. 250-254 (1969).
3. M. Teichmüller, "Über Neue Macerale der Liptinit-Gruppe und die Entstehung von Micrinit," *Fortschr. Geol. Rheinld. und Westf.*, Vol. 24, p. 37-64 (1974).
4. P. van Gijssel, "Polychromatic UV Fluorescence Microphotometry of Fresh and Fossil Plant Substances with Special Reference to the Location and Identification of Dispersed Organic Material in Rocks", *Petrographie Organique et Potentiel Pétrolier*, ed. by B. Alpern, pp. 67-91, CNRS, Paris (1975).

5. K. Ottenjann, M. Teichmuller, and M. Wolf, "Spectral Fluorescence Measurements in Sporinites in Reflected Light and Their Applicability for Coalification Studies", in Petrographie Organique et Potentiel Petrolier, ed. by B. Alpern, pp. 49-65, CNRS, Paris (1975).
6. W. Spackman, A. Davis, and G.D. Mitchell, "The Fluorescence of Liptinite Macerals", Brigham Young University Geology Studies, Vol. 22, pp. 59-75 (1976).
7. M. Teichmuller and M. Wolf, "Application of Fluorescence Microscopy in Coal Petrology and Oil Exploration", J. of Microscopy, Vol. 109, pp. 49-73 (1977).
8. P. van Gijssel, "Recent Developments in the Application of Quantitative Fluorescence Microscopy in Palynology and Paleobotany", Annales des Mines de Belgique, pp. 165-181, July-August (1978).
9. K. Ottenjann, M. Wolf, and E. Wolf-Fischer, "Beziehungen zwischen der Fluoreszenz von Vitriten und den Technologischen Eigenschaften von Kohlen", Proc. of the International Conference on Coal Science, Dusseldorf, Germany, IEA, pp. 86-91 (1981).
10. W.L. Borst, H.A. Hamid, J.C. Crelling, "Laser Induced Fluorescence Microscopy", Int. Conf. on Coal Sci., Pittsburgh, Penn; publ. by Int. Energy Agency, pp. 649-652 (1983).
11. W.L. Borst, G.W. Sullivan, H.A. Hamid, "Pulsed Laser Induced Fluorescence Microscopy for Materials Characterization", Bull. of the Amer. Phys. Soc., Vol. 28/29, p. 1335 (1983).
12. G.W. Sullivan and W.L. Borst, "Introduction to Fluorescence Spectroscopy of Coal Macerals", NATO Advanced Study Institute on Application of New Spectroscopic Techniques to Coal Science, St. Francis Xavier University, Antigonish, Canada, August 1984 (in press).
13. W.L. Borst, G.W. Sullivan, and R.N. Zitter, "Laser Induced Fluorescence Spectroscopy", NATO Advanced Study Institute (same as above; in press).
14. G.W. Sullivan, W.L. Borst, M.W. Pleil, and C.L. Landis, "The Application of Pulsed Laser Fluorescence Microscopy to Coal Maceral Characterization", NATO Advanced Study Institute (same as above; in press).
15. D.V. O'Conner, W.R. Ware, and J.C. Andre, J. Phys. Chem., 83, p. 1333 (1979).
16. A. Grinvald, I.Z. Steinberg, Anal. Biochem., 59, p. 583 (1974).
17. R.B. Cundall, R.E. Dale, "Time-Resolved Fluorescence Spectroscopy in Biochemistry and Biology", Plenum Press, New York (1983).
18. J.R. Lakowicz, "Principles of Fluorescence Spectroscopy," Plenum Press, New York (1983).
19. W. Demtroder, "Laser Spectroscopy - Basic Concepts and Instrumentation", Springer Verlag; Berlin, New York (1981).
20. P.R. Bevington, "Data Reduction and Error Analysis for the Physical Sciences", McGraw-Hill, New York (1969).
21. M.H. Barrows, R.M. Cluff, AAPG Memoir 35: Petroleum Geochemistry and Basin Evaluation, p. 111 (1984).
22. M.H. Barrows, R.M. Cluff, R.D. Harvey, Proc. 3rd Eastern Gas Shale Symp., p. 85 (1979).
23. G.E. Cox, M.S. Thesis, Southern Illinois University at Carbondale (1985).
24. Pieter van Gijssel, "Applications of the Geomicrophotometry of Kerogen, Solid Hydrocarbons, and Crude Oils to Petroleum Exploration", publ. in Organic Maturation Studies and Fossil Fuel Exploration, ed. J. Brooks, Academic Press (London, 351-377 (1981)).

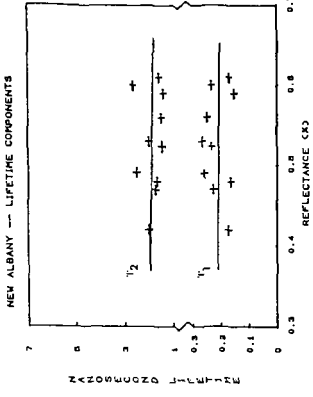


Figure 4a. The two fluorescence decay times in alginite samples from the New Albany formation (Illinois Basin) as a function of vitrinite reflectance (rank). Each data point is an average over 3 to 5 materials and over the fluorescence emission spectrum.

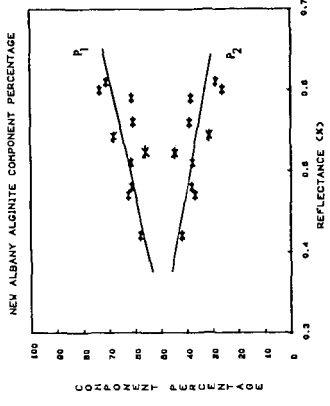


Figure 4b. The percentage contributions to the fluorescence from the two time-resolved components in alginite as a function of vitrinite reflectance. The averaging is the same as in Figure 4a.

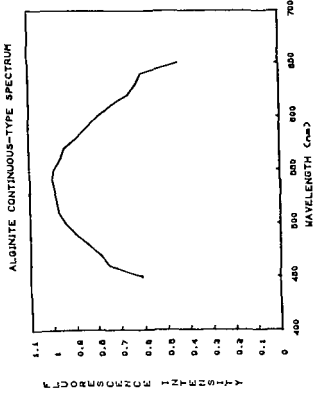


Figure 3a. Composite fluorescence spectrum from an alginite maceral in New Albany shale. The spectrum was obtained by integrating the fluorescence plates over time and is similar to that measured with continuous wave excitation.

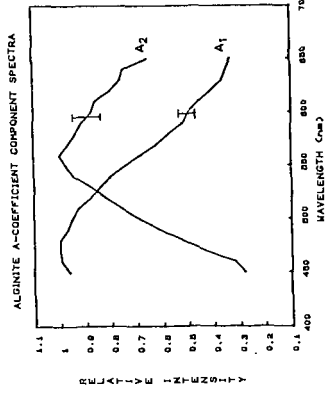


Figure 3b. Resolution of the composite spectrum above into two time-resolved component spectra (normalised to the same height). The vertical uncertainty bars indicate the 2 σ - range of the two individual spectra for 45 alginite macerals of different rank.

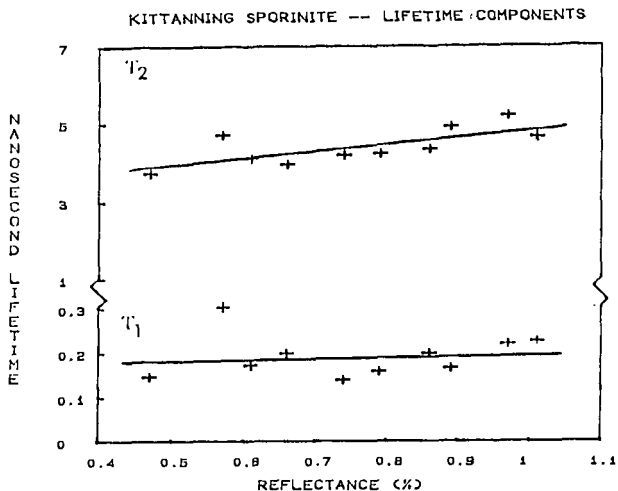


Figure 5a. The resolved fluorescence decay times from sporinite coal macerals from the lower Kittanning seam (Pennsylvania and Ohio) as a function of rank. (See also caption to Figure 4a.)

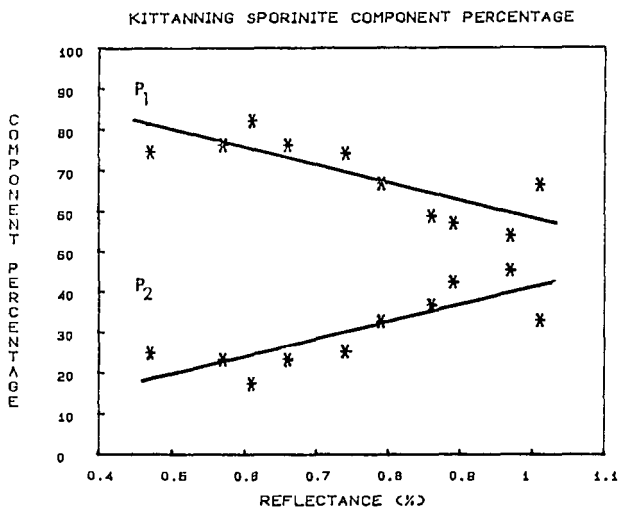


Figure 5b. Percentage contributions to the fluorescence from the two major fluorescing components in sporinite as a function of vitrinite reflectance. (See also caption to Figure 4b.)

MECHANICAL CHARACTERIZATION OF COALS IN THEIR RUBBERY STATE

Douglas Brenner

Corporate Research Science Laboratories
Exxon Research and Engineering Company
Annandale, N.J. 08801

INTRODUCTION

The macromolecular structure of a material affects a range of physical characteristics. It affects whether the material is a hard solid or a soft rubber, or whether it is a viscoelastic fluid or a low viscosity liquid. The macromolecular structure affects such properties as solubility, penetration by liquids and gases, and the ease of breaking down the structure. For coals, the macromolecular structures play a significant part in a number of processes. By understanding the macromolecular structure better we may hope to more effectively utilize coals.

Mechanical measurements on a material above its glass transition is one of the most effective means of probing its macromolecular structure (1,2). However, for undegraded coals above their glass transition in their rubbery state, no information has been available. Virtually all of the numerous mechanical measurements on undegraded coals have been below the glass transition temperature where the coals are in a glassy or semicrystalline state. This is to be expected since this is the natural state of coals under ambient conditions. On the other hand, the macromolecular chain segments have very limited mobility below the glass transition temperature, so they can not be probed very effectively. It is desirable to make measurements on coals in their rubbery state where the macromolecules can move and respond to stimuli. Measurements of the degree of swelling (3,4) have given some information on solvent-swollen coal, but the information that can be obtained is limited. Also the interpretation of those results depends on solution thermodynamics, and the need to determine the interaction parameter is a particular problem.

Previously we had been able to demonstrate that high volatile bituminous coals could attain a rubbery state when immersed in an appropriate solvent (5,6). Having established this, it became highly desirable to characterize macromolecular parameters of the rubbery coals using mechanical measurements. Unfortunately, though, satisfactory samples of rubbery coals had never been prepared. The problem which prevented the preparation of adequate samples of rubbery coals was the tendency of the coal to decrepitate when it is immersed in a good swelling solvent (7). In fact, solvent-swelling has been proposed as a beneficiation process to break down coal into particles (8). However, in our earlier work we had shown that coals in the form of thin sections could be swollen without much damage occurring. But such thin samples are not amenable to mechanical measurements. For this reason a program was undertaken to determine whether it was possible to develop new techniques for preparing adequate samples.

EXPERIMENTAL

A procedure has now been developed which for many coals enables the preparation of samples in the rubbery state which are satisfactory for mechanical measurements. The technique involves selecting relatively homogeneous regions of vitrinite which have low mineral matter content. The selected region of the sample is isolated by cutting on a wafering saw or by grinding away the unwanted material using a coarse grit. The isolated region is further ground to remove microcracked or weakened parts. The samples are ground dry on a revolving horizontal grinder using a SiC disk. Prior to swelling, typical samples are from 0.5 to 2.0 mm thick with top and bottom surfaces roughly 20 sq. mm in area. In the final grinding of the samples the top and bottom surfaces are ground parallel on a 600 grit SiC disk.

Sometimes samples can be swollen in the liquid form of the swelling agent without appreciable crack formation; but there has been better success by more slowly swelling the sample in the vapor of the solvent wherein its vapor pressure is well below its saturation value. Usually conditions have been used in which the swelling occurs over about one day. Although after swelling the top and bottom surfaces may no longer be precisely parallel, they are generally sufficiently parallel to be satisfactory for measurements. The effect of the deviation from parallelity can be observed in stress-strain curves as a "foot" or as a lower modulus region at the start of the curve. Once they are swollen, the samples are not allowed to dry. Drying usually causes many more cracks than the swelling does. The fully swollen samples have excellent retention of the original shape, and contain few, if any, cracks.

With the coherent specimens of solvent-swollen coals, physical qualities could be readily observed. The highly solvent-swollen specimens of coal have a distinct rubbery feel when pressed between the fingers -- somewhat firmer than a typical rubber band. However, the coals are poor quality rubbers. They split easily when stretching forces are applied to them so they have low tensile strength. The splits tend to have relatively smooth sides, and once a small split forms only a small force is needed to lengthen the crack. On the other hand, under compression the rubbery coals can generally undergo compressions of 15% or even more without splitting occurring.

The coals used in this study were Illinois No. 6, which is of high volatile C rank, and Pittsburgh No. 8, which is of high volatile A rank. The samples were extracted in pyridine prior to the measurements. The measurements were made at room temperature. The apparatus utilized was an Instron mechanical tester Model No. 1122. The measurements were made in the compression mode. Measurements in the tensile mode are disadvantageous because of the difficulty in clamping the rubbery coal and because it is very weak under tensile stresses. The samples were fully immersed in pyridine during testing.

RESULTS and DISCUSSION

Stress-Strain Measurements

Stress-strain measurements involve compressing the sample at a constant rate until the desired degree of deformation is obtained. Then instantaneously the direction of movement of the crosshead is reversed and the sample undergoes decompression. When more than one cycle was taken, there was a one minute waiting period between the end of the previous cycle and the start of the next cycle. This allows for some recovery of the sample between cycles.

Stress-strain results for pyridine-immersed, rubbery Illinois No. 6 coal are shown in Figure 1. The curve actually consists of two compression/expansion cycles. The closeness of the two cycles demonstrates excellent reproducibility. At the maximum strain the compression was about 10%. The stress-strain behavior of the pyridine-swollen coal is characteristic of a rubbery material. The modulus is in the range of conventional rubbers, there is rapid rebound during the decompression, and the curves exhibit good reproducibility over successive cycles.

The stress-strain curve for pyridine-immersed rubbery Pittsburgh No. 8 coal is shown in Figure 2. Two stress-strain cycles are shown. The heavy curves are the first cycle and the light lines are the second cycle. It is seen that the first and second cycles are very close to the same shape, but there is a slight displacement of the second cycle with respect to the first. The displacement is caused by incomplete recovery of the rubbery coal after the first cycle; a slight deformation or "set" was retained in the sample. Some of this "set" relaxes if a longer waiting time between cycles is used.

The shape of the decompression curve in the region of low force for the Pittsburgh No. 8 coal is considerably different from the Illinois No. 6 coal shown in Figure 1. The curve for the Pittsburgh No. 8 coal actually reaches zero force well before the crosshead returns to its initial position. This is a manifestation of incomplete recovery of the Pittsburgh coal at the test rate used. The macromolecular chains in the coal are not able to reorient fast enough to keep up with the crosshead. The point at which the force becomes non zero near the start of the second cycle for the Pittsburgh coal is at a considerably lower strain than where the force became zero during the decompression of the first cycle. This demonstrates that during the one minute waiting period before starting the second cycle, the coal has recovered to near its original height.

The slope of the stress-strain curve gives the dynamic Young's modulus. The dynamic moduli of the Illinois No. 6 and Pittsburgh No. 8 coals determined near the top of the compressional part of their stress-strain curves are given in Figure 3. Both elastic and viscous effects contribute to the dynamic Young's modulus. The elastic component is caused by the instantaneous effective cross-link density in the coal including temporary entanglements. The viscous drag results from the resistance of the macromolecular chain segments sliding past each other. The dynamic Young's modulus of the coals is influenced by how fast the macromolecular chain segments are able to

reorient in response to the applied stresses. If the reorientation is fast compared to the imposed strain rate, then the modulus should show relatively little dependence on the strain rate; whereas, if the reorientation rate is comparable to the strain rate, a large dependence on strain rate would be expected. The dynamic modulus is also affected by some of the solvent being squeezed out of or absorbed into the rubbery coal during portions of the cycle.

Figure 4 shows the effect of deformation rate on the dynamic Young's modulus of the coals. For a change in deformation rate of a factor of 25, the Pittsburgh No. 8 coal shows relatively little change in modulus. For the Illinois No. 6 coal the change in modulus is slightly larger even though the difference in rate is a factor of 10 rather than 25. It is not clear whether this change is related to the higher deformation rates used with the Illinois No. 6 coal (which would suggest that more of the macromolecular relaxation occurs at higher rates) or whether the change is indicative of structural differences between the Illinois No. 6 and Pittsburgh No. 8 coals.

The area enclosed by the stress-strain curve is the integral of force times distance over the cycle, so it is the net work done by the apparatus on the rubbery coal. This energy is dissipated in the sample as heat. The energy dissipation arises from the viscous movements of the macromolecular chain segments and also from some solvent being released from or absorbed by the rubbery sample during the cycle. The ratio of the net energy dissipated over the cycle to the maximum energy stored in the sample during the cycle is commonly used as a figure of merit to quantify the energy dissipation of a rubbery substance. A table showing the energy dissipations of the Illinois No. 6 and Pittsburgh No. 8 coals is given in Figure 5. The Pittsburgh coal exhibits a particularly high energy dissipation. Both coals show high energy dissipation as compared to most conventional rubbers, such as the rubber band.

Stress-Relaxation Measurements

The stress-relaxation behavior of macromolecular materials is an important probe of the rates of segmental motion of the substance. In a stress-relaxation measurement the sample is rapidly compressed by a selected amount, after which the deformation is held fixed. The stress on the sample is then measured as a function of time.

A stress-relaxation curve for Illinois No. 6 coal in its pyridine-swollen rubbery state is shown in Figure 6. The observed behavior can be explained as follows. As the sample is rapidly compressed, the structure deforms and the stress increases. When the sample first attains the selected deformation after the rapid compression, the macromolecular chains have not yet reached their equilibrium state. With time the macromolecular chain segments rearrange (within the constraints of the cross-links) to more probable configurations. As the macromolecular chain segments move past each other and the reorganization proceeds to a more entropically favorable state, the stress exerted by the rubber on the fixed constraining plates decreases. This is seen as a downward slope in a plot of stress versus time, such as is seen in Figure 6. Some degree of stress relaxation is characteristic of most rubbery materials. Slow

stress-relaxation indicates low mobility of some of the macromolecular chain segments, or high internal viscosity.

For liquid-saturated rubbers some of the liquid is squeezed out under compressive stress. This loss of liquid contributes to the stress-relaxation, though, it is a diffusional process involving small solvent molecules as contrasted to the segmental rearrangement of the macromolecular structure. For most swollen polymers this loss of fluid is small. For the pyridine-immersed coal samples there will also be loss of some liquid as a result of compression and it will contribute to the stress-relaxation. The extent of fluid loss under compression for coals has not been established. It is thought that the slower relaxation at longer times is caused primarily by this diffusion of solvent out of the rubbery coal.

SUMMARY

The first mechanical measurements on satisfactory samples of rubbery coals have been made. The rubbery character of highly solvent-swollen coals has now been substantiated by direct mechanical measurements. The techniques developed allow us to apply many of the methods and approaches of polymer science to the understanding and characterization of macromolecular properties of coals.

REFERENCES

1. Flory, P. J. 'Principles of Polymer Chemistry', Cornell University Press, Ithaca, 1953
2. Treloar, L. R. G. 'The Physics of Rubber Elasticity', 3rd Edition, Clarendon Press, Oxford, 1975
3. Sanada, Y. and Honda, H. Fuel ,1966, 45 , 295
4. Larsen, J. W. in 'Chemistry and Physics of Coal Utilization' (Eds. B. R. Cooper and L. Petrakis), Am. Inst. of Physics. New York, 1981, p. 1
5. Brenner, D. Fuel , 1984, 63 ,1324
6. Brenner, D. Fuel , 1985, 64 , 167
7. Dryden, I. G. C. Fuel 1951, 30 , 39
8. Keller, D. V. and Smith, C. D. Fuel , 1976, 55 , 273

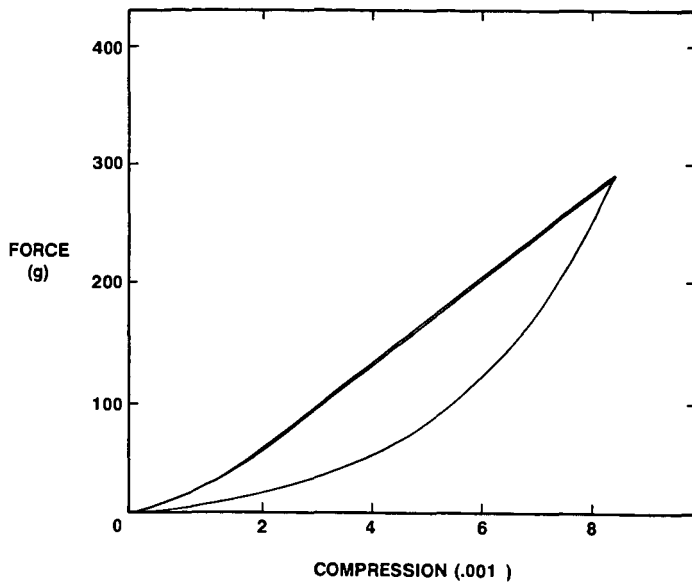


Fig. 1. Stress-strain curve for pyridine-immersed rubbery Illinois No.6 coal

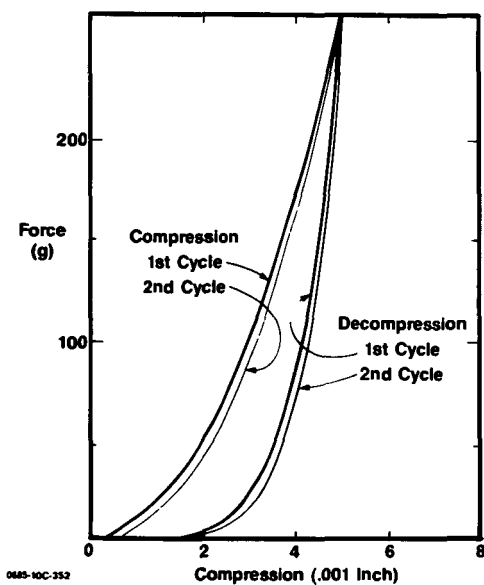


Fig. 2. Stress-strain curve for pyridine-immersed rubbery Pittsburgh No.8 coal

Fig. 3. RUBBERY MODULI OF COALS FROM STRESS-STRAIN CURVES

<u>COAL</u>	<u>%C (dmmf)</u>	<u>MODULUS (psi)</u>
Illinois No. 6	80	600
Pittsburgh No. 8	85	300

Fig. 4. EFFECT OF DEFORMATION RATE ON MODULUS

<u>COAL</u>	<u>%C</u>	<u>HIGH Deformation Rate (inch/min.)</u>	<u>LOW Deformation Rate (inch/min.)</u>	<u>Ratio of Moduli Low Rate High Rate</u>
ILLINOIS No. 6	80	.2	.02	.7
PITTSBURGH No. 8	85	.05	.002	.8

Fig. 5. ENERGY DISSIPATION BY COALS IN THEIR RUBBERY STATE

<u>COAL</u>	<u>%C</u>	<u>RATIO OF ENERGY DISSIPATED PER CYCLE TO MAXIMUM WORK OF DEFORMATION</u>
ILLINOIS No. 6	80	.30
PITTSBURGH No. 8	85	.50

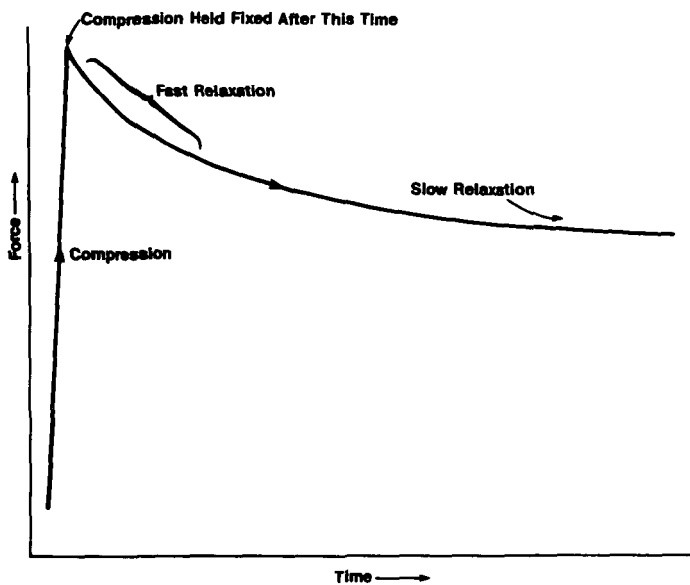


Fig. 6. Stress relaxation of pyridine-immersed rubbery Illinois No.6 coal

THE APPLICATION OF INVERSE GAS CHROMATOGRAPHY TO COALS AND OXIDIZED COALS*

P. H. Neill and R. E. Winans
Chemistry Division, Argonne National Laboratory
9700 South Cass Avenue, Argonne Illinois 60439

Introduction

In a previous paper (1) we reported the preliminary results concerning the application of Inverse Gas Chromatography (IGC) to coals. This paper will cover the extension of the technique to coals of various ranks and degrees of air oxidation.

The objective of this study is to provide detailed information on possible changes in the chemical and physical structures of the Argonne Premium Coal Samples during storage. In meeting this objective, new fundamental data will be obtained on this unique set of coal samples. The use of a broad range of experiments is planned in this study, but only one approach will be described here. While it is known that subtle changes in the physical and chemical structure of bituminous coals can effect changes in the plasticity upon heating, the techniques traditionally used to measure plasticity do not yield information which can be used to understand these changes.

A new approach, inverse gas chromatography (IGC), a technique widely used for studying polymers, is being used to study phase transitions in coals upon heating. Inverse GC has been applied to polymers to measure the glass transition temperature, the degree of crystallinity, melting point, thermodynamics of solution, and chemical composition (2-4). In contrast to classical GC, inverse chromatography probes the stationary phase, a coal, by determining the retention time of known compounds on it. This transposition of known and unknown in the GC experiment gives rise to the term "inverse chromatography". The coal samples will be chosen to examine variations with rank and to investigate structural changes in ground coals, both in air and in the absence of air, as a function of time. These approaches show promise for providing chemical information on subtle variations in coal structure.

Experimental

The coals used in this study included an Illinois No. 2 hvC bituminous, an Upper Freeport mv bituminous which is, an Argonne Premium Coal Sample, and a Bruceton hvA bituminous. The elemental compositions are shown in Table 1. The Illinois No. 2 was ground to -100 mesh and Soxhlet extracted with an azeotropic mixture of benzene and ethanol, and dried under vacuum at 110°C. The other two fresh coals were used as received. The oxidized Upper Freeport was exposed to air in an oven at 100°C for 90 hrs. The coals were thoroughly mixed with non-porous glass beads (-40 to -60 mesh) to give a mixture approximately 10% coal on a weight basis. The six foot by 1/4" glass columns were packed with ca. 30 grams of the mixture.

*Work performed under the auspices of the Office of Basic Energy Sciences, Division of Chemical Sciences, U.S. Department of Energy, under contract number W-31-109-ENG-38.

The submitted manuscript has been authored by a contractor of the U.S. Government under contract No. W-31-109-ENG-38. Accordingly, the U.S. Government retains a nonexclusive, royalty-free license to publish or reproduce the published form of this contribution, or allow others to do so, for U.S. Government purposes.

The GC equipped with a single FID could be controlled, within one degree C, from an external computer. The injector was a computer controlled Carle gas sampling valve in a thermostated box. Flow control was provided by two flow controllers one with a 0-5 ml/min. element and the second with a 0-60 ml/min. element. The 0-60 ml/min. controller was connected to the injector through a computer controlled solenoid. The experiment was controlled and the data analyzed by a IBM PC computer. The probe, methane, was injected onto the column and its retention time at the specific temperature was determined. In the experiment chromatograms were obtained in three degree increments between 50 and 450°C. The injector was held at 100°C and the detector at 400°C.

Results and Discussion

The retention volume may be related, through the partition coefficient, to the free energy or enthalpy of adsorption, and a plot of $\ln t_{ret}$ vs. $1/T$ gives a slope proportional to ΔH_a . Changes in the thermodynamics of retention result in discontinuities or changes in the slope of the plot. Plots of the three unoxidized coals are presented in Figure 1, with temperatures of significant transitions given in Table 2. They do not appear to vary greatly in an overall gross sense. Each has what appears to be a transition at relatively low temperatures as illustrated by T_A in the figure. This transition is most likely due to the loss of water from the surface and from the pores of the coal. The second region of interest is at T_B . This dip in the otherwise smooth portion of the curves can be attributed to the loss of chemical water. This transition varies in temperature with the coal, however there does not appear to be a rank dependence. The Bruceton coal seems to lose its water at the lowest temperature while the Upper Freeport at the highest.

At T_C a number of small transitions begin to occur for each of the coals. This is also the region where relatively large amounts of volatile material is beginning to be released. Due to the small thermodynamic changes in the interaction between the probe and the coal it is difficult to assign a starting temperature for this region, however it does appear to begin at a higher temperature for the Upper Freeport mv coal than the Bruceton hvA coal. Comparisons between the Illinois No. 2 hvC coal and the others would be speculative since this coal was pre-extracted. Thus, a large percentage of the volatile matter has been removed.

The primary transition in the plots occurs at T_P . In each case there is a marked increase in the retention time followed by a rapid decrease. This transition correlates well with the onset of plasticity in each of the coals, occurring 10 to 15°C before the initial softening temperature. The temperature at which the major transition occurs is also correlated with rank. The Illinois No. 2 exhibits the transition at a lower temperature, followed by the Bruceton and the Upper Freeport. The Bruceton hvC coal is the only one that appeared to have a leveling off of the slope of the curve by T_P . The Giesler plasticity measurement shows that this coal resolidifies just above the maximum temperature of this experiment. Thus, it appears that some of the post fluid pore structure has appeared and is showing up in the IGC data.

Figure 2 illustrates the effect of oxidation on the IGC pattern. There does not seem to be much effect on the lowest temperature transition although it may occur at a slightly higher temperature. The loss of water seems to occur at a significantly lower temperature. This is not surprising since the oxidized coal was heated in air at 100°C for 90 hrs. A vast majority of the water in this sample should be loosely held since it probably adhered to the surface of the coal after it was cooled. The major difference between the two coals is in the transition that should occur at higher temperatures. In the heavily oxidized sample there is almost no change in slope in this region indicating that the coal has probably not gone

fluid. There does appear to be some change occurring, which is a transient at approximately 330°C.

Overall IGC appears to be a very sensitive method for following the chemical and physical changes that occur when coals are heated in an inert atmosphere. Differences between coals of various ranks can be seen easily, as can the drastic effects of air oxidation.

Acknowledgments

The coal analysis were provided by I. Fox and P. C. Lindahl of the Argonne Analytical Chemistry Laboratory. The Bruceton coal was provided by J. W. Larsen of the Dept. of Chemistry, Lehigh University.

References

1. R. E. Winans, J. P. Goodman, P. H. Neill, and R. L. McBeth, ACS Fuel Chemistry Division Preprints, 30(4), 427 (1985).
2. S. G. Gilbert, in "Advances in Chromatography", Vol. 23, J. C. Giddings, E. Grushka, J. Cazes, and P. R. Brown, Eds., Marcel Dekker, New York (1984).
3. V. G. Berezkin, V. R. Alishoyev, and I. B. Nemirovskaya, J. Chromatography Library, 10, 197-223 (1977).
4. J. E. Guillet, in "New Developments in Gas Chromatography", J. H. Purnell, Ed., Wiley, New York, (1973).

TABLE 1. Composition of the Three Coals Studied.

Coal	% C (dmf)	Empirical Formula
Upper Freeport mv Bituminous	89.0	C ₁₀₀ H ₇₀ N _{1.5} S _{0.5} O _{2.5}
Bruceton hvA Bituminous	82.3	C ₁₀₀ H ₇₈ N _{1.6} S _{0.3} O _{9.3}
Illinois No. 2 hvC Bituminous	73.4	C ₁₀₀ H ₈₇ H _{1.3} S _{0.8} O ₁₈

TABLE 2. Transition Temperatures for IGC Data Shown in Figure 1.

Sample	Temperature °C					
	T _A	T _B	T _C	T _D	T _E	T _F
Illinois No. 2 hvC	111	138	240	326	352	398
Bruceton hvA	110	130	230	341	368	429
Upper Freeport MV	115	158	248	360	370	430

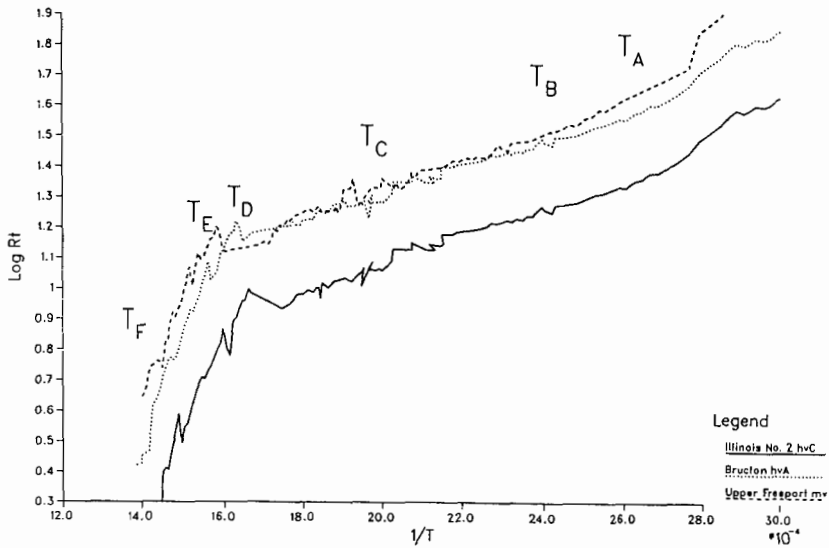


Figure 1. Data from inverse GC experiments. V_{ret} represents the retention volume; T is temperatures in $^{\circ}K$. Values for T_A - T_F are given in Table 2. — Illinois No. 2 hvC bituminous coal, Bruceton hvA bituminous coal, --- Upper Freeport mv bituminous coal.

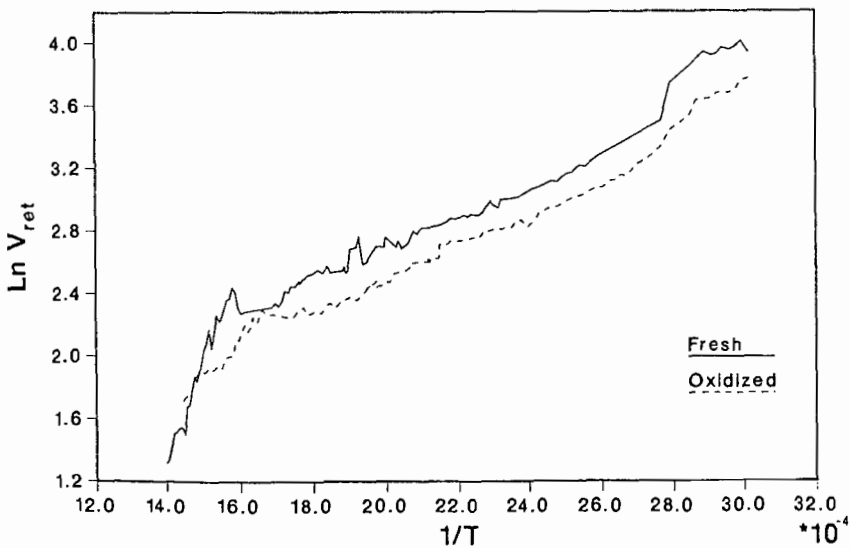


Figure 2. Comparison of data from an oxidized and a fresh sample of Upper Freeport mv bituminous coal.

ELECTRON MICROPROBE TECHNIQUE FOR QUANTITATIVE ANALYSIS OF COAL AND COAL MACERALS

Frank R. Karner, Jean L. Hoff, Tim P. Huber, and Harold H. Schobert

University of North Dakota Energy Research Center
Box 8213, University Station
Grand Forks, North Dakota 58202

Electron microprobe analysis is a powerful tool for analyzing the chemical composition of component grains and whole samples when sample quantities are too small for other analytical techniques. A quantitative procedure for microanalysis of elements such as Na, Mg, Al, Si, P, S, Cl, K, Ca, Ti, Mn, Fe, Sr, Ba in coal and coal macerals is highly desirable but development of quantitative techniques for microanalysis of organic materials has lagged behind progress in the material sciences. The heterogeneous character, low density, and light element composition of organic materials present special problems not accounted for in the usual microanalytical methods employing standard ZAF correction procedures applicable to mineralogy and metallurgy.

Alternative procedures developed by workers in the biological sciences, which minimize the problems specific to work with organic materials, might be better suited for analysis of coal than standard ZAF techniques. Quantitative methods have been most extensively developed for thin-sectioned specimens. Those techniques, which include Hall's (1968) peak-to-continuum and Russ's (1974) elemental ratio methods, rely on the assumption that absorption and fluorescence effects may be neglected because of the extremely short path length for exiting x-rays. For thick specimens these assumptions must be modified. Techniques include the standard ZAF correction procedures for material with light element matrices (Love and Scott, 1980) and peak-to-background methods (Miller and Corbet, 1972). Other techniques closely related to our approach are the peak-to-continuum (P/C) methods used for the analysis of particles by Statham and Pawley (1978) and Small and others (1980).

Most of the P/C methods rely on the hypothesis that, as an initial approximation, continuum and characteristic radiation are similarly affected by changes in particle-size, density, or specimen thickness. Thus the ratio of peak intensity to continuum intensity is approximately constant for a given elemental concentration. The P/C method should thus solve the major problems with microanalysis of organic materials: a dominantly light elemental composition which is not directly measurable by microprobe techniques, inhomogeneity, and variable density. Even though the analyzed elements have a low concentration in a light-element matrix the question remains as to whether the assumption of negligible absorption and fluorescence effects is valid for this method.

Methods

A set of organic reference standards has been analyzed as the first step in establishing a P/C procedure for electron microanalysis of minor and trace elemental concentrations in organic materials such as coal macerals. The one-to-one linearity of published to observed elemental concentrations is used as a test of the validity of the P/C method and its internal assumptions. Programmed correction factors relating peak intensity to concentration are obtained from best fit procedures and are then used for analysis of unknowns of similar composition.

Nine National Bureau of Standards (NBS) reference standards of selected organic materials were chosen for this evaluation of the P/C method. The standards consist of four bituminous and two subbituminous coals, citrus and tomato leaves, and pine needles. Samples were ground to a fine powder, vacuum-dried, and compressed under 10 tons pressure to form two flat pellets for each standard. The pellets were then carbon-coated for electron microprobe analysis.

Microprobe operating conditions during acquisition of chemical analyses were 15 keV accelerating voltage and 920 picoamperes beam current. The probed area was approximately one square millimeter. Fifty-three 400 second analyses were obtained during May and June 1985. Five analyses of incompletely ground and/or improperly coated samples were removed from the data set.

Between four and ten analyses were combined to obtain a single averaged spectrum for each reference standard. The region 2.00-5.00 keV was chosen for measurement of continuum intensity. A reference library of pure element and oxide standard spectra was used with the Tracor-Northern XML least squares fitting routine to generate peak-to-continuum elemental ratios for each averaged spectrum. This ratio was computed by the relationship: $\text{correction factor} \times (\text{peak intensity}) / (\text{continuum intensity})$.

The peak-to-continuum ratio, assumed in the P/C method to be proportional to absolute elemental concentration, was plotted against reported concentration for each element of interest (Na, Mg, Al, Si, P, S, Cl, K, Ca, Ti, Fe). The amount of deviation of the best-fit line through the origin from the hypothetical one-to-one relationship between observed P/C and reported concentrations was used to change the reference library stored correction factors. The peak-to-continuum ratios were then computed with the adjusted correction factors and final plots for each element were made.

Results

Results are summarized in Table 1 and Figures 1 and 2. Some questions to be considered while evaluating the peak-to-continuum results include: whether the data show the linear one-to-one relationship between reported element concentration and P/C ratios that would indicate the method and its assumptions are valid for the elements examined; whether scatter in the data indicate possible additional effects on x-ray intensities or analytic or sample preparation problems; and what trends are specific to certain elements or appear to affect all elements. Examination of the data for each element of observed versus literature-reported concentrations yield the following observations:

1. Silicon, phosphorus, and chlorine were not present in both observed and reported analyses of enough standards to generate a significant number of data points. Although the three data points graphed for each of these elements appear to show the desired linearity, they are too few to permit conclusive interpretation of the results.
2. Magnesium and titanium were only present in very low concentrations, mostly as less than 0.2 wt%. The data points thus cluster near the origin. Mg does show linearity with two points at slightly higher concentrations, but the clustered data points of both elements show some scatter from the linear relationship. In part, this may be accounted for by the detectability limits of the EDS microprobe system and by the relatively higher error of 5%-10% reported in microanalysis of organic materials as compared to work in the material sciences.
3. Aluminum (Figure 1), calcium, sulfur, and potassium show a linear relationship between observed and literature values. Data points are spread over a range of concentration values of up to 7% and show a low degree of scatter. These elements appear to be behaving in conformity with the assumptions of the peak-to-continuum method and might be expected to yield valid results for unknowns.
4. Sodium, known to be subject to elemental mass loss problems during sample preparation and microprobe analysis, is only present in concentrations of <0.3 wt%. Most data points cluster near the origin but do not show as much scatter as would be expected if mass loss had occurred.

Table 1. Results of Microprobe Analysis of NBS Coal and Botanical Standards Comparing Observed and Reported Weight Percentages

	REF STD	H	C	N	O	Na		Mg	
						RPT	OBS	RPT	OBS
1	1632	3.85	66.00	1.23	18.80	0.08	0.07	0.12	0.13
2	1635	4.07	62.60	1.26	24.60	0.24	0.19	0.10	0.10
3	2682	4.70	75.00	0.80		0.10	0.08	0.20	0.19
4	2683	5.00	79.00	1.60		0.05	0.05	0.05	0.06
5	2684	4.80	68.00	1.60		0.03	0.05	0.08	0.12
6	2685	4.60	66.00	1.10		0.08	0.11	0.10	0.16
7	1572							0.58	0.57
8	1573	5.08	37.80	4.97		0.06	0.10	0.69	0.62
9	1575	6.48	51.40	1.20		0.01		0.13	0.13

	REF STD	Al		Si		P		S		Cl	
		RPT	OBS								
1	1632	3.01	2.79	6.01	5.65	0.03		1.58	1.46	0.08	0.08
2	1635	0.31	0.29	0.54	0.61	0.01		0.33	0.42	0.00	
3	2682	0.46	0.41		0.60			0.47	0.58		0.09
4	2683	0.86	0.75		1.27			1.85	1.93		0.19
5	2684	1.10	1.21		2.73			3.00	3.12		0.09
6	2685	1.70	1.93		3.95			4.62	4.16		0.06
7	1572	0.01	0.02		0.21	0.13	0.14	0.41	0.52		0.10
8	1573	0.09	0.09		0.55	0.34	0.28		0.62	1.07	1.07
9	1575	0.05	0.06	0.03	0.20	0.12	0.14	0.10	0.19	0.01	0.04

	REF STD	K		Ca		Ti		Fe	
		RPT	OBS	RPT	OBS	RPT	OBS	RPT	OBS
1	1632	0.42	0.45	0.24	0.23	0.17	0.11	1.12	1.04
2	1635	0.01		0.55	0.66	0.02		0.23	0.37
3	2682	0.01		1.10	1.35	0.05	0.05	0.24	0.40
4	2683	0.08	0.09	0.20	0.18	0.04	0.05	0.76	0.47
5	2684	0.20	0.27	0.44	0.33	0.06	0.06	1.50	0.90
6	2685	0.26	0.38	0.52	0.53	0.09	0.10	2.90	1.23
7	1572	1.82	1.72	3.15	2.95			0.01	0.07
8	1573	4.42	4.17	2.92	2.69	0.01		0.02	0.10
9	1575	0.37	0.37	0.42	0.43			0.02	0.10

5. Iron data (Figure 2) shows the least linearity and greatest scatter of the analyzed elements. Observed values of samples with the least iron are too large; measured values for samples with higher iron content are too low. There does not appear to be a consistent trend to these variations. Iron is the heaviest element analyzed in the organic standards and the assumption of negligible fluorescence and absorption effects may not be valid. However, such effects would be expected to cause data points to be consistently offset in one direction and cannot fully explain what is observed.

The peak-to-continuum method has performed well for certain elements - Al, Ca, S, K. Evaluation of standards with a greater range in concentration is required to confirm that the method works as well for elements such as Mg, Ti, and Na. Problems with evaluating Fe content might be elucidated by analysis of additional reference standards or a set of standards created using standard additions of known quantities of Fe.

Application

Initial studies using the peak-to-continuum method for microprobe analyses of organic materials (Karner and others, 1984, Karner and others, 1985) show excellent potential for obtaining valuable geochemical data for coal lithotypes and macerals. The first survey of lithotypes in lignite of the Beulah-Zap bed of the Sentinel Butte Formation (Paleocene) in North Dakota examined vitrain, fusain and attritus at several locations within the seam (Karner and others, 1984). Common inorganic elements associated with these lithotypes included Na, Mg, Al, Si, S, K, Ca, and Fe. Samples of vitrain from a single vitrain layer in the seam have quite uniform elemental compositions while vitrain from different levels in the seam have significantly different concentrations of elements particularly Mg, S, and Ca. Fusain and attritus were quite different from vitrain in chemical composition, generally containing higher Ca, Mg, and Si, and lower Al, S, and Fe.

A survey (Karner and others, 1985) of the inorganic chemistry of huminite group macerals in four low-rank coals included analyses of ulminite representative of the Beulah-Zap (BZ) and Hagel (HG) lignites, ND, the Martin Lake (ML) lignite, TX, and vitrinite of the Rosebud (RB) subbituminous coal, MT. Major differences in maceral chemistry between coals and compositionally distinct maceral types within coals are shown by characteristic analyses given in Table 2.

Table 2. Characteristic Compositions Determined by Microprobe Analyses of Huminite Group Macerals in Four United States Low-Rank Coals Given in Weight Percent.

		Na	Mg	Al	Si	S	Ca	Fe	Sr	SUM
Beulah-Zap	(BZ) Ulminite 1	0.32	0.11	0.22	0.10	0.45	0.49	0.51	0.04	2.24
Beulah-Zap	(BZ) Ulminite 2	0.54	0.38	0.18	0.12	0.43	1.54	0.79	0.06	4.04
Hagel	(HG) Ulminite 1	0.06	0.15	0.16	0.08	0.59	1.03	0.24	0.01	2.32
Hagel	(HG) Ulminite 2	0.07	0.42	0.24	0.17	0.51	2.40	0.68	-	4.49
Martin Lake	(ML) Ulminite 1	0.15	0.38	0.32	0.28	1.25	1.69	0.45	0.05	4.57
Martin Lake	(ML) Ulminite 2	0.06	0.42	0.16	0.07	1.16	1.67	0.36	0.06	3.96
Rosebud	(RB) Vitrinite 1	0.06	0.20	0.33	0.05	0.76	0.71	0.08	0.03	2.22
Rosebud	(RB) Vitrinite 2	0.12	0.32	0.18	0.11	0.73	0.86	0.06	0.04	2.42

Comparing the four coals: BZ ulminites have high Na and Fe and low S and total constituents; HG ulminites have high Ca and low Na and S; ML ulminites have low Na and high Mg, S and total constituents; while RB vitrinite has moderate to low values for all elements. Within the coals BZ and HG ulminites tend to occur as either low or high Na+Mg+Ca types; ML ulminite as a low or high Al+Si type and RB vitrinite types vary from low to high Mg/Al. The chemistry of the huminite group macerals and the bulk compositions of the four coals have striking similarities, including the

high Na and low S for BZ, high Ca and low Na and S for HG, and low Na and high S for ML. Ullminite chemical variation between coals and within seams suggests the importance of hydrogeochemical processes during diagenesis.

The results of these studies show important patterns of concentrations and variability of numerous inorganic elements. These geochemical characteristics may have great significance for development of our understanding of coal formation and utilization.

References

Hall, T.A., 1968, Some Aspects of the Microprobe Analysis of Biological Specimens: in Heinrich, K.F.J., ed., Quantitative Electron Probe Microanalysis; N.B.S. Spec. Pub. 298, p 269-299.

Karner, F.R., D.R. Kleesattel, S.A. Benson, and H.H. Schobert, 1984, Optical and Microbeam Investigation of Lithotypes of Beulah-Zap Lignite, North Dakota. Geological Society of America Abstracts with Programs, v. 16, p. 555.

Karner, F.R., D.R. Kleesattel, H.H. Schobert, and T.P. Huber, Inorganic Chemistry of Huminite Group Macerals in Four Low-Rank Coals of the Western United States. Geological Society of America Abstracts with Programs 1985 Annual Meeting, p. 623.

Love, G. and V.D. Scott, 1980, New Developments in EMPA Correction Procedures: in Brederroo, P., and V.E. Cosslett, Electron Microscopy 1980, v. 3, Analysis, 7th Eur. Congr. Electron Microsc. Found. (Leiden), p. 146-147.

Millner, R., and U. Cobet, 1972, Quantitative Electron Beam Analysis of Thick Biological Tissue Samples: Phys. Med. Biol., v. 17, p. 736.

Russ, J.C., 1974, The Direct Element Ratio Model for Quantitative Analysis of Thin Sections: in Hall, T.A., P. Echlin, and R. Kaufmann, Microprobe Analysis as Applied to Cells and Tissues, Academic Press (London), p. 269-276.

Small, J.A., K.F.J. Heinrich, D.E. Newburg, R.L. Myklebust, and C.E. Fiori, 1980, Procedure for the Quantitative Analysis of Single Particles with the Electron Probe, in Heinrich, K.F.J., ed., Characterization of Particles, N.B.S. Spc. Pub. 533, p. 29-38.

Statham, P.J., and J.B. Pawley, 1978. A New Method for Particle X-ray Microanalysis Based on Peak to Background Measurements: Scanning Electron Microscopy/1978/I; SEM Inc., AMF O'Hare (Chicago), p. 469-478.

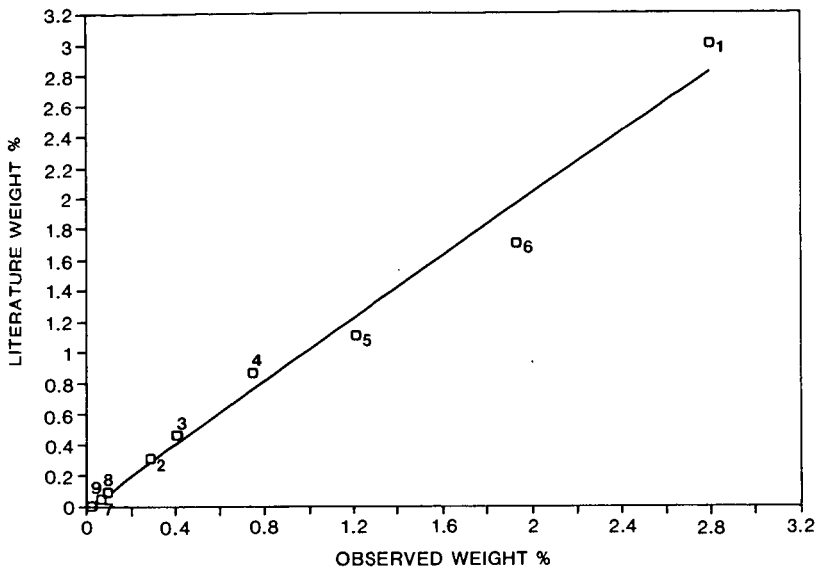


Figure 1. Aluminum calibration curve. Peak to continuum method.

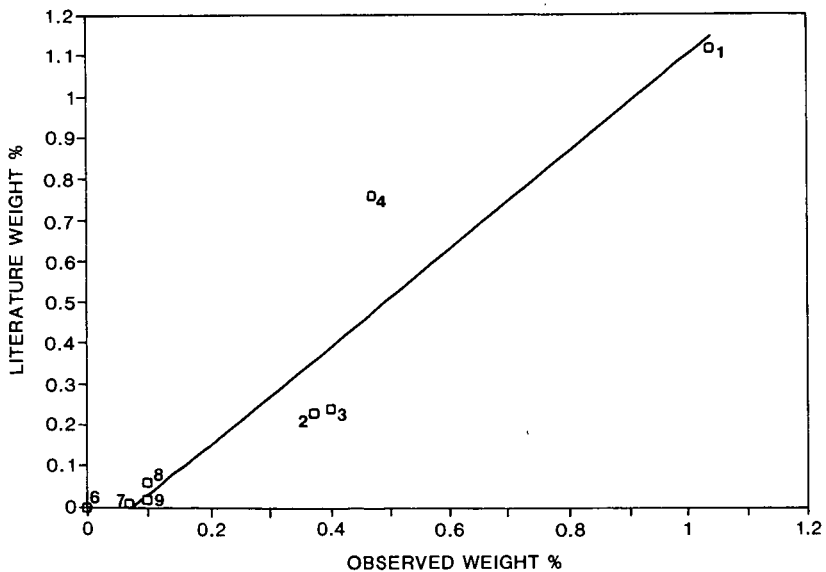


Figure 2. Iron calibration curve. Peak to continuum method.

PIXE - A NEW ANALYTICAL TECHNIQUE FOR THE
ANALYSIS OF COAL AND COAL DERIVED FUELS

Swadesh S. Raj

Department of Chemistry, William Paterson College, Wayne, N.J. 07470

ABSTRACT

A new technique, PIXE - particle induced x-ray emission scanning, for analyzing concentrations of sodium through uranium with detection limits in the order of ppb and ppm is explained in this paper. The accuracy of scan is $1 \mu\text{m}$ and the target can be moved over a distance of 8 inches in any direction for surface or depth analysis. PIXE is performed by scanning the target, in increments ranging from 1 to 8 mm adjustable diameter of proton beam, line by line, using a computer controlled Deadal motor driven linear translation stage in the needed directions.

The experimental results obtained from a number of coal and ash samples, using PIXE technique are presented. The degree of accuracy of the PIXE technique relative to other techniques is also discussed. The technique is very useful for coal and ash analyses, deposit analysis, and analyses of corroded and eroded surfaces using coal and coal derived fuels. PIXE is a unique technique which provides quantitative data on concentration of inorganic constituents, its oxidation state and depth simultaneously. Total analyses time in this technique, including sample preparation, varies from 8 - 10 minutes per sample.

INTRODUCTION

Coal is a heterogeneous assembly of macerals and minerals schematically shown in Fig. 1 {1}. This figure is similar to Schlosberg of Exxon. A number of investigators; Given {2}, Wiser {3} and Larsen {4} etc. have attempted to formulate a model for the organic components of coal (Figures 2,3 & 4) based upon the cumulative experimental results. The experimental results were obtained through different experimental techniques and using wide variety of analytical tools. In this regard a substantial understanding of coal structure has been obtained. However, these structures still do not provide clues to the solution of many engineering problems experienced due to coal utilization. Some of these problems may be attributed towards the poor understanding of chemical, thermodynamic and kinetic reactivity of coal in the process of combustion or conversion. The resolution to the engineering problems; deposits, corrosion, erosion, slag formation, NO_x , SO_x , and particulate emission, with the use of coal in industry can be achieved if multidimensional properties of coal are studied simultaneously. Industrial experience with coal {5} indicates that coal can be best analyzed for its structure (organic, inorganic, trace elements, porous and petrographic structure) under two main methods of study: Direct and Indirect.

In the Direct method, coal can be analyzed for its gross characteristic such as elemental composition, petrographic composition, Btu value, calorific value, etc. using conventional analytical tools. The results obtained through the Direct methods do not provide reasons for two coals exhibiting different chemical behavior although possessing similar gross characteristics and vice versa. Indirect methods, on the other hand, provide the core information most essential to the understanding of reaction mechanism and cause of many industrial problems {5}. Under Indirect methods controlled conditions may be used to obtain the recognizable chemical units of coal (representative of whole coal) without altering the chemical nature of coal. It is only through the Indirect methods that the composition of inorganic and organic constituents can be established {6,7}.

Inorganic constituents of coal and coal products are analyzed by a number of techniques. These techniques are reviewed in references {8 & 9} by Weaver and Fuller. The analytical techniques used are AAS, NAA, ICP, DCP, XRF, SEM, etc. Some of the techniques used are time consuming, some possess lower detection limits and some do not provide multi-elemental detections with depth profile. The PIXE (particle induced x-ray emission) technique overcomes the above mentioned difficulties. This technique even differentiates between the oxidation state of ions. According to Khan and Crumpton {10}, the PIXE technique is reliable and repeatable. PIXE technique has been widely used in the study of biological tissue {11}, meteoritic samples {12}, rain and snow {13 & 14}, and environmental samples {15} to analyze concentrations of trace elements sodium through uranium in ppb. In this paper, PIXE technique is reviewed and preliminary results on coal and coal ash using PIXE are presented.

EXPERIMENTAL THEORY

PIXE (particle induced x-ray emission) in general involves bombardment of elements with any particles: alpha, beta, gamma, electron, proton, etc. In the present study, however, the instrument generated a proton beam to excite electrons of K and/or L shells of atoms. The spectra of K and K x-rays and L and L x-rays are sufficient to detect even heavy elements. Proton beam with the energy strength of 4 MeV bombards K and L shells of electrons of an element {15,16}. The electrons after absorbing the proton energy migrate to higher energy levels and leave the vacant spots in K and L orbits. The transition of electrons from higher energy "allowed" orbitals takes place to fill the vacant spot in the K and L orbits. The transition of electrons from higher energy to lower energy orbits accompanies with the emission of electromagnetic radiations. The emitted radiation carries an amount of energy equivalent to the energy difference between two shells of the electron transition. These emissions correspond to K and L x-ray radiations. The wave length of the produced radiations are characteristic of the elements and varies from element to element. The corresponding K and L x-ray intensities are recorded in the form of a spectrum. Since these x-rays are characteristic for each element, the fingerprints of the x-ray emission attributes to the elemental identification. The area covered under a peak in the spectrum directly relates to the concentration of individual elements. The principle of PIXE and the development of PIXE is explained in great detail by Johansson and Johansson {17}.

EXPERIMENTAL METHOD

The experimental program was conducted in three steps. The first step was involved with the generation of the homogeneous beam of protons with a given intensity. The second step dealt with the preparation of samples and exposing the samples to the beam of protons. The third step was carried out to obtain the elemental x-ray spectra and compare it with that of standard elements.

Homogeneous beam of protons, with the energy of the order of 4 MeV, is generated using Tandem/Van de Graff accelerators. This energy is sufficient to detect heavy metals. The beam of protons travels a long way before it hits the coal sample. The proton beam passes through a diffuser foil, several collimators and finally through a 25 μ m diameter Kapton window. The purpose to pass the beam through a number of obstacles was to scatter the beam to obtain uniformity and subsequently to refocus it to obtain homogeneity. The homogeneity of the beam was checked by using known standard element. The test section where the sample was introduced was filled with helium. The beam when projected on a sample covered an estimated diameter of 8 mm. The Kapton window in the set up was changed every 12 hours so as to avoid pick up of any interaction effects in the final spectra. The Faraday cup was used to integrate the charge. This cup was mounted downstream of the sample. The detection was done by the Ge Princeton Gamma Tech. detector. This detector possessed energy resolution of 150 eV at the Mn 5.9 KeV K line.

Several other protective measures were taken in the PIXE set-up to maintain the sensitivity of the experiment. The sample slides were mounted in a slide projector. The insertion and the removal of the slides was controlled automatically.

Coal and ash samples were analyzed as a thin slide on kimfol film. Samples were mixed with an appropriate binding agent and the mixture was then transferred on to kimfol film slides. Binding agent used for coal was cellulose acetate (Polystyrene) in toluene where as ash samples were mixed with 6F HNO₃ doped with 100 ppm yttrium. Coal and ash samples were mixed with their appropriate binding agent in the ratio of 300 mg to 300 μ l of this mixture were deposited on the kimfol film slides and irradiated directly. Kimfol is a polyvinyl very thin material, easy to handle, resistant to chemical attack and can withstand high proton beam currents.

The concentration of an element in a sample was determined by comparing the area of the K (or L) peak of the element of interest with that of a reference element that contained Argon, Rhodium or yttrium as the internal standard. The standard reference spectra were obtained from bombarding high purity atomic absorption standards in a matrix of boric, perchloric, nitric, and hydrofluoric acid under the same conditions (i.e. target thickness, type of backing and its thickness, integrated charge, and current) as the samples. This normalization procedure removed uncertainties due to x-ray absorption and x-ray production cross sections. The data acquisition system and the slide projector are automatically controlled by a PDP 11/44 computer [16]. The thickness profile is obtained by bombarding the sample with variable proton energies that can pass through the sample. The stopping power of proton (depth penetration) is a function of its energy and the thickness of the sample under study.

EXPERIMENTAL RESULTS, DISCUSSION AND CONCLUSIONS

The characteristics of coal samples analyzed by PIXE methods are shown in Table 1.

TABLE 1
COAL AND ASH SAMPLES

<u>Sample #</u>	<u>Origin</u>	<u>Rank</u>	<u>% C dmmf</u>	<u>% MM Dry</u>
1. Coal - PSOC 95	(Washington)	HVA	84.39	23.75
2. Coal - PSOC 124	(W. Virginia)	HVA	83.48	9.71
3. Coal - PSOC 245	(No. Dakota)	Lignite	73.39	15.38
4. Coal - PSOC 251	(Kansas)	HVA	83.73	19.99
5. Coal - Low Temp. Ash	From coal sample #1			
6. Coal - Low Temp. Ash	From Coal sample #3			

Inorganic constituents in coals are detrital and authigenic. Minerals which are formed as a result of coalification process consists of montmorillonite, chlorite, kaolite, pyrite, gypsum, hematite, siderite and calcite. The detrital constituents include monmorillonite, quartz, plagioclase, alkali feldspar, biolite, chlorite, volcanic glass and rock fragments. Na, Mg, Al, K, Ca, Ti, Fe, Sc, V, Cr, Mn, Co, Ni, Zn, As, Se, Ru, Ag, Cd, Sb, Cs, Ba, Sm, La, Ce, Eu, Yb, Th, U etc. are the inorganic elements responsible for the formation of the mineral matter in coals. Major mineral matter which is not bonded with the organic structure of coal is widely known and can be taken out in the cleaning processes by physical or chemical means. However, this is cumbersome, expensive and time consuming process and changes the chemistry of whole coal. These are some of the reasons why direct use of coal is encouraged.

In the present investigation, powder form of coal samples was used. Therefore, the PIXE analysis of coal samples presented contain elemental concentration of total mineral contents. Fig. {5} through {10} illustrates the concentration distribution of various major elements in the sample. Some of the peaks are not seen on

plots due to scaling. These hidden peaks represent the elemental concentration the order of one ppm. In between the adjoining peaks, there are also elements less than 1 ppm which have not been identified due to presence of one of the elements in far excess compared to others and which controlled the vertical scale. Detection of the elements below 1 ppm concentration may be possible in future work. Since it is a preliminary investigation, it provided us an input to set up scales for future work on the coal mineral and ash investigation. Nevertheless, it was the first effort to analyze coal using the PIXE technique.

Presence of Na, Al, Si, K in large quantities also interfered with the Ar - standard used to identify trace elements. Fe, Ca, Al, Na, Si, K, Mg, Ba, etc. are not trace elements (concentration range is higher). These elements come from pyrite, silicates and quartz incorporated into coal during the coalification process. Mn, Co, V, Zn, Sr, Cr, As, Se, Sm, Pb, Cu, Th, U etc. are the trace elements. Concentration of these elements vary from few ppm to below hundreds.

Results of PIXE analysis are summarized in Table 2. The identified elements and their concentration levels match with the ones obtained from other methods given in references 7, 9 and 18, which demonstrates the accuracy of the method.

TABLE 2
GENERAL TREND IN
CONCENTRATION OF ELEMENTS (PPM)

Coal Sample	Concentration of Elements Na, Ca, Mg, Fe, Al, Si, K, Ba	Concentration of Elements Se, V, Ti, Co, Zn, Sc, Cr, As, Pb, Cu, Cd, Sr, Sb, Cs, Sm, Th, U
Washington HVA	Hundreds	Under One
W. Virginia HVA	To	To
Kansas HVA		
North Dakota LIGNITE	Thousands ppm	Under Hundred ppm
Coal Ash		
Coal Ash		

ACKNOWLEDGEMENT

The experiment was conducted while the author was at the Rutgers University. The author expresses her gratitude to Dr. G. Hall for arranging the spectra presented in this paper.

REFERENCES

Raj, S., and Raj, R., ASME Proc., IGTC, Coal Utilization, No. 82-GT-116, 1982.

2. Given, P.H., *Fuel*, 39, 1960.
3. Wisler, W.H., *DOE Sym. Ser.*, 46, 1978.
4. Larsen, J.W., *ACS Proc. Sym.*, *Fuel Chem.*, 30-4, 1985.
5. Raj, S., and Raj, R., paper submitted to ASME IGTC, *Coal Utilization*, 1985.
6. Gorbaty, M.L., Larsen, J.W., and Wender, I., *Coal Structure*, Academic Press, New York, 1982.
7. Meyers, R.A., *Coal Structure*, Academic Press, New York, 1982.
8. Weaver, J.N., *Methods for Coal and Coal Products*, Academic Press, New York, 1978.
9. Fuller, E.L., *ACS Sym. Ser.* 205, 1982.
10. Khan, Md. R., and Crumpton, D., *CRC Critical Reviews in Analytical Chemistry*, May, June 1981.
11. Walter, R.L., et al, *Analytical Chem.*, Vol. 46, 843, 1974.
12. Herzog, G., and Kuzel, H.W., *Nuclear Instrum. Methods*, Vol. 142, 301, 1977.
13. Tanks, S., Darzi, M., and Winchester, J.W., *Environ. Sci. & Tech.*, Vol. 15, 355, 1981.
14. Jervis, R.E. et al, *Nuclear Instrum. Methods*, Vol. 193, 323, 1982.
15. Raj, S., et al, *Internatl. Conf. on PIXE*, Max Plank Inst. Fur Kernphysik, Heidelberg, 1983.
16. Raj, S., Raj, R., and Hall G., *ASME Proc.*, IGTC, *Coal Utilization*, No. 84-GT-213, 1984.
17. Johansson, S.A.E., and Johansson, T.B., *Nucl. Instrum. Methods*, Vol. 137, 275, 1976.
18. *ACS Preprints*, Div. of Fuel Chem., 1983, 1984.

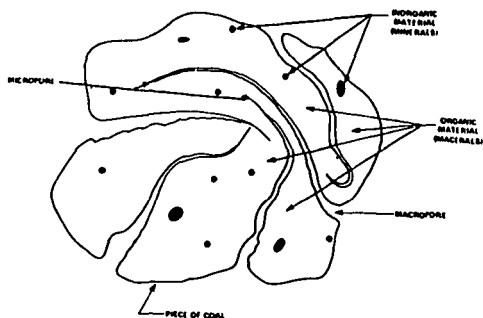


Fig. 1: Heterogeneous Assembly of Macerals and Minerals with Pores in a Piece of Coal.

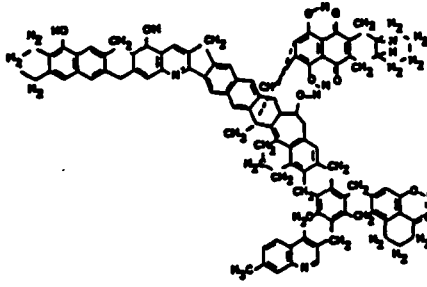


Fig. 2: Hypothetical Chemical Structure of Coal Molecule by Given.

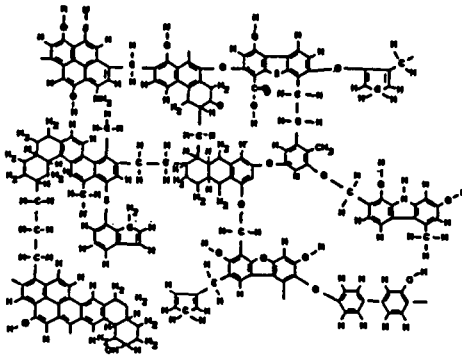


Fig. 3: Schematic Representation of Chemical Structure of Coal by Wiser.

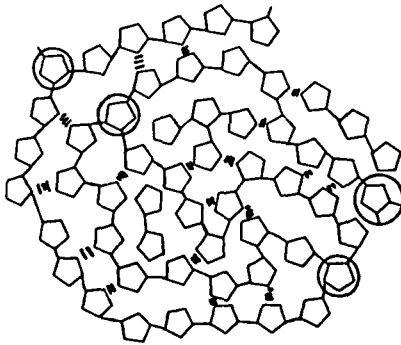


Fig. 4: Macromolecular Structure of coal by Larsen.

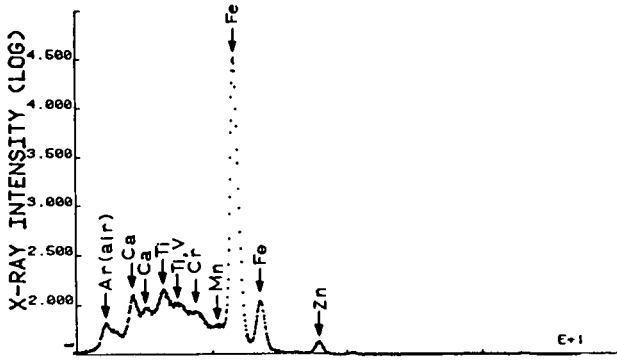


Fig. 5: X-Ray Spectra of Coal Sample 1.

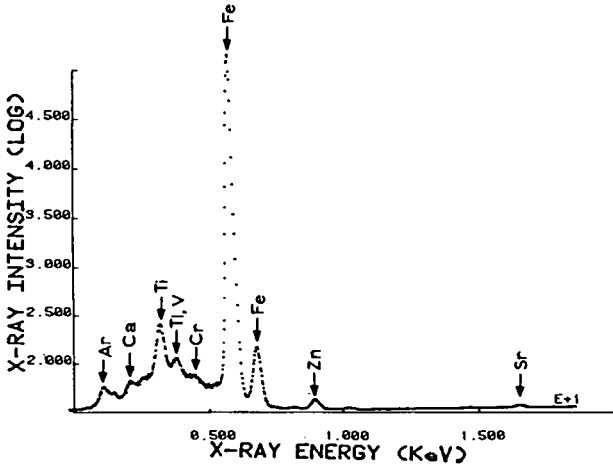


Fig. 6: X-Ray Spectra of Coal Sample 2.

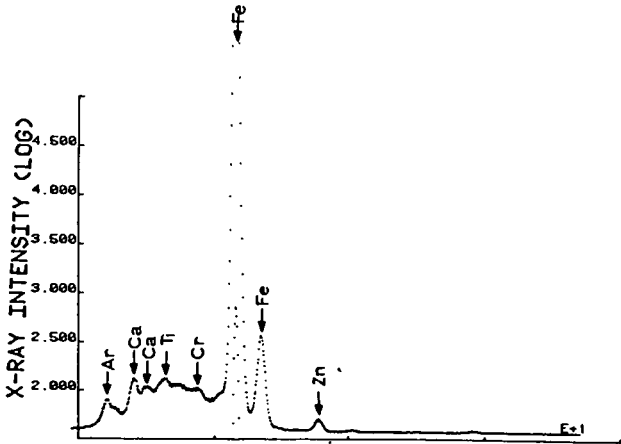


Fig. 7: X-Ray Spectra of Coal Sample 3.

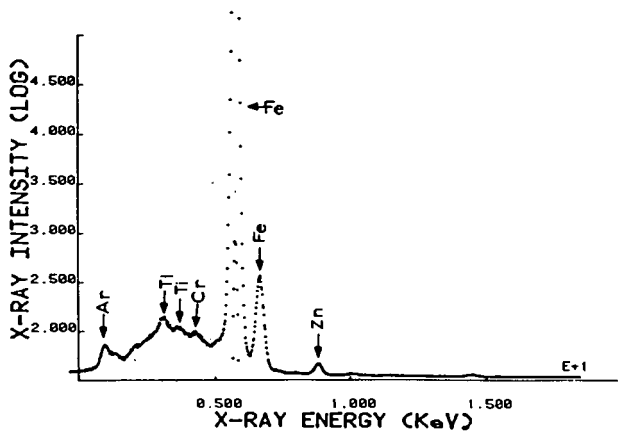


Fig. 8: X-Ray Spectra of Coal Sample 4.

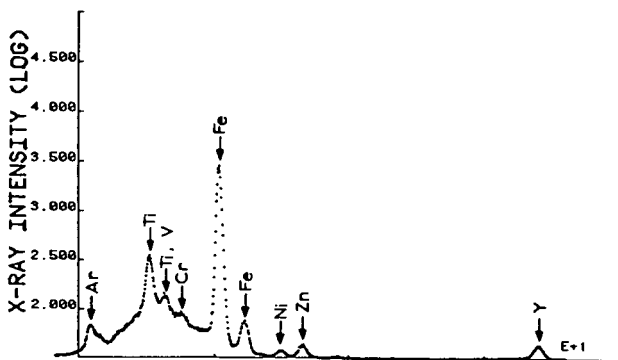


Fig. 9: X-Ray Spectra of Coal Ash Sample 1.

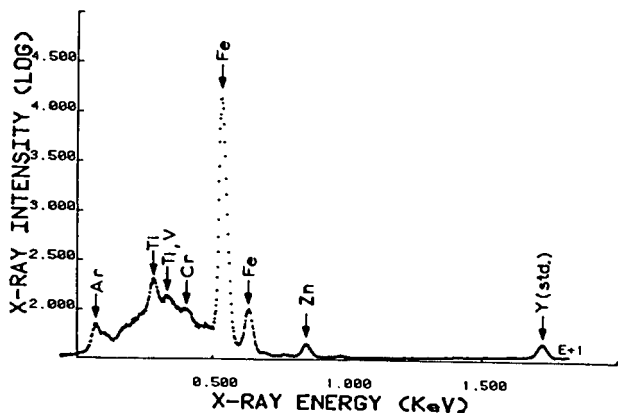


Fig. 10: X-Ray Spectra of Coal Ash Sample 2.

DETECTION BY PHOTOACOUSTIC INFRARED FOURIER TRANSFORM SPECTROSCOPY
OF SURFACE PEROXIDE SPECIES IN CHEMICALLY AND THERMALLY MODIFIED COALS

Brian M. Lynch, Lai-Im Lancaster, and James T. Fahey

Coal Characterization Group
Department of Chemistry
St. Francis Xavier University
Antigonish, Nova Scotia B2G 1C0, Canada
(902)-867-3992

ABSTRACT

Work in our laboratories over the last three years has demonstrated that PhotoAcoustic infrared Fourier Transform (PAIFT) spectroscopy provides unique qualitative and quantitative information about the surface functionalities of bituminous coals.

We now report evidence detected by PAIFT techniques of new carbonyl-type oxygen functionality in such coals, which is generated both by base-promoted and thermal decomposition of precursor peroxide species, which we propose are ubiquitous constituents of the surfaces of all except the most freshly prepared samples of powdered bituminous coals.

INTRODUCTION

Over the past three years, PhotoAcoustic Infrared Fourier Transform (PAIFT) spectra of coal samples have been acquired in our laboratory for a data base now amounting to some 6000 spectra. Various preliminary reports of our results have been presented (1-5).

Among the manifold advantages of PAIFT spectroscopy in the study of coals are minimal sample preparation, insensitivity of signal to degree of subdivision, and the ability to observe surface infrared absorbing features generated by chemical manipulation. Subtraction to yield difference spectra revealing such introduced features is straightforward and avoids arbitrary scaling procedures.

Although it is often stated that application of FTIR spectroscopy has revitalized the applications of infrared spectroscopy to coals, the truly new results reported as a consequence of this revitalization are very limited, and the recent literature contains several examples of unwarranted and probably incorrect conclusions arising from subjective applications of curve-resolving techniques and calibrations of relative intensities of spectral features.

In this paper, we report detection by PAIFT spectroscopy of new oxygen functionality produced by base-promoted decomposition of precursor peroxide species ubiquitously present at the surface of all except the most freshly prepared samples of powdered bituminous coals. The occurrence of this reaction process has escaped detection previously since KBr-pellet transmission FTIR and Diffuse Reflectance FTIR measurements involve randomization of the superficial infrared-absorbing groups as a consequence of the grinding procedures associated with sample preparation using these techniques.

EXPERIMENTAL

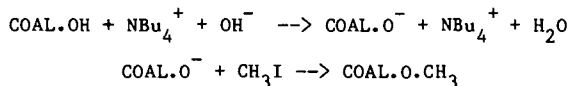
PAIFT spectra were acquired using a Bruker IFS110 purge-type Infrared Fourier System employing a Ge on KBr beamsplitter. The spectrometer was interfaced to an E G & G Princeton Applied Research Model 6003 Photoacoustic Accessory equipped with a zinc selenide window and the amplified photoacoustic output was transmitted to the data acquisition system of the IFS110. The purge flow was interrupted during scanning.

Coal samples were ground to finer than 60 mesh under liquid nitrogen using Brinkmann Pulverizer, and dried at 100 degrees C under vacuum before transfer to the sample cup of the photoacoustic accessory. For routine operation, 10-50 mg of dried coal were placed in the sample cup, and 128 photoacoustic interferograms were collected at 8 cm^{-1} resolution with a zero-filling factor of 2, corresponding to a final transformed spectrum encoded every 4 cm^{-1} . Photoacoustic spectra were obtained by ratioing against the energy output (black-body response) from a similarly prepared sample of Fisher Carbon Lampblack C-198.

The interferometer mirror velocity was $0.08333 \text{ cm s}^{-1}$, and spectra were acquired from $400\text{-}4,000 \text{ cm}^{-1}$.

DISCUSSION AND RESULTS

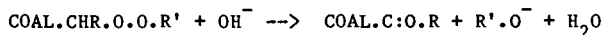
Bituminous coal samples may be methylated quantitatively using the phase-transfer catalyzed process developed by Liotta and co-workers at Exxon Research and Engineering Company (6,7). The procedure involves initial formation of anionic centres and associated swelling of the coal by treatment with tetrabutylammonium hydroxide in aqueous tetrahydrofuran under nitrogen, followed by $\text{S}_{\text{N}}2$ reaction with methyl iodide, that is:



PAIFT spectra for a typical sample of freshly ground, newly mined bituminous coal (from Cape Breton Island, Nova Scotia) and of its quantitatively methylated species are reproduced in the two spectra of Figure 1.

In previous work (1-4) we observed that many methylated coals exhibit distinct carbonyl absorption in the region $1680\text{-}1705 \text{ cm}^{-1}$, which is not present in the starting coal. Although we thought at first that a high-frequency shift of a pre-existing carbonyl species (occurring as a consequence of the elimination of hydrogen-bonding interactions) accounted for this phenomenon, further work shows that the new carbonyl is generated irreversibly at the stage of formation of the coal anions (that is, before methylation) (see the overlay spectrum of Figure 2), and is unchanged by re-acidification of the reaction mixture; thus the new peak cannot involve displacement of a carboxylate/carboxylic acid ratio, nor a simple frequency shift accompanying methylation.

We attribute the formation of the new absorbing entity to the base-promoted decomposition of peroxide species, that is:



R = alkyl or aralkyl, R' = H, alkyl, or aralkyl

This is a well documented reaction (8-10) whose possible relevance to coal transformations has not been recognized previously to our findings. The difference spectrum between the sample of Figure 1 and the corresponding reprotonated (re-acidified and washed) "coal anion", which was presented in overlay form in Figure 2, is reproduced as Figure 3, and exhibits a maximum at 1686 cm^{-1} . We have been able to define the nature of the carbonyl feature as ketonic, since it is quantitatively reduced to an alcohol species by tetrabutylammonium borohydride in aqueous tetrahydrofuran.

Derivatization of the same coal through acetylation using the standard procedure where the coal is heated to reflux with acetic anhydride dissolved in pyridine does not produce added ketone-type carbonyl species (see Figure 4). Under these conditions, we suggest that it is likely that the peroxide species transfers oxygen directly to the pyridine solvent, and the formed pyridine-1-oxide undergoes the known rearrangement/hydrolysis to give 2-acetoxypyridine and thence 2-pyridone.

Although the overlay and difference spectra referred to above bear a general resemblance to those observed for oxidation at higher temperatures (see Figures 5 and 6), the band shapes are different, with the carbonyl peaks from the base-generated ketones obviously being simpler, and the carbonyls shown in Figure 6 possessing multiple contributing components. Also we wish to point out that the intensity of the ketone carbonyl peaks in the difference spectra derived from base-treatment of coals stored in the laboratory at around 20°C for six and for twelve months (Figures 7 and 8) increases progressively: "fresh" coal, 0.020 intensity units, after six months, 0.059; after 12 months, 0.089.

Finally, we find that thermal decompositions of these coal samples occur in vacuo between 150 and 200 degrees C to generate carbonyl functions whose origin we are confident lies with surface peroxides, although the course of these reactions is more complex than for the base-promoted decompositions.

CONCLUSIONS

PAIFT spectroscopy of coals treated with phase-transfer base followed by reacidification provides evidence that previously unquantified and undetected peroxide species are significant features of coal surfaces exposed to air at ambient temperatures; thermal decompositions at coal surfaces similarly involve contributions from peroxide \rightarrow carbonyl conversions. The proportion of peroxides on a coal surface is surely playing an important, hitherto unguessed, role in determining the course of coal pyrolyses.

ACKNOWLEDGEMENTS

We wish to thank Dr. J. A. MacPhee (Energy Research Laboratories, Ottawa), Drs. J. Gethner and R. Liotta (Exxon Research and Engineering Company), and Dr. R. A. Durie (R. W. Miller Holdings, Sydney, Australia) for useful discussions.

The research work leading to this paper was supported by Energy, Mines, and Resources Canada through the Department of Supply and Services, Contract Serial No. OST83-00347. J. T. Fahey thanks the Natural Sciences and Engineering Research Council, Ottawa, for a 1985 Summer Undergraduate Research Assistantship.

REFERENCES

1. Campbell, M., Lancaster, L., Lynch, B. M. and MacEachern, A. M., Abstract 054, Pittsburgh Conference on Analytical Chemistry & Applied Spectroscopy, Atlantic City, New Jersey, March 1983.
2. Lancaster, L., Lynch, B. M., MacEachern, A. M., Donini, J. C., Hamza, H., and Michaelian, K. H., Abstract 158, 57th Colloid & Surface Science Symposium, American Chemical Society, Toronto, Canada, June 1983.
3. Lynch, B. M., and MacEachern, A. M., Proc. 1983 International Conference on Coal Science, Pittsburgh, Pennsylvania, pp.653-654.
4. Lynch, B. M., Lancaster, L., MacEachern, A. M., and Khan, M. A., Paper 161, Eastern Analytical Symposium, American Chemical Society, New York City, November 1983.
5. Lynch, B. M., Bull. Am. Phys. Soc., 30, 504-505 (1985).
6. Liotta, R., Fuel, 58, 724 (1979).
7. Liotta, R., Rose, K., and Hippo, E., J. Org. Chem. 46, 277 (1981).
8. Kornblum, M., and de la Mare, H. E., J. Am. Chem. Soc. 73, 880 (1951).
9. Sprinzak, Y., J. Am. Chem. Soc., 80, 5449 (1958).
10. Plesnicar, B., in The Chemistry of Peroxides. Patai, S., Editor. John Wiley & Sons, Inc., p. 573 (1979).

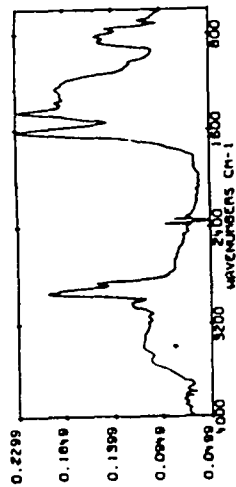


Figure 1. Typical PAFT spectra of Cape Breton Island bituminous coal and of its product of quantitative methylation.

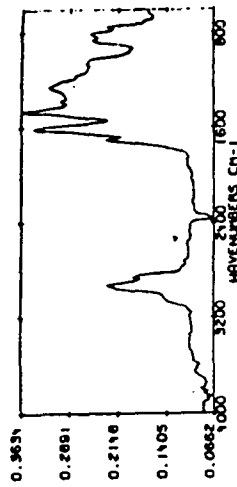
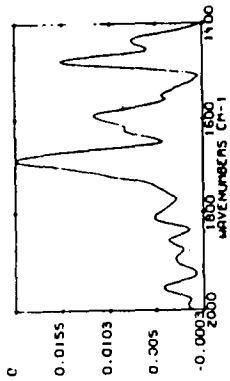
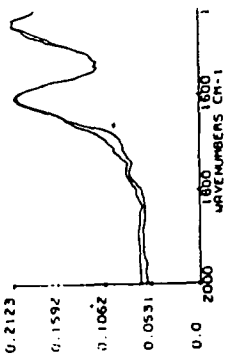


Figure 2. Overlay spectrum of the coal of Figure 1, before and after coal anion generation.



PRINTED CONTINUED

Figure 3. Difference spectrum, coal after minus before coal anion generation.

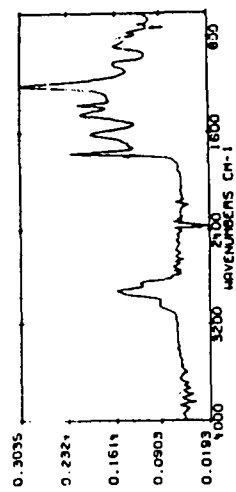


Figure 4. PAFT spectrum of quantitatively acetylated bituminous coal of Figure 1.

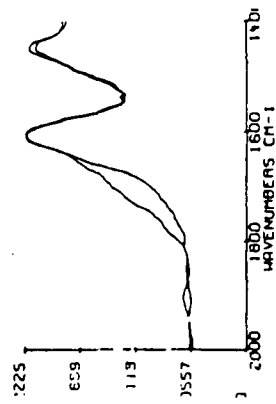


Figure 5. Overlay spectrum of thermally oxidized bituminous coal (before and after 192 h oxidation in air at 105°C).

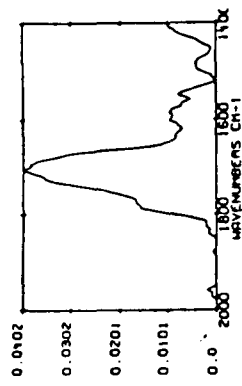


Figure 6. Difference spectrum, thermally oxidized coal (see Figure 5).

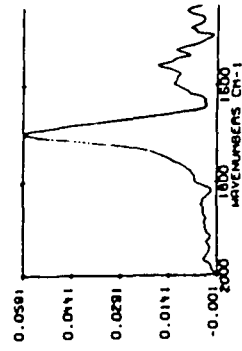


Figure 7. Difference spectrum, after minus before coal anion formation, for coal of Figure 1 stored six months.

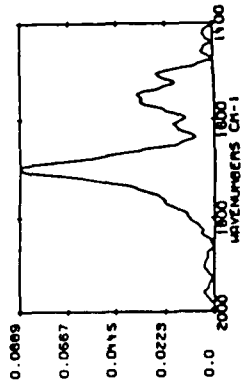


Figure 8. Difference spectrum after minus before coal anion formation, for coal of Figure 1 stored twelve months.

THE RUTHENIUM(VIII)-CATALYZED OXIDATION OF ILLINOIS NO. 6 BITUMINOUS COAL. AN
APPLICATION OF GC-FTIR SPECTROSCOPY FOR STRUCTURAL ANALYSIS.

Leon M. Stock and Shih-Hsien Wang

Department of Chemistry, University of Chicago, Chicago, IL 60637 USA

INTRODUCTION

Sharpless and his coworkers pointed out that ruthenium tetroxide could be used very effectively for the oxidation of aromatic compounds in the presence of acetonitrile (1). For example, 4-(1-pentyl)biphenyl is converted almost quantitatively to a mixture of hexanoic acid, benzoic acid and 4-pentylbenzoic acid. This reagent has been used successfully for the oxidation of Illinois No. 6 coal and the quantities of many aliphatic and aromatic mono-, di-, tri-, and tetracarboxylic acids have been determined for several different coals (2-5). Mass spectroscopy has been used almost exclusively in these studies. In related work, Mallya and Zingaro (6) investigated the ruthenium ion-catalyzed oxidation of Texas lignite using infrared spectroscopy. They pointed out that the stretching bands of the carbon-carbon bonds of the aromatic ring at 1600 cm^{-1} decreased and a new carbonyl band at 1700 cm^{-1} appeared. Their work and other factors prompted us to consider the utilization of GC-FTIR spectroscopy for the further analysis of the product distribution obtained in the oxidation of Illinois No. 6 coal.

EXPERIMENTAL PART

Coal Sample.--Illinois No. 6 coal [77.2%C, 5.6%H, 0.68%N, 0.15%Cl, 2.95% organic S, 0.89% pyritic S, 0.00% sulfate, and 12.5% O (by difference)] was obtained from the Peabody mine in Pawnee, Illinois. The sample was extracted before oxidation with aqueous hydrochloric acid, aqueous sodium hydroxide, benzene-methanol, and chloroform as described by Hayatsu and coworkers (7).

Oxidation Procedure.--The oxidation reactions were carried out as described previously (3,4,5) using coal (400 mg), ruthenium(III) chloride trihydrate (12 mg), and sodium periodate (4g) in a mixture of carbon tetrachloride (8 ml), acetonitrile (8 ml) and water (12 ml). The mixture was stirred for about 24 hours at room temperature. The solids were separated by filtration and the organic and the aqueous phases were retained. The mildly acidic aqueous layer was washed with four portions of ether (15 ml). The solid was also washed with ether. All the organic extracts were combined and dried with sodium sulfate. The solvents were removed with a rotary evaporator at 40°C . The acids in the concentrated solution were methylated using 0.35M diazomethane in ether (10 ml). The ether was carefully removed using a rotary evaporator at room temperature. This procedure was repeated three times and the final solution was examined by gas chromatography-Fourier transform infrared spectrometry and mass spectrometry.

Gas Chromatography-Fourier Transform Infrared Spectrometry.--An HP Model 5890 gas chromatograph and a Nicolet Model 60SX Fourier Transform Infrared Spectrometer were used in this study. The chromatograph was equipped with a 0.53mm X 25 meter, OV-1701 megabore column supplied by J & W Scientific, Inc.

Typical conditions for the analysis are noted: injection port, 250°C; the oven temperature was programmed to hold at 50°C for one minute then to heat to 270°C at the rate of 4°C/min and then to hold at 270°C. For all the spectra, 4 scans measured at 4 cm⁻¹ resolution were co-added.

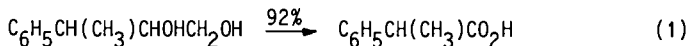
Gas Chromatography-Mass spectrometry.--The GC-MS results were obtained using an HP Model 5790A gas chromatograph with a VG Model 70-250 mass spectrometer. The chromatograph was equipped with a 50 meter, 0V-1701 (0.25μ) capillary column supplied by Quadrex Corporation, Inc. The conditions for the analysis are noted: injection port, 250°C; the oven temperature was programmed to hold at 50°C for one minute then to heat to 270°C at the rate of 7°C/min and then to hold at 270°C. One scan per second was recorded in these low resolution, electron impact mass spectral analyses.

RESULTS AND DISCUSSION

The ruthenium(VIII) ion-catalyzed oxidation reaction of Illinois No. 6 bituminous coal produces a large array of different carboxylic acids. These acids were quantitatively converted to the corresponding methyl esters by repetitive esterification reactions with diazomethane. The GC-FTIR chromatograms obtained using conventional capillary columns were not entirely suitable. However, the separations obtained using megabore capillary columns were more than satisfactory and suitable infrared spectra could be recorded for most of the reaction products. Chromatographic procedures were developed to enable facile comparison of the mass and infrared spectra.

Many aliphatic di-, tri-, and tetracarboxylic acids as well as the benzenedi-, tri-, tetra-, and pentacarboxylic acids can be readily detected and identified by GC-MS procedures (4,5). However, certain of the products cannot be unambiguously identified by MS tactics alone. We were particularly concerned that certain hydroxyacids and lactones might have escaped detection.

Inasmuch as sharp oxygen-hydrogen stretching frequencies are readily observed in the vapor phase, the infrared spectra were systematically scanned for the appearance of this absorption. Only three compounds among the host of reaction products exhibited this absorption. Inasmuch as these substances are produced only in trace amounts, this finding confirms the previous conclusion that aromatic hydroxylic compounds such as naphthol are oxidized to benzenedicarboxylic acid and that aliphatic hydroxylic compounds are degraded to simple aliphatic mono-, di-, and tricarboxylic acids. The absence of significant amounts of hydroxy compounds in the reaction product is in accord with the observations of Sharpless and coworkers (1) who reported that 3-phenyl-1,2-butanediol is oxidized to 2-phenylpropanoic acid under the experimental conditions, equation (1).



The position of the carbon-oxygen double bond stretching frequency is very dependent upon its structural environment with significant differences in the absorption frequencies of aromatic and aliphatic esters, lactones, anhydrides and so forth. The carbonyl stretching frequencies of the methyl esters of aliphatic acids, for example, dimethyl butane-1,4-dioate, appear near 1760 cm⁻¹, whereas the corresponding frequencies of methyl benzenecarboxylates, for

example, trimethyl benzene-1,2,3-trioate, appear near 1750 cm^{-1} . The carbonyl frequencies were examined to establish that proper structural assignments had been made in the previous work. No discrepancies were uncovered. However, several new compounds were detected. The carbonyl frequencies for these rather non-abundant compounds, not more than 1% of the abundance of dimethyl butane-1,4-dioate are listed in Table 1.

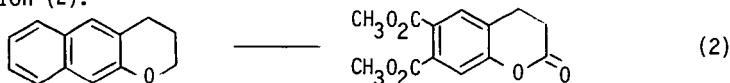
Table 1. The carbonyl bands of several novel substances in the oxidation of Illinois No. 6 coal

Compound	Frequency and Intensity
1	1720 (vs), 1704 (vs)
2	1820 (s), 1755 (s)
3	1824 (m), 1758 (vs)
4	1806 (m), 1755 (vs)
5	1809 (m), 1754 (vs)
aliphatic ester	around 1760
aromatic ester	around 1751

Compound 1 is quite volatile and exhibits a very intense carbonyl absorption centered at 1710 cm^{-1} . The absence of significant intensity in the carbon-hydrogen stretching region indicates that the substance is not a methyl ester. Indeed, the infrared spectrum is reminiscent of butane-2,3-dione. Hence, we infer that this non-abundant substance may be a 1,2-diketone produced as a byproduct of the principal reaction sequence.

Compound 2 exhibits two broad, equally intense carbonyl absorptions at 1755 and 1820 cm^{-1} . These observations and the strong absorption at 742 cm^{-1} imply that this substance is an aryl anhydride derivative.

Compounds 3, 4, and 5, which differ considerably in volatility, exhibit very similar carbonyl absorption frequencies. In each case, there are two relative sharp bands in the carbonyl region. The weaker band is centered between 1804 and 1809 cm^{-1} and the stronger band is centered between 1754 and 1758 cm^{-1} . These compounds all exhibit rather intense carbon-hydrogen absorptions. We postulate that these compounds are lactones with from one to three ester groups in the same molecule. These substances may form as illustrated in equation (2).



The abundance of lactones in the oxidation products of this bituminous coal appears to be much less than in the oxidation of Texas lignite (6).

CONCLUSION

Gas chromatography infrared spectroscopy provides useful information concerning the oxidation products of coals. The new data obtained by this technique confirm earlier conclusions concerning the low abundance of hydroxyl compounds among the oxidation and indicate that lactones are formed in low relative abundance during the oxidation of a bituminous coal.

REFERENCES

- 1) P.H.J. Carlsen, T. Katsuki, V.S. Martin and K.B.J. Sharpless, J. Org. Chem., 46, 3936 (1981)
- 2) L.M. Stock and K.-T. Tse, Fuel, 62, 974 (1983)
- 3) L.M. Stock and S.-H. Wang, Fuel, 64, 1713 (1985)
- 4) L.M. Stock and K.-T. Tse and S.-H. Wang, ACS, Division of Fuel Chem., Preprints, 30(4), 493 (1985)
- 5) L.M. Stock and S.-H. Wang, Fuel. Accepted for publication (1986)
- 6) N. Mallya and R.A. Zingaro, Fuel, 63, 423 (1984)
- 7) R. Hayatsu, R.E. Winans, R.G. Scott and R.L. McBeth, Fuel, 60, 158 (1981)

THE DEVELOPMENT OF LASER MICROPYROLYSIS OF COAL MACERALS

F. J. Vastola

Department of Materials Science and Engineering
The Pennsylvania State University
University Park, PA 16802

L. J. McGahan

Texas Instruments, Inc.
Semiconductor Division
19505 Hamelton St.
Torrance, CA 90502

INTRODUCTION

Since the development of the laser several workers have used its unique characteristics to study the pyrolysis of coal (1-11). The use of a focused laser beam to pyrolyze organic materials offers three advantages. The high degree of localization of surface heating allows the selective pyrolysis of micro components in a heterogeneous material such as the macerals in coal. The species resulting from laser heating are emitted from the heated solid surface with a minimum of interaction with the solid or other pyrolysis products thus increasing the probability of detecting primary structural fragments of the solid rather than products formed as a result of secondary reactions. Pyrolysis conditions can be set where selective bond breakage occurs, such as the rupture of alkyl bridges in coal.

The coupling of laser micropyrolysis with mass spectrometric detection of the emitted species offers a method of structural analysis of nonvolatile organic solids.

EXPERIMENTAL

The laser micropyrolysis mass spectrometer used in this investigation is an upgraded version of the one used in previous studies (1). The heating source used was a 0.1 J pulsed ruby laser. The laser output was focused by a 2X microscope objective lens onto the surface of a polished coal sample placed in the ionization chamber of a CVC 12-107 time-of-flight mass spectrometer. The area to be pyrolyzed was selected by viewing the surface through the same optical system as used to focus the laser beam. The zone of pyrolysis ranges between 10 and 200 μm in diameter, the size being dependent upon the power setting of the laser. The highly localized heating allows the selective pyrolysis of individual coal macerals to be made.

The pyrolysis products formed by laser heating are ionized by a 500 ns pulse of 18 eV electrons. Mass resolution is accomplished by accelerating the ion packet and measuring the time of flight of the respective ions in the packet over a given distance. The duty cycle of the spectrometer is governed by the flight time of the heaviest ion. For the work with coal, a cycle time of 50 μs was sufficient to scan to mass 400. The major modification of the micropyrolysis mass spectrometer was the replacement of the oscilloscope-photographic recording system with an ultra high speed analog to digital converter (TRW model TDC 1007) coupled to a specially designed cache memory which allows the digitization and storing of 32 sequential spectra over a 1.6 ms period. A major difficulty in analyzing the spectrum produced by a single pulse of a TOF spectrometer is that the small number

of ions produced during a single ionization pulse results in a large statistical variation in peak intensity between spectra of the same material whether they are taken successively or in different experiments. By taking a suite of 32 sequential spectra, computer averaging can be used to greatly improve the reproducibility of the spectra. For the analysis of coal pyrolysis products it was found that the optimum results were obtained when the acquisition of spectra commenced after the laser pulse. During the period of laser irradiation there is extensive fragmentation of the products due to their interaction with the laser beam. For a period of approximately 2 ms after the laser is extinguished pyrolysis products can be detected, by recording spectra during this period analysis is confined to those species being emitted from a hot coal surface.

RESULTS AND DISCUSSION

The spectra for the suite of coals listed in table 1 are shown in figures 1a and 1b. Several factors are discerned in the examination of the spectra. The resolution of a mass spectrum is not sufficient to give unit mass resolution, what is detected is a series of mass clusters. These clusters are numbered from 1 to 15 with the number being equivalent to the number of carbon or carbon plus oxygen atoms that characterize the species contained in a given cluster. Table 2 lists some of the most likely species that would account for each mass cluster.

There is a high degree of similarity between the pyrolysis spectra of the different coals, the major difference being the relative intensities and shapes of the mass clusters. Analysis of these variables reveals several rank related trends. Each mass cluster encompasses a mass range. The location of the cluster is determined by the number of carbon or carbon plus oxygen atoms in the pyrolysis fragments, while the width of the cluster is determined by the distribution of species of varying degrees of hydrogen saturation plus the occurrence of oxygen containing species. These characteristics can be seen by examination of the dashed lines on figures 1a and 1b which are drawn at mass positions 78 and 128, these masses represent one ring and two ring aromatic species, benzene and naphthalene. Both clusters 6 and 10 overlap these mass lines, ion intensity on the high mass side of the line is an indication of hydroaromaticity, the overlap on the high mass side of the mass 128 line is greater than that of the 78 mass line indicating that hydronaphthalene derived species are more prevalent than cyclohexane derived species. It can also be seen that the high mass overlap increases as rank decreases and the H/C ratio increases. The overlap of the clusters on the low mass side is indicative of the free radical nature of the pyrolysis products. There is a general trend of an increase in cluster width to height ratio as the rank of the coal decreases and the H/C and O/C ratios increase.

The aromaticity of the pyrolysis products can be determined by examination of mass clusters 6 and greater. For comparison the aromatic mass region can be divided into two families. The first, clusters 6,7,8 and 9, consists of single ring species plus single ring species with 1,2 and 3 substituent groups, the second family, clusters 10,11,12 and 13, comprises the same pattern for two ring species. Examination of these families reveals that alkyl and hydroxy substituted ring structures are more prevalent than unsubstituted ring structures, i.e., clusters 7,8,9 > 6 and 11,12,13 > 10. A trend with rank is seen with the shift of the major cluster in the two ring family. In the higher rank coals, those with a vitrinite reflectivity greater than 0.7 percent, disubstituted species, cluster 12, dominate the two ring region. For the lower rank coals, those with a vitrinite reflectivity less than 0.7 percent, trisubstituted products, cluster 13, are the major group in the region. This trend in a shift of the major cluster to products with a higher degree of substitution as rank decreases is found as well in the single ring family. The distribution of clusters in these two families indicates that the

process of laser pyrolysis is selective in bond breakage. Bond rupture occurs predominately at the weaker aliphatic linkages as evidenced in the much greater abundance of di- and tri- substituted products. The stronger aryl-alkyl bond results in a much lower concentration of mono- and unsubstituted ring fragments where at least one aryl-alkyl bond would have to be broken.

Another trend that can be observed in the high mass region is the appearance and increasing intensity of clusters 14 and 15 as rank decreases, the increase of the H/C and O/C ratios with decreasing rank results in a higher probability of finding ring structures with substituent groups. Although cluster 14 would be the first possible occurrence of three ring structures the fact that unsubstituted one and two ring pyrolysis fragments have lower concentrations than their substituted products would lend support to the conclusion that clusters 14 and 15 are predominately highly substituted two ring species. For the case of the lowest ranked coals the relative intensity of the high mass fragments rapidly diminishes leaving one ring structures as the major species.

Further information can be derived from the lower molecular weight clusters. Cluster 1 is due to water, it is interesting to note that methane or methyl groups are not a major product resulting from laser pyrolysis. Cluster 2 is dominated by carbon monoxide and nitrogen, species present as background gases in the mass spectrometer in addition to being generated by the pyrolysis process. Aliphatic fragments resulting from coal pyrolysis can be seen in clusters 3,4,5 and part of 6. Cluster 3 shows a bimodal distribution in many of the spectra. The low mass peak of this cluster corresponds to potassium, mass 39, under conditions of laser heating potassium is thermally ionized, greatly increasing its detection sensitivity (12). The major fragment ions for the C3-C6 alkane series would appear at masses 43, 57, 71 and 85, clusters 3, 4, 5 and 6. For each of these clusters there is little evidence of the presence of these ions, the mass of major intensity for each of these mass clusters is lower by 2-4 mass units indicating that the alkyl fragments are hydrogen deficient. This hydrogen deficiency indicates that the species detected tend to be unsaturated. In addition, it is likely that thermally generated free radical fragments of the pyrolysis process are being detected. Additional evidence for the detection of free radical species can be seen at mass locations 78 and 128, the dashed lines on figures 1a and 1b. At the low ionization potentials used to obtain these spectra the major ion peak for benzene and naphthalene would be their molecular ion at mass 78 and 128 respectively. However in the coal pyrolysis spectra the peaks associated with these species appears on the low mass side of these assignments indicating that benzyl and naphthyl free radicals are being detected. The most likely origin of the low molecular weight hydrocarbon clusters is from alkyl aromatic linkages and the fragmentation of hydroaromatic structures.

CONCLUSION

Under the conditions used for laser micropyrolysis of coal, primary products including free radical species emanating from a heated coal surface can be detected. By minimizing secondary condensation or cracking reactions the complexity of coal pyrolysis product analysis is greatly reduced. The pyrolysis mass spectra of the vitrinite portion of a series of coals has shown that as the degree of coalification changes there is a continuous variation in the relative distribution of a small number of primary coal pyrolysis products. These pyrolysis products tend to indicate that the primitive structures found in coal consist mostly of one and two ring aromatic and hydroaromatic groups linked by short aliphatic bridges.

ACKNOWLEDGEMENT

The authors wish to thank the Basic Research Program of the Gas Research Institute for the support of this work under contract no. 5082-260-0720.

REFERENCES

1. Vastola, F. J., and Pirone, A. J., *Am. Chem. Soc., Div. Fuel Chem., Preprint*, 10(2), 53-58, 1966.
2. Joy, W. K., Ladner, W. R., and Pritchard, E., *Nature (Lond.)*, 217, 640, 1968.
3. Vastola, F. J., Pirone, A. J., Given, P. H., and Dutcher, R. R., *Spectrometry of Fuels*, Plenum Press, 29-36, 1970.
4. Joy, W. R., Ladner, W. R., and Pritchard, E., *Fuel*, 49, 26-38, 1970.
5. Joy, W. K., and Reuben, B. G., *Dyn. Mass Spectrom.*, 1, 183-97, 1970.
6. Denoyer, E., Mauney, T., Natuch, D. F., and Adams, F., *Microbeam Anal.*, 17th, 191-6, 1982.
7. Dutta, P. K., and Talmi, Y., *Fuel*, 61, 1241-4, 1982.
8. McGahan, L. J., M.S. Thesis, Department of Materials Science and Engineering, The Pennsylvania State University, 1982.
9. Vanderborgh, N. E., Jones, and Roland, C. E., *Anal. Chem.*, 55, 527-32, 1983.
10. Denoyer, E., Natuch, D. F., Surkyn, P., and Adams, F. C., *Environ. Sci. Technol.*, 17, 457-62, 1983.
11. Gaines, A. F., and Page, F. M., *Fuel*, 62, 1041-5, 1983.
12. Vastola, F. J., Mumma, R. O., and Pirone, A. J., *Org. Mass Spectrom.*, 3, 101-4, 1970.

TABLE 1

COAL SAMPLES

<u>PSOC #</u>	<u>Rank</u>	<u>Province</u>	<u>Region</u>	<u>% RO</u> *	<u>% C</u> (dmmf)	<u>% O</u> (dmmf)	<u>% Vic</u> (dmmf)
263	MVB	Rocky Mountain	Uinta	1.44	90.4	2.2	93
12	HVA	Eastern	Appalachian	0.90	85.5	6.9	47
337	HVA	Eastern	Appalachian	0.89	86.1	5.8	75
1142	HVA	Eastern	Appalachian	0.88	85.9	6.3	87
505	HVA	Rocky Mountain	Uinta	0.75	83.5	8.7	86
330	HVB	Eastern	Appalachian	0.76	83.4	5.4	84
401	HVA	Interior	Western	0.73	82.5	7.9	88
461	HVA	Rocky Mountain	Uinta	0.68	82.5	10.1	88
235	HVB	Rocky Mountain	Uinta	0.68	81.0	11.2	87
854	HVB	Rocky Mountain	Uinta	0.67	81.6	10.6	93
1113	HVB	Rocky Mountain	Uinta	0.59	79.4	12.8	82
437	HVA	Rocky Mountain	Uinta	0.56	80.2	11.8	92
453	HVA	Rocky Mountain	Uinta	0.52	81.2	10.9	88
457	HVB	Rocky Mountain	Uinta	0.52	80.2	11.9	96
500	HVB	Rocky Mountain	Uinta	0.58	80.8	11.2	92
232	HVC	Rocky Mountain	Green River	0.55	77.4	15.3	89

TABLE 2
CHEMICAL ASSIGNMENTS FOR MASS CLUSTERS

<u>Cluster #</u>	<u>Mass Range</u> <u>m/z to m/z</u>	<u>Chemical Identification</u>
1	15 -- 18	CH ₃ , CH ₄ , and H ₂ O
2	28 -- 34	C ₂ alkanes and alkenes, N ₂ , CO, CO ₂ , and H ₂ S
3	39 -- 44	C ₃ alkanes and alkenes, K ⁺ , and CO ₂
4	55 -- 58	C ₄ alkanes and alkenes, and ketones
5	65 -- 72	C ₅ alkanes and alkenes, and dienes
6	77 -- 86	C ₆ alkanes, cycloalkanes, alkenes and benzene
7	91 -- 96	Methyl benzenes, phenols and cycloalkenes
8	105 -- 110	Dimethyl, hydroxy methyl and dihydroxy benzenes
9	119 -- 124	Alkyl and hydroxy-alkyl benzene and indans
10	128 -- 134	Naphthalene, hydroxy-alkyl benzene and dihydronaphthalene
11	141 -- 146	Methyl and hydroxy naphthalene and cycloalkanes
12	155 -- 160	Alkyl and hydroxy-alkyl naphthalenes and tetralins
13	166 -- 172	Alkyl and hydroxy-alkyl naphthalenes and fluorenes
14	178 -- 186	Phenanthrenes, anthracenes and alkyl naphthalenes
15	192 -- 196	Alkyl phenanthrenes and anthracenes

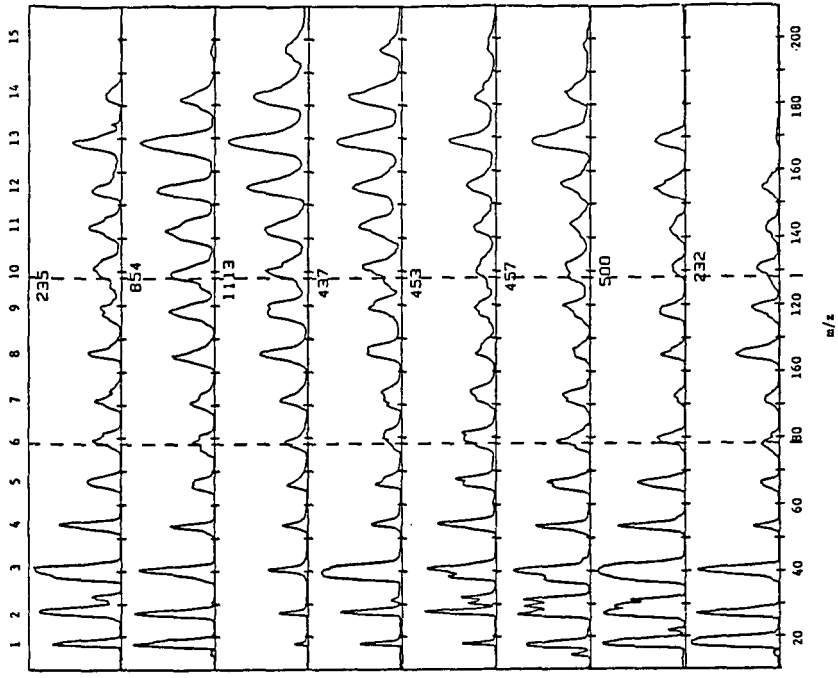


Figure 1b. Averaged Vitrinite Spectra

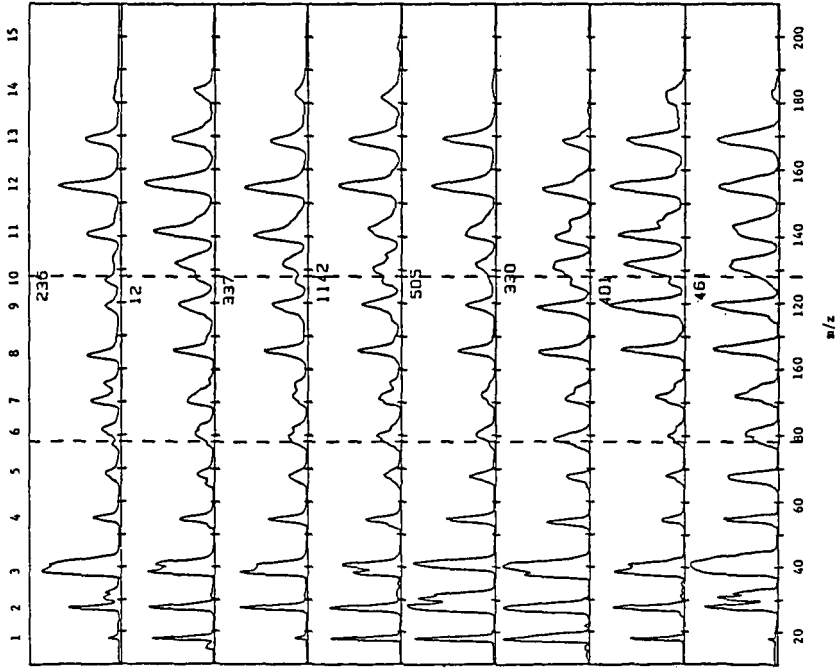


Figure 1a. Averaged Vitrinite Spectra

EFFECT OF WATER ON CP/MAS ^{13}C NMR SPECTRA OF LOW-RANK COALS

Sylvia A. Farnum, Donald D. Messick and Bruce W. Farnum

University of North Dakota Energy Research Center
Box 8213, University Station
Grand Forks, North Dakota 58202

Studies are being carried out directed toward elucidating the structure of low-rank coals and the mechanisms of their combustion, gasification, slurry preparation and liquefaction at the University of North Dakota Research Center. As a part of this research, our interest in the carbon structure of coals before and of residues after processing led us to develop solid ^{13}C CP/MAS NMR techniques suitable for our samples. As we surveyed the existing literature (1,2,3) and the results obtained in our laboratory for low-rank coals, we noted apparent intensity discrepancies. Some samples gave stronger signals than others when the same amount of carbon was in the rotor. In addition to variable intensities, the aromatic to aliphatic ratios and the relative intensities of prominent peaks varied for duplicate samples run under the same conditions. The effect of mineral matter in the high ash coals or the effect of free radicals in the coal were suggested as possible causes of these difficulties (4,5). However, in the case of our samples, these explanations failed to account for the variability we saw in samples. We had none of these problems obtaining spectra of the insoluble organic matter (IOM) after liquefying these coals, even though the IOM contained up to 70 weight percent ash and was greater than 90% aromatic carbon. Signals from the IOM samples were apparently proportional to the amount of carbon present and did not vary.

We had already optimized all of the variables required by our initial study. Each variable was important and needed to be carefully assessed directly on the coal samples to be used for further work. The work of many investigators emphasizes that when proper care is exercised, representative coal spectra may be obtained (1,6,7,8,9). Our conclusions were in accord with those previously reported with one important exception. For low-rank coals, peats and other solids that contain more than a trace of moisture, this study shows that the presence of moisture is the overwhelming factor in determining spectral intensity.

Experimental

Our NMR work was carried out at 50.3 MHz using our Varian XL-200 NMR. A Doty Scientific, Inc. high sensitivity carbon solids probe was interfaced directly with the standard Varian solids amplifier. The magic angle was adjusted for minimal line width with hexamethylbenzene, the probe was tuned for the decoupler and the observe signal with the coal sample in the probe, the field was centered and shimmed, the power level of the decoupler was accurately set, the 90° and 180° flip angles were adjusted ($+0.1\mu\text{s}$), the contact time for cross-polarization was selected to best fit the $T_{1\rho}$ values for the coal and an appropriate delay was chosen. The pulse sequence used was a typical cross-polarization experiment which provided an accurate 90° flip for the proton reservoir followed by a 90° proton phase alteration (spin-lock). The contact time, 1ms, fulfilling the Hartmann-Hahn condition ($\nu_{\text{H1H}} = \nu_{\text{C13C}}$), was followed by four timed 180° pulses of the TOSS echo sequence to refocus the spinning sidebands back into the isotropic peak(10). The acquisition of 4 K data points was carried out with high power proton decoupling. The selected recycle time was 1 s. Minimal data enhancement, consisting of 15 Hz line-broadening, apodization function of 0.020 was used.

Results and Discussion

Intrinsic water in low-rank coals plays a role in reactivity that has never been properly defined. It became apparent to us that water was also important in solid CP/MAS ^{13}C NMR spectroscopy. We found little in the literature that addressed the practical aspects of this problem, therefore, we initiated a preliminary screening

of the effect. We selected two coals as representatives of low-rank coals in general, a North Dakota lignite from the Indian Head mine and a Texas lignite from the Big Brown mine (Table 1). A sample of each was divided into two portions. One portion was dried overnight under partial vacuum in a desiccator containing drierite. The other portion was retained as received. ASTM moisture determinations were run on these samples and on all other samples before ^{13}C spectra were acquired.

Table 1. Lignite Analyses

	Indian Head (ND)	Big Brown (TX)
Moisture, wt %	22.2	23.1
<u>Proximate Analysis</u> (wt. % dry basis)		
Ash	10.5	12.1
Volatile Matter	37.2	45.9
Fixed Carbon	52.3	42.0
<u>Ultimate Analysis</u> (wt/ % mf)		
C	68.1	63.1
H	4.5	4.6
N	1.2	1.3
S	0.9	1.0
O	14.8	17.9

The vacuum dried coal was loaded into a 7 mm sapphire cylindrical rotor and placed in the Doty probe. The rotor was spun at 3000 rps and introduced into the 47 KGauss field of our NMR. The observe and decoupler signals were carefully tuned before the sample spectrum was acquired using the optimized conditions for the dried coal sample. The dried sample was replaced by the same weight of the AR coal sample and another spectrum was acquired in exactly the same manner. The AR coal spectrum gave approximately 1/5 of the absolute intensity of the carbon spectrum of the dried coal. For the Indian Head Zap lignite, fa for the dried sample was 0.67 and for the AR sample, only 0.48 (Table 2).

Table 2. Indian Head Lignite Changes Due to AR Moisture Solid ^{13}C CP/MAS NMR Data

% H ₂ O	Absolute Intensity C Signal	% Caromatic	% Caliphatic
0	242.0	67.6	32.4
1.8	198.2	69.4	30.6
7.6	189.5	69.0	31.0
13.0	133.0	65.0	35.0
22.0 (AR)	50.7	47.7	52.3

A series of partially dried coal samples were prepared for comparison with the completely vacuum dried coal and the AR coal. The spectra of these samples recorded

at various moisture levels are presented in Figure 1. The absolute intensities for each spectrum and their apparent % C aromatic and % C aliphatic are given in Table 2.

It is apparent from these values that the presence of water detunes the probe. When an attempt is made to tune the observe and decoupler coil with the "wet" AR coal in the coil, it is seen that the capacitance of the coil is changed a great deal by the presence of the small amount of water. Modern commercial probe design does not allow for large changes in capacitance of the decoupler coil. Tuning the observe coil is possible but only with broad-band probes. Carbon-only probe observe signal variable capacitance cannot accommodate these large changes.

Even if the operator could optimize the critical tune of the decoupler coil for the cross-polarization, "correct" spectral intensities of "wet" AR coals could not be reliably obtained because under rapid rotation and high power ^1H decoupling, there is a small gradual drying of the coal. And, of course, as the coal changes even slightly in water content, detuning during acquisition causes a loss of signal intensity and introduces errors in the aromatic to aliphatic ratios (Figure 1, Table 2).

The capacitance changes observed for the coal appear to be dependent on the dielectric constants of the included liquid. Liquids of high dielectric, as is expected, cause the greatest changes in capacitance, hence in tune and signal intensity (Table 3). The values of ϵ (dielectric constant) are given for liquids external to the magnetic field.

Table 3. Dried Indian Head Lignite Changes Due to Added Liquid Solid ^{13}C CP/MAS NMR Data

Dried Coal + Liquid, %	Absolute Intensity C Signal	% C aromatic	% C aliphatic	ϵ
H ₂ O, 19.9	17.8	45.6	54.4	80,78
H ₂ O, 11.2	127.0	68.6	31.4	
D ₂ O, 22.0	18.4	44.6	55.4	78
Ethanol, 22.5	3.9	51.6	48.4	24
CCl ₄ , 20.0	20.0	68.1	31.9	2
i-Octane, 20.7	216.0	64.7	35.3	2

The capacitance (and dielectric constant) of the system are also temperature dependent. Changes in wet and dry coal spectra as the temperature is lowered are shown for one of the lignites (Big Brown) in Figure 2. The spectra are all recorded in the absolute intensity mode. Other factors also become important as the temperature is lowered (11), but it is obvious that great caution must be exercised in acquiring and interpreting the data.

From the investigation reported here, it appears that under the "best" conditions fairly representative, reproducible solid ^{13}C spectra of low-rank coal can be obtained from vacuum dried samples. The contact time that yields maximum intensity is near 1000 μs for the aromatic portion of both lignites and slightly shorter for the aliphatic portion. Thus, the selection of 1000 μs as the optimum contact time slightly favors the aromatic part of the spectrum. This positive effect is offset by some aromatic signal loss, estimated at <3%, during spinning sideband suppression (10). We are currently investigating the relationship between signal intensity and the amount of dry coal carbon in the rotor both by absolute intensity measurements and by internal standard spin-counting experiments. It appears that the dried coal samples give much better signal intensity relationships than coals containing small amounts of water.

Performing CP/MAS ^{13}C experiments with complex solid samples such as coal and peat is becoming more common. This technique has opened exciting new areas of structural investigation in coal science and will certainly continue to grow rapidly in popularity. The coal scientist will have to become thoroughly conversant with such concepts as the decoupler power requirements, 90 and 180° flip angles, $T_{1\rho}$ values for his samples, optimal cross polarization times, correct delay, spinning speed, presence of radicals, effect of coal ash and many other factors. As each new experiment is designed, new variables may be introduced. Each variable must be carefully scrutinized, particularly for obvious effects such as the one reported here. When a series of coal samples are compared, or when low-rank coal spectra are being acquired, the samples must be dry enough to allow tuning within the range of the NMR probe or erroneous intensities and fa values will result.

References

1. Wilson, M.A., Pugmire, R.J. and Grant, D.M., 1983, Org. Geochem. 5, 121-129.
2. VanderHart, D.L. and Retcofsky, H.L., Fuel, 1976.
3. Gerstein, B.C., Chow, C., Pembleton, R.G., and Wilson, M.A., J. Phys. Chem., 1977, 81, 565.
4. Yokono, T., Miyazawa, K., Sanada, Y. and Marsh, H., 1979, Fuel, 58, 896-897.
5. Wind, R.A., Trommel, J. and Smidt, J., 1980, Fuel, 58, 900-901.
6. Hagaman, E.W. and Chambers, R.R., 1985, American Chemical Society Fuel Div. Prepr. 30 (1), 188-191.
7. Perdue, E.M., 1984, Geochimica et Cosmochimica Acta, 48, 1435-1442.
8. Hatcher, P.G. "The Origin, Composition, Chemical Structure and Diagenesis of Humic Substances, Coals, and Kerogens as Studied by NMR", 1980, PhD dissertation, University of Maryland.
9. Miknis, F.P., Sullivan, M., Bartuska, V.J. and Maciel, G.E., 1981, Org. Geochem., 3, 19-28.
10. Dixon, W.T., Schaefer, J., Sefcik, M.D., Stejskal, E.O., and McKay, R.A., 1982, J. Magn. Reson., 49, 341-345.
11. Macho, V., Kendrick, R. and Yannoni, C.S., 1983, J. Magn. Reson., 52, 450-456.

WATER STUDY

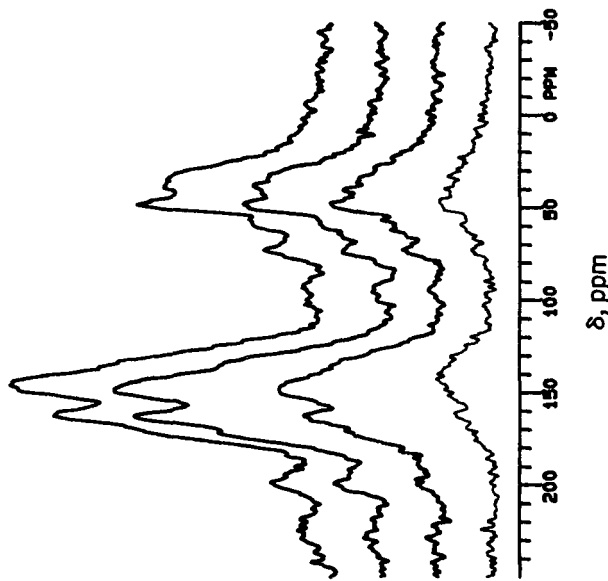


FIG. 1. Indian Head ^{13}C NMR Water study, top-dry, 2nd -7.6% water, 3rd, -13.0% water, bottom -22% (AR) water.

TEMPERATURE STUDY



FIG. 2. Wet and Dry Big Brown lignite, ^{13}C NMR spectra at 20, -5, -30, and -55°C.

NOVEL METHODS FOR FTIR
ANALYSIS OF COAL

Paul Painter, Brenda Bartges, Diane Plasezynski,
Thaddeus Plasczynski, Andrew Lichtus and Michael Coleman

Polymer Science Section
Penn State University
University Park, PA 16802

FTIR was first applied to the characterization of coal structure during the late 1970's and has now been applied to a range of problems in fuel science. Although the technique can therefore be considered established, in some very fundamental ways it is still evolving. Novel sampling methods, principally diffuse reflectance and photoacoustic techniques, have been applied; in addition, new software with the potential for extracting additional information from the spectrum has been developed. The basic thrust of our research is still the accurate quantitative determination of structural parameters, but in this context we have been studying alternative methodologies. Here we will report an examination of the use of diffuse reflectance methods together with two data processing routines; self-deconvolution and a program that can generate the spectrum of components from the spectra of a series of mixtures.

The application of diffuse reflectance and self-deconvolution to the study of coal has been pioneered by Peter Griffiths and co-workers (1,2). We originally considered the advantages in ease of sample preparation (compared to standard KBr pellets) to be relatively minor, given the greater difficulty in obtaining reproducible quantitative results; band intensities not only vary with particle size but are also affected by packing within the sample cup. If we work with the ratio of various bands, however, such factors can be largely eliminated (particularly for modes that are close in frequency and hence are almost equally affected by scattering factors) and we found that for a particular set of samples we obtained information that could not be determined by standard KBr techniques.

As mentioned above, we are still concerned with the measurement of functional groups, particularly aliphatic and aromatic CH content. We have discussed the difficulties associated with various methodologies in various papers and a recent review article (3). We postulated that if we could obtain a set of samples where most of the hydrogen was tied up in one type of functional group, then it should be a relatively straightforward task to obtain accurate absorption coefficients by relating band intensities to elemental hydrogen. Accordingly, we obtained a set of high rank coals (carbon content > 92%) from the Penn State coal bank, choosing those coals that also had an elemental hydrogen content of the order of 3% or more. To our surprise, we could not obtain spectra using standard KBr pellets, while diffuse reflectance revealed bands characteristic of a coal with a high aromatic CH and very low aliphatic CH content. The region between 2000 and 500 cm^{-1} is illustrated in figure 1 and it can be seen that the spectrum of the standard KBr pellet reveals no coal bands whatsoever. We presume that this is due to scattering factors associated with the difficulty in adequately reducing the particle size of such hard coals. Clearly, diffuse reflectance has overwhelming advantages in the characterization of high rank coals. We are now comparing results for lower rank coals obtained by diffuse reflectance and KBr pellets in order to determine whether the ratio of absorption coefficients for aliphatic and aromatic bands is the same for the two methods.

The infrared spectrum of coal is characterized by a set of broad, overlapping

bands. We could certainly obtain a greater insight into structure if various contributions to specific spectral regions could be separated or deconvoluted. In previous work, we have used second derivative spectra as a starting point for curve-resolving, while Griffiths and co-workers (2) have recently applied a novel self-deconvolution procedure. In refining spectra by improvement of the spectral resolution, deconvolution and derivative analysis can be considered alternative treatments of choice. An asymmetric spectral profile composed of two or more overlapped lines, is resolvable (in principle) into at least two component lines, within the limits imposed by the signal to noise ratio and instrument line shape of the original spectrum. It should be noted that no line in the refined spectrum may be narrower than the instrument line shape, unless continuation of the interferogram is performed on the spectrum.

The problem that arises in deconvolution is that neither the line shape nor the full width at half height of the overlapped constituent lines is known. To effect deconvolution, a line shape must be chosen which is considered a reasonable approximation to that of the individual overlapped lines. An optimum band width is then selected empirically from a series of deconvolutions of the overlapped spectral region such that ringing in the refined spectrum is reduced to a minimum.

This empirical technique may well be difficult to apply in practice, however, since the effects of over-deconvolution may be misinterpreted as significant spectral information. The sidelobes so introduced, when superimposed upon the residual spectrum, can easily take on the appearance of legitimate spectral detail, but are in effect artifacts of the technique. This ambiguity in the refined spectrum can be minimized by noting that a symptom of over-deconvolution is the "shifting" of lines in direct relation to the extent of deconvolution.

Although deconvolution appears to provide more information than derivative analysis, they are fundamentally related. Cameron and Moffatt (4) have demonstrated that both techniques rely upon the application of a weighting function in Fourier Space. This function is of the form

$$(2kt)^n$$

where n is the order of the derivative. This may be contrasted with the deconvolution weighting function, for a Lorentzian line shape, of the form

$$(e^{-bt})$$

Because both procedures rely on such weighting functions, similar limitations exist with respect to discrimination against noise. Deconvolution does have the advantage of retaining the integrated intensity and does not suffer the phase inversion characteristic of the second derivative, but has the disadvantage of more easily introducing artifacts. In this respect it should be kept in mind that coal bands are inherently broad due to the chemical heterogeneity of the material and instrumentally cannot be resolved into a series of sharp overlapping bands. Accordingly, deconvolution should be applied with extreme caution.

The final topic we wish to consider is the application of a routine capable of obtaining the spectra of individual components from those of a mixture. There are a number of approaches to this problem, including factor analysis, that could be useful in the analysis of coal spectra. We have developed a program based on a procedure described by Honigs et al. (5) that is most commonly used in near-infrared analysis of foodstuffs. Essentially, the known concentrations of a particular component in a set of mixtures are used as weighting factors to reconstitute the spectrum of that component from those of the mixtures. The application is illustrated in figure 2, which compares the spectra of three

"mixtures", each represented by a single band. The spectrum of a pure component was easily generated and is shown at the bottom of the figure. This method has several intriguing possibilities when applied to coal. For example, we have obtained the spectra of several coal extracts, where the aromatic and aliphatic hydrogen content is known from proton nmr measurements. Using the aromatic (or aliphatic) CH contents as weighting factors we should be able to generate a spectrum characteristic of those parts of the molecule associated with such groups, a sort of functional group based deconvolution.

The method is promising but preliminary results indicate that a careful choice of samples is required. In initial work we considered the spectra of extracts obtained from PSOC's 785, 801, 1192, 1195, 1196 and 1198. For clarity of illustration just the CH stretching region of the spectra, with the OH bands removed by curve-resolving and subtraction, are illustrated in figure 3. Note that the aliphatic CH stretching bands of the PSOC 785 extract, the top spectrum in this series, are stronger and sharper than those of the other extracts, indicating a higher concentration of long chain alkanes. Accordingly, when the program was applied to these spectra we not only obtained the bands characteristic of the aromatic CH stretching mode, but also negative peaks associated with sequences of CH₂ units, as shown in figure 4. In other words, PSOC 785 did not belong in this set. The character of its CH₂ groups is different to those of the other samples (which were obtained from much higher rank coals) and this resulted in the negative sharp peaks. We are presently obtaining the spectra of a wider range of samples so that we can "clump" similar spectra together for analysis. Nevertheless, this preliminary application illustrates the potential of the technique and also indicates that it might find additional utility in identifying different types of structural features.

References

1. Fuller, M. P., Hamadeh, I. M., Griffiths, P. R. and Lowenahupt, D. E., Fuel, 61, 529 (1982).
2. Griffiths, P. R., Wang, S. H., Hadeh, I. M., Yang, P. W. and Henry, D. E., ACS Fuel Chemistry Preprints, 28(1) 27 (1983).
3. Painter, P. C., Starsinic, M., and Coleman, M. M. in Fourier Transform Infrared Spectroscopy; Applications to Chemical Systems. Vol. 4, p.169, (Edited by J. R. Ferraro and L. J. Basile) Academic Press (1985).
4. Cameron, D. G., and Moffatt, D. J., JTEVA 12, 78 (1984).
5. Honigs, D. E., Hieftje, G. M. and Hirschfeld, T., Applied Spectroscopy, 38, 317 (1984).

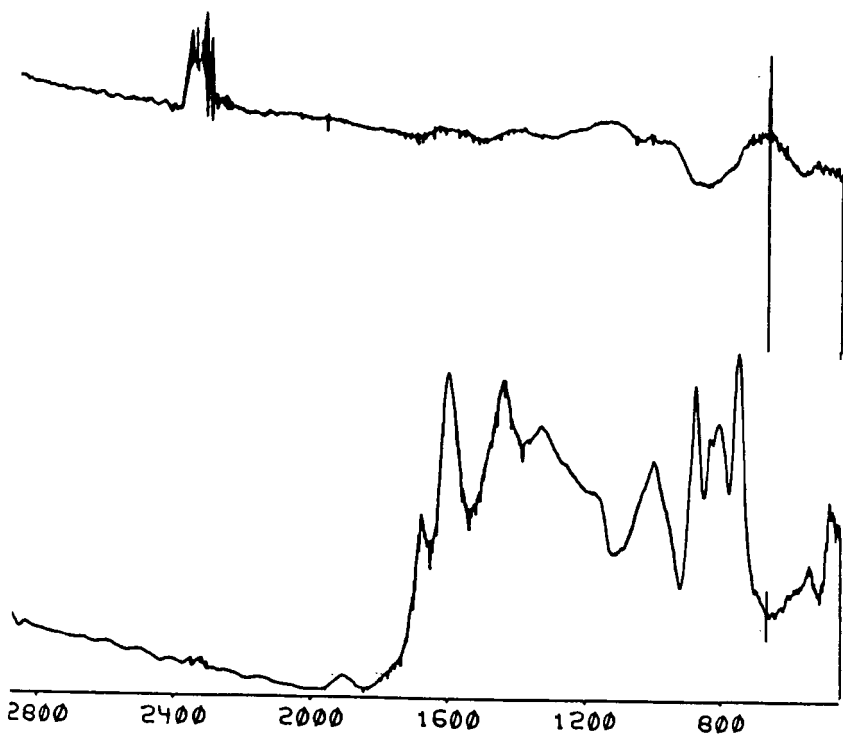


Figure 1. Top; Spectrum of PSOC 161 (92% C) prepared as a KBr pellet.
Bottom; same sample run in diffuse reflectance.

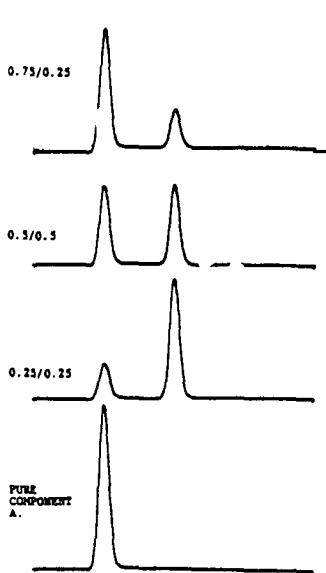


Figure 2. Top to bottom, spectra of a mixture of two components and the generated spectrum of the pure component.

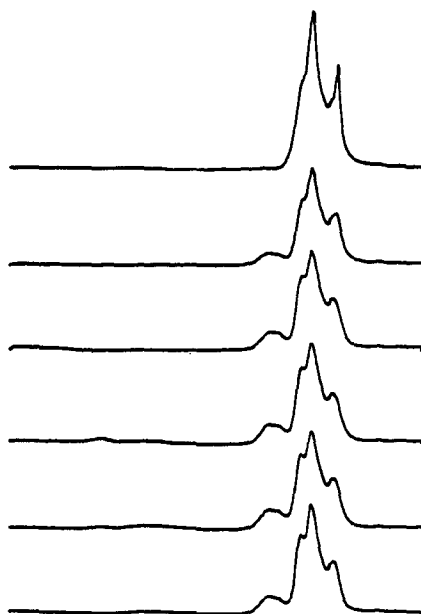


Figure 3. Top to bottom, CH stretching modes of pyridine extracts of PSOC's 785, 801, 1192, 1195, 1196 and 1198.



Figure 4. Generated spectrum of aromatic CH component.

SULFUR IN COAL BY PROGRAMMED-TEMPERATURE OXIDATION

Robert B. LaCount,* Richard R. Anderson,
Sidney Friedman, Bernard D. Blaustein

U.S. Department of Energy
Pittsburgh Energy Technology Center
Pittsburgh, Pennsylvania 15236

*Permanent Address: Waynesburg College, Waynesburg, PA 15370

ABSTRACT

A controlled-atmosphere, programmed-temperature, oxidation apparatus has been constructed and used to characterize organic-sulfur distribution in coals, partially desulfurized coals, and model systems. Samples were diluted with W_0 , and heated, in a stream of Ar containing 10% O_2 , at a programmed-temperature increase of $30^\circ/\text{min}$. Concentrations of SO_2 , CO_2 , CO, O_2 , and H_2O in the effluent gas were continuously measured until the runs were completed at 1000°C . Evolution patterns produced by the oxidation products characterize the coal and, upon integration, provide total C-H-S analyses consistent with classical coal analysis methods. The SO_2 derived from coal pyrite evolves with a maximum at about 430°C , and that from the organic portion of coal produces principal evolution maxima at about 320°C (attributed to nonaromatic coal structures) and at about 480°C (attributed to aromatic structures). During oxidation the H/C ratio decreases with increasing temperature to about 0.6-0.7 at 400°C . The NMR spectrum of residue isolated to 400°C shows a sharp decrease in aliphatic carbon compared to the original coal.

INTRODUCTION

A number of precombustion chemical-beneficiation procedures have been developed that remove most of the inorganic sulfur (pyritic and sulfate) and some of the organic sulfur from coal. These have recently been reviewed by Morrison (1). A method to distinguish among the organic-sulfur functional groups or to classify the organic sulfur present in untreated or treated coals would be an asset to those involved in coal desulfurization research. The predictive value of such a method would also be useful in selecting coals that will be most improved by beneficiation methods. Calkins recently described pyrolysis experiments aimed at the determination of organic-sulfur-containing structures in coal and briefly reviewed work in this area (2). The present work is a continuation of our efforts toward an oxidative-degradation procedure useful for characterization of the organic sulfur in coal (3,4). A controlled-atmosphere, programmed-temperature oxidation (CAPTO) apparatus has been constructed and used to characterize organic-sulfur distribution in coals, partially desulfurized coals, and model systems. The system monitors the evolution of SO_2 , CO_2 , CO, O_2 , and H_2O from coal samples thermally degraded in the presence of oxygen and a solid diluent-oxidation catalyst. Distinctive patterns of SO_2 , CO_2 , and H_2O evolution during programmed-temperature oxidation provide insights into the structural characteristics of the organic matrix of coal samples.

EXPERIMENTAL

A diagram of the apparatus used in this study is shown in Figure 1. A mass-flow-controlled mixture of Ar (90 mL/min) and O_2 (10 mL/min) was passed through minus-200-mesh samples dispersed (1:30) in W_0 , (diluent-oxidation catalyst) and pre-positioned on quartz fibers (wool) near the center of a 1.2-cm (i.d.) x 72.2-cm vertical quartz combustion tube. A spring-loaded tube assembly held the combustion tube in position between neoprene seals. Samples were positioned at the midpoint of a 30.8-cm vertical tube furnace that surrounds the reaction tube. A microprocessor was used to temperature program the furnace (normally at a rate

of $30^\circ/\text{min}$). A type K dual-head, isolated-junction thermocouple extends through a quartz capillary rod (used to minimize dead volume) and is inserted into the center of the sample. One of the thermocouple signals was sent to a strip chart recorder, and the other, after amplification, to a digital data system. A quartz rod was inserted below the sample to reduce dead volume.

A 1.9-cm x 6.7-cm secondary furnace was mounted directly below the primary furnace. The reaction tube in the secondary furnace hot zone contains 3.0 g of WO_3 supported on quartz fibers. This furnace, maintained at 1050°C , was utilized to convert CO to CO_2 , and COS to CO_2 and SO_2 , and to maintain a constant SO_2/SO_3 ratio in the exit gas stream (5). A pressure transducer located just after the reaction tube continuously monitored the pressure of the system throughout the run.

The effluent gas flowed from the reaction tube through 1/16-in.-i.d. Teflon tubing to the infrared analyzers that continuously monitored the concentration of H_2O , SO_2 , CO_2 , and CO. A $\text{Mg}(\text{ClO}_4)_2$ drying tube located just after the H_2O analyzer removed H_2O from the gas stream before it entered the SO_2 analyzer. A CO analyzer was utilized; however, under normal operating conditions, all CO was converted to CO_2 . A paramagnetic oxygen analyzer was used for detection of the oxygen content of the effluent gas. A mass flow monitor was used to measure the total flow of the gas stream. All detector signals were sent to a multichannel strip chart recorder and a digital data system. The strip chart recorder provided immediate feedback on the progress of the experiment. The data system acquired raw data, applied corrections, integrated, and provided qualitative and quantitative information for the effluent gas components over any desired temperature range. These methods are described in an earlier report (4).

A typical experiment consisted of thoroughly mixing 200 mg of minus-200-mesh coal (dried at 105°C) with 6.0 g of WO_3 and drying the mixture in a vacuum oven at 100°C . A 3.0-g portion of WO_3 was placed on quartz wool in the combustion tube and positioned at the hot zone of the secondary furnace. The tube was placed in position, and the secondary furnace stabilized at 1050°C . The analyzers were standardized and the sample was added to the combustion tube. A flow of 90 mL/min Ar and 10 mL/min O_2 was continued as the sample was heated from ambient temperature to 1000°C at a rate of $30^\circ/\text{min}$.

RESULTS AND DISCUSSION

The CAPTO instrumentation provides time-resolved data for the concentration of SO_2 , CO_2 , CO, H_2O , and O_2 in the effluent gas stream as a sample is oxidized at a programmed rate of temperature increase. The total flow, the pressure, and the temperature are also monitored throughout the oxidation. The gas composition profile with increasing temperature for untreated Indiana Minshall coal is shown in Figure 2. Similar information has been obtained from other coals, model sulfur systems, and pyrite. Initially, several heating rates, flow rates, compositions of the O_2 - Ar mixture, diluents, and sample/diluent ratios were examined (3,4). Variation of gas evolution patterns with particle size was also studied. Particle size studies (minus-48-mesh x 0; minus-100-mesh x 0; minus-400-mesh x 0) were completed on Pittsburgh Seam (Ohio No. 8) and several other coals. Little or no change in gas evolution patterns with increasing temperature was noted over the particle size range studied.

Temperatures of Sulfur Dioxide Evolutions from Coals

The SO_2 evolution temperature maxima of seven coals oxidized using the CAPTO unit are shown in Table 1. A few show small SO_2 evolutions in the 170°C - 200°C region. This is consistent with the presence of sulfur and/or volatile sulfides that sublime up to 200°C and are oxidized by the secondary furnace to produce SO_2 evolution maxima. Principal SO_2 evolution maxima occur in three

temperature ranges centered near 320°C, 430°C, and 480°C. So that these SO₂ evolution maxima could be assigned to coal structures, the CAPTO unit was used to oxidize (1) coal treated to partially remove pyrite, (2) coal pyrite, and (3) a series of model sulfur-containing systems. Figure 3 compares the CAPTO results of untreated (ROM) and treated (Float 1.60; Float 1.30; ASTM HNO₃) Pittsburgh Seam coal. Each sample contained a different pyrite concentration. The sharp peak at 430°C decreases with decreasing pyrite concentrations and was tentatively assigned to SO₂ evolution from the coal pyrite. A Deister table sample of coal pyrite obtained from the Robena Mine and oxidized using the CAPTO unit shows sharp SO₂ evolution at 430°C and confirms the above assignment.

A series of sulfur-containing model systems (6) was oxidized in the CAPTO unit, and the SO₂ evolution maxima temperatures were recorded. The results are summarized in Table 2. Note that polythiophene, polydibenzothiophene, polyarylsulfides, and polyarylsulfones all show SO₂ evolution maxima temperatures of 450°C or greater. All of these evolutions fall near or above the highest SO₂ evolution maxima observed from coals oxidized in the CAPTO unit. Poly(thiophene-tetrahydrothiophene) shows two SO₂ evolution maxima temperatures (300°C and 475°C). This polymer contains alternating cyclic sulfide and thiophenic sulfur structures. The lower temperature SO₂ evolution is ascribed to oxidation of the cyclic sulfide structure; and the higher temperature evolution, present in approximately an equal amount, to oxidation of the thiophenic structure. Based upon the model system results, the principal coal SO₂ evolution maximum near 320°C is consistent with nonaromatic sulfide oxidation, and the principal maximum near 480°C is consistent with thiophenic, aryl sulfide, and aryl sulfone oxidation.

Quantitative Evaluation of the Effluent Gas Components

The CAPTO unit was initially constructed to characterize partially desulfurized coals produced from Pittsburgh Energy Technology Center oxydesulfurization experiments (7). These oxydesulfurized coals had most of the pyrite and 40%-60% of the organic sulfur removed; however, most of the mineral matter was retained. Figure 4 shows the CAPTO data for oxydesulfurized (pyrite-free) Indiana Minshall coal. The higher temperature SO₂ evolution maximum is broadened and shifted to a somewhat lower temperature (centered at 450°C). The atomic H/C and C/S ratios with progressive oxidation are calculated and plotted from continuous measurements of the H₂O, CO₂, and SO₂ concentrations in the effluent gas stream. A plot of these ratios for the oxydesulfurized Indiana Minshall coal is reported in Figure 5. The H/C ratio is abnormally high near the beginning of the oxidation due to H₂O released from the mineral matter along with H₂O produced from coal oxidation. The H/C ratio at the 320°C SO₂ evolution maximum is about 2.40 and that for the evolution centered at 450°C is about 0.40. The H/C ratio decreased to 0.7 at 400°C. This sharp decrease in H/C ratio up to 400°C was observed for all coals oxidized in the CAPTO unit for which the H/C ratio was plotted.

The oxydesulfurized Indiana Minshall coal was also oxidized in the CAPTO unit up to a maximum temperature of 400°C, and the oxidized coal was separated (float-sink) from WO₃. The ¹³C CP-MAS NMR of the product is shown in Figure 6. A sharp decrease in aliphatic carbon is noted, but the coal has not been deeply oxidized. The SO₂ evolution maximum observed near 320°C must be associated with loss of these nonaromatic coal structures. Additionally, the SO₂ evolution observed beyond 400°C must be associated with oxidation of the aromatic coal structures. Integration of the SO₂ data up to 400°C and beyond 400°C reveals that 41% of the sulfur is associated with loss of nonaromatic carbon and about 59% is associated with oxidation of aromatic carbon. Similar data have been tabulated (Table 3) for a number of pyrite-free coals. The results for poly(thiophene-tetrahydrothiophene) are also presented in Table 3. A bimodal SO₂ evolution pattern exists and approximately one-half of the sulfur was lost up to 400°C. This is consistent with SO₂ evolution from oxidation of nonaromatic carbon followed by oxidation of the aromatic structures.

The total C-H-S content can be calculated from the integrated data. The unit was not specifically designed to provide elemental analysis results; however, the values serve as indicators of complete oxidation. The analytical results of four oxydesulfurized coals oxidized in the CAPTO unit are shown in Table 4 and are in good agreement with classical coal analyses results of these coals.

Gravimelt-Treated Coals

The CAPTO apparatus has been used to oxidize a number of raw and treated coals. The results provide information about the sulfur removed and remaining after coal beneficiation processes. Samples of untreated and Gravimelt-treated (8) Pittsburgh Seam coal were obtained from TRW. A portion of the untreated coal was treated with HNO₃ (1:9) overnight (ASTM Method) and washed until acid free. The untreated, HNO₃-treated, and Gravimelt-treated coals were oxidized in the CAPTO unit. The results are shown in Figure 7. The untreated coal produces SO₂ evolution maxima at 320°C, 430°C, and 480°C. The 430°C SO₂ maximum due to pyrite is no longer present in the HNO₃-treated coal. The Gravimelt-treated coal shows approximately the same SO₂ evolution at 320°C, but no 430°C SO₂ evolution is present, and the 480°C SO₂ evolution maximum has been strikingly diminished. The Gravimelt process appears to have removed the pyritic sulfur and most of the thiophenic and/or aryl sulfide sulfur. Integration of the SO₂ data up to 400°C (H/C ratio at 0.7) shows 55.5% of the remaining 0.75% coal sulfur to be nonaromatic, and integration beyond 400°C shows 44.5% in aromatic coal structures. The available analytical results for these coals are shown in Table 5. Note that the H/C ratio of the Gravimelt-treated coal is considerably below that of the untreated coal. This is consistent with the ¹³C NMR results, which show a sharp increase in aromaticity (9).

CONCLUSIONS

Distinctive SO₂ evolution maxima are produced at about 320°C, 430°C, and 480°C for coals mixed with a diluent and oxidized at a programmed rate of temperature increase.

The SO₂ evolution maxima temperatures for coal have been correlated with those produced from the oxidation of model organosulfur-containing systems and pyrite. The coal SO₂ evolution near 320°C is ascribed to sulfur in nonaromatic structures; that near 430°C, to oxidation of pyrite; and that near 480°C, to oxidation of thiophenic and aryl sulfide type structures.

ACKNOWLEDGMENT

The authors wish to thank several Oak Ridge Associated Universities (ORAU) students -- Murphy Keller and Robert Wright, both ORAU Interns, and Bryan Warner, an ORAU Student Research Participant -- for their precise work in experiments completed using the CAPTO apparatus. We are also indebted to Eugene J. Volker, ORAU Faculty Research Participant, and Bonnie Brooks, ORAU Student Research Participant, for preparing several of the model sulfur systems utilized in this work. We also wish to thank Richard F. Sprecher of the Pittsburgh Energy Technology Center, Analytical Chemistry Division, for the ¹³C NMR spectral information, and TRW for a sample of Gravimelt-treated coal. We thank the Coal Preparation Division, Pittsburgh Energy Technology Center, for funding the work, and Robert P. Warzinski for his interest and planning during the early phase of this work.

DISCLAIMER

Reference in this report to any specific product, process, or service is to facilitate understanding and does not necessarily imply its endorsement or favoring by the United States Department of Energy.

REFERENCES

1. Morrison, G.F., "Chemical Desulfurization of Coal," ICTIS/TR15, London, UK, IEA Coal Research, 72 pp. (1981).
2. Calkins, W.H., ACS Div. of Fuel Chem. Preprints, 30(4), 450 (1985).
3. LaCount, R.B., Gapen, D.K., King, W.P., Dell, D.A., Simpson, F.W., and Helms, C.A., New Approaches in Coal Chemistry, ACS Symposium Series 169, pp. 415-426 (1981).
4. LaCount, R.B., Anderson, R.R., Helms, C.A., Friedman, S., and Romine, W.B., "Construction and Operation of a Controlled-Atmosphere, Programmed-Temperature Reaction Apparatus," DOE/PETC/TR-83/5, (DE83011164) 1983.
5. Cullis, C.F., and Mulcahy, M.F.R., "The Kinetics of Combustion of Gaseous Sulfur Compounds," Combustion and Flame, 18, 1972, pp. 225-292.
6. Lin, J. W-P., and Dudek, L.P., J. Polym. Sci., Polym. Chem. Ed. 18, 2869 (1980); Yamamoto, T., et al., J. Polym. Sci., Polym. Lett. Ed. 18, 9 (1980); Kovacic, P., and McFarland, K., J. Polym. Sci., Polym. Chem. Ed., 1963, 17, (1979).
7. Warzinski, R.P., Friedman, S., Ruether, J.A., and LaCount, R.B., "Air/Water Oxydesulfurization of Coal-Laboratory Investigation," DOE/PETC/TR-80/6 (1980).
8. "Gravimelt Process Development," Final Report, TRW Energy Development Group, Contract No. DOE/PC/42295-T7, June 1983; Meyers, R.A., Hart, W.D., McClanathan, L.C., "Gravimelt Process for Near Complete Chemical Removal," Coal Process Technol. 1981, 7, 89-93.
9. Private Communication, Sprecher, R.F., Pittsburgh Energy Technology Center.

TABLE 1.
TEMPERATURES OF SULFUR DIOXIDE EVOLUTION
MAXIMA FROM COALS

COAL	TEMPERATURES (°C)
Middle Kittanning Oxydesulfurized	320 ... 445
Kentucky No. 11 ROM	320 450 490
Indiana Minshall ROM	295 440 490
Oxydesulfurized	310 ... 450
Illinois No. 6 ROM	310 440 455
Oxydesulfurized	320 ... 440
Upper Freeport Float 1.40	322 ... 475
Oxydesulfurized	200 325 500
Pittsburgh Seam (Ohio No. 8)	180 320 430 475
PETC (ROM)	325 440 485
PETC (Float 1.30)	325 435 480
TRW (ROM)	320 ... 492
TRW (Gravimelt)	328 ... 488
TRW (ASTM-HNO ₃)	322 430 475
Pittsburgh Seam (W.Va.) ROM	322 ... 480
ASTM-HNO ₃	170 ... 480

TABLE 2.
TEMPERATURES OF SULFUR DIOXIDE
EVOLUTION MAXIMA FROM MODEL SYSTEMS

MODEL SYSTEMS	TEMPERATURES (°C)
<u>Thiophenes</u>	
Polythiophene	450
Polydibenzothiophene (Grignard)	540
Polydibenzothiophene (AlCl ₃)	540
Poly(thiophene-tetrahydrothiophene)	300 475
Poly(thiophene-benzene)	540
<u>Aryl Sulfides</u>	
Polydiphenylsulfide-benzene)	550
3,3'-Thiobis-(7H-Benz[de]Anthracen-7-one)	530
<u>Aryl Sulfones</u>	
Poly(p-phenylene Ether Sulfone)	540
<u>Sulfate</u>	
Ferrous Sulfate	620

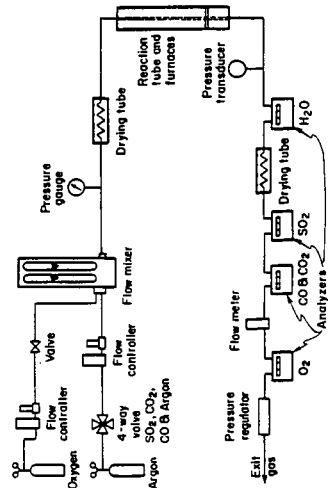


Figure 1. Controlled-atmosphere, programmed-temperature apparatus flow system.

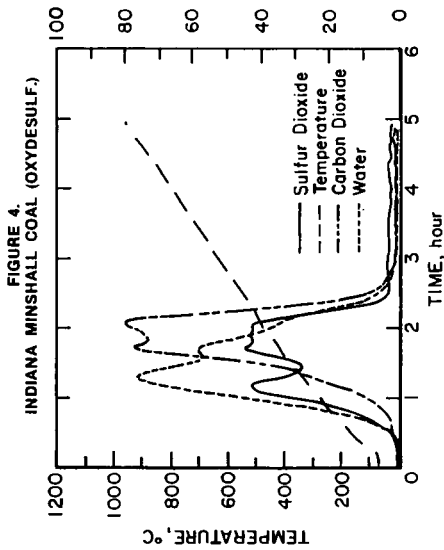
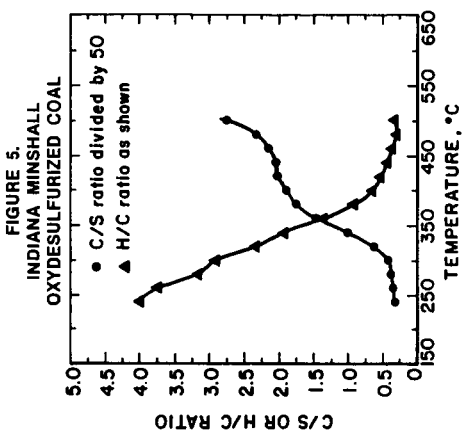
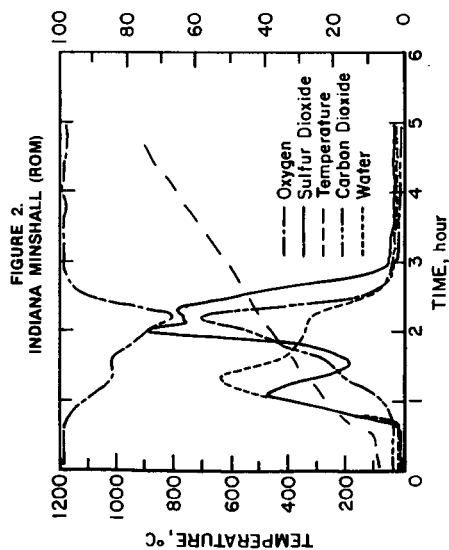
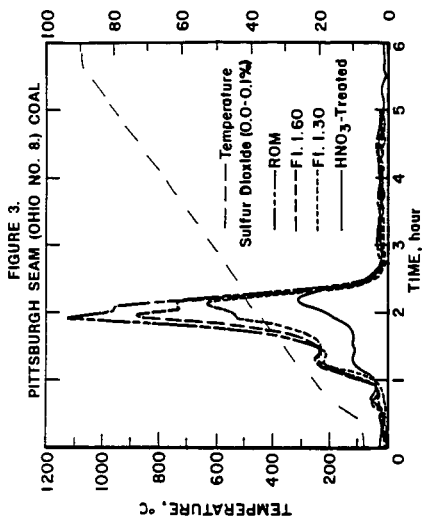


FIGURE 6.
¹³C NMR OF INDIANA MINSHALL COAL

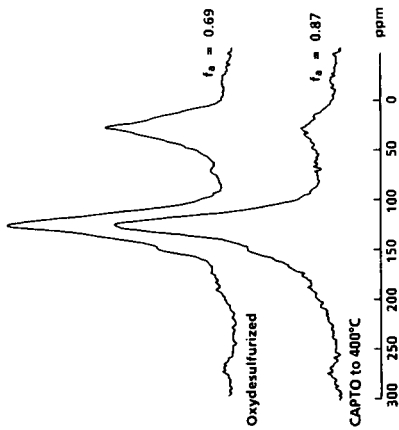


TABLE 3.
 NONAROMATIC -- AROMATIC SULFUR

COAL	NONAROMATIC	AROMATIC	SULFUR (%)	
			CAPTO	COAL ANALYSIS
Upper Freeport	21.7	78.3	0.38	0.60
Float 1.40				
Pittsburgh Seam (Ohio No. 8)	55.5	44.5	0.75	0.75
TRW Gravimelt	25.4	74.6	2.02	---
TRW Starting Coal (ASTM-HNO ₃)				
Pittsburgh Seam (W. Va.)	30.4	69.7	1.39	---
(ASTM-HNO ₃)				
Indiana Minshall	41.4	58.6	2.42	2.50
Oxydesulfurized				
Middle Kittanning	34.7	65.3	0.73	0.67
Oxydesulfurized				
Illinois No. 6	50.9	49.1	2.27	2.42
Oxydesulfurized				
Poly (Thiophene-Tetrahydrothiophene)	51.5	48.5	36.67	35.75

FIGURE 7.
 PITTSBURGH SEAM (OHIO NO. 8) COAL

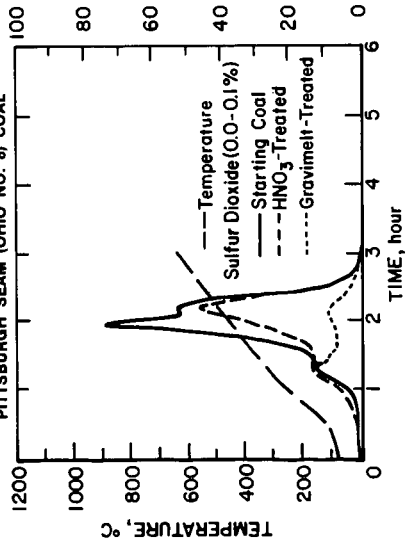


TABLE 4.
ANALYSIS OF OXYDESULFURIZED COALS
(moisture-free)

COAL	TREATMENT	METHOD	ASH %	C %	H %	S %	H/C	C/S
Indiana	None	Coal Anal.	14.7	61.0	4.5	6.3	0.88	26
Minshall	Oxydesulf.	Coal Anal.	13.1	64.0	4.2	2.5	0.78	69
Rank: HvBb	Oxydesulf.	CAPTO	---	67.0	4.2	2.4	0.74	74
Illinois	None	Coal Anal.	11.6	68.4	4.6	3.7	0.80	49
No. 6	Oxydesulf.	Coal Anal.	9.77	65.7	4.3	2.4	0.79	72
Rank: HvCb	Oxydesulf.	CAPTO	---	67.1	4.3	2.2	0.79	81
Middle	None	Coal Anal.	16.9	64.6	4.4	1.1	0.81	160
Kittanning	Oxydesulf.	Coal Anal.	16.2	61.9	4.0	0.67	0.77	247
Rank: HvCb	Oxydesulf.	CAPTO	---	63.3	4.0	0.60	0.75	280
Upper	None	Coal Anal.	16.2	72.3	4.3	1.6	0.71	122
Freeport	Oxydesulf.	Coal Anal.	15.3	72.0	4.2	0.76	0.70	253
Rank: Mvb	Oxydesulf.	CAPTO	---	70.4	4.1	0.71	0.69	265

TABLE 5.
TRW GRAVIMELT-TREATED
PITTSBURGH SEAM (OHIO NO. 8) COAL

Coal	Analytic Method	Ash	Total S	%C	%H	H/C	C/S
Raw *	Coal Anal.	10.15	4.22	---	---	---	---
Raw	CAPTO	---	3.93	73.1	5.1	0.83	50
HNO ₃	CAPTO	---	2.02	71.2	4.8	0.81	94
(ASTM)							
**	Coal Anal.	1.26	0.75	---	---	---	---
**	CAPTO	---	0.75	84.7	4.1	0.57	303

*Raw coal was analyzed as containing 0.20% sulfate sulfur, 1.78% pyritic sulfur, and 2.24% organic sulfur.

**Coal was treated at 370°C with 80/20 NaOH/KOH melt. Product was washed with water, 10% H₂SO₄, filtered; and washed 2 times with water.

HIGH RESOLUTION X-RAY FLUORESCENCE SPECTROSCOPY
A POTENTIALLY USEFUL TECHNIQUE FOR CHEMICAL BONDING STUDIES
IN FOSSIL FUELS

G. Andermann and F. Fujiwara

Department of Chemistry
University of Hawaii
Honolulu, HI 96822

and

J. Worman

University of North Dakota Energy Research Center
Box 8213, University Station
Grand Forks, North Dakota 58202

Introduction

One of the key problems in fossil fuel analysis is the determination of various functional groups associated with C, N, S, and O atoms. While a number of analytical techniques have been utilized to accomplish this objective, to date none of these techniques provide bulk information in a non-destructive manner. Thus, for example, when photoelectron spectroscopic methods are used in a non-destructive mode, because of the nature of the photoelectron escape depth ($\sim 10 \text{ \AA}$), they provide useful information only about surface composition. In order to get bulk analysis with these techniques, it is necessary either to average a large quantity of surface data by running different samples, or to destroy the sample, layer by layer, and average the resultant data. Of course, any sort of surface layer destruction is bound to alter the sample and provide inaccurate chemical bonding information. Mass spectrometric methods, which constitute another way of studying coal samples, are destructive by nature and do not yield totally reliable answers.

Aside from the above considerations, another problem presents itself if one considers coal to be an ensemble of randomly variable huge macromolecules. The size of the macromolecule by itself guarantees that the valence electron structure will be very complex, i.e., that there is a "forest" of valence molecular orbitals. Consequently, any spectroscopic technique which provides only a single valence electron spectrum per molecule is practically useless. It is, for this reason that UV absorption, UV and X-ray valence photoelectron spectroscopies are not effectively useful in coal functional group analysis. What is needed is a spectroscopic method which is able to provide different views of a complex "forest" of valence molecular orbitals. While it is certainly correct to say that X-ray core photoelectron spectroscopy provides some useful information because for each kind of atom (with $Z \geq 3$) there exists at least one specific and characteristic core photoelectron signal, it is equally true that the correlation between core photoelectron shifts due to changes in valence electron structure are not always readily decipherable in the case of large organic macromolecules.

It is the objective of this paper to present X-ray fluorescence in a new role at high optical resolution, namely, as a potentially useful tool for a direct determination of the valence electron structures around the different kinds of atoms of interest. Stated somewhat differently, it will be shown that XFS is an atomic probe to sample molecular valence electron structure, and because of the very nature of this probe, the complex "forest" of molecular orbitals becomes more decipherable than with any other technique.

Theory and Background Information on Pure Substances

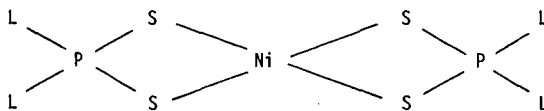
While Urch (1) has recently reviewed the overall capabilities of XFS for chemical bonding studies, his review did not direct the reader toward the analytical

possibilities of this technique. Thus, it appears to be useful to show how molecular XFS "works." Figure 1 is a comprehensive view of the energy level diagram of a hypothetical diatomic molecule A-B, where both atoms A and B have filled core levels, K, L₁, L₂, L₃, and where the molecule AB possesses a manifold of filled molecular orbitals ψ_i 's and a manifold of unfilled (antibonding) ψ_i 's. The various spectroscopic techniques are illustrated by appropriately labelled arrows, with each arrow representing a typical one-electron transition. Besides XFS, XPS (X-ray photoelectron spectroscopy), XAS (X-ray absorption spectroscopy), UAS (ultraviolet visible absorption spectroscopy) and UPS (ultraviolet photoelectron spectroscopy) transitions are shown.

As stated before, one of the fundamental differences between XFS and other spectroscopic methods used for electronic structural studies of molecules is that with all of the other methods one obtains a single spectrum per molecule. If one were interested in studying the valence electron structure of 10-thioxanthone (a likely constituent to be found in coal) by UAS, UPS, and XPS, each of the techniques would yield a single valence electron spectrum. Using XFS a carbon K emission spectrum, an oxygen K emission spectrum, as well as sulfur K and sulfur L emission spectra, can be obtained.

With XFS not only is there a heteroatom capability and possibly even multiple spectra per each heteroatom, but also electric dipole selection rules provide additional simplification in case the symmetry is high enough. Simplified spectra are obtained especially if the core vacancy is on an atom with a centro or pseudo centrosymmetric position.

The use of XFS to determine the position and type of heteroatom has enormous practical analytical consequences (2-5). If the core vacancy is on a central atom, and if the valence electron charge density is sufficiently localized, then XFS can be used for ligand identification. Thus, if the central atom A is in a 4-fold coordination with ligands L₁, L₂, L₃, L₄ and if L₁ = L₂ = L₃ = L₄, namely, A-(L₁)₄ but it is changed to L₂-A-(L₁)₃, then the XFS spectra will reflect this substitution of L₂ for one of the L₁-s by showing a new transition. Note that the ligands can be atoms or molecular fragments. Additional examples were studied by Whitehead (6). The central atom in this case was sulfur and S-K β spectra were obtained for Na₂SO₄, KHSO₄, Na₂SO₃, NaHSO₃, KC₂H₅SO₄, (C₄Hg)₂SO₂, (CH₃C₆H₄)₂SO₂, and C₆H₅SO₂NH₂. Typical examples are shown in Figures 2 through 5. Identical capability is achieved when the core vacancy is on a pseudo-central atom. The PK β spectrum of a large molecule of the type II shows individual transitions that correspond to the



II

different ligands as the ligand is changed from -OCH₃, to OC₂H₅, to CH₃ to C₂H₅. What is significant is that it is possible (4,5) to identify "fingerprint" transitions of the type: P_{p3}-S_{3p}; P_{3p}-S_{3p}; P_{3p}-O_{2p}C_{2p}; P_{3p}-O_{2p}C_{2p}C_{2p}; P_{3p}-C_{2p}; P_{3p}C_{2p}-C_{2p}; P_{3p}-O_{2s}; P_{3p}-C_{2s}.

Another interesting and unique aspect of using XFS as an atomic probe to characterize valence electron structure can be illustrated when the initial state core vacancy is on a ligand atom which itself is attached to a ring system. This was demonstrated by Whitehead (6,7). The Cl-K β spectra of p-chloroaniline, p-dichlorobenzene, and p-nitrochlorobenzene were different precisely because of the difference in the electron donating and withdrawing powers of the -NH₂, -NO₂, and -Cl functional groups. Equally interesting was Whitehead's demonstration of the ability of XFS as a ligand atom probe to differentiate among the o,m-, and p-chlorobenzoic acid isomers by studying the Cl-K β emission spectra.

It is appropriate to indicate the power of XFS as a heteroatom probe when studying sulfur bearing heterocycles since several types are present in coal. Phillips (8) studied the S-K β spectra of 19 different sulfur-bearing heterocycles which included thiophene, saturated sulfur heterocycles, various mono- and di-substituted thiophenes and a few heterocycles containing both sulfur and nitrogen. Figure 6 shows the S-K β spectrum of thiophene. Accordingly, there are several prominent features, namely, band A at 2456 eV corresponding to a transition from a σ bond of S(3p_x)-C(2s) character, band B at 2460 eV reflecting σ bonding of S(3p_y)-C(2p)-C(2p) character, band C around 2464 eV reflecting π bonding with S(3p_z)-C(2p_z) as well as S(3p_y)-C(2p_y) character, band D at 2466 eV reflecting π S(3p_x)-C(2p) σ bond, and the only sharp band E at 2468 eV corresponding to the nonbonding S(3p_z) orbital. In reality each of the broad bands A, B, and C involve several unresolved transitions, and the lack of resolution is primarily due to the initial state--S-K level broadening.

In going from thiophene to the other heterocycles, the overall pattern in terms of the number of bands and the relative positions of the bands remains the same. This should not be too surprising since the basic C-S-C structure is retained. The relative peak heights for bands A and B also remain the same. However, in going from an unsaturated to a saturated sulfur heterocycle, inserting a nitrogen into the ring system, or using dichloro substitution in the ring, the amount of S-3p character in molecular orbitals corresponding to transitions C, D, and E is altered. For the spectra of thiophene and tetrahydrothiophene (Figure 7), the integrated intensity ratio of D/E changes from 1.4 to 0.8. The introduction of a nitrogen atom in the ring, or dichloro substitution causes the D/E ratio to decrease to 0.9.

When the immediate environment of S is drastically altered from C-S-C to C-S-N as in isothiazole (Figure 8), or to N-S-N as in 2,1,3 - benzothiadiazole, then new bands appear, corresponding to C(2p)-S(3p)-N(2p) or N(2p)-S(3p)-N(2p) bonding, etc. The D/E intensity ratio for saturated sulfur heterocycles is in the range of 0.7 to 0.8, and since for unsaturated sulfur heterocycles this ratio is in the range of 1.2 to 1.4 with the exact value depending upon the nature of the substituent, it appears that this ratio gives a reliable value for the relative amount of saturated sulfur heterocycles. The introduction of one or more nitrogen atoms adjacent to S drastically alters the S-K β spectra and the S-N and N-S-N functional content also appears to be discernible. Consequently, it appears that there may be several useful analytical capabilities attainable from the S-K β emission spectra of sulfur heterocycles.

Another problem in electron structural studies is to examine whether or not a particular technique is capable of distinguishing between different kinds of carbon-oxygen bonding. This area was investigated by Burkard and Kim (9,10). The following substances were studied by Burkard: p-benzoquinone (PBQ), anthraquinone (AQ), acridone (ACR), acenaphthalenequinone (ANQ), and phenanthrenequinone (AQ). The oxygen K α spectra of all of the quinones show three basic features, namely, an intense and relatively sharp band around 527 eV corresponding to transitions from lone pair (lp) orbitals, a relatively diffuse and broad π band region about 2 eV below the lp peak, plus a very broad and diffuse σ region around 522 eV. There are significant differences in all of the spectra. For ACR the lone pair peak, probably due to the presence of the N heteroatom causes a low energy shift for the lone pair lp band. Moreover, the widths of the lp bands as well as their contours seem to provide useful lp-lp interactions. One of the more obvious lp-lp interactions, as illustrated in Figures 9 and 10, is due to ortho vs. para positions of the oxygen atoms yielding a very broad lp band for ANQ as compared with AQ. There appears to be some limited analytical potential in using O-K α emission spectra to distinguish among various quinones.

Kim's C-K α and O-K α studies included lithium carbonate, urea, lithium acetate, magnesium oxalate, and squaric acid. The spectra for the latter three are illustrated in Figures 11-13. According to the spectra, it appears that when there is a monocarboxylic acid (LiAC) as compared with a dicarboxylic acid, the halfwidth of the lone pair band A is considerably narrower. Thus, the halfwidth of the lone pair may be a useful tool for differentiating between mono and polycarboxylic

acids. Finally, as shown in Figure 13 for squaric acid, XFS can differentiate between C=O and C-OH functional groups (see bands A vs. A' and D vs D', respectively, in the O-K emission spectrum).

Instrumentation and Experimental Procedures

All of the S-K β , Cl-K β and P-K β spectra were obtained on a double crystal instrument developed by Andermann's group at the University of Hawaii (11). This instrument represents the addition of a second crystal to a standard Norelco vacuum emission spectrograph. Using calcite crystals, the instrumental broadening was about 0.7 eV. Spectra taken on this instrument were obtained point by point typically in 2 to 4 hours.

All of the O-K α and Cl-K β spectra were obtained on a 5M focal length grating spectrometer also developed by Andermann's group (12-14). The instrumental resolution at O-K α can be as low as 0.05 eV, and at C-K α , as low as 0.02 eV. These resolution limits are not achievable with the present photographic and scanning photoelectric detection methods, but the use of position sensing detection, etc. should allow the utilization of the instrument at the high resolution limits with exposure times well below 1 hr. (15).

With the double crystal spectrometer, helium was used to allow optical transmission, but with the grating spectrometer, vacuum has to be employed for O-K α and C-K α studies. It should be noted, that with the grating spectrometer a sample chamber pressure of 10^{-2} torr is adequate. Cryogenic sample handling currently under development will allow the irradiation and analysis of samples, such as coal, which contain volatile compounds.

Discussion of Analytical Capabilities for Functionality Characterization

While it may be premature to assert with any degree of certainty the potential analytical capabilities of XFS for characterizing the nature and amount of different functional groups, a few generalizations are in order. Judging from the position of the oxygen lone pair peaks in squaric acid, it should be feasible to distinguish between -C=O and -C-OH groups. In the case of carboxylic acids the C-K emission is highly simplified and the halfwidth of the lone pairs should provide a handle on the presence and quantity of mono or polycarboxylic acids. An unsaturated ring system provides a unique C $_{2p}$ -C $_{2p}$ π band, and conceivably, the integrated intensity might yield useful information about the extent of unsaturation. XFS to determine sulfur functionality, as discussed before, appears to provide a unique capability in determining the degree of saturation in the sulfur heterocyclic substances, as well as the capability in determining the nature of the atoms directly linked to the sulfur atom.

While the above fundamental studies appear to be encouraging, clearly it will be necessary to evaluate directly the analytical capabilities of XFS for coal characterization. Preliminary studies are currently under way.

Acknowledgement

The fundamental research undertaken at the University of Hawaii has been supported in part by the National Science Foundation. The preliminary analytical studies on coal are being supported by the Department of Energy under Contract. No. DE-FC21-83FE6D181.

References

1. Urch, D.S., X-ray Emission Spectroscopy, "Electron Spectroscopy, Theory, Techniques and Application," Acad. Press, N.Y. 3, 1-39 (1979).
2. Myers, K., M.S. Thesis, University of Hawaii (1972).
3. Myers, K., Andermann, G., Chem. Comm. 16, 934 (1972).
4. Myers, K., Andermann, G., J. Phys. Chem. 76, 3915 (1972).
5. Myers, K., Andermann, G., J. Phys. Chem. 77, 280 (1973).

6. Whitehead, H.C., Ph.D. Dissertation, Univ. of Hawaii (1975).
7. Whitehead, H.C., Andermann, G., J. Phys. Chem. 378, 2592 (1974).
8. Phillips, D., Ph.D. Dissertation, University of Hawaii (1976).
9. Burkard, F., M.S. Thesis, University of Hawaii (1981).
10. Kim, R., M.S. Thesis, University of Hawaii (1986).
11. Whitehead, H.C., Layfield, J., Andermann, G., Rev. Sci. Instr. 43, 50 (1973).
12. Andermann, G., Bergknut, L., Karras, M., Griesehaber, G., Spectr. Letters, 11 (8) 571 (1978).
13. Andermann, G., Bergknut, L., Karras, M., Griesehaber, G., Rev. Sci. Instr. 51 (6), 814 (1980).
14. Andermann, G., Burkard, F., Kim, R., Fujiwara, F., Karras, M., Spec. Letters, 16 (12), 891 (1983).
15. Andermann, G., Kim, R., Burkard, F., AIP Conf. Proceed. 75, 309 (1981).

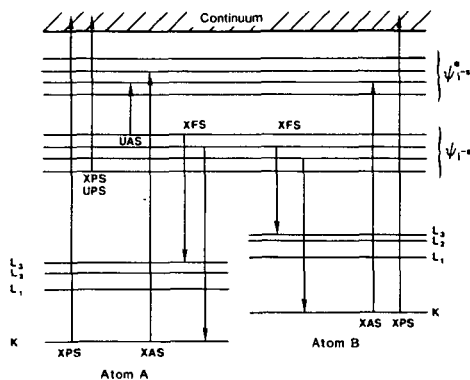


FIGURE 1. Energy Level Diagram For Diatomic Species A-B.

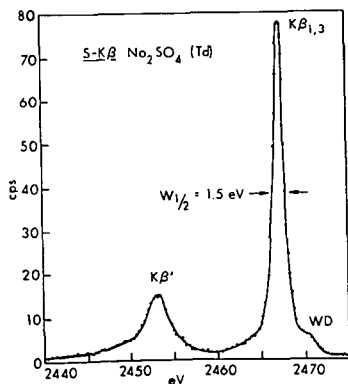


FIGURE 2. S-K β Spectrum of Na₂SO₄.

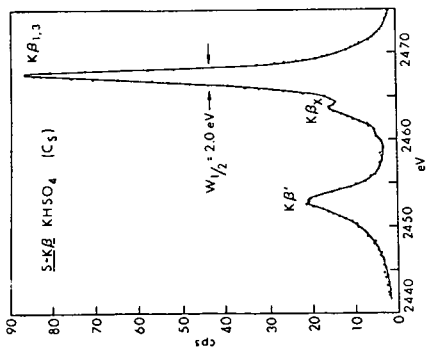


FIGURE 3. S-K α Spectrum of KHSO $_4$.

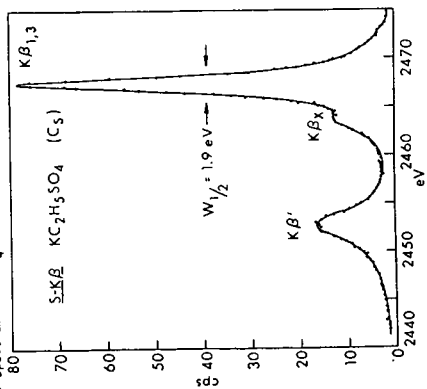


FIGURE 4. S-K α Spectrum of KC $_2$ H $_3$ SO $_4$.

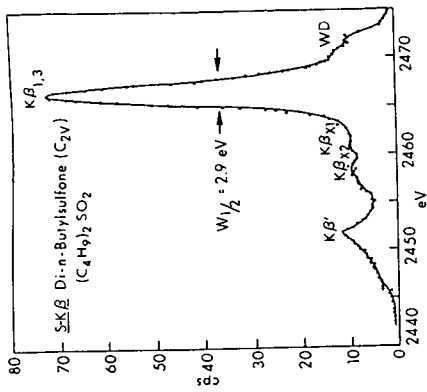


FIGURE 5. S-K α Spectrum of Di-n-Butylsulfone.

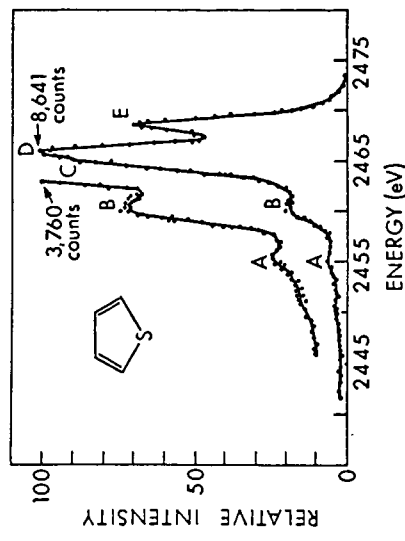


FIGURE 6. S-K α Spectrum of Thiophene.

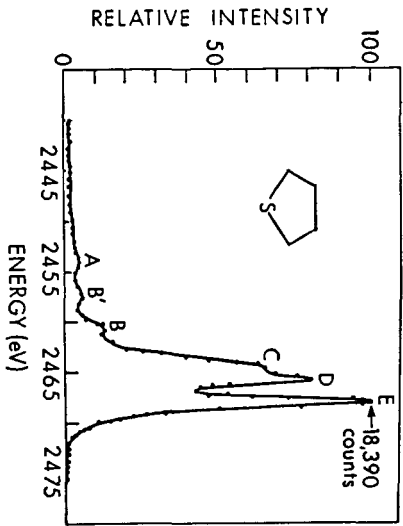


FIGURE 7. S-K α Spectrum of Tetrahydrothiophene.

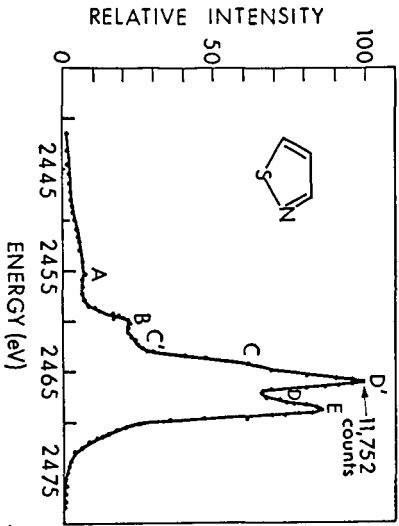


FIGURE 8. S-K α Spectrum of Isothiazole.

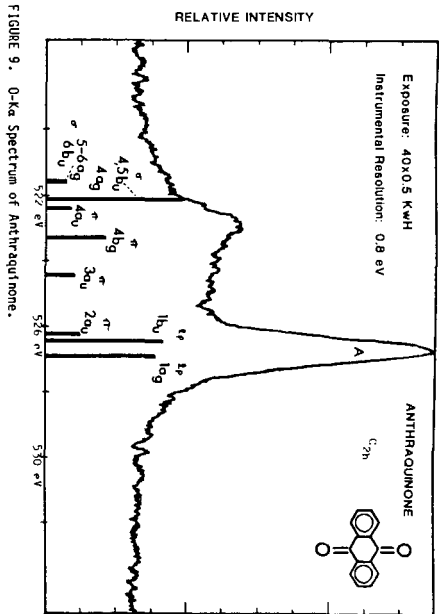


FIGURE 9. O-K α Spectrum of Anthraquinone.

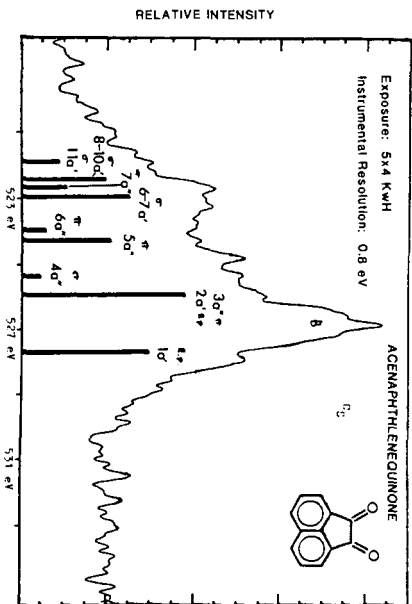


FIGURE 10. O-K α Spectrum of Acenaphthenequinone.

MATRIX ISOLATION EPR STUDIES OF COAL TAR MOLECULES

C. Judith Chu, Robert H. Hauge and John L. Margrave
Department of Chemistry, Rice University, Houston, Texas 77251

ABSTRACT

EPR studies of matrix isolated tar molecules have demonstrated for the first time the presence of free radical sites in the original gaseous tars evolved from coal over the 350-500°C temperature range. Matrix isolated tars exhibit considerably more structure than does the coal itself. It is initially isolated in carbon dioxide at liquid nitrogen temperature. The EPR spectra suggest the presence of four or more randomly oriented planar free radical molecules, some of which may be assignable to sulfur, nitrogen and oxygen containing heterocyclic aromatics. The parallel component (g_{\parallel}) is sensitive to the structure and/or composition of tar. The respective perpendicular (g_{\perp}) components are insensitive to tar structure and similar to the free electron value. The free radical species disappear as the coal tar is warmed to room temperature. This strongly suggests that the usual tar products that are formed from devolatilized coal are free radical polymerized polymers which are formed from smaller free radical species.

INTRODUCTION

Considerable literature (1-5) has been published concerning the existence of free radical ESR signals in coals. The reported coal ESR literatures have been mainly concerned with either coal, pyrolyzed coal, solvent refined coal or coal liquefaction products. The g -values of a large number of coals have been studied extensively by Retcofsky(1) and Yen (4) independently. It was found that g values are dependent on the heteroatom contents of the coal. In general, the higher the nitrogen, oxygen and sulfur contents, the higher the g values from that of the free electron. Evidence also suggests that the coal free radical ESR signal is associated with the organic structure of coal and not the mineral matter.

We have studied extensively the pyrolysis processes of coals using matrix isolation FTIR techniques. Since the primary step in coal gasification and coal pyrolysis presumably involves the thermal decomposition of coal to produce free radicals, it would be of interest to study the primary pyrolysis products to determine the existence of free radicals. This involves experimental techniques which allow the formation of primary pyrolysis products and the utilization of matrix isolation techniques which traps the reactive intermediate free radicals in an inert matrix gas at low temperatures and quenches further reaction. Using these techniques, we have identified all of the slow pyrolysis products of four different ranks of coal through matrix isolation FTIR spectroscopy (6,7), however, evidence of free radical formation was not observed except in the case where tar molecules were flash pyrolyzed at 1100°C and methyl radicals were observed for the first time. Other slow pyrolysis products identified through matrix isolation FTIR are: CO, CO₂, H₂O, CH₄, C₂H₄, C₂H₆, HCN, H₂S, CS₂, COS, SO₂, and tar molecules. If the existence of free radicals were to be found from the thermal decomposition of coal, the most likely free radicals would be that of tar molecules which are structurally similar to the parent coal and are considered to be smaller fragments of the original coal. To consider this possibility and the existence of other free radicals not identifiable through matrix isolation FTIR, we have matrix isolated tar molecules along with other pyrolysis products of four coals, Pittsburgh bituminous, Illinois #6, Rawhide sub-bituminous and Texas Lignite, and studied them by Electron Spin Resonance or Electron Paramagnetic Resonance Spectroscopy.

EXPERIMENTAL

Studies were performed on four coals donated by Exxon Research and Engineering Co., Baytown, Texas. They are:

1. Illinois #6, high volatile C bituminous
2. Pittsburgh, high volatile A bituminous
3. Rawhide, sub-bituminous C rank, Wyoming
4. Texas lignite, lignite rank

Elemental analysis of these coals are listed in Table I and slow pyrolysis behavior of these four coals has been described in detail in another paper.(6,7) The coal samples were ground and sifted under inert nitrogen atmosphere to prevent oxidation and only the -500 mesh coal particles of less than 25 microns were used in the experiments.

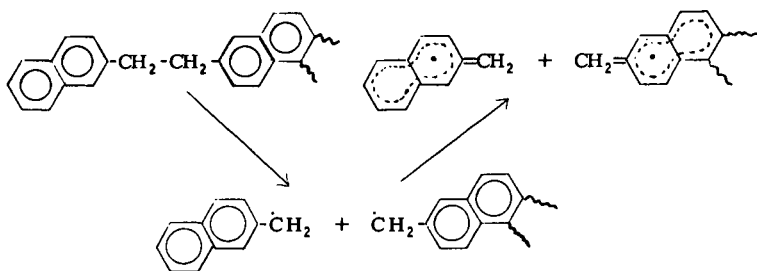
A detailed schematic diagram of the matrix isolation EPR apparatus is shown in Figure 1. The apparatus is constructed of stainless steel and pumped by a mechanical pump - 4" diffusion pump combination and maintained at 10^{-7} torr pressures except during deposition when the pressure rises to 10^{-5} torr due to excess inert matrix gas. The entire apparatus is mounted between the magnets of a Varian E-9 EPR spectrometer. The coal sample was placed in a slow pyrolysis reactor (6,7) situated in the furnace chamber directly facing a single crystal sapphire rod cooled to 77K. The coal particles were slowly heated to promote the evolution of pyrolysis products which exit the reactor and are then immediately co-condensed onto the liquid nitrogen temperature sapphire rod with carbon dioxide as the matrix gas. After deposition, the sapphire rod attached to a moveable liquid nitrogen cooled tube is slowly lowered into a 1/2" o.d. thin wall quartz tube situated in the microwave cavity and an EPR spectrum of the products obtained.

RESULTS AND DISCUSSION

Results obtained from the matrix isolated EPR spectra demonstrated for the first time the presence of free radical sites in the original gaseous tars evolved from coals over the 350-500°C temperature range. The assignment of the observed EPR spectrum to volatilized tar molecules is based on the temperature at which EPR spectra first begin to appear (i.e., <350°C). EPR spectra of Illinois #6 tar molecules are shown in Figure 2 which illustrates the appearance and gradual increase of the EPR spectra from 314°C to 564°C. FTIR matrix isolation studies of the coals also indicate extensive evolution of tar at <350°C to 500°C. This temperature range has been designated as the high temperature tar evolution temperature range. Another less intense low temperature tar evolution was observed from FTIR studies at ~100°C to 300°C. It is interesting to note that the low temperature tars (100-300°C) do not exhibit free radical character. Thus only the high temperature tars are formed by actual bond breakage. It seems likely that the low temperature tars are formed through the dissociation of hydrogen bonding in the coal. We have found that a disruption of the hydrogen bonding in coal by O-methylation of the coal hydroxyl functional groups dramatically increases the evolution of low temperature tar but not that of high temperature tar.(8)

Retcofsky et.al. (5) have reported the EPR behavior of a heat treated Ireland Mine hvAb coal. The results show an increase in spin concentration for the coal heat treated to 450°C, approximately 7 times that of the original unheated coal. The same coal heat treated to 350°C showed only a slight increase in spin concentration. Khan (9) has also reported increases in electron spin

concentration, in the same order of magnitude as Retcofsky, for Pittsburgh and Illinois #6 coals heat treated to 460°C. These results complement our findings since concurrent with the observation of free radical tar formation at 350°C to 500°C, the pyrolyzed residual coal particles must also be experiencing a gradual increase in electron spin concentration as more free radicals are formed through bond breakage in this temperature region. Retcofsky reported that the g value obtained for the heat treated coal at 450°C is 2.0028 which is in the spectral range generally attributed to π -hydrocarbon radicals. The observed g -anisotropy of the matrix isolated tar spectra is understandable if the tar molecules are also of a π -hydrocarbon free radical type. This indicates that during the tar evolution process, the σ -type free radicals formed as a result of bond breakage of linkage groups in coal are not as stable as π -hydrocarbon free radicals. Therefore the σ -free radical site must be preferentially transferring and delocalizing the free electron to adjacent aromatic π -ring systems, i.e.,



The smaller π -free radical fragments formed evolve as tar molecules and the remaining π -free radicals attached to the main skeletal structure of the coal stay in the residue and are the cause for the observed increase in spin concentration of the heat treated coal.

The EPR spectra of the randomly oriented but rigidly held tar molecules of the four coals are shown in Figure 3. The spectra obtained are similar to a "powder pattern" spectra exhibiting g anisotropy and no hyperfine splitting. The matrix isolated EPR spectrum of Illinois #6 tar is compared to the EPR spectrum of the original coal powder diluted in high vacuum grease in Figure 4. It is clear that the matrix isolated tar molecules exhibit considerably more structure than the coal itself. In fact peaks labeled a, b, c, and d can be identified with distinctly different free radical sites in the tar molecules. From similarities between the matrix isolated tar spectrum and the spectrum simulated by Weltner (10,11) of randomly oriented and rigidly held planar aromatic molecules, peaks a-d can be labeled as parallel components representing different free radical tar species. The parallel components ($g_{||}$) are apparently sensitive to the structure and/or composition of tar. The respective perpendicular (g_{\perp}) components are relatively insensitive to tar structure and similar to the free electron value.

Differences in the parallel ($g_{||}$) components of the tar are clearly observed between the four coals (Figure 3). The relative abundance of the a-d peaks varies significantly from coal to coal. In fact, the coal exhibiting the most distinct $g_{||}$ components is Illinois #6. Since it is known that the g values of the coal are dependent on the heteroatom contents of the coal,^(1,2,4) tar

molecule g values must also be effected by the heteroatom contents. Flash pyrolysis studies of the coal tars at 1100°C has shown the tar molecules to contain considerable sulfur, nitrogen and oxygen heteroatoms.⁽¹²⁾ Illinois #6 contains a much higher percentage of sulfur than the other coals (see Table I), this suggests that one of the g_{II} peaks may be associated with a sulfur containing free radicals. The other peaks may be attributed to either a pure aromatic free radical or nitrogen and oxygen containing heterocyclic aromatic free radicals. The experimentally calculated g_{II} , g_I and g^0 ($g^0=1/3(g_{II}+2g_I)$) values for the four matrix isolated tars are listed in Table II. Table III lists the g values of some of the possible organic free radicals in coal compiled by Petrakis and Grandy.⁽²⁾ By comparing the ordering of the tar g^0 values to that of the g values for hetero-atom containing free radicals (see Table IV), one can assign peak a to sulfur containing, peak b to oxygen containing, and peak c to nitrogen containing π aromatic free radicals. Peak d, nearest to the g_I component of the tar, is assigned to pure π aromatic free radicals containing no hetero-atoms. The higher g^0 values of the tar molecules may be a result of matrix isolation and will be further investigated. The assignment of peaks a-d indicates that potential exists for a direct measurement of the relative amounts of nitrogen, sulfur, and oxygen heterocyclics. Figure 5 shows the disappearance of the free radical species as the coal tar is warmed to room temperature. The tar molecules were initially isolated in carbon dioxide at liquid nitrogen temperature. This strongly suggests that the usual tar products formed from devolatilized coal are re-polymerized polymers formed from smaller free radical species.

More work will be done to conclusively characterize the types of free radicals present in tar. Work with model polymers containing appropriate heterocyclic aromatic structures will be very useful. It is already clear, however, that volatilized tars can be distinguished by the number and types of free radical sites present. An understanding of these differences could play a very important role in the choice of other processing steps which lead to the production of useful fuels.

ACKNOWLEDGEMENT

We gratefully acknowledge support of our work by the Department of Energy, Morgantown, West Virginia and in particular the support of Dr. Sophia Lai.

REFERENCES

1. Retcofsky, H.L., "Magnetic Resonance Studies of Coal", Coal Science, vol. 1, Gorbaty, M.L., Larson, J.W., and Wender, I., Academic Press, p. 43-82, 1982.
2. Petrakis, L., and Grandy, D.W., "Free Radicals in Coals and Synthetic Fuels", Coal Science and Technology 5, Elsevier, 1983.
3. Retcofsky, H.L., Maguire, M.M., and Clarkson, R.B., "Nature of the Free Radicals in Coals, Pyrolyzed Coals, Solvent-Refined Coal and Coal Liquefaction Products", Coal Structure, Adv. in Chem. Ser. 192, eds. Gorbaty, M.L. and Ouchi, K., p. 37-58, 1981.
4. Yen, T.F., and Sprang, S.R., "Contribution of ESR Analysis Toward Diagenic Mechanisms in Bituminous Deposits", Geochimica et Cosmochimica Acta, 41, 1007-1018, 1977.
5. Retcofsky, H.L., Hough, M.R., Maguire, M.M., Clarkson, R.B., "Some Cautionary Notes on ESR and ENDOR Measurements in Coal Research", Applied Spectroscopy, vol. 36, no. 2, 187-189, 1982.

6. Chu, C.J., Fredin, L., Hauge, R.H., and Margrave, J.L., "Studies of Pyrolysis Processes of Illinois #6 Coal and its Tar Using Matrix Isolation FTIR Spectroscopy", High Temperature Science, 20, 51-73, 1985.
7. C.J. Chu, S.A. Cannon, R.H. Hauge and J.L. Margrave, "Matrix Isolation FTIR Studies of the Slow Pyrolysis Processes of Four Coals", submitted for publication.
8. C.J. Chu, S.A. Cannon, R.H. Hauge and J.L. Margrave, to be published.
9. Khan, M.R., Fifth Annual Gasification Projects Contractors Meeting, U.S. Department of Energy, Office of Fossil Energy, Morgantown, WV, June 1985.
10. Weltner, W., Jr., Adv. High Temp. Chem. 2, 85, 1969.
11. Weltner, W., Jr., Magnetic Atoms and Molecules, Scientific and Academic Editions, 1983.
12. Chu, C.J., Hauge, R.H., and Margrave, J.L., "Matrix Isolation FTIR Studies of the Flash Pyrolysis of Tar Molecules at 1100°C", to be published.

Table I. Analytical Data of Four Coal Samples*

	<u>Texas</u> <u>Lignite</u>	<u>Rawhide</u> <u>Sub-bitum.</u>	<u>Illinois #6</u> <u>Bituminous</u>	<u>Pittsburgh</u> <u>Bituminous</u>
Moisture, Wt%	21.1	15.4	10.3	7.6
Ash, Wt%	9.35	8.64	9.28	6.04
Mineral matter, Wt%	6.9	7.1	10.9	7.8
Vol. matter, Wt%	48.2	47.3	41.6	37.2
Carbon, Wt%	68.0	68.3	70.9	78.9
Hydrogen, Wt%	4.99	4.84	5.08	5.25
Nitrogen, Wt%	1.06	0.82	1.18	1.28
Sulfur, total, Wt%	0.96	0.92	3.94	2.29
Sulfur, pyritic, Wt%	0.04	0.01	1.17	0.69
Sulfur, organic, Wt%	0.92	0.91	2.77	1.60
Oxygen, organic, Wt%	18.3	18.2	9.4	5.6
Density, g/cc	1.44	1.45	1.37	1.33
Btu/lb	11720	11710	12857	14312

*Samples supplied by Exxon Research and Engineering Co.

Analysis based on moisture free coal.

Ash contents of samples supplied may not be same as those indicated.

TABLE II. g Values for Matrix Isolated Tars*

Coal ----	g_{II} ---	g_I ---	g^O ---
Illinois #6			
a	2.037	2.002	2.014
b	2.029	2.002	2.011
c	2.025	2.002	2.010
d	2.010	2.002	2.005
Pittsburgh			
a	-----	-----	-----
b	2.030	2.003	2.012
c	-----	-----	-----
d	2.011	2.003	2.006
Rawhide			
a	-----	-----	-----
b	2.029	2.001	2.010
c	-----	-----	-----
d	2.010	2.001	2.004
Texas Lignite			
a	2.038	2.003	2.014
b	2.030	2.003	2.012
c	-----	-----	-----
d	2.011	2.003	2.006
O-methylated Illinois #6			
a	2.037	2.002	2.014
b	2.029	2.002	2.011
c	2.025	2.002	2.010
d	2.011	2.002	2.005
Coal (unheated)			2.0025-2.0045
Free Electron			2.0023
Graphitized carbon film			2.0107

$$*(g^O=1/3(g_{II}+2g_I))$$

Table III. g Values of Possible Free Radicals in Tars⁽²⁾

<u>Free Radical</u>	<u>g Value</u>	
Aromatic Hydrocarbons		
π Radicals	2.0025	(cation)
1-5 Rings	2.0026-2.0028	(anion)
7 Rings	2.0025	(cation)
7 Rings	2.0029	(anion)
Aliphatic Hydrocarbons		
σ Radicals	2.0025-2.0026	(neutral)
Oxygen Containing Free Radicals		
σ Type	2.0008-2.0014	(neutral)
π Type		
Quinones 1-3 rings	2.0047-2.0038	
Ethers		
i-ring, Mono-, Di-, Trimethoxybenzene	2.0035-2.0040	
N-Containing Radicals	2.0031	
S-Containing Radicals	2.0080-2.0081	
Graphite	2.0025-2.015	

Table IV. Comparison of Tar g-Values with Other Free Radicals

Tar	$\frac{a}{2.014}$	$\frac{b}{2.011}$	$\frac{c}{2.010}$	$\frac{d}{2.005}$
π Aromatic Free Radicals	$\frac{\text{Sulfur}}{2.008}$	$\frac{\text{Oxygen}}{2.004}$	$\frac{\text{Nitrogen}}{2.003}$	$\frac{\pi \text{ Aromatic}}{2.0025}$

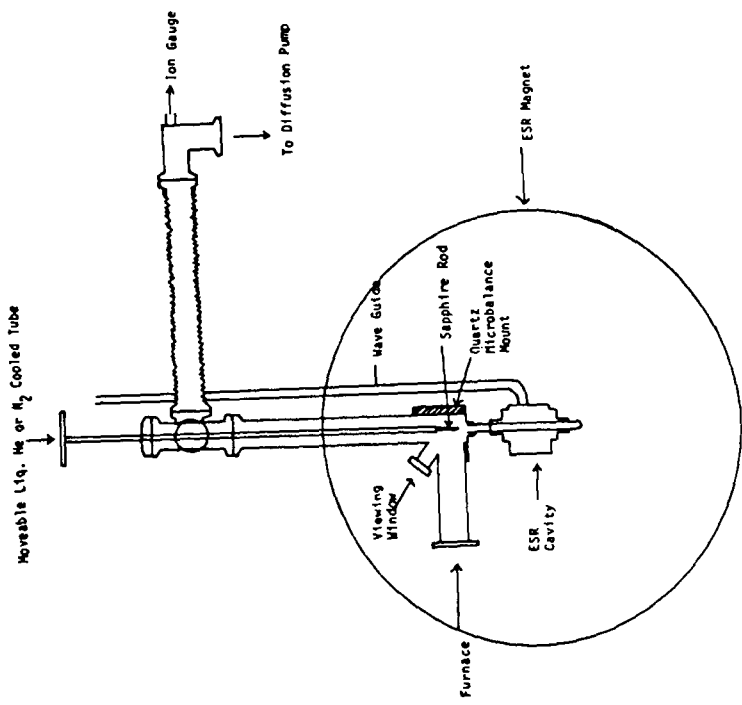
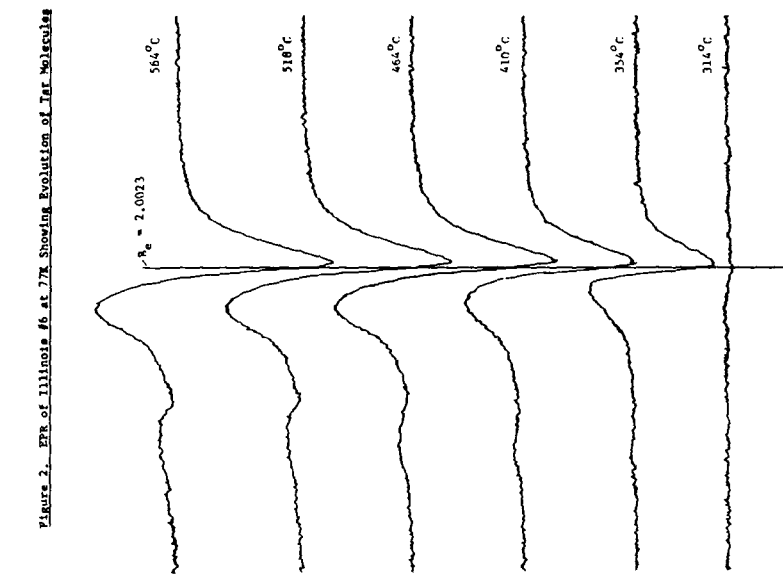


Figure 1. Matrix Isolation ESR Apparatus

Figure 4. Comparison of Illinois #6 and Its Matrix Isolated Tar

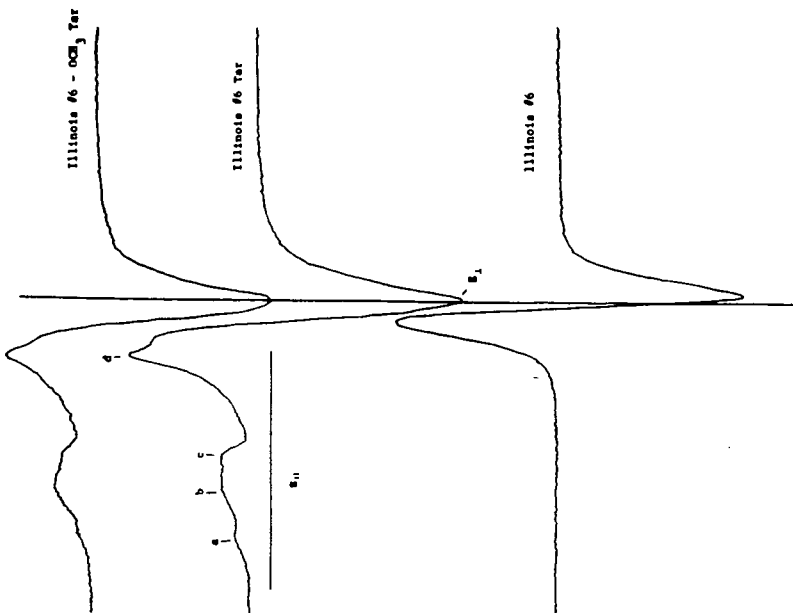


Figure 3. EPR of Matrix Isolated Tar Molecules at 77K

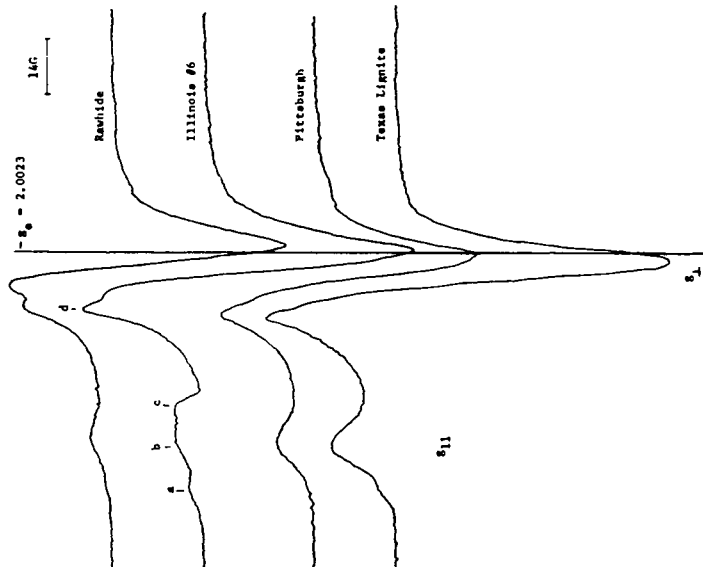
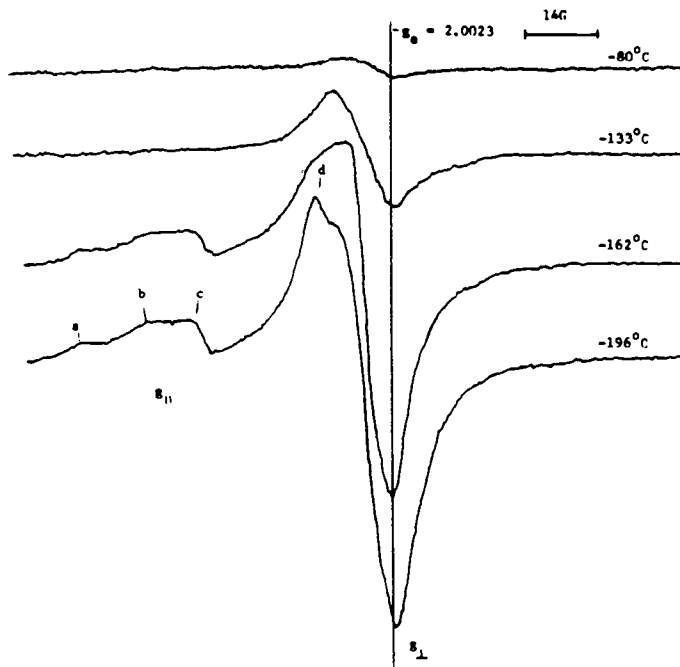


Figure 5. Warm Up of Matrix Isolated Illinois #6 Tar



LOW-RANK COAL STRUCTURE ELUCIDATION WITH RUTHENIUM TETROXIDE

E.S. Olson, J.W. Diehl, M.L. Froehlich, D.J. Miller
University of North Dakota
Energy Research Center
Box 8213, University Station
Grand Forks, North Dakota 58202

The goal of these studies was to elucidate the structural features of coals which are believed to be important in conversion processes. Of special interest are the nature of the hydroaromatic groups and the bridging groups between aromatic moieties, because of their roles in thermal cleavage and depolymerization processes and the hydrogen shuttling which occurs during the depolymerization and stabilization of cleavage products. The first objective was the development of new methods for the isolation or solubilization of the aliphatic groups in the coal, which may then be related to these hydroaromatic systems and bridging groups. We have successfully used ruthenium tetroxide in a two phase solvent system with a phase transfer catalyst to selectively oxidize the aromatic groups (1). Stock has used ruthenium tetroxide in the presence of acetonitrile to oxidize a Texas lignite and Illinois No. 6 coal (2,3). These procedures are a more viable alternative than the use of trifluoroperacetic acid which was used in earlier studies by Deno (4) and whose difficulties have been pointed out (1,2).

The oxidation of a North Dakota lignite with ruthenium tetroxide with the phase transfer catalyst proceeded rapidly at ambient temperature giving carbon dioxide and carboxylic acid products which were converted to methyl esters by diazomethane for qualitative analysis using GC and GC/MS. A very complex mixture of aliphatic mono and polycarboxylic acids and aromatic polycarboxylic acids was formed in the reaction. In contrast to the trifluoroperacetic acid studies, no oxiranepolycarboxylic acids were found. Keto acids were also found to be absent. An ion trap mass spectrometer was found to be useful in these analyses since an M+1 peak was found for many of the esters which normally do not exhibit any molecular ion.

A major effort was expended to find a reliable and accurate method for the quantitative analysis of carboxylic acid products. Loss of dicarboxylic acids and esters during extraction and conversion to methyl esters was a major problem. Analysis of the low molecular weight monoacids was carried out on a calibrated capillary GC using direct on-column injection of the distilled reaction products. High pressure liquid chromatography of the diacids directly on an Aminex HPB7H resin was unsuccessful due to interferences between aliphatic and aromatic acids, even though satisfactory resolution of the aliphatic diacids was obtained using two columns in series (5). Ion exchange chromatography both as a cleanup for the Aminex resin and analytical separations by itself was also unsuccessful. A calibrated GC method using an internal standard added to the acid mixture before cleanup and methylation also failed to give reproducible results, especially for the aromatic polycarboxylic acids. Finally, several deuterated acid standards were prepared or purchased so that isotope dilution methods using quadrupole GC/MS analysis of the methyl esters could be carried out. Calibration curves were highly linear ($r^2 = 0.99$) over a wide range. A series of repetitive oxidations on the same Beulah lignite sample gave highly consistent results, especially for the adipic and phthalic acids which were labeled with four deuteriums. The average deviations were in the second decimal place and thus are no more limiting than the proximate analysis data.

In order to interpret the data, a number of model compounds have been oxidized using the ruthenium tetroxide with a phase-transfer catalyst. Some of these data were reported previously (1). Basically alkyl substituents are converted in very high yield to the monocarboxylic acids. Hydroaromatics give a mixture of products consisting of the α -ketone, the diacid which maintains the same number of methylene

carbons as in the hydroaromatic ring, and smaller amounts of the diacid corresponding to loss of one methylene group. Stock obtained less of the ketone and more of the larger diacid. One-carbon methylene bridges are oxidized to ketones or carboxylic acid groups, but the arylacetic acid may be isolated in good yield. Malonic acid which would have resulted from oxidation of the second benzene ring is not found. Unfortunately it is not stable in the oxidizing system, in contrast to other carboxylic acids. Dimethylmalonic acid was isolated as a product from 2,2-diphenylpropane. Thus it probably not possible to determine one-carbon bridges in the structure using this reagent, unless they are quaternary. Two carbon methylene bridges gave succinic acid and hydrocinnamic acid. 9,10-Dihydrophenanthrene, however, gave succinic and diphenic acid, the major product from phenanthrene. Phthalic and other aromatic polycarboxylic acids are products from various polynuclear aromatic systems.

The effect that oxygens in the structure of hydroaromatics exert on the product yield was studied because of the prevalence of hydroxyl-substituted hydroaromatics in the devolatilization products of lignites. Oxidation of 6-hydroxytetralin with RuO_4 gave no ketone and more degradation to glutaric and succinic than that which occurred in the oxidation of tetralin. 6-Methoxytetralin behaved similarly. 5,6,7,8-Tetrahydronaphthoquinone gave a considerable amount of succinic acid in addition to the adipic. 1-Tetralone gave no reaction, however 2-tetralone was oxidized to succinic acid.

A comparison of three oxidation methods, the ruthenium tetroxide with phase transfer catalyst, the ruthenium tetroxide with acetonitrile and the trifluoroacetic acid, was carried out on the same sample of Beulah lignite. There was no significant difference in the amounts of acid products between the two ruthenium tetroxide methods (Table 1). Thus whatever differences exist between these reagents in their reactions with model compounds, no differences are apparent in the products from lignite oxidation. This may be a reflection of the more complete oxidation expected for hydroxyaromatics at the ends of the aliphatic bridging groups and for hydroxyhydroaromatic groups or perhaps the absence of tetralin groups in the coal structure. No evidence for a tetralone type of structure in the products of oxidation has been found. The lower yields of aliphatic acids found when the Deno oxidation with trifluoroacetic acid was used reflect the same problems encountered with model compound oxidations with this reagent.

Table 1. Comparison of Oxidation Methods on Same Beulah Lignite Sample

Method	SU	GL	AD	PT	PH	BT
RuO_4/PTC	3.04	0.49	0.14	0.55	0.05	0.67
RuO_4/CH_3CN	2.93	0.57	0.14	0.49	0.08	1.01
CF_3CO_3H	0.93	0.30	0.09	0.14	0.02	2.25

A number of low-rank coals were oxidized for comparison purposes. Values for the amounts of six carboxylic acid products which were determined using the isotope dilution method are reported in Table 2. The amounts of the six acids in the oxidation products generally increase with coal rank or % C. There is a little variation in the three North Dakota lignites (Beulah, Gascoyne and Velva), which have about 71% C. There is a greater variation in acids from the Texas lignites (San Miguel - 67% C and Martin Lake - 73% C) and the subbituminous coals (Wyodak - 73% C and Decker - 76% C). This trend is consistent with the hypothesis that the western subbituminous coals have a higher algal lipid-derived aliphatic component than the lignites. A Pittsburgh bituminous coal was also oxidized and found to have

a much lower aliphatic acid content, but higher aromatic acid content, consistent with the hypothesis that it has been aromatized to a greater extent than the subbituminous coals. It was not possible to find a correlation between these data in Table 2 and corresponding published tubing bomb liquefaction data for these coals (6).

Table 2. Results of Coal Oxidations with RuO₄ (% maf Basis)

<u>COAL</u>	<u>SUC</u>	<u>GLU</u>	<u>AD</u>	<u>PT</u>	<u>PH</u>	<u>BT</u>
Beulah	2.38	0.59	0.11	0.70	0.07	1.53
Gascoyne	2.58	0.56	0.13	0.62	0.07	1.60
Velva	2.71	0.56	0.16	0.73	0.05	1.37
Martin Lake	2.50	0.96	0.27	0.76	0.09	1.55
San Miguel	2.94	0.61	0.12	0.62	0.04	0.73
Wyodak	3.74	0.89	0.23	0.82	0.08	1.64
Decker	4.17	1.69	0.30	0.75	0.09	1.66

A comparison of all the major acid products for two coals, Beulah lignite and Wyodak subbituminous is given in Table 3 and 4. Amounts of those acids not determined by isotope dilution were obtained by a calibrated FID method.

Table 3. Oxidation of Beulah Lignite and Wyodak Coal (% of maf Coal)

<u>Aliphatic Acids</u>	<u>Beulah</u>	<u>Wyodak</u>
Succinic*	2.38	3.74
2-Methylsuccinic	0.41	0.11
Glutaric*	0.59	0.89
2-Methylglutaric	0.26	0.14
Adipic*	0.11	0.23
2-Methyladipic	0.07	0.15
Pimelic	0.04	0.11
Suberic	0.12	0.10
Azeleic	0.04	0.12
Sebacic	0.01	0.05
Octanoic	0.02	0.04
Nonanoic	0.00	0.00
Lauric	<0.01	0.00
Myristic	0.01	0.02
Palmitic	<0.01	0.02
1,2,3-Propanetricarboxylic*	0.70	0.82
1,2,4-Butanetricarboxylic	0.31	0.40

*determined by isotope dilution, the others by fid calibration

Table 4. Oxidation of Beulah Lignite and Wyodak Coal (% of maf Coal)

<u>Aromatic Acids</u>	<u>Beulah</u>	<u>Wyodak</u>
Phthalic*	0.07	0.08
1,2,3-Benzenetricarboxylic	0.23	0.32
1,2,4-Benzenetricarboxylic	0.30	0.32
1,3,5-Benzenetricarboxylic	0.01	0.01
1,2,3,4-Benzenetetracarboxylic	1.5	1.7
1,2,4,5-Benzenetetracarboxylic*	1.53	1.64
1,2,3,5-Benzenetetracarboxylic	1.5	1.7
Benzenepentacarboxylic	1.5	1.4
Benzenhexacarboxylic	0.01	0.37

Three lithotypes have been separated from Beulah lignite on the basis of physical properties and have been extensively studied at the University of North Dakota Energy Research Center (7). Oxidation of the vitrain, durain and fusain lithotypes gave a wider variation in the amounts of the six carboxylic acids (Table 5) than did oxidation of many of the samples from different mines (Table 2). The durain and fusain appear to be more aromatized than the vitrain. The main point is that a great variability is likely to be found in the samples obtained from one mine, depending on the lithotype composition, and consequently one should not attempt to correlate any data from different experiments unless they are all done with the same sample.

Table 5. Oxidation of Beulah Lignite Lithotypes with RuO₄

<u>Lithotype</u>	<u>SU</u>	<u>GL</u>	<u>AD</u>	<u>PT</u>	<u>PH</u>	<u>BT</u>
Vitrain	2.41	0.60	0.08	0.58	0.02	0.71
Durain	2.10	0.50	0.12	0.52	0.08	1.38
Fusain	1.38	0.33	0.10	0.27	0.15	1.40

Since the aliphatic diacids which are found in the products from ruthenium tetroxide oxidation may have been derived from either a hydroaromatic or a bridging group, a number of experiments have been attempted to try to distinguish the amount of diacids which are derived from each type of precursor. One of these experiments was a dehydrogenation of the lignite prior to oxidation with ruthenium tetroxide. Water was removed from Beulah lignite by Dean-Stark distillation with xylene under nitrogen and the lignite suspension in xylene was then refluxed with dichlorodicyanoquinone. The dehydrogenated coal was then oxidized with ruthenium tetroxide. The resulting acids were analyzed (Table 6). The amount of succinic acid decreased substantially, however the amount of adipic decreased very little. This result implies that about half of the succinic may be derived from the hydrophenanthrene or dihydropyrene type of hydroaromatics, whereas about 10% of the adipic acid may have been derived from the tetralin type of hydroaromatics. The increase in the amount of phthalic acid resulting from oxidation of the dehydrogenated lignite may also be noteworthy. Dehydrogenation of dihydrophenanthrene or dihydroanthracene structures to the polynuclear aromatics may explain this increase in phthalic acid.

Table 6. Effect of Dehydrogenation on Beulah Lignite

<u>SU</u>	<u>GL</u>	<u>AD</u>	<u>PH</u>
1.42	0.38	0.12	0.22

An experiment was carried out to determine the extent to which the original carboxylic acid groups of the coal make up the acid groups found in the products obtained after oxidation with the ruthenium tetroxide. In order to label the original carboxylic acid groups, a sample of Beulah lignite was methylated with methyl-d₃ iodide using Liotta's procedure (8). This sample containing the methyl-d₃ labelled ester groups was subsequently oxidized with ruthenium tetroxide and the ratio of labelled to unlabelled ester groups determined using mass spectrometry. The ratio of M+1 to M+4 was determined under CI conditions, since the molecular ions are not usually present. For the aliphatic acids, about 10% of the esters were labelled, indicating that 10% of the aliphatic diacid products resulted from oxidation of arylalkanoic acids, such as succinic from 3-arylpropanoic acid.

References:

1. E.S. Olson and J.W. Diehl, ACS Division of Fuel Chem. Preprints, 29(6), 217 (1984).
2. L.M. Stock and K.T. Tse, Fuel, 62, 974 (1983).
3. L.M. Stock, K.T. Tse and S.H. Wang, ACS Division of Fuel Chem, Preprints, 30(4), 493 (1985).
4. N.C. Deno, B.A. Greigger and S.G. Stroud, Fuel, 57, 455 (1978).
5. E.S. Olson, J.W. Diehl and M. Froehlich, Pittsburgh Conf. (1985), Abstracts, p 1074.
6. V.I. Stenberg, M.B. Jones and N.J. Suwarnasarn, Fuel, 64, 470 (1985).
7. H.H. Schobert, F.R. Karner and E.S. Olson, Int. Chem. Cong. of Pac. Basin. Soc., Honolulu, HI, (1984).
8. R. Liotta, G. Brons and J. Issacs, Fuel, 62, 7B1 (1983).

MOLECULAR WEIGHTS OF LIGNITE MACROMOLECULES

Edwin S. Olson, John W. Diehl, and Michael L. Froehlich

University of North Dakota Energy Research Center
Box 8213 University Station
Grand Forks, North Dakota 58202

Introduction

A knowledge of how to determine molecular weights and molecular weight distributions of coal macromolecules has been a long-standing goal of coal scientists (1). A fundamental understanding of the chemical and physical units in coals requires a knowledge of the population of various sizes of molecular entities in the coal. Information on the molecular weight distribution of coal macromolecules can aid in understanding the behavior of the macromolecules in various chemical and physical processes. In the high temperature processes such as liquefaction and pyrolysis, many bonds in the coal are broken and relatively small molecular weight material is obtained. These products have been extensively studied and are not the concern of this paper.

The goal of our research is to apply reliable and accurate polymer characterization methods to the high molecular weight macromolecules of the lignite. We have utilized low-angle laser light scattering (LALLS) photometry in a static mode and also coupled with size exclusion chromatography (SEC) for the determination of weight average molecular weights and molecular weight distributions. Polymers can be separated on the basis of size by SEC, thus providing information about molecular weight distributions; however, molecular weight values depend on calibration data which are subject to large errors (2). These errors result from the lack of similarity between the shapes and polarities of the calibration standards and the materials whose molecular weights are to be determined. Since light scattering techniques give absolute molecular weight values, a LALLS photometer was used as an on-line detector in an SEC system and no error prone calibrations of the size exclusion column were necessary. A refractive index (RI) detector was used in series with the LALLS flow cell to provide concentrations of the eluting solute.

Measurement of the molecular weights of the coal macromolecules of course requires that they be solubilized. Our initial studies (3) were carried out with humic acids from a North Dakota lignite (Beulah-Zap seam), mainly because the humic acids are conveniently obtained by extraction with base at ambient temperatures. Thermal cleavage reactions which could have extensively degraded or depolymerized the coal macromolecules would not have occurred under these conditions, although base initiated depolymerizations may have occurred.

In order to observe the scattering and interpret the results without complications, it is important that the optical absorbance of the macromolecules at the laser wavelength of 633 nm be negligible. Obviously coal-derived macromolecules must be decolorized and considerable effort was expended in finding the best way to reduce the molar absorptivity of the humic acids. The most successful method was found to be reduction of the exhaustively methylated humic acid with zinc dust in acetic anhydride (3). The resulting light powder was soluble in THF and exhibited satisfactory chromatographic profiles in the SEC, indicating that significant adsorption of the material to the SEC column was not a problem.

Results and Discussion

Having reduced the molar absorptivity of the methyl humates, we were able to determine Rayleigh factors for solutions in THF using the static LALLS cell. A linear dependence of Kc/R_{90} with c was obtained ($r^2 = 0.99$) (Figure 1). Thus the weight average molecular weight could be obtained from the intercept (1.3×10^6) (Table 1). These data contrast significantly with those of Hombach (4) where a nonlinear scattering plot was obtained. In that case, it was necessary to introduce a modification to the virial equation so that the non-linear curve could be resolved into a linear and an exponential component. A theoretical justification for the modification was not presented. Our data required no such manipulation, which would have made calculations of molecular weight distributions from the flow cell interfaced with the SEC system more complex. Furthermore the reduction eliminates the fluorescence which would cause an additional complication in determining the molecular weight from scattering plots (5).

Table 1. Molecular weights for humic acid and oxidized lignite derivatives

	Reduced methyl humate	Reduced oxidation product
<u>Static LALLS:</u>		
M_w	1.3×10^6	1.3×10^6
dn/dc	0.22	0.18
A_2	-4.2×10^{-5}	-3.6×10^{-5}
<u>SEC-LALLS:</u>		
M_n	9.7×10^5	6.6×10^5
M_w	1.4×10^6	7.8×10^5
M_z	1.8×10^6	9.1×10^5
$M_z:M_w:M_n$	1.9:1.3:1	1.4:1.1:1

A solution of the reductively acetylated methyl humate in THF was characterized in the SEC-LALLS-RI system. The LALLS chromatogram exhibited a single symmetrical curve whereas the corresponding RI chromatogram was nearly symmetrical (Figure 2). Values for the number average, weight average, and z average molecular weights were calculated from the LALLS and RI data ($M_n = 9.7 \times 10^5$, $M_w = 1.4 \times 10^6$, $M_z = 1.8 \times 10^6$) with polydispersity ratios of $M_z : M_w : M_n = 1.9 : 1.3 : 1$.

Thus the humic acid extracted from lignite with base is a large macromolecule; the relationship between the molecular weight of this material and that of the macromolecules which comprise the major humin portion of the coal must next be established. Although increased yields of humic acids can be obtained by more severe treatments with base (higher temperatures or ultrasonication), the issue of thermal degradation reactions of the macromolecules cannot be neglected in materials obtained from lignite under these conditions. Instead a mild oxidative reaction was chosen to obtain soluble material from the lignite. This oxidation was carried out with 4-nitroperbenzoic acid, a reagent which was recently reported to be effective for the cleavage of benzyl ethers (6). Benzyl ether linkages occur in the lignin

structure between the coniferyl groups and have been suspected to be present in coals as linkages between aryl groups (perhaps largely between coniferyl-derived groups or conjugates thereof). Treatment of the Beulah lignite with 4-nitroperbenzoic acid in refluxing chloroform gave only a small amount of material soluble in organic solvents; this material was similar in composition to the waxy material normally extracted from lignites with organic solvents. After removal of 4-nitrobenzoic acid and 4-nitroperbenzoic acid with hot methanol, the residue was extracted with base to give large amounts of humic acids in yields up to 90 % (on a maf basis). Thus the reagent was presumed to have converted the major portion of the lignite humin to a base-soluble form by cleavage of sufficient number of cross-linking groups of the benzyl ether or some other oxidatively labile type to give carboxylic acid and phenolic groups. The reaction rates and yields varied considerably depending on the particle size and length of sample storage; these oxidation studies are still under investigation. Oxidations of model compounds indicate that carbon bridges between aryl groups (such as in diphenylmethane) are not cleaved by this reagent. However polynuclear aromatic systems (such as in phenanthrene and anthracene) may be oxidized to quinones or other products.

A sample of the base-extractable product from the 4-nitroperbenzoic acid oxidation of lignite was converted to the methylated derivative with dimethyl sulfate followed by diazomethane in DMF-ether, and was reductively acetylated with zinc dust in acetic anhydride as in the humic acid derivatization above. A light tan THF-soluble material was obtained. The molecular weight was determined in the static LALLS cell in THF solution. A linear relationship was obtained in the Kc/R_{90} versus c plot ($r^2 = 0.95$) (Figure 3). The molecular weight obtained for the derivative of the oxidation product (1.3×10^6) was the same as the value obtained for the humic acid derivative.

The reductively acetylated oxidation product was also examined with the SEC-LALLS-RI system. A symmetrical peak was observed for the LALLS response, and a non-symmetrical peak for the RI response (Figure 4). Somewhat lower values for the number average, weight average and z average molecular weights were calculated from these data ($M_n = 6.5 \times 10^5$, $M_w = 7.8 \times 10^5$, $M_z = 9.1 \times 10^5$).

These data indicate that by oxidatively cleaving the benzyl ether groups with the peracid, a substantial macromolecule is produced which is comparable in size to that obtained by simple base extraction of the lignite. This implies that there is some basic unit of this molecular weight making up the coal structure, and that in base extraction some of these units are released, whereas in peracid oxidation a large number of them are released by scission of cross-linking bonds.

Experimental

Humic acids were isolated from lignite from the Beulah mine in Mercer Co. ND (Beulah-Zap seam, Sentinel Butte formation, Fort Union Region) and methylated with dimethyl sulfate followed by diazomethane as described in reference 3. The methyl humate was reduced with zinc dust in acetic anhydride.

Oxidation of the lignite was carried out by refluxing 11 g of Beulah lignite with 12.4 g of 4-nitroperbenzoic acid in 150 ml of chloroform for 20 hours. The mixture was filtered while hot and the residue was extracted with hot methanol to remove the 4-nitrobenzoic acid. A 3.8 g portion of the residue was extracted with NaOH solution and the resulting solution was treated with dimethyl sulfate as in the preparation of methyl humates. The methylated product was acidified with HCl, centrifuged, and dried to give a 1.75 g yield of methylated oxidation product. This material was treated with diazomethane in DMF-ether followed by zinc dust in acetic anhydride to give 0.70 g of reductively acetylated methylated product.

Rayleigh scattering was measured with a KMX-6 LALLS photometer in THF solution. The dn/dc values were determined using a KMX-16 differential laser refractometer at several concentrations in THF solution. The size exclusion chromatography was carried out with a 30 cm by 7.5 mm 105 A PLgel column in THF at a sample concentration of 2 mg/ml. The KMX-6 LALLS photometer with a flow-through

cell and a Model 401 RI detector were used for measurement of the Rayleigh scattering and RI response of the effluent from the SEC column. Data were acquired at 3.5 points/sec for each detector. The LALLS and RI peaks were divided into 100 area slices each for calculation of the molecular weights.

References

1. "Basic Coal Sciences Project Advisory Committee Report", prepared by Science Applications, Inc. for Gas Research Inst., 1980, p. 4.1.
2. R. L. Wershaw and D. J. Pinckney, U.S. Geological Survey Jour. Research, 1 (1973) 361.
3. E. S. Olson and J. W. Diehl, J. Chrom., in press.
4. H.-P. Hombach, Fuel, 60 (1981) 663.
5. C. Gourlaouen and N. Petroff, Characterization of Heavy Crude Oils and Petroleum Residues, Symp. Intern., Lyon, (June 25-27, 1984).
6. H.-J. Schneider, A. Ahlhelm and W. Muller, Chem. Ber., 117 (1984) 3297.

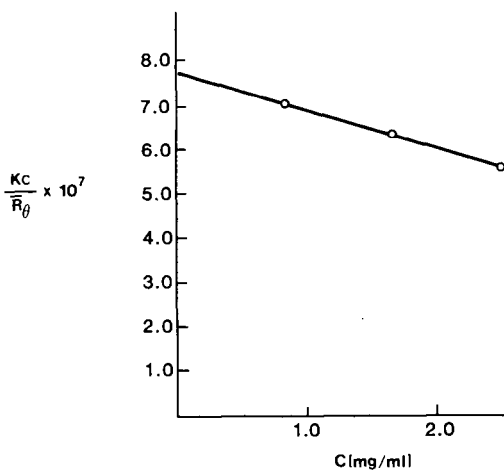


FIG. 1. Kc/\bar{R}_0 versus c plot for reduced methyl humate.

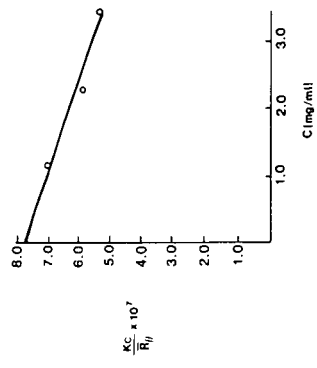


FIG. 3. Kc/\bar{R}_g versus c plot for reduced lignite oxidation product.

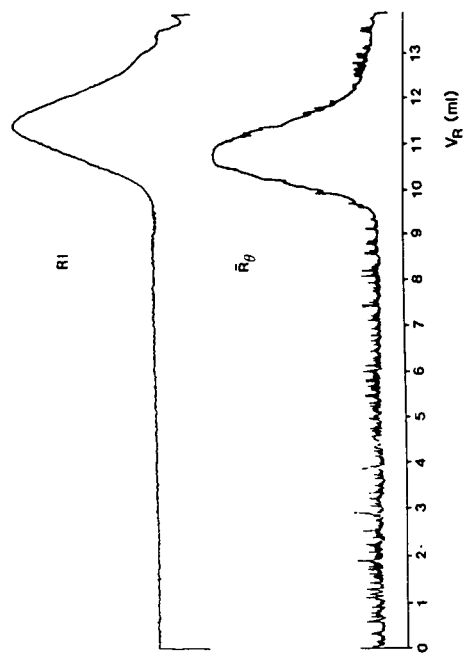


FIG. 2. SEC-LALLS of reduced methyl humate.

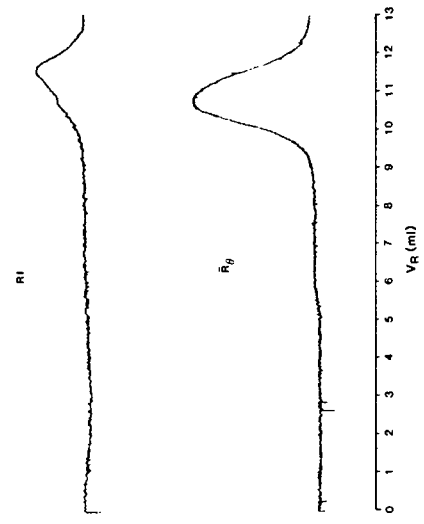


FIG. 4. SEC-LALLS of reduced lignite oxidation product.

FUNCTIONAL GROUP ANALYSIS OF COAL AND COAL PRODUCTS BY
X-RAY PHOTOELECTRON SPECTROSCOPY

David L. Perry and Alan Grint

BP Research Centre, Sunbury on Thames, Middlesex, TW16 7LN, UK.

The functional group composition of coal and coal products has a determining influence on their properties, affecting efficiency of utilisation. Also, it is well established that the oxidation which occurs when fresh coal is exposed to the atmosphere causes a marked deterioration in coal quality, affecting properties such as heating value, floatability and coking potential. The application of techniques such as Fourier transform infra-red (FTIR) spectroscopy and magic angle spinning nuclear magnetic resonance (NMR) spectroscopy has led, in recent years, to significant improvements in our understanding of the nature of carbon-oxygen functional groups in coal and the changes induced by different coal treatments.

In a number of technologies such as polymers and carbon fibres, where there is a similar interest in the nature of organic functional groups and their effect on material performance, the technique of x-ray photoelectron spectroscopy (XPS), also known as electron spectroscopy for chemical analysis (ESCA), has been applied successfully to a wide range of problems. However XPS is a technique which is little used in coal science. Since it has high surface sensitivity and the specific surface properties of coals play an important role in a number of coal technologies, e.g. floatation and agglomeration, it is perhaps surprising that XPS is not used more extensively. The reasons for this may lie in some of the discouraging references in the literature. For example early work by Frost et al (1) found no relationship between oxygen concentrations determined by XPS and the bulk analysis of a series of float-sink fractions. More recently Huffmann et al (2) observed that oxidation of bituminous coals for up to 383 days at 50°C in air completely destroyed Geiseler fluidity but neither XPS nor DRIFT (Diffuse Reflectance FTIR) spectroscopy could detect any parallel changes in the functional group composition of the coal.

This paper describes the application of XPS to coal, coal reactions and coal products. The aim is to present a critical evaluation in the context of other techniques which are applied to coal.

THE XPS TECHNIQUE

X-ray photoelectron spectroscopy is fully described in a number of reviews e.g. (3). It involves measurement of the kinetic energies of core and valence electrons photoemitted from a (usually) solid sample when irradiated by soft x-rays (normally Mg or AlK α). The experiment is carried out within a vacuum system (pressure < 1 x 10⁻⁵ Pa). Since core electrons have characteristic binding energies, the photoelectron spectrum provides an analysis for all elements except hydrogen and helium. The electrons detected are emitted only from the outermost 3-4nm of the solid; the analysis is therefore of a few atomic layers at the exposed surface. Different oxidation states or functional groups give rise to chemical shifts in the characteristic binding energies of contributing elements. For carbon (1s) spectra in coal the chemical shifts show themselves as a peak broadened to higher binding energy by the presence of different carbon-oxygen functional groups. The broadened spectra can be resolved into components corresponding to the functional group types which are assumed to contribute to the peak envelope. An example for a lignite C(1s) spectrum is given in Figure 1. The separation of the components depends upon the carbon oxidation state as follows: State CI (hydrocarbon) at 285eV, CII (singly bonded carbon-oxygen i.e. hydroxyl or ether) at 286.6eV, CIII (carbonyl) at 288eV and CIV (carboxyl, acid or ester) at 289.2eV (4). The positions of these components

relative to the principle hydrocarbon component are well established from model compound studies both reported in the literature and confirmed by the present authors.

Peak synthesis routines however do not provide a unique solution. Their accuracy is dependent on the suitability of transferring chemical shifts from simple model compounds to a more complex material. Uncertainty in peak synthesis arises from a lack of definition of the fundamental spectral lineshape for each component. Standard routines use Gaussian or Gauss/Lorentzian mixtures. Because of the aromatic nature of coal the fundamental lineshape is thought to be asymmetric but the precise shape has yet to be determined (5). The effect of using symmetric components rather than the correct lineshape, may be to exaggerate the concentration of carbon attached to oxygen, particularly in the CII state.

The most important features of XPS when compared with other instrumental techniques are:-

- 1) High surface sensitivity (information about the bulk of coal particles can be obtained by grinding to a smaller particle size).
- 2) Although different carbon-oxygen functional groups are not well-resolved, the constant sensitivity of XPS to the element rather than the functional group, means that functional group analysis is quantitative within the accuracy of the peak synthesis routine.
- 3) Quantitative functional group and elemental analysis in the same experiment allows validation of interpretation e.g. the changes in the carbon-oxygen functional groups can, in principle, be correlated with the oxygen concentration changes.
- 4) Functional group analysis can be applied to other elements of interest e.g. sulphur and nitrogen.

SURFACE COMPOSITION OF COALS

An example of the difference which can exist between the surface and bulk composition of coal particles, and hence the importance of appropriate sample preparation when using XPS, is illustrated in Table 1. The bituminous coal fines (particle size 500-38 μ) show very different surface compositions when examined as received, compared with the same material after grinding under heptane to <5 μ . The coal is clearly very heavily surface oxidised, having twice as much organic oxygen as the heptane ground exposed surfaces. Such differences between surface and bulk oxygen

TABLE 1: SURFACE ANALYSIS OF BITUMINOUS COAL BY XPS (% ATOM RATIOS)

<u>Element</u>	<u>As Received</u> (500 - 38 μ)	<u>Heptane Ground</u> (< 5 μ)
C	100	100
O Total	52	29
O Mineral	28	17
*O Organic	24	12
Si	10.0	6.3
Al	5.0	3.0

* Organic oxygen cannot be resolved from mineral oxygen. It is calculated by subtraction of mineral oxygen (calculated from Si and Al concentrations assuming stoichiometry SiO₂ and Al₂O₃) from the measured total oxygen concentration.

and the lack of correction for mineral oxygen, probably accounts for the poor XPS/bulk correlations obtained by previous authors (1). When a rank range of coals are prepared by grinding under heptane or under nitrogen just prior to analysis, a good correlation can be obtained between surface organic oxygen and bulk analysis (4). For a series of preasphaltenes the correlation for oxygen, sulphur and nitrogen is similarly good (6).

The distribution of oxygen between surface and bulk following weathering or deliberate oxidation is of particular significance for those coal technologies, such as froth flotation and oil agglomeration where surface properties govern the efficiency of the process.

THERMAL OXIDATION STUDIES

There has been considerable interest in recent years about the nature of carbon-oxygen functional groups introduced by thermal oxidation. FTIR studies have generally concluded that incorporation of oxygen as carbonyl or carboxyl groups is the dominant effect of oxidation (7,8).

We have previously shown (9) in XPS studies of the inhibition of Geiseler fluidity by oxidation, that exposure to air at 100°C causes predominantly a surface oxidation to occur and that oxygen is incorporated almost entirely as alcoholic or phenolic OH groups. This study has been extended by looking at the oxidation of Pittsburgh coal (<450 μ) in flowing air at three temperatures; 100, 150 and 200°C. Plots of the oxygen uptake by the surface and the bulk (revealed by heptane grinding after oxidation) are shown in Figure 2. A common feature of these data is the difference between the surface and bulk concentration of oxygen as the coal particle is oxidised. The concentrations diverge with time and the surface to bulk ratio is greater at the higher temperatures. At 100°C very little bulk oxidation of the coal is observed. It is clear that oxidation of these coal particles is diffusion limited at all three temperatures. This result appears to contradict the conclusions drawn by Chien et al (10) who concluded from FTIR-photoacoustic studies that oxidation of Illinois No 6 coal at 150°C was not diffusion limited. However this could be explained by differences in coal porosity, the Pittsburgh coal being mainly microporous.

Figure 3 shows the changes which occur in the carbon (1s) spectra on oxidation at 200°C. Evidence of carbon-oxygen groups formed is clearly visible on the high binding energy side of the peak; these being much more evident on the surface than in the bulk. The results of curve fitting the spectra are in Table 2. At all temperatures the formation of singly bonded species ie ether or OH groups, referred to as state CII in the peak synthesis, dominates in the early stages of oxidation. Even at 200°C, where carboxyl group formation is clearly favoured on the surface,

TABLE 2: CARBON (1s) PEAK SYNTHESIS OF OXIDISED PITTSBURGH COAL
(ATOM % TOTAL CARBON)

	Fresh Coal	Oxidised 100°C		Oxidised 200°C	
		48 hours		48 hours	
	Surface & Bulk	Surface	Bulk	Surface	Bulk
0 organic	8.7	11.0	10.2	38.6	20.0
CI	80.0	78.8	79.9	61.0	66.9
CII	12.3	12.7	12.0	20.0	17.0
CIII	2.0	2.4	2.0	5.3	2.8
CIV	1.6	1.6	1.5	7.7	4.7

the increase in carboxyl oxygen (2 x CIV) does not exceed greatly the increase in CII oxygen up to 48 hours of oxidation. This agrees with our previous results on temperature programmed oxidation of a bituminous coal (4), later confirmed by FTIR, that carboxyl group formation only became dominant above 200°C. The results from the most heavily oxidised coal indicate some limitations in the present methods of carbon (1s) peak synthesis since there is a lack of correlation between the oxygen increase and the carbon functional group analysis.

The results of our XPS study are in disagreement with previous FTIR studies. Painter et al (7) have reported that there is no evidence for OH formation on oxidation of a caking coal. In a subsequent study, on a different bituminous coal, Rhoads et al (8) report an initial increase in phenolic OH after ten hours at 140°C, though over 280 hours there is a decrease to a level below that of the fresh coal. In both cases the spectra are dominated by carbonyl and carboxyl peaks. NMR studies (11) of the same oxidised coal, however, showed no evidence for carbonyl or carboxyl group formation; changes involving oxygen incorporation were restricted to phenol formation up to 16 days at 140°C followed by condensation to form ethers at longer oxidation times.

The apparent disagreement between results from different techniques can be explained in general terms by the use of different coals, different oxidation conditions and the high sensitivity of FTIR spectroscopy to C=O groups. To resolve these differences there is a clear need to apply XPS, NMR and FTIR to an examination of the same samples of oxidised coal. The use of chemical derivatisation is likely to be an aid to spectral interpretation. An example of this combined approach applied to some preasphaltes will be described in a later section.

COAL OXIDATION BY WEATHERING

The laboratory simulation of the effects of weathering on the chemistry of coal is usually carried out by thermal oxidation i.e. exposure of beds of coal to air at an elevated temperature. Unlike weathering studies of polymer films and coatings, the influence of photoinduced reactions through exposure to light are not generally considered. This is probably realistic for simulation of weathering on stockpiled coal where the surface area of coal exposed to light is negligible. The effect of light does however have potential consequences for the storage of small quantities of coal for laboratory experiments, particularly when surface properties are being investigated.

The effect of daylight on the oxygen content of exposed coal surfaces has been tested by taking a sample of Pittsburgh No 8 coal, ground under heptane, and mounted on a sample probe for analysis by XPS. Before analysis the sample was exposed to a north facing window for a period of five days at an ambient temperature of 18°C. The changes induced by this exposure to diffuse sunlight are presented in Table 3. The degree of surface oxidation is substantial; oxygen is incorporated into the surface at a level not reached after 24 hours oxidation at 150°C. The peak fitting shows significant increases in all oxygen groups, with substantial formation of OH and carboxyl groups.

TABLE 3: CARBON (1s) PEAK SYNTHESIS OF 5 PITTSBURGH COAL EXPOSED TO DAYLIGHT FOR FIVE DAYS (ATOM % TOTAL CARBON)

	<u>Fresh</u>	<u>Exposed</u>
O Organic	8.7	23.3
CI	80.0	72.6
CII	12.3	14.9
CIII	2.0	3.5
CIV	1.6	5.0

FUNCTIONAL GROUP ANALYSIS OF PREASPHALTENES BY DERIVATISATION

Derivatisation of OH groups by acetylation is a widely used technique to enhance the sensitivity and resolution of infra-red spectroscopy. It can also be used in XPS to enable the discrimination of OH from ethers in the CII state by conversion of OH groups to esters (CIV). We have applied this technique to preasphaltenes in the first instance since the reaction can be carried out in solution. This avoids problems of selective extraction when solid coals are treated with organic solvents.

Preasphaltenes (THF soluble, toluene insoluble) obtained from a bituminous coal in tetralin and hydrogen were acetylated at 40°C for 24 hours using pyridine and acetic anhydride. The resultant solution was rotary evaporated to dryness using toluene and dried in a vacuum oven. Table 4 shows the data obtained from peak synthesis of the carbon (1s) envelope, revealing the nature of the surface groups of an acetylated and unacetylated preasphaltene. The increase in the CIV carbon state (3.6%) of the derivatised sample shows that acetylation has occurred. This is in reasonable agreement with the observed increase in organic oxygen (4.7 O/C atomic %). As expected no increase was observed in the CII carbon state (singly bonded carbon-oxygen), though a reduction in carbonyl was a reproducible feature.

TABLE 4: CARBON (1s) PEAK SYNTHESIS OF ACETYLATED PREASPHALTENE
(Atom % Total Carbon)

	<u>Preasphaltene</u>	<u>Acetylated Preasphaltene</u>
Oxygen	10.8	15.5
CI	77.9	72.3
CII	14.4	14.9
CIII	1.9	1.1
CIV	1.5	5.1

In order to evaluate the XPS data obtained from this experiment a series of preasphaltenes were analysed and quantified using four techniques in parallel: (XPS, FTIR (12) and ¹³C NMR) on acetylated preasphaltenes, plus enthalpimetric titrations (13) on the original preasphaltenes. Table 5 reports the results obtained. All techniques are in reasonable agreement validating the use of XPS to give a quantitative assessment of the hydroxyl content in carbonaceous materials. Generally the enthalpimetric technique gives the highest value for oxygen as hydroxyl whereas FTIR and XPS gave similar but lower values. The good agreement between the different techniques suggests that combined FTIR, NMR and XPS studies of acetylated coals after oxidation might resolve some of the existing differences in the literature.

TABLE 5: OXYGEN AS OH IN PREASPHALTENES MEASURED BY NMR, FTIR, XPS AND ENTHALPIMETRIC TITRATION

<u>Sample</u>	<u>Analysis</u>	<u>Oxygen as OH Relative to C = 100</u>			
		<u>NMR</u>	<u>FTIR</u>	<u>Titration</u>	<u>XPS</u>
1	C ₁₀₀ H ₈₇ O ₉	5	4.5	5.4	4.0
2	C ₁₀₀ H ₈₃ O ₈	3	3.8	5.0	3.8
3	C ₁₀₀ H ₇₆ O ₅	3	3.0	3.9	3.1

NITROGEN GROUPS IN COAL

Although the role of nitrogen in coal is not thought to be of direct importance in determining coal properties, there is interest in determining the fate of nitrogen

during combustion or liquefaction. This requires identification of the nitrogen functional group type at each processing stage. Previous work had shown that the nitrogen (1s) peak in coal could be resolved into two components corresponding to pyrrole and pyridine type groups (14). We have confirmed this model and shown that over the rank range of coals the preparation of each component remain approximately constant at around 2:1 pyrrole to pyridine. Carbonisation increases the proportion of pyridine groups.

Examination of some chemically separated asphaltene fractions has validated the analysis of the N(1s) peak by showing that in basic fractions the pyridine type groups are the major component (15). Examples of the spectra are shown in Figure 4. The asphaltene has a similar nitrogen group distribution as the parent coal.

Assignment of the pyridine component has been further supported by derivatisation experiments to form the pyridinium ion. This species can be readily distinguished by XPS (15).

CONCLUSIONS

These studies have demonstrated that XPS has specific and unique advantages for the examination of coal surfaces. Determination of the carbon-oxygen functional group chemistry at coal particle surfaces should enable a better fundamental understanding of many coal beneficiation and utilisation processes. However when proper consideration is given to sample preparation XPS can also contribute to improvements in our fundamental understanding of bulk coal chemistry. Developments are required to improve the accuracy of curve resolution methods, probably involving chemical derivatisation. Studies of Pittsburgh No 8 oxidation have revealed the distribution of oxygen and carbon-oxygen species between surface and bulk and have indicated the importance of OH group formation during oxidation. In several respects XPS can be seen to complement more conventional spectroscopies. This applies especially to sulphur and nitrogen functional group chemistry in which there is increasing interest due to environmental pressures. XPS is likely to be one of the more useful spectroscopic techniques for looking at these groups and their reactions during utilisation.

ACKNOWLEDGMENTS

Permission to publish this paper has been granted by the British Petroleum Company plc.

REFERENCES

- (1) Frost, D.C., Leeder, W.R. and Tapping, R.L., *Fuel*, 53, 206, (1974).
- (2) Huffmann, G.P., Huggins, F.E., Dunmyre, G.R., Pignocco, A.J. and Lin, M.C., *Fuel*, 64, 89, (1985)
- (3) PRACTICAL SURFACE ANALYSIS BY AUGER AND X-RAY PHOTOELECTRON SPECTROSCOPY, edited by Briggs, D. and Seah, M.P., John Wiley, (1983).
- (4) Perry, D.L. and Grint, A., *Fuel*, 62, 1024, (1983).
- (5) Cheung, T.T.P., *J. Appl. Phys.* 55, 1388, (1984).
- (6) Perry, D.L. and Grint, A., Unpublished Work.
- (7) Painter, P.C., Coleman, M.M., Snyder, R.W., Mahajan, O., Komatsu, M. and Walker, P.L., *Appl. Spectrosc.* 35, 106, (1981).

- (8) Rhoads, C.A., Senftle, J.T., Coleman, M.M., Davis, A. and Painter, P.C., *Fuel*, 62, 1387, (1983).
- (9) Grint, A. and Perry, D.L., Proceeding of 1985 International Conference on Coal Science, Sydney, Australia, 1985, p 879.
- (10) Chien, P.L., Markuszewski, R. and McClelland, J.F., ACS Division of Fuel Chemistry Preprints, 30 (1), 21 (1985).
- (11) Havens, J.R., Koenig, J.L., Kuehn, D., Rhoads, C.A., Davis, A. and Painter, P.C., *Fuel*, 62, 936, (1983).
- (12) Snyder, R.W., Painter, P.C., Havens, J.R. and Koenig, J.L., *Appl, Spectrosc.* 37, 497, (1983).
- (13) Vaughan, G.A. and Swithenbank, J.J., *Analyst*, 95, 890, (1970).
- (14) Jones, R.B., McCourt, C.B., and Swift, P., Proceedings of International Conference on Coal Science, Dusseldorf, 1981, p 657.
- (15) Bartle, K.D., Perry, D.L., and Wallace, S., Paper to be presented at First International Rolduc Symposium on Coal Science, The Netherlands 1986.

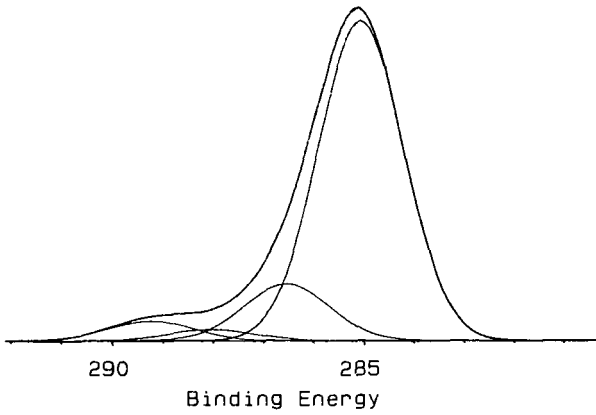


FIG 1. EXAMPLE OF C(1s) PEAK SYNTHESIS FOR A LIGNITE

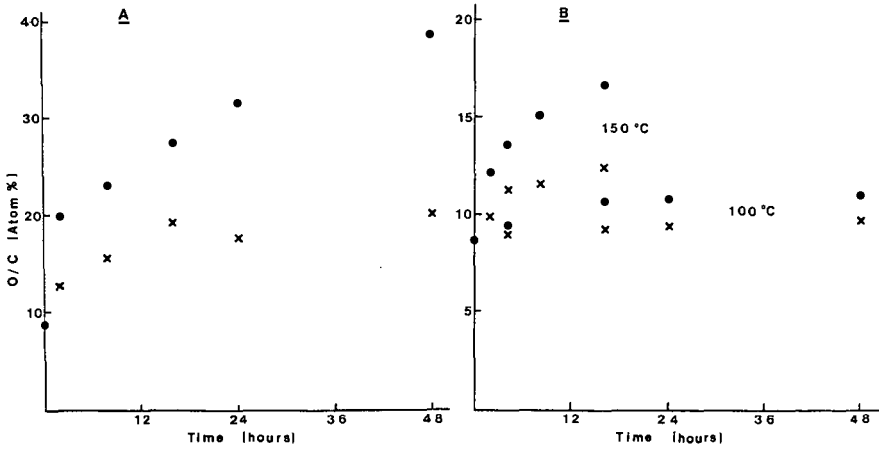


FIG 2. CHANGES IN ORGANIC OXYGEN CONCENTRATION FOR OXIDISED PITTSBURGH COAL: A-200°C, B-150 AND 100°C, ● - SURFACE, x - BULK.

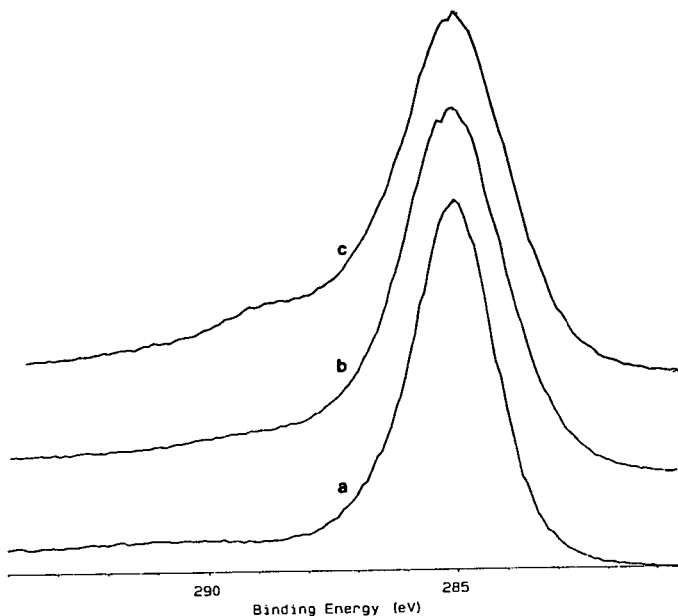


FIG 3: COMPARISONS OF C(1s) SPECTRA OF PITTSBURGH COAL OXIDISED AT 200°C
 a) INITIAL COAL, b) OXIDISED 48 HOURS - BULK, c) OXIDISED 48 HOURS - SURFACE .

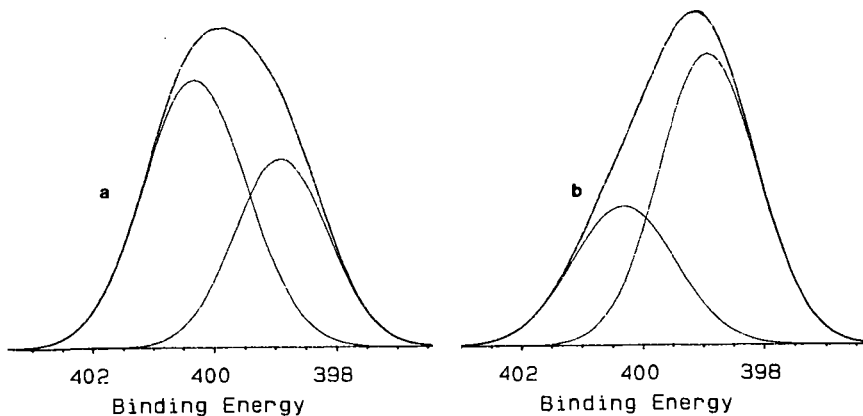


FIGURE 4: N(1s) SPECTRA OF a) ASPHALTENE, b) BASIC FRACTION OF ASPHALTENE (PYRIDINE COMPONENT AT 398.8eV, PYRROLE COMPONENT AT 400.2eV).

RAPID DETERMINATION OF NITROGEN IN COAL

Richard Markuszewski

Iowa State Mining and Mineral Resources Research Institute

Iowa State University, Ames, IA 50011

and

Scott V. Brayton

Hach Company, Ames, IA 50010

ABSTRACT

A simple and rapid colorimetric method for the determination of total nitrogen in coal has been developed. The method is based on the rapid digestion of the coal sample with a mixture of 50% hydrogen peroxide plus concentrated sulfuric acid and subsequent color development with Nessler's reagent for the determination of ammonium nitrogen. In this procedure, 250 mg of finely ground coal are digested within 30 minutes by heating with 25-60 ml of a 4:1 mixture of H_2O_2 - H_2SO_4 in a special Digesdahl® apparatus. After boiling to destroy excess hydrogen peroxide and cooling, subsequent color development and spectrophotometric measurement at 460 nm take only about 5 minutes. Application of this procedure gave good results for the nitrogen values of two NBS coal samples and reasonably good agreement for Illinois and Iowa (run-of-mine and physically and chemically cleaned) coal samples analyzed by a modified Kjeldahl procedure.

INTRODUCTION

The determination of total nitrogen in coal is usually performed by ASTM Method D-3719 (1) or by using commercial C, H, N, analyzers. The former procedures are based on the time-honored Kjeldahl method, involving long digestion times, difficult distillations, and tedious titration finishes. The fact that the literature is extensive (2) on various modifications of the Kjeldahl method for nitrogen in coal points to the inadequacies which plague this difficult but necessary procedure. The instrumental methods, on the other hand, require fairly expensive apparatus and may suffer in accuracy because the very small sample sizes combusted could be not too representative of the entire batch.

Recently, the determination of organic nitrogen has been simplified by a rapid and reliable procedure for digesting agricultural samples (3). The digestion is readily accomplished in a simple apparatus by the powerful mixture of hydrogen peroxide and sulfuric acid, and the final measurement is made spectrophotometrically using Nessler's reagent. Most of the necessary digestion parameters have been already established in that work.

The utility of this simple apparatus has been also demonstrated on the rapid digestion of coal samples by a mixture of nitric, phosphoric, and perchloric acids for the subsequent determination of sulfur and iron in coal (4). Because of the success of this method on agricultural samples and because of the ease of using the digestion apparatus, this work was undertaken to apply it to the determination of total nitrogen in coal.

EXPERIMENTAL

Coal Samples

The three coals in sample series 101-304 were high volatile C bituminous coals. The ROM Illinois No. 6 coal came from the Elm Mine, near Trivoli, Illinois. The Iowa coal in the series 201-204 was freshly mined near Lovilia, Monroe County, Iowa, and subsequently cleaned at the Iowa State University coal preparation research facility, using a heavy-media (magnetite) process at 1.3 sp. gr. The ROM coal in the series 301-304 came from the same region in Iowa but it was stored in the laboratory for a prolonged period; thus it was probably heavily oxidized. The chemical desulfurization treatment consisted of leaching with hot Na_2CO_3 solutions containing oxygen under pressure. Subsequent extractions were conducted with boiling 1:7 HNO_3 for 30 minutes. Further description of these samples and chemical treatments is provided elsewhere (5).

Sample No. 500 was an Upper Freeport coal provided by the Massey Coal Co., Inez, Kentucky. The NBS samples were obtained from the National Bureau of Standards.

Apparatus

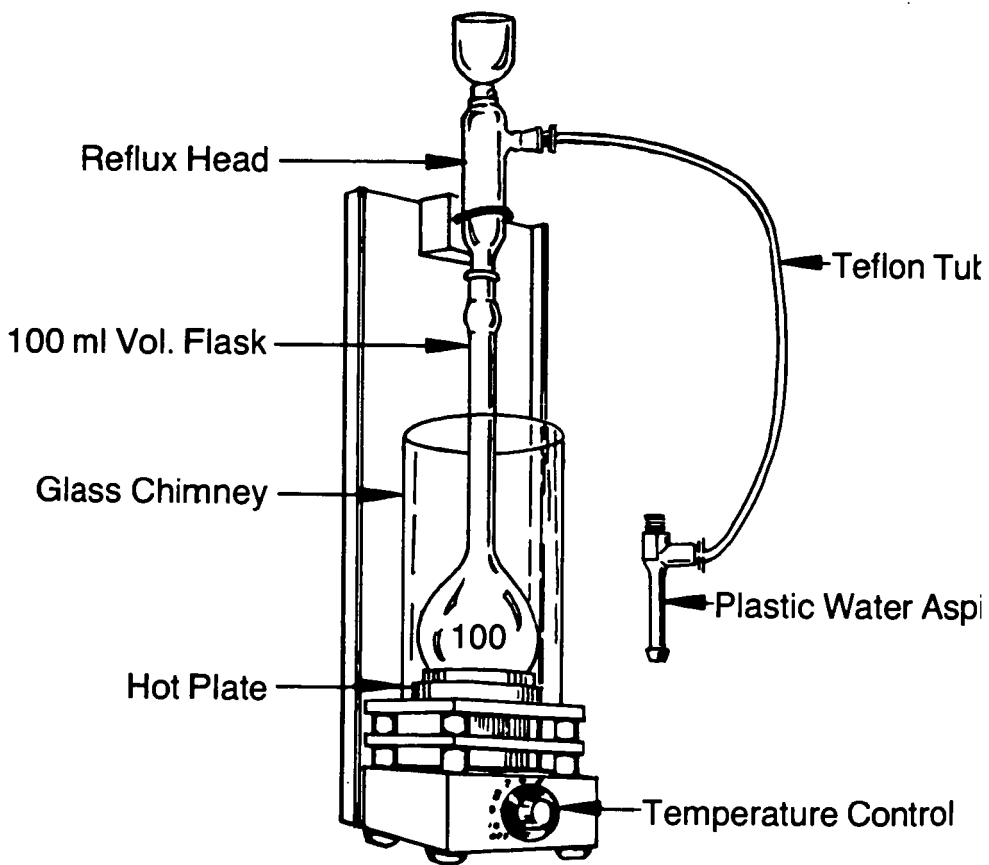
The samples were digested in a Hach Model 21400 Digesdahl® apparatus consisting of a heating unit, a 100-ml volumetric flask, surrounded by a glass chimney to diminish heat loss and thus reduce the digestion time, and a reflux head manifold at the top of the flask, connected via a Teflon tube to a plastic water aspirator to remove fumes. This simple and inexpensive apparatus is depicted in Fig. 1. The 25-to-250 watt disc-element heater is supplied with a solid-state controller. The colorimetric measurements were made at 460 nm with a Hach Model DR/2 single-beam spectrophotometer using a 2.5-cm flow-through cell.

Reagents

The digestion mixture was premixed using 4 parts of 50% hydrogen peroxide and 1 part concentrated sulfuric acid. CAUTION: This reagent is a powerful oxidizer and should be handled very carefully. However, it is stable during prolonged storage. The Nessler's reagent and the polyvinyl alcohol (as a 0.1 g PVA solution per liter) were obtained from the Hach Company.

Digestion Procedure

A weighed sample (~250 mg) of finely ground coal (60 mesh) is placed in the 100-ml volumetric flask. (As a convenience, the sample can be weighed onto a piece of plastic kitchen wrap which is then folded up and pushed down the neck of the flask). About 4-5 ml of concentrated H_2SO_4 is added to the flask, the flask is placed on the heater, and the reflux head manifold is attached to the top of the flask and connected to a water aspirator. The mixture is digested for ~5 min. at a medium-to-high setting to carbonize the sample, until the H_2SO_4 solution refluxes to the top of the head. The flask is then removed from heat, allowed to cool for ~2 min., and ~20 ml of the 4:1 H_2O_2 - H_2SO_4 digestion reagent is cautiously added through the side arm funnel of the manifold. (If the addition is too fast, some spattering may occur.) The flask is returned to the heater for further digestion. After ~5 min., more of the reagent can be added through the side arm and boiling is continued until the solution is fairly clear. Additional boiling for ~5 min. is then required to remove excess H_2O_2 , until refluxing of H_2SO_4 is observed. The



DIGESDAHL DIGESTER

Fig. 1. Digesdahl apparatus for rapid digestion of coal samples.

digested sample is then removed from the heater, cooled, and diluted to the 100-ml mark with deionized water.

Spectrophotometric Measurements

A 0.5-ml aliquot of the diluted digestate is pipetted into a 25-ml mixing cylinder and diluted to mark with the 0.1 g/L PVA solution. Then 1.0 ml of Nessler's reagent is added, and the cylinder is stoppered and inverted several times to mix the contents. The mixture is poured immediately into the flow-through cell of the spectrophotometer that has been zeroed and standardized with the 0.1 g/L PVA solution at 460 nm, and the % transmittance is read to determine the nitrogen level from a standard calibration curve.

Calibration Procedure

The calibration standards can be conveniently prepared using Voluette Ampule Standards for ammonium nitrogen (160 mg N/L) in the amounts of 0.01, 0.2, 0.3, and 0.4 ml. To each, 0.5 ml of a blank digest is added and dilution to 25.0 ml is made with the PVA solution. After addition of 1.0 ml of Nessler's reagent to each mixing cylinder, the % transmittance is measured as above. The standards represent 0, 0.64, 1.28, 1.92, and 2.56 mg of N/L which corresponds to 0, 1.28, 2.56, 3.84, and 5.12% N in coal, respectively.

RESULTS AND DISCUSSIONS

The percent nitrogen values determined by this new method for various coal samples are presented in Table 1. In most cases, there is reasonable agreement between these values and conventionally determined values. Except for samples 101 and NBS 1635, the nitrogen values obtained by this method are slightly lower in every other case. This "apparent loss" needs to be studied further in order to decide which method is subject to a possible systematic error. The precision of our method, as illustrated by the results in Table 2, appears to be good. But there may be sources of error which could be eliminated or minimized in order to bring our results in closer agreement with conventional results.

Of course, the coal samples in series 101-304 are very unusual in that they have been chemically treated and probably nitrated during the extraction with nitric acid. The effect of such chemical alteration of coal samples on the determination of nitrogen by this method needs to be examined.

CONCLUSIONS

The simple and rapid digestion of organic samples with a 4:1 mixture of $H_2O_2-H_2SO_4$, previously developed for protein nitrogen in agricultural samples, has been adapted for the determination of total nitrogen in coal. The digestion is usually complete within 30 minutes, and the subsequent spectrophotometric measurement after Nesslerization requires about 5 minutes. The results of this method agree reasonably well with those of conventional methods. Although the precision is good, the absolute values are slightly lower than those obtained by Kjeldahl procedures, pointing to the necessity of further research to minimize this discrepancy. The clear digestate could be possibly used for additional analyses for such elements as phosphorus, calcium, magnesium, and other metals.

Table 1. Total nitrogen values in various coal samples, determined by conventional methods and by the new method described.

Sample No.	Coal Description	% Nitrogen Sample	
		Conventional ^a	New Method
101	Illinois No. 6 coal, ROM	0.82	0.90 ^b
102	#101 after chemical desulfurization	0.93	0.90
103	#101 after HNO ₃ extraction	4.26	3.91
104	#102 after HNO ₃ extraction	3.66	3.42

201	Iowa coal (ISU precleaned)	1.31	1.20
202	#201 after chemical desulfurization	1.43	1.17
203	#201 after HNO ₃ extraction	4.63	4.23
204	#202 after HNO ₃ extraction	3.73	3.45

301	Iowa coal, ROM	1.15	0.85
302	#301 after chemical desulfurization	1.17	0.84
303	#301 after HNO ₃ extraction	3.74	3.55
304	#302 after HNO ₃ extraction	3.43	2.99
500	Upper Freeport	1.30	1.27 ^c
NBS 1632a	Penn Seam Bituminous	1.27	1.26
NBS 1635	Colorado Subbituminous	1.0-1.3	1.38

^a Conventional N values for the series 101-304 were provided by a modified Kjeldahl method in which 1.8 g of coal was digested with HgSO₄ catalyst at about 390-400°C. Sample 500 was analyzed by a commercial laboratory using an ASTM procedure. Values for the NBS coals were obtained from a literature compilation study (6).

^b Average of triplicate determinations.

^c Average of duplicate determinations.

Table 2. Reproducibility of nitrogen determinations by new method described.

Sample No.	Description	% Nitrogen	
		Replicate Detns.	Average
101	Same sample as in Table 1	(0.92, 0.89, 0.90)	0.90
500	Same sample as in Table 1	(1.23, 1.31)	1.27
NBS 1635	Different split, analyst, and time than in Table 1	(1.24, 1.26, 1.32)	1.28

ACKNOWLEDGMENTS

This work was supported, in part, through a Research Grant from the Hach Company. Special thanks are due to Professor Mark H. Love, Department of Food and Nutrition, for supplying the modified Kjeldahl analyses, and to Glenn A. Norton and Neal Adams for technical assistance.

LITERATURE CITED

1. 1984 Annual Book of ASTM Standards; Section 5, Petroleum Products, Lubricants, and Fossil Fuels, ASTM, Philadelphia, PA.
2. See, for example, R. B. Bradstreet, The Kjeldahl Method for Organic Nitrogen, Academic Press, New York, 1965.
3. C. C. Hach, S. V. Brayton, and A. B. Kopelove, "A Powerful Kjeldahl Nitrogen Method Using Peroxymonosulfuric Acid," J. Agricultural and Food Chemistry, 1985 (in press).
4. R. Markuszewski, B. C. Wheeler, R. S. Johnson, and C. C. Hach, "Rapid Dissolution of Coal for Analysis for Sulfur, Iron, and Other Elements," Am. Chem. Soc. Div. Fuel Chem. Preprints, 28(4), 292 ff. (1983).
5. R. Markuszewski, L. J. Miller, W. E. Straszheim, C. W. Fan, T. D. Wheelock, and R. T. Greer, "Evaluation of the Removal of Organic Sulfur from Coal," in New Approaches in Coal Chemistry, B. D. Blaustein, B. C. Bockrath, and S. Friedman, eds., American Chemical Society, Washington, D. C., 1981, pp. 401-414.
6. E. S. Gladney, Compilation of Elemental Concentration Data for NBS Biological and Environmental Standard Reference Materials, Report No. LA-8438-MS, Los Alamos Scientific Laboratory, July, 1980.

CHEMISTRY OF COAL FROM ELECTRON MICROSCOPY MEASUREMENTS

C. A. Wert, K. C. Hsieh and H. Fraser

Department of Metallurgy and Mining Engineering
and Materials Research Laboratory
University of Illinois at Urbana-Champaign
1304 West Green Street
Urbana, Illinois 61801

ABSTRACT

Well established techniques of analytical electron microscopy have applications to the chemistry of coal. The techniques use one or another of several interactions which occur when electrons are incident on a specimen. Two such interactions are discussed in this paper: 1: X-ray emission spectroscopy and 2: Electron energy loss spectroscopy. Both methods are used in the study of metallic and ceramic systems. The principles of the technique are illustrated by applications to metallic and ceramic systems; initial applications to coal are then described.

INTRODUCTION

Many interactions occur when electrons are incident upon a solid. X-ray and optical photons may be emitted, electrons may back-scatter, secondary electrons may be emitted and changes in energy of transmitted electrons may occur for thin specimens. These phenomena have been utilized in the electron microprobe, the scanning electron microscope, in other electron and photon spectroscopic instruments and in the transmission electron microscope. We consider two of these spectroscopies in this paper: utilization of the characteristic x-ray lines from atoms in the solid and measurement of the loss-of-energy of the transmitted electrons when ionizing collisions are made with atoms in a thin foil.

The use of x-ray emission spectroscopy has been made extensively using the electron microprobe and the scanning electron microscope. In that case, a thick specimen is used in which the electrons are stopped in the specimen. Characteristic x-ray lines from specific atoms in the solid are counted either with a crystal detector or with an energy dispersive detector to deduce the composition of the solid. This technique has been applied extensively to metals and alloys (1-5) and also for determination of the organic sulfur content of coal (6-10). That application has been generally successful. Calibration of the system has been made using known sulfur-bearing standards. Such calibration requires that a matrix of about the composition of coal must be used since fluorescence and absorption corrections are significant. Fortunately, a single calibration constant applies to all coals without much error.

The biggest difficulty with these measurements is the relatively large volume of material from which the x-rays come. Because of electron scattering and fluorescence, the volume of measurement is about $100 \mu\text{m}^3$. Thus, homogeneity in the specimen over this volume must exist for the measurement to be reliable. For measurement of organic sulfur in coal, this has posed some problems, since one can never be sure that small sulfide particles may not

exist under the surface, unseen by examination of the surface features. Procedures have been established by a number of investigators to circumvent this problem.

This technique has been heavily exploited by mineralogist and extensive procedures have been developed to make quantitative measurement of the mineral concentrations in ores (11-14). This technique also has been used for pyrite in coal using programmed scanning of polished surfaces.

We have developed techniques of transmission electron microscopy for examination of minerals in coals (15-17) and also for examination of the concentration of organic elements in coal. Principles of these techniques are described in the next section and applications are presented for measurement of sulfur, chlorine and other organic constitutions of coal.

X-RAY EMISSION SPECTROSCOPY

Chemical analysis using emission spectroscopy is based on the measurement of characteristic $K\alpha$ or $L\alpha$ lines upon excitation with incident electrons. In transmission electron microscopy the detector is almost always an energy-dispersive detector with a resolving power of about 150 eV. This limits the detectability of adjacent elements in the periodic table, but the variety of elements present in coal is so small that no serious difficulty arises from this source. A schematic of the apparatus is sketched in Fig. 1. The spectrum displayed in the multi-channel analyzer consists of two parts, characteristic lines of the elements present and a background radiation. The background is utilized in the quantitative determination of concentration of elements present, since it can be used to deduce the volume of the specimen. A sketch of a typical spectrum for sulfur is shown in Fig. 2.

The quantitative determination of the concentration of organic elements present in the specimen depends on a method developed for biological materials by Professor T. Hall and his colleagues (18-21). The count rate for the $K\alpha$ line of sulfur is proportional to the number of sulfur atoms in the volume. Hall showed that the volume from which that radiation came could be conveniently measured by simultaneously counting the background counts -- it is known that the background (or bremsstrahlung) count rate is proportional to the total number of atoms in the volume, the radiation from each type of atom being weighted according to its atomic number. The weight percent of sulfur in the volume is proportional to the ratio of the count rate for sulfur divided by the count rate for the bremsstrahlung radiation.

$$S \text{ (wt \%)} = A C_S/C_b$$

The measurement is therefore a simple one -- the concentration of sulfur in the specimen is given by the ratio of two count rates which can be measured in a few minutes of counting time in the electron microscope.

We have developed this system and made three principal applications to coal, oil shale and amber:

1. The technique can be used to measure the average organic sulfur concentration in fuels (16). Since the organic sulfur content varies among the maceral types, it is necessary to average the measurements over a number

of independent determinations to get a good mean value. We have found that 50 measurements over random spots in a coal specimen is sufficient; Raymond has noted that only 15 measurements are needed in his SEM method, if the measurements are made over only vitrinite macerals. A plot showing measurements on four coals using our TEM method compared with standard ASTM measurements is shown in Fig. 3.

2. The TEM method is valuable to measure variation of organic sulfur content among maceral types: the general variation had been known from earlier measurements, but the TEM method shows finer variation than is possible by gross techniques.

3. We have followed the loss of organic sulfur during heating of coal. Our measurements of loss of sulfur were made for inert, oxidizing and reducing atmospheres.

OXYGEN: Determination of the oxygen content of coal by standard methods is a complex chemical analysis. In principle, the same x-ray technique we have used for sulfur might be used to determine the oxygen content directly. The main difficulty is that the $K\alpha$ x-ray line of oxygen comes at 535 eV, compared with the value of 2300 eV for sulfur. Consequently absorption problems in the detector window are much more severe for oxygen.

Even so, we have made such a measurement using window-less detector on a Philips 420 microscope. An example is given in Fig. 4. We can observe both the oxygen line and the carbon line on the same scan and thus have the possibility to compare their magnitudes to get a general notion of the relative concentration of these two elements.

In practice, the measurement is extremely difficult. The weak lines of oxygen and carbon are absorbed by the matrix. Even more, oxygen and carbon come on opposite sides of the C $K\alpha$ absorption edge: oxygen is on the high absorption side. Therefore, absorption corrections must be made even for the thinnest coal samples. Even more, surface contamination of the specimen may produce additional absorption of the two x-ray lines. Therefore, the measurement is not straightforward. Even so, using polymeric films as standards, we have made measurements on macerals of vitrinite; we are also in process of making measurements on fusinite and resinite. Clearly this technique is expensive enough that it will not be heavily used for oxygen analysis routinely. However it does offer the possibility of mapping out variations in oxygen content of coals from maceral to maceral and of measuring the spatial variation of oxygen within a given maceral.

ENERGY LOSS SPECTROSCOPY

Electrons passing through a solid make both elastic and inelastic collisions with the electrons in the material. The elastic collisions have important uses in diffraction and other features of examination of materials. However, the inelastic collisions also produce a beam of electrons containing important information. In the last twenty years, a spectroscopy termed ELECTRON-ENERGY-LOSS-SPECTROSCOPY (EELS) has come to be recognized as an important tool in study the chemistry of solids. A number of excellent review papers exist (22,23) and an enormous number of examples of application of the techniques to studies of the physics and chemistry of alloys and compounds has

been published. Consequently only a few examples will be given here to show the general characteristics of the technique and the potential for its application to the study of the chemistry of the coal and other hydrogen carbon materials.

The study of the chemistry of light elements in solids by EDAX uses rather low energy x-rays -- from perhaps 250 to 3000 eV. The x-ray detecting systems are attuned to that energy range. The energy loss spectroscopic techniques, on the other hand, use the high energy range of the incident electron beam, since the composition of the specimen is deduced from the high-energy part of the loss spectrum; i.e., the accelerating voltage of the microscope (typically 100 keV) minus the inelastic collision energies of a few hundred to a few thousand eV. This requires quite a different spectroscopy.

In practice, energy loss spectroscopy has utilized either electrostatic or magnetic means for separating the transmitted beam of electrons into energy regimes which reflect the elemental composition of the material. A typical instrumental scheme is sketched in the lower half of Fig. 1. There the transmitted electrons are separated into two groups, one a group of electrons which have traversed the specimen suffering no inelastic collisions, the other a group of electrons which have suffered an inelastic collision of energy ΔE . The increment of energy loss is typically in the range of a few hundred to a few thousand eV.

A great many studies have been made on metals, alloys and compounds. Details of these studies can be seen by the examination of the many reviews and original papers. However, we present two studies to show the power of the technique.

The first study is an examination of the alloy system V + 5%Ti + a small amount of carbon. When heat treated appropriately an extremely fine precipitate of a vanadium-titanium-carbide forms in a vanadium matrix. A micrograph of that precipitate is shown in Fig. 5. Spectra for the vanadium solid solution and for the carbide are shown in Fig. 6 superimposed on each other. The matrix of vanadium shows a strong vanadium absorption peak for the L edge at 520 eV. A small carbon edge is seen at about 285 eV. The L edge of vanadium is lost in the background at 460 eV. The same spectrum for the beam focused on the precipitate shows very clearly all three elements, the vanadium L edge the titanium L edge and the carbon K edge.

The analysis of this spectrum combined with analyses made by an x-ray emission spectrum of the same carbides and additional diffraction measurements gave the complete solution to this microstructure. The precipitate is a structure of vanadium-titanium-carbide of composition about VTi_4C_5 . This is a hexagonal carbide whose basal plane rests against the (110) plane of the vanadium matrix. The successful analysis of this material was made possible by the combined spectroscopies and diffraction techniques available in a modern analytical electron microscope (24).

A second example from our laboratory was based on an analysis of a precipitate in a crystal of titanium diboride, TiB_2 . An electron micrograph of that specimen showed a matrix containing some precipitates on well defined crystal planes (25). Energy loss spectra of both the titanium diboride matrix and the precipitate are shown in Fig. 7. The pertinent lines come at energies

of 460 eV for the L edge of Ti, 284 eV for the K edge of C and 188 eV for the K edge of B. This analysis shows that the precipitate is titanium-carbide embedded in titanium-diboride. Further diffraction analysis in the microscope showed that the carbide is an FCC structure embedded in a hexagonal matrix of the diboride. The geometry of the matching plane has also been deduced by these investigators.

Many other measurements might be cited to show the power of this effect. We have made energy loss spectra of coal and can observe the carbon and oxygen K absorption edges. An example is shown in Fig. 8. A great deal more work will be required to put this on a quantitative basis since the absorption edge for oxygen is barely visible for the short counting time used in this feasibility measurement. However, techniques are improving rapidly, and this surely means that the application is possible.

SUMMARY

Spectroscopic methods using both emission and absorption characteristics of the interaction of electrons with atoms in a solid are common in metallurgy and ceramic investigations. Each has unique characteristics and applications, but they are even more powerful when they are used in combination. Analytical electron microscopy is in its infancy for coal and oil shale, but the potential is plainly evident.

ACKNOWLEDGEMENT

The authors acknowledge support from the Division of Materials Science, DOE, under contract DEAC02-76-1198.

REFERENCES

1. Petric, A. and Jacob, K. T., Met. Trans., 16A, 503-510 (1985).
2. Brown, J. M. and Sekhar, J. A., Met. Trans., 16A, 29-31 (1985).
3. Kaufman, M. J. and Fraser, H. L., Acta Met., 33, 191-203 (1985).
4. Konitzer, D. G., Muddle, B. C. and Fraser, H. L., Met. Trans., 14A, 1979-1988 (1983).
5. Kaufman, M. J., Fades, J. A., Loretto, M. H. and Fraser, H. L., Met. Trans., 14A, 1561-1571 (1983).
6. Sutherland, J. K., Fuel, 54, 132-134 (1975).
7. Solomon, P. R. and Manzoine, A. V., Fuel, 56, 393-396 (1977).
8. Straszheim, W. E., Greer, R. T. and Markazuszewski, R., Fuel, 62, 1070-1075 (1983).
9. Raymond, R. Jr. and Gooley, R., Scanning Electron Microscopy /1978/I, 93-107 (1978).
10. Clark, C. P., Freeman, G. R. and Hower, J. C., Scanning Electron Microscopy /1984/II, 537-545 (1984).
11. Reid, A. F., Gottlieb, P., MacDonald, K. J. and Miller, P. R., OEM*SEM Image Analysis of Ore Minerals, p. 191-204 in Applied Mineralogy, Eds. Park, W. C., Hansen, D. M. and Hagni, R. D., Met. Soc. of AIME, Warrendale, Pennsylvania (1984).
12. Sen, R., Yasar, R., Spottiswood, D. J. and Schowengerdt, F. D., Application of Quantitative Mineralogy to the Concentration of a Latenite Ore, p. 441-466 in Applied Mineralogy, Eds. Park, W. C., Hansen, D. M. and Hagni, R. D., Met. Soc. of AIME, Warrendale, Pennsylvania (1984).
13. Keller, W. D., Applications of SEM to Clays and Other Fine-Grained Minerals, p. 245-261 in Process Mineralogy II, Ed. Hagni, R., Met. Soc. of AIME, Warrendale, Pennsylvania (1982).
14. Boulmier, J. L., Oberlin, A., Rouzand, J. N. and Uilley, M., Scanning Electron Microscopy /1982/IV, 1523-1538 (1982).
15. Wert, C. A. and Hsieh, K. C., Scanning Electron Microscopy /83/III, 1123-1186 (1983).
16. Hsieh, K. C. and Wert, C. A., Fuel, 64, 255-262 (1985).
17. Tseng, B. H., Buckentin, M., Hsieh, K. C., Wert, C. A. and Dyrkacz, G. R., Fuel, in press.
18. Hall, T. A. and Werba, P. R., Proc. 25th Anniversary Meeting of the Electron Microscopy and Analysis Group, the Inst. of Metals, London, p. 146 (1971).
19. Hall, T. A., Jour. of Microscopy, 117 145-163 (1979).
20. Hall, T. A., Anderson, H. C. and Appleton, T. C., Jour. of Microscopy, 99, 177 (1973).
21. Shuman, H., Somlyo, A. V. and Somlyo, A. P., Ultramicroscopy, 1, 317 (1976).
22. Hren, J. J., Goldstein, J. I. and Joy, D. C., Eds. Introduction to Analytical Electron Microscopy, Plenum, New York (1979).
23. Colliex, C., Electron Energy Loss Spectroscopy in the Electron Microscope, p. 65-177 in Advances in Optical and Electron Microscopy, vol. 9, Eds. Barer, R. and Cosslett, V. E., Academic Press, London, New York (1984).
24. Bruemmer, S. M., Fluhr, C. P., Peggs, D. V., Wert, C. A. and Fraser, H. L., Met. Trans., 11A, 693-699 (1980).
25. Mochel, P., Allison, C. and Williams, W. S., Jour. Am. Cer. Soc., 64, 185-187 (1981).

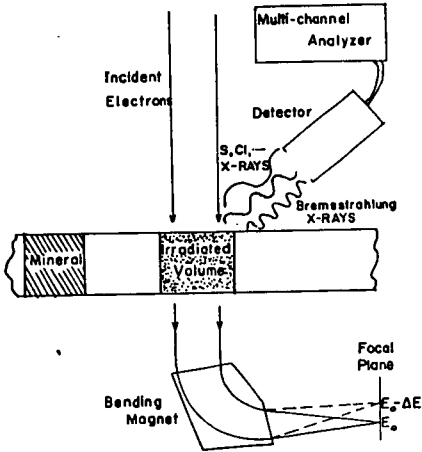


Fig. 1 Sketch of TEM with EDAX and EELS Capability.

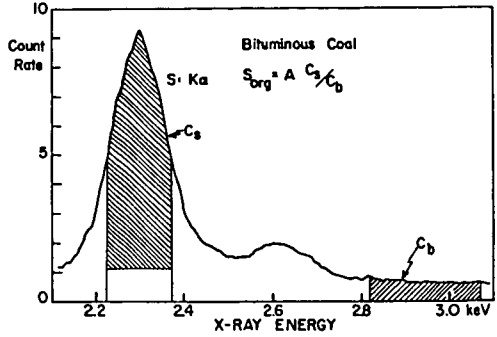


Fig. 2 EDAX Spectrum for S.

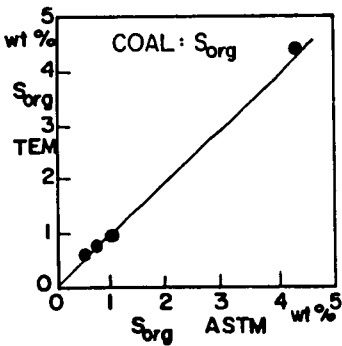


Fig. 3 Comparison of TEM and ASTM Analyses of Coal.

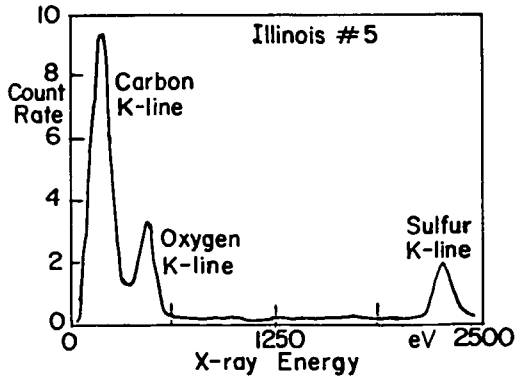


Fig. 4 Light-Element Spectrum: C and O X-ray lines.



Fig. 5 TEM Micrograph of a V-Ti-C Carbide.

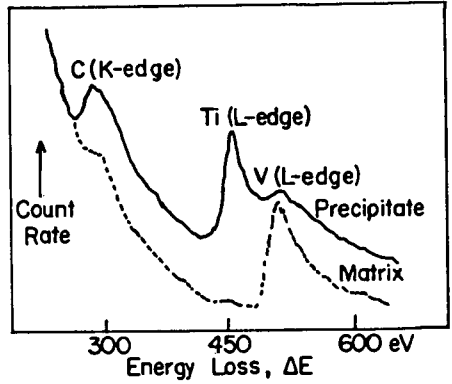


Fig. 6 EELS Spectrum of matrix and VTi_4C_5 Carbide.

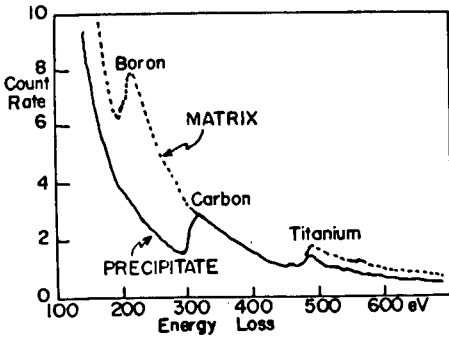


Fig. 7 EELS Spectrum for TiC in a TiB_2 matrix.

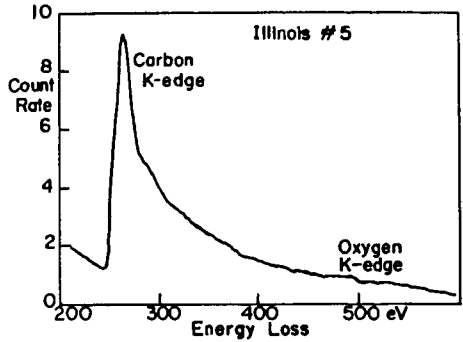


Fig. 8 Energy Loss Spectrum of a Bituminous Coal.

DIRECT DETERMINATION OF ORGANIC OXYGEN IN COAL USING SCANNING ELECTRON
MICROSCOPY WITH WAVELENGTH-DISPERSIVE X-RAY ANALYSIS

G. A. Norton, W. E. Straszheim, K. A. Younkin, and R. Markuszewski

Ames Laboratory*, Iowa State University

Ames, Iowa 50011

ABSTRACT

Illinois No. 6, Pittsburgh No. 8, and Dietz No. 1 and 2 coals were analyzed directly for organic oxygen content by using scanning electron microscopy and wavelength-dispersive x-ray analysis. The technique is a modified extension of a method previously developed for the direct determination of organic sulfur in coal. To assure statistical validity, 12 particles were analyzed for each coal at two different points per particle. Mean organic oxygen values were obtained, as well as inter- and intra-particle variations in the oxygen content. The mean values for organic oxygen obtained by this technique agreed favorably with values calculated from previously obtained data by prompt neutron activation analysis and by the indirect ASTM method.

INTRODUCTION

The organic oxygen content of coal is an important parameter in coal characterization and utilization and is a part of routine coal analyses. It must be known in order to perform some of the process calculations for coal combustion and various coal conversion technologies such as liquefaction and gasification (1). The organic oxygen content of coal is generally determined by ASTM Method 3176, the Standard Method for Ultimate Analysis of Coal and Coke (2). In this method, oxygen is the only element comprising the organic coal matrix which is not determined directly. Rather, it is determined by difference from the ultimate analysis, using the equation:

$$\%O = 100 - (\%C + \%H + \%N + \%S + \% \text{ ash}) \quad \text{Eq. 1}$$

Thus, the accuracy of this indirect oxygen determination suffers from cumulative errors inherent in the analytical methods used for each of the other elements. In addition, it is dependent on the ash content which is obtained by heating the coal at about 700°C for one hour; but since the ash produced at these temperatures is not directly relatable to the original mineral matter in the coal, another source of error is thereby introduced into the oxygen determination.

Furthermore, if the coal has been subjected to chemical treatment which alters the ash-forming mineral matter, the definition of "ash" used in Eq. 1 becomes a problem.

Although various methods for determining oxygen in coal directly have been employed, including neutron activation analysis (NAA) and oxidative or reductive techniques, analyses by these methods include all or some of the inorganic oxygen. Therefore, coal demineralization or corrections for inorganic oxygen must be performed in order to obtain the organic oxygen content.

*Ames Laboratory is operated for the U.S. Department of Energy by Iowa State University under Contract No. W-7405-Eng-82.

In this study, the feasibility was explored for using a scanning electron microscope (SEM) in conjunction with energy- and wavelength-dispersive x-ray analysis (EDX and WDX, respectively) to determine the organic oxygen content of coal directly. The technique is similar to methods used previously for the direct determination of organic sulfur levels in coals (3-8). In one such technique, a transmission electron microscope was used to quantify the sulfur content of the organic coal matrix (3). Other studies used an electron microprobe to determine organic sulfur in coal (4, 5). In one of those studies, the organic oxygen content of various macerals in a Kentucky No. 3 coal also was determined (5). By knowing the petrographic composition of the coal and the average organic oxygen content of each maceral examined, a weighted average was used to obtain an oxygen concentration for the organic matrix as a whole. The organic oxygen concentration thus obtained was in good agreement with the concentration obtained by the indirect ASTM procedure.

A third method used scanning electron microscopy coupled with energy-dispersive x-ray analysis (SEM-EDX) to obtain organic sulfur levels in raw and chemically desulfurized coals (6-8). In two of the studies using the SEM-EDX technique, mineral portions of the coal were avoided by locating organic maceral components of coal using 5000x magnification with the SEM and by monitoring the levels of Fe, Ca, Al, and Si (6, 7). Sulfur values which were obtained only for those areas where the other elements were not detected were assumed to be associated with the organic portion of the coal. Analyses were usually performed on 12 vitrinite particles by examining at least two points (with volumes of 2-3 microns in diameter) per particle. This was sufficient to obtain data with a precision of $\pm 10\%$ (relative) for organic sulfur levels. The results were comparable to those obtained by the common indirect ASTM method.

In our study, a similar SEM technique was used to determine organic oxygen levels in coal along with inter- and intra-particle variations. Organic oxygen values obtained by this technique were compared to values obtained by the indirect ASTM procedure and by neutron activation analysis.

EXPERIMENTAL

Channel samples of Illinois No. 6 (Captain Mine, Percy, Illinois), Pittsburgh No. 8 (Grafton Mine, Churchville, West Virginia), and Dietz No. 1 and No. 2 (Decker Mine, Decker, Montana) coals were powdered, dried, and subsequently mounted in one-inch pellets of epoxy. After polishing the mounted samples to a smooth cross section with silicon carbide sandpaper and alumina, they were coated with approximately 50 Å of carbon by evaporation in order to provide a conductive surface.

A JEOL (Japan Electron Optics Laboratory) model JSM-U3 scanning electron microscope (SEM) was used in conjunction with a Microspec WDX-2A wavelength-dispersive x-ray analysis system to perform quantitative oxygen determinations on the coals. Oxygen was determined by wavelength-dispersive x-ray analysis (WDX) because it could not be detected by the EDX system, being an element of low atomic number.

Samples were examined in the SEM with an accelerating voltage of 15 kV and a current of about 30 nA with an x-ray take off angle of 25°. The SEM was allowed to stabilize for 15 to 30 minutes after sample changes before collecting x-ray intensities. X-ray data were collected from square sample areas of 20 μm on a side. A square raster was used for the analyses instead of the traditional spot mode due to the high beam currents used. Prior to analysis, mineral portions of the coal were avoided by examining the sample visually at a magnification of 5000x in the SEM. Energy-dispersive x-ray analysis (EDX) was then performed with a KEVEX Si(Li)

detector and a Tracor Northern Model TN-2000 energy-dispersive x-ray analysis system to monitor the particles for Al, Ca, Fe, and Si. The absence of these elements ensured that mineral inclusions were excluded from the sampled areas. Since oxygen was determined by WDX only when significant levels of the elements screened by EDX were absent, the oxygen was assumed to be associated with the organic matrix.

Because organic sulfur and small amounts of Al, Si, Ca, and Fe were present in the analyzed particles, EDX spectra for a set of standards containing these elements were collected prior to analyzing the coal. Silica (SiO₂) was chosen for the oxygen standard since organic compounds which were tested did not hold up well under the electron beam. Organic compounds which were tested for use as a standard included urea, acetanilide, and citric acid. After analyzing a coal for organic oxygen content, one of the inorganic standards for the other elements was run for a second time to make sure that no significant drift in beam current occurred.

In this study, no attempt was made to distinguish between different maceral types. Two points within each of 12 particles were analyzed for each coal. EDX spectra and total oxygen counts obtained by WDX were each collected for 30 seconds. The total oxygen intensity was then transferred to the EDX unit for data reduction. The Tracor Northern program Super ML was used to reference the coal spectra against the standards, while the Tracor Northern ZAF correction program was used to correct for atomic number, absorption, and fluorescence matrix effects. In addition to mean organic oxygen concentrations, inter- and intra-particle variations in oxygen content were obtained.

RESULTS AND DISCUSSION

Average organic oxygen concentrations obtained by SEM-WDX on each of the coals are shown in Table 1. For comparative purposes, data obtained previously by neutron activation analysis (NAA) and by the indirect ASTM procedure are also included.

Table 1. Organic Oxygen Content of Illinois, Pittsburgh, and Dietz Coals.¹

Analytical Procedure	Coal		
	Illinois #6	Pittsburgh #8	Dietz #1 & 2
SEM-WDX	11.94	11.55	16.67
ASTM	9.44	8.07	20.67
NAA ²	10.67	7.85	22.70

¹ Values are in % on a dry mineral matter free basis.

² Organic oxygen content was obtained from total oxygen values by estimating the inorganic oxygen concentration and subtracting from total oxygen, as discussed in text.

The SEM values represent averages for the 24 sampled areas for each coal; ASTM and NAA data represent averages of duplicate determinations. Only total oxygen values were available in the original NAA data. For comparison on the same basis, the raw data obtained by NAA were used to estimate organic oxygen concentrations (shown in Table 1) by subtracting inorganic oxygen levels from the total oxygen levels. For these calculations, the inorganic oxygen values were estimated by first using a modified Parr formula (9) to approximate the mineral matter content

based on the known ash and pyritic sulfur contents for each coal. This formula is:

$$\%MM = 1.13 (\% \text{ ash}) + 0.47 (\% \text{ pyritic sulfur}) \quad \text{Eq. 2}$$

The amount of inorganic oxygen was then estimated using the equation

$$\%O_{\text{Inorg}} = 0.5 (\% \text{ MM}) \quad \text{Eq. 3}$$

This equation has been reported to give good inorganic oxygen estimations for well-known coals with relatively low ash contents (10). Thus, organic oxygen levels were obtained by calculating the difference in levels of total and inorganic oxygen. The mineral matter content of each coal, as calculated using the modified Parr formula, was used to convert the NAA and ASTM values to a mineral matter-free basis. The SEM-WDX data required no corrections for mineral matter because mineral inclusions were avoided during those analyses.

In view of the analytical uncertainties in each of the techniques, the SEM-WDX values agreed favorably with the values obtained by NAA and ASTM procedures. For the Pittsburgh No. 8 and Illinois No. 6 coals, there was a significant lapse in time between the SEM-WDX analyses and the determinations made by NAA and ASTM procedures. The coals were used frequently over this time period and often had been in contact with air. Thus, it is likely that some oxidation would have occurred during this time and that the somewhat elevated SEM-WDX data for these two coals reflect this oxidation.

For the Dietz coal, the SEM-WDX value is significantly lower than the values obtained by the other methods. This may be somehow connected with the fact that the Dietz coal is subbituminous, as opposed to the bituminous ranking of the other coals. More study is needed to resolve this discrepancy.

Also, although the same coals were used for the analyses by SEM-WDX, NAA, and the ASTM procedure, analyses by SEM-WDX were performed on different sample splits than the ones used for analysis by the other techniques. Coal composition between various splits from standard riffing procedures is generally comparable, but variations in chemical composition may still occur as a result of sample inhomogeneity and difficulties involved with obtaining representative samples of coal.

Thus, discrepancies between analytical data obtained by the various techniques may reflect actual differences in composition in addition to possible errors associated with the analytical methods. Future work will include more rigid monitoring of the various sample variables than was done in this preliminary study.

Statistical parameters for the SEM-WDX data are shown in Table 2. Details on the statistical parameters employed have been described previously (6, 7). These analyses enabled estimates for deviations from the sample mean within the particles (intra-particle deviations) and deviations from the sample mean between different particles (inter-particle deviations) to be calculated.

It is interesting to note that for each coal, intra-particle variations were larger than inter-particle variations. For the Illinois coal, analysis of variance gave a negative number for the inter-particle variation. Therefore, a value of zero is reported. Between coals, the inter-particle variations were less consistent than the intra-particle variations. This implies that some coals may require more extensive analyses due to a less uniform distribution of organic oxygen. One factor which could be important is the maceral distribution for a given coal.

Table 2. Statistics for Organic Oxygen Levels Obtained by SEM-WDX.

Coal	Org. O ^a (%)	S \bar{x} ^b	S _a ^c	S _p ^d
Illinois No. 6	11.94	0.37	1.43	0.00 ^e
Pittsburgh No. 8	11.55	0.24	0.97	0.45
Dietz No. 1 & 2	16.67	0.44	1.40	1.16

^a Values are on a dry mineral matter free basis.

^b S \bar{x} is the standard deviation in the sample mean.

^c S_a is the standard deviation within particles.

^d S_p is the standard deviation between particles.

^e Value of zero reported since analysis of variance gave a negative number.

Since the organic oxygen content can vary considerably between different macerals (5, 11), the maceral composition and distribution could have a large effect on the intra- and inter-particle variations.

The SEM-WDX technique may be particularly useful for determining organic oxygen in chemically cleaned coals, especially since ASTM procedures sometimes give questionable ash results for such coals (12), thereby throwing a large error into the ASTM organic oxygen determination.

CONCLUSIONS

Examination of the SEM-WDX results indicates that this technique has good potential for the direct determination of organic oxygen in coal. Analysis of inter- and intra-particle variations provides useful information on the distribution of organic oxygen in the coal. Because mineral phases are excluded from the analysis, a sample with a representative ash content is not nearly as important for this procedure as it is for NAA and ASTM procedures where ash corrections are necessary. However, since the SEM-WDX technique is surface-sensitive, extra care must be taken to keep the coal from oxidizing. Because of the numerous operating parameters involved in the analyses by SEM-WDX, the procedural details of this technique require optimization. In addition, applicability to a broad spectrum of raw coals and to chemically cleaned coals needs to be shown.

ACKNOWLEDGMENTS

This work was supported by the Assistant Secretary for Fossil Energy, Division of Direct Coal Utilization, through the Pittsburgh Energy Technology Center.

LITERATURE CITED

1. Hamrin, C. E. Jr.; Maa, P. S.; Chyi, L. L.; Ehman, W. D. "Organic Oxygen Determination of Kentucky No. 9 Coal by Fast-Neutron Activation Analysis," Fuel **54**, 70 (1975).
2. "1982 Annual Book of ASTM Standards, Part 26: Gaseous Fuels; Coal and Coke; Atmospheric Analysis," ASTM, Philadelphia, PA.
3. Hsieh, K. C.; Wert, C. A. "Direct Determination of Organic Sulphur in Coal," Fuel **64**, 255 (1985).
4. Raymond, R.; Gooley, R. "A Review of Organic Sulfur Analysis in Coal and a New Procedure," In Scanning Electron Microscopy, Vol. I, (Ed. O. Johari), 1978, pp. 93-107.
5. Friel, J. J.; Mitchell, G. D. "Organic Oxygen and Sulfur Analysis of Various Coal Macerals," In Microbeam Analysis, R. H. Geiss, Ed.; San Francisco Press: San Francisco, 1981; pp. 148-150.
6. Straszheim, W. E.; Greer, R. T. "Direct Determination of Organic Sulfur in Coal with Estimates of Intra- and Inter-Particle Variation," In Scanning Electron Microscopy, Vol. III, (O. Johari, Ed.), 1982, pp. 1013-1024.
7. Straszheim, W. E.; Greer, R. T.; Markuszewski, R. "Direct Determination of Organic Sulphur in Raw and Chemically Desulphurized Coals," Fuel **62**, 1070 (1983).
8. Maijgren, B.; Hubner, W.; Norrgard, K.; Sundvall, S.-B. "Determination of Organic Sulphur in Raw and Chemically Cleaned Coals by Scanning Electron Microscopy and Energy Dispersive X-ray Spectrometry," Fuel **62**, 1076 (1983).
9. Given, P. H.; Yarzab, R. F. "Analysis of the Organic Substance of Coals: Problems Posed by the Presence of Mineral Matter," In Analytical Methods for Coal and Coal Products, Karr, C., Jr., Ed.; Academic Press: New York, 1978; Vol. II, pp. 3-41.
10. Kinson, K.; Belcher, C. B. "Determination of Oxygen in Coal and Coke Using a Radio-Frequency Heating Method," Fuel **54**, 205 (1975).
11. Winans, R. E.; Hayatsu, R.; Scott, R. G.; McBeth, R. L. "Reactivity and Characterization of Coal Macerals," in Chemistry and Characterization of Coal Macerals, R. E. Winans and J. C. Crelling, Eds., American Chemical Society, Washington, D. C., 1984, pp. 137-155.
12. Meyers, R. A. Personal communication, 1985.

Non-intrusive Optical Techniques for the Study of Pulverized Coal Particles during
Devolatilization and Combustion*

D. K. Ottesen and J. C. F. Wang

Sandia National Laboratories
Livermore, CA 94550

This paper will discuss applications of Fourier transform infrared (FT-IR) spectroscopy and laser spark spectroscopy (LSS) as in situ diagnostics for disperse phase combustion environments. The ultimate goal of the FT-IR work is the identification of gas phase species, and the determination of their temperature and concentration during the combustion of pulverized coal particles. We are developing LSS as a complementary technique for the in situ elemental analysis of coal, char, and ash particles in combustion environments.

Fourier transform spectroscopy

We have made infrared absorption measurements for sized coal particles entrained in a laminar flow reactor. The combustion is initiated by hot bath gases produced in a $H_2/O_2/N_2$ flat flame at the base of the reactor. The interface between the flow reactor and the FT-IR system is shown in Figure 1; detailed descriptions of the experimental apparatus and typical infrared absorption spectra have been given elsewhere (1).

FT-IR spectroscopy has been shown to be an effective technique for detection of many different species simultaneously over a wide spectral bandwidth when conditions permit time-averaged measurements along a line-of-sight (1,2). This past year has seen the extension of these measurements into the high resolution domain and the careful quantitation of the technique's ultimate sensitivity for several molecules.

Fast absorption measurements have been plagued by the infrared emission of hot coal particles passing through the detector field-of-view. These signals act as an additional noise source, and are mitigated only somewhat by laborious time-averaging. This has prevented the measurement of spectra at a resolution greater than 0.5 cm^{-1} . We have found, however, that this particle generated "noise" occurs at Fourier frequencies lower than the pertinent bandwidth containing infrared spectral information. Electronic filtering of the detector output has greatly reduced this particle noise, and allowed us to make the first reported measurements of pulverized coal combustion products at a spectral resolution of 0.08 cm^{-1} .

Although these measurements are more time consuming than those at lower resolution, they allow a more accurate determination of both the molecular rotational temperature and concentration. This is due principally to the lessened interference of nearby absorption lines from other species (mainly water) and higher excited state transitions. These measurements have also allowed us to observe that the measured line width of CO and CO_2 transitions is considerably greater than the reported values of 0.04 cm^{-1} at temperatures around 1300 K. Measured widths at half maximum are 0.105 cm^{-1} , and we postulate that the additional width is caused by collisional broadening with the copious quantity of water present (15 mol %). An example is shown in Figure 2 for a portion of the CO P-branch rotation-vibration band produced during the combustion of a pulverized western Kentucky bituminous coal. The CO rotational temperature determined from the relative intensities of the absorption lines was $1218 \pm 28\text{ K}$ and was in good agreement

with a temperature of 1247 +/- 22 K derived from the CO₂ ω₃ R-branch rotation-vibration during the same experimental measurement.

Reduction of the noise caused by particulate emission has increased our sensitivity for many small infrared-active molecules (CO, CH₄, NO, HCN, H₂S) to about 100 ppm at combustion temperatures in the presence of coal particles. Current efforts at detecting minor products of combustion in situ have been hampered by the low particle number density we have been able to entrain in our flow reactor (2 cm⁻³), and by the serious overlap of water absorption lines with N- and S-containing species of interest.

Concentration measurements were made by entraining known amounts of carbon dioxide and nitric oxide into the flow reactor. Using literature values of line strengths, the corresponding experimental intensities could be theoretically calculated for a variety of other molecular species in our FT-IR/flow reactor system. This approach is effective in minimizing uncertainties in absolute intensity measurements which arise from line-shape distortions caused by our instrument. In Figure 3 we show the measured concentration of CO and CO₂ at 38 msec residence for coal particles in the +30/-50 micrometer size range as a function of excess oxygen in the flow reactor.

Laser spark spectroscopy

We have developed the technique of laser breakdown spectroscopy for analyzing the composition of particles and droplets suspended in air (3). As such, this technique should prove invaluable as an in situ real-time diagnostic for application to fundamental studies of the combustion or gasification of coal, coal-derived liquids and coal-water slurries.

A high-power pulse was generated by a Nd:YAG laser and focused on individual coal particles carried in a gas flow. Absorbed energy was sufficient to completely vaporize the particles, and to cause avalanche breakdown of the vapor. The emission spectra from the plasma were analyzed to identify lines characteristic of the specific elements. Because of the strong continuum emission at early time of the spark, a time-gated optical multichannel analyzer was used to record the emission spectra. Timing and spectral windows were carefully selected to minimize the continuum emission, and to eliminate interference from nearby or overlapping lines from the atoms of interest. We succeeded in isolating spectral features of the major elements: carbon, nitrogen, oxygen, as well as hydrogen, sodium, and chlorine.

A two-color cross-beam laser technique was developed to provide a simultaneous trigger for the breakdown laser and a measurement of the size of the particle being analyzed. A schematic diagram of the experimental apparatus is shown in Figure 3. With this apparatus it is possible to correlate the emission spectrum and intensity with the particle size. In addition, detection limits of various species of interest were deduced from these cross-correlation measurements.

Laboratory experiments were conducted using pulverized bituminous coal particles and water droplets with added impurities. The latter experiments used a piezoelectric droplet generator for the purpose of creating a series of water particles of carefully controlled diameter. This greatly facilitates the calibration of spectral emission with such variables as the droplet size, atomic concentration, incident laser energy, and spectrometer response. An emission spectrum is shown in Figure 4 for the sodium 5890 Å line (grating resolution was not sufficient to resolve the doublet in this spectrum). This spectrum originated from the vaporization of a single water droplet 70 micrometers in diameter, containing 0.1% Na by weight.

REFERENCES

1. Ottesen, D. K. and Thorne, L. R., 1983 Intl. Conf. on Coal Science, Pittsburgh, PA, p. 621, August, 1983.
2. Solomon, P. R., Hamblen, D. G., Carangelo, R. M. and Krause, J. L., 19th International Symp. on Combustion, The Combustion Inst., pp. 1139-49, 1982.
3. Schmieder, R. W., "Techniques and Applications of Laser Spark Spectroscopy", Sandia Natl. Laboratories Report, SAND83-8618, March, 1983.

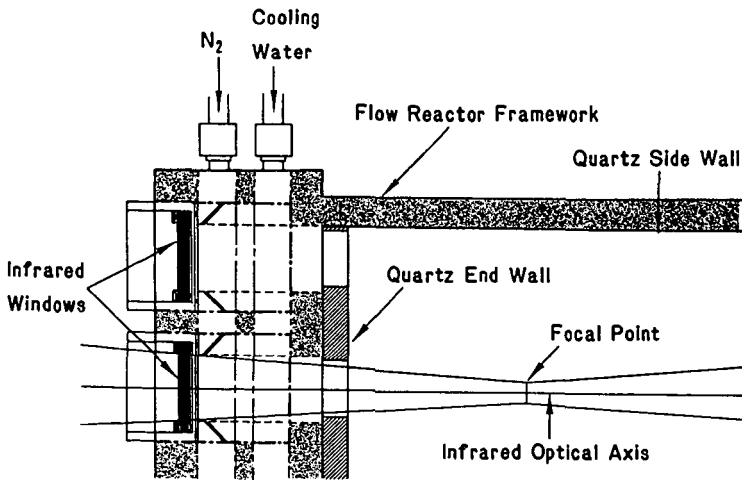


Figure 1. Schematic diagram of FT-IR / flow reactor interface.

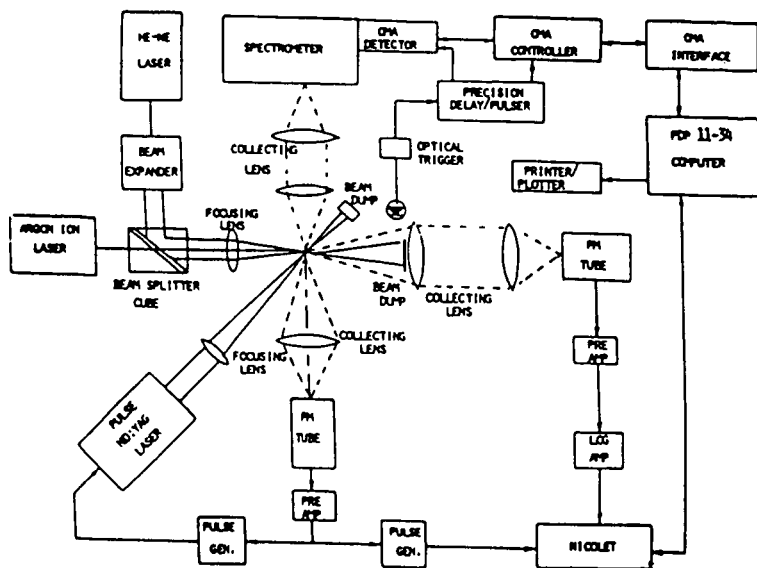


Figure 4. Schematic diagram of Laser Spark Spectroscopy apparatus.

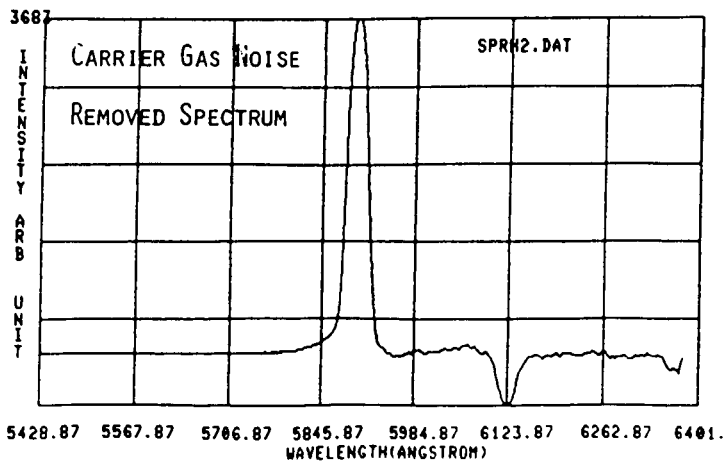


Figure 5. Na emission spectrum produced during laser spark vaporization of water droplet.

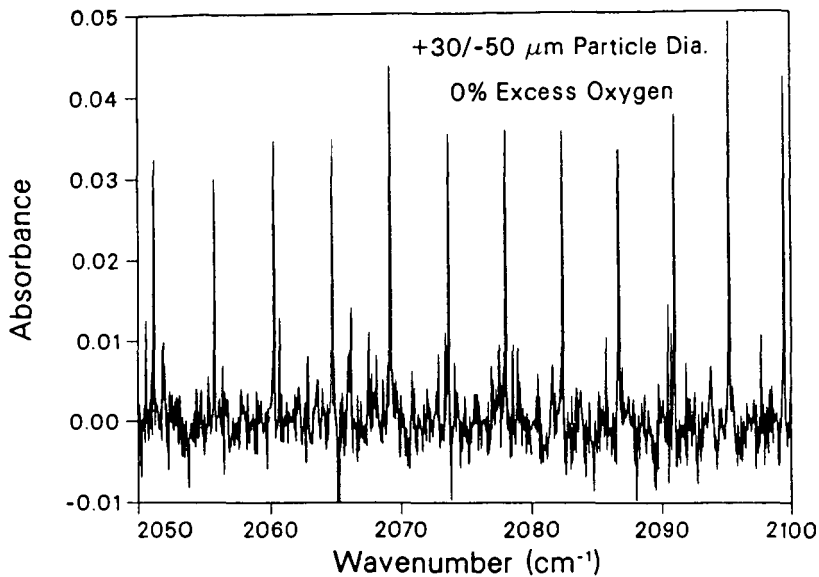


Figure 2. Absorbance spectrum of CO produced during pulverized coal combustion.

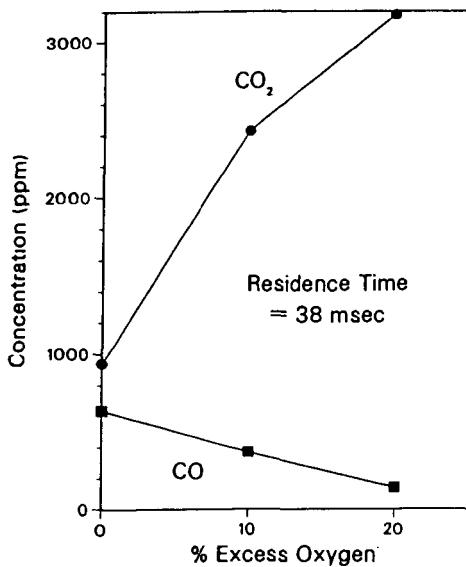


Figure 3. CO and CO₂ concentration in flow reactor as a function of excess oxygen.

**ANALYSIS OF PARTICLE COMPOSITION, SIZE AND TEMPERATURE
BY FT-IR EMISSION/TRANSMISSION SPECTROSCOPY**Peter R. Solomon, Robert M. Carangelo, Philip E. Best,
James R. Markham and David G. Hamblen

Advanced Fuel Research, Inc., 87 Church Street, East Hartford, CT 06108

Many chemical and energy conversion processes involve multi-phase feed or product streams. Streams can consist of mixtures of solids, liquids and gases and in some cases, the important species may be in transition between phases (e.g. liquid fuel combustion which involves liquid fuel droplets, vaporized fuel and soot). Process monitoring requires the measurement of parameters for the separate phases. There are requirements for monitoring feedstocks and samples of the process stream as well as for in-situ monitoring. Fourier Transform Infrared (FT-IR) absorption spectroscopy has been used previously as an in-situ diagnostic for both gas species concentration and gas temperature determinations (1-9). This paper describes a new method being developed for on-line, in-situ monitoring of particle streams to determine their chemical composition, size, and temperature. The technique uses a FT-IR spectrometer to perform both emission and transmission (E/T) spectroscopy for a stream of particles. The technique has been applied to measure particle properties under a variety of circumstances and several examples are presented for measurements of temperature, composition and size.

The method was employed to address a controversy concerning coal optical properties recently raised by Brewster and Kunitomo (10). Their recent measurements suggest that previous determinations for coal of the imaginary part of the index of refraction, k , may be too high by an order of magnitude. If so, the calculated coal emissivity based on these values will also be too high. The E/T technique was employed to determine directly the spectral emittance, ϵ_{ν} , of coal and char particles as a function of coal rank, extent of pyrolysis and temperature. For one coal, the measured spectral emittance was compared with a calculated value obtained from the material's complex index of refraction $N = n + ik$, and particle size, using Mie theory. The complex index of refraction was determined using an extension of Brewster and Kunitomo's method for measuring k . The technique employs KBr and CsI pellet spectra and uses Mie theory and the Kramers-Kronig transforms to separate scattering and absorption effects. Good agreement has been obtained between the calculated and measured values of (ϵ_{ν}) confirming the contention that previously measured values of k are too high.

EXPERIMENTAL

Apparatus - The apparatus employed in the experiments consists of an FT-IR spectrometer coupled to a reactor, such that the FT-IR focus passes through the sample stream as shown in Fig. 1. Emission measurements are made with the movable mirrors in place. Transmission measurements are made with the movable mirror removed. The Fourier transform technique, in contrast to wavelength dispersive methods, processes all wavelengths of a spectrum simultaneously. For this reason it can be used to measure spectral properties of particulate flows, which are notoriously difficult to maintain at a constant rate. The emission and transmission can be measured for the same sample volume. The technique is extremely rapid; a low noise emission or transmission spectrum at low resolution (4 cm^{-1}) can be recorded in under a second. Also radiation passing through the interferometer is amplitude modulated, and only such radiation is detected. Because of its unmodulated nature, the particulate emission passing directly to the detector does not interfere with the measurements of scattering or transmission.

In an ideal emission-transmission experiment both measurements are made on the identical sample. In our case the emission and transmission measurements are made sequentially in time along the same optical path, for a sample flowing through the cell in a nominal steady condition.

Measurements - To determine the temperature, size or composition of particulate samples, measurements are made of the transmittance and of the radiance, from which we calculate a quantity which we call the normalized radiance. The normalized radiance is the radiance divided by (1-transmittance) (which in the absence of diffraction effects is a measure of intersected particle surface area for samples whose index of refraction is sufficiently different from the surrounding medium). This normalization allows the radiance from particles which fill only a fraction of the FT-IR aperture to be compared to a black-body standard obtained for the full aperture.

The transmittance, γ_{ν} , at wavenumber ν , is measured in the usual way

$$\gamma_{\nu} = I_{\nu} / I_{0\nu} \quad (1)$$

where $I_{0\nu}$ is the intensity transmitted through the cell in the absence of sample, while I_{ν} is that transmitted with the sample stream in place. The geometry for the transmittance measurement is illustrated in Fig. 2. With a particle in the focal volume, energy is taken out of the incident beam by absorption and scattering. The figure illustrates scattering by refraction of energy at the particles surfaces. Scattering will also be caused by reflection and diffraction. For particles $> 50 \mu\text{m}$ whose index of refraction is sufficiently different from the surrounding medium, almost all the energy incident on the particle is absorbed or scattered.

To measure the sample radiance, the power from the sample with background subtracted, S_{ν} , is measured, and converted to the sample radiance, R_{ν} , in the following way

$$R_{\nu} = S_{\nu} / W_{\nu} \quad (2)$$

where W_{ν} is the instrument response function measured using a cavity radiator. The radiance measurement detects both radiation emitted by the particle itself, as well as wall radiation scattered or refracted by the particle as illustrated in Fig. 2.

We calculate the normalized radiance (which we refer to as the E/T spectra), R^n , in the following way,

$$R^n = R_{\nu} / (1 - \gamma_{\nu}). \quad (3)$$

The complete analysis for the normalized emission will be presented elsewhere (11). For this discussion we consider the limit where particles are sufficiently large that they effectively block all the radiation incident on them, and their diffraction pattern falls completely within the angular acceptance aperture of the spectrometer. Then the normalized radiance has the simple form,

$$R^n = (1 - \epsilon_{\nu}) R_{\nu}^b(T_w) + \epsilon_{\nu} R_{\nu}^b(T_p) \quad (4)$$

where ϵ_{ν} is the spectral emittance and $R_{\nu}^b(T_w)$ and $R_{\nu}^b(T_p)$ are the theoretical black-body curves corresponding to the temperature of the wall (T_w) and particle (T_p), respectively. This equation will be used in the discussion of results to follow.

RESULTS

Temperature and Emisivity - To illustrate the measurements, we consider several simple cases. First we consider hot particles such as coal or char surrounded by cold

walls ($T_p \gg T_w$). Then according to Eq. 4,

$$R_{\nu}^n = \epsilon_{\nu} R_{\nu}^b(T_p). \quad (5)$$

If T_p is known, then ϵ_{ν} can be determined and vice-versa.

The first example is for char under conditions where the particles first reach equilibrium with a heated tube reactor (HTR) and then exit the reactor and pass the FT-IR aperture. The reactor has been described previously (12-14). The gas-particle mixture cools about 75°C between the reactor and the FT-IR focus as determined with a thermocouple (14). In Fig. 3 we show the radiance, (R_{ν}), 1- transmittance, ($1-\tau_{\nu}$), and the normalized radiance, (R_{ν}^n), from char emerging from the HTR at a temperature of 983 K. ($1-\tau_{\nu}$) is a measure of the intersected surface area of particles, i.e., 4% of the beam is blocked. The normalized radiance is compared with a number of grey body curves at different values of constant ϵ . The $\epsilon = 0.87$ curve at 1000 K gives best fit with the experimental data. The temperature is in good agreement with the thermocouple measurement.

The second example is for lignite particles at a temperature of 782 K, before any pyrolysis has occurred. The normalized radiance spectrum in Fig. 4a is compared to a grey-body ($\epsilon = .90$) at the average thermocouple temperature of 782 K. While the previously formed char shows a grey-body shape close to the average temperature, the lignite does not have a grey-body shape. The black-body and experimental curves are close only in the range 1600-1000 cm^{-1} where the emissivity, calculated from Eq. 5, (Fig 4b) is close to 0.9. These and other measurements (12-16) show that the particle's emissivity is size and temperature dependent. For the size of coal particles used here, only specific bands between 1600 cm^{-1} and 1000 cm^{-1} (corresponding to the strongest absorption bands in coal) have a spectral emittance near 0.9.

The result can be understood by considering that a particle's emittance is related to its absorbance. By Krichoff's law, particles will emit only where they have absorption bands. As discussed by Hottel and Sarofim (17), for large particles (where diffraction can be neglected) the absorption can be calculated from geometrical optics considering all possible rays through the particles. The absorption within the particle can be calculated using absorbance values measured by the KBr pellet method (15,18). Figure 4c shows the absorbance measured by the KBr pellet method. The correspondence between the high absorbance bands and the regions of high emissivity are apparent. The most significant difference between the spectra of Figs. 4a and 4c is the presence of a steeply sloping background going toward large wavenumbers in the pellet spectrum (Fig. 4c) and its absence in the emittance spectrum (Fig. 4b). The pellet spectrum is from a transmission measurement which does not distinguish between the absorption and scattered components of the total cross section. This problem is treated in the section on Calculated Emissivity.

The emittance varies with particle size as shown in Fig. 5. R_{ν}^n is smallest for small particle sizes and approaches the black-body curve for large size particles.

The spectral emittance varies with rank as shown in Fig. 6. The strongest feature is the emittance above 1700 wavenumbers which increases above 90% carbon. The increase in emittance above 90% carbon is consistent with a corresponding increase in the broad sloping absorbance observed in KBr pellet spectra for high carbon coals. This absorbance is believed to be due to electronic absorption of multi-ring aromatic hydrocarbons (19). The emittance of anthracite is close to grey body. The spectral emittance variation with rank is consistent with the functional group variation with rank.

Having demonstrated that the FT-IR method does give an appropriate temperature assuming $\epsilon \approx 0.9$ in the 1600 cm^{-1} to 1000 cm^{-1} region, the technique was used to determine particle temperatures for non-isothermal conditions in the HTR reactor (13,14). Figure 7 shows the E/T spectra for increasing time in the reactor. The FT-IR temperatures are in good agreement (within 25°C) with calculated temperatures and temperatures measured with a thermocouple (14).

We can also observe in Fig. 7, changes in emittance of particles as a function of the extent of pyrolysis. At 883 K all the bands present in coal can be seen, except that the hydroxyl peak is noticeably depleted. At 963 K a broad continuum, characteristic of char, is beginning to grow. By 1050 K we see almost a grey-body continuum with CO_2 and H_2O peaks superimposed. From the spectra discussed so far we can say that the spectral emittance of lignite of this size range increases continuously with pyrolysis, reaching a constant maximum of about 0.9 when pyrolysis is sensibly complete. The relationship of the development of the continuum char spectrum with the extent of pyrolysis will be the subject of a future investigation.

The other examples are from a reactor where the particles are surrounded by hot walls. For the case where the particles are at wall temperature, $T_p = T_w$, Eq. 4 reduces to

$$R_{\nu}^n = R_{\nu}^b(T_p) \quad (6)$$

Figure 8a displays R_{ν}^n in one such case. In this case we don't have to include particle emittance in the analysis, as it can be shown and Eq. 6 indicates, that any lack of emittance must be made up by scattered and reflected radiation. Indeed, the normalized emission is close in shape and amplitude to a black-body at the measured window height wall temperature (1225 K). The determination of T_p when T_p is of the same order of magnitude as T_w requires a knowledge of ϵ_{ν} at some wavenumber and use of the complete expression for R_{ν}^n (Eq. 4). Examples are discussed in reference (11).

Two additional examples are shown for the case $T_p \ll T_w$. Then Eq. 4 reduces to

$$R_{\nu}^n = (1 - \epsilon_{\nu}) R_{\nu}^b(T_w) \quad (7)$$

Figure 8b is for KCl, a non-absorbing particle and Fig. 8c is for coal which absorbs in specific bands. By Eq. 7, $R_{\nu}^n = R_{\nu}^b(T_w)$ for KCl, since $\epsilon = 0$. R_{ν}^n matches the black-body curve at the wall temperature of 1060 K. The E/T spectrum of the coal sample matches the wall black-body in regions where the coal is transparent (i.e., $\epsilon \approx 0$) but is lower where the coal has absorption bands. We can determine the emissivity $\epsilon = 1 - R_{\nu}^n/R_{\nu}^b(T_w)$ from these spectra. The emissivity for the lignite of Fig. 8c is shown in Fig. 8d. When compared to the emittance for the same coal at 782 K in Fig. 4b, the most significant difference is the larger hydroxyl band at low temperatures due to hydrogen bonding.

Composition - As illustrated in Fig. 2b, the normalized radiance, R_{ν}^n , is the wall radiance $R_{\nu}^b(T_w)$ attenuated over the chord d at the particle's absorbance bands. We can, therefore, use R_{ν}^n (e.g., Fig. 8c) to obtain the absorbance of the particle if we know the average chord length, d . This has been done using a ray optics model and a computed probability density function $P(d)$ for all possible chords d . A more detailed discussion will be presented elsewhere (20). Figure 9 shows a comparison between the absorbance spectra obtained for the same coal by three methods: a) a quantitative spectrum (i.e. for a known sample density) of a finely dispersed coal in a pressed KBr pellet; b) a non-quantitative photoacoustic spectrum for fine particles suspended on a thin membrane (21); and c) a quantitative E/T "absorbance" spectrum considered to

arise from the black-body furnace spectrum being attenuated by the particle over some effective sample thickness related to the shape and size of the particle. The details of the analysis to obtain the E/T absorbance spectra from the E/T spectra are discussed in (20).

The spectra have a number of similarities and differences. To compare the spectra, it should be noted that the KBr pellet absorbance spectrum is the sum of absorption plus a sloping background due mostly to scattering of radiation. The KBr pellet spectrum also has distortion of the bands (a dip at the high wavenumber side of the band and a sloping tail at the low wavenumber side of the band) due to the Christiansen effect (22). This effect is caused by variation in the real part of the index of refraction near the absorption band, which effects the scattering contribution. The photoacoustic spectrum is free of the scattering and Christiansen effects, but is non-quantitative and appears to be more sensitive to mineral components than to the organic components. On the other hand, the E/T absorbance spectra is free from scattering and band distortions and appears in reasonable quantitative agreement with the absorption component of the KBr pellet spectrum.

Size - Size information can be obtained from the $(1-\gamma)$ or R_{∞}^n spectra. Figure 5 shows the increase in the emissivity with particle size, especially in the region above 1700 wavenumbers. The average particle size can be determined from R_{∞}^n if the complex index of refraction of the material is known. Alternatively, $(1-\gamma)$ contains size information for particles with $D < 80 \mu\text{m}$. For example $(1-\gamma)$ in Fig. 3b increases at low wavenumbers (long wavelengths) due to diffraction effects. The shape may be calculated using Rayleigh theory for large particles (23) or Mie theory for small particles (24). While the effect is small for particles near $80 \mu\text{m}$ diameter, the diffraction effect increases as the particles decrease in size, and is very sensitive to size in the 1-30 μm range.

CALCULATED EMISSIVITY

The determination of spectral emittance is important for two reasons. The first is that knowledge of the spectral emittance is necessary for the measurement of particle temperatures. The second is that the spectral emittance or the emissivity (the average emittance over all wavelengths) must be known to calculate both the rate of particle heatup and the radiative energy released by the particle during gasification or combustion. For small particles, the spectral emittance is usually not measured. Rather, it is calculated using the complex index of refraction, $N = n + ik$, from the standard equations of electromagnetic theory. For spherical particles these calculations are performed using Mie theory.

Unfortunately, some controversy surrounds the value of k for coal. The problem was recently considered by Brewster and Kunitomo (10). Large variations in the value of k have been reported in the literature ranging from less than 0.1 to more than 0.5. Brewster and Kunitomo have suggested that a possible reason for these discrepancies is that previous measurements of k for coal using reflection measurements were highly inaccurate due to an inherent limitation in the ability to get sufficiently smooth, and homogeneous coal surfaces. Using a transmission technique for small particles in KBr, they obtained values of k which are more than an order of magnitude lower in most regions of the spectrum. If the previously measured values of k are too high, then values of emissivity based on them are also too high. Based on the values of emissivity presented above, this is indeed the case.

In this section, we compare the measured values of ϵ_p to predictions of Mie theory. For these calculations, the value of n and k were determined using KBr and CsI pellet spectra for coal, in an extension of the method of Brewster and Kunitomo (10). The results confirm the low values of k measured by Brewster and Kunitomo.

To determine $N = n + ik$ from pellet spectra we use Mie theory and the Kramers-Kronig transform. Mie theory is a general solution of Maxwell's equations for an isotropic, homogeneous sphere of index of refraction N_{ν} , imbedded in a medium of index of refraction \tilde{N}_{ν} (24). In general, the complex index of refraction contains all of the electromagnetic properties of the material, but the real and imaginary parts, n_{ν} , and k_{ν} , must be Kramers-Kronig transforms of each other (24). Physically, this relationship arises by requiring causality, i.e., the material cannot respond to radiation until after the incident radiation hits the material. In practice, we determine k_{ν} , perform a Fourier Transform into the time domain, force causality in the time domain, and then transform back to the frequency domain to obtain n (25). The complete description of the method will be the subject of a future publication, but briefly our procedure for determining n and k is as follows: 1) with trial values of $n = n_0$ (a constant) and $k = 0$ and a particle diameter D , for coal in KBr, we use Mie theory to calculate a smooth scattering curve. 2) This scattering curve, plus a constant to account for reflection from the pellet surface, is subtracted from the experimental spectrum and the result is assumed to be a pure absorption, A_{ν} , where

$$A_{\nu} = \frac{4\pi}{2.3026} \frac{k_{\nu}}{\lambda} \times \frac{\text{volume of coal}}{\text{area of pellet}} \quad (8)$$

3) Calculate k_{ν} from Eq. 8 and use the Kramers-Kronig transform to determine the correction to n . 4) Using these values of n , k , and D , Mie theory is used to predict a CsI pellet spectrum. Since the scattering above 4000 cm^{-1} depends largely on the product $(n_{\text{coal}} - n_{\text{medium}})D$, this 4th step allows us to determine D and n_0 . This procedure is repeated until we can predict both the KBr and CsI spectra with the same n , k and D . The results of this procedure are shown in Fig. 10. Figure 10a and 10b are the KBr and CsI pellet spectra for a Montana Rosebud coal. Values of $n_0 = 1.66$ and $D = 2.6$ microns were found to give reasonable fits to the data. Figure 10c shows the calculated n and k ; and Fig. 10d shows the absorbance due to k (which now depends only on the coal, not the pellet material). Figures 10a and 10b also show the calculated scattering contribution to the absorbance spectrum (which depends on the difference between the n for the coal and medium). The structure in the scattering curves is the Christiansen effect, and as can be seen from Figs. 10a and 10b, it is in the opposite direction for the KBr and CsI pellets. Figure 10d shows the calculated total spectrum for the CsI pellet which is the sum of the absorption and scattering comparison with the measured spectra (Fig. 10b). The agreement is quite good, most obviously for the Christiansen effect on the minimum near 1700 cm^{-1} .

For a particle radius of 25 microns, we use Mie theory with the n_{ν} and k_{ν} from Fig. 10c to predict the emittance spectrum of cold coal, Fig. 10e. This is compared to the measured emittance in Fig. 10f. The agreement is good.

ACKNOWLEDGEMENTS

The general E/T method development and measurements of temperature and emissivities were performed under DOE contract #DE-AC21-81FE05122, the measurement of composition and size under NSF SBIR Grant #CPE-8460379, the measurement of index of refraction and calculating of emissivities under DOE SBIR contract #DE-AC01-85ER80313. We wish to thank Woodrow Fiveland and Richard Wessel of Babcock and Wilcox for helpful discussions on the coal emissivity problems and John McClelland of Ames Laboratory for supplying the PAS spectrum.

REFERENCES

1. Liebman, S.A., Ahlstrom, D.H., and Griffiths, P.R., *Applied Spectroscopy*, **30**, #3, 355, (1976).
2. Erickson, M.D., Frazier, S.E., and Sparacino, C.M., *Fuel*, **60**, 263, (1981).
3. Solomon, P.R., Hamblen, D.G., Carangelo, R.M., and Krause, J.L., Coal Thermal Decomposition in an Entrained Flow Reactor; Experiment and Theory, 19th Symposium (International) on Combustion, 1139, The Combustion Institute, Pittsburgh, PA, (1982).
4. Solomon, P.R., Hamblen, D.G., and Carangelo, R.M., Applications of Fourier Transform Infrared Spectroscopy in Fuel Science, ACS Symposium Series, 205, 4, 77, (1982).
5. Ottensen, D.K. and Stephenson, D.A., *Combustion and Flame*, 46:95 (1982).
6. Ottensen, D.K. and Thorne, L.R., 1983 International Conference on Coal Science, Pittsburgh, PA, pg. 621, (Aug. 15-19, 1983).
7. Solomon, P.R., "Pyrolysis", in Chemistry of Coal Conversion, R.H. Schlosberg, Editor, Plenum Publishing, New York, NY, (1985) in press.
8. Solomon, P.R. and Hamblen, D.G., Measurements and Theory of Coal Pyrolysis, A Topical Report for U.S. Department of Energy, Office of Fossil Energy, Morgantown Energy Technology Center, Contract No. DE-AC21-81FE05122, (1984).
9. Solomon, P.R., Hamblen, D.G., and Carangelo, R.M., "Analytical Pyrolysis", K.J. Voorhees, (Editor), Butterworths London, Chapter 5, pg. 121, (1984).
10. Brewster, M.Q. and Kunitomo, T., *Trans. ASME*, **106**, 678, (1984).
11. Best, P.E., Carangelo, R.M., Markham, J.R., and Solomon, P.R., "FT-IR Emission - Absorption Measurements from Coal and Char: Temperature and Emittance", submitted to *Combustion and Flame*, (1985).
12. Solomon, P.R., Hamblen, D.G., Carangelo, R.M., Markham, J.R. and DiTaranto, M.B., ACS Div. of Fuel Chemistry Preprints, **29**, #2, 104, (1984).
13. Solomon, P.R., Serio, M.A., Carangelo, R.M., and Markham, J.R., ACS Division of Fuel Chemistry Preprints, **30**, #1, 266 (1985).
14. Solomon, P.R., Serio, M.A., Carangelo, R.M., and Markham, J.R., Very Rapid Coal Pyrolysis, Accepted for publication in *Fuel* (1985).
15. Solomon, P.R., Hamblen, D.G., Carangelo, R.M., Markham, J.R., and Chaffee, M.R., Application of FT-IR Spectroscopy to Study Hydrocarbon Reaction Chemistry, ACS Division of Fuel Chemistry Preprints, **30**, #1, 1, (1985).
16. Best, P.E., Carangelo, R.M. and Solomon, P.R., FT-IR Determination of Coal and Soot Particle Temperatures During Pyrolysis, ACS Div. of Fuel Chem. Preprints, **29**, #6, 249, (1984).
17. Hottel, H.C., and Sarofim, A.F., "Radiative Transfer", McGraw Hill Book Co., New York, (1967).
18. Solomon, P.R. and Carangelo, R.M., *Fuel*, **61**, 663, (1982).
19. van Krevelen, D.W., Coal, Elsevier Co., Amsterdam, (1961).
20. Solomon, P.R., Carangelo, R.M., Hamblen, D.G., and Best, P.E., "Infrared Analysis of Particulates by FT-IR Emission/Transmission Spectroscopy", submitted to *Applied Spectroscopy* for publication (1985).
21. This technique was developed by John McClelland of Ames Laboratory and the spectra were supplied by him.
22. Laufer, G., Huneke, J.T. Royce, B.S.H. Teng, Y.C., *Appl. Phys. Lett.*, **37**, 517, (1980).
23. Gumprecht, R.O. and Slipeivch, C.M., *J. Phys. Chem.*, **57**, 90, (1953).
24. Bohren, C.F. and Huffman, D.R., "Absorption and Scattering of Light by Small Particles," John Wiley and Sons, NY (1983).
25. Peterson, C.W. and Knight, B.W., *Journal of the Optical Society of America*, **63**, No. 10, pg. 1238 (1973).

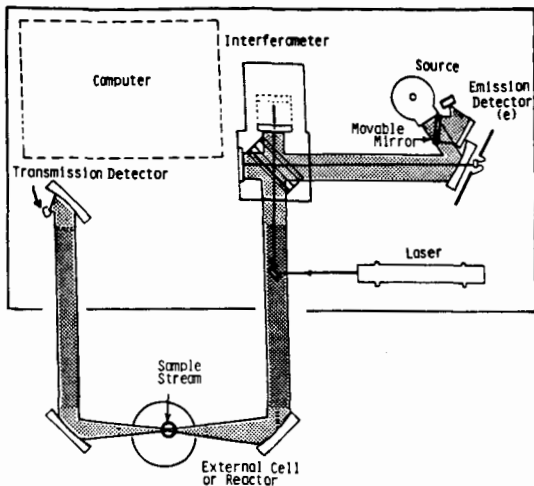


Figure 1. FT-IR Spectrometer with External Cell or Reactor.

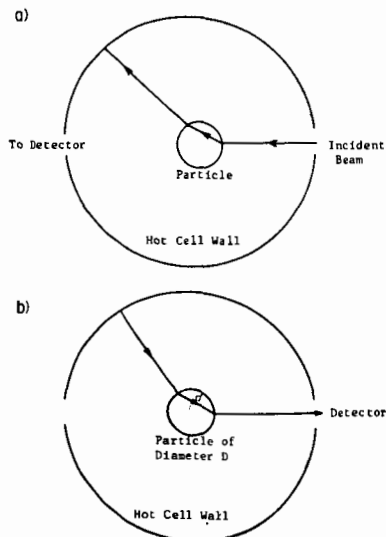


Figure 2. Measurement Geometry. a) Geometry of Transmission Measurement showing the Incident Beam Reflected by the Particle Out of the Beam; b) Geometry of Radiance Measurement showing Wall Radiance Refracted through a Particle to the Detector.

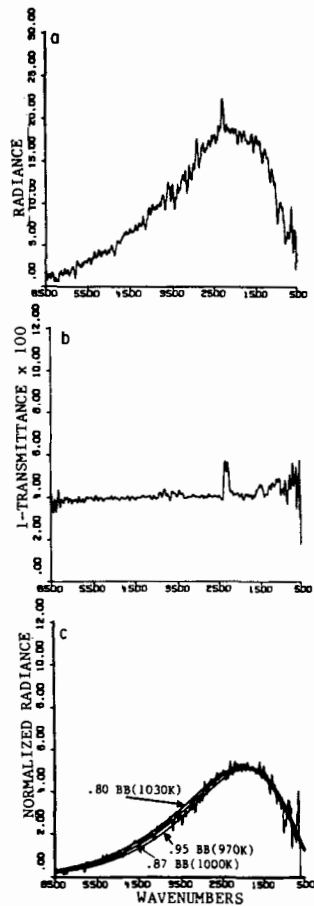


Figure 3. a) Radiance, b) (1-transmittance) and c) Normalized Radiance $R/(1-\tau)$ from Char Previously formed at 1300°C at an Asymptotic Tube Temperature of 1075 K , 115 cm Reaction Distance. In c) the Experimental Data is Overlaid by 3 Black-body Curves, the 1000 K being the Best Fit.

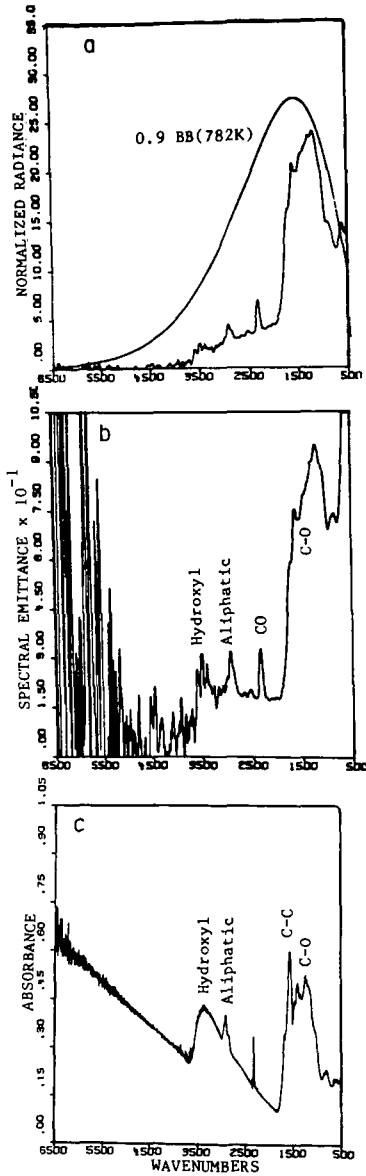


Figure 4. Spectra for Zap North Dakota Lignite a) Normalized Radiance, b) Spectral Emittance, and c) KBr Pellet Spectrum.

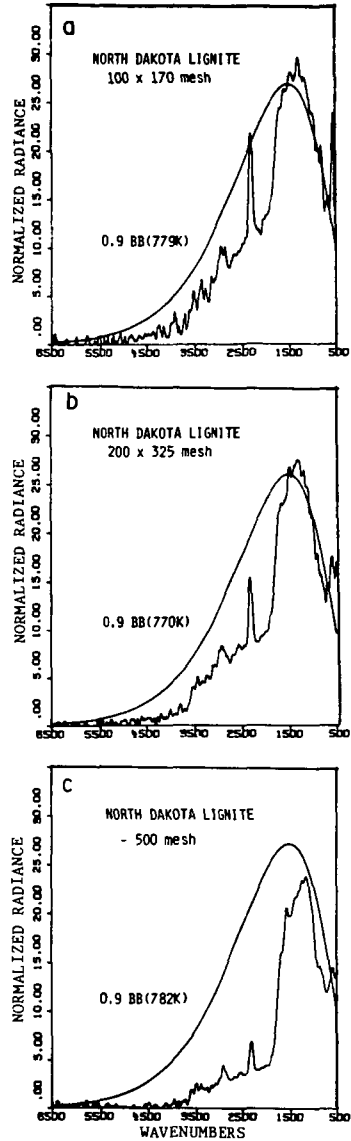


Figure 5. Normalized Radiance for Different Size Fractions of North Dakota Lignite.

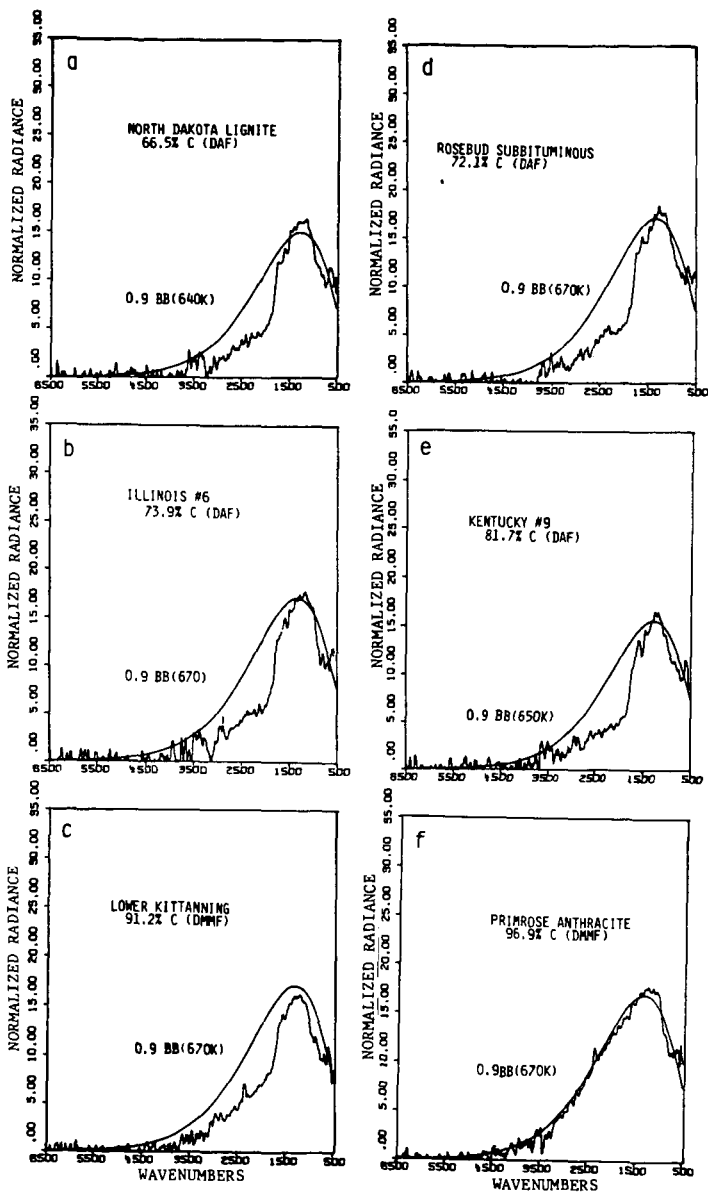


Figure 6. Comparison of Normalized Emission (Radiance) with Theoretical Grey-body Curves ($\epsilon = 0.9$) for Coals of Different Rank.

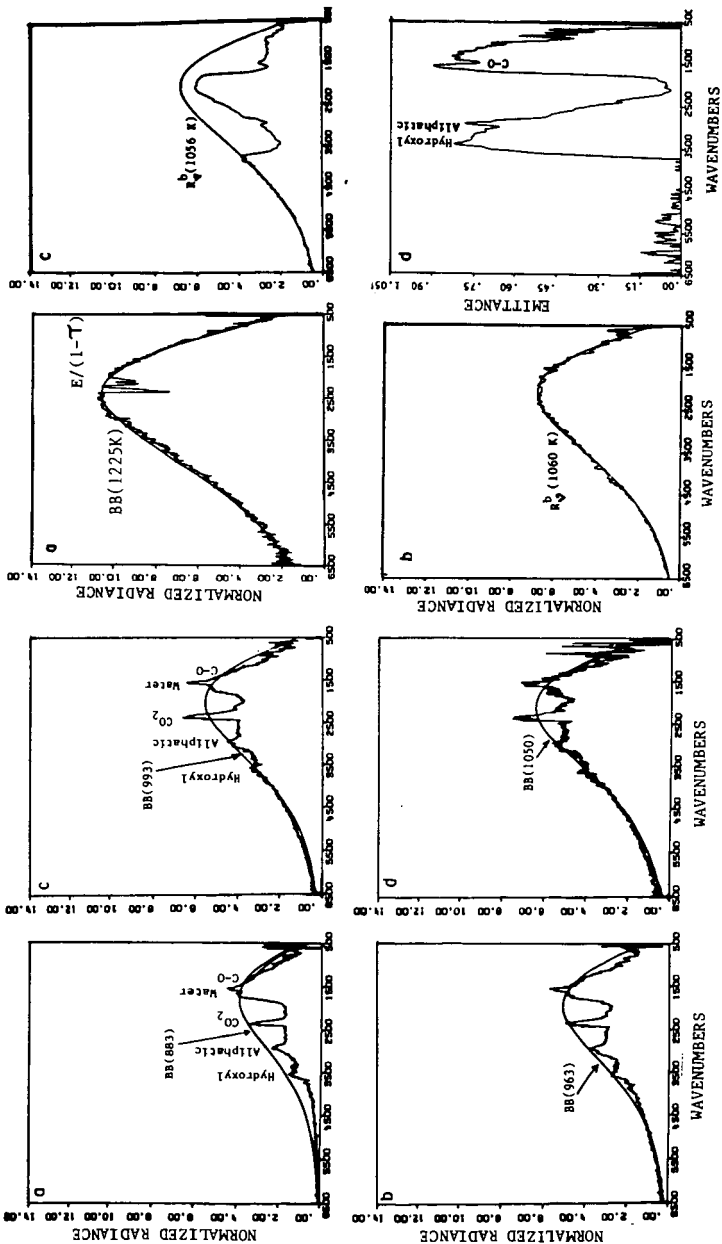


Figure 7. Comparison of Normalized Radiance with Theoretical Grey-Body Curves ($\epsilon = 0.9$) for Charts at Increasing Extents of Pyrolysis.

Figure 8. a-c) Comparison of Normalized Radiance with a Theoretical Black-body Curve for Several Cases. a) Coal, $T_p = T$; b) KCl, $T_p = 1060 >> T$; c) Coal $T_p = 1056 >> T$; d) Emission derived from c) using Eq. 7.

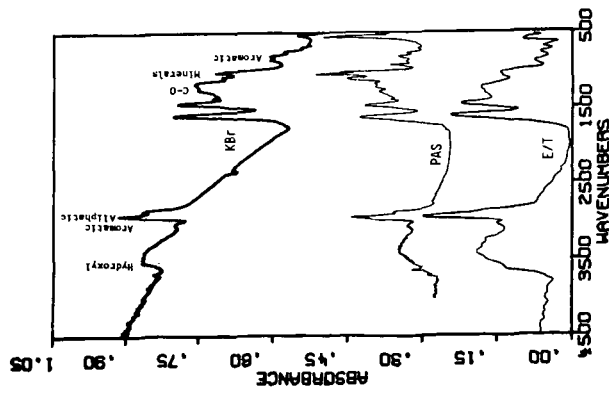


Figure 9. Comparison of Absorbance Spectra Obtained by KBr Pellet, Photoacoustic Spectroscopy (PAS), and E/T Methods. The KBr and E/T Spectra are Normalized to a 1 mg Sample in a 1.33 cm² area. The PAS Spectrum is Non-Quantitative.

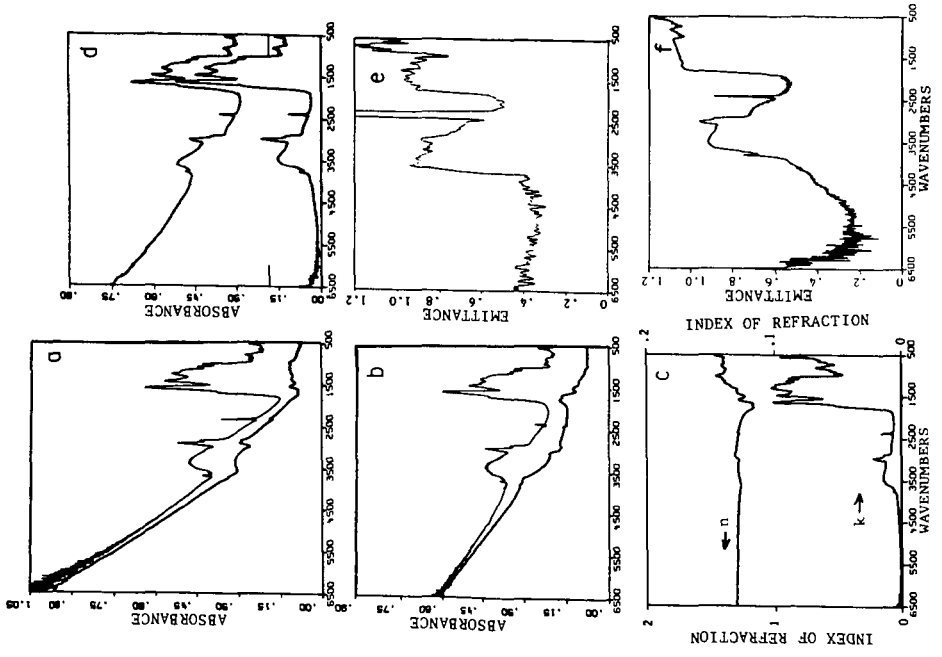


Figure 10. a) Measured Spectrum for Montana Rosebud in KBr with Part of Spectrum due to Scattering. b) Measured Spectrum for Montana Rosebud in Csi with Part of Spectrum due to Scattering. c) Real and Imaginary Parts of the Index of Refraction, $N = n + ik$. d) Upper Curve is Calculated Spectrum for Montana Rosebud in Csi, Lower Curve is Calculated Absorbance of Montana Rosebud without Scattering. e) Measured Emittance for Montana Rosebud, and f) Calculated Emittance for Montana Rosebud.

APPLICATION OF TGA/FT-IR TO STUDY HYDROCARBON STRUCTURE AND KINETICS

Carangelo, R. M. and Solomon, P. R.
Advanced Fuel Research, Inc., 87 Church Street, E. Hartford, CT 06108
and Gerson, D.J., IBM Instrument, Danbury, CT 06810

For the characterization of fossil fuels, thermal analysis methods have proven to be a useful technique for probing the organic and mineral composition of these typically insoluble materials. In thermal analysis, the sample is taken through a temperature excursion and its weight loss or evolved products are monitored. Examples include: the use of thermogravimetric analysis (TGA) for performing coal proximate analysis (1); pyrolysis with detection of total hydrocarbons for petroleum source rock evaluation (2,3) and pyrolysis with trapping of evolved products for analysis by GC for source rocks and sediments (4-7).

This paper describes a new instrument which couples thermogravimetric analysis (TGA) with evolved gas analysis (EGA) performed with a Fourier Transform Infrared (FT-IR) spectrometer. A unique feature of the system is its ability to provide continuous monitoring of the infrared spectra of evolving liquids as well as quantitative analysis of gases during pyrolysis or other reactions. The complementary TGA/EGA data provide a wealth of information regarding composition, structure, and kinetics for hydrocarbons. This technique offers advantages compared to GC in speed, and compared to GC and MS in ability to identify heavy tarry materials. FT-IR studies of chars and tars at various stages of pyrolysis by KBr pellets help complete the story by showing what functional groups in the sample are actually changing when specific pyrolysis products are released. While the instrument typically provides slower sample heating than is encountered in practical coal conversion processes, the use of slow heating in pyrolysis experiments provides data on individual reactions which often cannot be distinguished in flash pyrolysis because they occur simultaneously. Slow heating conditions often resolve such reactions into separate gas evolution peaks. These peaks provide low temperature data for gas evolution kinetics.

This apparatus has been used to analyze coal, char, tar, lignins, wood, polymers, oil shale and source rock. The technique has been useful in elucidating the source and kinetics of many of the pyrolysis products of the above hydrocarbons. The technique will be discussed and examples presented for several materials.

EXPERIMENTAL

The apparatus, illustrated in Fig. 1, consists of a sample suspended from a balance (Mettler, model AE160) in a gas stream within a furnace. As the sample is heated, the evolving tars and gases are carried out of the furnace directly into a gas cell for analysis by FT-IR (IBM Instruments, model IR 85). The FT-IR can obtain spectra every 0.2 sec to quantitatively determine the evolution rate and composition of most pyrolysis products. The system allows the sample to be heated in a gas flow of arbitrary composition on a preprogrammed temperature profile at rates between 3°C/min and 100°C/sec up to a temperature between 20°C and 1000°C and held for a specified time. The system continuously monitors the time dependent evolution of: i) the gases (including specific identification of the individual species such as, CO, CO₂, H₂O, CH₄, C₂H₆, C₂H₄, C₂H₂, C₃H₈, benzene, heavy paraffins, heavy olefins, HCN, HCl, NH₃, SO₂, CS₂, COS, CH₃OH, CH₃COOH and CH₃COCH₃); ii) tar amount and infrared spectrum with identifiable bands from the functional groups; and iii) weight of the non-volatile material (char plus mineral components). An analysis of C, H, and S in the residue at the end of the experiment can be obtained by introducing oxygen to burn the residue and measuring the combustion products.

APPLICATIONS

Coal Pyrolysis - We consider first the use of the TGA/EGA to follow the pyrolysis chemistry of coal. Figure 2 presents a series of spectra obtained during pyrolysis at 0.5°C/sec. The spectra show absorption bands for CO, CO₂, CH₄, H₂O, SO₂, COS, and C₂H₄. In other samples, bands for HCl, NH₃, and HCN can be identified. The spectra also show aliphatic, aromatic, hydroxyl and ether bands from tar, which form an aerosol. Figure 3 shows spectra during tar evolution which identifies these bands. The higher aromatic content of the higher rank coals is evident. At the end of the run the temperature was reduced to 700°C and oxygen was added to the flow to combust the remaining char.

Integrations over specific regions of the spectra provide the concentrations of each species as a function of time as shown in Fig. 4. Evolution curves are shown for 8 species. The tar weight is determined from its concentration of aliphatic, aromatic and ether functional groups. In addition, the absorptivities of each species have been calibrated to provide the weight loss for each species, which is also plotted. The individual constituents can be summed and compared with the char weight loss, as shown in Fig. 4. The directly measured weight loss is very close to that determined from the individual species. The final evolution of H₂O, CO₂, and SO₂ determines the C, H and S composition of the char.

For coal, the relative pyrolysis kinetics can be determined from the position of the peaks (8-11). Figure 5 compares the tar evolution peaks for coals of increasing rank. There is a systematic shift from lignites (lower temperature peaks, higher rates) to bituminous coals (higher temperature peaks, lower rates). The pyrolysis kinetics can be correlated with the coals' ignition properties.

The reactivities of the coal char can also be studied by dropping the temperature at the end of pyrolysis from 900°C to a lower temperature (eg. 300 - 450°C) and measuring the weight loss rate when oxygen is added.

Sulfur Forms - Because of the problems of acid rain, the determination of sulfur forms (e.g. pyrite, calcium sulfate, thiols, thiophenes, etc) is important in evaluating energy resources. Methods employing reductive (12,13) and oxidative (14) pyrolysis at a programmed heating rate have been employed. These methods are based on the concept that the differences in reactivity of each sulfur form will result in separate evolution peaks. Using the TGA/EGA, the determination of sulfur species can be made by following the evolution of SO₂, COS, CS₂ and H₂S. This method of determining sulfur species is an improvement of the reductive pyrolysis method proposed by Attar (12,13) because of the addition of COS, CS₂ and SO₂ species. Figure 6 presents the SO₂ evolution curves from several coals. The profiles are reproducible for repeat analyses. They show peak evolution profiles indicative of separate species as their source. Some peaks appear in all samples (e.g. the peak at 300°C). The Kentucky coal which has the highest pyrite content has a large peak at about 500°C. Also, it is interesting that while the high rank coals retain much of the sulfur in the char (which is released as SO₂ during the combustion cycle) the lignite retains very little. The addition of oxygen to the volatiles shows additional sulfur evolution. These SO₂ evolution curves, together with those of COS and CS₂ must be analyzed to determine whether a relation to specific sulfur forms can be obtained. Sulfur identification could also be made under oxidizing conditions as in the oxidative thermal analysis method discussed by LaCount (14).

Sources for Evolved Products - An excellent way of studying the chemistry of hydrocarbon pyrolysis is to combine analysis of the evolved products with an analysis of the source of the evolved products. Figure 7 presents a series of infrared spectra of chars obtained by stopping the pyrolysis at intermediate temperatures. The loss of

functional groups in the char can be correlated with the appearance of the evolved products. For example, the loss of aliphatic C-H (plotted as solid circles) is clearly correlated with the appearance of the tar as shown in Fig. 4a. Similar correlations can be made between methyl group loss and methane evolution, and ether group loss and carbon monoxide evolution.

An extension of the method is to employ labeled functional groups in the organic material. As an example, we consider perdeutero-methylated coal (15). The coal was chemically altered by substituting CD_3 groups for H on all hydroxyl and carboxyl groups in the coal. The decomposition of these groups is studied by following the appearance of deuterated compounds in the pyrolysis products. In the infrared spectra, the deuterated compounds are shifted with respect to their hydrogen analogs. Figure 8 presents the evolution of CD_3H which occurred just below $450^\circ C$. To study the source for this product, chars were prepared by heating to 300, 400, 500 and $600^\circ C$. The intensity of the CD_3 groups in the char are also plotted (solid circles) on Fig. 8, and it is clear that the loss of CD_3 groups in the char matches the appearance of CD_3H in the gas. Methylated coals also produce methanol at low temperatures.

The chemistry learned from this set of experiments is most relevant to very low rank coals and lignins which have methoxyl groups. Pyrolysis experiments, at a heating rate of $30^\circ C/min$, were performed on several samples including: a) a lignin, b) a coal, c) a methylated coal, d) the perdeutero-methylated coal, e) a polymer with methoxyl groups and f) the same polymer with methyl groups. Where methoxyl groups are present (a,c,d,e, and f) there is a methane peak at a consistent temperature of $450^\circ C$, independent of the other reactions, such as tar formation. In the absence of methoxyl groups, methane evolution starts coincident with tar formation or at $500^\circ C$. The interpretation is that the methoxyl groups decay via homolytic cleavage of the relatively weak O-C bond to form methyl groups which abstract hydrogen to form methane. In the absence of methoxyl groups, initial methane evolution comes from a substitution reaction in which H radicals, believed to be formed during tar evolution, replace the methyl groups. In the absence of H radicals, methane evolution above $500^\circ C$ comes from homolytic cleavage of methyl groups.

Oil Shale - To provide a survey of the yields from reactions occurring in oil shale as a function of temperature, TGA/EGA analyses were performed on samples of shale at a heating rate of $30^\circ C/min$ from 0 to $900^\circ C$ at 1 atmosphere. Figure 9a presents the weight loss as a function of temperature for a 350 mg sample of an Israeli oil shale. Figures 9c-9i present the evolution rate (in arbitrary sample units) as a function of temperature for the major evolved species; oil, COS, SO_2 , methane, ethylene, CO_2 , water, and CO. The individual contributions to the weight loss are also presented on each figure. The sum of these contributions is presented in Fig. 9b.

The weight loss (Figs. 9a and 9b) occurs over three regions. The first, below $150^\circ C$, is due to the loss of moisture. Between 300 and $600^\circ C$ the main source of weight loss is from oil evolution. There is also a significant contribution from CO_2 and minor contributions from CO, H_2O , hydrocarbon gases, and sulfur species. It is interesting that COS and SO_2 evolutions precede that of the oil. Weight loss above $700^\circ C$ is due to carbonate decomposition to produce CO_2 and some CO. The main source of the high temperature CO_2 is the calcite.

An important feature of this analysis is the ability to determine the infrared spectrum for evolved oil. Figure 10 compares the oil spectrum of an eastern and a Colorado oil shale. As can be seen, the Eastern shale oil has a higher level of aromatic components. This is in agreement with the observation that the organic material in the Eastern shales are more aromatic.

Information can also be obtained on the temperature, T_{max} of the oil peak (S2 peak). Figure 11 compares a Colorado and an Israeli oil shale. T_{max} for the Israeli shale appears to be about 20°C lower than T_{max} for the Colorado oil shale. This is consistent with the observation that the Israeli oil shale is more prone to cracking under pyrolysis (16).

Oil Source Rock - The objective in petroleum source rock evaluation is to determine the petroleum generation potential of the sample and its relationship to neighboring samples. Current methods determine the parameters S1, (the height or area under the first oil evolution peak), S2 (the height or area under the second oil evolution peak) and T_{max} (the temperature of the maximum of the second peak). We employed the TGA/EGA analysis of the aliphatic peak to determine the evolution rate and integrated weight loss for several samples of source rock. Examples of the evolution of the aliphatic components for several source rock samples are presented in Fig. 14. The figure shows the evolution rate and the integrated weight loss. A comparison of results of the TGA/EGA with results obtained at Woods Hole Oceanographic Institute (17) are presented in Table I.

TABLE I

SAMPLE	S1 Weight %	S2 Weight %	T_{max} (°C)	
S. Meade 2930-2960	.007	.070	498	Pyroprobe (WHOI)
	.015	.055	470	TGA/EGA (AFR)
S. Meade 6100	.009	.040	540	Pyroprobe (WHOI)
	.040	.040	505	TGA/EGA (AFR)
Ikpikpuk 790	.010	1.0	500	Pyroprobe (WHOI)
	.010	4.0	450	TGA/EGA (AFR)

The values are in qualitative agreement. The TGA/EGA yields are, however, typically higher. This may be reasonable in view of the possible losses of some heavy species in the pyroprobe sample transfer lines.

SUMMARY

For coal, the TGA/EGA is capable of providing a proximate analysis. In addition, the analysis provides not only the total volatile material, but also the individual volatile species. The relative amounts of oxygen and hydrocarbon species provide a good measure of rank and the concentration of functional groups. The evolution of sulfur species provide data on the sulfur forms. Ignition and char reactivity information can also be obtained. The changes in the coal functional group composition during pyrolysis as determined by FT-IR are well correlated with the evolved products (also determined by FT-IR). Analysis of oil shales and source rocks also provides useful data on the organic structure, yield and reactivity of these materials.

ACKNOWLEDGMENT

The work on coal was performed under DOE Contract DE-AC21-81FE05122. Work on oil shale was sponsored by PAMA (Israeli Resources LTD). The authors would like to thank Ron Liotta of Exxon Research and Engineering Company for supplying the sample of perdeutero-methylated coal, and Jean Whelan of Woods Hole Oceanographic Institute for the source rock samples and data.

REFERENCES

1. Ottaway, M., *Fuel*, **61**, 713, (1982).
2. Espitalie, J., Madec, M., Tissot, B., Mennig, J.J., and Le Plat, P., "Source-Rock Characterization Method for Petroleum Exploration", 9th Offshore Technology Conference Paper No. 2395, (1977).
3. Madec, M. and Espitalie, J., *Fuel*, **63**, 1720, (1984).
4. Whelan, J.K., Hunt, J.M., and Huc, A.Y., "Applications of Thermal Distillation-Pyrolysis to Petroleum Source-Rock Studies and Marine Pollution", *J. Anal. Appl. Pyrolysis*, **2**, 79-96, (1980).
5. Huc, A.Y., and Hunt, J.M., "Generation and Migration of Hydrocarbons in Offshore South Texas Gulf Coast Sediments", *Geochim Cosmochim Acta*, **44**, 1081-1089, (1980).
6. Whelan, J. K., Fitzgerald, M., and Tarafa, M. E., "Analyses of Organic Particulates from Boston Harbor by Thermal Distillation-Pyrolysis", *Environmental Science and Technology*, **17**, 292-298, (1983).
7. Huc, A.Y., Hunt, J.M., and Whelan, J.K., "The Organic Matter of a Gulf Coast Well Studied by a Thermal Analysis-Gas Chromatography Technique", *Journal of Geochemical Exploration*, **15**, 671-681, (1981).
8. Juntgen, H. and van Heek, K. H., *Fuel Processing Technology*, **2**, 261, (1979).
9. Solomon, P. R. and Hamblen, D. G., "Pyrolysis", in *Chemistry of Coal Conversion*, R. H. Schlosberg, Ed., Plenum Pub., NY, (1984) in press.
10. Solomon, P. R. and Hamblen, D. G., "Measurements and Theory of Coal Pyrolysis", U.S. DOE (METC) Topical Report No. DOE/FE/05122-1668, (1984).
11. Solomon, P. R. and Hamblen, D. G., "Finding Order in Coal Pyrolysis Kinetics", U.S. DOE (METC) Topical Report No. DOE/FE/05122-1485, (1983). *Progress in Energy and Combustion Science*, **9**, 323, (1983).
12. Attar, A. and Dupuis, F., ACS Div. of Fuel Chem. Preprint, **23**, 2, 44, (1978).
13. Attar, A. and Hendrickson, G.G., "Coal Structure", (R.A. Meyers, Ed.), Academic Press, NY, Chptr. 5, pg. 131, (1982).
14. Robert LaCount, Private Communications.
15. The samples were supplied by Ron Liotta of the Exxon Corporation by methods described in, Liotta, R., *Fuel*, **58**, 724, (1979).
16. Solomon, P. R., Carangelo, R. M., and Horn, E., "The Effects of Pyrolysis Conditions on Israeli Shale Oil Properties", submitted to *Fuel*, (1985).
17. These results and samples were supplied by Dr. Jean Whelan of Woods Hole Oceanographic Institute.

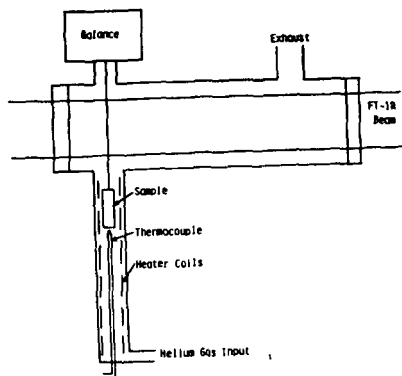


Figure 1. Schematic of TGA/EGA.

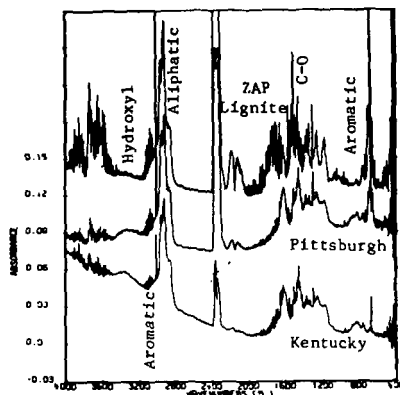


Figure 3. Spectra of Evolved Products Showing Tar Absorption Bands During Pyrolysis of Two Bituminous Coals and a Lignite.

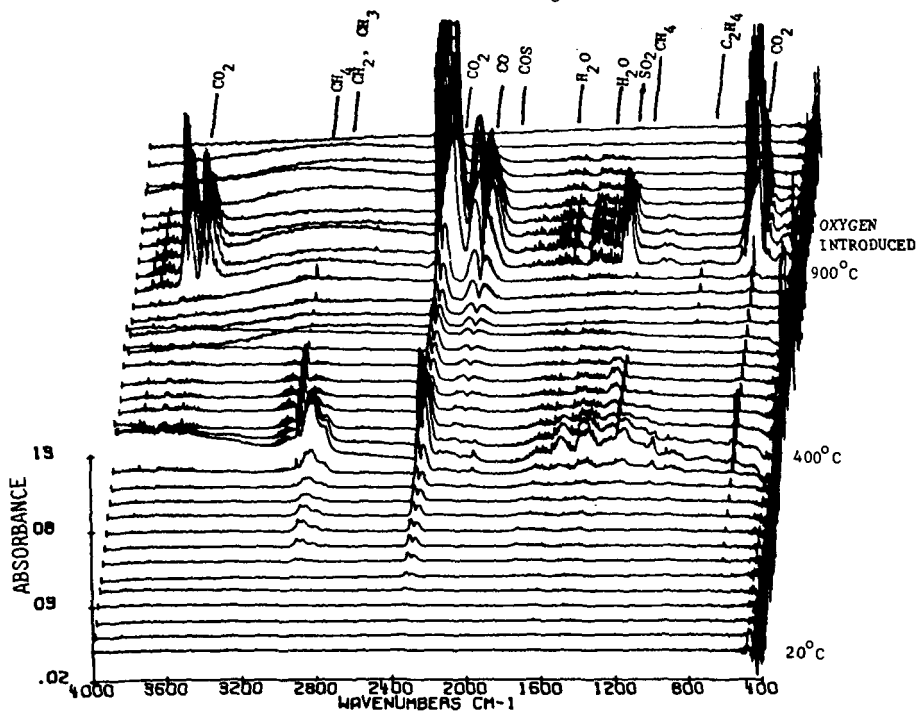


Figure 2. Spectra from TGA/EGA. Heating Rate is 0.5°C/sec from 20°C to 900°C. The Remaining Char is then Burned at 700°C.

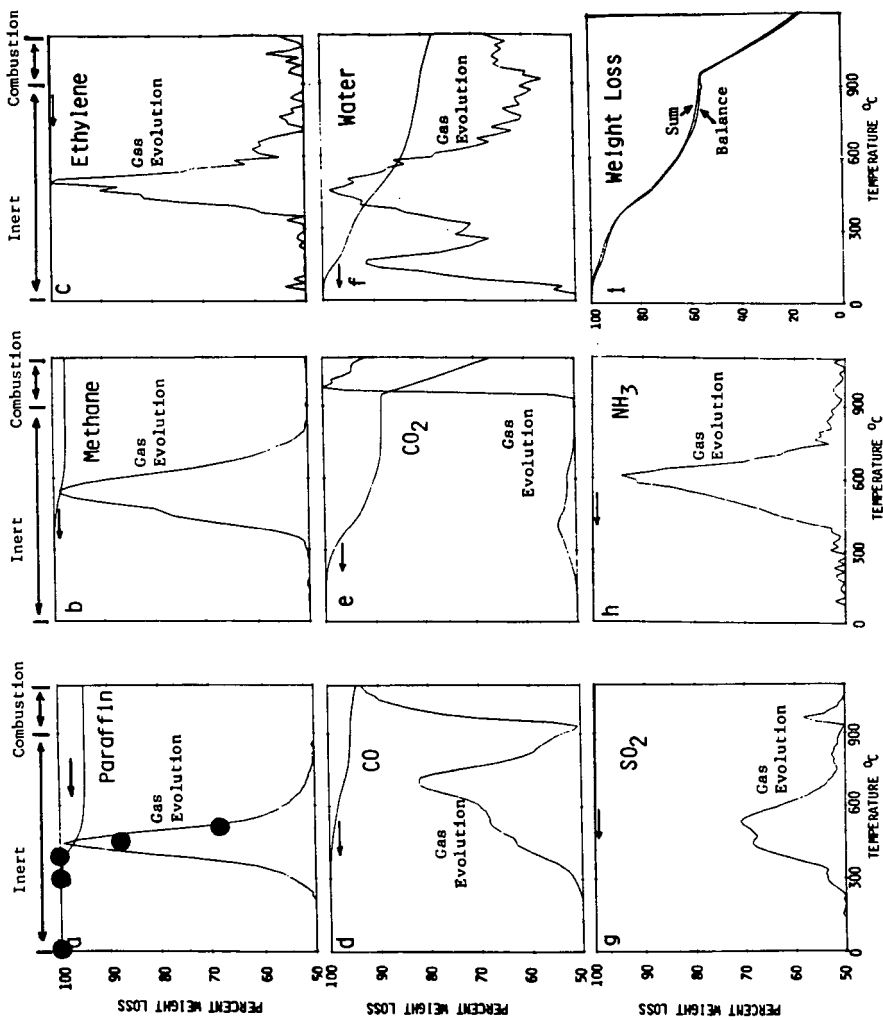


Figure 4. Thermogravimetric/Evolved Gas Analysis (TGA/EGA) of Zap Lignite. a-h) Evolution Rate (in arbitrary units) and Weight Loss from Individual Gas Species, and i) Measured Weight Loss and Sum of Weight Loss from Individual Gas Species. Heating Rate = 30°C/min.

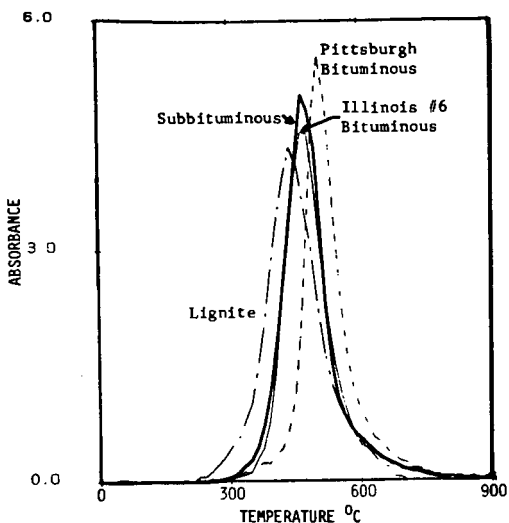


Figure 5. Paraffin Evolutions from Three Coals and a Lignite. T_{max} Varies with Coal Rank Heating Rate = $30^{\circ}\text{C}/\text{min}$.

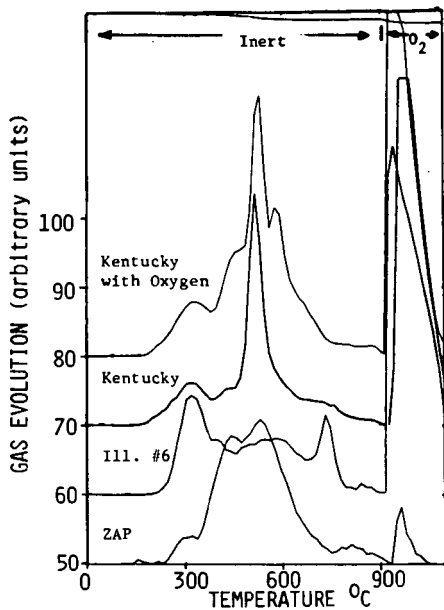


Figure 6. SO_2 Evolutions from Two Coals and a Lignite. The Curves for the Kentucky Bituminous are Present with and without Oxidation of Volatiles.

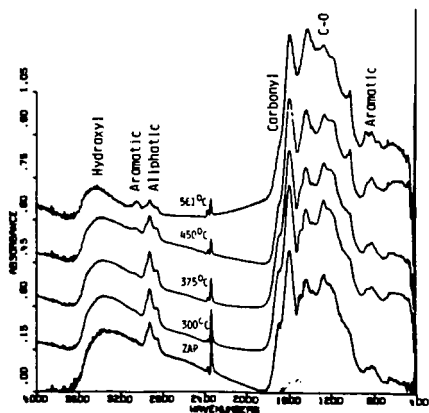


Figure 7. FT-IR Spectra of Chars at Successive Stages of Pyrolysis for ZAP North Dakota Lignite.

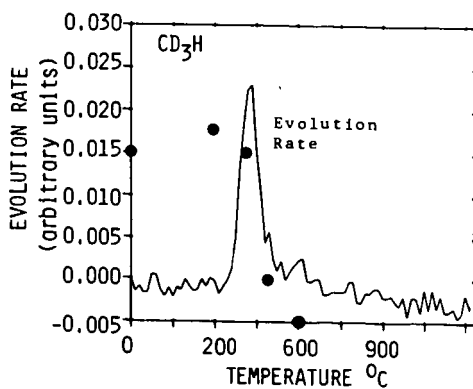


Figure 8. Evolution of CD_3H During Pyrolysis of Perdeutero-Methylated Coal. Heating Rate = $30^{\circ}\text{C}/\text{min}$.

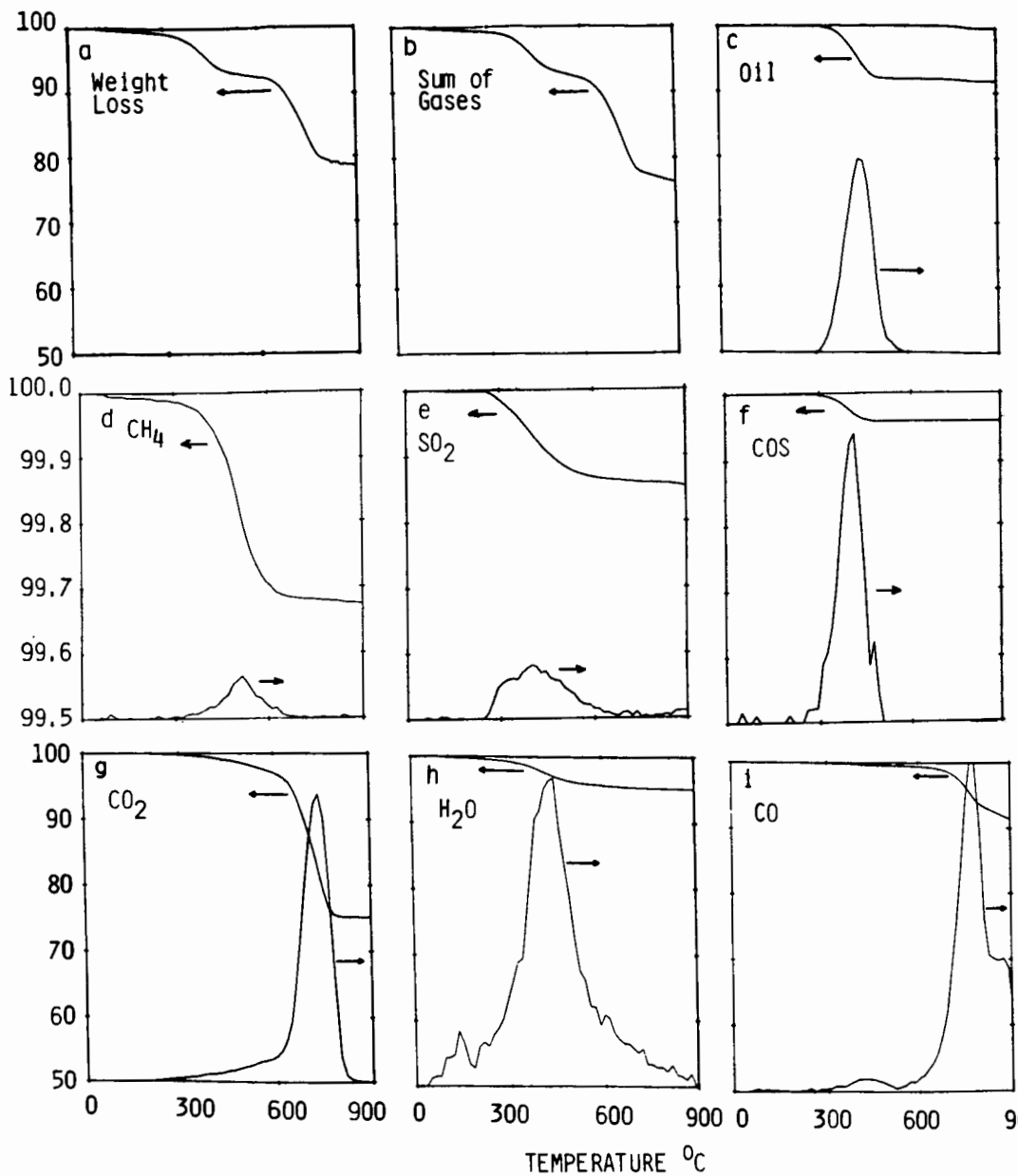


Figure 9. Thermogravimetric/Evolved Gas Analysis (TGA/EGA) of Israeli Oil Shale. a) Measured Weight Loss, b) Sum of Weight Loss from Individual Gases. c-i) Evolution Rate and Weight Loss from Individual Gas Species. Heating Rate = 30°C/min.

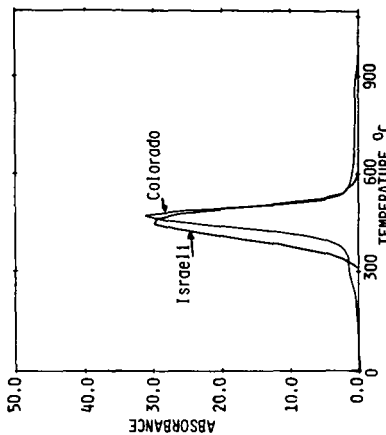


Figure 11. Comparison of Paraffin Evolutions from Israeli and Colorado Oil Shales. The Israeli Oil Shale Appears to be Slightly More Reactive with T_{max} about 20 °C Lower than for the Colorado Oil Shale. Heating Rate = 30 °C/min

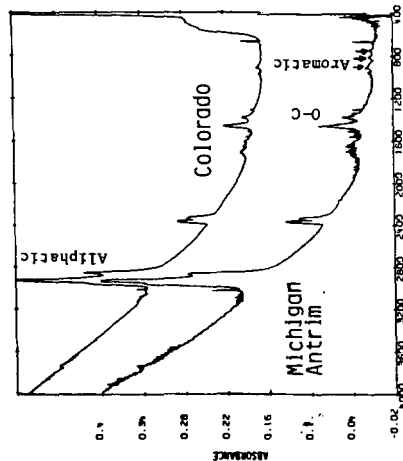


Figure 10. FT-IR Spectra of Evolved Products from Colorado and Michigan Antrim Oil Shales. The Spectra show a Higher Level of Aromatic Hydrogen in the Michigan Antrim Oil Shale.

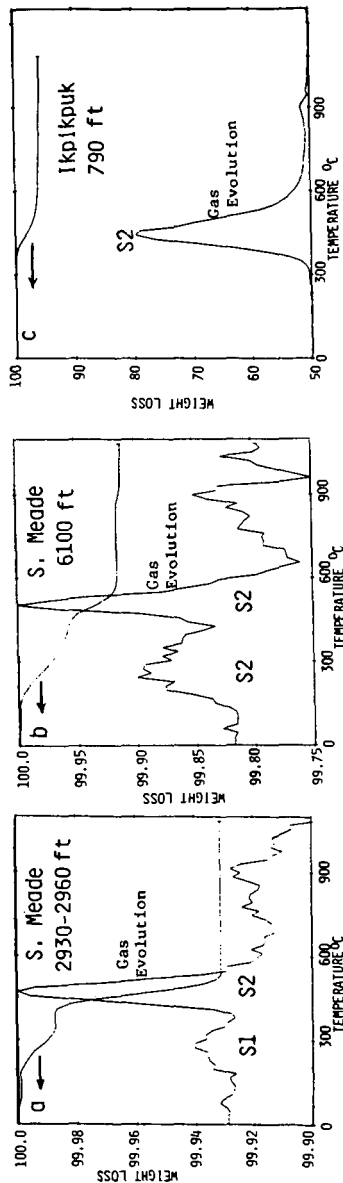


Figure 12. Determination of S1 and S2 and T_{max} for Three Source Rocks using the TGA/EGA. The Parameters are Compared in Table I to those Obtained by Pyroprobe at WHOI. Heating Rate = 30 °C/min.

INTERACTION BETWEEN COAL AND METHANE
DURING ENTRAINED-FLOW FLASH PYROLYSIS
IN RELATION TO ENHANCEMENT IN ETHYLENE YIELD

Muthu S. Sundaram* and Meyer Steinberg
Process Sciences Division
Brookhaven National Laboratory
Upton, NY 11973

ABSTRACT

The flash pyrolysis of coal in a methane atmosphere leads to a significant improvement in total ethylene production by comparison with pyrolysis in an inert helium atmosphere. A study was undertaken to determine the fractional contribution of coal and methane feed toward formation of ethylene. The analytical method entails determination of ^{13}C distribution in coal, methane feed, and product ethylene. The ^{13}C distribution in alkyl side chains (or polymethylene moieties) of coal, which are considered to be likely precursors for ethylene, was found to be higher than in the remaining carbon skeleton. The data available show an interaction between methane and coal during entrained-flow flash pyrolysis of coal with methane with respect to the increase in ethylene yield. At 1000°C and 50 psi methane, with a methane to coal ratio of 1.2, ethylene concentration in the product stream is 1.3% by volume. Of this, 41.8% is produced from coal and the remaining 58.2% is from methane feed. This corresponds to a carbon conversion of 1.9% from methane and 1.6% from coal.

KEYWORDS: Coal; pyrolysis; gasification; methane; ethylene; isotope ratio; carbon.

INTRODUCTION

Traditionally, flash pyrolysis of coals for the production of fuels and chemicals has been carried out in a reactive hydrogen atmosphere and non-reactive helium, nitrogen, and argon atmospheres. The fundamental aspects of primary devolatilization of coal and secondary cracking of volatiles in the above gas media have been investigated extensively under various reaction conditions.

Over the past few years, Brookhaven National Laboratory has investigated the possibility of using methane (or natural gas) as an entraining gas in coal pyrolysis studies. Pyrolysis of coal in a methane atmosphere resulted in enhanced ethylene and BTX yields over those obtained by the flash pyrolysis of coal in an inert helium atmosphere under the same conditions of temperature and pressure.^(1,2)

The objective of the present study was to understand the role of methane in enhancing ethylene production. Originally, experiments were

*To whom correspondence should be addressed.

planned tagging the methane gas with a known amount of $^{13}\text{C}\text{H}_4$. However, this approach was economically impractical, since each experiment would use several hundred litres of expensive CH_4 - $^{13}\text{C}\text{H}_4$ gas mixture. This prompted us to look for other alternatives, and a successful attempt was made taking advantage of the small difference in the natural abundance of ^{13}C in coal and methane.

The focus was on product ethylene rather than on producing a complete ^{13}C material balance. Accordingly, this paper deals with the question: How much of the ethylene in the product stream is produced from coal and how much from methane feed?

EXPERIMENTAL

The flash pyrolysis experiments were carried out in an externally heated 1-in.-diameter-by-8-ft-long downflow entrained tubular reactor. Preheated helium and unlabeled methane gases were fed into the reactor to a pressure of 50 psi. A New Mexico subbituminous coal, with analysis shown in Table 1, was used in the study. The coal, premixed with 10% by weight of Cab-O-Sil (a fumed silica powder) to prevent agglomeration, was dried in a vacuum oven overnight. The particle size of the coal was 150 μm or less, and coal from the same batch was used in pyrolysis experiments reported here. The high temperature gas feed is mixed at the top of the reactor preheating the gases at optimum conditions of temperature, coal-feed rate and gas-feed rate chosen from previous studies so that a high concentration of ethylene was obtained in the product stream.

Routine gas analyses were performed in an on-line GC. In addition, grab samples of product gas mixture were collected in steel gas cylinders, and the components in the gas mixture were separated from each other in a conventional GC/MS system using a 6-ft Carbosieve S column. The compositions of normal ethylene (C_2H_4) and heavy ethylene ($^{13}\text{C}\text{C}\text{H}_4$) in the mixture were determined by selectively monitoring ions due to masses 28 and 29. A typical example of ion profiles for masses 28, 29, 30, and 44 is shown in Figure 1. The nitrogen peak is an impurity arising from the use of a gas-tight syringe for transfer of gas samples from steel cylinders to the injection port of the GC/MS. From the integrated peak area, the $^{13}\text{C}/^{12}\text{C}$ ratio for product ethylene is readily calculated.

RESULTS AND DISCUSSION

The natural abundance of ^{13}C isotope is 1.1%. During the process of photosynthesis, there is a discrimination against $^{13}\text{C}\text{O}_2$ in the rate of assimilation when compared to that of CO_2 .⁽³⁾ As a result of this isotope fractionation, wood, crude oil, and coal are enriched in ^{12}C by about 20 to 30 ‰. The isotopic constitution of carbon in some samples of coal, wood, and methane gas frequently used in our laboratory is shown in Table 2. Methane is lighter than either coal or biomass. An appreciable difference in ^{13}C enrichment between coal or biomass and methane is seen

Table 1

Analysis of New Mexico Coal (wt %)

Rank: Subbituminous

Moisture (as received): 7.8

Proximate Analysis (dry):

Volatile Matter : 34.9
 Fixed Carbon : 42.4
 Ash : 22.4

Ultimate Analysis (dry):

Carbon : 55.9
 Hydrogen : 4.3
 Nitrogen : 1.1
 Sulfur : 1.0
 Oxygen : 14.9
 (by diff.)

Table 2

Isotopic Constitution of Carbon in Selected Materials

Feedstock	$\delta(^{13}\text{C}), \text{‰}^*$	$^{13}\text{C}/^{12}\text{C}$	$^{12}\text{C}/^{13}\text{C}$
Douglas Fir Wood	-23.3	0.01098	91.11
Sugar Pine Wood	-24.1	0.01097	91.19
Illinois No. 6 Bituminous Coal	-25.7	0.01095	91.34
New Mexico Subbituminous Coal	-27.0	0.01093	91.46
Methane	-41.4	0.01077	92.85

*Analyses reported in parts per mil (‰) and computed as follows:

$$\delta^{13}\text{C}_{\text{sample}} = \frac{^{13}\text{C}/^{12}\text{C}_{\text{sample}}}{^{13}\text{C}/^{12}\text{C}_{\text{standard}}} - 1 \times 1000$$

where, $^{13}\text{C}/^{12}\text{C}_{\text{standard}}$ is CO_2 from *Belemnitella americana*, Cretaceous, Peedee formation, South Carolina, USA, Chicago (PDB) standard.

and $^{13}\text{C}/^{12}\text{C}_{\text{standard}} = 0.0112372$

in Table 2. A small enrichment in ^{13}C is observed in a higher-rank Illinois No. 6 bituminous coal when compared with a lower-rank New Mexico sub-bituminous coal. Monin reported a progressive increase in $\delta(^{13}\text{C})$ found in a series of coals from the Mahakam delta, Indonesia.⁽⁴⁾ The $\delta(^{13}\text{C})$ value increased from -29.5 ‰ at the peat-lignite level to -27.6 ‰ at the bituminous A level.

A vast literature exists on the partial oxidation and thermal cracking of methane under various conditions. An excellent review of articles on this subject is available in Reference 6. Methane, however, did not undergo homogeneous decomposition in the BNL reactor. The Cab-O-Sil additive, spent char, and reactor walls made of Inconol 617 alloy were also found not to promote the cracking of methane to ethylene in the absence of coal.

The New Mexico subbituminous coal was pyrolyzed in a methane atmosphere at 1000°C . The same coal was pyrolyzed in a helium atmosphere for comparison. The gas feed rates, in terms of lb-mole per hour, were kept identical in both atmospheres. The reaction conditions and the product yields are shown in Table 3. The yields are customarily reported as percent conversion of carbon contained in the feed coal to product.

The $^{13}\text{C}/^{12}\text{C}$ ratios of product ethylene under various experimental conditions obtained from GC/MS analyses with an error of $\pm 2\%$, are shown in Table 4. The following points are noteworthy: (1) In inert helium atmosphere, the $^{13}\text{C}/^{12}\text{C}$ ratio for ethylene is higher than for the original coal. If ^{13}C atoms were uniformly distributed throughout the coal "structure," one would not expect this fractionation effect. To explain this nonhomogeneity in ^{13}C distribution in the coal matrix, it is suggested that the ^{13}C distribution in alkyl side chains (or polymethylene moieties) of coal, which are considered to be likely precursors for ethylene,⁽⁵⁾ is higher than in the remaining carbon skeleton. This suggests that the origin of these alkyl side chains is different from the rest of the coal. This might be due to a different kind of plant material, a diagenesis organism, or something else. (2) In helium atmosphere, the concentration of ethylene in the product stream decreases from 0.65% at 900°C to 0.35% at 1000°C . However, the concentration in the product stream or the pyrolysis temperature does not affect the $^{13}\text{C}/^{12}\text{C}$ ratio for ethylene. (3) Ethylene concentration increases substantially when the coal is pyrolyzed in methane. (4) The $^{13}\text{C}/^{12}\text{C}$ ratio for ethylene from methanolysis experiments lies between that from a helium run and the $^{13}\text{C}/^{12}\text{C}$ ratio for methane feed. This indicates that a part of ethylene in the product stream comes from coal and the remaining from the methane feed.

On the basis of ^{13}C material balance with respect to product ethylene, the actual fractional contributions of coal and methane feed in the formation of ethylene can be determined. For this analysis, the following assumptions are made:

Table 3

Product Yield Data

Reactor Temperature, °C	900	1000	1000
Entraining Gas	He	He	CH ₄
Gas Pressure, psi	50	50	50
Coal Feed Rate (lb/hr)	1.81	1.81	3.84
Gas Feed Rate (lb/hr)	1.04	1.04	4.74
Gas Feed Rate (lb-mole/hr)	0.26	0.26	0.29
Particle Residence Time (sec)	1.5	1.5	1.5
<u>Product Yields*</u>			
CH ₄	5.4	6.7	ND
C ₂ H ₄	3.3	1.7	3.2 ⁺
C ₂ H ₆	0.3	0	0.5
BTX	3.5	3.3	5.9
CO	4.6	7.2	5.3
CO ₂	1.8	2.1	1.8

* All yields based on the carbon contained in coal.

⁺ Corrected to 1.6% after subtracting the contribution from the methane feed.

Note: The difference in the coal flow rates was not great enough to cause a significant change in ethylene yields.

Table 4

Isotopic Constitution of Carbon in Product Ethylene

Entraining Gas	Temperature °C	Ethylene Concentration (mole %)	13C/12C*	
			13C/12C*	13 _δ ⁺
Helium	900	0.65	0.01295	0.01278
"	1000	0.35	0.01295	0.01278
Methane	1000	1.3	0.01167	0.01154
"	-	-	0.01077	0.01065

* Average of three analyses from samples collected under specified conditions.

⁺ Not to be confused with $\delta(^{13}\text{C})$, ‰.

This is concentration of ¹³C atoms in the total of (¹²C + ¹³C).

- (1) At given temperature and pressure conditions, the devolatilization characteristics of coal are the same in both helium and methane atmospheres.
- (2) The $^{13}\text{C}/^{12}\text{C}$ ratio is not affected by the coal feed rate.
- (3) The kinetic isotope effect involving ^{13}C and ^{12}C atoms is negligibly small.

Setting up a material balance for ^{13}C in ethylene, we have

$$W_m f_m {}^{13}\delta_m + W_c f_c {}^{13}\delta_c = \Delta_e {}^{13}\delta_e \quad (1)$$

- W_m = Amount of carbon in methane feed.
 W_c = Amount of carbon in coal feed.
 f_m = Fraction of carbon in methane converted to ethylene.
 f_c = Fraction of carbon in coal converted to ethylene.
 Δ_e = Total carbon in product ethylene.
 ${}^{13}\delta_m$ = Concentration of ^{13}C in methane feed.
 ${}^{13}\delta_c$ = Average concentration of ^{13}C in coal.
 and ${}^{13}\delta_e$ = Concentration of ^{13}C in product ethylene in methane atmosphere.

The effective concentration of ^{13}C in coal involved in the formation of ethylene, as measured in an inert helium atmosphere, can be related to the average concentration of ^{13}C in whole coal by the following expression:

$${}^{13}\delta_c = \alpha {}^{13}\delta_H \quad , \quad (2)$$

where

- ${}^{13}\delta_H$ = effective concentration of ^{13}C in coal involved in the formation of ethylene
 α = inhomogeneity factor.

Substituting for ${}^{13}\delta_c$ and dividing both sides of Eq. (1) by Δ_e we have

$$X_m {}^{13}\delta_m + X_c {}^{13}\delta_H = {}^{13}\delta_e \quad , \quad (3)$$

where

$$X_m = W_m f_m / \Delta_e \quad (4)$$

= ratio of ethylene produced from methane feed to total ethylene produced.

$$X_c = \alpha W_c f_c / \Delta_e \quad (5)$$

= ratio of ethylene produced from coal to total ethylene produced.

From the definitions for X_m and X_c in Eqs. (4) and (5), it follows that

$$X_m + X_c = 1.0 \quad (6)$$

$^{13}\delta_m$, $^{13}\delta_H$, and $^{13}\delta_e$ are experimentally determined and α can be calculated from $^{13}\delta_H$ and $^{13}\delta_C$. Now, Eqs. (3) and (6) can be solved to obtain the values for X_m and X_c .

Using the data shown in Table 4, X_m and X_c are calculated to be 0.5822 and 0.4178, respectively, which, since the kinetic isotope effect between ^{13}C and ^{12}C is negligibly small, means that 58.22% of the ethylene in the product stream is produced from methane feed and the remaining 41.7 originated in coal under the conditions employed. This corresponds to a carbon conversion of 1.92% from methane and 1.58% from coal. The effect of interaction between coal and methane in enhancing the total yield of ethylene is, thus, clearly indicated. Conversion of methane to ethylene in the presence of coal, as observed by the authors is somewhat higher than the 0.9 - 1.0% conversion reported by Calkins from pyrolysis of methane alone at 850°C for 0.5 sec in a fluidized-bed reactor after having pyrolyzed Alcoa Texas lignite in it.⁽⁷⁾ The higher carbon conversion in BNL experiments is attributed to the higher temperature (850°C vs. 1000°C) and increased residence time (0.5 sec vs. 1.5 sec). Furthermore, the mineral matter or char from the New Mexico sub-bituminous coal used in our study could have been catalytically more active than the lignite used by Calkins et al.

Though this study establishes that interaction between coal and methane effects total ethylene production, it is still not clear whether the yield enhancement is due to catalytic cracking of methane on the coal surface or due to chemical reaction of methane with "reactive" (free radical) species generated from coal. It is our speculation that the mechanism is associated with reaction of methane gas with high-temperature-coal-pyrolysis tar. Reaction studies using representative model compounds can give greater insight into the actual mechanism. Further investigation with a complete ^{13}C material balance between reactants and all products under different coal and methane feed rates is warranted.

CONCLUSION

Pyrolysis of coal in methane atmosphere leads to a significant improvement in total ethylene production when compared to pyrolysis in an inert helium atmosphere. This is due to an interaction between methane and coal during entrained-flow flash pyrolysis. At 1000°C and 50 psi pressure of methane, and a methane-to-coal ratio of 1.2, 1.9% carbon from the methane feed, and 1.6% carbon from the coal feed were converted to produce ethylene resulting in a concentration of 1.3 vol. % in the effluent gas stream.

ACKNOWLEDGMENT

This work was performed under the auspices of the U.S. Department of Energy, Washington, D.C., under contract No. DE-AC02-76CH00016. The authors would like to thank Dr. Alan Goland for his suggestions and helpful comments during this research. Our thanks are due to Prof. William Calkins for a critical review of the manuscript.

REFERENCES

1. Steinberg, M. and Fallon, P.T., Hydrocarbon Processing **61**(III), 92 (1982).
2. Sundaram, M.S., Steinberg, M., and Fallon, P.T., ACS Fuel Div. Prepr. **29**(2), 129 (1984).
3. Rankama, K., Progress in Isotope Geology, Chapter 12, Interscience Pub., John Wiley and Sons, New York, 1963.
4. Monin, J.C., Bondon, J.P., Durand, B., and Oudin, J.L., Fuel **60**, 957 (1981).
5. Calkins, W.H., ACS Fuel Div. Prepr. **28**, 85 (1983).
6. Back, M.H., and Back, R.A., "Thermal Decomposition and Reactions of Methane", Chapter 1 in "Pyrolysis Theory and Industrial Practice", pp. 1-23, Ed., Albright, L., Crynes, B.L., and Corcoran, W.H., Academic Press, New York (1983).
7. Calkins, W.H., and Bonifaz, C., Fuel **63**, 1716 (1984).

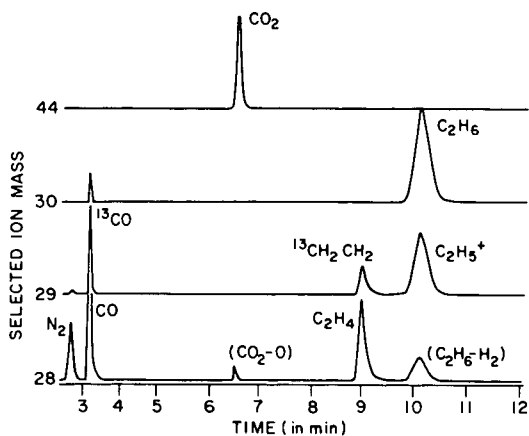


Figure 1. Selected Ion Chromatogram of Gaseous Products from Pyrolysis of New Mexico Sub-bituminous Coal in 50 psi Methane at 1000°C.

UV RESONANCE RAMAN SPECTROSCOPY: A NEW TECHNIQUE FOR SPECIATION OF AROMATICS IN COMPLEX MATRICES.

Sanford A. Asher and Colleen M. Jones

Department of Chemistry
University of Pittsburgh
Pittsburgh, Pa. 15260

Vibrational spectroscopic techniques such as IR and Raman are exquisitely sensitive to molecular structure. These techniques yield incisive results in studies of pure compounds or for rather simple mixtures, but are rarely used for the analysis of complex systems. Indeed, IR can be utilized for quantitative investigations in special cases for complex systems if the analyte of interest shows an infrared absorption spectrally resolved from that of other species in the sample.

Recent advances in laser and optical detection instrumentation permit the development of major new spectroscopic techniques. One of these, UV resonance Raman spectroscopy (1), appears to be uniquely suited for studies of aromatic species in fuels, coal liquids and in petroleum fractions(2,3). It is possible to selectively excite the vibrational spectra of particular ring systems in a complex sample to separately determine the types and concentrations of conjugated rings present in a sample. Our laboratory has pioneered the development of this spectroscopy over the last few years and this report reviews our accomplishments and presents our view of the future.

PHENOMENOLOGY

Excitation of a molecule with monochromatic light results in an induced dipole moment proportional to the magnitude of the electric field of the incident light and to the polarizability of the molecule. The induced dipole moment which oscillates at the frequency of the incident light derives from oscillating charges which are accelerating and decelerating in time. An accelerating charge must radiate light and this induced moment is responsible for the elastic Rayleigh scattering observed for molecules in the gas or condensed phase. Molecular vibrations modulate the molecular polarizability. The molecular vibration couples and beats against the oscillations of the induced dipole moment. This results in a component of oscillation which has a frequency offset from the monochromatic light source by a vibrational frequency of the molecule. This is the origin of Raman scattering (4).

The proportionality between the intensity of Raman scattered light and the intensity of incident light is measured by the Raman cross section, σ . The Raman cross section is proportional to the fourth power of the frequency and to the square of the

Raman polarizability. The Raman polarizability is a strong function of excitation frequency. Excitation within a molecular electronic absorption band can result in a Raman cross section increase of as much as seven orders of magnitude. This occurs because of an increase in the magnitude of the induced moment oscillating at the Raman frequency. This increase occurs because of the dramatic polarizability increase of the molecule for excitation frequencies within the molecular electronic absorption band. Excitation in "resonance" with an absorption band results in a resonance Raman spectrum.

The excitation frequency dependence of the Raman cross section can be utilized to selectively enhance the vibrational Raman spectrum of one component within a complex mixture provided excitation can selectively occur within a discrete absorption band of the analyte. Over the last few years we have examined the factors which permit this selective enhancement. We have developed new instrumentation, clarified the spectroscopic fundamentals, and have begun to apply this new analytical technique to polycyclic aromatic hydrocarbons (PAH's).

INSTRUMENTATION

We recently described the construction of a UV and visible wavelength Raman spectrometer which is continuously tunable from 217 to 800 nm and which is discretely tunable at shorter and longer wavelengths using stimulated Raman shifting in a hydrogen cell (5,6). A block diagram of the instrument is shown in Figure 1. The excitation source derives from a Nd-YAG laser whose 1064 nm output is frequency doubled or tripled or quadrupled by using nonlinear optical techniques. The frequency doubled or tripled Yag excitation pumps a dye laser giving tunable light from 370-800 nm. UV light is generated by either frequency doubling the dye laser output or by combining the doubled dye laser output with the YAG fundamental. Excitation further in the UV derives from Raman shifting of the quadrupled Yag in hydrogen.

The UV excitation beam is diffusely focused on the sample which either flows through the excitation beam in a stream free of any sample walls, or flows in a quartz capillary. The Raman scattered light is collected by reflective optics to avoid lens chromatic aberrations and this light is focused onto the entrance slit of a Spex Triplemate spectrometer-spectrograph. The double spectrometer stage rejects the Rayleigh scattered light by using subtractive dispersion. The spectrograph stage disperses the Raman scattered light onto an EG&G PAR OMA II intensified Reticon array. This optical multichannel detector simultaneously detects the entire Raman spectrum dispersed across its active surface and avoids the signal-to-noise limitation associated with the pulse-to-pulse fluctuations in effective pulse energy of the laser. Except in the case of nonlinear phenomena the signal-to-noise-ratios for typical signal levels appear to be limited by photon shot noise.

FUNDAMENTALS

3

We developed a new technique to measure, for the first time, absolute Raman cross sections (7). We examined small molecules such as CH_3CN , SO_2 , NO_2 , acetone, N-methyl acetamide as well as other species and found that the intensities derived from preresonance enhancement by transitions in the vacuum UV. Species such as NO_2 and N-methyl acetamide which have clearly assigned $\pi \rightarrow \pi^*$ transitions show Raman cross sections which are essentially dominated by these strong absorptions (8). The other species show no discrete, easily assignable transitions in the vacuum UV and show Raman cross sections which increase relatively slowly (almost as ν^4). A major point of these studies is that no interference will occur from the resonance Raman scattering of small molecules for excitation at wavelengths greater than 210 nm. For example, the carbonyl functional group of acetone and the amide functional group of acetamide show $n \rightarrow \pi^*$ transitions between 200 and 280 nm; however, these absorptions result in negligible resonance Raman scattering. It is clear that species containing these functional groups will not congest the Raman spectra of mixtures. It should be realized, however, that the signal-to-noise ratio of the spectra will decrease to the extent that the excitation beam is absorbed by the absorption bands of these species.

Little resonance Raman intensity is evident from the 260 nm absorption spectrum of benzene (9). Indeed, the Raman intensity observed for benzene with visible wavelength excitation derives from excited states in the far vacuum UV spectral region. Major increases in benzene Raman intensity occurs only for the ν_1 , symmetric ring stretch at 992 cm^{-1} . This enhancement which appears to derive from both the B_{1u} and E_{1u} transitions is only evident for excitation below 230 nm. Thus, benzene is a relatively weak Raman scatterer in the 215-300 nm spectral region. Substituted benzene derivatives, in contrast, show strong resonance enhancement from their L_u (in benzene B_{1u}) transitions (10). The aromatic ring modes increase in intensity by a factor of 1000 compared to that in benzene excited between 215-240 nm. This occurs primarily because ring substitution breaks the ring symmetry and allows many ring vibrations to be Raman allowed. Figure 2 compares the resonance Raman spectra of benzene, toluene and phenylalanine with 230 nm excitation. The shaded peaks derive from Raman bands of the solvents. Obviously, selective enhancement is present for substituted benzene derivatives.

Substituted benzene derivatives such as phenol, p-cresol, tyrosine, phenolata and tyrosinate have strong absorption bands shifted to longer wavelength than that of alkyl substituted benzenes (10,11). The oscillator strengths of the absorption bands increase and a large increase occurs in their UV Raman intensities. Indeed, the L_u transitions of p-cresolate, tyros-

inate, and phenolate are shifted to 240 nm and excitation in these absorption bands result in large resonance Raman intensities.

Polycyclic aromatic hydrocarbons show strong absorptions in the UV (12). In general, the maximum wavelength for absorption increases as the number of fused conjugated rings increase. Although the longest wavelength absorption bands often show modest oscillator strengths the second and higher singlet transitions are strong. Figure 3 shows the absorption spectra of a variety of polycyclic aromatic hydrocarbons. The absorption spectrum of a solution of a coal liquid in water is shown as the topmost spectrum. The broad strong absorptions of the coal liquid sample derive from the numerous polycyclic hydrocarbon ring systems present in the sample. Figure 4 illustrates the UV resonance Raman spectra displayed by the different PAH's at excitations close to their absorption spectral maxima.

The different PAH's can be selectively studied by utilizing their unique vibrational spectral features and by selectively exciting each PAH in its relatively unique absorption band (12). Ring substitution alters the Raman spectra as can be seen by comparing the UV Raman spectra of naphthalene and its 1- and 2- hydroxy derivatives (Fig. 5). Thus, the spectra are diagnostic of ring substitution patterns. Indeed, the substitutional isomers show absorption spectral shifts which can be utilized to separately and selectively excite the individual derivatives in mixtures.

The magnitude of resonance enhancement for these derivatives is huge. For example, the Raman cross section for pyrene excited at its 240 nm absorption spectral maximum is significantly greater than 4×10^{-23} cm²/sr molc. This compares to a cross section of close to 10^{-27} cm²/sr molc for an alkane in this spectral region. Thus, a dramatic selectivity exists for resonance enhancement of polycyclic aromatic hydrocarbons versus saturated hydrocarbons and nonaromatic ring systems. As discussed later, our values for the cross sections of pyrene are underestimates because saturation phenomena have prevented the penultimate measurements of the cross sections. It is, however clear from figure 6 that the detection limit for pyrene in acetonitrile solution is less than 20 ppb. Recent improvements have decreased the detection limit to less than 1 ppb. This limit derives from optical saturation phenomena due to the high laser peak powers, and is not the ultimate detection limit.

APPLICATIONS

We are able to selectively enhance polycyclic aromatic ring systems in complex samples of industrial analytical interest. For example, our recent UV Raman study (2,3) of a coal liquid dissolved in acetonitrile demonstrates that the spectra are characteristic of the polycyclic ring systems present in the coal liquid samples (Figure 7). Different excitation wavelengths result in spectral changes which reflect alterations in the

selective enhancement of the polycyclic aromatic ring systems in the sample. The fact that UV Raman measurements of these ring systems is possible indicates that UV Raman spectroscopy is apparently immune from the fluorescence interference phenomena which plague normal visible wavelength Raman measurements of typical environmental and industrial samples. This immunity stems from the fact that few, if any, compounds show fluorescence below 250 nm in condensed phase matrices (2).

The future is especially bright for the application of UV Raman measurements to petroleum and coal liquid samples. Information is available on conjugated fused ring systems. As libraries of data become available on model systems it will become practical to analyze typical samples for aromatic ring content and overall substitution patterns. Unfortunately, the technique is relatively insensitive to the exact structure of the ring substituent unless it is unsaturated and conjugated with the ring. The spectra are, however, sensitive to the ring substitution position.

Extraordinarily complex samples will require pre-separation prior to spectral identification of individual components. The high sensitivity of UV Raman measurements can be effectively utilized in the detection of polycyclic aromatic hydrocarbons eluting from an HPLC column as is illustrated in figure 8.

The utility of UV Raman spectroscopy for studies of fuels is just now being investigated. Many of the ongoing studies focus on characterizing the spectroscopic phenomena involved and relating spectral data to detailed ring structure. Other studies involve developing new sampling methodologies. The present UV laser excitation sources are pulsed with low duty cycles. These pulses which are typically less than 5 nsec in duration have extraordinarily high peak powers. These high peak powers can result in peculiar optical phenomena which limit spectral sensitivity and/or result in the creation and observation of photochemical transient species (11). For example, recent studies of tyrosine and phenol displayed spectral features assignable to phenoxy and tyrosyl radical species which were formed due to photon absorption from the incident laser pulse. A subsequent photon from the same excitation pulse was resonance Raman scattered from the transient radical species. It was interesting that the phenoxy radical forms only transiently and decays back to ground state phenol with a milli- to micro-second lifetime.

A more insidious limitation of the high peak power excitation pulses is optical saturation phenomena (13). Figure 9 shows three resonance Raman spectra of pyrene in acetonitrile. The acetonitrile peaks are shaded. The differences between the spectra derive from changes in the incident excitation pulse power density. The important feature to note is that the

relative pyrene intensities compared to acetonitrile intensities increase dramatically as the pulse power density decreases. Indeed, no intensity is evident for the acetonitrile at the lowest laser excitation power. The acetonitrile intensities are directly proportional to laser power. Thus, the acetonitrile cross sections do not depend on the excitation power. In contrast, the pyrene cross sections are obviously decreasing as the excitation power density increases. Thus, the optimal cross section for pyrene would occur for low power excitation. Unfortunately, this condition is accompanied by low net Raman intensities, poor signal-to-noise ratios and high detection limits.

We are in the process of developing a quasi-CW UV laser excitation source to improve the sensitivity of UV Raman spectral measurements. The likely detection limits for pyrene in pure acetonitrile solutions, for example, are likely to be in the part per trillion range. It should be realized that this represents less than a femtogram of pyrene in the sample volume probed by the laser. Further, we are in the process of examining cryogenic sampling methodologies such as Shpol'skii and matrix isolation. These techniques will lead to increased sensitivity and selectivity. Increased selectivity derives directly from narrowing of vibrational Raman bands which permit finer resolution between Raman bands of different species, and also the narrowing of the Raman excitation profiles which permit higher resolution excitation for the Raman spectra of individual species. Increased sensitivity derives from the accompanying dramatic increases in Raman intensity due to decreased homogeneous and inhomogeneous linewidths of the electronic absorption bands.

We expect the next few years to result in major new advances in the demonstrated utility and utilization of UV Raman spectroscopy as a technique for the study of PAH's in complex samples. In addition to an increased understanding of the fundamental spectroscopic processes involved, the development of a library of spectral data, and the development of simple sampling methodologies we expect major improvements in instrumentation which will make the technique routine and permit the commercialization of a reasonably priced instrument.

REFERENCES

1. Jones, C. M.; Naim, T.; Ludwig, M.; Murtaugh, J.; Flaugh, P. F.; Dudik, J. M.; Johnson, C. R.; Asher, S. A.; Trends Anal. Chem. 1985, 4, 75.
2. Asher, S. A.; Johnson, C. R.; Science 1984, 225, 311.

3. Johnson, C. R.; Asher, S. A.; Anal. Chem. 1984, 56, 2258.
4. Long, D. A.; "Raman Spectroscopy"; McGraw Hill: New York, 1977.
5. Asher, S. A.; Johnson, C. R.; Murtaugh, J.; Rev. Sci. Instru. 1983, 54, 1657.
6. Asher, S. A.; Appl. Spectrosc. 1984, 38, 276.
7. Dudik, J. M.; Johnson, C. R.; Asher, S. A.; J. Chem. Phys. 1985, 82, 1732.
8. Dudik, J. M.; Johnson, C. R.; Asher, S. A.; J. Phys. Chem. 1985, 89, 3805.
9. Asher, S. A.; Johnson, C. R.; J. Phys. Chem. 1985, 89, 1375.
10. Asher, S. A.; Ludwig, M.; Johnson, C. R.; J. Am. Chem. Soc. 1985, submitted.
11. Johnson, C. R.; Ludwig, M.; Asher, S. A.; J. Am. Chem. Soc. 1985, in press.
12. Asher, S. A.; Anal. Chem. 1984, 56, 720.
13. Jones, C. M.; Ludwig, M.; Asher, S. A.; Appl. Spectrosc. 1986, in preparation.

ACKNOWLEDGEMENTS

We gratefully acknowledge partial support of this work from NIH grant 1-R01GM30741-04 and by EG&G Princeton Applied Research. Sanford A. Asher is an Established Investigator of the American Heart Association; this work was done during the tenure of an Established Investigatorship of the American Heart Association and with funds contributed in part by the American Heart Association, Pennsylvania affiliate.

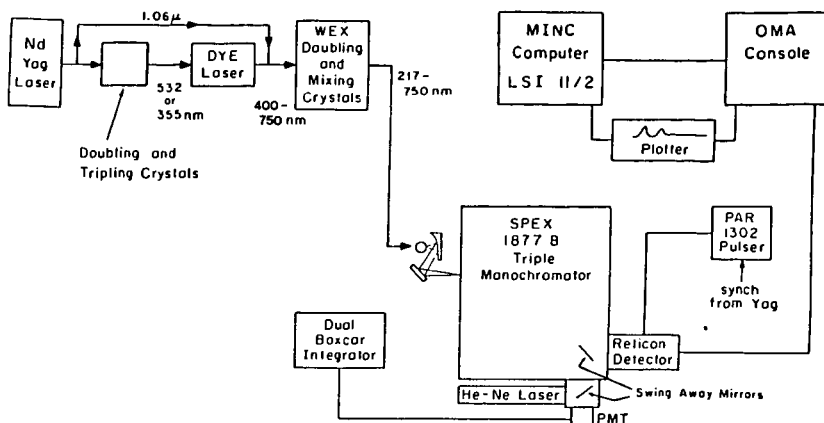


Fig 1. Block diagram of UV Raman Spectrometer. Taken from reference 1.

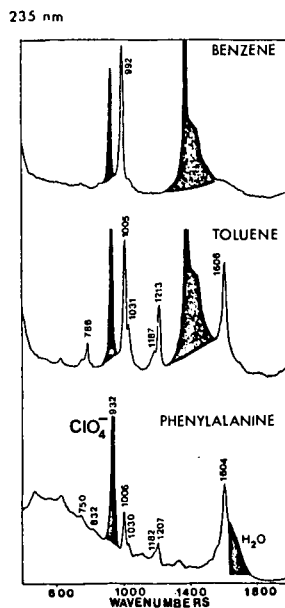


Fig 2. UV resonance Raman spectra of solutions of benzene and toluene in acetone/nitrite and phenylalanine in water excited at 235 nm. The darkened peaks derive from the solvent and ClO_4^- anion. Adapted from reference 10.

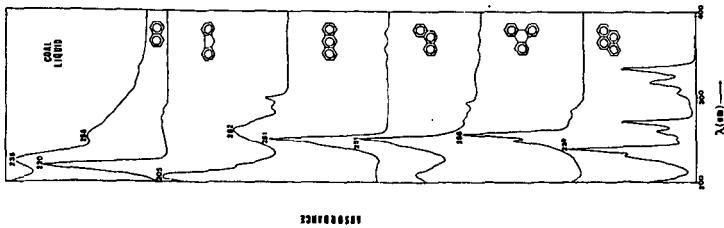


Fig 3. Absorption spectra of various polycyclic aromatic hydrocarbons in acetone. Taken from reference 3.

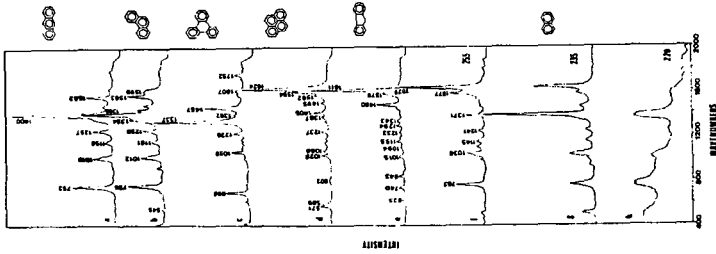


Fig 4. UV resonance Raman spectra of various polycyclic aromatic hydrocarbons in acetone. Except where explicitly indicated excitation occurred at 235 nm. Taken from reference 3.

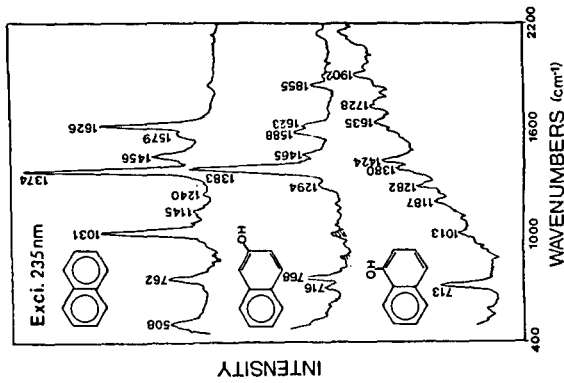


Fig 5. UV resonance Raman spectra at 235 nm of derivatives of naphthalene dissolved in acetonitrile. The bands of the solvent have been numerically subtracted.

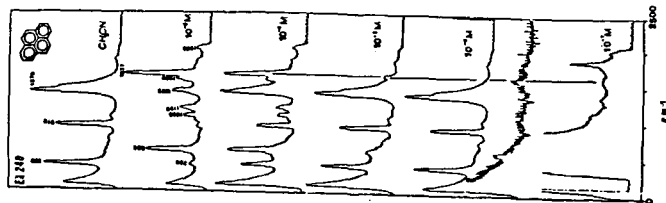


Fig. 6. UV Resonance Raman spectra of Pyrene in acetone/nitrile at different concentrations. Top spectrum is the Raman spectrum of a 10⁻⁴ M solution of Pyrene in water. The bottom spectrum is of 10⁻¹ M Pyrene in acetone/nitrile. The second from the bottom spectrum is from the 10⁻² M solution after subtraction of the spectrum of the acetone/nitrile. Excitation is at 240nm. Taken from reference 12.

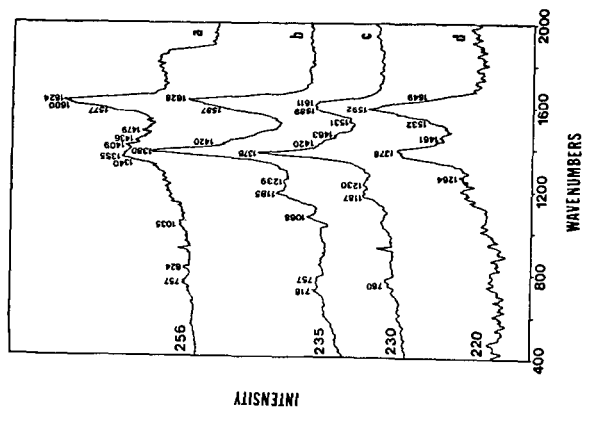


Fig. 7. UV resonance Raman spectra of a solution of a coal liquid sample dissolved in acetone/nitrile at various excitation wavelengths. Taken from reference 3.

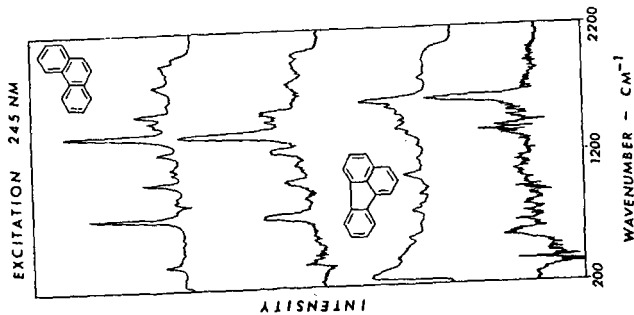


Fig B. UV resonance Raman spectra of phenanthrene and fluorene eluting in real time from an HPLC column. The top spectra are from pure samples in static solutions while the shaded regions were measured during the elution of the components from the column. Scan duration 58 one minute.

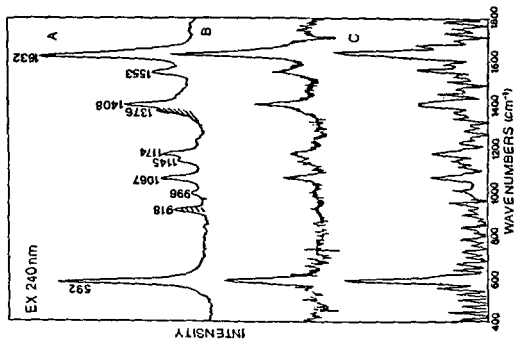


FIG P. UV resonance Raman spectra of a 10^{-4} M pyrene solution in acetonitrile as a function of laser power. A, maximum pulse energy; B, 50 % of maximum; C, 30 % of maximum. Acetonitrile bands are shaded in the figure.

COAL TAR ANALYSIS BY LC/MS

A.A. Herod, W.R. Ladner, B.J. Stokes

National Coal Board, Coal Research Establishment,
Stoke Orchard, Cheltenham, Glos. GL52 4RZ, UK

A.J. Berry and D.E. Games

Department of Chemistry, University College,
P.O. Box 78, Cardiff, CF1 1XL, UK

SUMMARY

The application of LC/MS to the analysis of an aromatic fraction of a hydroxyrolysis tar is described. The results are compared with those obtained by GC/MS, low eV probe mass spectrometry and field desorption mass spectrometry.

INTRODUCTION

The production of liquids from coal gives rise to complex intermediates which require detailed analysis to understand the processes occurring and to make effective use of the products. Analysis has hitherto been based on structural parameters from NMR methods (1) to give the average characteristics of the sample, supplemented by molecular information from GC and GC/MS. The gas chromatographic approach to molecular information is often hampered by lack of volatility and is generally limited to aromatic systems of five or six condensed rings with molecular weights up to about 300 (2). For samples with number average molecular weights over 300, the molecular information available through GC/MS describes less than half of the compounds present. To improve this situation we have investigated LC in conjunction with mass spectrometry for the analysis of coal tar.

Liquid chromatographic separations of coal-derived oils have been followed off-line by GC (3-6) and by probe-mass spectrometry (6). Directly combined LC/MS studies of coal-derived samples are rare (7,8), although LC/MS of standards found in coal tars (9) and of aromatic material from petroleum (10), as well as super-critical fluid chromatography/MS applied to a coal tar extract (11), have been described.

This paper describes the application of LC/MS to the analysis of an aromatic fraction of a hydroxyrolysis coal tar and compares the results with those obtained by GC/MS, by mass spectral probe at low ionising voltage and by field desorption mass spectrometry.

EXPERIMENTAL

Tar Sample and Fractionation

The tar chosen for study was produced by the hydroxyrolysis of a high volatile bituminous coal (82.9% C; 5.3% H) at 500°C in 150 bar hydrogen in a fixed bed reactor. The tar was first separated by solvent extraction into pentane solubles, asphaltenes (pentane insoluble-benzene soluble) and preasphaltenes (benzene insolubles); the pentane soluble fraction was further subdivided into saturates, aromatics and polars by column chromatography on silica (12). The separation scheme is shown in Figure 1 where yields for the various fractions are given relative to the starting weight.

Standard compounds

Standard compounds used to establish the mode of separation of the LC column were cyclohexane, perhydropyrene, benzene, toluene, pentyl benzene, sym-octahydrophenanthrene, naphthalene, methylnaphthalene, acenaphthene, diphenyl, dibenzofuran, 9,10 dihydroanthracene, fluorene, phenanthrene, methyl phenanthrene, pyrene, chrysene, perylene, dibenzanthracene and dibenzopyrene.

EQUIPMENT

The LC was performed using an analytical 3.9 x 300 mm stainless steel $10\ \mu\text{m}$ Bondapak NH_2 column with hexane as the mobile phase pumped at $1\ \text{ml}\ \text{min}^{-1}$ by a Waters 6000A pump. Detection was either by a variable wavelength Cecil 272 detector at 254 nm or a Finnigan 4000 mass spectrometer equipped with a moving belt interface and an Incos data system.

GC/MS examination was carried out using a Perkin-Elmer F17 gas chromatograph with a 42 m glass SCOT capillary column coated with SP2100 phase which was interfaced by a glass jet separator to a Kratos MS30 double beam mass spectrometer fitted with a DS55 data system. Mass spectrometric resolution of 3000 and a scan rate of 3 s/decade of mass enabled accurate mass measurement of all the spectral peaks. The gas chromatograph temperature-programme was from 85° to 285°C at 4°min^{-1} .

MS 30 examination of the aromatics (at 10 eV) was achieved using a solids injection probe heated from ambient temperature to 350°C . Field desorption mass spectrometry on the same sample was performed using a Varian CH_3 double focussing instrument.

RESULTS AND DISCUSSION

The full ultimate and proximate analyses of the coal and tar asphaltenes and aromatics are given in reference (1); the whole tar contained 82.2% C and 7.0% H while the aromatics fraction contained 87.5% C and 7.7% H. Number average molecular weights of the whole tar and the aromatics were 260 and 250 respectively.

LC of standards and aromatic fraction

The LC/UV separation of some of the standards is shown in Figure 2. This separation gave a linear relationship between log capacity factor (corrected for column dead volume) and the number of double bonds in the standard compound as indicated in Figure 3. Thus, the elution volume is controlled by the aromaticity of the compound and classes of similar compounds elute together with their alkyl derivatives. This separation is significantly different from that obtained by GC where the compounds elute in approximate boiling point order which means that long chain alkyl aromatics coelute with unsubstituted but much more condensed aromatics. Figure 4 shows that the LC/UV and LC/MS profiles of the aromatic fraction are similar; any differences are due to the changes in UV adsorbance with increasing aromaticity compared with the total ion current. The first peaks in the LC/MS profile correspond to cycloalkanes, including the biomarkers, pentacyclic triterpanes such as hopanes revealed by an intense m/z 191, which have no significant UV adsorption. Their presence indicates that the saturates/aromatics split is not complete, possibly because the boiling range of the sample exceeds that originally intended for the method (12).

Figures 5 to 8 show mass spectra of some of the more prominent peaks in the total ion current profile of Figure 4. In each spectrum we have linked the fragment or molecular ion peaks for the various Z series of hydrocarbons by

solid lines. Z is defined by the general hydrocarbon formula C_nH_{2n+Z} and denotes the hydrogen deficiency compared with alkanes (where Z = +2) since each double bond or ring adds (-2) to the Z number. The graphically represented Z series indicate the range of homologues present in the spectrum but not the aromatic structure since all structural isomers elute close together. The mass spectra reveal that homologous series are prominent and extensive; Table 1 numerises the Z series found with the maximum alkyl chain homologues detected. Other evidence for long alkyl chains ($> C_8$), for example, from NMR analysis is given in reference 1. Long Z series aliphatic and aromatics were also found in off-line LC-field ionisation MS on two non-distillable SRC-I coal liquids(5), these extended to over mass 700 and revealed long homologous series for the different Z series. This similarity is not surprising since the SRC-I process and hydrolysis at 500°C use very similar severities of treatment.

GC/MS

The GC/MS study revealed a complex alkylated aromatic mixture but only extending to about mass 240. The total ion current profile in Figure 9 shows that the number of structural isomers of overlapping alkylated aromatic types was so great that the GC resolution was insufficient to cope and broad multiple peaks were evident. The main unsubstituted aromatics are indicated in the Figure and components found are listed in Table 2 which shows that there are numerous highly alkylated aromatics.

Mass Spectrometry Probe

Figure 10 shows an averaged mass spectrum of the aromatic fraction obtained by low ionising voltage probe MS. It reveals a complex series of aromatic molecular ions with components such as alkyl-naphthalenes, alkyl-diphenyls, alkyl-perylenes etc. up to mass 600, the upper limit of the mass range. The average molecular weight, calculated as the 50% intensity of the averaged spectrum is 260, i.e. close to the number average molecular weight determined isopiesticly.

Field Desorption Mass Spectrometry

Figure 11 shows the field desorption spectrum. There is no significant intensity below mass 200 but a complex series of masses extending, at low intensities, beyond mass 1000; the low molecular weight material observed by LC/MS and GC/MS has presumably been pumped away in the mass spectrometer.

GENERAL DISCUSSION

This study indicates that on-line LC/MS gives chemical information on the coal-derived aromatics which has not previously been obtained by other methods. On the other hand, probe experiments have revealed the presence of high molecular weight material which is not detected by LC/MS, most probably because this material was not volatilised from the moving belt interface and therefore did not enter the ion source (13).

The complex alkylated aromatics with evidence of the biomarkers pentacyclic triterpanes of the hopane type indicate that there has not been undue degradation of the molecular structures and evidence from NMR (1) indicates that the loss of hydroaromatic groups by aromatisation is one of the main reactions taking place during mild hydrolysis; the small quantity of low carbon number hydrocarbon gas (less than 5 wt % daf coal) produced during the hydrolysis reinforces this view.

Alkylated material, including up to C₁₀ - alkyl naphthalenes, has also been observed (14-16) to evaporate from coals at low temperatures (>300°C) and has been described as the remains of the oil produced during coalification the bulk of which has migrated from the coal measures to oil and gas fields. The aromatics fraction described in this work probably corresponds to a slightly modified, wider molecular weight range fraction of the oil remnant.

CONCLUSIONS

LC/MS gives significant chemical information on a wide boiling sample of aromatics derived from coal by revealing both the extent of the homologous series, up to C₂₀ alkyl substituents, and the size of the aromatic systems, up to seven rings. This information is not revealed by other techniques such as NMR, MS, or GC/MS. Although the method works satisfactorily on-line, there is still discrimination against high molecular weight material.

ACKNOWLEDGEMENTS

The work was carried out as part of the analytical support for the IEA coal pyrolysis project being undertaken by Bergbau Forschung in Germany. A.J. Berry acknowledges financial support from SERC. The views expressed are those of the authors and not necessarily those of the Board.

REFERENCES

1. C.E. Snape, W.R. Ladner and K.D. Bartle, *Fuel* 64, 1394, 1985.
2. P. Burchill, A.A. Herod and R.G. James in *Carcinogenesis*, Vol.3, Polynuclear Aromatic Hydrocarbons ed. P.W. Jones and R.I. Freudenthal, Raven Press NY, p.35, 1978.
3. B.A. Drew and S.C.F. Robinson, *Fuel* 64, 861, 1985.
4. R.B. Lucke, D.W. Later, C.W. Wright, E.K. Chess and W.C. Weimer, *Anal. Chem.* 57, 633, 1985.
5. H. Uchino, S. Yokoyama, M. Satou and Y. Sanada, *Fuel* 64, 842, 1985.
6. T.W. Allen, R.J. Hurtubise and H.F. Silver, *Anal. Chem.*, 57, 666, 1985.
7. W.A. Dark, W.H. McFadden and D.L. Bradford, *J. Chrom. Sci.* 15, 454, 1977.
8. W.A. Dark and W.H. McFadden *J. Chrom. Sci.* 16, 289, 1978.
9. K.J. Krost, *Anal. Chem.*, 57, 763, 1985.
10. R.W. Smith, D.E. Games and S.F. Noel, *Int. J. Mass Spectrom. and Ion Physics* 48, 327, 1983.
11. R.D. Smith, H.T. Kalinoski, H.R. Udseth and B.W. Wright, *Anal. Chem.*, 56, 2476, 1984.
12. K.D. Bartle, W.R. Ladner, T.G. Martin, C.E. Snape and D.F. Williams, *Fuel* 58, 413, 1979.
13. D.E. Games in 'Soft Ionisation Biological Mass Spectrometry', *Proc. Chem. Soc. Symposium on Advances in Mass Spec. Soft Ionisation Methods*, ed. H.R. Morris London, p.54, July 1980.
14. A.A. Herod, N.J. Hodges, E. Pritchard and C.A. Smith, *Fuel* 62, 1331, 1983.
15. A.A. Herod and C.A. Smith, *Fuel* 64, 281, 1985.
16. A.A. Herod, W.R. Ladner and B.J. Stokes, *Proc. 10th Int. Mass Spec. Conf. Swansea, UK, Paper 400, 9-13 September 1985.*

TABLE 1

Aromatic types detected by LC/MS

Mass of parent of homologous series	Z No. $C_n H_{2n+Z}$	Name of one isomeric structure	Maximum alkyl chain detected
78	-6	Benzene	>15
118	-8	Indan	>20
116	-10	Indene	>20
128	-12	Naphthalene	>21
154	-14	Diphenyl	>19
166	-16	Fluorene	>19
178	-18	Phenanthrene	>12
204	-20	Phenyl-naphthalene	12
202	-22	Pyrene	15
228	-24	Chrysene	11
226	-26	Benzo(ghi)fluoranthene	11
252	-28	Benzopyrene	10
278	-30	Dibenzanthracene	10
276	-32	Naphthylphenanthrene	7
302	-34	Dibenzopyrene	8
300	-36	Coronene	9

TABLE 2

Aromatic types detected by GC/MS

Mass of parent of homologous series	Z No. $C_n H_{2n+Z}$	Name of one isomeric structure	Maximum alkyl chain detected
78	-6	Benzene	5
118	-8	Indan	5
116	-10	Indene	0*
128	-12	Naphthalene	6
154	-14	Diphenyl	5
166	-16	Fluorene	4
178	-18	Phenanthrene	4
204	-20	Phenyl-naphthalene	2
202	-22	Pyrene	2

* Components of Z = -10 are not normally detected at masses less than mass 186 corresponding to octahydro-phenanthrene although indene is the lowest "parent" of the series.

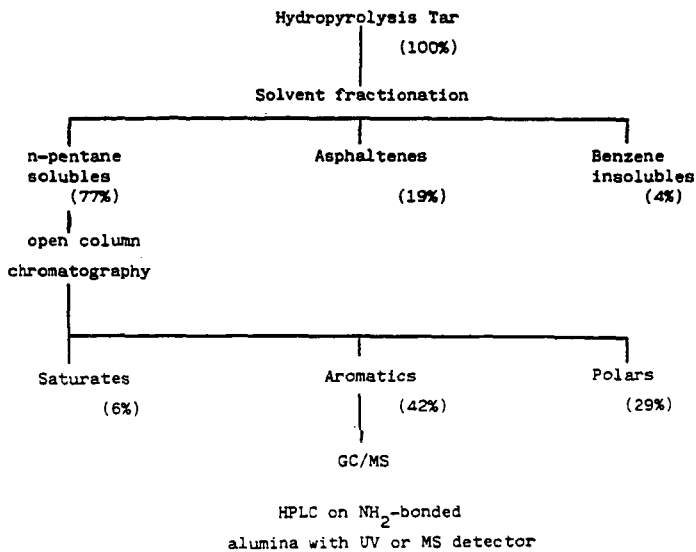


Figure 1: Separation Scheme

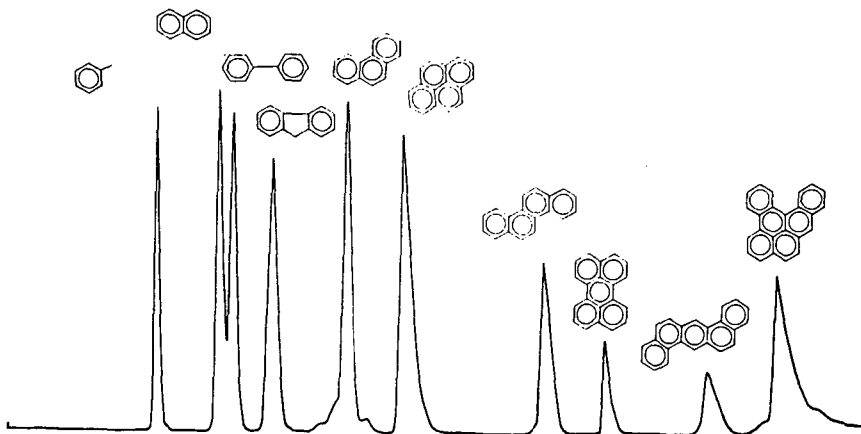


Figure 2: LC/UV separation of some standards

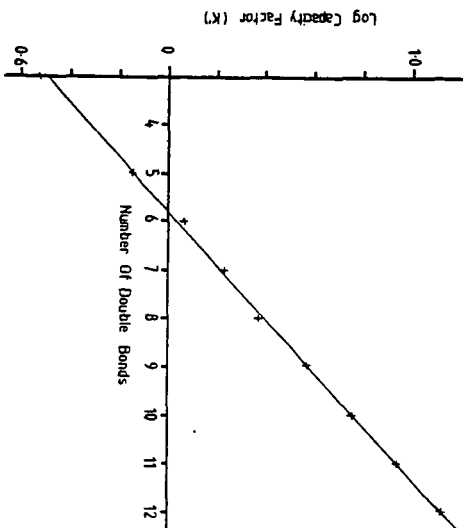


Figure 3: Relationship between number of double bonds in various aromatic molecules and log capacity factor (K'), where $\log k' = 1 + [(V_R - V_M) / V_M]$; V_R and V_M are the elution volumes of the aromatic and cyclohexane respectively.

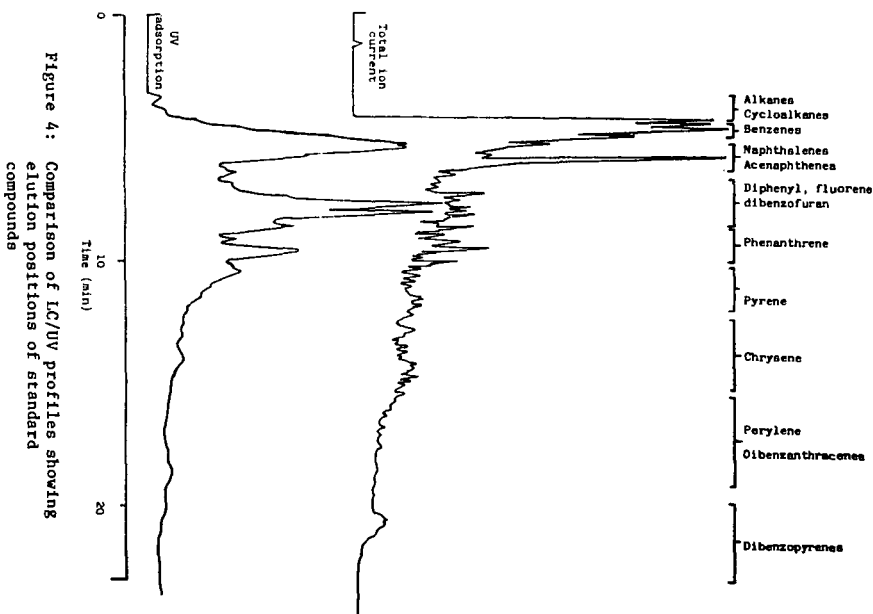


Figure 4: Comparison of LC/UV profiles showing elution positions of standard compounds

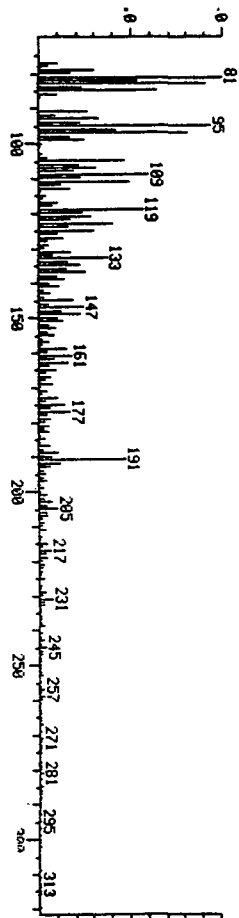


Figure 5: Mass spectrum of saturates showing m/z 191

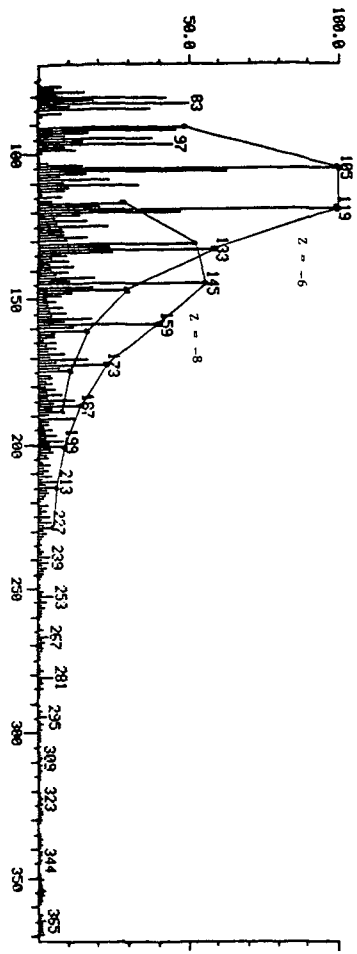


Figure 6: Mass spectrum showing Z=-6 and Z=-8 fragment ions

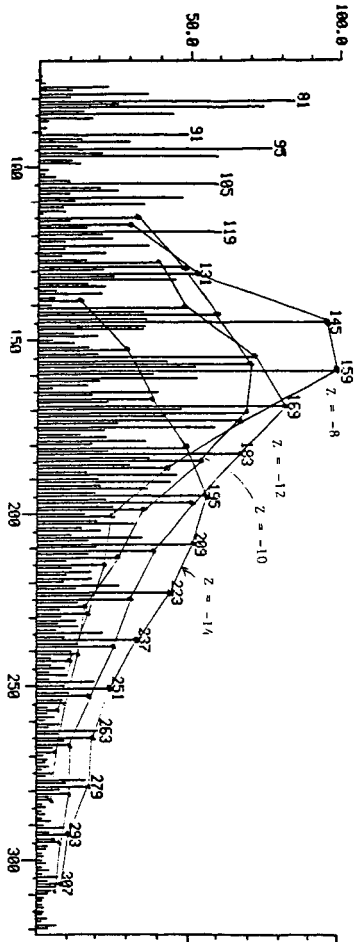


Figure 7: Mass spectrum showing Z=-8, Z=-10, Z=-12, and Z=-14 fragment ions

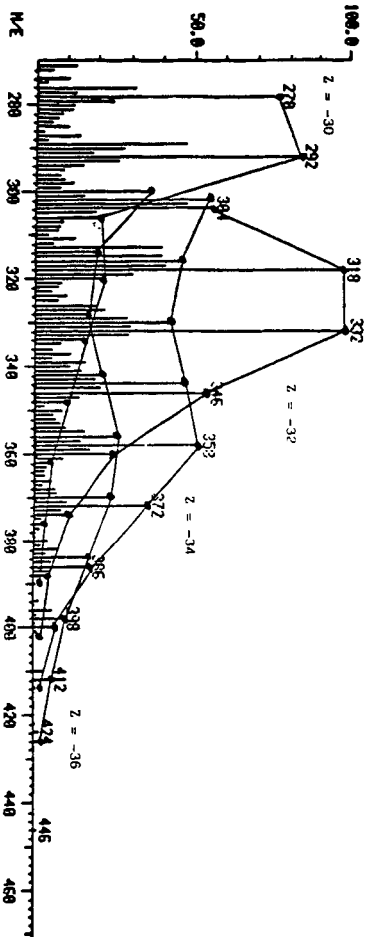


Figure 8: Mass spectrum showing Z=-30, Z=-32, Z=-34 and Z=-36 molecular ions

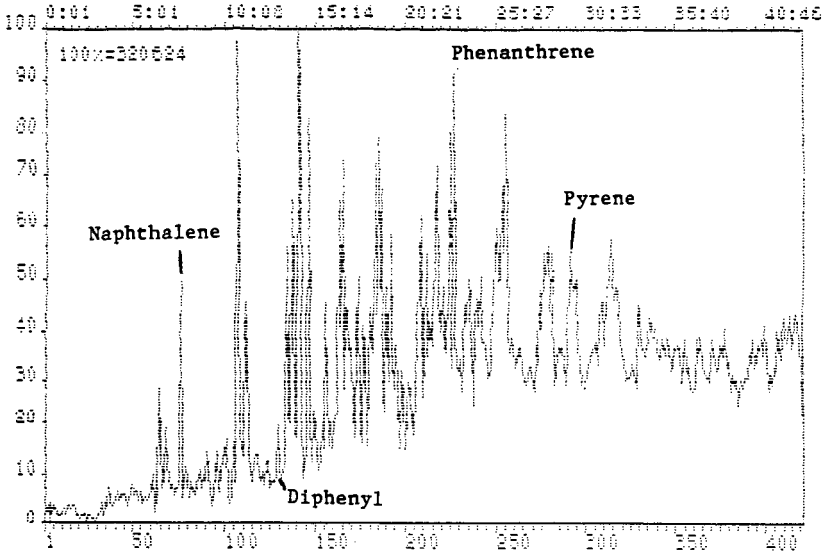


Figure 9: Aromatics by GC/MS

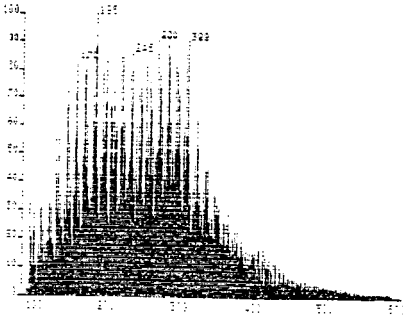


Figure 10: Averaged spectrum at low eV of aromatics

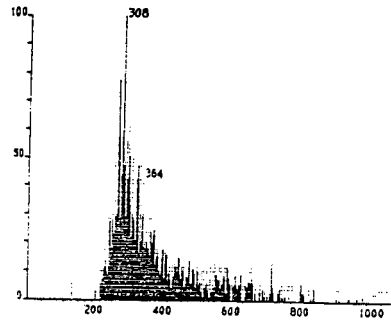


Figure 11: Field desorption profile of aromatics

Negative Ion Processes for the Unambiguous
Identification of Polycyclic Aromatics*

M. V. Buchanan and M. B. Wise

Oak Ridge National Laboratory
P. O. Box X
Oak Ridge, Tennessee 37831

The unambiguous identification of polycyclic aromatic hydrocarbons (PAH) in a complex mixture is a difficult analytical problem. Combined gas chromatography/mass spectrometry is one of the most frequently used techniques for the analysis of PAH in complex mixtures due to its ability to separate components prior to detection by the mass spectrometer. Conventional electron impact ionization is often limited in its ability to identify PAH at the isomeric level because PAH generally yield strong molecular ions with little or no fragmentation which would allow isomeric species to be differentiated. The presence of a particular isomer in a mixture can have a profound effect on the mixture's biological activity. For example, benzo(a)pyrene is a well-known potent carcinogen, whereas its isomer, benzo(e)pyrene is relatively inactive. Therefore, it is important to be able to identify these compounds and even quantitatively determine their levels in the presence of each other in order to fully assess a mixture's potential risk with respect to human health.

A number of mass spectral techniques have been reported in recent years as a means of differentiating isomeric PAH, including mixed charge exchange chemical ionization (1,2), pulsed positive and negative chemical ionization using mixed reagents (3,4), and metastable ion spectra (5). These methods rely upon comparing the ratios of the observed ion intensities for the differentiation of the isomeric compounds. This would limit the usefulness of these techniques to compounds for which standards were available. Ideally, one would like an analytical technique which would not rely on the availability of authentic compounds. This is particularly true in the case of PAH and alkyl-substituted PAH, where thousands of isomers are possible, but relatively few are commercially available.

Recently, we have been investigating the use of electron capture negative ion processes for the differentiation of isomeric PAH (6). Most PAH have positive electron affinities ranging in magnitude from a few tenths to over one electron volt (7). Electron capture reactions of PAH using both electron capture chromatographic detectors (8,9) and negative ion chemical ionization mass spectrometry (6,10-12) have been reported. In this paper, negative ion processes have been investigated for the differentiation of isomeric PAH based upon relative differences in electron affinities. The use of these processes in both negative ion chemical ionization mass spectrometry and a newly developed chromatographic detector will be discussed.

In the electron capture negative ion chemical ionization (CI) experiments, methane was used as a buffer gas and introduced into the ion source of a Hewlett-Packard 5985B quadrupole mass spectrometer at a pressure of a few tenths of a torr (6). Electron bombardment was used to ionize the methane. Under these conditions, electrons with nearly thermal energy are produced and can be captured by compounds to form anions. Initial experiments using these conditions revealed that some PAH undergo electron capture to form molecular anions, M^- , whereas others did not ionize, as shown in Figure 1.

*Research sponsored by the Office of Health and Environmental Research, U.S. Department of Energy under Contract No. DE-AC05-84OR21400 with Martin Marietta Energy Systems, Inc.

Further studies using over forty PAH suggested that the ionization behavior of the PAH under electron capture conditions was related to their electron affinities. Electron affinities (EA) of complex molecules are difficult to measure experimentally (7). However, EA values may be estimated from Hückel molecular orbital calculations (13). The EA of a PAH is linearly related to the energy of the lowest unoccupied molecular orbital, ϵ_{LUMO} , where

$$\epsilon_{LUMO} = \alpha + m_{m+1} \beta \quad 1)$$

and α and β are defined as the Coulomb and resonance integrals, respectively, and m_{m+1} is the coefficient of energy for the LUMO. The values of m_{m+1} have been calculated for a large number of PAH and are available in a number of compilations (14-16). Because m_{m+1} is linearly related to ϵ_{LUMO} , which is in turn linearly related to the electron affinity of a molecule, m_{m+1} values may be used as a relative measure of EA values (6).

Using adiabatic EA values which had been calculated by Younkin et al., (17), as well as m_{m+1} values, it was found that the ionization behavior of the PAH fell into two groups with respect to their EA values, as shown in Table 1. Those with EA values greater than 0.5 eV (or m_{m+1} values greater than -0.42) ionized to produce molecular anions. Compounds with lower EA values did not ionize and thus were not observed. This difference in ionization behavior permits a number of isomeric PAH to be distinguished. For example, fluoranthene and pyrene, both with a molecular weight of 202, are readily distinguished under the negative ion CI conditions, with only fluoranthene yielding a molecular anion. Perhaps the most important differentiation, however, is between the two benzopyrene isomers. As stated previously, benzo(a)pyrene is a much more potent carcinogen than its isomer, benzo(e)pyrene. Under negative ion CI conditions, only benzo(a)pyrene is ionized, allowing it to be identified readily and quantitatively determined in the presence of its isomer without interference.

The addition of alkyl groups to a PAH is predicted to alter the α term in Equation 1 only slightly and thus have little effect on EA value of the alkylated PAH (13). This prediction has been confirmed in studies using alkyl-substituted PAH, which show that these compounds may be differentiated in a manner similar to their parent compounds. This eliminates the need for standard compounds to differentiate these compounds as well.

A number of nitrogen-substituted PAH have also been studied by the electron capture negative ion CI techniques, and the same type of isomeric differentiation is observed. A few of the compounds which have been studied are shown in Table 2. The addition of a nitrogen into the ring system of a PAH raises the electron affinity of the azaarene slightly above that of the parent PAH. This is observed clearly in the case of acridine, which yields molecular anions, in contrast to the corresponding PAH, anthracene, which does not ionize.

An example illustrating the use of electron capture negative ion CI is shown in Figure 2. In this figure are three total ion chromatograms of a PAH isolate from a coal-derived liquid. The lower trace was obtained by conventional electron impact ionization. The middle trace was obtained by methane chemical ionization in the positive ion mode. In both of these chromatograms, all of the compounds are ionized and the profiles appear essentially identical. The upper trace was obtained in the electron capture negative ion CI mode using methane as the buffer gas. In this chromatogram, only compounds with EA values over 0.5 eV are observed, allowing a number of isomers to be distinguished. Most notable is the differentiation of fluoranthene (peak 1) and pyrene (peak 2), as well as the C₂-substituted fluoranthenes (peak 4) and the C₂-substituted pyrenes (peak 5). Another feature of this technique is also observed in Figure 2. Higher molecular weight compounds are often difficult to observe using chromatographic methods. This is due to the fact that the chromatographic efficiency drops off as the compounds are retained on the

column for longer periods of time. In the negative ion CI mode, however, these higher molecular weight PAH are more clearly observed than with either electron impact or positive ion chemical ionization. The higher sensitivity of the compounds in the electron capture process is due to the faster reaction rates of electron-molecule reactions, in general, and the higher capture cross-section and electron affinities of these larger PAH. The ability to detect these larger-ring PAH is especially important in the analysis of complex mixtures with respect to human health risks because these compounds generally have higher biological activity than compounds with fewer aromatic rings. Compounds with molecular weights in excess of 350 have been observed in coal-derived liquids using this technique.

Electron capture detectors (ECD), which are widely used in chromatography, employ chemical processes which are similar to those used in electron capture negative ion CI experiments. In the case of an ECD, the detector is operated at atmospheric pressure instead of a few tenths of a torr, and a source of β -radiation, usually ^3H or ^{63}Ni , is used instead of an electron filament for the ionization of the buffer gas. Typically, a mixture of 10% methane in argon is used as the buffer gas. The particles collide with the argon to produce metastable ions, which then ionize methane to produce thermal electrons. As a compound enters the detector cell and captures these electrons, the current measured at the anode decreases, producing the resulting signal.

Studies of PAH using an ECD have shown that some differentiation may be obtained based on the relative responses of the isomers (19). This differentiation can be enhanced with the addition of dopants to the buffer gas, such as oxygen and ethyl chloride (19,20). The similarity in the chemical processes used in an ECD and the negative ion CI experiments prompted the investigation of whether a chromatographic detector similar to an ECD but operated at lowered pressures would yield the same type of distinct responses for isomeric PAH as was observed in the mass spectrometry experiments.

A vacuum chamber was designed to contain a conventional ECD cell with a ^{63}Ni source. The chamber was constructed so that the pressure could be varied from a few tenths of torr to atmospheric. A separate line supplied the buffer gas to the cell and a fused silica capillary column was connected directly to the detector. A more detailed description of the detector design has been submitted for publication.

A mixture of four PAH, phenanthrene, anthracene, fluoranthene, and pyrene, were first studied with the detector at atmospheric pressure. As shown in Figure 3a, only three of the four compounds were detected with the detector operated in the conventional ECD mode. Phenanthrene has a low electron affinity (0.03 eV), and does not undergo electron capture (17,19). When the pressure in the detector was lowered to about one torr, the direction of the chromatographic peaks were reversed, as shown in Figure 3c. This reverse response indicates that the electron population in the cell increased as the compounds eluted, representing electron emission by the compounds themselves. The emission process yields approximately equal response for all four compounds, in contrast with the distinctly different relative responses observed in the electron capture mode at atmospheric pressure.

When the pressure within the variable pressure detector was increased to approximately 200 torr, a third type of response was observed, as shown in Figure 3b. The peaks for the two isomers fluoranthene and pyrene are in the electron capture and electron emission modes, respectively, allowing them to be readily distinguished. The peak for phenanthrene is in the electron emission mode and that for anthracene is at a cross-over point between emission and capture modes. At lower pressures, the peak would be negative, indicative of electron emission, and at higher pressures, the peak would be positive, indicative of electron capture. This demonstrated that differentiation of various isomers can be

obtained with this new detector by selecting pressures where one isomer would be in the electron capture mode, while the other isomer would be in the electron emission mode. An example of this is shown in Figure 4. In the top profile, the detector was operated in the emission mode and all components of a mixture of alkyl-substituted phenanthrenes and anthracenes are observed. Raising the pressure to 175 torr causes the substituted anthracenes to cross-over to the electron capture mode, allowing them to be clearly differentiated from the isomeric alkyl-substituted phenanthrenes.

This variable mode ionization detector can be operated in three distinct modes just by changing the pressure within the cell. At atmospheric pressure, it can be operated as a conventional ECD. At low pressures, it can be operated in the electron emission mode and very level responses for each compound can be obtained, not unlike electron impact ionization or flame ionization response. Finally, at intermediate pressures, a high degree of selectivity for various compounds may be obtained. In this latter mode, the same type of isomeric differentiation observed in the negative ion CI mass spectrometry experiments can be obtained, but without the need for the mass spectrometer. Not only can the detector be used in this mode to distinguish various isomers, but also to selectively detect one class of compounds in the presence of other classes.

References

1. M. L. Lee and R. A. Hites, *J. Am. Chem. Soc.* **99**, 2008, (1977).
2. W. J. Simonsick, Jr. and R. A. Hites, *Anal. Chem.*, **56**, 2749-2754 (1984).
3. D. F. Hunt, C. N. McEwen, and T. M. Harvey, *Anal. Chem.* **47**, 1730 (1975).
4. D. F. Hunt, G. C. Stafford, Jr., F. W. Crow, and J. W. Russell, *Anal. Chem.* **48**, 2098 (1976).
5. B. Shushan and R. K. Boyd, *Org. Mass Spectrom.* **15**, 445 (1980).
6. M. V. Buchanan and G. Olerich, *Org. Mass Spectrom.*, **19**, 486, 1984.
7. L. G. Christophorou, *Atomic and Molecular Radiation Physics*, pp 565-584, Wiley-Interscience, New York (1971).
8. W. E. Wentworth and R. S. Becker, *J. Amer. Chem. Soc.* **84** (1962) 4263.
9. L. Wojnarouits and G. Foldiak, *J. Chromatogr.* **206**, (1981) 511.
10. Y. Iida and S. Daishima, *Chem. Lett.* **273**, (1983).
11. M. Oehme, *Anal. Chem.* **55**, (1983), 2290.
12. L. R. Hilpert, G. D. Byrd, and C. R. Vogt, *Anal. Chem.* **56**, (1984), 1842.
13. A. Streitwieser, Jr., "Molecular Orbital Theory for Organic Chemists," pp. 175-185, John Wiley and Sons, New York (1961).
14. E. Heibronner-Straub, "Huckel Molecular Orbitals," Springer Verlag, Berlin (1966).
15. A. Streitwieser, Jr. and J. I. Brauman, "Supplemental Tables of Molecular Orbital Calculations," IFI/Plenum, New York (1970).

16. R. Zahradnik and J. Panai, "HMO Energy Characteristics," IFI/Plenum, New York (1970).
17. J. M. Younkin, L. J. Smith, and R. N. Compton, *Theor. Chem. Acta.* (Berlin) **41**, 157 (1976).
18. E. P. Grimsrud, "Electron Capture, Theory and Practice in Chromatography," ed., A. Zlatkis and C. F. Poole, Elsevier, Amsterdam, 1981, pp. 91-117.
19. E. P. Grimsrud and C. A. Valkenburg, *J. Chromatogr.* **302** (1984) 243.

Table 1. Electron capture CI response of PAH

Compound	Molecular weight	$-m_{m+1a}$	EAB ^b	Base peak m/z
Acenaphthylene	152	0.285	0.77	152
Anthanthrene	276	0.291	- ^c	276
Indeno(1,2,3-cd)pyrene	276	0.293	-	276
Benzo(i)fluoranthene	252	0.312	-	252
Benzo(a)pyrene	252	0.371	0.64	252
Fluoranthene	202	0.371	0.63	202
Benzo(b)fluoranthene	252	0.377	-	252
Benzo(ghi)fluoranthene	226	0.378	-	226
Azulene	128	0.400	0.77	128
Benzo(k)fluoranthene	252	0.401	-	252
Anthracene	178	0.414	0.49	- ^c
Dibenzo(a,i)pyrene	302	0.522	-	302
Dibenzo(a,e)pyrene	302	0.422	-	302
Benzo(ghi)perylene	276	0.439	0.51	276
Pyrene	202	0.445	0.45	-
Benzo(a)anthracene	228	0.452	0.42	-
Dibenzo(a,i)anthracene	278	0.492	0.33	-
Benzo(e)pyrene	252	0.497	0.35	-
1,2,3,4-Dibenzanthracene	278	0.499	0.34	-
Picene	278	0.502	0.29	-
Chrysene	228	0.520	0.26	-
1-Phenylnaphthalene	204	0.522	-	-
Coronene	300	0.539	0.32	-
Benzo(c)phenanthrene	228	0.568	0.18	-
2-Phenylnaphthalene	204	0.565	-	-
p-Terphenyl	230	0.593	-	-
Phenanthrene	178	0.605	0.03	-
Naphthalene	128	0.618	-0.06	-
Biphenyl	154	0.705	-	-

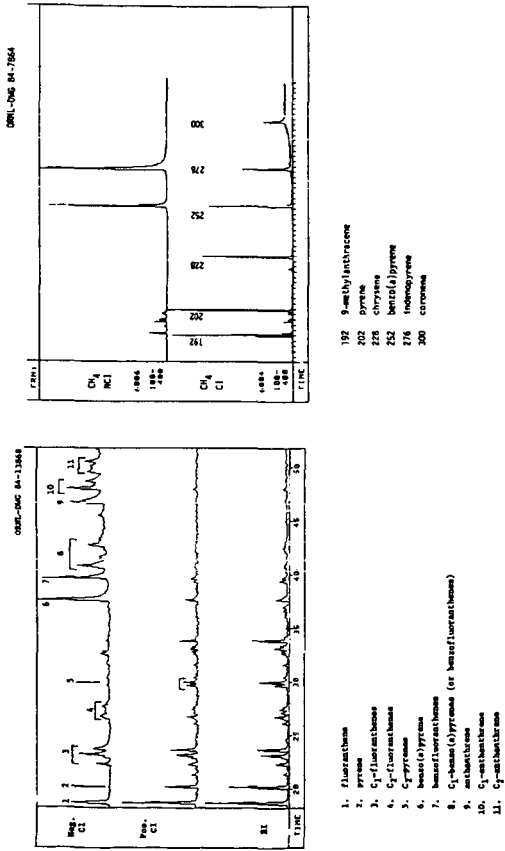
^aCalculated coefficient of energy for LUMO from Refs. 14, 15, and 16.

^bCalculated electron affinity values from Ref. 17.

^cThe - signifies that no response was observed.

Table 2. Negative ion CI response of selected azaarenes

	MW	Negative Ion CI Response
Acridine (9-azaanthracene)	179	179
Phenanthridene (9-azaphenanthrene)	179	-
2-azafluoranthene	203	203
1-azapyrene	203	203
1-azachrysene	229	-
10-azabenz(a)pyrene	253	253



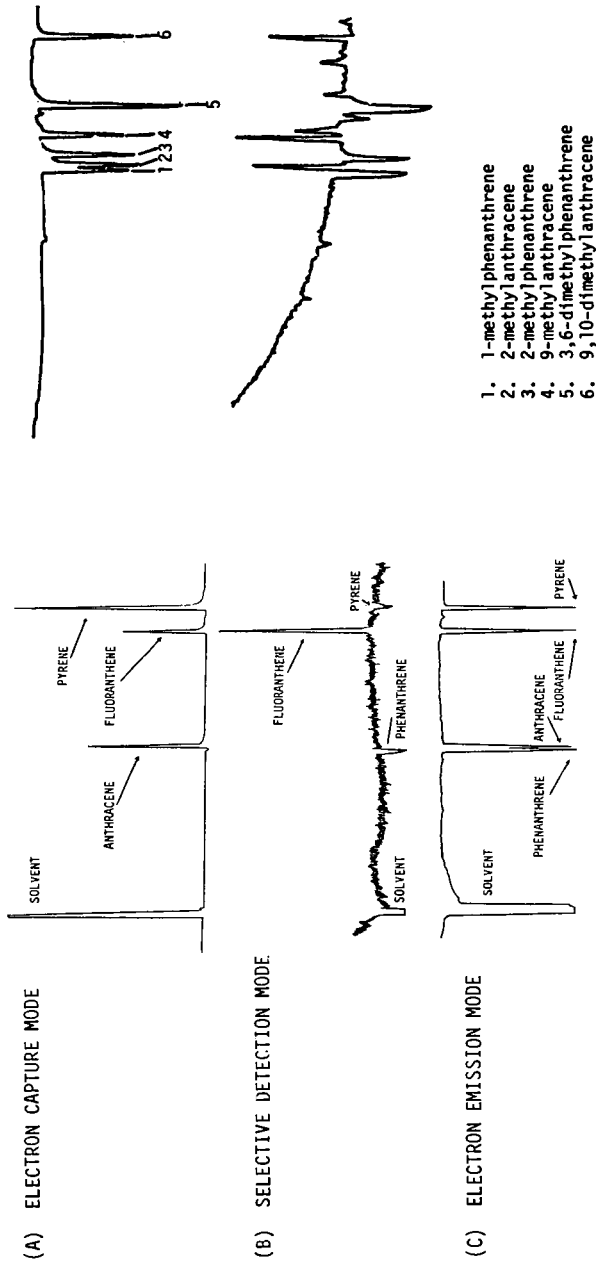
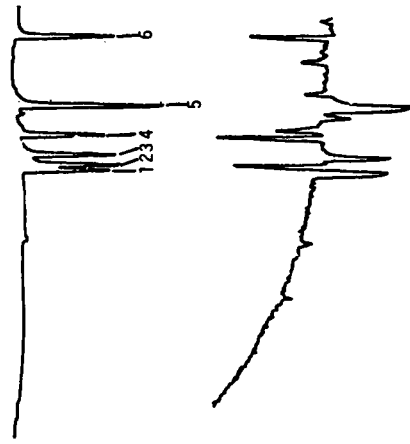


Fig. 3. Different modes of operation of variable pressure detector at atmospheric pressure (A), 200 torr (B), and 1 torr (C).



1. 1-methylphenanthrene
2. 2-methylanthracene
3. 2-methylphenanthrene
4. 9-methylanthracene
5. 3,6-dimethylphenanthrene
6. 9,10-dimethylanthracene

Fig. 4. Variable pressure ionization detector response at low pressures (emission mode, top), and at intermediate pressures (selective mode, bottom).

SEPARATION AND ANALYSIS OF HYDROXYAROMATIC SPECIES IN LIQUID FUELS. I. ANALYTICAL METHODOLOGY

J. B. Green, J. S. Thomson, S. K-T Yu, C. A. Treese,
B. K. Stierwalt, and C. P. Renaudo

Department of Fuels Research
National Institute for Petroleum and Energy Research
Division of IIT Research Institute
P. O. Box 2128
Bartlesville, OK 74005

INTRODUCTION

The analysis of hydroxyaromatics (ArOH) in fuels has received considerable attention for the last 20-30 years. Interest was especially high in the late 1970's and early 1980's during the "synfuels boom" because of the relatively high concentrations of ArOH in shale oils and especially coal liquids. ArOH as a class are important because they impact fuel properties such as its stability, viscosity, water miscibility and toxicity as well as its behavior in refinery processes. For example, Hara, *et al.* (1) and White *et al.* (2) found that phenolic compounds contributed to sediment formation in SRC-II coal liquid through oxidative coupling. In addition, ArOH are believed to increase viscosity by hydrogen bonding to nitrogen bases (3). Finally, ArOH and cyclic ethers are believed to control the rate of hydrodeoxygenation of coal liquids during hydrotreating processes (4).

The approach most commonly used for analysis of ArOH involves a preliminary step for their isolation from the bulk fuel matrix followed by analysis of the ArOH concentrate. Aqueous extraction and liquid chromatography are the most common methods for isolating ArOH; GC, GC/MS, MS, NMR, IR, and UV have all been used singly or in combination for analysis of the ArOH concentrate.

While any of the published methods will work on fuels rich in ArOH, unsatisfactory results are often obtained on samples such as petroleum which are low in ArOH as well as with samples with a higher average molecular weight or boiling point. For example, aqueous-alcoholic NaOH extraction yields negligible amounts of acidic material from high-boiling petroleum distillates and residues which actually contain 10-20 weight-percent acidic compounds (5). The hydrophobic nature of larger molecular weight acids prevents them from partitioning into the aqueous phase.

Liquid chromatography on alumina probably has the widest applicability for isolation of ArOH from fuels (6-11), although methods using silica as the adsorbent have also been reported (11-17). Reportedly, the silica-based methods have yielded ArOH fractions also containing nitrogen compounds (11,13, 14) but Schabron *et al.* (16) and Hurtubise *et al.* (17) reported that pre-treating the silica with HCl eliminates this problem by forming HCl-salts of nitrogen bases on the column, thereby preventing their coelution with ArOH. Coelution of nitrogen compounds with ArOH has also been reported to be a problem with alumina-based separations (10,15). On the other hand, nonaqueous ion exchange chromatography has been used to obtain ArOH concentrates, either

by sequential elution of the ion exchange resin (3,18,19) or by subfractionation of the total acid concentrate on alumina (20,21). Since nitrogen bases are trapped by a cation resin and ArOH by an anion resin in that procedure, overlap of those classes is minimal. Finally, size exclusion chromatography with THF eluent separates ArOH as a class from coal liquids (22,23). Reportedly, phenols hydrogen bond to THF, thereby effectively increasing their molecular size and decreasing their elution volume from the size exclusion column.

Chemical derivatization of ArOH often facilitates subsequent chromatographic and/or spectroscopic analysis. Acylation with fluorinated acid anhydrides or acid chlorides has been used in conjunction with GC (24) and especially NMR methods (25-29). This reaction has also been used extensively to determine primary aromatic amines in coal liquids. Similarly, silylation with a variety of reagents enables specific ArOH analysis by NMR (13,30) and GC/MS (31,32). Chemical derivatization is useful from both qualitative and quantitative standpoints because 1) it eliminates many potential O-containing interfering compound classes which will not react (e.g., ketones, ethers), 2) it adds a chemical moiety containing elements not commonly in fuels (e.g. F,Si) allowing for specific detection of ArOH, 3) it significantly adds to the molecular weight of the ArOH which facilitates mass spectral analysis because the derivatized ArOH molecular ions are at significantly higher mass than interfering compounds, 4) it improves gas chromatographic resolution of ArOH, and 5) it alters the polarity of ArOH which can enable their further separation from interfering compound classes.

The ArOH analysis method described here is based on 1) initial isolation of a total acid concentrate by nonaqueous ion exchange chromatography, 2) subfractionation of the acids into compound class fractions by HPLC, 3) chemical derivatization via acylation or silylation, and 4) GC/MS analysis of the derivatized ArOH concentrate. The objective of the scheme is to provide detailed analysis of ArOH species regardless of fuel type and overall concentration of ArOH present. Because the ultimate analysis is by GC/MS, the method is limited to distillates boiling below approximately 500° C (932° F).

Nonaqueous ion exchange chromatography was chosen for the first step because it separates acidic types from the bulk hydrocarbon matrix as well as from basic nitrogen compounds. As discussed previously, many of the published schemes based on silica or alumina overlap some nitrogen compound types into the ArOH fraction. This presents a serious interference for GC/MS analysis because nitrogen compounds yield even-numbered fragments which can partially or completely obscure parent ArOH ions. Chemical derivatization alone frequently cannot compensate for this interference because many N-compounds also derivatize. HPLC was chosen over the previously cited open-column separation methods for subfractionating acids because of its higher chromatographic resolution, use of automated instrumentation, use of detectors which continuously monitor the separation, and microprocessor-controlled solvent gradient and pump. The above factors coupled with the fact that a single column may be used for numerous samples result in much higher quality, more reproducible ArOH concentrates. This dual-liquid chromatographic approach has the following inherent advantages: 1) acidic compounds are concentrated in the first step from bulk fuel components and then subfractionated in a second step -- this approach is especially suited to fuels which contain low amounts of ArOH, 2) extremely hydrophobic or hydrophilic ArOH which are incompletely recovered

In aqueous extraction procedures pose no special problems for this procedure, 3) the complementary selectivities of the ion exchange and HPLC separations yield ArOH concentrates relatively free of other compound classes, 4) it has been evaluated using numerous pure compounds as well as a wide variety of fuels, and 5) it yields concentrates of other major acidic compound classes suitable for detailed analysis.

EXPERIMENTAL

Preliminary Fractionation of Fuels

Details of distillation (4,33) and nonaqueous ion exchange isolation of acid concentrates (5) appear elsewhere. Distillation was not absolutely necessary for analysis of ArOH, but the level of information obtained on higher boiling ArOH was enhanced if the bulk of the phenols and indanols/tetralinols were distilled into a light (ca. 200-325° C) boiling fraction.

Preparative HPLC Subfractionation of Acid Concentrates

A preliminary evaluation of HPLC methods for acid subfractionation (34) and a study of the liquid chromatographic behavior of acidic compounds on silica using mobile phases spiked with tetraalkylammonium hydroxides (35) give background information on the HPLC method used here. Table 1 shows details of the equipment and conditions for the acid subfractionation.

TABLE 1. Conditions for HPLC Subfractionation of Acid Concentrates

Column - 30 cm X 2.5 cm (I.D.) 316 ss
Packing-Adsorbosil-LC (Alltech Assoc. -10 μ prep grade silica)
N (average plates/m) - 15,000-20,000
Flow rate - 28 mL/min
Chart speed - 0.5 cm/min
Temperature - 35.0° C
Detector (uv) - ISCO UA-5, 1 mm path cell, 280 nm, 0-2 AUFS
Apparatus - Spectra Physics M8000 HPLC
Injection vol (mL) - 1.8
Injection amount (mg) - 300
Gradient - (linear)

Time (min)	Volume Percent		
	A	B	C
0	88	12	0
2	88	12	0
17	78	22	0
30	20	80	0
38	20	80	0
50	0	30	70
51	0	30	70
53	88	12	0

A: Methyl t-butyl ether (MTBE)

B: 70 percent (V/V) MTBE, 30 percent (V/V) methanol, 0.03 percent tetramethylammonium hydroxide

C: Methanol with 0.03 percent tetramethylammonium hydroxide.

Chemical Derivatization of ArOH

Acylation was done at room temperature by bubbling trifluoroacetyl chloride (TFACl) (SCM Speciality Chemicals, Gainesville, FL) into 0.5 mL of benzene containing 0.05 M triethylamine catalyst and 1-2 mg ArOH for 30 minutes. Nitrogen gas was passed through the reacted ArOH for 10 minutes to remove residual TFACl, and the reaction mix was transferred to a 1-mL propylsulfonic acid-bonded silica cartridge (PRS Bond Elute, Analytichem International, Harbor City, CA) and eluted with 10 mL dichloromethane. The bonded silica cartridge removed triethylamine catalyst and trifluoroacetic acid produced as a by-product from reaction of TFACl and water. Either of the above contaminants gave rise to a large, poorly eluting GC peak which interfered with analysis of C₀-C₃ phenols.

Silylation was accomplished by heating a mixture of 0.5 mL BSTFA containing 10 percent TMCS catalyst (N,O-bis(trimethylsilyl)-trifluoroacetamide, 10 percent trimethylchlorosilane; Regis Chemical, Morton Grove, IL) and 4 mg ArOH dissolved in 1.0 mL benzene at 60° C for one hour.

The silylated and acetylated ArOH were concentrated to 0.1-0.2 mL under nitrogen prior to injection into the GC.

GC/MS

A Kratos (Ramsey, NJ) MS-80 GC/MS system comprised of a Carlo Erba model 4662 temperature programmed GC, Scientific Glass Engineering (Austin, TX) open-split interface, EI source, MS-80 magnetic-scan mass spectrometer and Data General Nova 4-based DS-55 data system was used for all analyses. A 0.25 mm X 30 m, 0.25 µm film thickness J and W (Rancho Cordova, CA) DB-5 column was programmed from 50° C (initial time one minute) at a 5° C/min to 350° C (hold 20 minutes) for a typical ArOH concentrate. Other instrumental conditions were: injector - 300° C, 100:1 split; GC/MS interface - 300° C, He make up 1 mL/min (50 mL/min for solvent peak purge); column head pressure 1.25 Kg/cm² (1 mL/min He); mass spectral conditions - 70 eV ionizing voltage, 1,000 dynamic resolution, 0.5 sec/decade scan rate, source pressure 5 X 10⁻⁶ torr, and source temperature 300° C.

RESULTS AND DISCUSSION

HPLC Acid Subfractionation

Figure 1 shows UV detector traces from HPLC separation of typical acid concentrates obtained by nonaqueous ion exchange as well as a chromatogram of a synthetic blend (STD) of acidic compounds typical of those in fuels. Strong and weak acid concentrates are obtained from ion exchange separation of distillation residues (5); thus, Figure 1 shows traces from subfractionation of strong and weak acids from SRC-II >325° C and OSCR shale oil >200° C residues whereas total acids were separated from the Wilmington, CA, 370-535° C petroleum distillate.

As indicated in the figure, five or six subfractions are typically obtained from this separation. Fraction 1 contains very weak acids as well as any neutral compounds present as contaminants from the ion exchange procedure.

Fraction 2 is largely made up of pyrrolic benzologs. For example, GC/MS analysis of fraction 2 from the SRC-II >325° C weak acid concentrate showed it to contain largely C₀-C₄ carbazoles.

Originally, fraction 3 was isolated because it was uncertain whether this retention region would contain hindered phenols, strongly retained pyrrolic benzologs, or possibly amides (see corresponding compounds eluting in STD in Figure 1). Subsequent analysis of this fraction revealed it to usually contain hindered phenols; hence in much of the authors' current work, fraction 3 is combined with fraction 4 -- the main ArOH subfraction. Cut points for fraction 4 are usually defined by retention of 2,4,5-trimethylphenol and 2-naphthol (see STD, Figure 1). However, as indicated in the figure, sometimes the final cut point is extended beyond this range during separation of synthetic fuels or other fuels not likely to contain carboxylic acids. Subsequent work (35) with a chloroform-based mobile phase has indicated that much of the retention of polycyclic ArOH beyond that of 2-naphthol is due to their poor solubility in methyl t-butyl ether (MTBE). Hence, conditions specified in Table 1 are no longer used for subfractionation of nondistillable acids. Instead, an analogous mobile phase system is used where chloroform is substituted for MTBE as the bulk solvent. Details of this separation are available (36).

In separations of petroleum acid concentrates (Figure 1, Wilmington 370-535° C), fraction 5 cut points are set such that it will contain the bulk of the carboxylic acids present. A later eluting fraction 6 is then obtained which contains either very acidic (*i.e.*, condensed aromatic) carboxylic acids, dicarboxylic acids, and/or polyfunctional compounds. With synfuels, all compounds more retained than ArOH are usually lumped into the fifth subfraction. This subfraction probably contains dihydroxyaromatics as well as hydroxylated nitrogen heterocycles (35), such as those recently identified in a SRC-II coal liquid (37). As expected, weak acid concentrates show very little material eluting in fractions 4-6.

As stated previously, one of the objectives of the liquid chromatographic separations was to obtain ArOH fractions relatively free of nitrogen compounds. Figure 2 shows that this objective was largely met as evidenced by the dual FID/NPD GC chromatograms of representative ArOH subfractions. The sensitivity ratio of the FID/NPD detectors was adjusted such that carbazole gave an FID/NPD response ratio of two. The largest concentration of nitrogen compounds observed was in the fraction from OSCR shale oil. This observation is consistent with relatively high concentrations of amides such as 2-hydroxy pyridines in shale oil (21,38). Amides with two free hydrogens (*e.g.* benzamide) and amides analogous to 2-hydroxypyridine are known to elute into the ArOH subfraction in this HPLC system (35).

Chemical Derivatization

Tables 2 and 3 show yields of silylated and acylated hydroxy compounds, respectively. The highly hindered 2,4,6-tri-t-butylphenol did not react in either system, but most other ArOH reacted in good yield in both systems. As shown by Table 3, use of 6:1 molar ratio of catalyst to ArOH gave improved yields over those obtained using a 0.6:1 ratio. Triethylamine serves a dual role as catalyst and HCl scavenger (25,26); thus, an excess is necessary for quantitative yields.

TABLE 2. - Results of BSTFA silylation of pure alcohols and hydroxyaromatics¹

Compound	Percent Reacted
<u>Alcohols</u>	
1-Dodecanol	99.9
9-Hydroxyfluorene	99.7
1-Acenaphthenol	100.0
<u>Hydroxyaromatics</u>	
o-Cresol	98.3
2,6-Dimethylphenol	99.9
2,4,6-Tri- <i>t</i> -butylphenol	0
2-Naphthol	99.8
<u>Dihydroxyaromatics</u>	
Resorcinol	0,100 ²

¹ 10 Percent trichlorosilane catalyst.

² The first number indicates percentage reacted at one OH, the second number indicates the percentage reacted at both OH-sites.

GC/MS

Figures 3 and 4 show total ion current GC/MS profiles of ArOH, acylated ArOH, and silylated ArOH in SRC-II 200-325° C distillate and >325° C residue, respectively. Inspection of the figures and analysis of the resulting data lead to the following conclusions. 1) Acylated ArOH are more volatile than their underivatized counterparts while silylated ArOH are less volatile than plain ArOH. 2) Chemical derivatization greatly improves gas chromatographic resolution of ArOH on nonpolar columns. This feature is especially obvious in Figure 4, where the resulting mass spectra from the underivatized ArOH run were so complex they were essentially unanalyzable. Even in the case of the low boiling SRC-II ArOH (Figure 3), many more isomers of a given ArOH homolog were observed in GC/MS runs of derivatized ArOH. For example, only two C₂-phenols were resolved in GC/MS of underivatized ArOH (Figure 3A), whereas six were detected during analysis of both the acylated (Figure 3B) and silylated ArOH (Figure 3C). In the case of C₃-phenols, the number of isomers resolved in Figures 3(A-C) were 4, 9, and 5, respectively. 3) Mass spectra from acylated ArOH are much more characteristic and therefore more useful for qualitative identification of ArOH than either silylated or underivatized ArOH. However, silylated ArOH give stronger parent (M⁺) and M-15 ions which enables more sensitive detection of minor components in ArOH subfractions. These points are discussed in detail below.

TABLE 3. - Results of TFACl acylation of pure alcohols and hydroxyaromatics

Compound	Catalyst ratio ¹		
	0	0.6	6
	Percent Reacted		
<u>Alcohols</u>			
1-Dodecanol	100	100	100
9-Hydroxyfluorene	77	100	--
1-Acenaphthenol	10	100	--
<u>Hydroxyaromatics</u>			
o-Cresol	<1	43	100
2,4-Dimethylphenol	<1	80	100
2,6-Dimethylphenol	<1	8	100
2,4-Dimethyl-6-t-butylphenol	0	0	48
2,4,6-Tri-t-butylphenol	--	0	0
2-Hydroxybiphenyl	0	40	100
2-Naphthol	<1	89	98
9-Phenanthro1	<1	100	--
<u>Dihydroxyaromatics</u>			
Catechol	2,0 ²	15,79 ²	--
Resorcinol	0	12,88 ²	0,100

¹ Molar ratio of triethylamine catalyst to reactant.

² The first number indicates percentage reacted at one OH; the second number number indicates the percentage reacted at both OH-sites.

Figures 5 and 6 show mass spectra of individual peaks from GC/MS of ArOH fractions from fuels. Figures 5 (A-C) show representative spectra of phenol, a cresol and a C₂-phenol from silylated ArOH isolated from Wilmington <370° C distillate. Obviously, the dominant ions in the spectra are the parent ions (M+), M-15 ions produced from loss of a methyl group from the trimethylsilyl ether moiety, and m/e 73 ions from (CH₃)₃Si+. Spectra in Figures 5 (D-F) are all C₂-phenols obtained from GC/MS of acylated ArOH from the same Wilmington distillate. Parent ions (m/e 218) are certainly intense in the acylated C₂-phenols, but they do not overshadow the fragment ions to the extent observed in spectra of silylated ArOH. Also, M-97 ions (m/e 121) representing loss of the CF₃C(O)O+ functionality are apparent as well as m/e 69 ions from CF₃+. More importantly, loss of CH₃ in the ethylphenol (Figure 5F) can be used to distinguish it from dimethylphenols (Figures 5D and 5E) in the acylated fraction, whereas all silylated C₂-phenols show M-15 ions. Furthermore, spectra of the two acylated dimethylphenols are easily distinguished by the presence of the m/e 175 ion in only one as well as the large difference in intensity of the m/e 121 ion. Thus, Figure 5 demonstrates the greatly enhanced utility of acylation over silylation for identification of specific ArOH isomers. On the other hand, GC/MS of underivatized Wilmington <370° C

ArOH resolved only one cresol and only one C₂-phenol; thus, no isomeric information was obtained whatsoever from that analysis. All three cresols and up to six C₂-phenols have been observed from GC/MS of derivatized ArOH.

Figure 6 further illustrates points made by Figure 5; also, it shows the need for standard spectra of acylated ArOH to aid in identification of ArOH in fuels. Figures 6A and 6B show spectra of two C₇-indanols and Figure 6C shows a C₁-tetralinol from analysis of acylated SRC-II 200-325° C ArOH. Figure 6C can be identified as a 2- or 3-methyltetralinol by the fragment ion at m/e 216 produced from retro-Diels-Alder loss of propylene from the methyl-substituted six-membered saturated ring (39). Indanols do not show this type of fragmentation, but do readily lose any alkyl groups substituted onto the cyclopentyl ring. Thus, Figure 6A shows a C₇-indanol with one methyl group on the saturated ring (M-15 = 243) and Figure 6B shows what is probably an indanol with an ethyl group substituted on the cyclopentyl ring (m-29 = 229). With a sufficient library of standard acylated ArOH spectra, identification of a large number of phenol and indanol/tetralinol isomers would be possible.

Figures 6 (D-F) further emphasize the need for standard spectra. These spectra show mass 280 (184 underivatized) members of the C_nH_{2n-14}O series from OSCR >200° C shale oil (6D), SRC-II 200-325° C (6E) and SRC-II >325° C (6F) acylated ArOH fractions. Possible structures for this series include: hydroxybiphenyls, hydroxyacenaphthalenes, benzindanols and benztetralinols. Although the spectra in Figures 6 (D-F) are distinctively different, it is quite difficult to definitively assign a structure to each because of the lack of reference spectra. Usually, this series is referred to as hydroxybiphenyls in the literature; but, considering the differences in these and many other spectra not shown it appears very doubtful that all members of this series are hydroxybiphenyls. After phenols and indanols/tetralinols, this series is the most abundant in most ArOH concentrates. Current best guesses at assignment of Figures 6(D-E) are: (6D) C₁-hydroxybiphenyl, (6E) C₁-2-hydroxybiphenyl, and (6F) C₁-hydroxyacenaphthalene.

CONCLUSIONS

The combined liquid chromatographic-chemical derivatization-GC/MS approach can provide a detailed analysis of ArOH in fuels boiling below 500° C. Acylation is usually the preferred derivatization method because it enhances the volatility of ArOH and provides the most useful mass spectra for compound identification. Currently, the greatest limitation on the method is the unavailability of standard spectra for acylated ArOH. Part 2 of this series presents results from detailed analysis of ArOH from SRC-II coal liquid, OSCR shale oil and Wilmington, CA, petroleum (40).

ACKNOWLEDGMENT

The financial support of the U.S. Department of Energy and industrial sponsors under Cooperative Agreement DE-FC01-83FE60149 is greatly appreciated.

REFERENCES

1. Hara, T., L. Jones, N. C. Li and K. C. Tewari, Fuel, **60** (1981) 1143.
2. White, C. M., L. Jones and N. C. Li, Fuel, **62**, (1983) 1397.
3. Young, L.-J. S., T. Hara and N. C. Li, Fuel, **63**, (1984) 816.
4. Green, J. B., P. L. Grizzle, J. S. Thomson, R. J. Hoff and J. A. Green, Fuel, in press.
5. Green, J. B., R. J. Hoff, P. W. Woodward and L. L. Stevens, Fuel, **63**, (1984) 1290.
6. Later, D. W., M. L. Lee, K. D. Bartle, R. C. Kong, and D. L. Vassellaros, Anal. Chem., **53**, (1981) 1612.
7. Schiller, J. E., and D. R. Mathiason, Anal. Chem., **49**, (1977) 1225.
8. Snyder, L. R., B. E. Buell and H. E. Howard, Anal. Chem., **40**, (1968) 1303.
9. Boduszynski, M. M., R. J. Hurtubise and H. F. Silver., Anal. Chem., **54** (1982) 372 and 375.
10. Oderfer, G. A., L. R. Rudnick and D. D. Whitehurst, Amer. Chem. Soc., Div. Fuel Chem. Prepr., **22**(2) (1981) 89.
11. Whitehurst, D. D., S. E. Buttrill, F. J. Derbyshire, M. Farcasiu, G. A. Oderfer and L. R. Rudnick, Fuel, **61** (1982) 994.
12. Farcasiu, M., Fuel, **56** (1977) 9.
13. Seshadri, K. S., D. C. Young and D. C. Cronauer, Fuel, **64** (1985) 22.
14. Seshadri, K. S., and D. C. Cronauer, Fuel, **62** (1983) 1436.
15. McClennen, W. H., H. L. C. Meelaar, G. S. Metcalf and G. R. Hill, Fuel, **62** (1983) 1422.
16. Schabron, J. F., R. J. Hurtubise and H. F. Silver, Anal. Chem., **51**, (1979) 1426.
17. Hurtubise, R. J., T. W. Allen, J. F. Schabron and H. F. Silver, Fuel, **60** (1981) 385.
18. Jewell, D. M., J. H. Weber, J. W. Bunger, H. Plancher and D. R. Latham, Anal. Chem., **44**, (1972) 1391.
19. White, C. M., and N. C. Li, Anal. Chem., **54** (1982) 1570.
20. McKay, J. F., T. E. Cogswell, J. H. Weber, and D. R. Latham, Fuel, **54** (1975) 51.
21. McKay, J. F., M. M. Boduszynski and D. R. Latham, Liquid Fuels Technol., **1** (1983) 35.
22. Philip, C. V., and R. G. Anthony, Amer. Chem. Soc., Div. Fuel Chem. Prepr., **24**(3) (1979) 204.
23. Philip, C. V., and R. G. Anthony, Fuel, **61** (1982) 357.
24. Shulgin, A. T., Anal. Chem., **36** (1964) 920.
25. Sleavei, P., T. E. Glass and H. C. Dorn, Anal. Chem., **51** (1979) 1931.
26. Dorn, H. C., P. S. Sleavei, K. Koller and T. Glass, Amer. Chem. Soc., Div. Fuel Chem. Prepr., **24**(2) (1979) 301.
27. Baltisberger, R. J., K. M. Patel, V. I. Stenberg and N. F. Woolsey, Amer. Chem. Soc., Div. Fuel Chem. Prepr., **24**(2) (1979) 310.
28. Burke, F. P., R. A. Winschel and G. A. Robbins, "Recycle Slurry Oil Characterization," Final Rept. on U.S. Dept. Energy Contract No. DE-AC22-80PC30027, NTIS, 1985, p. 50.
29. Spratt, M. P. and H. C. Dorn, Anal. Chem., **56**, (1984) 2038.
30. Schweighardt, F. K., C. M. White, S. Friedman and J. L. Shultz, in "Organic Chemistry of Coal," J. W. Larsen (ed.), American Chemical Society, Washington, DC, 1978, pp. 240-257.
31. Novotny, M., J. W. Strand, S. L. Smith, D. Wiesler and F. J. Schwende, Fuel, **60** (1981) 213.

32. Nishioka, M., M. L. Lee, H. Kudo, D. R. Muchiri, L.J. Baldwin, S. Pakray, J. G. Stuart, and R. N. Castle, Anal. Chem., 57 (1985) 1327.
33. Hirsch, D. E., J. E. Doolley, H. J. Coleman and C. J. Thompson, "Compound-Type Separation and Characterization Studies for a 370-535° C Distillate of Wilmington, Calif., Crude Oil," U.S. BuMines Rept. of Investigation, RI 7893, 1974.
34. Green, J. B. and P. L. Grizzle, in "Trace Analysis," J. F. Lawrence (ed.), v. 2, Academic Press, New York, 1982, pp. 223-265.
35. Green, J. B., J. Chromatogr., in press.
36. Green, J. B., C. A. Treese and S. K-T Yu, "Chemical/Physical Separations of Alternate Petroleum Distillates III. HPLC Subfractionation of Acid Distillates," NIPER Topical Report No. 42, 1985.
37. Nishioka, M., R. M. Campbell, M. L. Lee, D. R. Muchiri, J. G. Stuart and R. N. Castle, Anal. Chem., 57 (1985) 2211.
38. Holmes, S. A., and L. F. Thompson, Fuel, 62 (1983) 709.
39. Wozniak, T. J., and R. A. Hites, Anal. Chem., 57 (1985) 1314.
40. Green, J. B., C. A. Treese, S. K-T Yu, J. S. Thomson, C. P. Renaudo, and B. K. Stierwalt, Amer. Chem. Soc., Div. Fuel Chem. Prepr., 31, spring 1986.

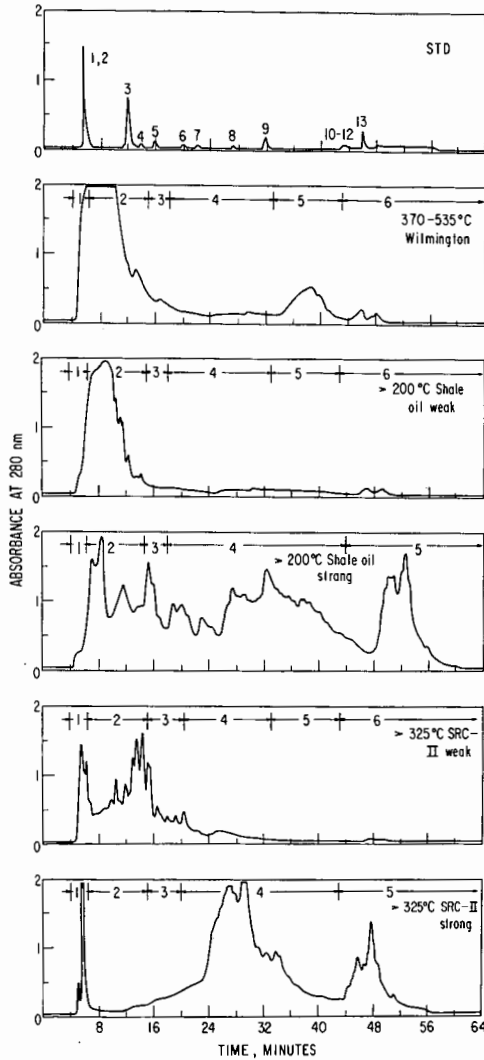


Figure 1. HPLC subfractionation of acid concentrates. Numbered peaks in STD are: 1) dibenzofuran, 2) benzophenone, 3) 13H-dibenzo[a,i]carbazole, 4) oxindole, 5) 2,4,5-trimethylphenol, 6) o-cresol, 7) 3,4-dimethylphenol, 8) phenol, 9) 2-naphthol, 10) 2,2-diphenylpropanoic acid, 11) p-toluic acid, 12) 1-fluorenicarboxylic acid, 13) 1-naphthoic acid. See text for explanation of retention regions 1-6 shown above chromatograms.

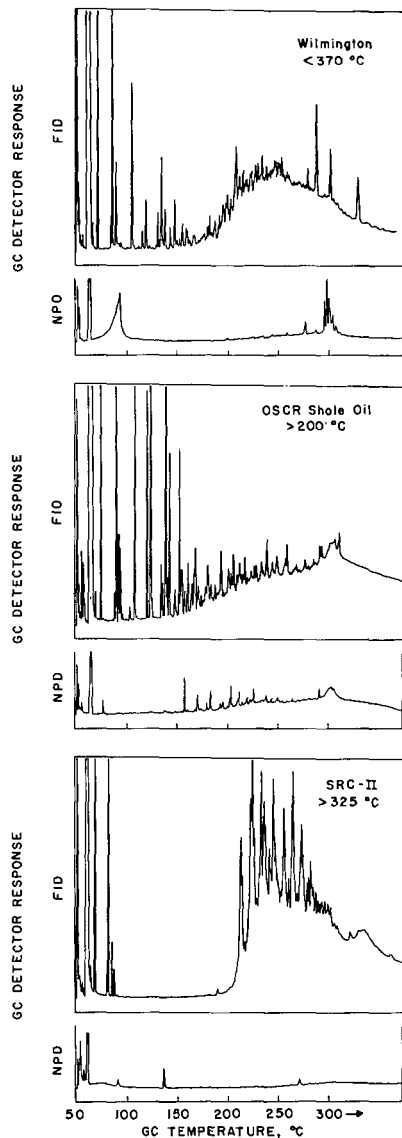


Figure 2. Gas chromatograms of selected underivatized ArOH fractions using dual FID/NPD (thermionic) detection. GC conditions were similar to those specified for GC/MS. Note the overall low levels of N-containing compounds in ArOH fractions.

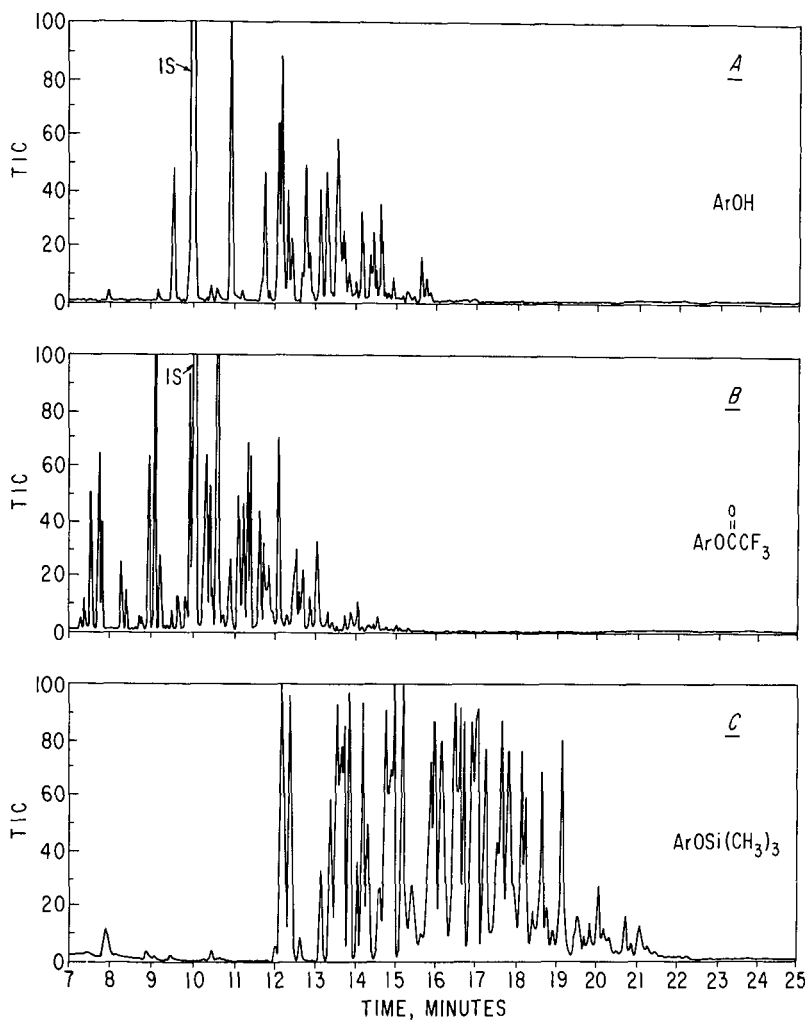


Figure 3. Total ion GC/MS traces of plain and derivatized SRC-II 200-325° C ArOH concentrate. Note the relative volatilities of acylated and silylated ArOH vs underivatized ArOH, as well as the enhanced GC resolution resulting from chemical derivatization.

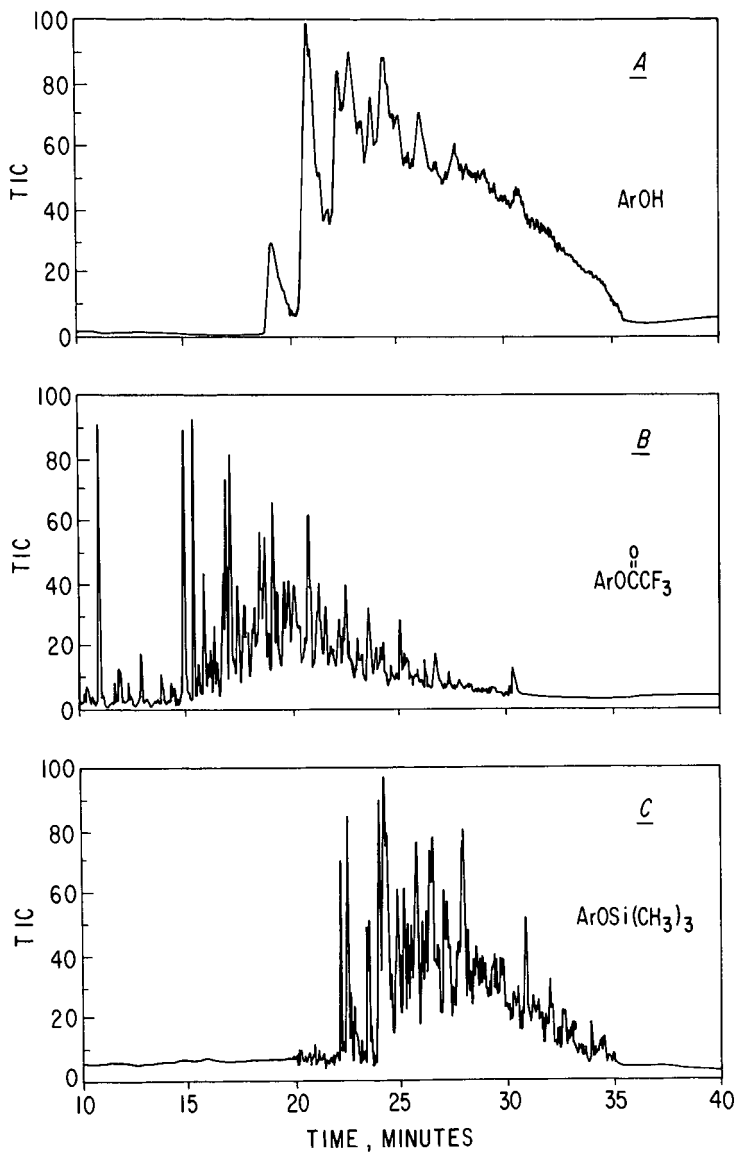


Figure 4. Total ion GC/MS traces of plain and derivatized SRC-II >325° C ArOH. The benefits of chemical derivatization are especially evident from analysis of higher boiling ArOH fractions. Higher molecular weight silylated ArOH (e.g. pyrenols) were not eluted from the GC column.

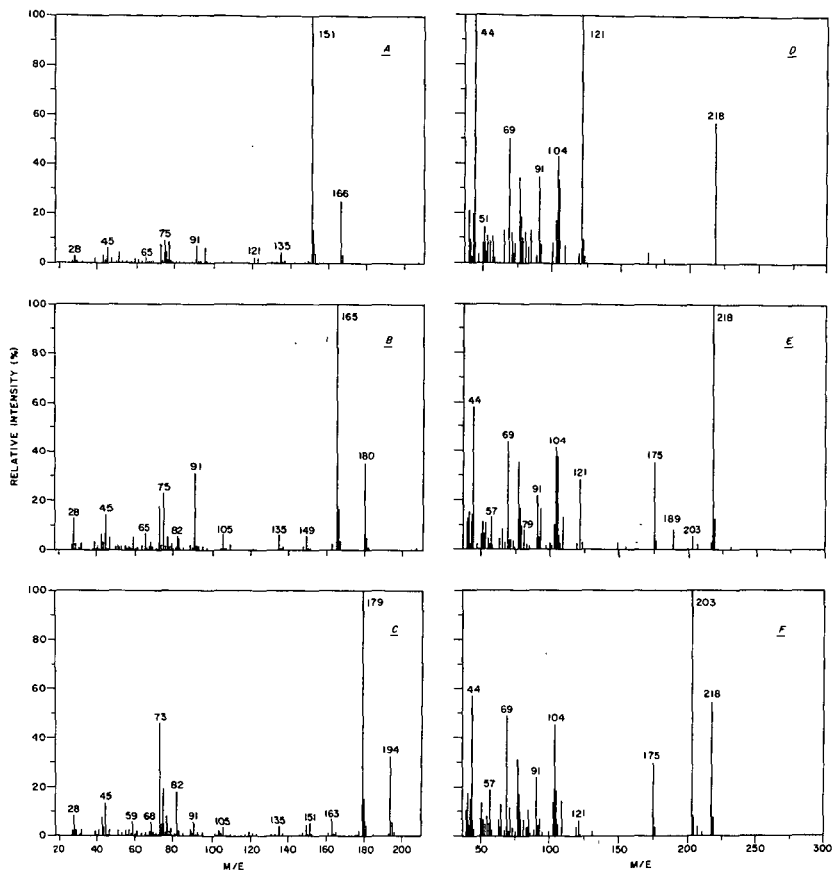


Figure 5. Mass spectra of silylated C₀-C₂ phenols (A-C) and acylated C₂-phenols (D-F) from analysis of Wilmington <370° C ArOH. Note the large M-15 fragment in A-C and see text for explanation of D-F.

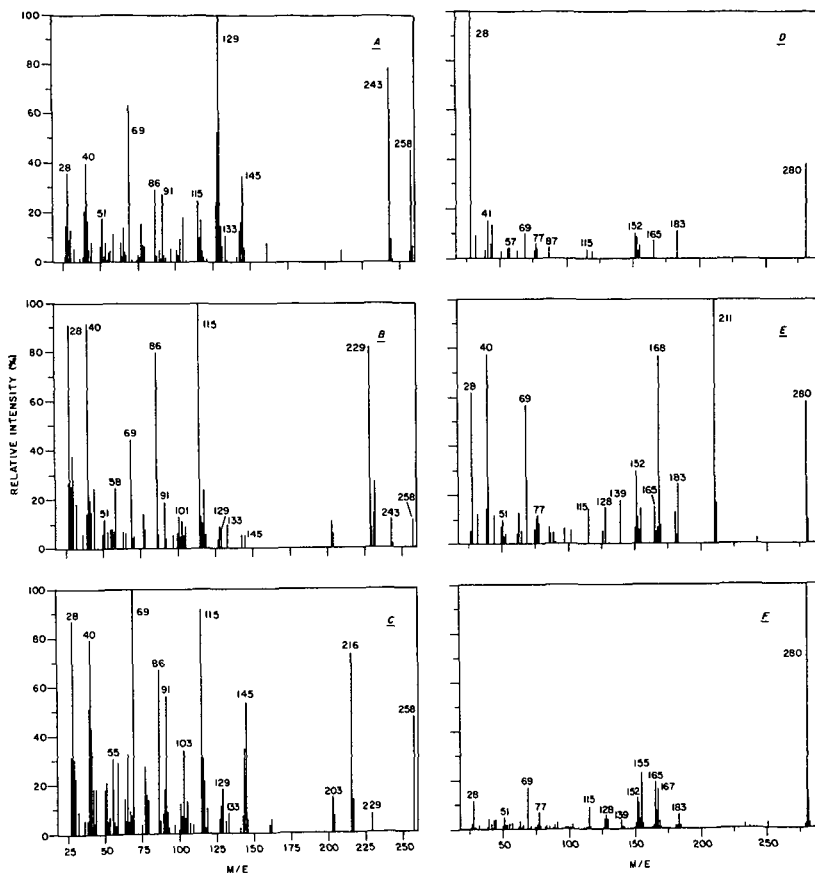


Figure 6. Mass spectra of acylated C_2 -indanols (A,B) and a C_1 -tetralinol (C) from SRC-II 200-325° C ArOH, and representative spectra from acylated members of the $C_{10}H_{2n-14}O$ series from <200° C shale oil (D), SRC-II 200-325° C (E) and SRC-II >325° C (F) ArOH fractions. See text.

STUDYING COAL MOLECULAR STRUCTURE WITH ELECTRON SPIN ECHO SPECTROSCOPY

R. B. Clarkson, R. L. Belford, J. Cornelius, and P. Snetsinger

Illinois ESR Research Center and Department of Chemistry
University of Illinois
Urbana, Illinois 61801

and

M. K. Bowman

Argonne National Laboratory
Argonne, Illinois

For several years, a major research goal of our laboratory has been the development of non-destructive spectroscopic techniques designed to study the molecular structure present in whole coal macerals. Our interest in this grows from our desire to know in more detail the microscopic structure of the organic components in coal in order to better determine the effects of various coal beneficiation technologies (e.g. various desulfurization techniques) on that structure. In this paper we wish to report on our progress using one very promising approach - Electron Spin Echo (ESE) spectroscopy. We will first briefly review the ESE technique and then present results obtained from Illinois #6 whole coal.

BACKGROUND

The physical and chemical characterization of whole coal by spectroscopic techniques presents several challenging problems. As Retcofsky points out in a good review of the applications of various spectroscopies to the coal system, the opaque, relatively non-volatile and insoluble nature of whole coal renders it a poor sample for conventional visible, UV, Raman, and mass spectrometry [1]. As a consequence of these difficulties, it has been customary to dissolve, extract, or volatilize coal prior to studying its atomic and molecular structure, and these pre-spectroscopic treatments have been shown to produce materials for examination that no longer represent the state of affairs in the whole coal itself. Magnetic resonance techniques (NMR, EPR, ESE, ENDOR) are not adversely effected by coal's physical properties, however, and these spectroscopies have played a role of ever increasing importance in coal characterization since 1954 when the first EPR spectrum of coal was obtained [2,3]. In particular, we know that new methods of performing the EPR experiment in the time domain hold exciting promise for the elucidation of the atomic and molecular structure of whole coal.

Electron Paramagnetic Resonance (EPR) looks at the energies associated with the magnetic dipole transitions of unpaired electrons. In coal, these unpaired electrons most often are associated with naturally occurring free radicals, which are present in all Illinois coals. While the stable free radicals in coal are interesting in themselves, they are of importance to our work in that they act as probes of the atomic environment in which they find themselves. Because of electron-nuclear dipole

interactions, the unpaired electrons "report" on the distance and orientation of neighboring nuclei with non-zero nuclear dipole moments (i.e. $I \neq 0$ nuclei) through the EPR signal. Such nuclei include hydrogen (^1H), carbon (^{13}C), and sulfur (^{33}S). Thus EPR is, in principle, able to give detailed information concerning the structure of coal. The excellent sensitivity of EPR (it can observe as few as 10^7 unpaired spins under favorable conditions) and the fact that it can be observed while subjecting coal to thermal and chemical treatments are other key benefits of studying coal by this spectroscopic technique.

In order to illustrate the main features of EPR spectra, and to gain insights into the characteristics of the EPR spectra from coal, let us consider a specific example. Figure 1 shows the EPR spectrum of a radical believed to occur naturally in coal[4]. This condensed ring aromatic, perylene, has three magnetically inequivalent protons which give rise to the complex and uniquely characteristic spectrum through their interaction with the unpaired electron of the radical. The excellent resolution of all the energies of interaction is due to the fact that the ion is freely tumbling in solution. If the species is immobilized by adsorption on a solid, a spectrum like that shown in Figure 2 results. Note that much of the resolution (detail) has disappeared. This spectrum no longer exhibits enough resolved information to identify the structure of the species giving rise to it; we will need somehow to extract the now unresolved information.

This example illustrates the key problem that needs to be addressed before EPR can be used to probe the atomic and molecular structure of coal. A new technique needs to be employed to resolve the important structural information that is obscured by so-called inhomogeneous broadening and various anisotropic interactions usually averaged to zero when the species are tumbling rapidly in solution. We have recently demonstrated that Electron Spin Echo spectroscopy (ESE) does, in fact, achieve this spectral resolution of the structural detail (hyperfine structure) from radicals in coal. Figure 3 is a Fourier transformed ESE spectrum of the adsorbed perylene radical showing the resolution of all three proton hyperfine couplings, including the weakest (about 2 MHz), which cannot be resolved by cw EPR [5]. This spectrum has the same format as an ENDOR spectrum, i.e.

$$f_i(\text{ENDOR}) = f(\text{proton}) \pm |A_i|/2, \quad 1)$$

where $f_i(\text{ENDOR})$ is the frequency of the i^{th} ENDOR transition, $f(\text{proton})$ is the precessional frequency of ^1H at the magnetic field of the experiment (in this case $f(\text{proton}) = 13.9$ MHz) and $|A_i|$ is the absolute value of the i^{th} proton hyperfine coupling constant. In Figure 3, only the frequencies below the ^1H precessional frequency are shown.

ELECTRON SPIN ECHO SPECTROSCOPY

Although the ideas behind ESE techniques are as old as magnetic resonance itself (1946), the general application of spin echo methods to paramagnetic systems has occurred in only the last few years with the advent of very high speed digital electronics under computer control. Unlike the familiar continuous wave (cw) EPR experiment, which has been available in commercial instrumentation for nearly 20 years, ESE spectroscopy is not yet commercially available, and only a dozen or so laboratories throughout

the world currently perform the experiment. For an excellent review of the theory and early applications of ESE spectroscopy, the book by Kevan and Schwartz is recommended [6].

Unlike cw EPR, ESE is a pulsed microwave experiment. Very short microwave pulses excite the paramagnetic spin system, and the time evolution of the magnetization is monitored. Certain pulse schemes, characterized by the number of degrees the magnetization vector is tipped by each pulse, are known to generate a strong instantaneous magnetization in the sample following the sequence. Typical pulse schemes known to induce this rephasing or "echo" effect are $90^\circ - T - 180^\circ$ (Hahn echo sequence) and the $90^\circ - t - 90^\circ - T - 90^\circ$ (stimulated echo sequence). We have found the latter (stimulated echo) sequence to be most useful in our coal work. The sequence is diagrammed in Figure 4.

ESE spectroscopy has many advantages over the more conventional cw EPR. Chief among the advantages for our coal work is that the technique may be used to obtain spectra which resolve hyperfine structure that is obscured in cw spectra by inhomogeneous line broadening. In order to understand how ESE can be made to accomplish this task, let us look at the characteristics of the information obtained in the experiment.

In a typical stimulated echo experiment done on coal, the time interval t between the first and second 90° pulse is set at a fixed value during the experiment, while the interval T between the second and third pulses is incremented in steps, as shown in Figure 5. The amplitude of the echo induced by the sequence is measured as a function of the delay time T between the second and third pulses. In the absence of any interactions between the unpaired electrons being observed and neighboring nuclei with non-zero magnetic moments, the variation of the echo amplitude V with the delay time T is given by the simple exponential function:

$$V_{\text{echo}}(2t + T) = V_0 \exp \{-(2t + T)/T_m\}, \quad 2)$$

where T_m is the phase memory time of the individual spin packets. The exponential decay curve describing the echo amplitude as a function of T is called the electron spin echo envelope.

If our unpaired spins experience hyperfine interactions with neighboring nuclei, these interactions will manifest themselves as modulation patterns in the ESE envelope. This phenomenon is thus known as electron spin echo envelope modulation (ESEEM). For an $S = 1/2$ system with isotropic g -values (a very good approximation in the case of coal) and two hyperfine interactions characterized by frequencies f_a and f_b , the ESEEM pattern compensated for echo decay is given by:

$$V_{\text{mod}}(2t + T) = 1 - k[\sin^2(f_a t/2)\sin^2(f_b(t+T)/2) + \sin^2(f_b t/2)\sin^2(f_a(t+T)/2)] \quad 3)$$

In this expression, k is the so-called modulation depth parameter, proportional to B_0^{-2} in the limit of small hyperfine interactions (B_0 being the value of the static external magnetic field).

What makes the ESEEM effect so important to us is that a Fourier transform of the ESEEM pattern results in a frequency domain spectrum exhibiting linewidths that are characteristic of individual spin packets rather than of the entire envelope of spin packets comprising the inhomogeneously broadened lines observed by cw EPR. Since the modulation frequencies can be analyzed in an ENDOR-like theory, this technique provides us with a potential way of resolving the hyperfine interaction energies normally obscured in the cw spectra of whole coal. This information, in turn, allows us to study the environment experienced by radicals in coal, giving us a route to explore the atomic and molecular structure of whole coal. An example of a Fourier transformed ESEEM data set for the coal model system of perylene on alumina was shown in Figure 3.

Our typical experimental procedure when working on coal is to first carefully evacuate samples that have been ground to 50-100 mesh (although we have performed ESE experiments on large fragments). We have noticed that the presence of adsorbed oxygen has a significant effect on T_m , reducing it by more than a factor of two and making the experiments more difficult to perform; we have reported similar effects of oxygen on ENDOR spectra of coal [7]. Samples evacuated to pressures less than 10^{-6} Torr for several days are then sealed in quartz glass tubes for study. Experiments typically are performed at liquid helium temperatures in order to make T_m and T_1 as long as possible. A typical ESEEM result from an Illinois #6 coal is shown in Figure 6.

One can see in Figure 6 that the depth of the ESEEM pattern on the overall envelope is quite small. This is true for all coal samples. Since the signal-to-noise of the Fourier transformed spectrum is proportional to the modulation depth, we seek always to find ways to improve this feature of our ESE work. One obvious approach to improve matters is to recall that k , the modulation depth parameter from Equation 2, is proportional to B_0^{-2} . The spectrum shown in Figure 6 was taken at $B_0 = 3400$ G. on the spectrometer built by Norris and Bowman at ANL. We currently are building a spectrometer operating at $B_0 = 1000$ G. This instrument should improve the ESEEM amplitude by a factor of 10, and will be much better suited for the special characteristics of coal samples.

RESULTS AND DISCUSSION

The result of a stimulated echo experiment performed on powdered Illinois #6 coal was illustrated in Figure 6. Information on the proton hyperfine coupling constants of the species under observation now is present in the form of different periods of modulation that comprise the ESEEM pattern. In order to extract this data, the overall echo envelope may be simulated, making use of equations similar to that given in Equation 3. Alternately, the echo envelope decay function can be subtracted from the data and the remaining ESEEM function can be Fourier transformed to generate a frequency domain spectrum similar to that obtained from a cw ENDOR experiment. The advantage of the latter data processing route is that the result is in a familiar spectral format; one difficulty is that the amplitudes and phases of the spectral lines obtained in this way may be very unreliable.

Recently, Barkhuijsen, et. al. published a technique for analyzing ESEEM data that may combine the best features of both the simulation and FT approaches [8]. Called LPSVD (linear prediction singular value

decomposition), the analysis first simulates the ESEEM data using a linear combination of exponentially damped sinusoidal functions. The frequency, amplitude, T_M , and phase data for each component is then used to construct a new data set which then may be Fourier transformed to give a "noise-free" frequency domain spectrum. We currently are studying this analysis technique, and a more efficient variation of it called LPQRD [9]. Figure 7 illustrates the result of processing the ESEEM data of Figure 6 by the LPQRD method.

Analysis of the spectrum shown in Figure 7 is by the standard ENDOR formula given in Equation 1. For proton couplings, we expect to find pairs of lines symmetrically positioned about the free precessional frequency of the proton, $f(\text{proton})$, which is marked by an arrow labeled ^1H . Three such pairs of lines are indicated by the brackets marked A_1 , A_2 , and A_3 , corresponding to coupling constants of 8.0, 14.7, and 17.9 MHz. A low frequency peak without the complimentary high frequency partner is also seen, indicating another coupling constant of 2.8 MHz. In addition to these lines, a line marked with an arrow labeled ^{13}C is also shown. This resonance appears at the free precessional frequency of ^{13}C , and may be due to this isotope of carbon.

Kevan and colleagues were the first to publish ESE spectra of whole coal, and they demonstrated the power of the technique by analyzing the lineshape of the ^1H resonance (called the proton matrix line) [10]. Das, and later Doetschman, have reported ESE results in which proton hyperfine couplings of 4.8 and 14.0 MHz were seen in a low sulfur Pittsburgh bituminous coal [11,12]. Such hyperfine constants are consistent with protons in conjugated aromatic molecules, and provide direct evidence for the existence of such species in whole coal. They also are in good agreement with the constants measured by Retcofsky, et. al. using ENDOR spectroscopy on several Pennsylvania coals [13].

Not only can ESE spectroscopy obtain information about the molecular structure of organic compounds in coal, it can probe their environment. Figure 8 shows the magnetic field dependence of the amplitude of the 12.4 MHz component of the ESEEM pattern. It represents an "echo-induced" EPR spectrum of an Illinois #6 coal. The unique shape is due to a phenomenon called instantaneous diffusion, and can be related to the amplitude of the dipolar field experienced by an unpaired electron due to neighboring unpaired electrons [14]. Bowman and Clarkson have analyzed this effect and calculate it arises from a coal maceral with a radical concentration of 5×10^{18} spins/cm³, quite close to the average value EPR measurement of 1×10^{19} spins/cm³ for this coal [15].

Figure 9 illustrates the field dependence of two different frequency components of the ESEEM data from the Illinois #6. As we have already seen, the 12.4 MHz component has a lineshape characteristic of instantaneous diffusion. The 2.9 MHz peak, on the other hand, does not exhibit this effect, indicating that it arises from a coal maceral of lower radical concentration. The centers of the two spectra do not coincide, further indicating that the two signals have different g-values. The g-value difference between the two peaks, Δg , is nearly 0.001. Assuming that the principal mechanism for differences in g-values is the variation in heteroatom (O,N,S) content in different macerals, this data is consistent with a picture indicating that the 12.4 MHz coupling constant arises from a radical in a maceral with a significantly higher heteroatom content than

that found in the maceral containing the 2.9 MHz species. Such observations lead us to hope that in the future, ESE data can help us to develop maceral-specific information about the molecular forms present in whole coal.

ACKNOWLEDGMENTS

The authors gratefully acknowledge support for this work from the Department of Energy University Coal Research program (grant no. DOE/PC/70782), the Illinois Coal Research Board/Center for Research on Sulfur in Coal (grant no. STILENR12CRGCLARK961), and the Illinois ESR Research Center (NIH grant no. PHS#RR01811-01).

REFERENCES

1. H. L. Retcofsky, Scientific Problems of Coal Utilization, U. S. Department of Energy Report, 1978, pp. 79 - 97.
2. J. Uebersfeld, A. Etienne, and J. Combrisson, *Nature, Lond.*, **174**, 615 (1954).
3. D. J. E. Ingram, J. G. Tapley, R. Jackson, R. L. Bond, and A. R. Murnaghan, *Nature, Lond.*, **174**, 797 (1954).
4. C. M. White and M. L. Lee, *Geochim. Cosmochim. Acta*, **44**, 1825 (1980).
5. R. B. Clarkson, R. L. Belford, K. Rothenburger, and H. Crookham, *J. Catalysis*, 1985 (submitted).
6. L. Kevan and R. L. Schwartz, Time Domain Electron Spin Resonance, Wiley-Interscience, New York, 1979.
7. H. L. Retcofsky, M. R. Hough, M. M. Maguire, and R. B. Clarkson, *Appl. Spectroscopy*, **36**, 457 (1982).
8. H. Barkhuijsen, R. de Beer, W. M. M. J. Bovee, and D. van Ormondt, *J. Mag. Res.*, **61**, 465 (1985).
9. J. Tang, C. P. Lin, M. K. Bowman, and J. R. Norris, *J. Mag. Res.*, **62**, 167 (1985).
10. S. Schlick, M. Narayana, and L. Kevan, *J. Am. Chem. Soc.*, **100**, 3322 (1978).
11. U. Das, D. C. Doetschman, P. M. Jones, and M. Lee, *Fuel*, **62**, 285 (1983).
12. D. C. Doetschman and D. Mustafi, in Magnetic Resonance, L. Petrakis and J. P. Fraissard, eds., D. Reidel, 1984, pp. 639 - 644.
13. H. L. Retcofsky, M. R. Hough, M. M. Maguire, and R. B. Clarkson, in Coal Structure, ACS Advances in Chemistry Series, Vol. 192, 1981, pp. 37 - 58.
14. K. M. Salikhov and Yu. D. Tsvetkov, in Time Domain Electron Spin Resonance, L. Kevan and R. N. Schwartz, eds., Wiley-Interscience, New York, 1979.
15. M. K. Bowman and R. B. Clarkson, *Fuel*, 1985 (submitted).

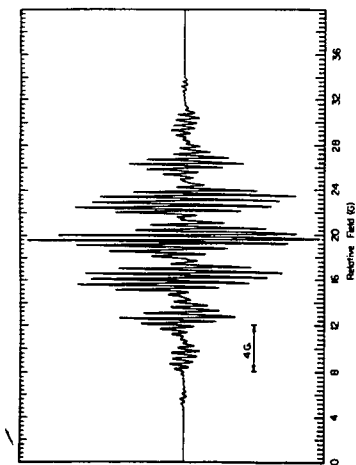


Figure 1. X-band EPR spectrum of the perylene cation radical in concentrated sulphuric acid.

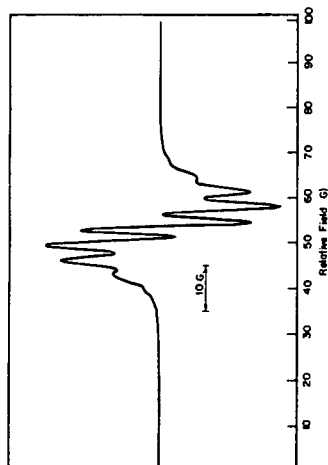


Figure 2. X-band EPR spectrum of the perylene radical adsorbed on alumina (11.5K)

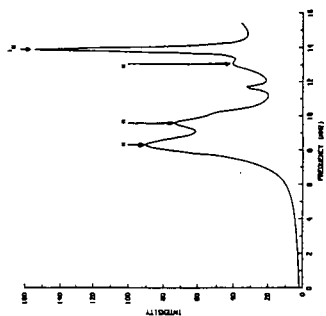


Figure 3. Processed ESE spectrum of the perylene radical adsorbed on alumina. Processing is through the LFQD version of Fourier transformation (see text) with conditioning to suppress features believed to be spurious. The three hyperfine transitions are marked with arrows labeled H, H', and H''. The peak marked H'' is the proton matrix line. T = 15K.

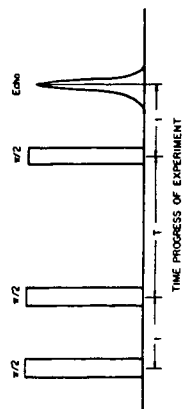


Figure 4. Timing diagram of the pulse sequence used to create a stimulated electron spin echo.

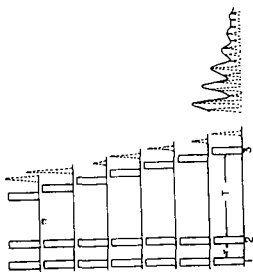


Figure 5. Diagram illustrating the formation of the ESEEM pattern in the context of a stimulated echo sequence. (after Kevan, [6])

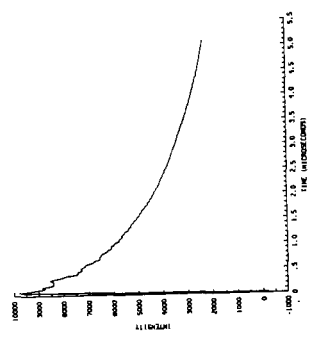


Figure 6. ESEEM effect in the echo envelope from an evacuated Illinois #6 whole coal. (15K).

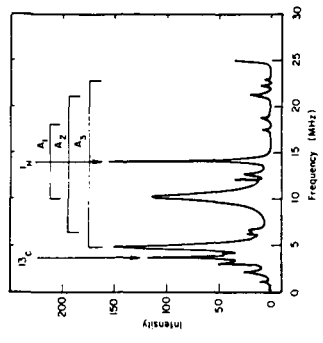


Figure 7. LFORD processed ESE spectrum of an evacuated sample of Illinois #6 whole coal. Resonances corresponding to the main proton hyperfine couplings are bracketed.

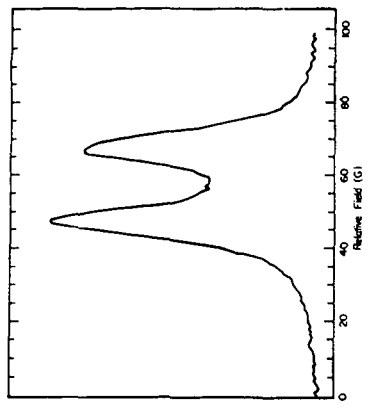


Figure 8. Plot of the magnetic field dependence of the amplitude of the 12.4 MHz modulation in the echo envelope of the evacuated Illinois #6 coal.

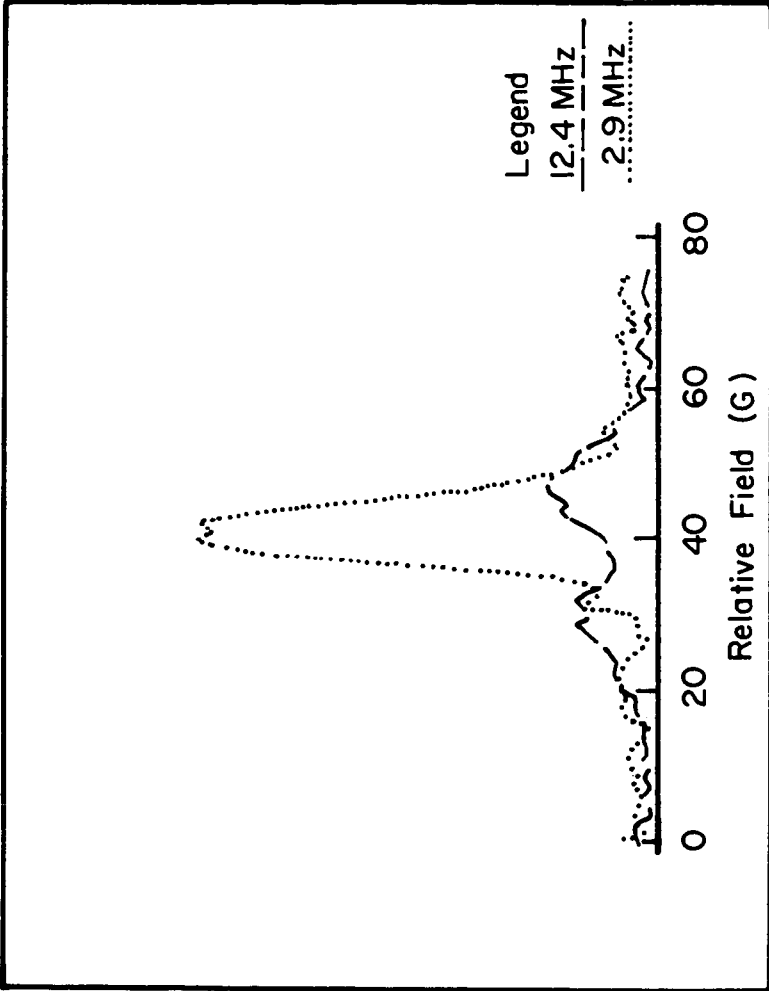


Figure 9. Plots of the magnetic field dependences of the amplitudes of the 2.9 and 12.4 MHz modulations in the echo envelope of the evacuated Illinois #6 whole coal.

THE USE OF DYNAMIC NUCLEAR POLARIZATION IN COAL RESEARCH

R.A. Wind

Dept. of Chemistry
Colorado State University
Fort Collins, Colorado 80523

1. Introduction

In a variety of articles it has been shown that the presence of unpaired electrons in coal makes it possible to enhance the ^1H and ^{13}C NMR signals of this material by irradiating at or near the electron Larmor frequency: the Dynamic Nuclear Polarization (DNP) effect (ref. (1)-(5) + references cited therein). It is found that in favourable cases the nuclear polarization can be enhanced by one to three orders of magnitude, which can e.g., be used as a fast method to characterize coal via ^{13}C NMR. In this paper the DNP enhancement will be investigated as a function of coal rank, and the observed behavior will be explained. Furthermore, special DNP experiments will be given which provide information about the carbon percentage detected via ^1H - ^{13}C cross-polarization (CP).

2. Experimental

For an extensive treatment of the experimental set-up we refer to the references (1) and (3). The external field strength was 1.4 T, corresponding to a proton Larmor frequency of 60 MHz, a ^{13}C Larmor frequency of 15 MHz and an electron Larmor frequency of 40 GHz. The microwave power was provided by a 10 W Klystron, in our set-up resulting in an amplitude B_1 of the microwave field of about .05 mT. All experiments shown in this paper except for the ^{13}C (DNP)-CPMAS experiments were performed on coal samples which were dried and degassed and have been put into pyrex tubes. (We found that both drying and degassing caused an increase in both the ^1H and ^{13}C Zeeman relaxation times as well as in the respective DNP enhancements). All measurements have been performed at room temperature.

3. The DNP enhancement as a function of coal rank.

In a solid several types of DNP effects can occur, depending on the nature and time-dependence of the spin-spin interaction term H_{en} between the electrons and the solids^{(3),(5)}: (i) an Overhauser effect is observed when H_{en} is time-dependent on a scale comparable to the inverse electron Larmor frequency ω_e^{-1} ; (ii) a solid state effect occurs when H_{en} is (partially) time-independent; (iii) a thermal mixing effect can be found when H_{en} is time-independent and when the electron concentration is so large that the broadening of the ESR line becomes homogeneous in character. In the latter case the polarization corresponding to this broadening can be enhanced via microwave irradiation, and this enhanced polarization is transferred towards the nuclear Zeeman system either via electron-nucleus relaxation interactions (the direct thermal mixing effect) or via so-called forbidden transitions (the indirect thermal mixing effect).

The ^1H and ^{13}C DNP enhancement in coal has been investigated extensively in the ref. (3) to (5). It has been found that, though all DNP mechanisms are present in the coal, the ^1H polarization enhancement becomes a maximum when the microwave frequency $\omega = \omega_e - \omega_H = \omega_e - 60$ MHz and that for this value of ω the enhancement is mainly due to a combination of the solid state effect and the indirect thermal mixing effect. The ^{13}C polarization becomes maximal when $\omega = \omega_e - \omega_H$, ω_H being the ESR linewidth (half width at half height) and is mainly caused by the direct thermal mixing effect. These results appeared to be the same for all coals we have investigated, with the exception of a meta-anthracite, where the Overhauser effect dominated.

We investigated the maximum ^1H and ^{13}C enhancements, $(P_{\text{H}})_{\text{max}}$ and $(P_{\text{C}})_{\text{max}}$, respectively, of more than sixty coal samples of different rank and origin, with a volatile matter percentage % VM varying from 6.8 to 91% (dmmf) and a carbon content %C varying from 96% to 66% (dmmf). The meta-anthracite has been omitted. We found that for a microwave amplitude B_1 of ca 0.05 mT $(P_{\text{C}})_{\text{max}}$ was about 8 times larger than $(P_{\text{H}})_{\text{max}}$, independent of the coal rank, so that we can confine ourselves by showing the proton results.

Figure 1 shows $(P_{\text{H}})_{\text{max}}$ as a function of %C, from which we observe that $(P_{\text{H}})_{\text{max}}$ becomes maximal when %C is 92% and that for %C < 75% no enhancement is found. In order to explain this we use an approximate equation for $(P_{\text{H}})_{\text{max}}$:

$$(P_{\text{H}})_{\text{max}} = 1 + c N_e (W_z^{\text{H}})^{-1} (\Delta B_z^{\text{H}})^{-1} \quad (1)$$

N_e is the number of organic radicals, W_z^{H} is the proton Zeeman relaxation rate, $\Delta B_z^{\text{H}} = 2g_e \omega_z$ is the ESR linewidth and c is a constant, among others proportional to B_1^2 . For $B_1 = 0.05$ mT c is given by $c = 2.4 \cdot 10^{-24}$, if N_e is expressed in m^{-3} (dmmf), W_z^{H} in sec^{-1} and ΔB_z^{H} in mT. As ΔB_z^{H} varies only between 0.8 and 1.3 mT for all the coal samples, the change in $(P_{\text{H}})_{\text{max}}$ as a function of coal rank is mainly due to variations in N_e and W_z^{H} . Figure 2 shows N_e as a function of % VM, from which we observe that N_e is decreasing for decreasing coal rank. In fact two dependencies are observed, curve 1 and curve 2, and it was found that the coals with the large N_e value (curve 2) almost all originated from the southern hemisphere. Moreover, it was found that for these coals only a part contributed to the DNP enhancement, so that presumably not all the radicals in these coals are present in the organic part of the coal. Figure 3 shows W_z^{H} as a function of the oxygen content. We observe that W_z^{H} increases with increasing %O, which probably means that a part of the oxygen is present as paramagnetic oxygen, because it is well-known that even a small percentage of paramagnetic oxygen causes a strong increase in the Zeeman relaxation rate. The increase in W_z^{H} for small oxygen percentages is caused by an increased number of organic radicals.

By inserting the observed values of ΔB_z^{H} , N_e (except for the coals of the southern hemisphere, where only a part of N_e is causing the DNP effect, see above) and W_z^{H} into Equation 1) it was found that this equation predicts the observed proton enhancement very satisfactorily. We like to emphasize that, as the constant c in Equation 1) is proportional to B_1^2 , both $(P_{\text{H}})_{\text{max}}$ and the region of coals for which a DNP enhancement is observed, will increase if more microwave power were available (this does not hold for the ^{13}C enhancement, as for the used B_1 value $(P_{\text{C}})_{\text{max}}$ is already close to the largest possible value).

4. How much carbon do we observe in coal?

A long standing problem is the percentage of carbons observed via the ^1H - ^{13}C cross-polarization technique, because it is possible that a substantial fraction of especially the aromatic carbons may be too remote from the protons to be measured via this method. In the literature this problem has been approached via a variety of different experiments¹⁰, and the found percentage differed between 50 and 100% so that the problem is still unresolved. The best way to determine this percentage is to compare the ^{13}C CP spectrum with the ^{13}C FID spectrum, where the ^{13}C signal is obtained after a 90° pulse applied at the ^{13}C Larmor frequency, but this is almost impossible to do because of the many scans needed and the long recycle delay between the scans. Therefore, we used an alternative approach and compared the ^{13}C CP spectra with ^{13}C FID spectra, obtained by enhancing the ^{13}C polarization via DNP. In figure 4, ^{13}C spectra are given of a medium volatile bituminous coal (31% VM, 87.4% C, 5.2% H, 5.3% O, all dmmf) obtained via CP, DNP-CP (here the ^1H signal was enhanced with a factor 16 via DNP before the CP experiment) and DNP-FID (here the ^{13}C signal was enhanced with a factor 130 before the 90° pulse), both with and without

Magic-Angle Spinning (MAS). We observe that within the signal-to-noise ratio the ^{13}C CP(MAS) and DNP-CP (MAS) spectra are the same, indicating that the proton polarization is enhanced uniformly. However, in the ^{13}C DNP-FID (MAS) spectra the aliphatic carbons are suppressed. Two explanations are possible: (i) in the DNP-FID experiment we are indeed observing more aromatic carbons than in the (DNP)-CP experiments; (ii) in the DNP-FID experiment, the DNP enhancement of the aliphatic carbons is less than that of the aromatic carbons, which is possible if the radicals are located mainly in the aromatic part of the coal. In order to investigate this we performed the following experiments:

a. $T_{1\rho}^{\text{C}}$ experiments. It is known that the electron Zeeman relaxation time T_{1e} in coal is of the order of μsec , which means that this provides an efficient way of relaxing the ^{13}C nuclei in the rotating frame, as T_{1e} is of the same order of magnitude as the inverse lock field. As the ^{13}C - ^{13}C spin diffusion is very slow, the relaxation of the ^{13}C magnetization M_{C} in the rotating frame is given by

$$M_{\text{C}}(t) = M_{\text{C}}(0) \exp\left\{-\left(t/T_{1\rho}^{\text{C}}\right)^{\frac{1}{2}}\right\} \quad (2)$$

Equation 2) holds provided that all the carbon nuclei are observed. If a percentage s of the carbons close to the electrons are not observed, Equation 2) is valid only for larger values of t , whereas for short values of t $M_{\text{C}}(t)$ is almost independent of t and given by 1-s.

Figure 5 shows the rotating frame relaxation of the aromatic carbons of the medium volatile bituminous coal, measured via the DNP-FID and DNP-CP experiment. It follows that in the first case we measure about 90% of the carbons, probably because carbons very close to the electrons are shifted out of the ^{13}C DNP-FID spectrum. In the DNP-CP experiment only 65% of the aromatic carbons are observed, which means that another 25% of the carbons are too remote from the protons to be observed via ^1H - ^{13}C cross-polarization.

b. The back-match experiment. The contact times T_{CH} between the carbons and protons, which determine the increase of the carbon polarization during a ^1H - ^{13}C CP experiment, depend on the strengths of the C-H interactions, and therefore on the carbon-proton distances. The values of T_{CH} can be determined by varying the matching time t_{M} during which the cross-polarization takes place. Figure 6a shows the result of such an experiment for the aromatic carbons in the medium volatile bituminous coal. We see that for about 35% of the carbons $T_{\text{CH}} = 30 \mu\text{sec}$ (direct C-H bonds) whereas for the remaining 65% $T_{\text{CH}} = 350 \mu\text{sec}$ (C-C-H bonds). Figure 6b shows a similar experiment, but now for a $\text{CH}_3\text{C} \rightarrow ^1\text{H}$ cross-polarization experiment (the 'back-match' experiment), after enhancing the ^{13}C polarization directly via DNP. We observe a much slower decay than in Figure 6a, because for about 40% of the aromatic carbons $T_{\text{CH}} = 1600 \mu\text{sec}$, which is not observed via the usual ^1H - ^{13}C CP experiment. Hence in the latter experiment about 40% of the aromatic carbons are not observed, a percentage which is comparable to the one obtained via the T_{CH} experiments. Similar results were obtained for a high volatile bituminous coal and an anthracite.

However, if we correct the aromatic part of the ^{13}C (DNP)-CP(MAS) spectra for the percentage of carbons not observed, still the percentage of aliphatic carbons in these spectra is larger than that obtained via the DNP-FID method. This means that indeed in the latter experiment the aliphatic carbons are enhanced less than the aromatic ones. Therefore, we conclude that both types of experiments are necessary to obtain the true percentages of the aliphatic and aromatic carbon atoms, and that the ^{13}C aromaticity in coal is larger than the apparent aromaticity following from the ^{13}C CP spectra.

References

1. R.A. Wind, F.E. Anthonio, M.J. Duijvestijn, J. Smidt, J. Trommel and G.M.C. de Vette, *J. Magn. Res.* **52** (1983), 424.

2. R.A. Wind, M.J. Duijvestijn, C. vd Lugt, J. Smidt and J. Vriend, Magnetic Resonance. Introduction, Advanced Topics and Applications to Fossil Energy. Eds. L. Petrakis and J.P. Fraissard. D. Reidel Publishing Co., Dordrecht 1984, p. 461.
3. R.A. Wind, M.J. Duijvestijn, C. vd Lugt, A. Manenschijn and J. Vriend, Progr. NMR Spectr. 17 (1985), 33.
4. C. vd Lugt, J. Smidt and R.A. Wind. Investigation of coal and coal products by means of ^1H and ^{13}C NMR in combination with Dynamic Polarization and ESR. Final report of the research project nr 4351, supported by a grant from the Project Office for Energy Research of the Netherlands Energy Research Foundation ECN, within the framework of the Dutch National Coal Research Program, 1985 (in Dutch).
5. M.J. Duijvestijn. The use of Dynamic Nuclear Polarization in ^1H and ^{13}C solid state NMR. Thesis. Delft University of Technology, Delft, 1985.
6. D.L. VanderHart and H.L. Retcofsky, Fuel, 55 (1976), 202.
7. F.P. Miknis, M. Sullivan, V.J. Bartuska and G.E. Maciel, Org. Geochem. 3 (1981), 19.
8. D.E. Wemmer, A. Pines and D.D. Whitehurst, Phil. Trans. R. Soc. Lond. A 300 (1981), 15.
9. E.W. Hagaman and M.C. Woody, Proc. Int. Conf. on Coal Science, Dusseldorf (Essen, FRG, Verlag Glueckauf), (1981), p. 807.
10. D. Tse and S.R. Hartmann, Phys. Rev. Lett. 21 (1968), 511.
11. M. Mehring, High Resolution NMR in Solids, Springer Verlag, Berlin, Heidelberg, New York, (1983).

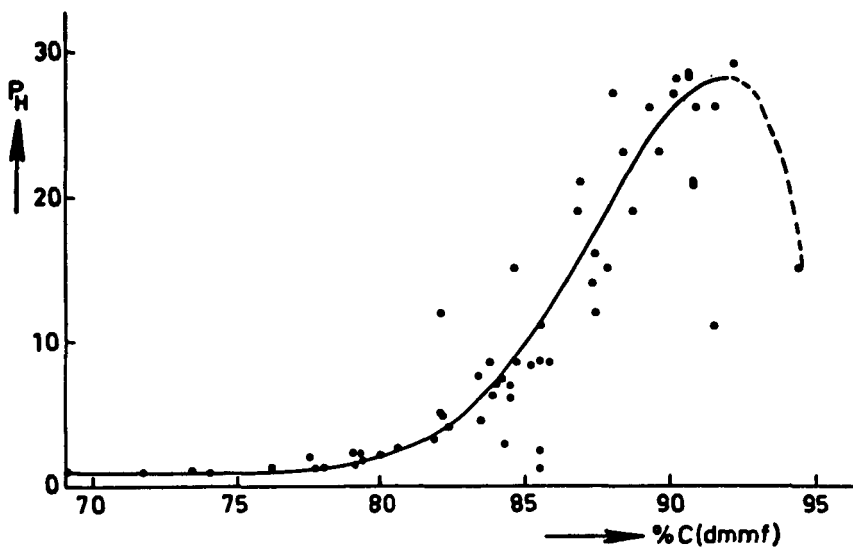


Figure 1. The maximum proton enhancement as a function of the carbon content.

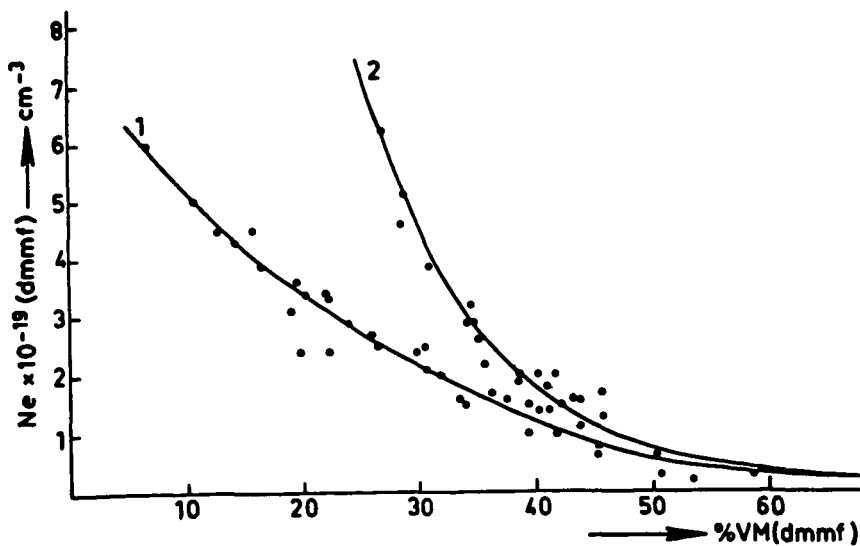


Figure 2. The number of unpaired electrons as a function of the percentage volatile matter.

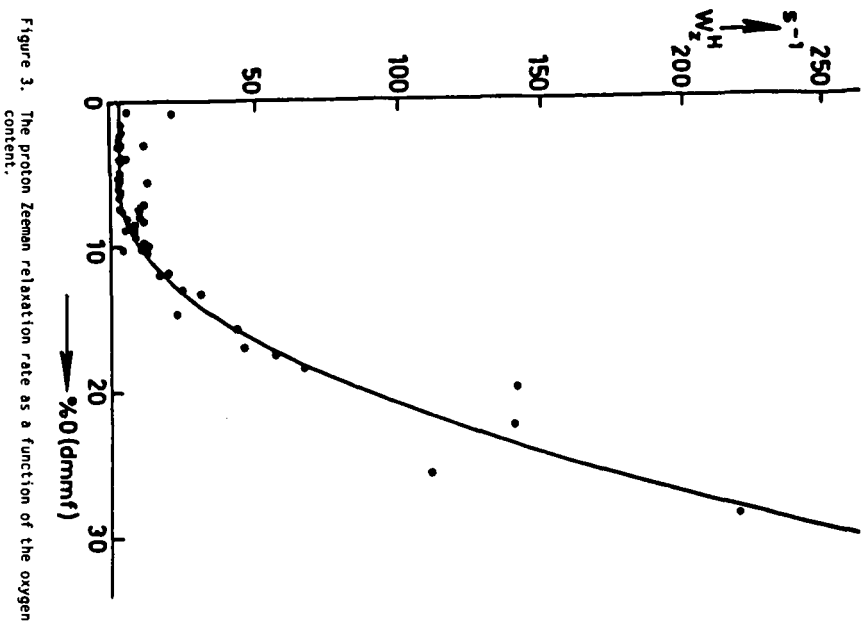


Figure 3. The proton Zeeman relaxation rate as a function of the oxygen content.

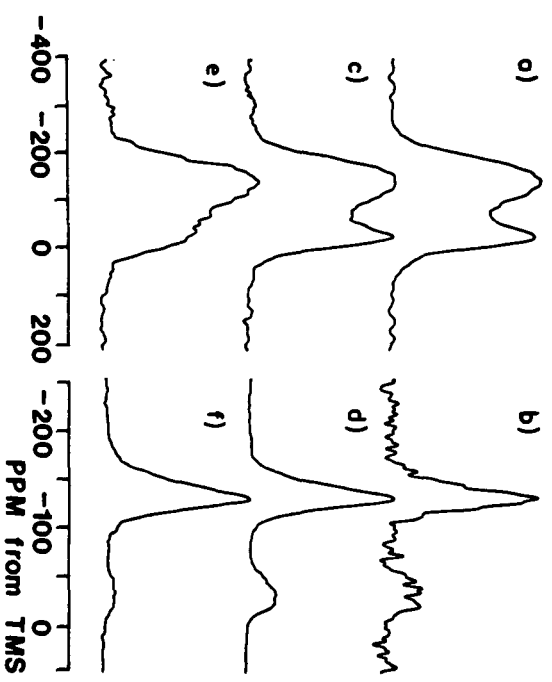


Figure 4. ¹³C spectra of a medium volatile bituminous coal measured via different techniques: a) CP. Match time = 0.9 msec; acquisition time = 5 msec; match field = proton decoupling field = 50KHz; number of scans = 20,000; recycle delay = 0.6 sec. A Lorentzian broadening of 200 Hz is applied. b) CPMAS. Spinning frequency = 3.5 KHz; acquisition time = 15 msec; number of scans = 10,000; no broadening is used. Other parameters as in a). c) DNP-CP. Number of scans = 400. Other parameters as in a). d) DNP-FID. Duration of pulse = 6 msec; acquisition time = 5 msec; proton decoupling field = 50 KHz; number of scans = 8; recycle delay = 60 sec; Lorentzian broadening = 200 Hz; e) DNP-FIDMAS. Spinning frequency 3.4 KHz; acquisition time = 15 msec; number of scans = 70; no broadening. Other parameters as in e).

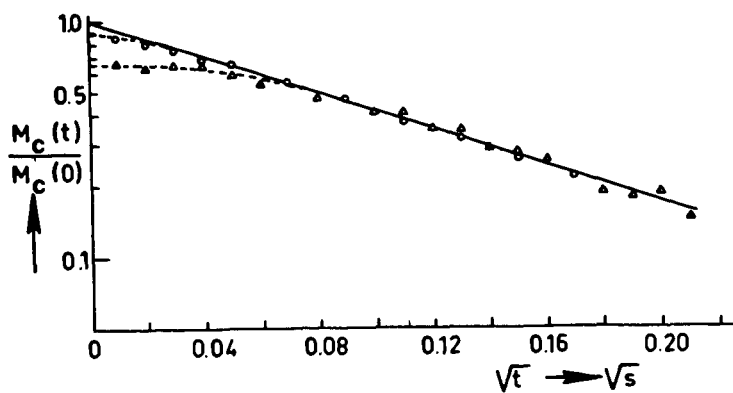


Figure 5. The rotating frame relaxation of the aromatic carbons of a medium volatile bituminous coal. The amplitude of the lock field = 40 KHz. circles : measured via DNP-FID; triangles: measured via DNP-CP.

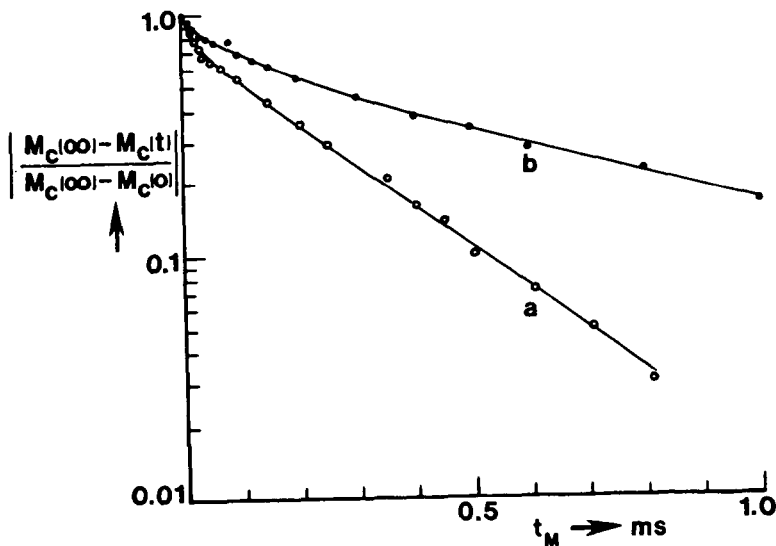


Figure 6. The magnitude of the aromatic ^{13}C signal as a function of the matching time. a: After ^1H DNP and $^1\text{H} - ^{13}\text{C}$ CP; b: After ^{13}C DNP and $^{13}\text{C} - ^1\text{H}$ CP.

Zero Field and 2D NMR Methods: Applications to Fossil Fuels

K. W. Zilm, G. G. Webb

Department of Chemistry
Yale University
225 Prospect Street
New Haven, CT 06511

Introduction

A knowledge of the chemical structures present in coals is essential for developing a better understanding of coal chemistry. Therefore, the study of coal structure is important to the successful synthetic conversion of coal to a chemical feedstock or high quality fuel. A great deal has been inferred about coal structure from the study of liquid coal products by both classical chemical methods and modern spectroscopic techniques. This approach is attractive as most modern analytical methods are applicable only to liquid samples and are not suitable for solids. However, because of the heterogeneity of coals and the complexity of coal chemistry it is often difficult to extrapolate back to the structure of a whole coal solely from the characterization of liquid products and extracts. Over the last decade this has spurred the development of spectroscopic methods suitable for nondestructively analyzing the structures of whole coals in the solid state. The two most useful techniques to emerge so far have been Fourier transform infrared spectroscopy and carbon-13 solid state nuclear magnetic resonance. The latter technique in the form of the combination of cross polarization and magic angle sample spinning (CP/MAS) spectroscopy has proven the most useful in characterizing the functionalities present in the organic portion of coals(1,2). This method provides the best direct measure of carbon aromaticities and can also measure the relative amounts of protonated versus nonprotonated carbon when combined with dipolar dephasing techniques. Much more information is, in principle, contained in carbon-13 CP/MAS spectra, but the resolution typically obtained does not permit as detailed an analysis as is possible in the NMR of liquids. The situation for coal CP/MAS spectra is similar to that found in the NMR of complex biomolecules where the large number of resonances and broad natural linewidths result in incompletely resolved spectra. In solution studies these difficulties can often be overcome by the application of two dimensional (2D) NMR methods (3,4). In 2D NMR experiments a complex spectrum is separated into component subspectra on the basis of a second spectroscopic parameter. The subspectra are simpler, more resolved and thus easier to interpret.

Standard 2D NMR methods are not directly applicable to organic solids for a number of reasons, the main one being the strong dipolar couplings among the abundant protons. In this paper two 2D NMR methods are presented that overcome these problems and are suitable for solids. The first is an adaptation of heteronuclear shift correlation spectroscopy to solids (5,6). In this method the carbon-13 and proton chemical shifts of a solid are correlated with one another. This allows the spectroscopist to generate the carbon-13 spectra of all the species with a particular proton chemical shift and vice versa. The second method is a new variant of the dipolar-shift spectroscopy (DIPSHIFT) methods that have been developed to measure C-H distances from carbon-13 proton dipolar couplings (7). Since bonded C-H distances in organic solids are all very close to 1.09Å, the dipolar coupled patterns observed in DIPSHIFT spectra are principally determined by the number of directly attached protons. In this way the dipolar interaction is used to give the number of protons attached to a carbon-13 with a particular chemical shift. The last approach to high resolution solid state spectroscopy described here is deuterium zero field NMR (ZFDMR) (8). In most solid state NMR methods the large anisotropic solid state interactions are suppressed to give liquid like high resolution chemical shift spectra. However, by doing NMR in zero magnetic field these interactions can be used to spectroscopically discriminate

among different functionalities. For deuterium the spectra are determined by the electric field gradient tensor which is a measure of the amount of s-character in a C-D bond. The spectra so obtained give information equivalent to normal proton NMR spectra, however the resolution is now as good in the solid state as in solution. These methods have shown great promise in model systems and should prove useful in studies of coal structure. The first of these methods has already had some success when applied to coal. Hopefully the finer structural information made available by these techniques will make it possible to apply more sophisticated and selective chemistry to coal. In the following paragraphs the basic principles underlying these experiments are examined and some applications are given. The interested reader is referred to the papers referenced above and to the references contained therein for a more complete description of the theory and the experimental requirements of these methods.

Heteronuclear Shift Correlation Spectroscopy

The pulse sequence used in heteronuclear shift correlation is indicated in figure 1. The basic idea of this method is to separate the overlapping carbon-13 resonances on the basis of the differences in the chemical shifts of the protons attached to the carbon-13 nuclei and vice versa. During the t_1 interval the protons are allowed to evolve under their chemical shifts. To give optimal resolution the carbon-13 nuclei are decoupled from the protons and MREV-8 homonuclear decoupling is employed to remove the dipolar couplings among the protons. At the end of t_1 the proton evolution must be transferred to the carbon-13 nuclei. In solids this can be accomplished by applying a proton spinlocking radio frequency (RF) field and then cross polarizing. When the proton spinlocking RF is turned on only that portion of the magnetization that is parallel to the RF field is spinlocked. For the protons on resonance all of the magnetization is spinlocked independent of the initial t_1 period. On the other hand the protons off resonance go in and out of phase with the spinlocking field. This results a spinlocked magnetization that oscillates at the off resonance frequency as a function of t_1 . Since the carbon-13 signal produced in the CP step depends on the size of the spinlocked proton magnetization, the carbon-13 signal will also oscillate as a function of t_1 at the proton resonance offset. The Fourier transform of the carbon signal amplitude versus t_1 then gives the proton chemical shift. To produce a 2D spectrum a set of carbon-13 spectra for successively longer values of t_1 is acquired. A second Fourier transform versus t_1 results in a 2D spectrum in which the proton and carbon-13 chemical shifts are correlated. The CP mixing time is kept short to minimize the contribution to the carbon-13 signal from non-bonded interactions. This ensures that only directly bonded pairs are correlated. This short mixing time also reduces the spin diffusion among the protons during cross polarization which can degrade the resolution in the proton dimension. As a result, this experiment is sensitive only to the subset of carbons that have a directly attached proton. In addition the proton spectra are only representative of that portion of the protons in the coal attached to a carbon.

The most natural way to portray 2D spectra is in a contour plot with the contours being paths of constant amplitude. Peaks appear as sets of concentric contours in this type of plot. In figure 2 is the contour plot of the heteronuclear shift correlation spectrum of an Illinois #6 coal (6). Along the top and sides are the summations of the data set onto the two axes. These spectra are the same as the normal short contact time CP/MAS spectrum and the combined multiple pulse MAS proton spectrum. In the contour plot there are three clearly resolved peaks and two weaker peaks labelled 1-5. For the aromatic region there is one peak at $\delta^1\text{H} = 6.8$ ppm, $\delta^{13}\text{C} = 128$ ppm as expected for the protonated aromatics. The results in the aliphatic region are much more revealing. Here the two most clearly resolved peaks, 4 and 5, are attributed to methylenes with $\delta^1\text{H} = 2.1$ ppm, $\delta^{13}\text{C} = 29$ ppm, and to methyls with $\delta^1\text{H} = 1.0$ ppm, $\delta^{13}\text{C} = 18$ ppm. These peaks are clearly resolved in both proton and carbon shift in the 2D spectrum. As the spectra along the top and sides indicate this resolution is not possible in either the proton or carbon-13 one dimensional spectra. In addition there are two

other weak peaks, 2 and 3, that are observed as shoulders in the 2D spectrum, one at $\delta^1\text{H} = 3.5$ ppm, $\delta^{13}\text{C} = 40$ ppm, and a second at $\delta^1\text{H} = 0.8$ ppm, $\delta^{13}\text{C} = 35$ ppm. These peaks are probably due to methyl groups with the first corresponding to heteroatom substituted methyls of some type and the second to sterically hindered methyls. Taking into account the bias in intensities that the short CP mixing time produces, the relative amounts of methyl to methylene to aromatic hydrogen can be estimated as 1.0 : 0.9 : 0.7 respectively.

From this 2D spectrum one can easily appreciate the increase in resolution that the method has over the usual CP/MAS technique. It is also apparent that the distribution of protons in the organic portion is easily accessible without spectral interference from water or mineral protons as would be encountered in direct solid state proton spectroscopy of coals. As shown above the method should be particularly useful in disentangling the overlapping bands in the aliphatic portion of coal CP/MAS spectra.

Dipolar Resolved Chemical Shift Spectroscopy- DIPSHIFT

The previous method used solid state pulse sequence trickery to adapt a liquid state method to the solid state. In the method diagrammed in figure 3, the solid state interactions are actually put to good use rather than considered just a nuisance. Let us begin by first considering some of the fundamentals of the magic angle spinning experiment.

In an MAS experiment the sample spinning is typically used to average the anisotropic chemical shifts to their isotropic values producing liquid like spectra. If the spin rate does not exceed the width of the shift anisotropy in Hertz, the spectrum will contain spinning sidebands. In the limit of very slow MAS spinning the envelope of the sideband pattern is the same as the static powder pattern. If MREV-8 decoupling is used to remove the proton-proton dipolar couplings in a solid, the remaining carbon-proton dipolar interaction also acts like a shift anisotropy. The combination of MREV-8 decoupling and MAS then gives dipolar coupled carbon-13 spectra broken up into sideband patterns. From the envelope of the sidebands the dipolar couplings can be determined. This is the principle behind the DIPSHIFT methods used to measure C-H distances via carbon-proton dipolar couplings and their $1/r^3$ dependence. In the current application the strategy is to take advantage of the constancy of C-H distances in organic solids and to realize that the dipolar coupled spectral patterns thus depend only on the number of protons attached to a given carbon center. In figure 4 are typical dipolar coupled patterns for methylene, methine, rapidly rotating methyl and quaternary carbons using MREV-8 proton decoupling with CP/MAS. Note that the methylene pattern is approximately twice as wide as the methine pattern and that both are much wider than the methyl or quaternary patterns. The different widths of these patterns can be used to cleanly separate overlapping carbon-13 resonances that have different numbers of attached protons. Consider the case where the resonances for a methylene, methine and methyl carbon all overlap. In the MREV-8 decoupled CP/MAS spectrum the outermost sidebands will come only from the methylene carbon. Since the sideband intensity ratios in each pattern are fixed by the size of the carbon-proton dipolar coupling and the spin rate, the contribution of the methylene to the rest of the spectrum can be subtracted. In this resultant spectrum the outermost sidebands will now only be due to the methine. The subtraction operation used for the methylene can be repeated for the methine leaving only the methyl carbon spectrum. In this way the contributions to a line from methylene, methine and methyl plus quaternary carbons can be separated. This is a significant improvement over dipolar dephasing which cannot separate methylenes from methines. Also, since all carbons are observed at the same time, this type of technique avoids the problems with quantitation encountered in dipolar dephasing.

For a complex solid the dipolar coupled patterns are best obtained from a 2D experiment as in figure 3. During t_1 the carbon-13 nuclei evolve under the effect of MREV-8 decoupling and the carbon-proton dipolar coupling. Afterwards in t_2 the carbon signal is acquired under the influence of strong dipolar decoupling.

As before a set of carbon-13 spectra for successively longer values of t_1 is acquired. The second Fourier transform gives a 2D spectrum with the normal carbon-13 chemical shift along one axis and chemical shift plus dipolar couplings along the second axis. In other DIPSHIFT methods the chemical shifts are removed during the t_2 interval with a π refocussing pulse. To refocus the anisotropic as well as the isotropic shift the π pulse must be applied at an integral multiple of the MAS spinning cycle. Since accurately controlling MAS spin rates is difficult, an alternative method is attractive. In the new method presented here the chemical shift is kept in both t_1 and t_2 . Spectral distortions will occur in this experiment from the so-called phase twist problem (3) unless the carbon magnetization is projected at the end of t_1 . This is done by flipping a portion of the carbon-13 magnetization up along the applied field, waiting a short dephasing time to destroy any transverse magnetization, and flipping the spins back down into the x-y plane. This method has the advantage that none of the experiment need be done synchronously with the MAS rotation. In addition the MREV-8 sequence can be incremented a piece at a time giving a greatly increased bandwidth in the dipolar dimension. The pulses used in the projection step are also phase cycled in 90 degree increments for each successive point to simulate the effect of having the detector off-resonance during t_1 . This allows the carrier frequency to be placed in the center of the spectrum while appearing to be at the extreme edge and makes the most effective use of the available bandwidth in t_2 . This feature is especially important for methylenes because their dipolar coupled patterns are so wide.

By using the subtraction scheme outlined above on the 2D spectrum the methylene only, methine only and methyl plus quaternary only spectra can be generated. With suitable software routines the relative numbers of methylenes, methines and methyls plus quaternary carbons can also be extracted for the different resolvable spectral regions. Application of this method in model polymer systems has allowed separation of overlapping resonances such as the methine and methylene that overlap in polystyrene. Whereas the peak in question seems to be a single resonance in the normal CP/MAS spectrum, the dipolar slices taken in the 2D experiment clearly show that this line is a superposition of a methylene and methine. The advantage of this method over the heteronuclear shift correlation technique is that all carbons are detected as a long mixing time can be used and therefore the signal to noise obtained in a given amount of time is much better. The information obtained is complementary being in terms of proton multiplicity rather than chemical shift. For coals the method should prove particularly useful for separating and assigning the resonances observed in CP/MAS spectra.

Zero Field NMR

Another method that should prove useful in the study of coal structure is zero field NMR (ZFNMR). In the 2D methods described so far the basic strategy has been to use carbon-13 chemical shifts to identify different functional types of carbon. Then either proton chemical shifts or carbon-13 proton dipolar couplings are used to separate resonances that occur at the same shift. In ZFNMR a very different approach is used. Instead of suppressing the large solid state anisotropic interactions such as dipolar or quadrupolar couplings to obtain liquid like chemical shift spectra, these interactions themselves are used as the principal means of resolving different chemical species.

Consider the case of a spin 1 nucleus in a large static magnetic field. The main interaction that this nucleus feels is the coupling to the static field giving the usual Zeeman splittings observed in an NMR experiment. In a rigid solid a spin 1 nucleus also has a quadrupole coupling that produces an additional splitting of the energy levels. For deuterium in organic solids this interaction is a measure of the s-character in the C-D bond and in a sense is analogous to a chemical shift. Deuterium quadrupole couplings typically range from tens to hundreds of kHz. This is much larger than the spread of deuterium chemical shifts that span only 750 Hz at the highest fields available today. Thus quadrupole couplings could potentially be the basis for a deuterium spectroscopy with much

greater resolving power than standard NMR. Unfortunately the quadrupolar interaction does not simply add to the Zeeman interaction and the size of the splitting at high field depends on the orientation of the electric field gradient tensor with respect to the applied field. In a randomly oriented powder sample this results in a range of observed splittings and the spectra are broad overlapping powder patterns.

The application of a strong magnetic field produces powder broadening because it polarizes the nuclei along a particular direction in space. However in the absence of an applied field, all deuterium nuclei of the same type experience the same splitting of their energy levels independent of their absolute orientation in space and the spins are quantized in a molecule fixed frame. Thus the zero field deuterium NMR (ZFDNR) spectrum of a randomly oriented powder is the same as for a single crystal and has narrow resolved lines. This is the basic idea behind pure nuclear quadrupole resonance (NQR) spectroscopy as well. The trick is to do a high sensitivity experiment in the absence of an applied field. Several clever field cycling and double resonance techniques have previously been developed for pure NQR spectroscopy of nuclei such as deuterium (8). However all of the standard methods are either continuous wave techniques or involve low frequency detection. The ZFNMR method is more generally applicable to nuclei such as deuterium with relatively small quadrupole couplings. The method uses high frequency detection for good sensitivity and is also a Fourier transform technique. This latter feature gives ZFNMR a better inherent resolution than any of the continuous wave methods (8).

The magnetic field cycle used in the ZFNMR method is shown in figure 5. The first step is to polarize the nuclei in a high field magnet to produce a measurable signal. The sample is then mechanically removed to an intermediate region in the fringe field of the high field magnet. If this is done rapidly compared to the characteristic relaxation times of the sample, the high field polarization is maintained in the intermediate field system. As long as the intermediate field is chosen to give a Zeeman splitting several times larger than the quadrupole splittings, the polarization will continue to be aligned with the applied field axis. This intermediate field is suddenly removed by a set of pulsed coils that can collapse the field rapidly compared to the inverse of the NQR frequencies of the sample. The magnetization that was initially along the applied field axis now finds itself influenced solely by the quadrupolar interaction. Since the polarization at zero field would prefer to be aligned in the internal axis system of the electric field gradient tensor, any portion that is not so oriented now oscillates at the zero field NQR frequencies. If a receiving coil was in place around the sample at this point, a zero field free induction decay (FID) would be observed. The Fourier transform of this zero field FID would give the ZFNMR spectrum. Because of the low frequencies involved, it is better to turn this oscillation into a high field observable. This requires a 2D type of data taking sequence with the zero field time as t_1 . At the end of the zero field interval the intermediate field is suddenly pulsed back on trapping the component of the magnetization parallel to the applied field. After the sample is returned to the NMR magnet this component can be measured as a high field NMR signal. The amplitude of this signal naturally oscillates as a function of the length of time t_1 that the sample spent at zero field. A Fourier transform of the high field signal amplitude versus t_1 then results in the ZFNMR spectrum. Although a 2D type of data set is actually acquired, a full 2D transform is not performed since the high field spectra do not provide any additional information.

A typical result is shown in figure 6 where the ZFDNR 6a and high field MAS NMR 6b spectra of perdeuterated dimethoxy benzene are compared. In spectrum 6a the methyls give a resonance at about 40 kHz and the aromatics appear in the region around 135 kHz. This resolution is comparable to the resolution of the methyl and aromatic carbon-13 resonances in the CP/MAS spectrum. The two types of deuterium are barely resolved in spectrum 6b with the aromatics appearing at 2 and 4 ppm from the methyl. This set of spectra dramatically demonstrates the superior

resolving power of ZFDMR over the more conventional high field MAS technique. In fact the resolution of ZFDMR is comparable to high field deuterium NMR in solution and can discriminate among different functionalities as well as carbon-13 CP/MAS spectroscopy can. Thus the method should be the technique of choice for determining the different types of hydrogen in organic solids. For instance proton aromatics in coals could accurately be measured with ZFDMR. The successful application of this method will undoubtedly require additional developments to increase the sensitivity of the method such as combining ZFDMR with dynamic nuclear polarization (1) or indirect detection of the deuterium via the abundant protons (8). All experiments to date have used isotopically enriched samples because of the low natural abundance of deuterium. At present natural abundance studies are not feasible and in the immediate future the most fruitful contributions to coal chemistry will involve chemically modified coals either by using deuterated reagents or exchanging labile hydrogen for deuterium.

Conclusions

The increase in resolution made possible by these new 2D NMR and zero field NMR methods should make it possible to determine the chemical structures present in coals to a much finer degree than previously possible. With a better knowledge of the functional units in coals it should be possible to develop more sophisticated chemistry for converting coal to a chemical feedstock or fuel. These NMR methods are still in an early stage of development but have already had some success in application to polymers and coal. The question of quantitative response has yet to be fully addressed but at present there is no evidence to indicate that this will be any more of a problem than in standard carbon-13 CP/MAS spectroscopy. More development is needed to make these techniques generally accessible to the practicing chemist and work in this area is being actively pursued.

Acknowledgements

Acknowledgement is made to the donors of the Petroleum Research Fund, administered by the ACS for partial support of this work. Other financial support for this work was provided by the Department of Energy under grant number DE-FG22-83PC60791.

References

- 1) Magnetic Resonance Introduction, Advanced Topics and Applications to Fossil Energy" ed. by L. Petrakis and J. P. Fraissard, NATO ASI Series, D. Reidel, Holland, 1985
- 2) F. P. Miknis, Magn. Reson. Rev. 7 (1982) 87.
- 3) A. Bax, "Two Dimensional NMR Spectroscopy in Liquids" Reidel, Hingham.
- 4) K. Wuthrich, K. Nagayama, R. E. Ernst, Trends in Biochem. Sci. 4 (1979) 178.
- 5) J. E. Roberts, S. Vega, R. G. Griffin, J. Am. Chem. Soc. 106 (1984) 2506.
- 6) K. W. Zilm, G. G. Webb, Fuel in press
- 7) M. G. Munowitz, R. G. Griffin, G. Bodenhausen, T. H. Huang, J. Am. Chem. Soc. 103 (1981) 2529.
- 8) A. Bielecki, J. B. Murdoch, D. P. Weitekamp, D. B. Zax, K. W. Zilm, H. Zimmerman, A. Pines, J. Chem. Phys. 80 (1984) 2232

Fig. 1

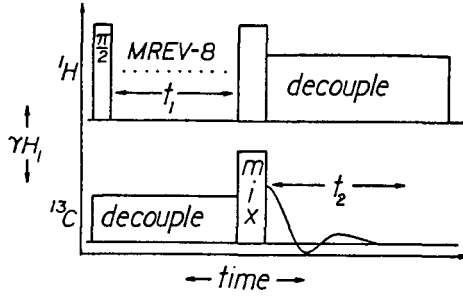


Fig. 2

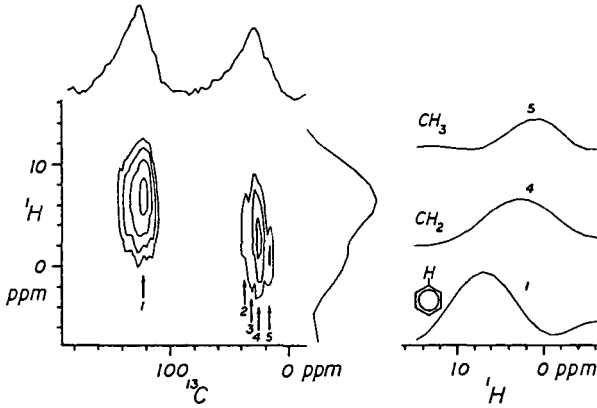


Fig. 3

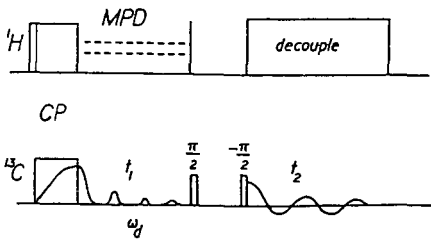


Fig. 4

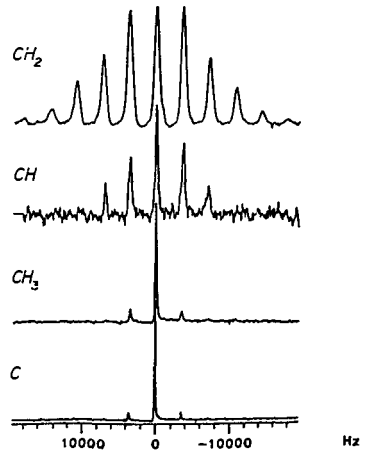


Fig. 5

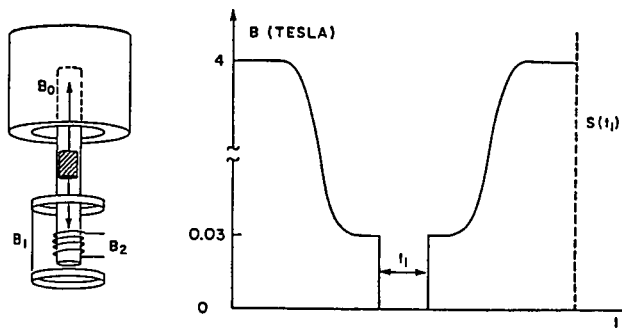
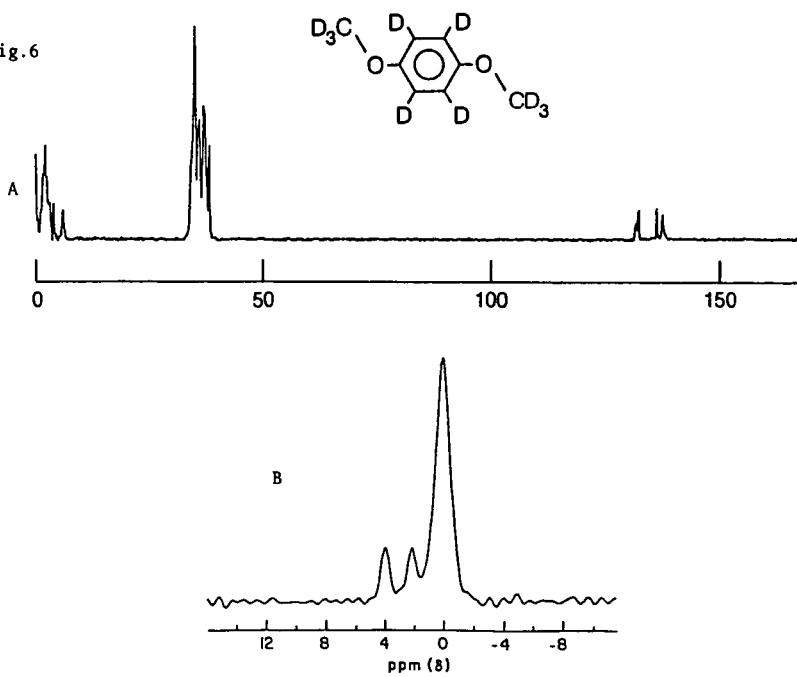


Fig. 6



**TEMPERATURE PROGRAMMED SOLUBILIZATION OF COAL:
CHARACTERIZATION OF PRODUCT FRACTIONS**

Bogdan Slomka, Tetsuo Aida, Yu-Ying Chen,
Gregor A. Junk and Thomas G. Squires

Ames Laboratory
Iowa State University
Ames, Iowa 50011

INTRODUCTION

For more than forty years, it has been recognized that the many interactive physical and chemical phenomena which comprise coal liquefaction fall into two functional categories: productive processes and counter-productive processes (1,2,3). Yet despite this understanding, the nature of these components and the contribution of each to the overall conversion have remained obscure. This can be attributed, in part, to the complex nature of coal but is also due to poor perception of the problem and to consequent deficiencies in experimental design.

The conversion of coal to liquid products is clearly a dynamic process. It is, therefore, quite curious that most coal scientists continue to employ investigative techniques more appropriate for measuring thermodynamic rather than dynamic phenomena. These techniques confine starting materials, intermediates, and products to the same reaction space throughout the primary product-determining segment of the conversion.

From this perspective, autoclaves (4,5), tubing bombs (6), and even staged flow reactors (7) are simply incapable of resolving productive and counter-productive processes. In these reactor systems, secondary processes are promoted rather than inhibited and, thus, obscure primary pathways in the conversion. Interpretations of the results from these experiments in terms of primary processes are beyond the capacities of mere mortals. On the other hand, fixed bed, flow mode reactors have the capacity to remove conversion products as they dissolve in the flowing phase; and, in this way, such reactors inhibit secondary reactions involving solubilized products.

Recently, we reported the development of a flow mode micro-reactor for the purpose of dynamically investigating the thermal dissolution of coal (8). Using this apparatus, we established characteristic staged temperature solubilization profiles for coals of various ranks and presented evidence that these dynamic profiles were comprised of (at least) two types of solubilization phenomena. In the present study, we have confirmed and extended these findings by using temperature programmed experiments to clearly resolve the benzene solubilization events and by characterizing the coal liquids produced during these events.

EXPERIMENTAL

General

Illinois No. 6 Coal from the Ames Laboratory Coal Library was used for these studies. The ultimate analysis for this coal (dmmf basis) is C: 80.60%; H: 5.63%; N: 1.56%; S_{org}: 2.35%; and O(diff): 9.81%. Ash (dry basis) and volatile matter (dmmf basis) contents are 10.0% and 40.4%, respectively. Prior to use, the coal was ground, sized to 200 x 400 mesh, riffled to insure uniformity, and dried at 110°C overnight under vacuum. Degassed HPLC grade benzene was used in the solubilization experiments; and samples and solvents were handled and stored under nitrogen.

Solubilization Procedures

Flow mode solubilization experiments were carried out in an improved version of our flow mode reactor. New features include continuous, "on-line" optical density monitoring of the reactor effluent; real time data acquisition of optical density, temperature, and pressure; and an improved time resolved product collection system. In a typical experiment, a preweighed amount (25-200 mg) of 200-400 mesh coal was placed in the tubular reactor, fixed in place by 2 μ stainless steel frits, and a shielded 0.062 inch o.d. chromel-alumel thermocouple was inserted into the coal bed. After connecting the reactor and purging the apparatus with nitrogen, the entire system was filled with benzene and pressurized to 3190 psi before adjusting the solvent flow to 1.0 ml/minute.

Two kinds of temperature programmed benzene solubilization experiments were carried out:

- (1) Staged temperature benzene solubilization and
- (2) Continuous temperature benzene solubilization.

In the former experiments, targeted temperatures were always attained and stabilized within 3 to 5 minutes. For all experiments, temperature was controlled during the conversion according to a predetermined program; and the optical density profile of the product stream, as well as temperature and pressure profiles of the coal bed, were recorded throughout the conversion. Products were collected at appropriate times on the basis of the optical density profile.

Chromatographic Analysis of Products

Samples were prepared for analysis by removing the solvent from the solubilization product at room temperature using a slow stream of nitrogen. The dried product was then dissolved in 0.2 ml of tetrahydrofuran and this solution was used for chromatographic analysis. Products were analyzed by Reverse Phase Liquid Chromatography (RPLC) on a 4.1 mm x 300 mm μ -Bondapak (phenyl/corasil) column (Alltech Associates), by Gel Permeation Chromatography (GPC) on 1000, 500, and 100 Angstrom μ -Styragel columns (Waters Associates), and by Capillary Gas Chromatography on a 30 meter DB-5 column (J&W Scientific).

RESULTS & DISCUSSION

Solubilization Profiles

Previous investigations in our laboratories (9) have provided persuasive evidence that coal solubilization in benzene proceeds via physical processes at temperatures below 300°C and that, as the temperature is increased beyond 300°C, thermal chemical processes become progressively more important. Staged temperature, flow mode experiments have proven useful as a means of investigating solubilization phenomena as a function of time and temperature (8). A staged temperature (260/390°C) solubilization profile for Illinois No. 6 coal is shown in Figure 1.

Under these conditions, it is not clear whether the maxima in effluent absorbance at 3 minutes and 24 minutes are due to distinct and resolvable conversion phenomena. The maxima coincide with heating ramps and could simply reflect a general temperature driven increase in all of the processes which contribute to solubilization. This question was addressed by carrying out the benzene solubilization experiment while programming the temperature continuously from 25°C to 420°C (Figure 2). The solubilization profile generated in this manner demonstrates conclusively that there are at least two distinct solubilization events: one in the 240 to 280°C region and the other in the 370-410°C region.

Characterization of Products

In order to further investigate the nature of these events, low temperature product (LTP) and high temperature product (HTP) fractions were collected during the times indicated in Figure 2. These fractions were then analyzed by Reverse Phase Liquid Chromatography (RPLC) and by Gel Permeation Chromatography (GPC), and the resulting chromatograms are shown in Figures 3 and 4, respectively. On the basis of RPLC, the High Temperature Fraction appears to have a larger polar component than the Low Temperature Fraction. However, these results are not unambiguous; the difference in RPLC patterns appears to be due to differences in the relative concentrations of components rather than the presence or absence of components in the product fractions. Furthermore, little difference is apparent in the GPC traces of the two fractions (Figure 4).

To clarify these results, products were collected from a three stage (260/340/420°C) solubilization experiment and analyzed by RPLC and GPC (Figures 5 and 6). The chromatograms reveal unambiguous differences in the products and provide the basis for two important conclusions. That the material produced at 420°C is distinctly more polar than products solubilized at lower temperatures is clear from the RPLC traces (Figure 5). It is equally apparent from the GPC traces (Figure 6) that the molecular weight of the product increases to a maximum between 260 and 420°C.

Thus, while the molecular weight distributions of the products at 260 and 420°C are quite similar (see also Figure 4), the products themselves are almost certainly generated by different

processes. It appears that the 260°C fraction is produced by physical dissolution processes which continue to dominate pyrolytic processes at 340°C. However, by 420°C, thermal chemical fragmentation processes are dominant and the average MW of the product has decreased while the polarity has increased.

FUTURE WORK

We have begun to test this hypothesis and to further elucidate the nature of these processes using GC/MS to analyze time and temperature resolved products from our experiments. In Figure 7, the capillary gas chromatograms of the 260 and 420°C fractions are compared with those of acetone extracts from whole coal and coal tar (420°C, vacuum). Major new components, absent in the low temperature extracts are apparent in both 420°C products and are now being analyzed by GC/MS.

ACKNOWLEDGEMENT

Portions of this research were supported by U. S. Department of Energy Grant No. DE-FG22-82PC50786 for which we are grateful. However, any opinions, findings, conclusions, or recommendations expressed herein are those of the authors and do not necessarily reflect the views of DOE.

REFERENCES

1. van Krevelen, D. W. in "Coal"; Elsevier: New York, 1961; pp. 201-216.
2. Neuworth, M. B. J. Am. Chem. Soc. 1947, 69, 1653.
3. Glenn, R. A.; De Walt, C. W. Fuel 1953, 32, 157.
4. Painter, P. C., et. al. Fuel 1979, 58, 233.
5. Ouchi, K.; Makabe, M.; Yoshimoto, I.; Itoh, H. Fuel 1984, 63, 449
- 6a. Neavel, R. C. Fuel 1976, 55, 273.
- 6b. Mitchell, T. O.; Whitehurst, D. D. Prepr. Pap.-Am. Chem. Soc., Div. Fuel Chem. 1976, 21(2), 127.
7. Burke, F. P.; Winschel, R. A.; Jones, D. C. Fuel 1985, 64, 15.
8. Aida, T.; Slomka, B.; Shei, J. C.; Chen, Y.-Y.; Squires, T. G. Prepr. Pap.-Am. Chem. Soc., Div. Fuel Chem. 1985, 30(4), 274.
9. Squires, T. G.; Aida, T.; Chen, Y. Y.; Smith, B. F. Prepr. Pap.-Am. Chem. Soc., Div. Fuel Chem. 1983, 28(4), 228.

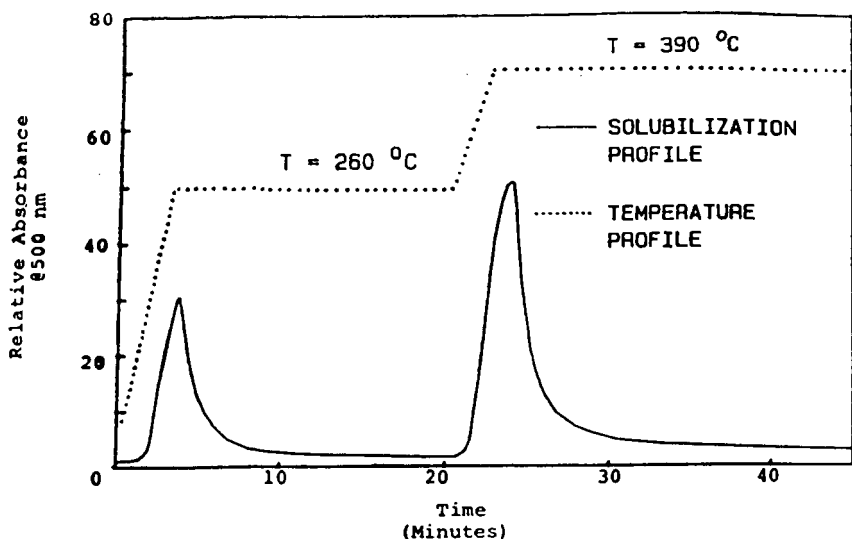


Figure 1. Staged Temperature Benzene Solubilization of Illinois No. 6 Coal. First Stage: 260°C/3180 psi; Second Stage: 390°C/3180 psi.

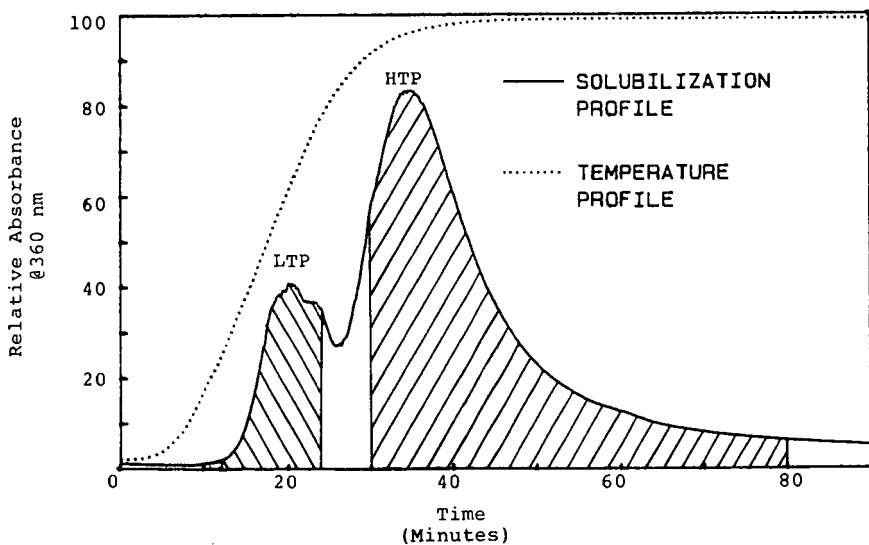


Figure 2. Continuous Temperature Benzene Solubilization of Illinois No. 6 Coal at 3180 psi. Initial Temperature: 20°C; Final Temperature: 420°C.

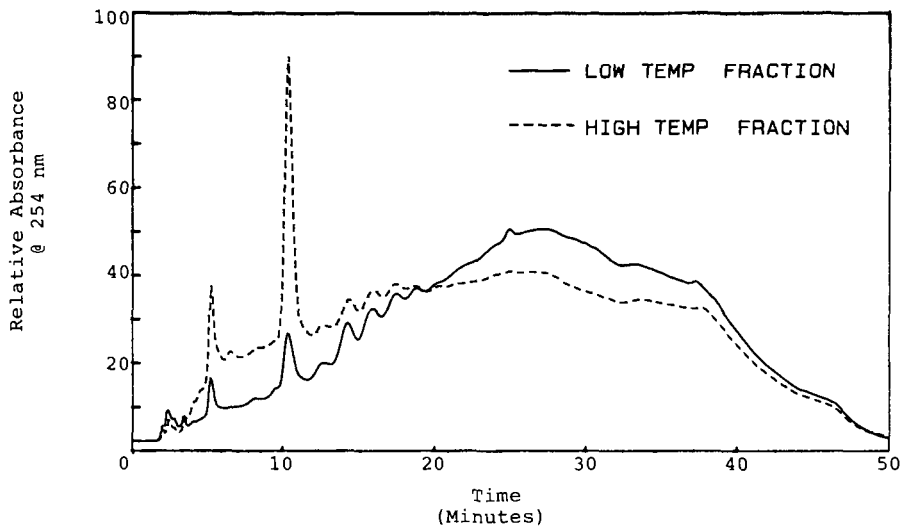


Figure 3. Liquid Chromatograms of Products from the Continuous Temperature Programmed Benzene Solubilization of Illinois No. 6 Coal.

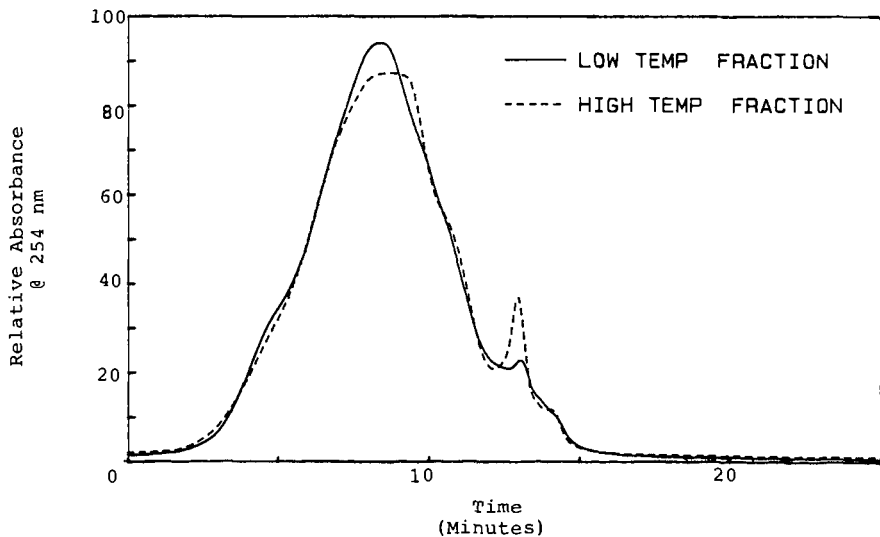


Figure 4. Gel Permeation Chromatograms of Products from the Continuous Temperature Programmed Benzene Solubilization of Illinois No. 6 Coal.

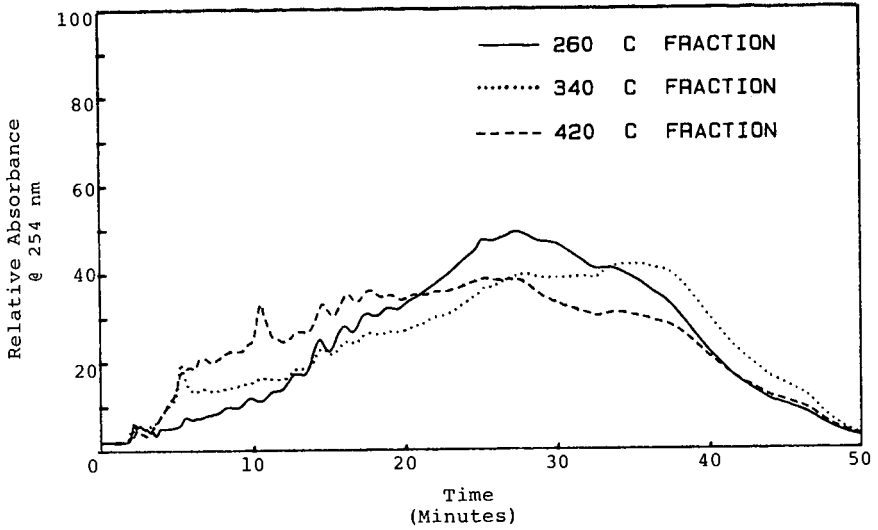


Figure 5. Liquid Chromatograms of Products from the Temperature Staged Benzene Solubilization of Illinois No. 6 Coal.

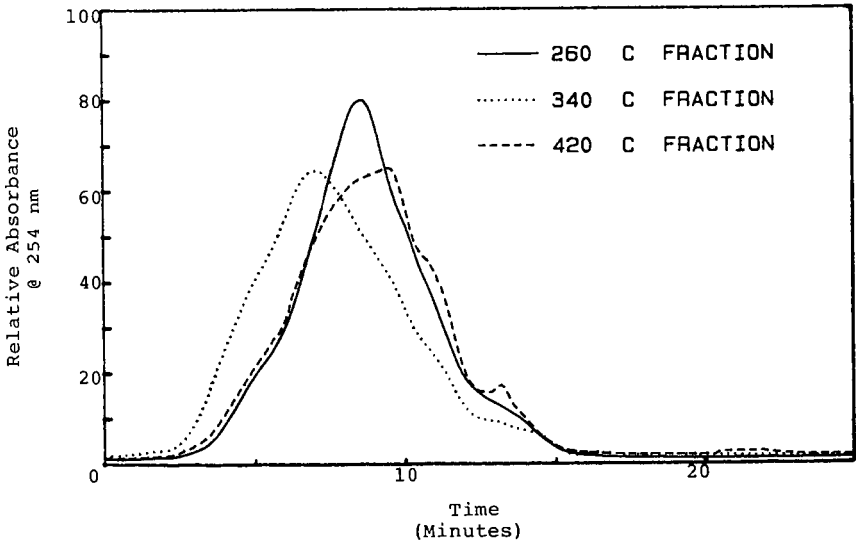


Figure 6. Gel Permeation Chromatograms of Products from the Temperature Staged Benzene Solubilization of Illinois No. 6 Coal.

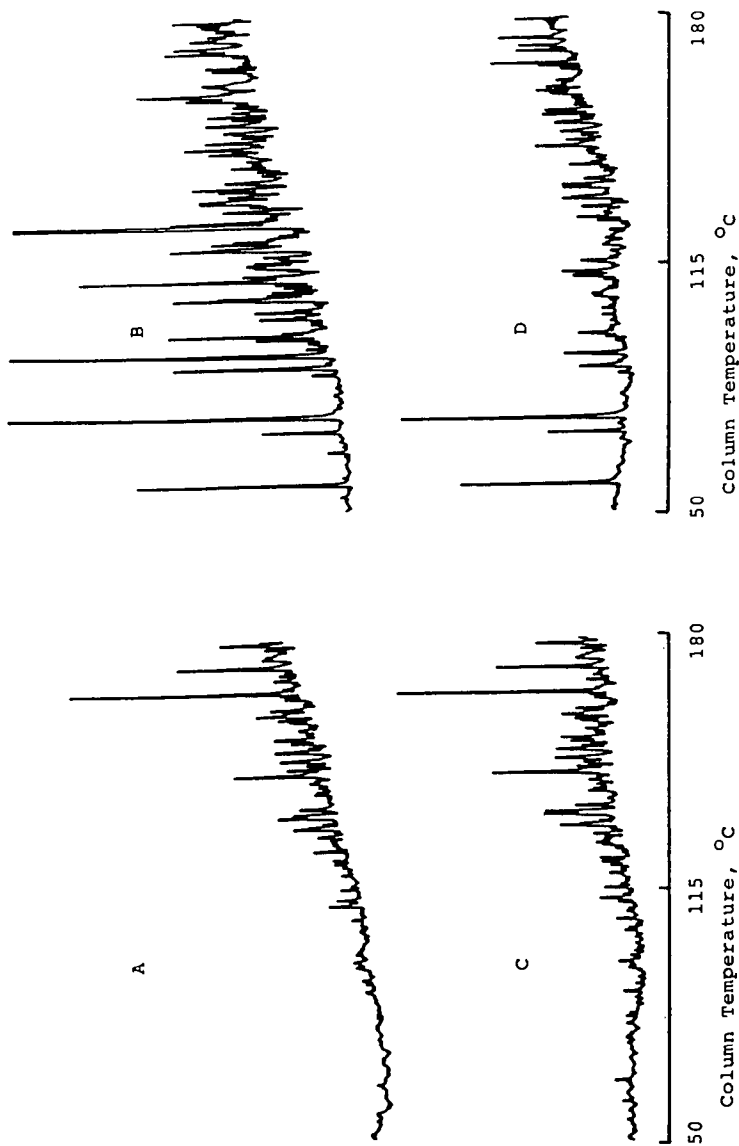


Figure 7. Capillary Gas Chromatography Data for the Benzene Solubilization and Pyrolysis Products from Illinois No. 6 Coal. A - Solubilization at 260 °C; B - Solubilization at 420 °C; C - Room Temperature Acetone Extract; D - Pyrolysis at 420 °C (Acetone Soluble Tar).

Determination of Liquid and Solid Phase Composition in Partially
Frozen Middle Distillate Fuels

T.L. Van Winkle, W.A. Affens, E.J. Beal, G.W. Mushrush,
R.N. Hazlett and J. DeGuzman

Naval Research Laboratory
Washington, D. C. 20362

INTRODUCTION

One of the tasks of the United States Navy Mobility Fuels program at the Naval Research Laboratory is to determine the effect of composition on the freezing properties of liquid fuels (1,2). The combination of requirements for ship and jet aircraft fuels of a low freezing point (to permit cold temperature operations around the world) and a flash point minimum (to reduce the hazard of storage and transport of liquid fuels on board ship) leads to opposing compositional needs. This is because many components of a fuel that tend to lower the freezing point (small hydrocarbons with higher vapor pressures) will also reduce the flash point. Because of these constraints, it is not always practical to produce fuels meeting these requirements from available crudes. This limits the amount of crudes and hence the amount of JP-5, the Navy fuel for carrier based aircraft, which can be produced from "a barrel of crude." With increased knowledge and understanding of the components that first crystallize out of a cold fuel, it may be possible to modify refining techniques to increase the yield of Navy liquid fuels per barrel of crude without compromising either the freezing point or the flash point restrictions.

Part of this task was a study of partially frozen fuels, in particular, to isolate and characterize the "precipitate" (solid crystals plus entrapped liquid) which can cause aircraft fuel-tank holdup, filter plugging, and related jet aircraft engine problems at low temperature operation. In order to accomplish this, the liquid "filtrate" had to be separated from the precipitate and a quantitative analysis made of several components (especially the normal alkanes) in the original fuel and in both fractions. The importance of the saturated hydrocarbon fraction, particularly the higher normal alkanes, in raising the freezing points of hydrocarbon fuels had been suggested by Dimitroff et al. (3-5); Petrovic and Vitorovic (6); Solash et al. (2); and others.

This paper deals with the method used to separate the liquid filtrate from the precipitate in fuels cooled to predetermined temperatures below their freezing points, the method of analyzing the fuel and fuel fractions, and the results obtained from a study of one particular jet fuel.

The fuel used to test the method was a shale-derived fuel (NRL No. J-22) from the Shale-II refining process conducted by the Standard Oil Company of Ohio (SOHIO) at their refinery at Toledo, Ohio (7-9). This fuel met the military specification requirements for Navy JP-5 jet turbine fuel (10); its actual freezing point of -48°C (11) was below the specification maximum requirement (10) of -46°C . This fuel, referred to hereafter as J-22, was chosen because the normal alkane concentrations in shale-derived fuels are considerably greater than those in petroleum-derived fuels (8). Table 1 lists the concentrations of the n-alkanes present in measurable amounts in the J-22 fuel.

TABLE 1. n-Alkane Concentrations in Filtrate of Fuel J-22
JP-5 Shale II, as a Function of Temperature

°C	Normalized Concentrations (X_F')*						
	Fuel Sample, X_0	-57.5	-55.3	-53.6	-51.4	-48.5	-48**
<u>n-Alkane</u>							
C ₁₀	4.50	1.04	1.03	1.01	1.00	0.98	0.97
C ₁₁	8.55	0.94	0.96	0.97	0.98	0.97	0.98
C ₁₂	7.10	0.71	0.77	0.83	0.91	0.95	0.99
C ₁₃	4.41	0.47	0.56	0.67	0.83	0.92	1.00
C ₁₄	1.36	0.42	0.51	0.57	0.70	0.91	0.94
C ₁₅	0.35	0.43	0.54	0.66	0.83	0.97	0.97

*Normalized data = concentration divided by concentration in original sample

**Data extrapolated to freezing point (-48°C)

ISOLATION OF PRECIPITATE FROM FILTRATE

A glass apparatus constructed for the isolation of the partially frozen precipitate is shown in Figure 1. The design was based on the fractional crystallization device used by Pitzer and Scott (12) and is similar to that of Dimitroff et al (5), at the U. S. Army Fuels and Lubricants Laboratory. It is referred to as a "Liquid-Solid separator" (LSS), as it was called by Dimitroff.

The LSS consisted of four components, A, B, C, and D, which were attached together by means of O-ring joints with clamps. Glass-metal joints connected the LSS to copper coils immersed in the bath, which carried dried nitrogen gas from the flow meters. The assembled LSS was immersed in a refrigerated and stirred methanol bath in a large clear-glass Dewar flask. Dry ice was added to the methanol to help cool the system rapidly to the freezing point of the fuel, at which time the fuel was added. A weighed sample of fuel (about 8 grams) was introduced through the open stopcock J by a hypodermic syringe with a long needle. A temperature controller then cooled the system to the desired temperature and maintained it to within $\pm 0.1^\circ\text{C}$ during crystallization and filtration. A very slow stream of nitrogen flowing through stopcock K (stopcocks I and L being closed), bubbling up through the fritted glass disc H and out through stopcock J prevented any liquid fuel from flowing down through the disc before and during crystallization. Approximately 20 minutes were allowed at the desired temperature for crystallization to be completed.

Stopcocks J and K were then closed, and L and I opened to allow a slow stream of nitrogen under pressure (up to 15 psig) through L to force the liquid filtrate through the fritted glass disc, and down the funnel M and into the preweighed filtrate cup D. Entrapped liquid was forced out of the precipitate by stirring and tamping. To carry this out, dome B was removed and the gelatinous precipitate stirred and pressed with a glass rod having a flattened end. The rod was either kept in the apparatus during the entire freezing process or cooled in dry ice just prior to insertion. In this way the precipitate was spread more evenly over the fritted glass disc, eliminating channels through which the nitrogen could pass. Attempts to compress the precipitate by the rod and thus force the liquid through the disc were unsuccessful. After stirring, dome B was replaced by a plain dome without a stopcock, B', and further filtering allowed to take place under nitrogen pressure. The plain dome eliminated nitrogen leakage through stopcock J. This

stirring process was repeated several times if necessary. Although the J-22 fuel separated quite easily without stirring and tamping, other fuels, especially diesel, proved quite difficult to separate, and much stirring was needed.

After the filtration was completed, the nitrogen flow was stopped. The Dewar flask was lowered until the glass-metal connectors to the nitrogen tubes were just out of the bath. The copper coils were disconnected, and the entire LSS removed from the bath. The filtrate cup was quickly detached, and a weighed glass vial placed under the glass funnel M before any melted precipitate appeared in the funnel.

The filtrate in the cup was weighed, and a sample taken for analysis. As the LSS warmed to room temperature most of the precipitate melted and flowed down into the vial. Nitrogen under low pressure helped force the flow. The residues on the fritted disc and stirring rod were washed down with n-pentane into another weighed vial. After removing the pentane by bubbling nitrogen through the solution at ambient temperature and pressure, the residue was weighed and combined with the precipitate in the first vial, which had also been weighed. After thorough mixing, a sample was taken for analysis. Careful tests showed that the higher n-alkanes (and other material) present in this residue were not swept out with the nitrogen sparging at a slow rate through the pentane solution. Since the amount of pentane present in the sample was readily determined, the composition of the precipitate was converted to a pentane-free basis.

SAMPLE ANALYSIS BY GAS CHROMATOGRAPHY

The concentrations of the n-alkanes in the original fuel samples, filtrates and precipitates were determined using an OV-101 fused silica capillary column, 0.2 mm i.d. x 50 m long, in a Hewlett-Packard Model 5880 gas chromatograph (GC). The inlet split ratio was 60:1; the column oven was temperature programmed from 50° to 200°C and the inlet and detector outlet temperatures were both 300°C. Iso-octane was used as the internal standard. Moreover, the concentrations of quantitatively prepared solutions of pure n-alkanes were accurately determined using iso-octane as the one internal standard.

Additional data were obtained when necessary by combined GC/MS (EI mode). The GC/MS unit consisted of a Hewlett Packard Model 5710 GC, a H-P Model 5980A mass spectrometer and a Ribermag SADR GC/MS data system. An all-glass GC inlet system was used in conjunction with a 0.31 mm x 50 m SP2100 (similar to OV-101) fused silica capillary column.

The gas chromatograms for the original fuel, the filtrates and precipitates are very similar, with differences noticeable only in the relative heights of the major n-alkane peaks. The chromatogram for J-22 fuel, shown in Figure 2, is relatively simple. The components are bounded by normal nonane, n-C₉, on the light end and by normal hexadecane, n-C₁₆, on the heavy end. The normal alkanes dominate the chromatogram, accounting for 26% by weight of the fuel (Table 1). There are a few other sharp, prominent peaks, some of which are labelled on the chromatogram for reasons discussed below.

CONCENTRATIONS OF n-ALKANES IN LIQUID AND SOLID PHASES

Filtrate

Normalized filtrate composition data as a function of temperature are listed in Table 1. For each n-alkane going from left to right these data approach unity at the freezing point of -48°C . Since this temperature (actually the melting point) is the point at which the last trace of solid material melts, or redissolves, the composition of the filtrate at this point should be the same as that of the liquid fuel. The descending columns in Table 1 show decreasing concentrations as the carbon number of the n-alkanes increases, showing that the higher the n-alkane the more readily it crystallizes, or freezes, out of solution. These data, when plotted as the logarithm of the n-alkane concentration in the filtrate vs. the reciprocal of the absolute temperature, form straight lines for all the n-alkanes, as would be expected for a Van't Hoff solubility plot.

Precipitate

Since the precipitate, a waxy crystal matrix, entrapped significant amounts of filtrate, the concentrations of the n-alkanes in the precipitate varied unpredictably depending on handling and treatment and were not used in this study directly. The interest lies rather in the n-alkane concentrations in the actual crystalline solids formed. Because the amount of entrapped liquid in the precipitate was large, only by indirect methods was it possible to estimate the amount of true solids present and the composition of those solids.

Estimating n-Alkane Concentration in Solids Fraction of Precipitate

Since the precipitate contains some solid crystals and some entrapped liquid, let Z equal the weight fraction of liquid entrapped in the precipitate:

$$W_L = ZW_P, \quad (1)$$

Based on mass balance considerations, and assuming that the liquid portion of the precipitate is entrapped filtrate, it can be shown (17) that

$$X_S = (X_P - ZX_F)/(1 - Z) \quad (2)$$

where X_S , X_P , and X_F are the concentrations of a given component in the solid fraction, precipitate, and filtrate respectively. Equation 2 expresses the concentration of any component A in the solid fraction of the precipitate as a function of its concentration in the filtrate (X_F) and precipitate (X_P), and the fraction of liquid in the precipitate (Z). We have determined X_F and X_P , and the problem is to estimate Z.

Estimation of Z

If there is a species k in the precipitate which has a very low freezing point and does not freeze (form crystals) under the conditions of the experiment, it would therefore be present only in the liquid fraction of the precipitate ($X_S = 0$). It is thus possible to estimate Z by making use of this information and applying Equation 2. Solving Equation 2 for Z, gives

$$Z = X_P/X_F \quad (3)$$

The Z obtained from Equation 3 for component k is also applicable to the solid A components since it is the result of the same dilution of the precipitate by liquid filtrate. Hence, we can estimate Z by means of the ratio of component k in the precipitate to that in the filtrate.

Estimating the Fraction of Solids in the Sample

From the weights of total material in the sample (W_0), filtrate (W_F), precipitate (W_P), the fractions of filtrate (F), precipitate (P), and solids (S) it can be shown (17) that:

$$F = W_F/W_0 \quad 4)$$

$$P = W_P/W_0 \quad 5)$$

$$S = W_S/W_0 = (1 - Z)P \quad 6)$$

Thus, by means of Equations 4, 5, and 6 and knowing Z, we can calculate F, P, and S.

Estimating Percent of n-Alkanes in Fuel Found in the Solid Phase

Not only is the concentration of each n-alkane in the crystalline solid of interest, but of even greater interest is the percent of each n-alkane or other frozen component present in the fuel that is found in the solid phase. If we define X_S as the percent of a given component present in the fuel that is found in the solid phase, then it can be shown (17) that

$$X_S = P(X_P - ZX_F)/X_0 \quad 7)$$

Thus X_S depends on directly determined experimental data and on the value of Z, which can be determined indirectly as explained previously.

Choice of Noncrystal-Forming Components for Estimating Z

After careful examination of the gas chromatograms for the jet fuel J-22, two k compounds were selected, labelled a and b in Fig. 2, which do not form solid crystals. The retention time of a was between that of C_{10} and C_{11} , and that of b between C_{12} and C_{13} . They were identified by GC/mass spectrometry as 4-methyl decane and 2-methyl dodecane. The freezing point (T_m) of 4-methyl decane is -92.9°C , (13), well below the temperatures of these experiments. The drastic difference in freezing points effected by branching is typical of branched isomers vs straight-chain alkanes ($n-C_{11}$, $T_m = 25.6^\circ\text{C}$). These two compounds were selected because they exhibited sharp, distinct GC peaks, and because their concentrations in the filtrate and precipitate were essentially constant with temperature in both the filtrate and precipitate. The average normalized concentration data (relative to concentrations in the original sample) were slightly greater than unity (about 1.06) in the filtrate, and slightly below unity (about 0.91) in the precipitate. This would be expected for compounds which do not crystallize out, since their concentrations (relative to that in the sample) in the filtrate would rise as other materials precipitate out. Conversely, their concentrations in the precipitate (since they appear only in the liquid fraction of the precipitate) would decrease as the alkanes concentrate in the precipitate.

n-Alkane Concentrations in the Solids

By means of the concentrations of the k components a and b , Z values were calculated using Equation 3. Using Equation 2, and knowing Z , the concentrations of each alkane in the solids (X_S) were calculated. Normalized concentrations of each n-alkane in the solids are listed in Table 2. Average values of Z are shown later in Table 4.

Table 2. n-Alkane Concentrations in Solid Phase of Fuel J-22 JP-5 Shale II, as a Function of Temperature

°C	Normalized Concentrations (X_S')*				
	-57.5	-55.3	-53.6	-51.4	-48.5**
<u>n-Alkane</u>					
C ₁₀	0.42	0.44	0.33	0.31	0.08
C ₁₁	1.61	1.49	1.46	1.16	0.29
C ₁₂	4.26	3.90	4.42	3.68	0.96
C ₁₃	6.55	5.76	7.53	6.64	1.91
C ₁₄	8.01	7.57	9.85	9.48	2.76
C ₁₅	8.63	8.00	10.29	9.74	2.66

*Normalized data—concentration divided by concentration in original sample.

**Data listed here because they are useful later on. The value of Z at this temperature was very inaccurate.

It is apparent that the larger the n-alkane the greater is its concentration in the solid phase. The concentrations of the smaller n-alkanes generally show an increase in concentration in the solids as the temperature decreases. This is expected as more crystals freeze out of the liquid and form part of the solid phase. On the other hand, it can be seen that the reverse is true for the heavier n-alkanes in the solid phase. At the higher temperatures they will form most of the solid crystalline phase. As the temperature decreases and more of the lighter n-alkanes appear in the solid phase, the absolute proportion of the heavier n-alkanes must get smaller, and so the concentration decreases with decreasing temperature.

The values of the normalized n-alkane concentrations in the solid phase, X_S' , were calculated by dividing the values of X_S obtained from Equation 2 by the concentration in the fuel, X_0 , for each n-alkane. The sensitivity of X_S' to the accuracy of the value of Z can be readily seen: an error of 5% in the value of Z when $Z = 0.85$ causes an error of 25% in the value of X_S' , whereas an error of 5% in Z when $Z = 0.70$ causes an error of 11% in X_S' . Thus one of the more important and difficult tasks was obtaining accurate values of Z . The values of S , X_S and X_S' all depend on the factor $(1 - Z)$, the uncertainty of which increases as Z approaches unity. In general, however, the values of X_S' as a function of temperature show the expected relationship for a component freezing or crystallizing out of a liquid solution.

Percent of n-Alkanes in Fuel Found in the Solid Phase

Table 3 shows the variation of X_S' , the percent of the n-alkanes present in the original fuel that are found in the solid phase, using Equation 7 with the average value of Z. It is seen that the increase in the percent found in the solid phase increases with the carbon number and varies inversely with temperature for each n-alkane.

Table 3. Percent of Total Fuel n-Alkanes Found in Solid Phase as a Function of Temperature
Fuel: J-22, JP-5 Shale II

Percent of Total Fuel n-Alkanes: $X_S'' = X_S' \cdot S$					
°C	-57.5	-55.3	-53.6	-51.4	-48.5
n-Alkane					
C ₁₀	3.4	3.2	1.5	0.90	0.22
C ₁₁	13.2	10.9	6.6	3.4	0.78
C ₁₂	34.9	28.5	19.9	10.7	2.6
C ₁₃	53.7	42.0	33.9	19.3	5.2
C ₁₄	65.7	55.3	44.3	27.5	7.4
C ₁₅	70.8	58.4	46.3	28.2	7.2

Freezing point extrapolated for $X_S'' = 0$: range -48.7° to -47.2°
(average -47.9°C)

MATERIAL BALANCES

Overall Balance

By means of Equations 4, 5 and 6 the total overall material balances were estimated and the results listed in Table 4. The percent recovery, defined as 100 times the ratio of the weight of the filtrate plus precipitate to the weight of the original fuel, varied between 98.8 and 99.7%

Table 4. Total Material Balances-Fuel: J-22, JP-5 Shale II

°C	-57.5	-55.3	-53.6	-51.4	-48.5**
% Filtrate	44.7	67.8	79.6	90.1	83.9
% Precipitate	54.9	31.4	19.9	8.7	16.1
% Recovery	99.7	99.2	99.5	98.8	-
% Solids***	8.2	7.3	4.5	2.9	2.7
Z*	0.85	0.76	0.77	0.67	0.83

*Fraction liquid (filtrate) in precipitate, P
**Not accurate-some information lacking in these early runs
***Freezing point extrapolated for S = 0 is -48°C

n-Alkane Balance

Perhaps the most important check for self-consistency for the type of data gathered in this study is a material balance for each of the compounds present. For every run, a material balance for each of the n-alkanes and k compounds was carried out. Material balances are shown for all the n-alkanes present for one specific run at -53.6°C in Table 5.

Table 5. n-Alkane Balance, (mgs.) - Fuel: JP-5, J-22, -53.5°C, Z = 0.767

n-Alkane	Filtrate F	Precipitate (P)			Total Liq. F + L	Recovery F + P	Fuel Sample	Percent Recovery
		Liquid L	Solids S	Total L + S				
C ₁₀	282	55	6	61	337	343	357	96.1
C ₁₁	510	100	45	145	610	655	678	96.6
C ₁₂	362	71	111	182	433	544	563	96.6
C ₁₃	191	38	113	151	229	342	350	97.7
C ₁₄	47	9	48	57	56	104	108	96.3
C ₁₅	14	3	13	16	17	30	32	93.8
TOTAL	1406	276	336	612	1682	2018	2088	96.8
TOTAL FUEL	6292	1233	375	1608	7525	7900	7934*	99.6
Percent n-Alkane in Total	22.4	22.4	89.6	38.1	22.4	25.5	26.3	-

* Starting weight of sample used in Run No. 30

Only in one case was the discrepancy between the "input" (fuel) and the "output" (filtrate plus precipitate) greater than 4%. This occurred with C₁₅ where the concentrations were extremely low. The method of analysis by gas chromatography used in this study clearly gave consistently good results.

Determination of Z by Liquid Chromatography

Because the value of Z is of the greatest importance in this study, two other methods for determining it were investigated as a check on the accuracy of the method used, which we call the "k-component method." One of these methods was high performance liquid chromatography (HPLC) (14,15). Samples of fuel, filtrate, and precipitate for a particular run were analyzed for three classes of compounds: saturated, monocyclic, and dicyclic aromatic hydrocarbons. The fuel sample contained no internal standard, but the filtrate and precipitate each had an internal standard, iso-octane, added to it. Since iso-octane is a saturated hydrocarbon and was present to about 9% by weight, the percentages of the three fractions determined by HPLC had to be adjusted for no iso-octane present.

Table 6 gives the results of the HPLC analyses. Both the percentages obtained by HPLC analyses of the precipitate and filtrate containing iso-octane and the adjusted values are listed. As expected, the percent of saturated hydrocarbons is greater in the precipitate than in the filtrate, whereas the reverse is true for the monocyclic and dicyclic aromatic hydrocarbons. To calculate Z, we first assume that no dicyclic aromatic hydrocarbons freeze or crystallize out of the fuel. Then this fraction can be assumed to be a k compound. By Equation 3, $Z = 0.78/1.02 = 0.765$, total solids, $S = 4.8\%$ and saturated hydrocarbons making up 97.5% of S. By GC analysis, using components a and b as k compounds, Z for Run No. 30 was determined to be 0.766 and $S = 4.8\%$ with the normal alkanes comprising 89.6% of the solids.

Table 6. Hydrocarbon Fractions Determined by High-Pressure Liquid Chromatography - Fuel: J-22, JP-5 Shale II. Run No. 30: T = -53.6C

Hydrocarbon Fraction	Percent (w/w) in Fuel	Percent (w/w) in		Percent (w/w) in	
		Filtrate*	Precipitate*	Filtrate**	Precipitate**
Saturated	76.58	75.01	80.23	75.52	80.70
Monocyclic aromatics	22.45	23.99	19.00	23.46	18.51
Dicyclic aromatics	0.97	1.00	0.77	1.02	0.78

*iso-octane present as internal standard

**Adjusted for no iso-octane

If the assumption is made that neither monocyclic nor dicyclic aromatic compounds appear in the solid phase, the value of Z becomes 0.78, the average value taking both the monocyclic and dicyclic aromatic components as k compounds. The total solids S becomes 4.5% still in remarkably close agreement to the GC analysis.

The other confirmatory method involved the use of dye tracers to obtain the values of Z. This was suggested in a recent paper by Moynihan et al. (16). However, we were not able to use the dye method successfully for our purposes. Our work with the dye tracer method is reported elsewhere (17).

SUMMARY AND CONCLUSIONS

The liquid (filtrate) and the solid crystals containing a large portion of entrapped liquid (precipitate) from partially frozen samples of middle distillate fuels were separated from each other and collected by means of a liquid-solid separator (LSS) developed at NRL. This was done at several temperatures below the freezing point of the original fuel samples. The collected filtrates and precipitates along with original fuel samples were analyzed quantitatively for the normal alkanes and other specifically designated components (k-compounds) by gas chromatography.

The filtrate data were straightforward, and Van't Hoff plots of the n-alkane concentrations (log concentration vs. reciprocal temperature) formed straight lines. Their slopes demonstrated the importance of the higher n-alkane in fuel freezing, or crystallization, at low temperatures.

Since the precipitate consisted of a waxy crystal matrix in which significant amounts of liquid (filtrate) were entrapped, the data presented some problems of interpretation. Modifications in the method resulted in better separation, but it was still far from complete. An indirect method (using k-compounds) was derived to estimate the total solid fraction in the precipitate and also the individual n-alkane concentrations in the crystalline solids.

It was seen that the solid fraction increased with decreasing temperature, and that the fraction (or percent) of the n-alkanes in the original fuel that appeared in the solid phase increased with the carbon number and was inversely proportional to the temperature for an individual n-alkane.

Results of total material balances as well as of individual n-alkanes gave close agreement, within a few percent in nearly all cases. Tests using high pressure liquid chromatography further validated the method used.

ACKNOWLEDGMENTS

The authors wish to acknowledge the assistance of Drs. Dennis Hardy and Charles Sink for various analyses and Professor Cornelius Moynihan for helpful discussions and advice.

This work was sponsored by the Naval Air Propulsion Center and David Taylor Naval Ship Research and Development Center.

REFERENCES

1. W. A. Affens, J. M. Hall, S. Holt, and R. N. Hazlett, Fuel **63**, 543 (1984).
2. J. Solash, R. N. Hazlett, J. M. Hall, and C. J. Nowack, Fuel **57**, 521 (1978).
3. E. Dimitroff, J. T. Gray, Jr., N. T. Meckel, and R. D. Quillan, Jr., "Crystal-Liquid Fuel Phase Intersolubility and Pumpability," in Proc. 7th World Petrol. Cong., Vol. VIII, Part 2, 141 (Elsevier, New York, 1967).
4. E. Dimitroff and H. E. Dietzmann, preprints Petrol. Div., ACS **14**, B132 (Sept. 1969).
5. U. S. Army Fuels and Lubricants Research Laboratory, San Antonio, TX, "Procedure for Determining Fuel Low Temperature Pumpability Using a Liquid-Solid Separator Apparatus," Aug. 1969.
6. K. Petrovic and J. Vitorovic, J. Inst. Petrol. **59**, 20 (1973).
7. N. J. Waslik and E. T. Robinson, Ch. 15, ACS Symposium Series No. 163, Oil Shale, Tar Sands, and Related Materials, H. C. Stauffer, Ed., 1981.
8. J. Solash, R. N. Hazlett, J. C. Burnett, E. Beal, and J. M. Hall, Ch. 16, ACS Symposium Series No. 162, Oil Shale, Tar Sands, and Related Materials, H. C. Stauffer, Ed., 1981.

9. W. A. Affens, J. M. Hall, E. Beal, R. N. Hazlett, J. T. Leonard, C. J. Nowack and G. Speck, Ch. 17, ACS Symposium Series No. 163, Oil Shale, Tar Sands, and Related Materials, H. C. Stauffer, Ed., 1981.
10. Turbine Fuel, Aviation Grades, JP-4 and JP-5, MIL-T-5624L, 18 May 1979.
11. American Society for Testing and Materials, "Freezing Point of Aviation Fuels," ASTM D 2386-67.
12. K. S. Pitzer and D. W. Scott, JACS **65**, 803 (1943).
13. M. P. Doss, "Physical Constants of the Principal Hydrocarbons," The Texas Company, 4th Ed. 1943.
14. C. W. Sink, D. R. Hardy, and R. N. Hazlett, "Quantitative Determination of Compound Classes in Jet Turbine Fuels by High Performance Liquid Chromatography/Differential Refractive Index Detection", NRL Memo Report 5407, 13 September 1984.
15. C. W. Sink, D. R. Hardy, and R. N. Hazlett, "Quantitative Determination of Compound Classes in Jet Turbine Fuels by High Performance Liquid Chromatography/Differential Refractive Index Detection - Part 2", NRL Memo Report 5497, December 31, 1984.
16. C. T. Moynihan, R. Mossadegh, and A. J. Bruce, Fuel **63**, 378 (1984).
17. T. L. Van Winkle, W. A. Affens, E. J. Beal, R. N. Hazlett, and J. DeGuzman, "The Distribution of Higher n-Alkanes in Partially Frozen Middle Distillate Fuels," NRL Report 8869, April 10, 1985.

NOMENCLATURE

	Fuel Sample	Filter	Precipitate	Precipitate Solids	Precipitate Liquid
Total Material:					
Weight	W_s	W_f	W_p	W_s	W_l
Fraction of Sample		$F = W_f/W_s$	$P = W_p/W_s$	$S = W_s/W_s$	$L = W_l/W_s$
SPECIES A.W.S:					
Weight	w_i	w_j	w_k	w_i	w_k
Concentration (w/W)	$X_i = w_i/W_s$	$X_j = w_j/W_s$	$X_k = w_k/W_s$	$X_i = w_i/W_s$	$X_k = w_k/W_s$
$Z = W_i/W_s$					
c - Crystalline Species					
l - Monocrystalline Species					
Subscripts:			Superscripts:		
o - Original Sample				$'$ - Normalized Data (Concentration divided by that of original sample)	
F - Filter					
P - Precipitate					$"$ - Percent concentration of a species in the fuel found in the solid phase
S - Solids Fraction of Precipitate (Crystals)					
L - Liquid Fraction of Precipitate					
T - Total					

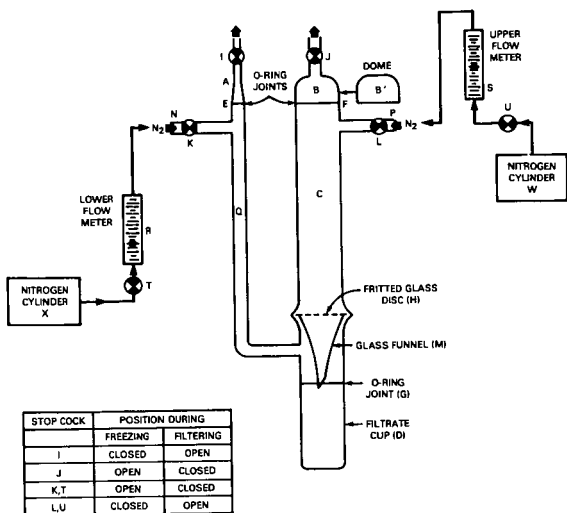


Fig. 1 - Liquid-Solid Separator

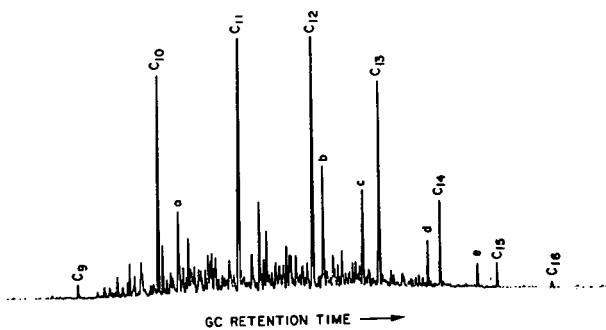


Fig. 2 - GC Trace
Fuel: J-22, JP-5 Shale II

T.L. Van Winkle, W.A. Affens, E.J. Beal, R.N. Hazlett and J. DeGuzman

"The Distribution of n-Alkanes in Partially Frozen Middle Distillate Fuels"

Naval Research Laboratory, Washington, DC 20375-5000

INTRODUCTION

This work on partially frozen fuels is one of a continuing series of studies on the effect of composition on the freezing properties of hydrocarbon fuels (1-6). The method used for this purpose was reported previously (4-7). By means of this method we were able to determine the composition of the liquid and solid phases in partially frozen mixtures consisting of liquid and of solid crystals plus entrapped liquid. This paper presents the results of this study on five different middle distillate fuels.

FUEL SAMPLES

Five fuel samples were used in this study: three Navy jet fuels (JP-5) and two Navy ship propulsion diesel fuels (DFM). The three jet fuels included a shale-derived fuel (NRL No. J-22) from the Shale-II refining process conducted by the Standard Oil Company of Ohio (SOHIO) at their refinery at Toledo, Ohio (8-10). The other two were conventional petroleum-derived JP-5 fuels (NRL Nos. 80-5 and 81-19). Fuel 81-19 contained very low concentrations of n-alkanes compared to those in the other two fuels. All three met the military specification requirements for JP-5 jet turbine fuel (11). The freezing points (12) of J-22, 80-5, and 81-19 fuels, -48° , -49° , and -53°C ., respectively, were below the specification requirement of -46°C maximum (11).

One of the samples of diesel fuel studied [82-8] was a conventional petroleum-derived DFM. The other [82-16] was a shale-derived fuel also from SOHIO's Shale-II refining process. The pour points (13) of the two DFM fuels, -11° and -23°C respectively, were well below the military specification requirement of -6.7°C maximum (11).

FUEL ANALYSES

Quantitative analyses of the n-alkane compositions in the fuels were made using a 50-m (OV-101), fused silica 0.2-mm i.d. capillary column in a Hewlett-Packard 5880 gas chromatograph (GC) or when necessary by combined GC/MS (EI mode). The n-alkane concentrations in all five original fuel samples are listed in Table 1.

PARTIALLY FROZEN FUELS

The residual liquid ("filtrate") from partially frozen fuel samples was separated from the "precipitate" (crystalline material plus entrapped liquid) and collected by means of the NRL liquid-solid separator apparatus (LSS) at several temperatures below the freezing points of the original fuel samples. The LSS method was described previously (6,7). The filtrate and precipitate were characterized by gas chromatography. The GC chromatograms for all five fuels and their associated filtrates and precipitates are all quite similar, although there are significant differences which affected the ease and accuracy of the quantitative analysis.

TABLE 1
n-Alkane Concentrations in Original Fuel Samples
($X_o = \% w_o/w_o$)

n-Alkane	JP-5			DFM		
	Shale II	Petroleum	Petroleum	Shale II	Petroleum	
	NRL No.	J-22	80-5	81-19	82-16	82-8
C ₈				0.07	0.07	
C ₉				0.17	0.12	
C ₁₀		4.50	1.01	0.21	0.53	
C ₁₁		8.55	4.36	0.82	1.11	
C ₁₂		7.10	5.35	1.01	1.61	
C ₁₃		4.41	3.78	1.30	2.54	
C ₁₄		1.36	1.67	0.82	2.91	
C ₁₅		0.35	0.54	0.45	2.66	
C ₁₆			0.15	0.16	2.30	
C ₁₇			0.06	2.26	1.63	
C ₁₈				1.60	1.22	
C ₁₉				0.68	1.08	
C ₂₀				0.06	0.71	
C ₂₁					0.50	
C ₂₂					0.30	
C ₂₃					0.16	
C ₂₄					0.07	
Total %		26.27	16.86	4.83	18.50	15.07

RESULTS AND DISCUSSION

Filtrate

The filtrate solubility data for the five fuels are plotted as the logarithm of n-alkane concentration in the filtrate (as weight percent) vs the reciprocal absolute temperature ($1000/T$ K). Three of these plots are shown in Figures 1-3. For each of the five fuels, the data for all the n-alkanes form straight lines, as would be expected for a Van't Hoff solubility plot. All of the slopes were determined by a least squares fit of the data.

The six n-alkanes present in measurable quantities in the J-22 jet fuel are plotted in Fig. 1. The slope of the line for the lowest n-alkane, n-C₁₀, is very slightly positive, and the next n-alkane, n-C₁₁, the line is almost horizontal. The data for the remaining n-alkanes show definite negative slopes which increase in magnitude with carbon number. The shaded points in Fig. 1 represent the original fuel concentrations for each alkane plotted at the freezing point (-48°C). Since this temperature (actually the melting point) is the point at which the last trace of solid material redissolves, the composition at this point should be the same as that of the liquid fuel. As expected, these concentrations fell close to the plotted lines in almost all cases.

The n-alkanes present in the petroleum-derived jet fuel 80-5 were n-C₁₀ - n-C₁₆. The slopes of the curves for the two smallest n-alkanes, n-C₁₀ and n-C₁₁, were perfectly flat. The data for fuels 80-5 and J-22 indicate that the normal alkanes behave in an identical manner when the fuels are partially frozen.

For the low-n-alkane jet fuel, 81-19, the data are plotted in Fig. 2 for the five highest n-alkanes. The lines for C₁₀ and C₁₁ (omitted for clarity) are perfectly flat, and the line for C₁₂ is almost so. The three highest n-alkanes, C₁₄

through C₁₆, show definite slopes which increase in magnitude with the carbon number, thus showing close agreement with the higher n-alkanes in the other fuels studied.

The data for C₁₃ in the 81-19 fuel, however, follow a different pattern, as is clearly evident. Not only are the data widely scattered from the straight line obtained by linear regression from the six data points, but the line itself shows a slight increase in concentration with decreasing temperature. Also, unlike the other n-alkanes, the extrapolated concentration at the freezing point is considerably lower than its concentration in the original fuel. This suggests that n-C₁₃ may have an opposite effect on the freezing point of fuels to that of the other n-alkanes. This anomalous effect of n-C₁₃ has been reported elsewhere (1,3,5), where the effect of n-C₁₃, in certain cases, was to lower the freezing point rather than to raise it.

The two diesel fuels show a much wider spectrum of n-alkanes, from n-C₈ to n-C₂₀ in the shale-derived 82-16, and from n-C₈ to n-C₂₄ in the petroleum-derived 82-8. The filtrate data for fuel 82-8 are plotted in Figure 3. For the sake of clarity the data for the lower alkanes were not plotted in Figure 3. The behavior of the n-alkanes in fuel 82-8, are very similar to that in the other fuels.

A careful study of the fuel and filtrate chromatograms failed to reveal any other components in any of the five fuels whose concentration in the filtrate was regularly lower than that in the fuel. Therefore a conclusion, indicated by a study of the filtrate data above, is that only the n-alkanes freeze or crystallize out of the fuel in the temperature ranges studied, which in each case was in the vicinity of the freezing point of that fuel. The filtrate data demonstrate the importance of the role of the higher n-alkanes in the freezing of jet and diesel fuels.

Precipitate

The precipitates for all five fuels consisted of a waxy crystal matrix and varying, significant amounts of entrapped liquid (filtrate). In the previous paper we have shown how the concentrations of the n-alkanes in the crystalline solids can be obtained from the filtrate and precipitate concentrations (7). The key to determining the concentrations in the solid phase was seen to lie in the value of "Z", (the liquid fraction of the precipitate), and this in turn depended upon the suitable choice of non-crystal-forming reference components.

Choice of *k* Components for Estimating Z

Two components (clearly defined in the GC traces and identified by GC-mass spectrometry as 4-methyl-decane and 2-methyl-dodecane) were chosen as *k*-components for the jet fuel J-22. Very satisfactory results were obtained by using them to determine the values of Z.

A study was made of the GC traces of each of the other fuels, from which a number of components were chosen as *k*-components. For each fuel, average Z-values were thus estimated. The details of the selection of *k*-components was described previously (6).

Variation of Solid Fraction with Temperature

Once the value of Z was determined, it was a simple matter to find the solid fraction in the precipitate, and then the percent solids in the partially frozen fuel sample (6,7). The percent of crystalline solids, S, as a function of temperature is shown for all five fuels in Fig. 4.

The lines in Fig. 4 may be extrapolated to zero (S = 0) with resulting temperatures corresponding to the freezing point (more correctly, the "melting

point"). This is because in the determination of the freezing point of fuels, the freezing point is defined as the temperature at which the crystals formed on cooling just disappear when the temperature is allowed to rise (12). The extrapolated temperatures are shown in Table 2. The experimentally determined freezing points for the JP-5 fuels (Table 2) are in agreement with the extrapolated values within experimental error. Furthermore, the extrapolated temperature of -46°C for the Shale-II JP-5 fuel (J-22) is in good agreement with the extrapolated data obtained by Moynihan et al (14) who investigated the same fuel in their studies of partially frozen fuels using a dye tracer technique for the separations.

TABLE 2
Extrapolated vs. Experimental Freezing Point Data

Fuel	Experimental (°C)		Extrapolated (°C)	
	Freezing Point (12)		S = 0	X _G " = 0*
JP-5 (J-22)	-48		-46	-48
" (80-5)	-49		-48	-48
" (81-19)	-53		-56	-54
DFM (82-16)	-23**		-14	-16
" (82-8)	-11**		- 4	- 4

* Averaged data

** Pour Point (13)

There are no freezing point requirements for DFM and therefore no corresponding data for the above DFM fuels. The pour points were determined (13), and are shown in Table 2. Since the pour point of a fuel is a function of flow properties (viscosity and amount of crystallization which has taken place) an increased quantity of solid material (relative to that at the freezing point) is involved. Since this requires further chilling (below the freezing point) it would be expected that pour points should be lower than freezing points. In this case the pour points are 9° and 7° below the extrapolated "freezing point" temperatures for the DFM fuels 82-16 and 82-8 respectively.

Total Material Balance

Table 3 lists the total material balances together with the values obtained for Z, the liquid fraction in the precipitate, and S, the weight percent of crystals

TABLE 3
Total Material Balances

Fuel	JP-5			DFM	
	Shale II	Petroleum	Petroleum	Shale II	Petroleum
NRL No.	J-22	80-5	81-19	82-16	82-8
Temp.(°C)	-53.6	-56.3	-64.4	-28.1	-11.1
% Filtrate (F)	79.6	73.2	69.4	79.8	87.0
% Precipitate (P)	19.9	26.3	29.6	19.6	11.7
% Recovery	99.5	94.5	99.0	99.4	98.6
% Solids (S)	4.5	5.3	1.7	5.5	2.6
Z*	0.77	0.80	0.94	0.72	0.78

*Fraction liquid (filtrate) in precipitate (P)

formed, from a typical run for each fuel. Data for all the experimental runs have been given elsewhere (5,6), but the data presented in Table 2, at roughly the middle of the temperature range investigated, give a good comparison of the values of Z obtained for each fuel.

n-Alkane Concentration in the Solids

The concentration of each n-alkane in the solid phase was calculated by the previously described method (6,7).

All five fuels show the same characteristic behavior: the higher the n-alkane the greater its concentration increase in the solid phase. The concentrations of the lighter n-alkanes generally show an increase in concentration in the solids as the temperature decreases, which is to be expected as more crystals freeze out of the liquid phase and form part of the solid phase. The heavier n-alkanes, on the other hand, form most of the solid phase at the higher temperatures, and will form a proportionately lower fraction as more of the other n-alkanes freeze out as the temperature decreases.

Percent of the n-Alkanes in the Fuel Found in the Solid Phase

Of great significance is the percent (or fraction) of each n-alkane present in the original fuel that appears in the solid phase, X_S'' . This tells us the distribution of the n-alkanes in partially frozen fuels. X_S'' depends on the concentration of the n-alkane in the original fuel, in the filtrate and in the precipitate, as well as on the value of Z (7).

Figs. 5-7 show the values of X_S'' plotted as a function of the temperature for three of the five fuels. In most cases the graphs are linear. In almost every case the rate of increase in the percent of n-alkane appearing in the solid phase increases with the carbon number.

For the fuel J-22, the data plotted in Fig. 5 show a slight but steady increase in the percent of n-C₁₀, the lowest n-alkane present that appears in the solid phase, reaching a value of about 4% at -58°C. The higher n-alkanes show increasing amounts appearing in the solid phase with over 75% of n-C₁₅ in the solids at -58°C. It may be, however, that there is no longer a straight-line relationship near this lower temperature for the two highest n-alkanes. Obviously the percent in the solids must approach 100% more slowly the closer it gets to 100%. If all the lines for the six n-alkanes are extrapolated to $X_S'' = 0$ (the freezing point temperature is found to be an average value of -47.9°C. Similar extrapolated data for all five fuels ($X_S'' = 0$) are shown in Table 2. These extrapolated freezing points ($X_S'' = 0$) compare well with actual freezing points, as well as with extrapolated data from $S = 0$, as can be seen in Table 2.

The normal alkanes are thus seen to behave as would be expected if they alone freeze or crystallize out of the fuel at temperatures below, but in the vicinity of, the freezing point. The higher the n-alkane the more completely it is removed from the liquid phase as the temperature decreases.

Individual n-Alkane Balances

For every run, a material balance for each of the n-alkanes and A-components present was carried out. With very few exceptions the amount of each n-alkane in the total liquid and in the solid was found to be within 5% of that in the original fuel. Where the concentrations were very low, as with n-C₂₃ and n-C₂₄ in fuel 82-8, the deviation approached 20%.

Composition of the Solid Phase

Probably the most important and certainly the most difficult task we had was the determination of the composition of the solid phase. The actual concentrations of the n-alkanes are not reported here, but they are obtainable from the earlier NRL studies (5,6).

In the case of the J-22 fuel, at two temperatures, -58° and -54°C , the n-alkanes account for over 95% of the solids formed. About 1% seems to be due to the k-compounds. There are undoubtedly some other compounds in the 67% of the J-22 fuel (that is not made up of n-alkanes or of the k-compounds) that form crystals in the solids. Nevertheless no compounds other than the n-alkanes could be found having higher concentrations in the precipitate than in the filtrate, and so no compounds other than n-alkanes form crystals to any great extent. The other fuels followed the same pattern, but the percentage of n-alkanes in the solid phase was not as high as that of the J-22 fuel.

Until other methods of analysis can be devised to measure accurately small amounts of many different components, or until the solid crystals can be separated completely from the entrapped liquid and then analyzed, the complete composition of the solid crystalline phase will remain undetermined. Further useful information, however, might be gathered, by partially freezing some mixtures of normal alkanes with one or two other components and determining their distribution coefficients. Extrapolation from this to their behavior in fuels might be made and tested.

SUMMARY AND CONCLUSIONS

The liquid (filtrate) and the solid crystals containing a large portion of entrapped liquid (precipitate) from partially frozen samples of five middle distillate fuels were separated from each other and collected by means of the NRL liquid-solid separator (LSS). The fuels consisted of three different types of JP-5 jet fuel and two different types of DFM Navy ship propulsion fuel. The separations were made at several temperatures, each below the freezing point of the original fuel samples. The original samples and the collected precipitate and filtrates were analyzed quantitatively by GC (or when necessary by combined GC/MS). The filtrate data for all five fuels were straightforward, and Van't Hoff plots of the n-alkane concentrations (log concentrations vs reciprocal absolute temperature) formed straight lines and their slopes demonstrated the importance of the higher n-alkanes in fuel freezing, or crystallization, at cold temperatures. The precipitates, which consisted of a waxy crystal matrix, all entrapped significant amounts of liquid (filtrate). An indirect method (using k-compounds), which was described in an earlier paper, was used to estimate the n-alkane concentrations in the solid fraction of the precipitate.

The solids data demonstrated that the higher n-alkanes play the key role in fuel crystallization at low temperatures, concentrating as much as tenfold in the crystallized solids compared to the liquid. Also it was shown that the n-alkanes form the major part, up to at least 95% by weight in some fuels, of the solid crystals formed.

ACKNOWLEDGEMENTS

The authors wish to acknowledge the assistance of Drs. Dennis Hardy, George Mushrush, and Charles Sink for various analyses; and Prof. Cornelius Moynihan for helpful discussions.

This work was sponsored by the Naval Air Propulsion Center and David Taylor Naval Ship Research and Development Center.

REFERENCES

1. W.A. Affens, J.M. Hall, S. Holt, and R.N. Hazlett, *Fuel* **63**, 543 (1981).
2. J. Solash, R.N. Hazlett, J.M. Hall, and C.J. Nowack, *Fuel* **57**, 521 (1978).
3. W.A. Affens, R.N. Hazlett, and D.E. Smith, "A Statistical Examination of the Effect of Composition on the Freezing Points of Hydrocarbon Mixtures," NRL Report 8692, July 21, 1983.
4. T.L. Van Winkle and W.A. Affens, "Jet Fuel Freezing Point and Composition," in *Shale Oil Upgrading and Refining*, S.A. Newman, Ed. (Butterworth, Boston, MA, 1983), Ch. 12.
5. T.L. Van Winkle, R.N. Hazlett, E.J. Beal, and G.W. Mushrush, "Liquid and Solid Phase Compositions in a Partially Frozen JP-5 Fuel Low in n-Alkanes," NRL Memorandum Report 5357, June 1984.
6. T.L. Van Winkle, W.A. Affens, E.J. Beal, R.N. Hazlett, and J. Deguzman, "The Distribution of Higher n-Alkanes in Partially Frozen Middle Distillate Fuels," NRL Report 8869, April 10, 1985.
7. T.L. Van Winkle, W.A. Affens, E.J. Beal, R.N. Hazlett, G.W. Mushrush, and J. DeGuzman, "Determination of Liquid and Solid Phase Composition in Partially Frozen Middle Distillate Fuels," this symposium.
8. N.J. Waslik and E.T. Robinson, Ch. 15, ACS Symposium Series No. 163, Oil Shale, Tar Sands, and Related Materials, H.C. Stauffer, Ed., 1981.
9. J. Solash, R.N. Hazlett, J.C. Burnett, E. Beal, and J.M. Hall, Ch. 16, ACS Symposium Series No. 163, Oil Shale, Tar Sands, and Related Materials, H.C. Stauffer, Ed., 1981.
10. W.A. Affens, J.M. Hall, E. Beal, R.N. Hazlett, J.T. Leonard, C.J. Nowack, and G. Speck, Ch. 17, ACS Symposium Series No. 163, Oil Shale, Tar Sands, and Related Materials, H.C. Stauffer, Ed., 1981.
11. Turbine Fuel, Aviation Grades, JP-4 and JP-5, MIL-T-5624L, 18 May 1979.
12. American Society for Testing and Materials, "Freezing Point of Aviation Fuels," ASTM D 2386-67.
13. American Society for Testing and Materials, "Pour Point of Petroleum Oils," ASTM D 97-66.
14. C.T. Moynihan, R. Mossadegh, and A.J. Bruce, *Fuel* **63**, 378 (March 1984).

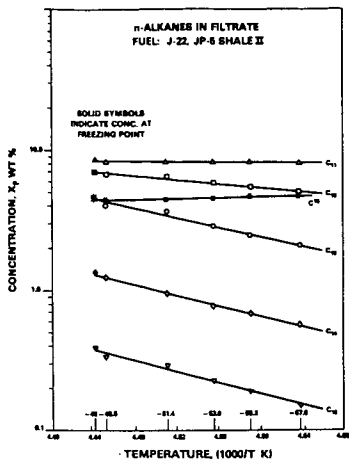


FIGURE 1

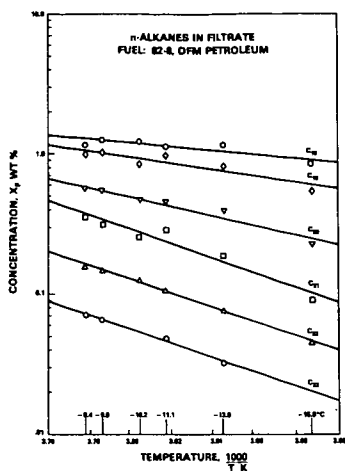


FIGURE 3

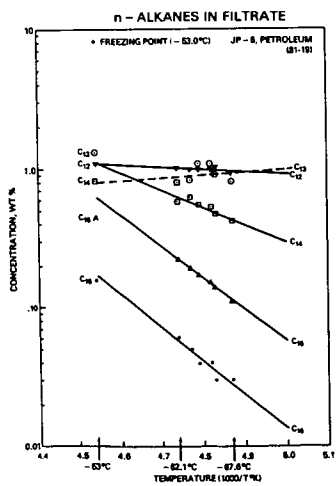


FIGURE 2

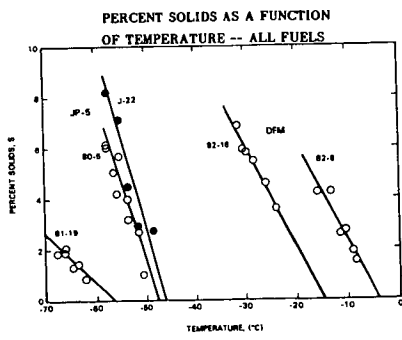


FIGURE 4

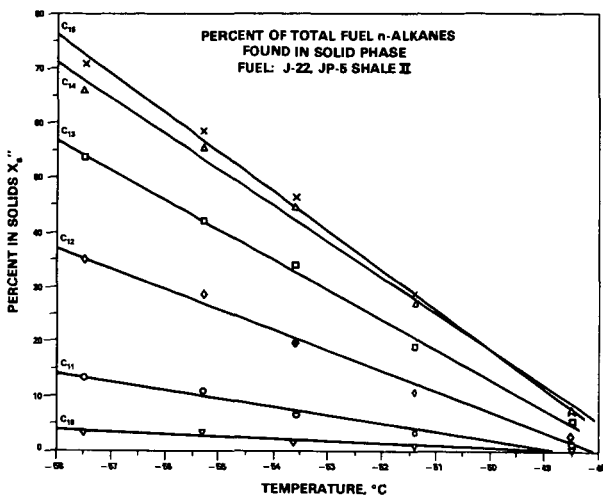


FIGURE 5

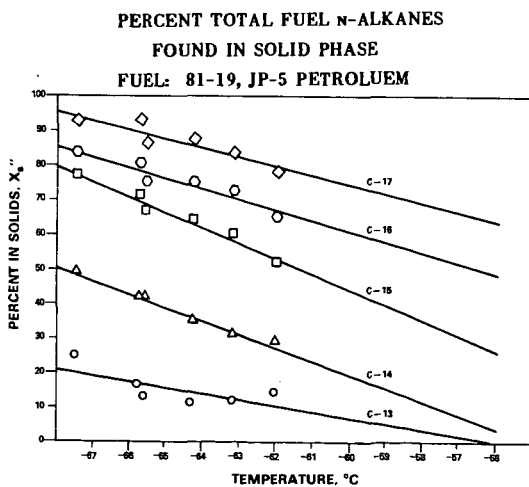


FIGURE 6

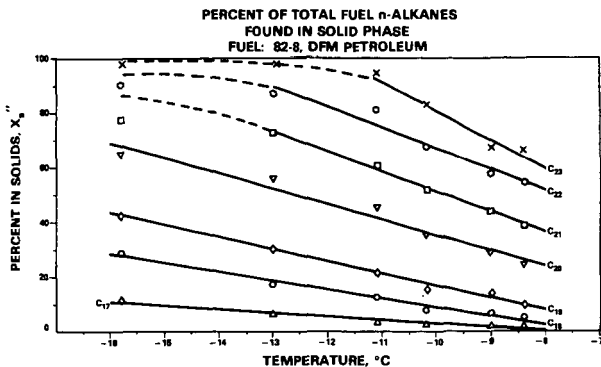


FIGURE 7

NOMENCLATURE

	Fuel Sample	Filtrate	Precipitate	Precipitate Fraction	
				Solid	Liquid
<u>Total Material:</u>					
Weight	W_0	W_f	W_p	W_s	W_L
Fraction of Sample		$F = W_f/W_0$	$P = W_p/W_0$	$S = W_s/W_p$	$L = W_L/W_p$
<u>SPECIES a or b:</u>					
Weight	w_a	w_f	w_p	w_s	w_L
Concentration (w/W)	$X_a = w_a/W_0$	$X_f = w_f/W_f$	$X_p = w_p/W_p$	$X_s = w_s/W_s$	$X_L = w_L/W_L$
$Z = W_L/W_p$					
a = Crystalline Species					
k = Noncrystalline Species					
<u>Subscript:</u>					
o = Original Sample					
f = Filtrate					
p = Precipitate					
s = Solids Fraction of Precipitate (Crystals)					
L = Liquid Fraction of Precipitate					
T = Total					
				<u>Superscript:</u>	
				* = Normalized Data (Concentration di-	
				vided by that of original sample)	
				** = Percent concentration of a	
				species in the fuel found in the	
				solid phase	

Limitations of Existing Analytical Methodologies-
Needs for Future Methods Development in The Analysis
of Fossil Fuels: Concluding Remarks

M.B. Perry, Division of Coal Science
U.S. Department of Energy, Pittsburgh Energy Technology Center

Introduction

Two of the challenges faced by fuel scientists with respect to a future fuel-processing technology are (1) the need to characterize highly complex samples in various stages of conversion, and (2) the need to aid in developing conversion processes that are economically feasible and yield a product that is environmentally acceptable. The Committee on Nuclear and Alternative Energy Systems concludes that coal and nuclear energy are the only potential major sources for electricity generation in this century.¹ For this reason, and since most of the papers in this symposium have been directed toward investigations relevant to coal, this discussion will focus on problems associated with the characterization of coal and its concomitant processing products.

An understanding of coal requires integration of the perspectives of investigators from various backgrounds. For example, even today there is still no consensus concerning the origins of the various forms of sulfur in coal that integrates the views held by scientists from different disciplines. Socolow² noted the various views of coal from miners, geologists, chemists, and biologists. Today, this list can be expanded to include views of coal from social scientists and environmentalists. Socolow quotes the noted geologist David White, who once said, "Coal is like character, the deeper you go into it, the more interesting it becomes." Thus, to a great extent each investigator becomes more or less captivated by these materials and the analytical challenges they offer, such that if the muse of fuel science were to appear to each of us and offer one gift of instrumentation, we would each of us request a different gift, the final assemblage of which would require standardization and cross calibration.

In the absence of a muse, it might be interesting to trace the stages of evolution of a new analytical method. Laitinen³ has described a set of seven phases through which an analytical method passes. The phases he describes are traced in terms of the history of infrared spectroscopy and can be summarized as follows:

First, there is a conception phase that occurs after a principle of physics (e.g., the absorption of infrared radiation) is recognized as a basis for identification and measurement. Second, the validity of the principle as a basis for useful measurements is established. Third, instrumental developments bring the method from a laboratory curiosity into the hands of a nonspecialist. Fourth, detailed studies of principles and mechanisms are pursued, and the method matures as an accepted procedure. (Laitinen identifies this stage as the crest of analytical research as distinguished from instrumentation research). Fifth, applications are enlarged with appropriate modifications in procedures. Sixth, well-established procedures are applied to new as well

as to old problems. Seventh, a period of senescence occurs while other developing methods surpass the method under consideration. Finally, a resurgence of these later phases may occur as new developments in instrumentation or theory come along.

Two questions come to mind in considering these stages of evolution of accepted analytical methodology: First, has physics recognized new principles that suggest new methods for probing fossil fuels; and second, are fuel scientists actively developing methods applicable to these materials or are we merely modifying methods that were originally developed for investigation of other sample types (i.e., polymers, proteins, amino acids, biological materials)?

"It has been said, perhaps cynically, that chemists can expect to see no further new analytical methods. Physicists have discovered the fundamental interactions of energy and matter, and combining existing techniques into hyphenated methods is all that remains." Is it reasonable to expect the development of new analytical methods for the analysis of fossil fuels? A historical view of coal utilization might produce some insights.

Past, Present, Future Trends

Some well-established laboratory techniques for the analyses of coal and petroleum have been identified and are accepted by the American Society for Testing and Materials (ASTM) as standard methods. There are, however, three other organizations that specify methods and procedures for coal analysis, including (1) International Organization for Standardization (ISO), (2) Deutsches Institut für Normung (DIN), and (3) British Standards Institution (BSI). Procedures recommended by these four standard-setting groups were compared at Conoco's Coal Research Division (Liberty, Pa.) using an Eastern United States high-sulfur coal.¹ They note that although the terms used by these different standard setting groups are the same, the procedures used for some of the determinations are not, and results obtained from these analyses show that differences exist. Finally, they conclude that "the increasing movement of coals from the U.S. or other parts of the world to Europe requires an understanding of the various methods of coal analysis used by coal buyers and sellers." Thus, a fundamental problem is confirmed that must be addressed by investigators of fossil fuels, the necessity for methods calibrations and standardizations.

Coal preparation (beneficiation) can be viewed as a form of coal processing that should be well understood. Coal prep has been used in the U.S. for approximately 100 years. In the 1960s, about 1/3 of the total coal mined was cleaned. As Klatt has pointed out,⁵ coal prep and flue gas desulfurization are the least costly ways of meeting New Source Performance Standards for SO₂ emissions.^{6,7} Yet, the application of analytical methodologies to the characterization of these materials and processes have been minimal. Klatt cites several reasons for this deficiency;⁵ he points out that fundamentally coal is undervalued relative to other fuels, and the coal industry has been reluctant to try new technology. As evidence of this observation, Klatt relates the cost of a modern coal prep plant is approximately \$75,000,000, with a total on-line instrumentation cost of about \$150,000 -- a much lower investment in instrumentation than is found in the

chemical industry. The economic rationale for the use of on-line process and quality control instrumentation, Klatt notes, has simply not been provided. Most laboratory techniques used to analyze coal cannot be transferred to on-line instruments because they do not satisfy principle design criteria (i.e., rapid response time and the ability to sample large quantities of materials). Other important criteria that must be considered include cost, reliability, and maintainability. Methods that use high-energy photons, gamma or X-ray, can meet the above design criteria. Consequently, essentially all systems developed or under development (i.e., Mossbauer spectroscopy, X-ray diffraction, and X-ray fluorescence) for the coal industry that yield elemental composition information employ methodology involving the measurement of gamma or X-rays.

The assessment of the mechanisms, efficiency, environmental acceptability, etc., of a particular processing technology may require knowledge of the functionalities present or a determination of the individual organic compounds present. Hertz et al.⁸ have briefly reviewed emerging methods for the analysis of individual organic compounds in petroleum, shale oil, and synthetic coal liquids. However, they note that none of these methods was developed for the accurate quantitative analysis of individual compounds. Because of sample solubility or volatility requirements, in many cases, the actual sample for which data are reported is a fraction or derivative of the material of interest that has been subjected to a variety of pretreatment procedures. Because of their carcinogenic potential and because they are present at significant levels in combustion products, polycyclic aromatic hydrocarbons and their heterocyclic analogue derivatives have been the focus of many recent investigations. Analytical methods that have been applied to the analysis of these sample constituents have been reviewed.^{9,10,11} Karasek et al.¹² and Janardan and Schaeffer¹³ have reviewed the mechanisms involved in the introduction of errors in the analysis of trace organics. Karasek et al. address problems associated with solvent purity, sample pre-concentration, and sample collection and handling; they suggest that a major problem with all techniques for trace analysis of organics is the lack of appropriate environmental standards.¹² They recommend specific changes in the design and use of glassware and other apparatus employed in sample preparation. Likewise, in an analysis of random errors in estimating levels of trace organics in environmental sources, Janardan and Schaeffer¹³ show that the estimated quantity is dependent on the capture efficiency and precision, the average recovery and reproducibility, and the sensitivity of the analysis. They concluded that "in order to insure the accuracy of such data, the scientist must control not only the analyses but, more importantly, the processes involved in obtaining the sample itself."¹³

Many of the future needs in fossil energy research are fundamental to the ordinary requirements for the analysis of any diverse complex sample type. There must be developed a series of suitable, universally acceptable standards that are appropriate for instrumental and methods calibration for routine analyses. Intermethod and intramethod calibration is vital if results and conclusions from the investigations of the various fossil fuel types are to be compared and contrasted. These tasks will require the expertise and background of the most reputable and credible fossil fuels scientists among us if their results and suggestions are to be widely accepted and implemented. This endeavor would be unique in that the study

would attract the worldwide interest and support of fossil fuels scientists. Finally, the translation of these laboratory methods into a form suitable for on-line process analyses with the appropriate cross-calibration and cross-validation of results should be forthcoming.

New Methods for Fossil Fuels?

Who will accept the risks and bear the costs of new analytical methods development in fossil fuels research? Few young investigators can accept a high risk of failure; certainly graduate students and nontenured professors have timetables that are relatively intolerant of failure. However, significant contributions have been made and should continue in incremental improvements in existing methodologies applied to fossil fuels; these investigations can be accomplished, in many cases, within a time frame and within a risk factor acceptable to the new researcher. The fresh approach and ideas of new investigators should be brought to bear on fundamental problems of fossil fuels research. Federal budgets are being increasingly scrutinized, and the requisite for fossil fuels development is being delayed. Increasingly, managers outside of academia are adopting the "publish-or-perish" criterion for promotion or even retention of entry level professionals. A conference, "Strategies for Innovation," sponsored by an international accounting firm, convened in London in June 1985.¹⁵ There Douglas Dybvig, managing director of Minnesota 3M Research, Ltd., pointed out that "the rising cost of innovation, pressures from investors for immediate gains, and economic pressures have helped reduce productive growth and concomitant growth in innovation." Two primary themes emerged from the conference. One was the need for companies to establish an atmosphere in which people are not afraid to fail; the second was the need for companies to be accepting of not only in-house ideas but also those from the outside. Without significant changes in this philosophy and these attitudes, it is reasonable to conclude that the risks of failure associated with new methods development will probably be the burden of established professionals -- established professionals who must consciously purge old biases and precepts, and bring a youthful approach to problems, established professionals who have secure and adequate budgets to staff their laboratories with capable personnel willing to endure the painstaking, slow, and patient approaches required of innovation and creativity.

References Cited

1. Brooks, H., Proc. Am. Philos. Soc., 125, 245 (1981).
2. Socolow, A.A., "Coal in Pennsylvania," Educational Series No. 7, Commonwealth of Pennsylvania, Department of Environmental Resources, Bureau of Topography and Geologic Survey, 1968.
3. Laitinen, H.A., Anal. Chem. 45, 2305 (1973).
4. Stinson, Stephen, C., C&EN 63, 21-32 (November 11, 1985).
5. Klatt, L.N., Analytical Instruments in the Coal Preparation Industry - Current Status and Development Needs, in "Coal and Coal Products: Analytical Characterization Techniques," E.L. Fuller, Jr., ed., ACS Symposium Series 205, American Chemical Society, Washington, D.C., 259-279, 1982.
6. "Engineering/Economic Analysis of Coal Preparation with SO₂ Cleanup Processes," EPA-600/7-78-002, U.S. Department of Energy, Pittsburgh, Pa., 1979.
7. "Environmental Assessment of Coal Cleaning Processes: Technology Overview," EPA-600/7-79-073e, U.S. Environmental Protection Agency, 1979.
8. Hertz, H.S., Brown, J.M., Chesler, S.N., Guenther, F.R., Hilpert, L.R., May, W.E., Parris, R.M., and Wise, S.A., Anal. Chem. 52, 1650-1657 (1980).
9. White, C.M., Determination of Polycyclic Aromatic Hydrocarbons in Coal and Coal-Derived Materials, in "Handbook of Polycyclic Aromatic Hydrocarbons," Alf Bjørseth, ed., Marcel Dekker, Inc., 1983, 525-616.
10. Lee, M.L., Novotny, M.V., and Bartle, K.D., "Analytical Chemistry of Polycyclic Aromatic Hydrocarbons," Academic Press, New York, N.Y., 1981.
11. Hurtubise, R.J., "Solid Surface Luminescence Analysis - Theory, Instrumentation, Applications," Marcel Dekker, Inc., New York, N.Y.
12. Karasek, F.W., Clement, R.E., and Sweetman, J.A., Anal. Chem., 53, 1050A (1981).
13. Janardan, K.G., and Schaeffer, D.J., Anal. Chem., 51, 1024 (1979).
14. "Comparison of ASTM, ISO, DIN, and BSI Methods of Coal Analysis," Technical Bulletin (TB-4 9/83 ELO), Coal Research Division, Conoco, Inc., Library, PA 15129.
15. C&EN, 63, 16 (July 1985).

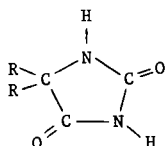
THE MECHANISM OF THE FORMATION OF HYDANTOINS

J.J. Worman, K. Uhrich, E. Olson, J. Diehl
S. Farnum, and S. Hawthorne

University of North Dakota Energy Research Center
Box 8213, University Station
Grand Forks, North Dakota 58202

Introduction

Hydantions, (1), are biologically active compounds which occur in nature and have been isolated from such sources as sugar beets and butterfly wings. Synthetic analogs have found widespread use as anticonvulsant drugs, bacteriocides, stabilizers in photographic film, and in the preparation of high temperature epoxy resins. Uses, preparation, and reactions of hydantions have been extensively studied and are reported elsewhere (1, 2).



(1)

Recently a number of hydantoin isomers have been detected and identified in coal gasification condensate water from the gasification of Indian Head (ND) lignite at the University of North Dakota Energy Research Center in a slagging fixed bed gasifier (3). The hydantions constitute a major portion of the organics in the condensate water and have recently been identified in water from other gasification processes (5). In general the concentrations of hydantions found in the condensate water from an ash gasifier are smaller than those found from the slagging process. There is also a relationship between the type of coal used and the amount of hydantions formed. Lignite coal reacting in a slagging gasifier gives the largest concentration of hydantions in the condensate water. The major isomer in the coal gasification condensate water is 5,5-dimethylhydantoin (DMH). It should be emphasized that DMH is formed from individual species (acetone, cyanide, ammonia, and carbonate) in the condensate water and does not form directly in the gasifier. Hydantions were shown to be either absent or present in low concentrations in water samples which were collected from side-stream samples in the UNDERC gasifier and quickly frozen. When this sidestream condensed water was heated in a constant temperature bath of 40°C, DMH concentrations increased in an approximately second order manner (6). The formation is believed to proceed by the Bucherer-Berg reaction, the same reaction used for commercial hydantoin synthesis (3).

The potential use of the slagger to produce economically useful synthetic fuel gas, both on the national and international scale, prompted an investigation into the kinetics and mechanisms of formation of DMH. It was impossible to obtain reliable and reproducible concentration data for acetone and cyanide in the raw gasifier condensate water due to reversible addition products (acetone cyanohydrin, etc), so a model system was chosen. Acetone cyanohydrin was reacted with excess ammonium carbonate at concentrations approaching those obtained in the condensate water. The experimental details and results have been recently reported (7). The rate of formation of DMH was first order in all of the reactants as expressed by Equation 1.

$$\text{Rate of formation of DMH} = [\text{Acetone}] [\text{HCN}] [\text{NH}_3] [\text{CO}_2] \quad 1)$$

This kinetic data is valuable in predicting the rate of formation of DMH in coal gasification condensate water, provided the model is applicable. The pH of the model solution and the condensate water remained constant at around 8.4, but the effects of small changes in pH on the rate are not fully known.

A mechanism consistent with the kinetic data and partially verified by others is shown in Scheme 1 (8, 9, 10). What remains to be studied is to obtain detailed evidence of the rate-determining step and to isolate intermediates VI, VII, and VIII. In this work we will show that the carbamate salt which results from the reaction of two moles of α -aminoisobutyronitrile with carbon dioxide gives an N-substituted hydantoin rather than the expected DMH. This either precludes the salt as forming in the gasifier water since the N-substituted hydantoins has not been identified in gasifier condensate water, or the salt reacts rapidly by an alternate mechanism to give DMH.

Experimental

α -Aminoisobutyronitrile (IV) - Ammonia gas was bubbled into 50 ml of acetone cyanohydrin (Aldrich) at 60°C for several hours. The product was distilled at 50-56° (20 mm) to give 90 percent yield. The structure was verified by IR, Mass Spec. and ¹³C NMR. The product was stored under nitrogen and refrigerated to prevent slow reverse hydrolysis and discoloration.

2-Cyanopropyl-ammonium 2-Cyanopropyl-2-Amino Carbamate (X) - Dry ice was added slowly to a 25-ml neat sample of α -aminoisobutyronitrile. This was continued until the entire system was solid, about one hour. Anhydrous ether was added and the mixture stirred and filtered. The resulting white solid reacts with dilute hydrochloric acid to give the starting aminonitrile hydrochloride salt and carbon dioxide. The carbamate had a m.p. of 210°C and gave peaks at m/e 212 and 168 via solid probe mass spectrometry. On hydrolysis, the compound gave acetone, ammonia, acetone cyanohydrin, and α -aminoisobutyronitrile as indicated by GC/MS.

N-(α -Carbamylisopropyl)-N'- α -isobutyronitrile urea (XI)

- A) Carbon dioxide was bubbled through a neat sample of a α -Aminoisobutyronitrile at room temperature. After one hour, the entire sample was solid. This solid was filtered and washed thoroughly with anhydrous ether to remove any unreacted starting material. All spectral properties and elemental analyses were consistent with the structure. The m.p. was identical to the structure proposed by Bucherer (8).
- B) Compound X was allowed to stand at room temperature for several days and after analysis proved to be identical to XI in all respects.

3-(α -Carbamylisopropyl)-5,5-dimethylhydantoin (XIII) - The N-substituted urea, XI, was allowed to stand at room temperature in water for 24 hours. The reaction was followed by ultraviolet spectroscopy and by gas chromatography which indicated the formation of an intermediate that disappeared slowly to give the final product. After evaporation of the water in a vacuum, the resulting white solid (50% yield) was identified as 3-(α -carbamylisopropyl)-5,5-dimethylhydantoin (XIII). The structure was verified by ¹³C-NMR and single crystal x-ray analysis. The properties of the solid were identical in all respects to that of a sample prepared by an alternate synthesis (11). The high resolution mass spectrum gave the correct molecular formula and a molecular ion of m/e 213 and a base peak at m/e 169.

Results and Discussion

In order to clarify further the mechanism of formation of DMH shown in Scheme 1, an attempt was made to isolate the carbamic acid salt of X. When solid dry ice was added to α -aminoisobutyronitrile, a white solid was isolated which by IR, mass spectrometry, elemental analysis, and its reaction with water and hydrochloric acid was best represented by structure XI. Salts of carbamic acids of similar structure have been reported previously and are more or less stable, depending on their specific structure (12). The carbamate X slowly rearranged at room temperature to the disubstituted urea, XI, shown in Scheme 2. This urea was also prepared by bubbling carbon dioxide gas through α -aminoisobutyronitrile at room temperature.

The compound was reported previously (8). Its structure was verified by spectroscopic techniques and elemental analysis.

What occurred next was unexpected. When the N, N'-disubstituted urea was placed in water at room temperature, changes began to take place. The ultraviolet absorption spectrum showed a gradual increase in an absorption at 257 nm. This peak began to disappear after twelve hours and after twenty-four hours was absent from the spectrum. GC analysis using a cool, on-column injection onto a 30 m OV-351 fused silica capillary column gave, as a major compound, the N-substituted hydantoin, XIII. The structure of XIII was proven by alternate synthesis, elemental and spectral analysis, and single crystal X-ray analysis. The carbamate salt in water gave similar results. Only trace amounts of DMH were observed by GC/MS.

The mechanism for the formation of the N-substituted hydantoin is shown in Scheme 2. Evidence for the structure of the bicyclic imino intermediate (XII) is based on several factors. The ultraviolet absorption spectrum is consistent with an $n \rightarrow \pi^*$ transition of an imine chromophore occurring at 257 nm (13) and the GC/MS of the intermediate gave a peak at m/e 195. This represented a loss of ammonia from the starting N-substitute urea, XI. The absence of a fragment peak at m/e 151 (m-44) is strong evidence that the intermediate, XII, does not contain a carbonyl or carboxyl group. That this highly strained bicyclic system would form at room temperature in water might at first appear unusual; however, a similar bicyclic system was isolated in the alternate synthesis of the N-substituted hydantoin (11).

Conclusion

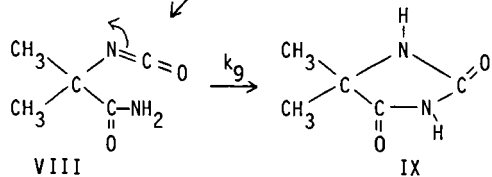
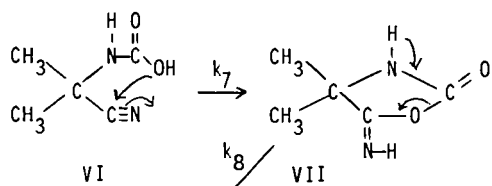
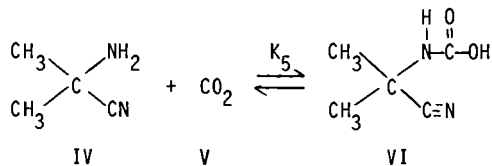
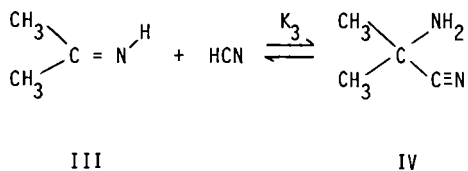
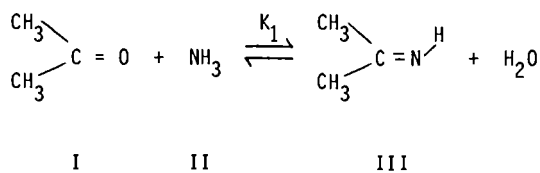
N-substituted hydantoin, specifically the N-(carbamyliisopropyl)-5,5-dimethylhydantoin, form in water at room temperature from the N- α -carbamyliisopropyl-N'- α -isobutyronitrile urea. Only a small amount of the 5,5-dimethylhydantoin, IX, is produced from the N-substituted urea, XI, or its carbamate salt, X. Thus, they are not likely intermediates in the formation of the DMH in water in the presence of acetone, hydrogen cyanide, carbon dioxide, and ammonia. Instead the hydantoin is believed to result from the hydrated conjugate base of the carbamic acid (VI) (Scheme 1).

Acknowledgement

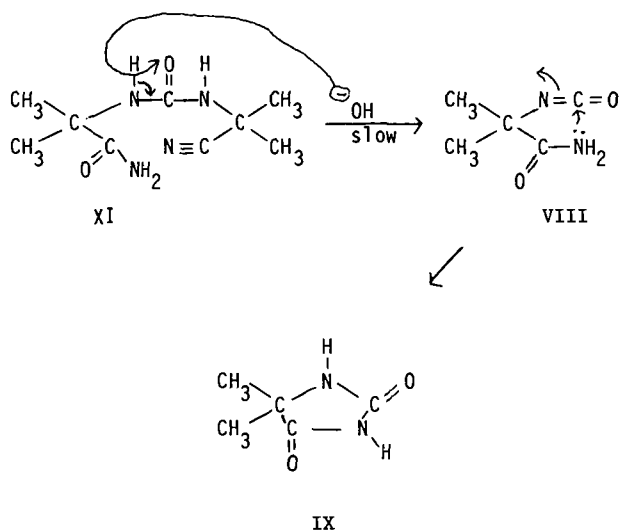
The advice of Dr. Warrack Willson, Manager of the Coal Conversion Research Division at the University of North Dakota Energy Research Center and the support from the U.S. DOE Grand Forks Project Office was appreciated.

References

1. Ware, E. *Chem. Rev.*, 1950, **47**, 438.
2. Dorfman, R.I. "Encyclopedia of Chemical Technology", 3rd Ed., Vol. 12, John Wiley, NY, 1978, p. 692.
3. Olson, E.S., Diehl, J.W., and Miller, D.J. *Anal. Chem.*, 1983, **55**, 1111.
4. Mohr, D.H. and King, J.C., *Environ. Sci. Technol.*, 1985, **19**, 929.
5. Private Communication - Proprietary Information from Privately Owned International Gasification Corporations.
6. Olson, E.S., Worman, J.J., and Diehl, J.W. "The Formation of Hydantoin in Gasifier Condensate Water", *American Chemical Society Division of Fuel Chemistry Preprints*, 1985, **30** (2), 288.
7. Diehl, J., Olson, E., and Worman, J., *Fuel*, 1985, **64**, 1019.
8. Bucher, H.T. and Steiner, W.J., *J. Pract. Chem.*, 1934, **140**, 291.
9. Taillades, J. and Commeyras, A., *Tetrahedron*, 1974, **30**, 3407.
10. Rousset, A., Lasperas, M., Taillades, J., and Commeyras, A., *Tetrahedron*, 1980, **36**, 2649.
11. McKay, A.F., Paris, G.Y., and Garmaise, D.L., *J. Am. Chem. Soc.*, 1958, **80**, 6276.
12. Caplow N., *J. Am. Chem. Soc.*, 1968, **90**, 6795 and references therein.
13. Nelson, D.A. and Worman, J.J., *Tetrahedron Letters*, 1966, 507.



Scheme 1. Mechanistic sequence for formation of DMH



Scheme 3. Possible mechanistic pathway for the formation of 5,5-Dimethyl-hydantoin from N- α -carbamylisopropyl-N'- α -isobutyronitrile urea (XI)

LIQUID PHASE OXIDATION OF ALKYL SULFIDES AND THIOLS BY HYDROPEROXIDES

By

George W. Mushrush, Dennis R. Hardy, Harold G. Eaton
and Robert N. Hazlett
The Naval Research Laboratory
Code 6180
Washington, D. C. 20375

INTRODUCTION

In general, jet fuels deteriorate in quality with time. One of the significant undesirable changes is the formation of insoluble material which can plug nozzles and filters and coat heat exchanger surfaces. Deposit formation in fuels is triggered by autoxidation reactions and is closely associated with hydroperoxide concentration (1-3). If the available oxygen is low and the temperature raised, the hydroperoxide concentration will be limited by free radical decomposition (2). This regimen (low oxygen and increasing temperature) is similar to the environment found in an aircraft fuel system.

The composition of deposits affords clues to the molecular species involved in deposit formation and the mechanism of formation. Hetero-atoms (oxygen, nitrogen and sulfur) and ash have been found to comprise up to 40% of such deposits (4-6). The sulfur content of these deposits has been found to vary from 1 to 9%. Sulfur (0.4% max. allowed) is the most abundant hetero-atom present in jet fuels.

This paper is concerned with the reaction between a primary autoxidation product, a hydroperoxide, and organo sulfides and thiols. Specifically, we examine the tert-butyl hydroperoxide oxidation of hexyl sulfide and dodecyl thiol in deaerated benzene at 120°C. The reactions were studied for time periods from 15 min to 180 min. Additionally, we have developed reaction conditions and an analytical method of high reproducibility which may be applicable to the study of other hydroperoxide oxidative processes.

EXPERIMENTAL

Reagents tert-Butyl hydroperoxide, tBHP, (90%), hexyl sulfide and dodecyl thiol were obtained from Aldrich Chemical Co. They were distilled in vacuo to 99.9% purity. Benzene (Aldrich Gold Label) was refluxed and distilled from CaH_2 .

Method. The reactions were carried out in sealed borosilicate glass tubes. The reagents (typically $3\text{-}9 \times 10^{-4}$ mol of tBHP and 6×20^{-4} mole of hexyl sulfide or 6×10^{-4} mole of dodecyl thiol in 3.6 m mol of solvent) were weighed into 6 in. long, 1/4-in. o.d. Pyrex tubes closed at one end and fitted at the other with a stainless steel valve via a Swagelok (Teflon ferrules) fitting. The tube was attached to a vacuum system, cooled to 77K and subjected to several freeze-pump-thaw cycles. The tube was then subsequently flame-sealed below the valve. The ullage volume (0.30 ml) was kept constant for all runs. The deaerated samples were warmed to room temperature and immersed in a Cole-Parmer fluidized sand bath. The temperature (120°C) was controlled by a Leeds and Northrop Electromax III temperature controller. The total pressure during each run was estimated to be 5.1 atm for the runs in benzene. After the reaction period the sealed tube was quenched to 77K and opened. The tube was capped, warmed to room temperature and the internal standards added. The solution was transferred to a screw cap vial (Teflon cap-liner) and stored at 0°C until analysis. Since a typical chromatogram required 90 min, two internal standards were added. One, p-xylene, afforded quantitation for peaks with short retention times, and a second, 1-phenyltridecane, for the peaks with longer retention times.

Samples were heated for time periods of 15, 30, 60, 120 and 180 min except for those runs with the more reactive mercaptan (60 min max). All tubes were subjected to the same cleaning procedure. They were filled with toluene, cleaned with a nylon brush, rinsed with toluene twice, then with methylene chloride, and dried in air at 150°C for 8 h. A search of the literature gives a few examples of catalytic behavior with glass systems (7,8); however, when a glass tube was filled with crushed Pyrex, thus increasing the surface area, the results at 120°C for the above time periods were not substantially altered.

The samples were analyzed by two techniques, both based on gas chromatography. Peak identification for both techniques was based on retention time matching with standards and mass spectrometry. In the first, a Varian gas chromatograph Model 3700 with flame ionization detector (F.I.D.) and equipped with a 50-m 0.20-mm i.d. wall-coated open tubular (OV-101) fused silica capillary column gave the necessary resolution to distinctly separate the individual components. A carrier gas flow of 1 ml/min was combined with an inlet split ratio of 60:1, a temperature program with an initial hold at 50°C for 8 min and a ramp of 4°/min to a final temperature of 260°C.

In the second technique, gases formed during the reaction were analyzed using a Perkin-Elmer Model Sigma 2 gas chromatograph equipped with a 6-ft 5A Molecular Sieve column or a 4-ft Porapak/S column. For the gas analysis, the column was operated at 55°C. The chromatogram was recorded and integrated on a Hewlett-Packard Model 3390A reporting integrator. For this procedure, the valve was left on the reaction tube and after the appropriate reaction period, the tube valve was connected directly to a GC gas sampling valve via a Swagelok connection. An external standard was used for calibration. A pressure gauge measured the pressure in the sample loop at the time of analysis.

A material balance was assessed for each compound. The principal peaks of the chromatogram accounted for approximately 90% of the original compounds.

The very small peaks account for another 5-10%. The product distribution was repeatable to within 2-3% for each component.

RESULTS AND DISCUSSION

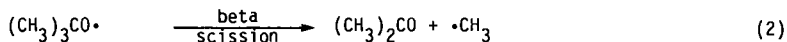
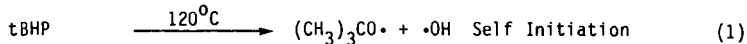
The thermal decomposition of an alkyl hydroperoxide is complex. At temperatures of 120°C or greater, tBHP decomposes by an autoinitiated pathway.⁹ The major reaction pathway in the 120°C decomposition of tBHP, however, involves its attack by free radicals in the solution. The detailed mechanism of tBHP decomposition is highly dependent upon the specific reaction conditions employed since radical behavior is sensitive to structural, solvent and stereoelectronic effects.

The results in Table 1 illustrate that the product distribution from the reaction of tBHP with hexyl sulfide in deaerated benzene solvent can be conveniently divided into lower and higher molecular weight products. The quantities in Table 1 are based on per cent conversion from the moles of reactants originally present. Products derived solely from hexyl sulfide are calculated on the basis of the starting amount of hexyl sulfide. The tBHP derived products (for example, t-butanol) are similarly calculated based on the starting amount of tBHP. Mixed condensation products (i.e., tBHP + hexyl sulfide) are calculated on the basis of moles of hexyl sulfide. The values in Table 2 were likewise calculated using dodecyl thiol.

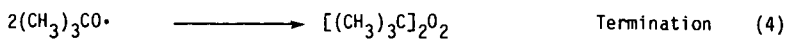
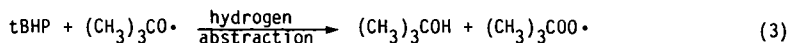
From tBHP, the major product was t-butanol. A small amount of acetone, methane, isobutylene and the tBHP radical termination product di-t-butylperoxide were also observed. From hexyl sulfide, lower molecular weight products included hexane, hexene and hexanal; higher molecular weight condensation products included the major product hexyl sulfoxide along with hexyl sulfone and hexyl disulfide. From dodecyl thiol, Table 2, lower molecular weight products included dodecane and dodecanol; higher molecular weight condensation products included the major product dodecyl disulfide along with dodecyl sulfoxide, dodecyl sulfide and dodecyl sulfone.

Solvent participation was noted by the formation of trace quantities of toluene and other substituted benzenes.

tBHP products The mechanism of autoinitiated tBHP decomposition can be depicted as follows:



Propagation



In aliphatic hydrocarbon solvent, it has been shown that beta-scission is favored over hydrogen abstraction at temperatures of 100°C or less. In the benzene solvent of this study, beta-scission was found to be less than competitive with hydrogen abstraction at 120°C. Small amounts of acetone were formed ranging from 1.5% for hexyl sulfide to 4.7% for dodecyl thiol at 60 min. By contrast, t-butanol was 75.4% for hexylsulfide and 76.7% for dodecyl thiol at 60 min. The greater yield of t-butanol compared to acetone definitively shows that hydrogen abstraction was favored over cleavage in benzene solvent under the conditions of this study. The increasing yield of acetone indicated, however, that at long reaction times beta-scission was a viable competing process.

Gaseous products The gaseous products formed included isobutylene, methane and a trace amount (0.1%) of ethane. No free oxygen was observed in any of the runs. As indicated in Table 1, isobutylene was 4.2% initially and decreased to 2.7% at 180 min. Methane increased from 0.8% at 15 min to 1.6% at 180 min. For dodecyl thiol, Table 2, isobutylene was 3.6% initially and decreased to 3.0% at 60 min. Methane increased from 0.9% at 15 min to 1.4% at 60 min.

Isobutylene probably resulted from the acid catalyzed dehydration of t-butanol. The decreasing yield was not surprising in light of the many pathways open to a reactive olefin in a radical environment.

The yield of methane was similar to that of acetone. This was an expected result since they both form via beta scission of the alkoxy radical (reaction 2). The reactive methyl radical easily abstracts hydrogen to yield methane rather than reacting with other radicals present in the system. This accounted for the low yield of methyl radical derived products.

The lack of measured oxygen does not mean that it was not formed. It could form from a non-terminating reaction of two t-butyl peroxy radicals and then be consumed immediately by any of several pathways.

Hexyl sulfide products The cleavage of a C-S bond in sulfides is known to occur in thermal and photochemical reactions.¹⁰ The most direct means of generating a sulfur centered radical is the homolysis of a bond to sulfur. However, most simple alkyl sulfides are thermally quite stable (C-S bond dissociation energies are ca. 74 kcal/mol) and quite unreactive toward oxygen.¹¹ In the presence of t-butyl hydroperoxide, the t-butoxy radical generated was found to abstract the hydrogen alpha to the sulfur. Thus for hexyl sulfide, observed products were the thiyl radical and hexene. An alternate pathway would involve the attack of an alkoxy by a S_H2 mechanism to yield both a thiyl radical and hexyl radical. That these processes were minor pathways can be seen from the results in Table 1. Hexane and hexene were present in low yields at all reaction times (hexane ca. 0.3% at 180 min and hexene 0.2%). Combination of thiyl radicals to form the disulfide was also a minor termination pathway (0.6% yield at 180 min).

Table 1

Mole % Conversion for the Reaction of Hexyl Sulfide with t-Butyl Hydroperoxide in Benzene Solvent at 120°C.

	Conversion (Mole %)				
	Reaction Time (min.)				
	15	30	60	120	180
<u>TBHP Products^a</u>					
Acetone	1.0	1.5	1.5	1.5	2.5
t-Butanol	55.5	59.5	65.9	69.8	75.4
di-t-butyl peroxide	0.5	0.7	0.7	0.7	1.0
<u>Hexyl sulfide Products^b</u>					
Hexene	0.1	0.1	0.1	0.3	0.2
Hexane	0.1	0.1	0.3	0.4	0.3
Hexanal	0.2	0.2	0.3	0.2	---
Hexyl disulfide	0.3	0.5	0.5	0.5	0.6
<u>Condensation Products^b</u>					
Hexyl sulfoxide	74.8	85.9	81.6	81.9	80.7
Hexyl sulfone	1.2	1.4	3.0	3.4	4.0
Hexyl thiosulfinate	0.1	0.1	0.1	0.1	---
<u>Gaseous Products</u>					
Methane	0.8	0.8	1.0	1.4	1.6
Isobutylene	4.2	3.9	3.6	3.1	2.7
<u>Unreacted</u>					
TBHP	28.9	23.9	8.7	3.9	1.8
Hexyl sulfide	22.5	13.9	8.2	3.9	2.9
<u>Trace Products^c</u>					
	6.7	7.8	9.7	10.1	8.1

a. based on the starting moles of TBHP

b. based on the starting moles of hexyl sulfide

c. summation of small peaks

The observed hexanal can be formed by several reaction pathways. Among these are the thermal rearrangement of the hexyl sulfoxide,¹² or more likely, the coupling of a t-butylperoxy radical with a thioacetal radical. Based on bond dissociation energy considerations alone, the t-butylperoxy radical was probably the least reactive and most plentiful radical present in the system.¹³ This would favor a termination step involving this radical over a termination involving the very reactive alkoxy radical which would be expected to propagate the chain.

The major higher molecular weight product observed from the oxidation of hexyl sulfide by tBHP was hexyl sulfoxide. Its yield varied from 74.8% at 15 min. to 85.9% at 30 min., gradually decreasing to 80.7% at 180 min. of reaction. Other products included: hexyl sulfone (1.2% at 15 min. gradually increasing to 4.0% at 180 min.), hexyl disulfide (0.3 to 0.6%) and a trace amount of dihexyl thiosulfinate (0.1%).

Table 2

Mole % Conversion for the Reaction of Dodecyl Thiol with t-Butyl Hydroperoxide in Benzene Solvent at 120°C

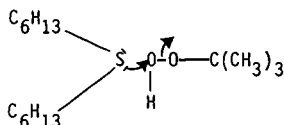
	Conversion (Mole %)		
	Reaction Time (min.)		
	15	30	60
<u>TBHP Products^a</u>			
Acetone	4.7	4.4	4.7
t-Butanol	59.2	65.4	76.7
di-t-butyl peroxid	1.6	1.6	1.9
<u>Dodecyl thiol Products^b</u>			
Dodecane	0.1	0.3	0.4
Dodecanal	0.6	0.7	1.1
Dodecyl sulfide	1.9	1.8	1.4
Dodecyl disulfide	74.4	78.8	74.1
<u>Condensation Products^b</u>			
Dodecyl sulfoxide	2.3	2.1	2.1
Dodecyl sulfone	0.9	1.5	1.7
<u>Gaseous Products</u>			
Methane	0.9	1.3	1.4
Isobutylene	3.6	3.3	3.0
<u>Unreacted</u>			
TBHP	19.7	12.6	1.3
Dodecylthiol	15.6	7.3	3.4
Trace Products ^c	4.6	6.7	9.4

a. based on the starting moles of TBHP

b. based on the starting moles of dodecyl thiol

c. summation of small peaks

The major product hexyl sulfoxide could result from at least two mechanisms: attack of oxygen-centered radicals (i.e., alkoxy) on sulfur followed by a beta scission;¹⁴ or alternatively, the sulfoxide may arise from the reaction of t-butyl hydroperoxide with the hexyl sulfide.



The resulting sulfoxide once formed is quite stable, as can be seen from the slight lowering of the yield at extended reaction times.

The hexyl sulfone yield in the present work varied from an initial 1.2% at 15 min. to 4.0% at 180 min of reaction. This very slight increase compared to the yield of hexyl sulfoxide at 180 min. (80.7%) definitively illustrates the stability of the alkyl sulfoxide in the presence of tBHP.

The further oxidation of a sulfide or a sulfoxide to a sulfone is believed to proceed by a mechanism similar to that for sulfoxide formation from an alkyl sulfide.¹⁵ The formation of an alkyl sulfone is a facile reaction only in the presence of a strong oxidant or when the reaction is catalyzed by transition metal ions.¹⁶

The hexyl disulfide product was a consequence of a self annihilation by dimerization of the thiyl radical. The thiyl radical was in low concentration at all reaction times (see hexyl termination products in the Table). As a result, the termination product hexyl disulfide was a minor product at all reaction times (1% at 180 min.). The other minor observed product forms as a direct result of the disulfide. The trace amounts of hexyl thiosulfinate observed (0.1% at all reaction times) resulted from the peroxidation of the disulfide.

Dodecyl thiol products. When thiols are oxidized by air or peroxides, disulfides are the major product regardless of the presence or absence of a catalyst.¹⁷ The mechanism of thiol oxidation has been the subject of discussion for many years. Some reports support ionic mechanisms while others support radical processes.¹⁸ The results in the present work, Table 2, support a radical mechanism. The t-butoxy radical generated from tBHP was found to abstract the thiol hydrogen. By contrast, hydrogen abstraction by the thiyl radical to yield a thiol is only observed in cases involving very stable thiyl radicals with active hydrogen donors.¹⁹ Actually, the problem with this hydrogen abstraction is not that the process is slow, but that abstraction of a hydrogen from a thiol is thermodynamically favorable. Likewise, the thiyl radical has not been observed to undergo a beta scission to yield a thione and a methyl radical.²⁰ In the present work, thiones and thiols were not detected, even in trace amounts, in the product mix.

The observed secondary reaction products dodecane, dodecanal and dodecyl sulfide were present in low concentration for all reaction time periods. Dodecyl sulfide, 1.9% at 15 min decreasing to 1.4% to 60 min, was probably formed by the reaction of dodecyl thiol with the condensation product dodecyl sulfoxide. The products of such a reaction would be dodecyl disulfide and dodecyl sulfide. Dodecyl sulfide once formed could then undergo other side reactions. The observed dodecane was the result of such a reaction scheme: an S_H2 reaction between the t-butoxy radical and dodecyl sulfide would result in both the dodecyl radical and a thiyl radical. The dodecanal product, 0.6% at 15 min increasing to 1.1% at 60 min, could result from several mechanisms. Among these are the thermal rearrangement of the sulfoxide or the coupling of the t-butyl peroxy radical with a thioacetal radical.

The major higher molecular weight product observed from the oxidation of dodecyl thiol by tBHP was dodecyl disulfide. Other products included dodecyl sulfoxide, dodecyl sulfone and trace but unreported amounts of dodecyl thiosulfinate.

Dodecyl disulfide, 74.4% at 15 min increasing to 78.8% at 30 min and then decreasing to 74.1% at 60 min, was formed by the direct oxidation of dodecyl thiol and subsequent dimerization of the thiyl radicals. An alternative side reaction for its formation would be the reaction of the

starting thiol with dodecyl sulfoxide to generate additional dodecyl disulfide.

The dodecyl sulfoxide, 2.3% at 15 min decreasing to 2.1% at 60 min, probably resulted from the same two pathways mentioned for hexyl sulfoxide.¹⁴ The dodecyl sulfoxide yield was not observed to increase significantly due to further oxidation to dodecyl sulfone or for example its reaction with the starting thiol. The latter reaction would produce both dodecyl disulfide and dodecyl sulfide.

The low yield of dodecyl sulfone, 0.9% at 15 min increasing to 1.7% at 60 min, indicated the stability of alkyl sulfoxides toward further oxidation by tBHP in the liquid phase at 120°C.

LITERATURE CITED

1. Hazlett, R.N., Hall, J.M. and Matson, M., *Ind. & Eng. Chem. Prod. Res. Dev.*, **16**, 171 (1977).
2. Hazlett, R.N., "Frontiers of Free Radical Chemistry"; Academic Press: New York, (1980).
3. Taylor, W. and Wallace, T., *Ind. & Eng. Chem. Prod. Res. Dev.*, **6**, 258 (1967).
4. Cullis, C.F., Hirschler, M.M. and Rogers, R.L., *Proc. R. Soc. Lond, Ser. A* **375**, 543 (1981).
5. Rogers, J.D., SAE Meeting, Preprint 103T, Los Angeles, CA Oct. 5-9, (1959).
6. Nixon, A.C., "Autoxidation and Antioxidants"; Wiley: New York, Chap. 17 (1962).
7. Hiatt, R.R. and Irwin, K.C., *J. Org. Chem.*, **33**, 1436 (1968).
8. Mushrush, G.W. and Hazlett, R.N., *J. Org. Chem.*, **50**, 2387 (1985).
9. Howard, J.A., "The Chemistry of Functional Groups, Peroxides"; Wiley: New York, Chap. 8 (1983).
10. Calvert, J.G. and Pitts, J.N., "Photochemistry"; Wiley: New York, Chap. 5 (1966).
11. Correa, P.E. and Riley, O.P., *J. Org. Chem.*, **50**, 1787 (1985).
12. Barnard-Smith, D.G. and Ford, J.F., *Chem. Commun.*, **2**, 120 (1965).
13. Mushrush, G.W., Hazlett, R.N. and Eaton, H.G., *Ind. & Eng. Chem. Prod. Res. Dev.*, **24**, 290 (1985).
14. Rahman, A. and Williams, A., *J. Chem. Soc. (B)*, 1391 (1970).
15. Curci, R., Giovine, A. and Modena, G., *Tetrahedron*, **22**, 1235 (1966).
16. Henbest, H.B. and Khan, K.A., *Chem. Commun.*, **17**, 1036 (1968).
17. Wallace, T.J., *J. Org. Chem.*, **31**, 1217 (1966); cf. also Schrauzer, G.N. and Sibert, J.W., *J. Amer. Chem. Soc.*, **92**, 3509 (1970).
18. Cohen, S.G. and Aktipis, S., *J. Amer. Chem. Soc.*, **88**, 3587 (1966); cf. also Wagner, P.J. and Zepp, R.C., *ibid.*, **94**, 285 (1972).
19. Kice, J.L., "Free Radicals", Wiley: New York, Chap. 24 (1973).
20. VanSwet, H. and Kooyman, E.C., *Rec. Trav. Chim.* **87**, 45 (1968).

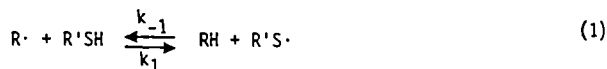
REACTIONS OF THE THIOPHENOXY RADICAL FROM THE
THERMAL AND PHOTOLYTIC DECOMPOSITION OF PHENYLDISULFIDE

M. S. Alnajjar and J. A Franz

Pacific Northwest Laboratory
P. O. Box 999
Richland, WA 99352

INTRODUCTION

The importance of sulfur-containing constituents or additives on the thermal degradation of coal has been recognized by many investigators.^{1a-d} Stock and co-workers^{1a,c} in a study of the hydrogen atom transfer reactions of tetralin-d₁₂ with coal, diphenylmethane, and other coal model-compounds have shown that sources of thiol radicals such as benzylphenylsulfide significantly accelerate the rate of hydrogen shuttling between benzylic positions of model structures. Studies of deuterium exchange between deuterated donors and coals^{2a} suggest that a higher sulfur content is correlated with a more rapid exchange of benzylic hydrogen with the deuterated donor. Activation barriers for abstraction of hydrogen atoms from thiols



(k_1) are less than a few kcal/mole, with the result that the reverse reaction, abstraction from hydrocarbons by thiol radical (k_{-1}) is very rapid, being limited only by ΔH^0 of the reaction. For example, for R = benzyl and R' = phenyl in (eqn. 1) $\log (k_1/M^{-1}s^{-1}) = (8.27 \pm 0.07) - (3.79 \pm 0.12)/\theta$, $\theta = 2.3RT$ kcal/mole.^{2b} For $\Delta H^0 = -6.5$ kcal/mole,^{2c} $\log (k_{-1}/M^{-1}s^{-1}) = (8.5 \pm 0.5) - (10 \pm 2)/\theta$. Thus, at coal liquefaction temperatures (450°C), k_1 is about $10^7 M^{-1}s^{-1}$ and k_{-1} is $3 \times 10^5 M^{-1}s^{-1}$, resulting in very rapid equilibration of hydrogen between benzylic sites. Rapid, reversible abstraction reactions of sulfur-centered radicals are well documented.³⁻⁸ Hydrogen sulfide, pyrite, elemental sulfur, and organic disulfides have been suggested to play significant roles in promoting the liquefaction of various coals.^{1,9-12} Displacement of aromatic substituents and dehydrogenation of hydroaromatic hydrocarbons facilitated by sulfur-centered radicals in reactions with sulfur and disulfides have been extensively studied.¹³⁻¹⁵

The rapid, reversible reactions of addition of sulfur-centered radicals to aromatic rings and readily reversible abstraction reactions (eqn.1) dominate mechanisms of structural evolution during liquefaction, by virtue of the weak S-S bond strengths of disulfides (54 kcal/mol for PhSSPh)¹⁶ which assure that



the sulfur-centered radicals are present in significant concentrations throughout the coal liquefaction process for any sulfur-containing coal. Although it is well known that sulfur-sulfur bonds in alkyl and aryl disulfides and sulfides readily undergo photolytic or thermal homolysis, and many studies¹⁷⁻²¹ have been devoted to the reactions of thiyl radicals with organic substrates, mechanistic aspects of the incorporation of sulfur into aromatic structure are perhaps less well developed, and detailed pathways of carbon-carbon and carbon-sulfur bond cleavage and formation reactions in the context of the thermal evolution of coal structure during liquefaction are lacking.

Thus, we present preliminary results of high-temperature reactions of phenyldisulfide and benzylphenyl sulfide with organic substrates (9,10-dihydroanthracene, diphenylmethane, bibenzyl, stilbene, and diphenylacetylene) which demonstrate mechanisms for the enhanced cleavage of $\text{sp}^2\text{-sp}^2$, $\text{sp}^2\text{-sp}^3$, and $\text{sp}^3\text{-sp}^3$ bonds mediated by thiophenoxy radical, and a series of addition-elimination, abstraction and rearrangement reactions leading to a series of thiophenes and related structures.

EXPERIMENTAL

General. NMR spectra were obtained with Varian FT-80 or Bruker AM-300 systems. Gas chromatography was performed with a Hewlett-Packard HP5890A instrument equipped with a 25-m, 0.32-mm i.d. J&W Scientific DB-5 capillary column. GC-mass spectrometry was performed with HP-5970 or HP-5992 systems. Products were identified by gc coinjection and comparison of mass spectra of authentic standards.

General Procedure for Thermolysis Reactions. In a typical reaction 0.05-0.10 mmole of phenyldisulfide or benzylphenylsulfide and an appropriate amount of

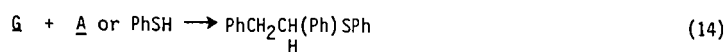
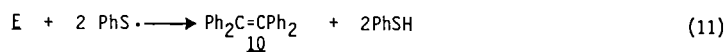
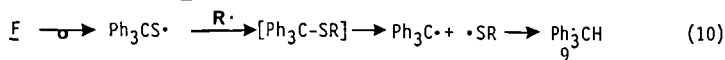
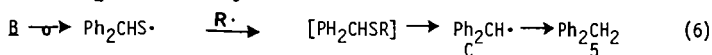
the desired additive were mixed in quartz tubes, freeze-thaw degassed, and sealed. The tubes were heated in a fluidized sand bath at $400\pm 5^{\circ}\text{C}$ for 30 min., cooled to room temp, opened under nitrogen, and transferred to a degassed methylene chloride solution containing naphthalene as an internal gc standard.

Thermolysis of Model Compounds in the Presence of Phenyldisulfide or Benzylphenylsulfide. Thermal decomposition of neat PhSSPh at 400°C produced the following products; thiophenol (1), diphenylsulfide (2), and thianthrene (3). Decomposition of neat benzylphenylsulfide produced the following products: toluene (4), 1, diphenylmethane (5), bibenzyl (6), 2, phenyldisulfide (7), 3, 2-phenylbenzothiophene (8), triphenylmethane (9) and tetraphenylethylene (10). The reactions of PhSSPh with additives are presented below, followed by major products in parentheses: PhSSPh + dihydroanthracene (1, 2, and anthracene); PhSSPh + diphenylmethane (1, 2, 4, 9 and 10); PhSSPh + bibenzyl (1, 2, 4, trans-stilbene (11), 8, 2,3-diphenylbenzothiophene (12), and 1,2,3,4-tetraphenylthiophene (13)); PhSSPh + trans-stilbene (1, 2, 4, 5, 8, 12, and 13); and PhSSPh + diphenylacetylene (1, 2, 4, 8, 12, and 13). The products listed accounted for typically 80% or more based on unrecovered starting material, with individual products varying from 5-10% to as high as 50%.

Preparation of 2,3-Diphenylbenzothiophene. Phenyldisulfide (0.50 mmol) and diphenylacetylene (0.50 mmol) were placed in a quartz tube, freeze-thaw degassed, and heated at 400°C for 30 min. The reaction mixture was transferred to hexane/ether solution (97/3 (v/v)) followed by flash liquid chromatography through a short silica column. Several fractions were taken for GC analysis. The fraction containing most of the product was concentrated. The residue was recrystallized from hexane to give 30% yield of 2,3-diphenylbenzothiophene:m.p. $114-115^{\circ}\text{C}$ (lit.²² 113-114). 300 MHz ^1H NMR (CDCl_3), 7.85 (m, 1H), 7.59 (m, 1H), 7.32 (m, 9H), 7.21 (m, 3H); 75 MHz ^{13}C NMR (CDCl_3), 140.87, 139.53, 138.84, 135.51, 134.22, 133.22, 130.42, 129.59, 128.62, 128.32, 127.67, 127.35, 124.50, 124.41, 123.33, 122.04; GC-MS, m/e (relative intensity) 287 (18, $\text{M}^+ + 1$), 286 (100, M^+), 285 (33), 284 (30), 282 (10), 271 (12), 252 (10), 44 (19).

Results and Discussion

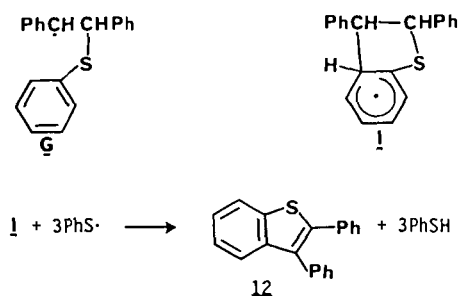
Pyrolysis of neat benzylphenylsulfide produced toluene, thiophenol, Ph_2CH_2 , Ph_2S_2 , Ph_3CH , Ph_2S , 2-phenylbenzothiophene and 2,3-diphenylbenzothiophene. With a central bond strength of $\approx 52 \pm 2$ kcal/mole,¹⁶ benzylphenylsulfide will exhibit a unimolecular half-life of about 5 seconds at 400°C . The elementary free radical reactions in eqns. 2-14 show the origin of abstraction (PhCH_3 , PhSH) rearrangement (Ph_3CH , Ph_2CH_2), and termination/oxidation ($\text{Ph}_2\text{C}=\text{CPh}_2$, $\text{PhCH}=\text{CHPh}$) products.



As noted, radical forming reactions for the weak C-S bonds (eqn. 2) are very rapid at 400°C resulting in the facile equilibria of eqns. 2 and 4. Ph_3CH and Ph_2CH_2 both must occur via 1,2-aryl migration of phenyl from sulfur to carbon (equations 6,10), since an alternate mechanism of ipso displacement by benzyl radical on benzylphenylsulfide has been rendered unlikely based on other model studies.^{15,23} Tetraphenylethylene (10) and stilbene (11) result from radical oxidation of the parent hydrocarbons $\text{Ph}_2\text{CHCHPh}_2$ and $\text{PhCH}_2\text{CH}_2\text{Ph}$.

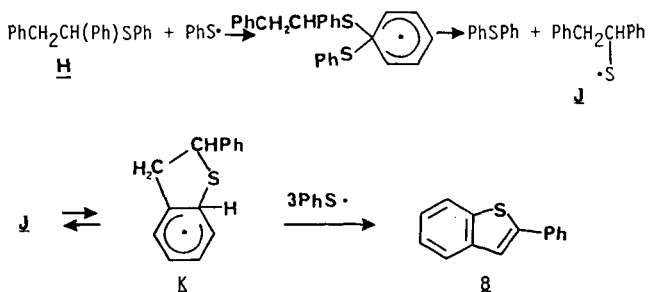
The formation of 2,3-diphenylbenzothiophene is a straightforward consequence of the formation of stilbene. Rapid, reversible addition of $\text{PhS}\cdot$ to stilbene followed by cyclization and oxidation provides the observed product as shown in Scheme I.

Scheme I

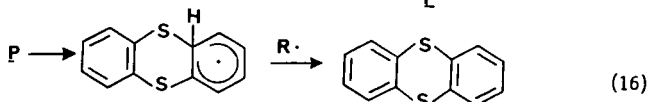
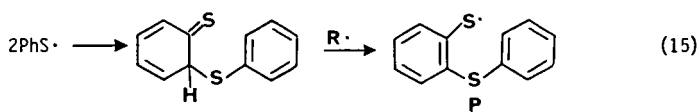


The formation of 2-phenylbenzothiophene must involve a displacement by the thiophenoxy radical on H as depicted in Scheme II.

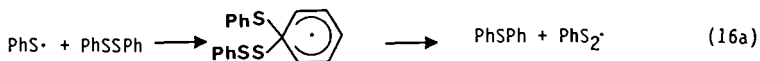
Scheme II



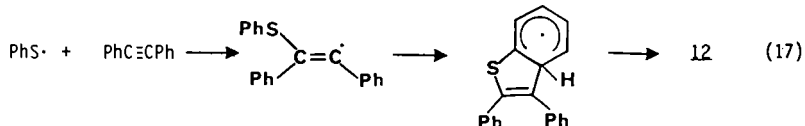
The displacement reaction of $\text{PhS}\cdot$ with **11** will be rapid at these temperatures (cf. the photolysis of Ph_2S_2 at 25°C efficiently produces Ph_2S as the major product), providing an unambiguous route to **13**. The thermolysis of neat phenyldisulfide provides thianthrene and phenylsulfide, the former product by a termination pathway (eqns. 15,16),



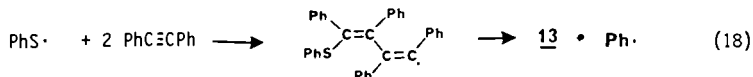
and the latter via direct displacement (eqn.16a).



The reaction of diphenylacetylene and Ph_2S_2 produced 2,3-diphenylbenzothiophene in synthetically useful yields, along with **13**. Production of 2,3-diphenylbenzothiophene (**12**) occurs in straightforward fashion (eqn. 17).

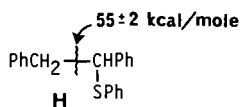


The formation of **13** is difficult to explain without proposing displacement by an intermediate vinylic radical at sulfur (eqn. 18). The displacement of



phenyl radical would be nearly thermoneutral in this case, and the 9-S-3 intermediate (or transition state) is quite plausible.

Finally, we note that significant yields of toluene were produced in reactions of stilbene and bibenzyl. The intermediacy of **H** is suggested.



The thermal C-C cleavage in H to produce $\text{PhCH}_2\cdot$ and species B is expected to be rapid since the estimated bond dissociation energy is comparable to that of PhSSPh (55 ± 2 kcal/mol). The net effect of the thiophenoxy radical in these reactions will have been to substantially enhance the cleavage of $\text{sp}^2\text{-sp}^2$ and $\text{sp}^3\text{-sp}^3$ bonds in these otherwise refractory systems.

Conclusions

The disulfide \rightleftharpoons thiophenoxy radical equilibrium, which models an important family of equilibrating sulfur-center radicals present during liquefaction of sulfur-containing coals, provides facile mechanisms for rapid hydrogen transfer, displacement and condensation reactions leading to enhanced cleavage of aralkyl structure on the one hand, and retrograde formation of nearly inert thiophene structures on the other hand. Further work is underway in this laboratory to determine the kinetics of 1,2-aryl migrations of phenyl from sulfur to carbon and to detect the intermediacy (if any), of 9-S-3 sulfur-centered radicals involved in radical displacement reactions at sulfur.

Acknowledgment

This work was supported by the Office of Basic Energy Sciences, U.S. Department of Energy, under Contract De-AC06-76RLO 1830.

References

- (a) Huang, C. B. and Stock, L. M., Prepr., Div. Fuel. Chem., Am. Chem. Soc. 1982, 27(3-4), 28.
(b) Attar, A., Fuel 1978, 57, 201.
(c) King, H.-H. and Stock, L. M., Fuel 1980, 59, 447.
(d) Yarzab, R. F., Given, P. H., Spackman, W. and Davis, A., Fuel 1980, 59, 81.
- (a) Franz, J. A. and Camaioni, D. M. Fuel 1984, 63, 990.
(b) Franz, J. A., Suleman, N. K. and Alnajjar, M. S., J. Org. Chem., in press.
(c) Benson, S. W., "Thermochemical Kinetics, 2nd Ed.," Wiley-Interscience, New York, New York, 1976.
- Pryor, W. A., Gojon, G. and Stanley, J. P., J. Am. Chem. Soc. 1978, 43, 793.
- Walling, C. and Rabinowitz, R., J. Am. Chem. Soc. 1959, 81, 1137.
- Walling, C. "Free Radicals in Solution", Wiley-Interscience, New York, New York, 1957.
- Kellogg, R. M. "Methods in Free Radical Chemistry," E. S. Huysen, Ed., Marcel Dekker, New York, NY, Vol. II, 1969.
- Tanner, D. D., Wada, N. and Brownlee, B. G., Can. J. Chem. 1973, 51, 1870.
- Poutsma, M. L., "Free Radicals", (Ed. Kochi, J.), Wiley, New York, NY, Vol. II, 1973.
- Baldwin, R. M. and Vinciguerra, S., Fuel 1983, 62, 498.
- Abdel-Baset, M. and Ratcliffe, C. T. Prepr. Div. Fuel. Chem., Am. Chem. Soc. 1979, 25, 1.
- Sondreal, E. A., Wilson, W. G. and Stenberg, V. I., Fuel 1982, 61, 925.
- Takeya, G., Pure and Appl. Chem. 1978, 50, 1099.
- Glass, H. B. and Reid, E. E., J. Am. Chem. Soc. 1929, 51, 3428.
- Oae, S. and Kawamura, S., Bull. Chem. Soc. Jap. 1963, 36, 163.
- Ritter, J. J. and Sharpe, E. D., J. Am. Chem. Soc. 1937, 59, 2351.
- Benson, S. W., Chem. Rev. 1978, 78, 23.
- Sayamoi, K. and Knight, A. R., Can. J. Chem. 1968, 46, 999.
- Pryor, W. A. "Mechanisms of Sulfur Reactions." McGraw-Hill Book Co., New York, NY, 1962.
- Kice, J. L. "Free Radicals", (Ed. Kochi, J.), Wiley, New York, NY, 1973, Vol. II, Chap. 24.
- Smisman, E. E. and Sorenson, J. R. J., J. Org. Chem. 1965, 30, 4008.
- Walling, C. and Rabinowitz, R., J. Am. Chem. Soc. 1959, 81, 1137.
- Capozzi, G., Melloni, G. and Modena, G., J. Chem. Soc. (c), 1970, 2621.
- Poutsma, M. L., Fuel 1980, 59, 335.
- Beak, P. and Sullivan, T. A., J. Am. Chem. Soc. 1982, 104, 4450.

COAL LIQUEFACTION IN A FLUOROCARBON MEDIUM. II.
KINETICS OF THE 1,2,3,4-TETRAHYDROQUINOLINE REACTION

Myron Kaufman, W. C. L. Jamison, S. Gandhi and Dennis Liotta

Department of Chemistry, Emory University, Atlanta, Georgia 30322

Introduction

Many coal liquefaction experiments involve heating coal in a medium which both reacts with the coal and simultaneously dissolves released coal fragments. One problem of this approach is that it is difficult to differentiate between physical interactions which result in solvent power and chemical reactions which disrupt the coal macromolecular network. A secondary problem of such experiments is that accurate measurements of coal conversion require considerable care in collecting all deposits adhering to the reactor walls.

We have reported that coal processed in a perfluorinated liquid medium with small amounts of additives does not dissolve, but in at least one case, that of 1,2,3,4-tetrahydroquinoline (THQ), the processed coal has considerably enhanced solubility. This increased solubility is attributed to a low temperature (200-250°C) reaction between THQ and coal. Since coal is recovered intact in these experiments, coal conversion can be measured by extraction of a fraction of the processed coal, without need for complete recovery of material from the reactor. In the present work, we present kinetic data in order to better understand the mechanism of this interesting coal transformation.

Experimental

These experiments were performed in FC-70 (3M Corp.), a mixture of perfluorinated tertiary aliphatic amines, with average molecular weight of 820 (primarily five-carbon chains), having a boiling point of 215°C. FC-70 has high solubility for gases such as H₂, but very low room temperature solubility for both polar and nonpolar organic molecules. However, at temperatures greater than 200°C, the solubility of THQ in FC-70 exceeds the concentrations employed in the present studies. (FC-70 is not recommended for coal liquefaction experiments at T > 350°C, since at these temperatures the perfluorinated liquid decomposes and polymerizes.) Experiments were performed on three very different coals with carbon contents ranging from 74-84% (MAF). Properties of these coals, as suggested by the Pennsylvania State University Coal Bank, are given in Table 1. In the present work, representative samples of these coals, as obtained from the Coal Bank, are employed without preliminary grinding, washing or sieving. Reactions are carried out in stainless steel tubing bombs (15 cm x 1.3 cm o.d.). Typically the reactor contains 0.5 g of coal, 0.1 g of THQ and 12 g of FC-70. After sweeping out dissolved air, the reactor is pressurized with 8 MPa of H₂ and sealed with a high-pressure valve. The bombs are heated in a fluidized sand bath while being agitated at 300 cpm. Processed coals are compared on the basis of their pyridine solubility.

Table 1. Coal Properties

PSOC Designation	<u>1104</u>	<u>247</u>	<u>1098</u>
Moisture (%)	1.95	30.36	4.19
Ash (% on dry basis)	3.43	11.29	15.86
Volatile Matter (% MAF)	43.83	46.22	41.78
C (% MAF)	84.47	74.44	80.20
H (% MAF)	5.66	4.93	5.73
N (% MAF)	1.46	1.49	1.45
S (% MAF)	1.86	0.53	4.73
O (by difference)	6.48	18.61	7.89

1104 - HVA bituminous coal from Elkhorn #3 Seam

247 - North Dakota lignite A from Noonan Seam

1098 - Illinois #6 coal

After an 8-12 hour Soxhlet extraction with acetone, the processed coals contain only 3-4% retained THQ (from nitrogen analysis). The light color of the acetone extract indicates that very little of the coal is removed in this step. Pyridine extraction was for a minimum of 8 hours in a micro-Soxhlet apparatus, followed by two-hour extractions with benzene and acetone, a procedure found necessary to remove adhered pyridine from the coal.¹⁻³ All weighings were done after an 8-hour vacuum drying at 110°C followed by equilibration with CaSO₄ in a desiccator.

Results

Coal heated at 250°C in FC-70 with low concentrations of THQ visually appears the same as untreated coal. After the coal particles settle, the FC-70 is transparent and uncolored. It is found, however, that the pyridine solubility of treated coal is increased substantially over its original value. As shown in Figure 1, the conversions of the three very different coals all asymptotically approach 33-35% in long (18 hour) runs, with no evidence of char formation, as indicated by decreased conversion at long time. The pyridine solubilities of the unprocessed coals are included as the t=0 points on these curves. To within the scatter of the data, the plots of $\log(C(\infty) - C(t))$ vs time, shown in Figure 2, are straight lines, in agreement with first-order approach to the ultimate conversions obtainable in these experiments. The least-squares slopes and correlation coefficients of these lines are: $-.62\text{hr}^{-1}$, $-.98$ (1104), $-.77\text{hr}^{-1}$, $-.99$ (247), and $-.57\text{hr}^{-1}$, $-.95$ (1098). These slopes are reasonably close. However, the lignitic coal (247) has very low unprocessed solubility, and undergoes a rapid initial increase in conversion to a value similar to those of the other two coals. If the unprocessed conversion of PSOC 247 coal is not included in the least-squares analysis,¹ the slope of its approach to ultimate solubility is even closer ($-.70\text{hr}^{-1}$, $-.999$) to the slopes for the other two coals.

Discussion

Most coal liquefaction studies emphasize variations in behavior between different coals. In this work we have demonstrated a mode of processing in which three very different coals approach almost identical ultimate conversions

at similar rates. The range of first-order rate constants for the three coals is 30% of their mean value. However, if the unprocessed value ($t = 0$) is not included in calculating the rate for the lignitic coal (PSOC-247), the range is only 20%. We have previously noted,¹ that it is relatively easy to induce small increases in the conversion of PSOC-247, perhaps because it is initially only 4% soluble in pyridine. For example, unlike a bituminous coal, the conversion of PSOC-247 increased 8% when quinoline rather than THQ is used in our experiment. Thus, it is likely that after an initial very rapid increase in conversion of PSOC-247, its approach to ultimate solubility is at a rate very close to that of the higher rank coals. These kinetics appear to be representative of a chemical reaction rather than of mass transport, since there is very little change in the rate of coal conversion when a fine sieved fraction of the coals is processed. (PSOC-1104, 100-200 μ particles, compared to the as-received coal, which has > 50% of its mass in particles larger than 400 μ .)

There are a number of reasons for preferring a mechanism for these observations that is based on breaking chemical bonds in the coal macromolecular network, rather than one based on physical effects, such as swelling due to relaxation of hydrogen bonds. First, physical effects are generally reversible,⁴ and we measure coal conversion after almost all the THQ is removed by 12-hour acetone extraction and the acetone is removed by drying at 110°C, a procedure which should allow reformation of hydrogen bonds. Second, when shorter acetone washes are employed, leaving ca. twice as much THQ on the coal, very similar results are obtained,⁵ whereas additional hydrogen-bond rupture would be anticipated with more adsorbed THQ. Third, using the strong bases triethylamine and ethylenediamine in place of THQ produces less than 5% increase in conversion (bituminous coals for 4½ hours). Ethylenediamine is a particularly good low-temperature solvent for coal,^{3,6} and would be expected to be effective in a purely physical mechanism. Last, NMR spectra of the evaporated acetone wash show considerable conversion of THQ to quinoline in these experiments. Without H₂ for reformation of THQ, conversions are somewhat reduced.¹ Although probably only a small fraction of the hydrogen transferred from THQ breaks bonds in the coal macromolecule, observation of THQ conversion is consistent with the chemical reaction mechanism. These four points provide a strong argument for a low temperature reaction between THQ and the macromolecular network of a variety of coals and offer an explanation for the unique efficacy of THQ as a coal liquefaction medium.

Although dehydrogenation of THQ is observed in this work, tetralin, another potent hydrogen donor, does not increase coal solubility in similar experiments. Thus, neither basicity nor hydrogen donor ability alone is sufficient for the liquefaction reaction, and it appears that the proximity of a lone pair of electrons to a labile hydrogen is necessary. There are model compounds, such as diphenyl disulfide, which are related to weak bonds in proposed coal structures,⁷ and react with THQ at 250°C. It is not yet known, however, which of these reactions satisfy the other criteria (kinetics, selectivity against tetralin, etc.) necessary to explain the results of our experiments. Experiments are continuing to further explore the parameters of this process and to find a mechanism to describe it.

Acknowledgment

This work has been supported by the U. S. Department of Energy under contract DE-FG22-82PC50785. A grant from the Emory University Research Committee is also acknowledged. Provision of perfluorocarbon materials by 3M Corporation is greatly appreciated.

References

1. Kaufman, M., Jamison, W. C. L. and Liotta, D., Fuel 65, 148 (1986).
2. Derbyshire, F. J., Odoerfer, G. A. and Whitehurst, D. D., Fuel 63, 56 (1984).
3. Collins, C. J., Hagaman, E. W., Jones, R. M. and Vernon, F. R., Fuel 60, 359 (1981).
4. Brenner, D., Nature 306, 772 (1983).
5. Dryden, I. G. C., Fuel 30, 39 (1951).
6. VanBodegom, B., vanVeen, J. A. R., vanKessel, G. M. M., Sinnige-Nijssen, M. W. A. and Stuiiver, H. C. M., Fuel 64, 59 (1985).
7. Whitehurst, D. D., Mitchel, T. O. and Farcașiu, M., Coal Liquefaction, Academic Press (1980) p. 22.

Figure 1. Coal Conversion with THQ in FC-70

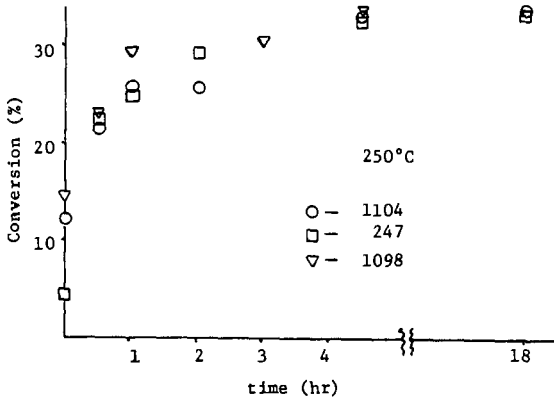
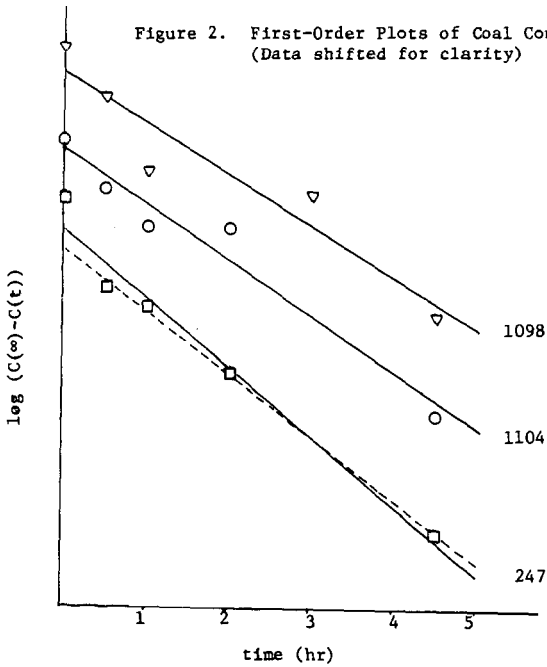


Figure 2. First-Order Plots of Coal Conversion (Data shifted for clarity)



LIQUEFACTION CO-PROCESSING OF COAL AND SHALE OIL

R. L. Miller

Chemical Engineering Department
University of Wyoming
Laramie, Wyoming 82071

ABSTRACT

Results are reported for a series of experiments in which Wyodak subbituminous coal and shale oil derived from medium grade Colorado shale were co-processed at typical coal liquefaction reaction conditions. Distillate yields in excess of 60 wt% MAF coal with corresponding hydrogen consumption values of less than 2.8 wt% MAF coal were obtained in a once-through process configuration. Encouraging results were also obtained from low severity experiments using CO/H₂O rather than H₂ as reducing agent. Prehydrotreatment of the shale oil, feed coal reactivity, and use of a disposable catalyst were shown to affect process performance.

INTRODUCTION

A number of studies have been reported in which coal and non-coal-derived heavy solvents were simultaneously converted to more valuable distillable liquid products (1 - 6). This type of once-through process, known as co-processing or liquefaction co-processing, has several potential advantages over conventional direct liquefaction:

- Two low grade feeds are converted to higher quality liquid products.
- Recycle solvent requirements are reduced or eliminated resulting in lower capital investment and operating costs.
- Existing petroleum refinery capacity can be utilized with minimal process modification.

However, liquefaction co-processing does suffer from a number of technical problems which must be solved before commercial development can proceed. Most non-coal-derived heavy oils derived from petroleum, oil shale, or tar sands are less aromatic than coal-derived liquids, and, not surprisingly, have been shown to be rather poor coal dissolution solvents. Typically, very severe thermal reaction conditions and/or use of expensive heterogeneous catalysts are utilized during co-processing to obtain sufficiently high levels of coal conversion. This generally results in excessive hydrogen consumption and cracking of distillable liquids to gases.

An alternate approach to the problem of increasing coal dissolution has been employed in the present study. Results of exploratory liquefaction co-processing experiments demonstrated that selected non-coal-derived heavy oils, each with a nitrogen content in excess of about 1.2 wt%, could be used to dissolve Wyodak subbituminous coal at typical coal liquefaction reaction conditions (7). This effect was not surprising, since quinoline-type nitrogen compounds such as tetrahydroquinoline (THQ) have been shown to greatly enhance coal dissolution in model compound studies (8 - 10). Based on encouraging results from the exploratory screening runs, additional co-processing studies using promising coal/heavy oil combinations were undertaken.

The objective of this paper is to report yield and conversion results from liquefaction co-processing experiments using Wyodak subbituminous coal and shale oil

derived from medium grade Colorado shale. Runs designed to demonstrate the effects of feed coal reactivity, mild hydrotreatment of feed shale oil prior to co-processing, and use of hydrogen or carbon monoxide/water as feed gas were included in this study.

EXPERIMENTAL PROCEDURE

Wyodak subbituminous coal samples Wyo-1 and Wyo-3 were used as feed coals in the liquefaction co-processing experiments. Ultimate analyses for these samples are presented in Table I. Sampling and preparation details of the coals have been reported elsewhere (11, 12). Previous reactivity studies performed on four Wyodak subbituminous coals including Wyo-1 and Wyo-3 indicated that Wyo-3 coal was an extremely reactive coal at representative direct liquefaction reaction conditions (11, 13). The high degree of reactivity was primarily attributed to the high organic sulfur and reactive maceral (vitrinite and exinite) contents of Wyo-3 coal. Wyo-1 coal was found to be much less reactive at liquefaction reaction conditions. Coal samples were dried to less than 1.0 wt% moisture content before use in the liquefaction co-processing experiments.

Two shale oil samples were used in the liquefaction co-processing runs. Solvent A-5 was a full boiling range sample of shale oil obtained from the Western Research Institute (formerly the Laramie Energy Technology Center of the Department of Energy). This sample was produced from thermal retorting of medium grade (29 gal/ton) Colorado oil shale. Solvent A-6 was prepared by mildly hydrotreating a portion of sample A-5 in a two liter batch Autoclave Magnedrive II reactor at 650°F for one hour with an initial cold hydrogen pressure of 2000 psig. Nalco 477 cobalt molybdate catalyst was used to hydrotreat the shale oil. Catalyst samples were thermactivated at 1000°F for two hours in a muffle furnace prior to use. Approximately 0.6 wt% hydrogen was consumed by the shale oil during hydrotreating. Properties of shale oil samples A-5 and A-6 are presented in Table II. Approximately 50 wt% of the nitrogen in these samples existed in quinoline-type or hydroquinoline-type molecular structures.

Iron oxide provided by the Kerr-McGee Corporation and carbon disulfide were used as disposable catalysts in some co-processing runs using hydrogen as feed gas. Each of these materials was added to the reaction mixture in an amount equal to 5 wt% of the dry feed coal. Iron sulfate (5 wt% MF feed coal) was used as catalyst in selected CO/H₂O experiments.

The liquefaction co-processing experiments were carried out in a 60 cm³ stirred microautoclave reactor system designed and constructed at the University of Wyoming. The reactor was similar to larger Autoclave batch reactors except that heating was accomplished with an external high temperature furnace. At the end of each run, the reactor and its contents were quenched with an icewater batch. This reactor system provided the benefits of small tubing bomb reactors [quick heatup (~2 min. from room temperature to 850°F) and cooldown (~30 sec. back to room temperature)], while at the same time insuring sufficient mechanical agitation of the reactants with an Autoclave Magnedrive II stirring assembly to minimize hydrogen mass transfer effects. The system was also designed so that the reactor pressure was very nearly constant throughout an experiment. Two iron-constantan thermocouples attached to a Fluke 2175A digital thermometer were used for temperature measurements. One thermocouple measured the temperature of the reactor contents, while the other measured the temperature of the reactor wall. Reactor pressure was monitored using a 0 - 5000 psi Marsh pressure gauge.

A majority of the liquefaction co-processing runs were completed at representative coal liquefaction reaction conditions: 825°F reaction temperature, 2000 psig initial cold hydrogen pressure, and 30 or 60 minutes reaction time. Some preliminary experiments were also completed at more mild reaction conditions using carbon

monoxide and water rather than hydrogen as the reducing agent. In these runs, hydrogen was produced from CO and H₂O via the water gas shift reaction. The CO/H₂O runs were completed at 600°F reaction temperature, 1500 psig initial cold carbon monoxide pressure, and 30 minutes reaction time. Distilled water in an amount equal to 50 wt% of the dry feed coal was added to runs using a carbon monoxide atmosphere.

Gaseous products were analyzed using gas chromatography. Water and distillate yields were measured by distilling portions of the combined liquid-solid product mixture to an 850°F endpoint in a microdistillation apparatus. Additional portions of the liquid-solid product mixture were extracted in a Soxhlet extraction apparatus using cyclohexane, toluene, and pyridine. Details of the experimental procedures used in this work have been reported (7).

RESULTS AND DISCUSSION

Using data collected with the analytical procedures described, detailed yield and conversion results were computed for each liquefaction co-processing run. Details of the computational methods used in this study have been described previously (7). For purposes of the present discussion, process performance will be monitored using the following three parameters: C₄-850°F distillate yield (wt% MAF coal basis), hydrogen utilization efficiency, and pyridine conversion (wt% MAF basis). Hydrogen utilization efficiency is defined as the mass of C₄-850°F distillate produced per unit mass of hydrogen consumed. The value of this parameter provides a good indication of the overall efficiency of hydrogen consumed in the co-processing experiments. Pyridine conversion is defined as a measure of the extent of conversion of all feeds (coal and non-coal-derived heavy oil) to pyridine soluble products. However, since both A-5 and A-6 shale oil samples were completely soluble in pyridine, the pyridine conversion values reported in this paper are direct measures of the extent of coal conversion in the co-processing runs.

Effect of Shale Oil Prehydro-treatment

The results from liquefaction co-processing experiments using Wyo-3 coal and A-5 or A-6 shale oil at 825°F and 2000 psig initial cold hydrogen pressure are shown in Figures 1 - 3. It is apparent from this data that mild prehydro-treatment of the shale oil prior to co-processing greatly enhances process performance. Distillate yields of 55 - 60 wt%, hydrogen utilization efficiencies of about 20, and pyridine coal conversion values of 68 - 85 wt% were obtained using Wyo-3 coal and A-6 shale oil. Similar enhancement effects were seen using Wyo-1 feed coal. Previous co-processing studies by Kerr-McGee using Ohio No. 5 bituminous coal and Canadian Cold Lake bitumen also demonstrated the beneficial effect of heavy oil hydro-treatment prior to co-processing (14).

At least two possible reasons exist for the effects shown in Figures 1 - 3. First, mildly hydro-treated A-6 shale oil acted as a more powerful hydrogen donor solvent than A-5 in promoting coal conversion and distillate production. Secondly, the quinoline-type nitrogen content of A-5 was approximately 0.7 wt%. Mild hydro-treatment of A-5 presumably converted a number of the quinoline structures to hydroquinoline structures. As mentioned earlier in this paper, hydroquinolines such as tetrahydroquinoline (THQ) have been shown to actively promote coal solvation in direct liquefaction. The data shown in Figures 1 - 3 suggest that a similar effect occurred during liquefaction co-processing with A-6 shale oil.

Effect of Feed Coal Reactivity

Figure 4 presents a comparison of yield results for co-processing runs using Wyo-1 and Wyo-3 coal. These data show that liquefaction co-processing performance is a strong function of feed coal reactivity as measured by the extent of dissolution to

pyridine solubles and distillate production. As shown in Figure 5, the detrimental effects of low feed coal reactivity can be partially offset by use of a disposable catalyst such as iron oxide/carbon disulfide.

Liquefaction Co-Processing Using Carbon Monoxide and Water

Several previous studies have reported the successful liquefaction of low rank coal at mild reaction conditions using carbon monoxide and water in place of hydrogen gas (5, 15, 16). In these runs, hydrogen was provided by the water gas shift (WGS) reaction involving carbon monoxide and water. In the aqueous phase, a number of catalysts such as alkali metal salts, alkaline earth salts, and organic nitrogen bases have been shown to catalyze the WGS reaction (17).

Hypothesizing that the high basic nitrogen content of A-6 shale oil would also catalyze the WGS reaction, several preliminary liquefaction co-processing experiments using Wyo-3 coal, A-6 shale oil, and CO/H₂O were completed. As shown in Figure 6, significant conversion of coal and 850°F⁺ shale oil to distillate liquids was obtained, even though the reaction conditions were very mild. Use of iron sulfate as a disposable catalyst provided some improvement in yield structure and coal conversion. Based on these encouraging results, a more extensive study of liquefaction co-processing using carbon monoxide and water is underway.

CONCLUSIONS

A series of liquefaction co-processing experiments has been completed using two Wyodak subbituminous coals and two shale oil feeds. Both hydrogen and carbon monoxide/water were evaluated as reducing agents. Results indicated that prehydro-treatment of the shale oil, feed coal reactivity, and to some extent, use of a disposable catalyst all affect process performance. Sample A-6 was found to be an attractive feedstock for liquefaction co-processing. Distillate yields in excess of 60 wt% MAF coal were obtained using Wyo-3 coal and A-6 shale oil at typical coal liquefaction conditions. Encouraging results were also obtained using CO/H₂O at much more mild reaction conditions.

ACKNOWLEDGEMENTS

Financial support for this research was provided by the Electric Power Research Institute under Contract Number RP 2383-01. Mr. Conrad Kulik of EPRI provided helpful comments.

REFERENCES

1. Yan, T.Y., and Espenscheid, W.F., *Fuel Proc. Tech.*, 7, 121, (1983).
2. Shinn, J.H., Dahlberg, A.J., Kuehler, C.W., and Rosenthal, J.W., "The Chevron Co-Refining Process," Proceedings of the Ninth Annual EPRI Contractors' Conference on Coal Liquefaction, Palo Alto, California, (May 1984).
3. Kelly, J.F., Fouda, S.A., Rahimi, P., and Ikura, M., "CANMET Coprocessing: A Status Report," CANMET Coal Conversion Contractors' Review Meeting, Calgary, Alberta, Canada, (November 1984).
4. Curtis, C.W., Guin, J.A., Pass, M., and Tsai, K.J., *ACS Fuel Chem. Preprints*, 29, 5, 155, (1984).
5. Ignasiak, B., Kovacik, G., Ohuchi, T., Lewkowicz, L., and duPlessis, M.P., "Two-Stage Liquefaction of Subbituminous Alberta Coals in Non-Donor Solvents," CANMET Coal Conversion Contractors' Review Meeting, Calgary, Alberta, Canada, (November 1984).

6. Miller, R.L., "Use of Non-Coal-Derived Heavy Solvents in Direct Coal Liquefaction," Proceedings of the Tenth Annual EPRI Contractors' Conference on Coal Liquefaction, Palo Alto, California, (April 1985).
7. Miller, R.L., "Use of Non-Coal-Derived Heavy Solvents in Direct Coal Liquefaction," Interim Report for EPRI Project RP 2383-01, (November 1985).
8. Atherton, L.F., and Kulik, C.J., "Advanced Coal Liquefaction," presented at the 1982 AIChE Annual Meeting, Los Angeles, California, (November 1982).
9. McNeil, R.I., Young, D.C., and Cronauer, D.C., Fuel, 62, 806, 1983.
10. Broderick, T.E., "Liquefaction of Wyodak Coal in Tetrahydroquinoline," M.S. Thesis, University of Wyoming, Laramie, Wyoming, (1984).
11. Miller, R.L., "Effect of Wyodak (Wyoming) Coal Properties on Direct Liquefaction Reactivity," Ph.D. Dissertation, Colorado School of Mines, Golden, Colorado, (1982).
12. Silver, H.F., Corry, R.G., and Miller, R.L., "Coal Liquefaction Studies," Final Report for EPRI Projects RP 779-23 and RP 2210-1, (December 1982).
13. Miller, R.L., and Baldwin, R.M., Fuel, 64, 1235, (1985).
14. Rhodes, D.E., "Comparison of Coal and Bitumen-Coal Process Configurations," Proceedings of the Tenth Annual EPRI Contractors' Conference on Coal Liquefaction, Palo Alto, California, (April 1985).
15. Ross, D.S., Blessing, J.E., Nguyen, Q.C., and Hum, G.P., Fuel, 63, 1206, (1984).
16. Hodges, S., and Creasy, D.E., Fuel, 64, 1229, (1985).
17. Elliott, D.C., and Sealock, L.J., I & EC Proc. Des. Dev., 22, 426, (1983).

Table I
Ultimate Analysis of Wyodak Subbituminous Coal Samples

Sample	<u>Wyo-1</u>	<u>Wyo-3</u>
Ultimate Analysis, wt% dry basis		
Carbon	69.8	58.2
Hydrogen	4.7	4.3
Nitrogen	0.8	0.8
Sulfur	0.3	2.9
Sulfate	0.0	0.8
Pyrite	0.0	0.9
Organic	0.3	1.2
Oxygen (difference)	18.3	13.9
Ash	6.1	19.9

Table II
Properties of Shale Oil Samples

Sample	<u>A-5</u>	<u>A-6</u>
Wt% Distilled		
Water	0.7	0.1
350°F	4.2	10.3
350°-500°F	9.6	18.3
500°-650°F	18.8	22.5
650°-850°F	39.0	29.8
850°F+	27.7	19.0
Ultimate Analysis, wt% dry basis		
Carbon	83.3	84.7
Hydrogen	12.1	12.9
Nitrogen	1.4	1.2
Sulfur	0.5	0.4
Oxygen (difference)	2.7	0.8
Ash	0.0	0.0

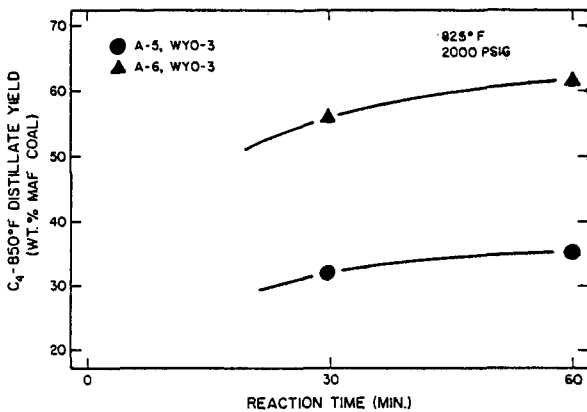


Figure 1. Distillate Yield as a Function of Reaction Time and Shale Oil Feed

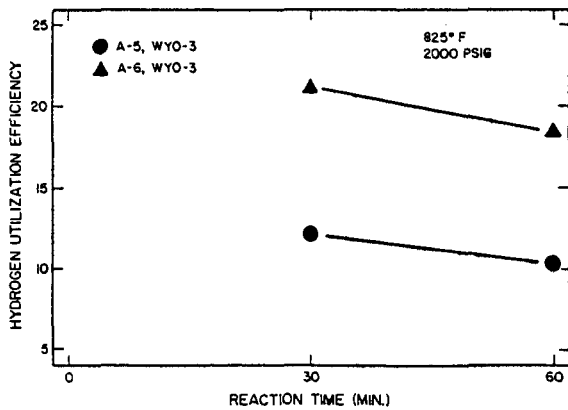


Figure 2. Hydrogen Utilization Efficiency as a Function of Reaction Time and Shale Oil Feed

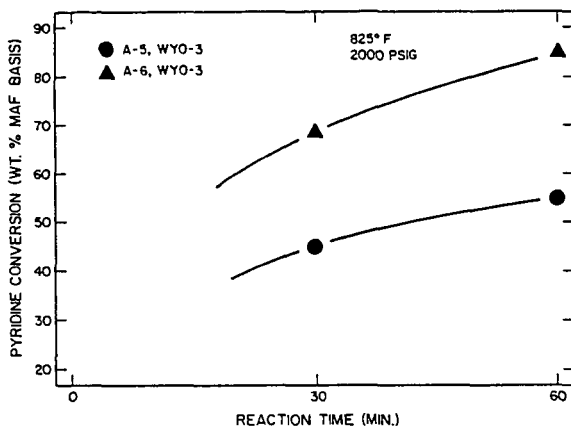


Figure 3. Pyridine Conversion as a Function of Reaction Time and Shale Oil Feed

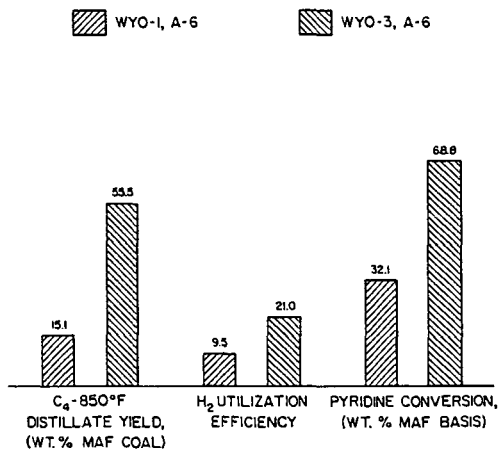


Figure 4. Effect of Feed Coal Reactivity on Process Performance (Reaction Conditions: 825°F, 2000 psig H₂, 30 min.)

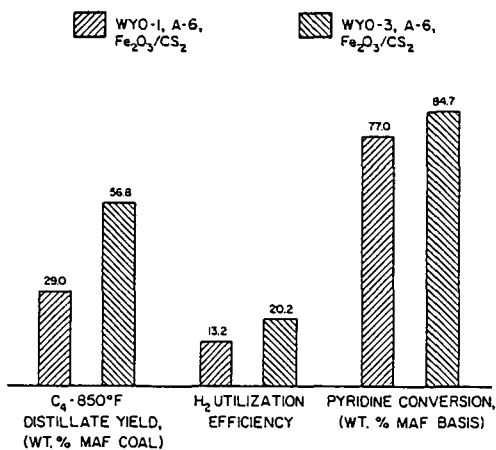


Figure 5. Effect of Feed Coal Reactivity on Process Performance (Reaction Conditions: 825°F, 2000 psig H₂, 30 min., Fe₂O₃/CS₂ Catalyst)

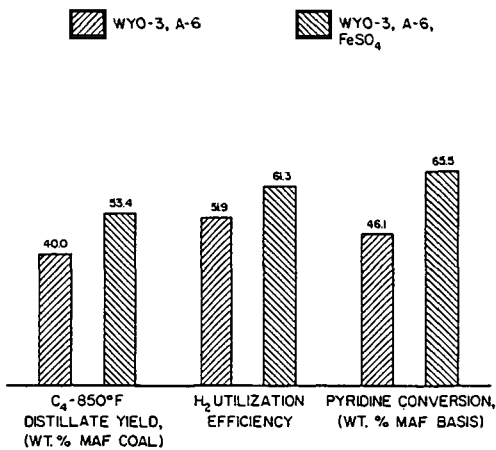


Figure 6. Liquefaction Co-Processing Yield Results using Carbon Monoxide/Water (Reaction Conditions: 600°F, 1500 psig CO, 30 min.)

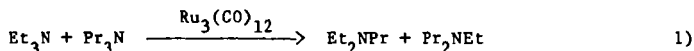
NEW CATALYSTS FOR HYDROTREATING COAL LIQUIDS

A. S. Hirschon, R. B. Wilson, Jr. and R. M. Laine*

SRI International, Menlo Park, CA 94025

The cost of hydrotreating coal liquids or heavy crudes is considerably higher than for light crudes because of the significantly higher amounts of sulfur, nitrogen and oxygen found in these hydrocarbon sources relative to light crudes. In particular, the current processes for the catalytic removal of nitrogen (HDN) and oxygen (HDO) consume excessive amounts of hydrogen due to concurrent hydrogenation of aromatics. The ideal HDN or HDO catalyst would be one that selectively cleaves C-N or C-O bonds with minimum consumption of hydrogen. This would reduce the overall hydrotreating costs for refining crude oil and could make synfuels a competitive energy source.

In this paper, we discuss the results of two approaches to the development of improved HDN catalysts. One approach focuses on the synthesis of high-activity, highly dispersed, "surface confined", catalysts using organometallic complexes. The other approach examines the hydrotreating activities of metals not currently used in HDN and HDO catalysis. This latter investigation arises as a consequence of our efforts to develop mechanistic models of HDN through studies of the homogeneous catalysis of the transalkylation reaction, (1,2) equation 1,



and through studies of quinoline HDN by bulk metals (3). In both the trans-alkylation and the bulk metal studies; ruthenium exhibits the highest activity for C-N bond cleavage. This suggests that it may be useful as an HDN catalyst.

We describe here the synthesis and HDN activities of catalysts prepared according to the principles established by these two separate approaches.

Experimental

Materials

The CoMo catalyst (HT-400, 3 wt% CoO, 15.1 wt% MoO₃, on Al₂O₃) was donated by Harshaw Chemical Company. The preparation of the sulfided catalyst has been described previously.⁴ γ-aluminum oxide was donated by Kaiser Aluminum and was made from Gibbsite (surface area = 210 m²/g and passed 400 mesh sieve.) The aluminum oxide was calcined at 400°C for 2h under flowing synthetic air. Ruthenium was obtained from Strem Chemical, and was heated at 400°C for 12 h first with flowing synthetic air to remove any surface sulfur, and then with flowing hydrogen to form the reduced metal. Ruthenium carbonyl [Ru₃(CO)₁₂] and nickel cyclooctadiene [Ni(COD)₂] were obtained from Strem Chemicals and used as received. Molybdenum(II) allyl dimer was prepared by modifying the method of Cotton and Pipal (5).

Preparation of a Conventional NiMo Catalyst

Ammonium molybdate tetrahydrate (2.10 g, 1.7 mol) and nickel nitrate hexahydrate (1.34 g, 4.6 mmol) were dissolved in 200 mL of water. Alumina, 10 g, was added to the metal salt solution and stirred for 24 h. The water was evaporated from the mixture, and the residue was slowly heated to 400 C under flowing synthetic air over a 2-h period. The heating was continued for 12 h. The process was repeated for another 12 h with flowing H₂S (10%)/H₂.

Preparation of Supported Organometallic Catalysts

Molybdenum Supported on Alumina. Molybdenum allyl dimer (1.0 g) dissolved in 10 mL of hexane was slowly added to a stirred slurry of 10 g of alumina in 20 mL of hexane. The mixture was stirred overnight, then washed with 20 mL of hexane to give a gray solid. The product was then heated at 200 C in flowing H₂S (10%)/H₂ for 12 h.

Bimetallic Metal Supported Catalysts. An aliquot (1 g) of the sulfided supported molybdenum catalyst was suspended in 10 mL of hexane. The desired amount of Ni (as Ni(COD)₂) in THF was added to the suspension and the mixture stirred overnight, washed with hexane, dried, and sulfided at 200 C as described above.

Ruthenium doped CoMo Catalyst (RuCoMo). Under nitrogen, ruthenium carbonyl (0.053 g), dissolved in 5 mL of hexane, was added to a stirred slurry of 2.00 g of the sulfided CoMo catalyst in 10 mL of hexane. The mixture was allowed to stir for 72 h. The hexane was then evaporated and the residue heated under vacuum at 76°C for 6 h. A portion of the doped catalyst was sulfided by treating with a flowing mixture of H₂S(10%)/H₂ at 200°C for 12 h.

Standard HDN Reaction Procedures

The following materials were placed in a quartz liner, under nitrogen in a 45-mL Parr bomb: the catalyst (0.100 to .250 g), a stirbar, and 10 mL of 0.197 M quinoline (0.151 M THQ for Ru reactions) and 0.098 M n-dodecane (as internal standard) in n-hexadecane. The bomb was pressurized with 500 psia of H₂, and heated at the desired temperature.

Results and Discussion

The HDN activities of the catalysts prepared by the various synthetic techniques were compared using a quinoline/hexadecane solution for model studies. As shown in Figure 1, quinoline HDN leads to two major HDN products; propylcyclohexane (PCH) and propylbenzene (PB). In comparing the catalytic properties of the various catalysts, we use two criteria, rate of HDN and, as discussed above, hydrogen consumption. The production of PCH requires 7 moles of H₂ per quinoline and typifies aromatic hydrogenation, whereas the production of PB requires only 3 moles; thus the relative ratios of PCH to PB are an excellent measure of hydrogen consumption.

Comparison of Conventional NiMo and Organometallic Origin NiMo Catalysts

Table 1 lists the estimated turnover frequencies (TF = moles THQ reacted/mole of metal catalyst/hour ± 10%) for THQ disappearance, and the appearance of PCH, PCHE, and PB, calculated based on initial rates. From this data we see that the organometallic origin or surface confined NiMo catalysts exhibit higher hydrogenation activity than a conventionally prepared NiMo catalyst. In a similar manner and from Figures 2a-c, it can be seen that the surface confined catalysts are superior in terms of C-N bond cleavage activity.

The total metal content in the catalysts is approximately the same, so that the activity and selectivity of these catalysts can qualitatively be compared. Figure 3 presents calculations of the total hydrocarbon conversion as a sum of PCH, PB and propylcyclohexene (PCHE) as a function of time.

To compare the relative PCH, PCHE and PB selectivities for the various catalysts, the relative distributions of these products, normalized to 5% total hydrocarbon conversion, were extracted from Figure 3 and are listed in Table 2. We see, in Table 2, that the product selectivities for the NiMo catalyst of organo-

metallic origin (surface confined catalyst) are essentially the same as those found with the conventionally prepared NiMo catalyst.

Table 1
TURNOVER FREQUENCIES^a

Catalyst	THQ	PCH	PB	PCHE
NiMo (conventional)	67.4	8.2	0.3	1.4
NiMo (0.83, 2.63)	111	26.5	1.4	--
NiMo (0.37, 2.81)	104	16.6	0.7	1.7
CoMo	54.0	8.9	0.5	0.8
RuCoMo	141	26.9	8.0	0

^aMoles product/moles metal catalyst/h.

Table 2
HYDROCARBON DISTRIBUTION AT 5 mol%
HDN CONVERSION^a

Catalyst	%PCH	%PB	%PCHE
NiMo (conventional)	76.2	5.2	18.6
NiMo (0.37% Ni, 2.81% Mo)	81.4	3.1	15.5
NiMo (0.83% Ni, 2.63% Mo)	76.0	5.0	19.0
CoMo	82.2	4.6	13.2
RuCoMo	76.6	23.4	0

^aReaction of 10 mL 0.197 M quinoline in n-hexadecane and catalyst at 350°C and 500 psig H₂.

Bulk Ruthenium HDN Catalysis

Figure 4 shows the product distribution from the reaction of bulk ruthenium with THQ at 200, 250 and 300°C. These results demonstrate ruthenium's high activity for C-N bond cleavage even at temperatures of 200°C. At 200 and 250°C the major HDN products are propyl- or ethyl- and methyl-cyclohexylamine, but at 300°C almost no nitrogen containing species remain after 3 hours of reaction time due to extensive

C-N and C-C bond hydrogenolysis. If the bulk ruthenium is exposed to sulfur in the form of CS₂ (20 µl to the standard reaction), then even at temperatures up to 350°C, no reaction of any type is observed. Thus, sulfur poisons bulk ruthenium's ability to catalyze both hydrogenation and C-N bond cleavage.

Ruthenium-Doped Harshaw CoMo Catalysts

In an attempt to overcome the difficulty of sulfur poisoning with the ruthenium, we doped a commercial CoMo catalyst with a ruthenium containing organometallic. Figure 5a and b show the product distribution after reaction with a sulfided Harshaw CoMo catalyst and the same catalyst doped with ruthenium. As seen in these figures, the doped catalyst is significantly more active, produces no PCHE, and gives a much higher ratio of propylbenzene to propylcyclohexane than does the "unpromoted" CoMo catalyst. As shown in Figure 3, the total hydrocarbon production is greater for the ruthenium-"promoted" catalyst than any of the other catalysts studied. This catalyst, as shown in Table 2, also produces the most propylbenzene of any of the catalysts studied. For instance, after 5% conversion, the fraction of propylbenzene in the hydrocarbon products has increased from 4.6% for the CoMo catalyst to 23.4% for the RuCoMo catalyst. Furthermore, when this catalyst was treated with carbon disulfide, as was the bulk ruthenium, the catalyst was even more active towards HDN activity.

Conclusions

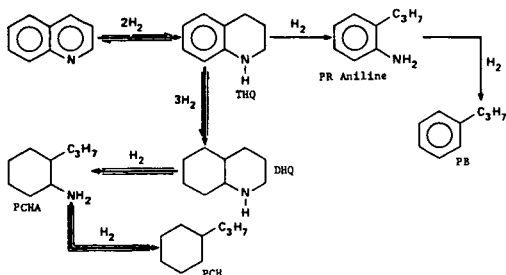
We have shown that the activity of HDN catalysts using conventional metals, such as nickel and molybdenum can be improved using organometallic precursors; although, in our hands, the selectivity of aromatic and aliphatic hydrocarbon products remained unchanged from that of conventional based catalysts. However, through the use of more active metals such as ruthenium, we can promote a conventional type catalyst to give a catalyst which is not only more active, but is more selective towards aromatic products, and remains sulfur tolerant.

Acknowledgements:

We would like to thank the Department of Energy, Pittsburgh Energy and Technology Center for support of this work through grants DE-FG22-83PC60781 and DE-FG-85PC80906. We would also like to thank NSF for partial support of this work through grant CHE 82-19541.

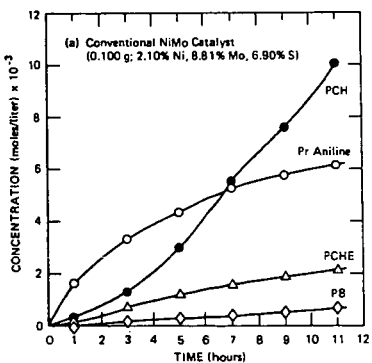
References

1. R. B. Wilson Jr. and R. M. Laine, J. Am. Chem. Soc. (1985) 107, 361-369.
2. R. M. Laine, D. W. Thomas, L. W. Cary, J. Am. Chem. Soc. (1982) 104, 1763.
3. A. S. Hirschon and R. M. Laine, manuscript in preparation.
4. A. S. Hirschon and R. M. Laine, Fuel (1985) 64, 868-870.



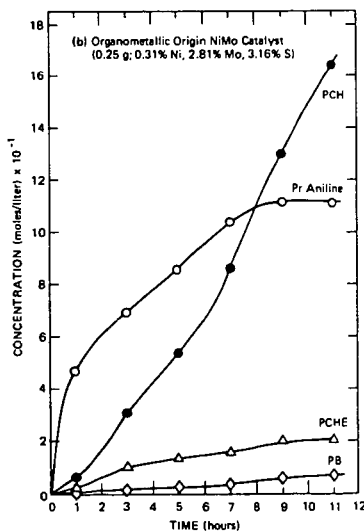
JA-6762-1

FIGURE 1 QUINOLINE HDN REACTION NETWORK



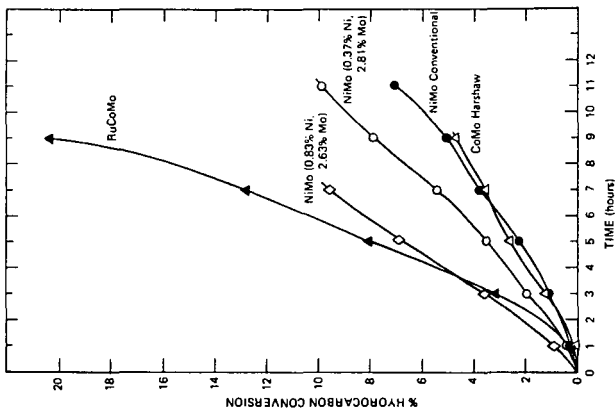
JA-6762-18A

FIGURE 2a PRODUCT DISTRIBUTION DUE TO CARBON-NITROGEN CLEAVAGE REACTIONS
10 mL of 0.197 M quinoline in *n*-hexadecane and sulfided NiMo catalyst at 350°C and 500 psia H₂.



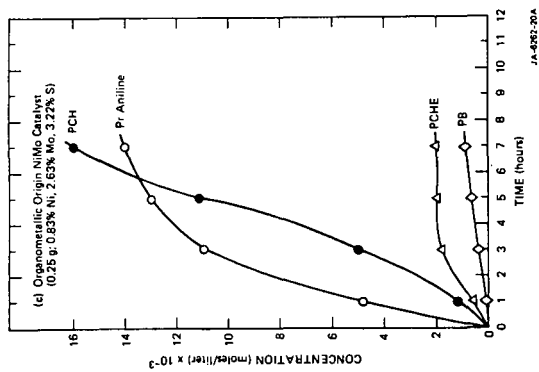
JA-6762-27A

FIGURE 2b PRODUCT DISTRIBUTION DUE TO CARBON-NITROGEN CLEAVAGE REACTIONS (Continued)
10 mL of 0.197 M quinoline in *n*-hexadecane and sulfided NiMo catalyst at 350°C and 500 psia H₂.



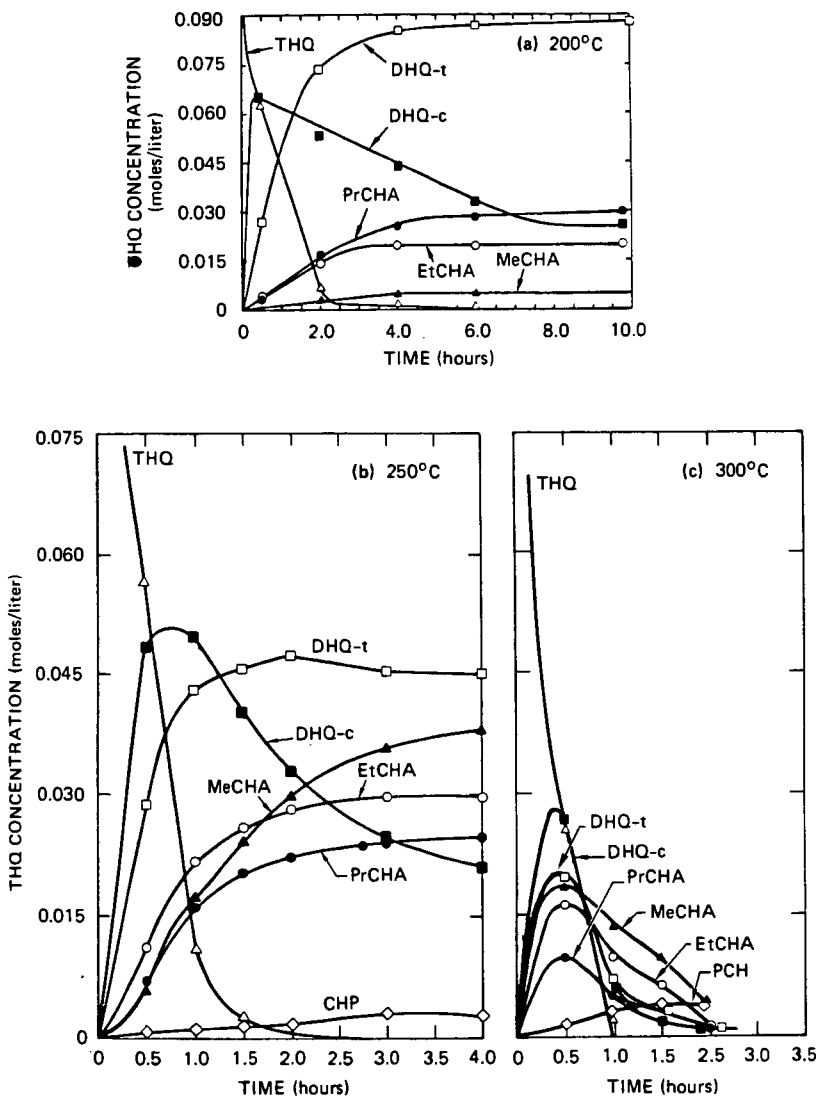
JA-4882-16

FIGURE 3 TOTAL HYDROCARBON CONVERSION



JA-4882-20A

FIGURE 2c PRODUCT DISTRIBUTION DUE TO CARBON-NITROGEN CLEAVAGE REACTIONS (Continued)
10 mL of 0.197 M quinoline in *m*-heptadecane and sulfided NiMo catalyst at 350°C and 500 psia H₂.



JA-6262-9A

FIGURE 4 PRODUCT DISTRIBUTION FROM REACTION OF THQ WITH RUTHENIUM AND 500 psi of H_2
 10 mL of 0.1506 M THQ and 0.100 g of Ru in hexadecane.

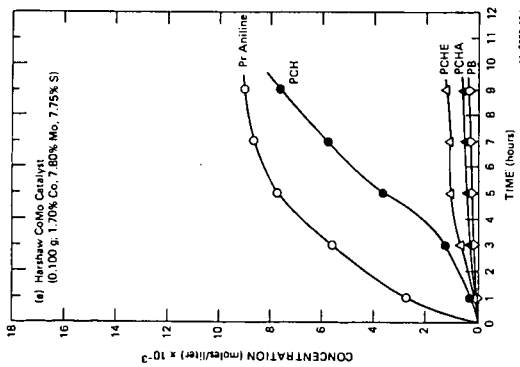


FIGURE 3a PRODUCT DISTRIBUTION DUE TO CARBON-NITROGEN CLEAVAGE REACTIONS WITH CoMo CATALYST
10 mL of 0.197 g/liter *m*-hexanamine and sulfided CoMo catalyst at 350°C and 500 psia H₂.

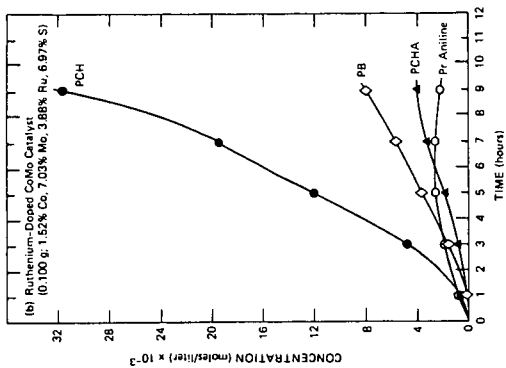


FIGURE 3b PRODUCT DISTRIBUTION DUE TO CARBON-NITROGEN CLEAVAGE REACTIONS WITH CoMo CATALYST (Continued)
10 mL of 0.197 g/liter *m*-hexanamine and Ru/CoMo catalyst at 350°C and 500 psia H₂.

FTIR SPECTROSCOPIC STUDIES OF COAL LIQUEFACTION PRODUCTS

Jack Youtcheff, Paul Painter and Peter Given

Mineral Industries Research Lab
University of Alaska
Fairbanks, Alaska 99701

AND

Materials Science Department
The Pennsylvania State University
University Park, PA 16802

Recent work in our laboratories has been concerned with obtaining a better understanding of the phenomena associated with coal liquefaction (1). An initial study of three bituminous coals discussed the changes that occur in oxygen containing functional groups (2). It was concluded that the initial large loss of so-called "unaccounted" oxygen was a result of a cleavage of ether groups to form hydroxyls, which were subsequently removed by dehydroxylation. These same samples were also characterized by FTIR and the results of this portion of the work are presented in this communication.

As might be expected, the most interesting changes occurred in the aliphatic and aromatic CH stretching regions of the spectrum. Samples were prepared for infrared analysis using established KBr pellet techniques (1,3) and representative spectra of the three coals, PSOC 521 (HVC), PSOC 767 (HVB) and PSOC 757 (HVA) are presented in figure 1. Even though the aromatic CH stretching modes between 3100 and 3000 cm^{-1} are relatively weak, it can be seen that there is still a degree of overlap that can lead to errors when band areas are determined by simple integration. Accordingly, a curve resolving procedure, described in previous publications (1,3), was used to separate the two contributions. In addition, it was found that there was a change in the relative proportion of various aliphatic CH groups. In order to sort this out second derivative methods were used to define the initial positions of five bands that were curve-fit to the difference spectrum obtained by subtracting the aromatic CH stretching modes, as illustrated in figure 2. These bands do not represent individual components, but are themselves composites (4). Nevertheless, the bands near 2956 and 2867 cm^{-1} are largely due to methyl groups, the bands near 2923 and 2852 cm^{-1} have a major contribution from methylene groups, while the band at 2893 cm^{-1} can be assigned to methine CH moieties.

Liquefaction reactions were carried out at temperatures of 350, 370, 400 and 425°C for periods of 2, 12, 22 and 32 minutes, as described previously (1,2). Overall, the spectra of the liquefaction products from a particular coal were surprisingly similar, supporting the notion that structural rearrangement under these reaction conditions is relatively limited. The integrated area of the aromatic CH stretching modes increases with the severity of the liquefaction conditions, but it should be kept in mind that to some extent this is an apparent increase that is due to the loss of oxygen containing functional groups. The pattern of out-of-plane bending modes between 900 and 700 cm^{-1} shows little change in the distribution pattern of hydrogen in aromatic units, supporting the inference that the changes in this region are largely due to the loss of other groups and hence an increase in the per unit weight concentrations of those left behind.

Although this factor also affects the aliphatic CH stretching modes, the changes in this region are far more pronounced. The overall aliphatic CH content appears to initially increase with conversion, but then drops off somewhat

at conditions of high conversion. The data, however, shows considerable scatter and such conclusions are only tentative. There are much clearer changes in individual curve-resolved bands, (measured as a fraction of total aliphatic CH area, in order to eliminate and reduce errors in sample preparation, etc.), with the most marked differences being observed in the 2956 cm^{-1} band. The relative area of this band is plotted as a function of reaction time and conversion in figures 3 and 4, respectively.

The Ohio coal (PSOC 757) showed no temperature dependence in the plot against time, in contrast to the other coals. When the 2956 cm^{-1} band is plotted as a function of conversion (figure 4), the points for all temperatures tend to lie in a single band. Visual inspection suggests that the band or line is somewhat curved. However, linear regressions were performed and gave surprisingly high variance, particularly for the Oklahoma and Wyoming coals. Nevertheless, the slopes of these least-squares fits suggest that the number or type of bonds broken during liquefaction are different for the three coals. For a slope of zero to exist in figure 4, the distribution of aliphatics in the parent coal and products would have to be the same. This would result if no chemical reactions were involved, and conversion results from the physical dissolution of the coal. An increase in this slope is indicative of an increasing number of alkyl ethers or aliphatic systems cleaved in converting a particular coal. If the increase in relative area of this band stems from methyl-generating reactions, for the Ohio coal (PSOC 757), only a few bonds need to be broken to drastically enhance its conversion.

In figure 5, the amount of "ethers" cleaved (loss of unaccounted oxygen from references 1 and 2) is plotted against the area of the 2956 cm^{-1} band as a fraction of the total area for aliphatic C-H stretching vibrations. Correlations are readily apparent for the coals having a higher number of cleavable ethers, namely the Wyoming and Ohio coals with 7.7 and 5.1 cleavable ethers per 100 carbon atoms, respectively. A least-squares linear regression was performed on the values at the three lowest temperatures for the Wyoming coal (Figure 5 (b)). The slopes and the R^2 values for this correlation between ether removal and relative area of the 2956 cm^{-1} band show a high proportion of variance explained. If the correlation is accepted, the obvious inference is that ether cleavages generate methyl groups (i.e. $-O-CH_2-$ bonds are cleaved forming OH and CH_3). It should be noted that the slopes of the least-squares fit for the lowest three temperatures are quite similar, whereas the curves for the Ohio coal (figure 5 (c)) increase more steeply with increasing temperature. For the latter case, one could infer that at the lower temperatures, labile ethers (aliphatic and benzylic) are cleaved; proceeding to higher temperatures, the more refractory type of ethers (diaryl) are likely to be cleaved. The fact that the slopes are similar for the Wyoming coal suggests that similar types of ethers are broken under these conditions. The relatively small slopes suggest that these ethers are predominantly aliphatic or aralkyl. The lack of correlation at 425°C for this coal and the poor correlation at all temperatures for the Oklahoma coal (though a trend similar to that of the Ohio coal exists) arises perhaps because any trend is marked by alkyl cleavage and other reactions that do not involve loss of unaccounted oxygen.

In conclusion, the FTIR results indicate that extensive structural rearrangements are not occurring during liquefaction. Rather, a few selected bridging units are broken, resulting in the formation of various fragments of different solubility. The increase in methyl groups and previously reported loss of ether oxygen indicates

that bonds between aliphatic methylene units, benzylic ethers and aryl alkyl ethers are the principal sites of cleavage.

References

1. Youtcheff, J. S. and Given, P. H. "The dependence of liquefaction behavior on coal characteristics" and references therein. Final Report to DOE under Contract No DE-AC22-81-PC-40784, September 1983.
2. Youtcheff, J. S. and Given, P. H. *Fuel*, 61, 980 (1982).
3. Sobkowiak, M., Reisser, E., Given, P. and Painter, P. *Fuel*, 63, 1245 (1984).
4. Painter, P. C., Starsinic, M. and Coleman, M. M. in "Fourier Transform Infrared Spectroscopy", Vol 4. (edited by J. R. Ferraro and L. J. Basile) pp 169-243 Academic Press (1985).

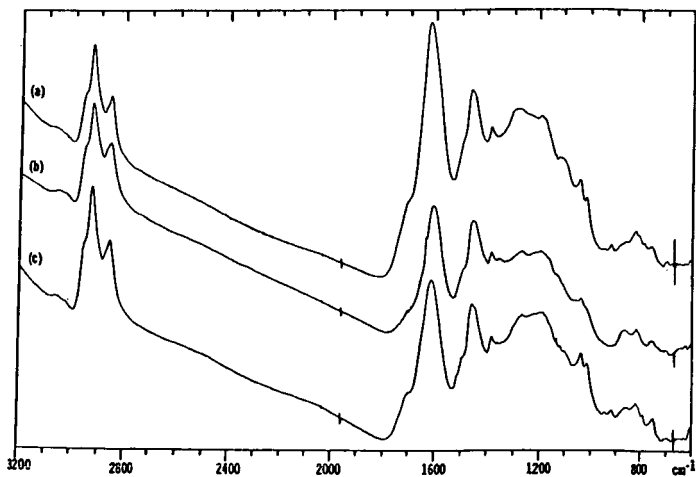


Figure 1. FTIR SPECTRA OF COALS (a) PSOC-521; (b) PSOC-767; (c) PSOC-757

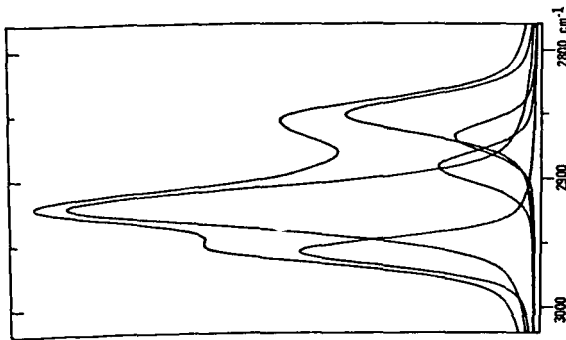


Figure 2. RESOLUTION OF THE DIFFERENCE SPECTRUM OF THE ALIPHATIC C-H STRETCH REGION INTO INDIVIDUAL BANDS (envelope synthesized by co-adding individual bands is superimposed)

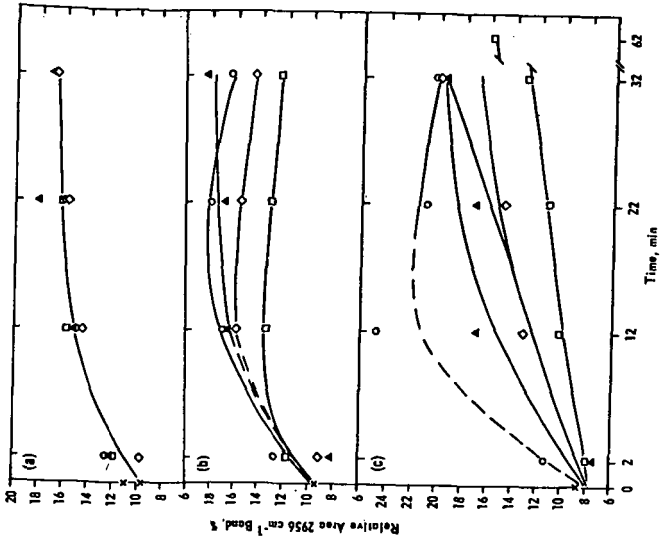


Figure 3. CHANGE IN RELATIVE AREA OF 2956 cm^{-1} BAND FOR COAL AS A FUNCTION OF TIME (a) PSOC-757; (b) PSOC-767 (c) PSOC-521
 o 425°C Δ 400°C \square 370°C 350°C

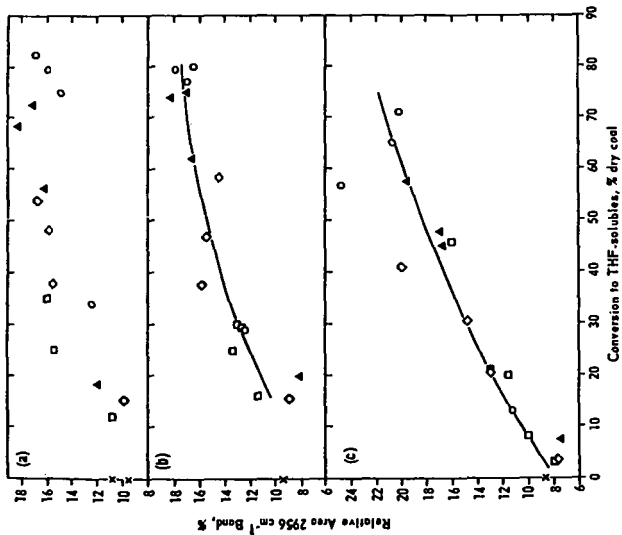


Figure 4. CHANGE IN RELATIVE AREA OF 2956 cm^{-1} BAND FOR COALS AS A FUNCTION OF CONVERSION TO THF-solubles, % dry coal
 (a) PSOC-757; (b) PSOC-767 (c) PSOC-521
 o 425°C 400°C 370°C 350°C

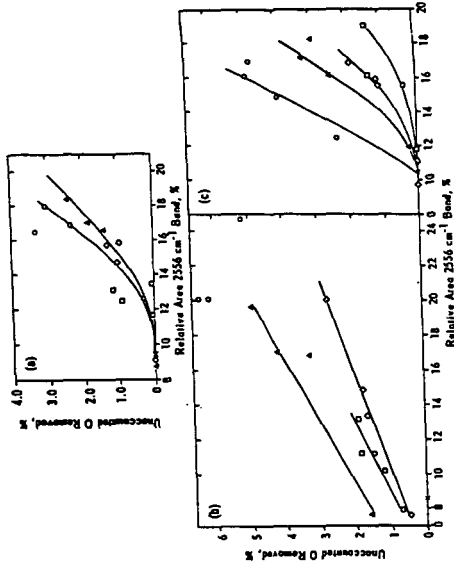


Figure 5. RELATION OF UNACCOUNTED O_1 REMOVED TO THE RELATIVE AREA OF 2956 cm^{-1} BAND
 (a) PSOC-767; (b) PSOC-521; (c) PSOC-757
 o 425°C 400°C 370°C 350°C

PHYSICAL BENEFICIATION OF CHAR AND CHEMICALLY CONDITIONED COAL

Robert P. Warzinski and Joseph A. Cavallaro

U.S. Department of Energy
Pittsburgh Energy Technology Center
Pittsburgh, Pennsylvania 15236.

ABSTRACT

Demineralization of coals and coal-derived chars is part of an effort to develop alternative fuels from coal. Pyrolysis and some gasification processes yield chars containing a large fraction of the calorific value of the feed coal and essentially all of its mineral matter. In the work reported here, three gasification chars produced from anthracite, bituminous, and subbituminous coals have been subjected to specific gravity separation to determine their yield-ash relationships. Either low yields or high ash levels in the float products were observed. Also reported is preliminary work concerning the use of chemical conditioning to enhance the cleanability of coal prior to physical beneficiation. Conditioning of an Illinois No. 6 River King Mine coal with either supercritical methanol or cyclohexane resulted in an improved yield-ash relationship, whereas similar treatment with supercritical toluene had a negative effect.

INTRODUCTION

Currently, there is increasing interest in the identification, development, and characterization of new coal-derived fuels which have application extending beyond traditional electric utility markets into the commercial, industrial, residential, and transportation sectors of our economy. To penetrate these markets, new fuels must be low in both total sulfur and mineral matter. Emphasis is therefore being placed on the development of new processes to provide ultraclean coal having less than one percent mineral matter. In one recent example coal is subjected to physical beneficiation, pyrolysis, and subsequent beneficiation of the char [1]. In this scheme, a portion of the char is combined with the pyrolysis liquids to produce a heavy oil substitute. In order for the process to be profitable, however, the excess char must be sold at a premium price, such as in the residential heating market.

Results from two different areas of research concerned with the development of alternative fuels from coal will be presented in this paper. The first area involves beneficiation of chars produced from coal. Such chars may be a major product of gasification and pyrolysis processes used to produce premium liquid and gaseous fuels. Since a large portion of the calorific value often ends up in the char, the beneficiation of this material to produce a premium fuel can be important from a process economics standpoint.

The second area of research is concerned with the use of a chemical pretreatment to improve mineral matter liberation during subsequent physical beneficiation. Advantages of this reversal of the conventional order of treatment have been discussed elsewhere [2]. Reported here are preliminary results from the use of supercritical fluids in the initial chemical-pretreatment step.

For reasons of clarity, the following discussion of methodology and results is divided into two parts. The first section describes the beneficiation of the gasification chars, and the second the work on conditioning of coal prior to its physical beneficiation. After this, an overall conclusion section summarizes both areas of research.

I. BENEFICIATION OF GASIFICATION CHARs

EXPERIMENTAL

Three gasification chars produced at the Pittsburgh Energy Technology Center were used for the beneficiation tests. These chars were formed from three different coals: a Pennsylvania anthracite coal, a Pittsburgh seam bituminous coal from the Bruceston Experimental Research Mine, and a Montana subbituminous coal from the Rosebud Mine. These coals were gasified at approximately 1160 K under a combined oxygen/steam pressure of 4.1 MPa in the Synthane Process Development Unit (PDU) gasification system. The PDU system combined the steps of fluidized-bed pre-treatment, free-fall carbonization, and fluidized-bed gasification [3]. Table 1 contains the analysis of the three chars used.

Beneficiation of the gasification chars involved a washability determination on the char as received and after additional crushing. A high-speed centrifuge equipped with four 0.5 L hourglass-shaped flasks was used to effect the specific gravity separations. Enough heavy organic liquid was added to fill each centrifuge flask just above the neck. The specific gravity was checked with a spindle hydrometer to within ± 0.001 of a specific gravity unit.

Four 25-gram samples were riffled from each char using a microsplitter. The 25-gram char samples were then added to the flasks along with enough additional liquid to bring the liquid level to within 1.5 cm of the top of the flask. The samples were centrifuged for 20 minutes at 1500 rpm, and the centrifuge was allowed to stop without braking. After removing the flasks, thin rubber inserts were put in the necks, and the float products were carefully poured off. The rubber inserts were removed to recover the sink products. Both products were vacuum filtered to remove the heavy liquid, air dried, and weighed.

The total sink product was divided into two or four equal portions by weight and then added to the centrifuge flasks containing the next higher specific gravity liquid. This procedure was repeated for each specific gravity. Each product was analyzed for calorific value, ash, and total sulfur. All results are tabulated as cumulative values and are reported on a moisture-free basis.

Another riffled portion of each char sample was crushed to either 200- or 325-mesh top size, and similar tests and analyses were performed to determine the effects of crushing on the liberation of ash and its subsequent removal.

DISCUSSION OF RESULTS

The results of the specific gravity separations for the three as-received and crushed chars are contained in Tables 2, 3, and 4. For the anthracite coal gasification char shown in Table 2, the as-received sample contained 69.7 wt% plus-200-mesh material. After crushing, 91.9 wt% of the sample was minus-325 mesh. For the as-received sample, 79.1 wt% could be recovered at 2.00 specific gravity, analyzing 7.6 wt% ash. This represents a 54% ash reduction. After crushing, only 44.0 wt% was recovered at the same specific gravity, and only a 10% ash reduction was observed.

The data for the bituminous coal gasification char are contained in Table 3. Initially 76.5 wt% of the char was plus-200 mesh. After crushing, all of the sample was minus-200 mesh. At a specific gravity of 1.80, 87 wt% of the char was recovered; however the ash reduction was only 28%. After crushing, the ash content of the float 1.80 specific gravity product was only 4.1 wt%, but the weight recovery was only 20.5%.

Table 4 contains the results for the subbituminous coal gasification char. The as-received char contained 44.7 wt% plus-200-mesh material. After crushing,

96.8 wt% was minus-200 mesh. The float-sink tests show a 72% ash reduction for the as-received material recovered at 1.80 specific gravity. However, as with the bituminous coal, the weight recovery is quite low. For this char, crushing appears to be of no benefit, as the yield/ash relationship for the crushed char is essentially the same as for the as-received material.

It is apparent from these washability data that the apparent particle density of the chars is higher than that observed for coal. In most of the tests, less than 20 wt% of the char would float in liquids of 1.80 specific gravity. For most raw coals, upwards of 70 wt% would float in such liquids, with only the concentrated mineral matter occurring in the sink product. Also, for coal, crushing to a finer size typically improves the yield/ash relationship. For the chars, crushing was either of no value or resulted in a poorer yield/ash relationship.

To explain these observations, phenomena occurring during the formation of the chars must be considered. Under the high-temperature gasification conditions, the pore structure of the coal may collapse or otherwise be destroyed; and as a result, a denser form of carbon would exist in the char. Also under these conditions, the volatile matter is driven off. Loss of this relatively light material would also cause an increase in the apparent particle density. Finally, encapsulation of the mineral matter by the organic phase would increase the apparent particle density and also result in a more homogeneous material that would be difficult to beneficiate by physical means. Encapsulation of the ash would also explain why these gasification chars were less responsive to grinding for release of mineral matter than typical coals, since there would be less segregation of the various materials. We have visually observed under the microscope such encapsulation of the ash in other chars produced by similar high-temperature processing.

II. CONDITIONING OF COAL PRIOR TO PHYSICAL BENEFICIATION

EXPERIMENTAL

A unit has been designed and constructed to process coal and coal-derived materials with supercritical fluids. Figure 1 contains a sectional view of the heart of this apparatus, the supercritical fluid extraction vessel. The vessel is constructed entirely of 316 stainless steel and can be operated at conditions up to 673 K at 27.6 MPa. In the work reported here, the reflux column, which consists of a packed bed and condenser section, was maintained at the same temperature as the extraction section. The use of a temperature difference across the column to exploit the properties of supercritical fluids to fractionate non-distillable coal-derived liquids has been reported elsewhere [4].

The coal used in this work was a channel sample of Illinois No. 6 coal from the River King Mine containing 8.31 percent moisture, 13.33 percent ash, and 4.68 percent sulfur. Supercritical methanol ($T_c = 512.6$ K; $P_c = 8.097$ MPa), cyclohexane ($T_c = 553.4$ K; $P_c = 4.074$ MPa), and toluene ($T_c = 591.7$ K; $P_c = 4.115$ MPa) were used in the treatment of this coal. The solvents were obtained in drum quantities at greater than 99 percent purity and used as received.

A 500-gram charge of the coal, crushed to minus-14 mesh, is first placed in the extraction section of the supercritical fluid extraction vessel. After the unit is stabilized at operating conditions under a nitrogen atmosphere, the supercritical fluid is introduced into the bottom of the vessel through the sparger, where it contacts the coal. The fluid phase containing extracted material continues up the column and exits at the top of the vessel. The extracted material leaving the column is separated from the supercritical fluid by partial depressurization. The fluid is then condensed for reuse. Before being recycled in the unit, the solvents are distilled on a rotary evaporator.

The Illinois No. 6 coal was processed with methanol, cyclohexane, and toluene at a T_r , or T/T_C , of 1.02, and at a P_r , or P/P_C , of 2.0. The runs were terminated when the rate of collection of extracted material was less than 1 gram in 30 minutes. This required from 5 to 9 hours of operation. The flow of solvent was maintained at 0.27 gram-moles/minute during most of this work. This rate was doubled in one of the toluene treatments. No appreciable change was observed in the yield of extract in this case. To provide sufficient material for characterization and physical beneficiation testing, two runs were made with each solvent, and the respective products were combined. The yields of treated coal on a moisture-free basis were 90, 89, and 75 weight percent for methanol, cyclohexane, and toluene, respectively. The overall material balance, defined as the total weight of recovered material divided by the weight of the coal initially charged, ranged from 95 to 102 percent for all the tests.

Specific gravity separations of the treated coals were performed using conventional static float-sink techniques to determine their beneficiation potential.

DISCUSSION OF RESULTS

Tables 5 through 8 contain the results from the washability analysis of the Illinois No. 6 coal before and after treatment. These data are cumulative values and are reported on a moisture-free basis. Also shown in these tables are ash, total sulfur, and calorific value data obtained on the bulk samples prior to the specific gravity separations. The agreement between the bulk values and the results reconstituted from the washability data is generally acceptable. Noteworthy exceptions are the total sulfur contents of the coals treated with methanol and cyclohexane and the ash content of the toluene-treated coal. Additional work is being performed to find an explanation for these differences.

Reduction in total sulfur concentration is only observed in the specific gravity separation products of the methanol-treated coal. The higher total sulfur levels resulting from the cyclohexane and toluene treatments are primarily due to the extraction of a portion of the organic phase, which concentrates the remaining sulfur in the treated coal. The extractable materials from all of the tests contain approximately 2.4 wt% sulfur and no mineral matter. Sulfur balances for the treated coals using the bulk sample sulfur data are between 95 and 99 percent.

Unusually low levels of pyritic sulfur are reported for the cyclohexane-treated coal. The total sulfur, however, did not decrease by a corresponding amount, indicating either that organic sulfur was formed from the sulfur originally contained in the pyrite or that the analysis for pyritic sulfur is in error. Under the relatively mild reaction conditions, it is not likely that sulfur from the pyrite has incorporated into the organic matrix of the coal. Rather, the pyrite has probably been transformed into a form that does not dissolve in the acid used for the pyritic sulfur determination.

In contrast to the other treated coals, the total and pyritic sulfur levels in the toluene-treated coal remain high, even in the low specific gravity fractions. One possible explanation is that the toluene treatment caused a softening of the organic portion of the coal, resulting in increased encapsulation of the mineral matter. This would make the material more homogeneous with respect to the specific gravity separations. Softening of the coal was evidenced by the fact that the coal was mildly agglomerated after the toluene treatment. After treatment with either methanol or cyclohexane, however, the product was free-flowing and similar in appearance to the starting material.

Microscopic analysis of the various specific gravity fractions shows the toluene treatment produces particles that contain relatively more and larger pore openings than the particles after methanol or cyclohexane treatment. This characteristic could decrease the apparent specific gravities of the coal particles and result in

the poor sulfur rejection observed for the toluene-treated coal. This phenomenon would explain the high yield in the Float-1.25 fraction. Several other coals have been treated to provide a larger frame of reference from which to investigate these observations.

In order to illustrate the changes in the true and/or apparent specific gravities of the coal particles resulting from the supercritical fluid treatments, the yield versus ash content data are plotted in Figure 2 for the raw and treated coals. In comparison with raw coal washability data, both the methanol and cyclohexane treatments marginally enhance the cleanability of the raw coal. In contrast, the toluene treatment makes it worse. Additional work with other solvents is in progress to determine if the positive trends observed with methanol and cyclohexane can be improved.

CONCLUSIONS

A set of three gasification chars have been subjected to physical beneficiation. In some cases, marginal improvements in the mineral matter content were achieved, but either unsatisfactory ash liberation or low yields were observed overall. The form of carbon in the ash is much denser than that typical for coal. One explanation for this observation is that some of the mineral matter has been encapsulated during the formation of the char. This is further evidenced by the poor response of the chars upon further size reduction. Other phenomena, such as loss of porosity and volatile matter, may also contribute to the poor separations observed. In summary, these observations highlight the inadequacy of conventional physical-cleaning methods for some coal-derived materials. If a clean char product is to be produced, either deeper initial cleaning of the coal is required or new techniques must be developed to separate the mineral matter from the resulting chars.

The washability of coal can be marginally improved through the use of an initial pretreatment with supercritical methanol or cyclohexane. Similar treatment with supercritical toluene has the opposite effect. While not presently practical from an economic standpoint, this work may provide new insights into possible avenues for producing alternative fuels from coal. More work needs to be done to determine if the mineral matter liberation can be further improved by varying the conditions and reagents used in the pretreatment.

ACKNOWLEDGMENT

The authors would like to thank Robert Kornosky for his assistance in obtaining the gasification chars used in this work and Geno Irdi for performing the microscopic analyses.

DISCLAIMER

Reference in this report to any specific product, process, or service is to facilitate understanding and does not necessarily imply its endorsement or favoring by the United States Department of Energy.

REFERENCES

1. McCown, F.E., Im, C.J., and Wolfe, R.A., Proceedings of the Second Annual Pittsburgh Coal Conference, 1985, 479.
2. Walters, A.B., ACS Fuel Division Preprints, 29(4), 1984, 337.
3. Kornosky, R.M., Gasior, S.J., Strakey, J.P., and Haynes, W.P., ACS Fuel Division Preprints, 22(2), 1977, 197.
4. Warzinski, R.P., ACS Fuel Division Preprints, 30(3), 1985, 139.

Table 1. Chemical Analysis of Gasification Chars

Coal Type	Subbituminous	Bituminous	Anthracite
Char Yield, wt% of Raw Coal	25	39	45
Proximate Analysis, wt%			
Moisture	1.8	1.3	0.5
Volatile Matter	5.8	1.7	3.1
Fixed Carbon	57.7	72.9	75.6
Ash	34.7	24.2	20.8
Ultimate Analysis, wt% mf			
Carbon	60.3	72.2	74.7
Hydrogen	1.2	1.4	1.1
Nitrogen	0.4	0.7	0.6
Oxygen	3.3	1.4	2.5
Sulfur	0.2	0.3	0.3
Ash	34.7	24.2	20.8
Calorific Value, Btu/lb	9,308	10,622	----

Table 2. Cumulative Washability Results for the Anthracite Coal Gasification Char

Products	--- As-Received ---				--- Crushed ---			
	Yield	Ash	Total Sulfur	Btu/lb	Yield	Ash	Total Sulfur	Btu/lb
	--- wt% mf ---				--- wt% mf ---			
Float 1.60	16.4	3.4	0.45	14,019	3.8	2.2	0.54	14,199
1.60 x 1.80	52.9	6.4	0.41	13,145	4.5	3.4	0.51	13,976
1.80 x 2.00	79.1	7.6	0.33	12,746	44.0	15.9	0.33	11,580
Sink 2.00	100.0	16.7	0.29	11,447	100.0	17.8	0.32	11,259

Table 3. Cumulative Washability Results for the Bituminous Coal Gasification Char

Products	--- As-Received ---				--- Crushed ---			
	Yield	Ash	Total Sulfur	Btu/lb	Yield	Ash	Total Sulfur	Btu/lb
	--- wt% mf ---				--- wt% mf ---			
Float 1.40	63.0	11.2	0.57	12,368	--0--	---	---	-----
1.40 x 1.60	77.2	11.5	0.53	12,265	19.5	3.8	0.80	13,100
1.60 x 1.80	87.0	12.8	0.49	12,103	20.5	4.1	0.78	13,041
1.80 x 1.90	100.0	17.8	0.45	11,354	23.0	5.1	0.73	12,894
1.90 x 2.00	----	----	----	----	98.5	15.7	0.35	10,991
Sink 2.00	----	----	----	----	100.0	17.0	0.35	10,953

Table 4. Cumulative Washability Results for the Subbituminous Coal Gasification Char

Products	--- As-Received ---				--- Crushed ---			
	Yield	Ash	Total Sulfur	Btu/lb	Yield	Ash	Total Sulfur	Btu/lb
	--- wt% mf ---				--- wt% mf ---			
Float 1.60	6.2	7.6	0.38	12,289	5.2	7.2	0.46	12,138
1.60 x 1.80	14.6	8.9	0.23	12,297	5.6	8.8	0.46	11,909
1.80 x 2.20	100.0	32.1	0.19	9,456	97.7	30.0	0.26	8,873
Sink 2.20	----	----	----	-----	100.0	30.1	0.28	8,860

Table 5. Cumulative Washability Results for Illinois No. 6 Coal

Products	Yield	Ash	Total Sulfur	Pyritic Sulfur	Btu/lb
	--- wt% mf ---				
Float 1.25	-0-	----	----	----	-----
1.25 x 1.28	3.4	3.1	2.60	0.45	13,777
1.28 x 1.30	12.8	2.6	2.67	0.37	13,836
1.30 x 1.40	67.5	5.4	3.12	0.78	13,492
1.40 x 1.60	86.4	7.6	3.40	1.14	13,450
Sink 1.60	100.0	13.8	5.02	2.92	12,410
Bulk Sample	-----	14.5	5.10	-----	11,713

Table 6. Cumulative Washability Results for Methanol-Treated Illinois No. 6 Coal

Products	Yield	Ash	Total Sulfur	Pyritic Sulfur	Btu/lb
	--- wt% mf ---				
Float 1.25	-0-	----	----	----	-----
1.25 x 1.28	8.5	1.9	2.50	0.25	13,781
1.28 x 1.30	30.9	2.4	2.59	0.29	13,653
1.30 x 1.40	69.3	5.3	2.86	0.68	13,202
1.40 x 1.60	82.7	7.2	3.14	0.96	12,877
Sink 1.60	100.0	15.3	4.74	2.84	11,485
Bulk Sample	-----	14.9	5.29	-----	11,601

Table 7. Cumulative Washability Results for Cyclohexane-Treated Illinois No. 6 Coal

Products	Yield	Ash	Total Sulfur	Pyritic Sulfur	Btu/lb
	--- wt% mf ---				
Float 1.25	7.4	2.3	2.88	0.41	13,847
1.25 x 1.28	25.5	3.4	2.90	0.19	13,826
1.28 x 1.30	42.7	3.1	3.02	0.16	13,713
1.30 x 1.40	72.7	5.5	3.42	0.17	13,339
1.40 x 1.60	86.4	7.5	3.85	0.18	13,036
Sink 1.60	100.0	14.7	4.38	1.03	12,031
Bulk Sample	-----	15.4	5.38	-----	11,808

Table 8. Cumulative Washability Results for Toluene-Treated Illinois No. 6 Coal

Products	Yield	Ash	Total Sulfur	Pyritic Sulfur	Btu/lb
		wt%	mf		
Float 1.25	42.4	8.3	3.22	1.44	12,885
1.25 x 1.28	50.0	8.5	3.24	1.48	12,869
1.28 x 1.30	53.6	8.3	3.21	1.46	12,938
1.30 x 1.40	73.0	8.6	3.22	1.50	12,863
1.40 x 1.60	83.5	9.8	3.41	1.70	12,672
Sink 1.60	100.0	17.3	5.51	3.92	11,465
Bulk Sample	-----	19.3	5.75	-----	11,263

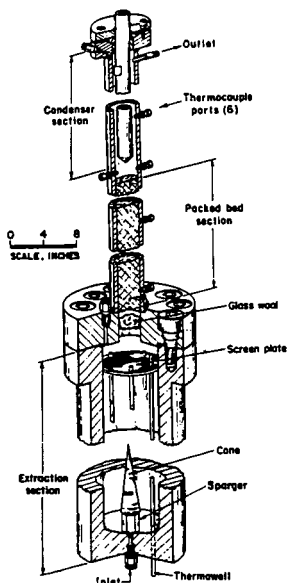


Figure 1. Sectional View of the Supercritical Fluid Extraction Vessel.

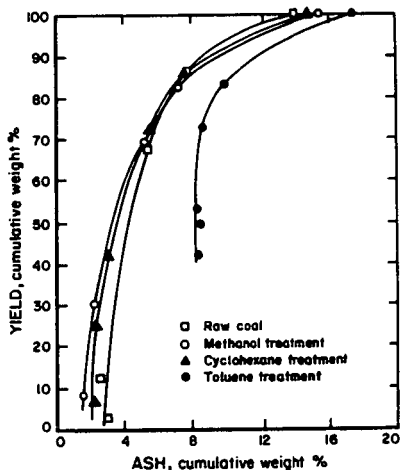


Figure 2. Comparison of Washability Data for Illinois No. 6 Coal Before and After Treatments with Supercritical Methanol, Cyclohexane, and Toluene.

NO. 6880